Jason B. West · Gabriel J. Bowen
Todd E. Dawson · Kevin P. Tu
Editors

Isoscapes

Understanding movement, pattern, and process on Earth through isotope mapping

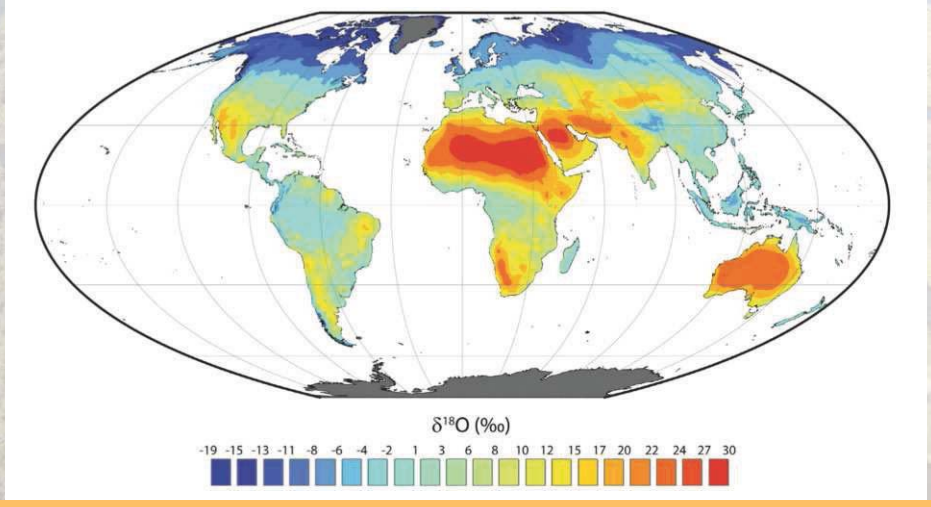

Springer

Isoscapes

Jason B. West · Gabriel J. Bowen
Todd E. Dawson · Kevin P. Tu
Editors

Isoscapes

Understanding Movement, Pattern, and Process on Earth Through Isotope Mapping

Springer

Editors
Jason B. West
Department of Ecosystem Science and Management
Texas AgriLife Research
Texas A&M University System
Uvalde, TX
USA
jbwest@tamu.edu

Gabriel J. Bowen
Department of Earth and Atmospheric Sciences
Purdue Climate Change Research Center
Purdue University
West Lafayette, IN
USA
gjbowen@purdue.edu

Todd E. Dawson
Department of Integrative Biology
Center for Stable Isotope Biogeochemistry
University of California
Berkeley, CA
USA
tdawson@berkeley.edu

Kevin P. Tu
Department of Integrative Biology
University of California
Berkeley, CA
USA
kevinptu@gmail.com

ISBN 978-90-481-3353-6 e-ISBN 978-90-481-3354-3
DOI 10.1007/978-90-481-3354-3
Springer Dordrecht Heidelberg London New York

Library of Congress Control Number: 2009934502

Cover illustration: Top right: A monarch butterfly. *Top center:* A Boreal landscape in northeastern Alberta, Canada. Oxbow lakes surrounding the Winifred River channel situated 4 km east of the Christina River confluence, looking north. Photo provided courtesy of Alberta Research Council (photo taken 13 September 2007). *Bottom center:* A leaf water isoscape provided courtesy of Jason West (see Chapter 8, this volume).

Printed on acid-free paper

Springer is part of Springer Science+Business Media (www.springer.com)

Preface

Context and Background for the Topic and Book

Since the discovery of isotopes and the development of precise instrumentation capable of measuring small differences in isotope abundances, there has been an interest in quantifying and understanding the spatio-temporal distributions of isotope ratio variation in natural systems. The wealth of information about spatially-distributed Earth system processes potentially available in these records drives this interest and includes insights to such processes as the origins and mixing of meteoric, surface and ground water, human movement, carbon cycling between vegetation and the atmosphere, and tracking of atmospheric pollution (Friedman 1953; Clayton et al. 1966; Zimmermann and Cegla 1973; Adar and Neuman 1988; Martinelli et al. 1991; Rozanski et al. 1991; Farquhar et al. 1993). The recent and continuing development of analytical tools for isotope analysis, in particular continuous-flow isotope ratio mass spectrometry (CF-IRMS) methods, as well as other newer approaches such as laser spectroscopy (e.g., Metzger 1978; Preston and Owens 1983; Marshall and Whiteway 1985; Jensen 1991; Lis et al. 2008), have led to dramatic increases in the availability of light stable isotope data, while advances in the measurement of radioactive isotopes (Wölfli 1987; Southon et al. 2004) and heavy stable, radiogenic isotopes (Capo et al. 1998; Barnett-Johnson et al. 2005) have also increased the availability of these data. In addition, an abundance of spatially-explicit datasets have emerged from a host of Earth-observing instruments (Justice et al. 1998; Njoku et al. 2003), and computer and software developments, especially in Geographic Information Systems (Goodchild 2003), continue to supply critical tools for exploring spatial variation in isotope ratios and its application to questions across a spectrum of scientific domains.

It was in this context that two of the editors of this book (West and Bowen) were engaged in research in the laboratories of Jim Ehleringer and Thure Cerling developing the capacity to reconstruct histories and origins of materials based on their isotopic composition. As we worked on these problems, including sampling the spatial isotopic variability of various systems, developing and evaluating models to describe and predict observations, constructing new approaches for mapping, and developing inferences and approaches to tackle unknowns, a common language and set of ideas

began to emerge that unified these efforts. An important element common to efforts to understand human movements over landscapes, the changing sources of water to cities, or the geographic origin of drugs or counterfeit money (taking some of our work as examples) is the development of maps of the spatial isotopic variation of the material(s) of interest. We have called these maps "isoscapes" from "isotope landscapes" and thought that, more than just a useful new term, this represented an opportunity to advance science by recognizing commonalities across disciplines through the expanding interest in isoscapes. Although perhaps not previously recognized as having a common ground, questions being addressed using isoscapes come from plant and animal ecology, geology, atmospheric sciences, anthropology, forensic science, and microbiology. We believed that there were significant and important commonalities in the ways questions were being asked, the models being developed and tested, the products derived from these modeling efforts and the conclusions drawn from them. It was these commonalities that promised to form the basis for new interactions and insights both within individual fields and across disciplines.

To foster these interactions, we envisioned a conference dedicated to isoscapes followed by publications highlighting advances across and between fields. This conference would assemble a diverse set of scientists and students interested in isoscapes and allow for synergistic interactions, generate new ideas and insights, and foster a kind of common arena for a community of scientists interested in isoscapes. The idea was strongly supported by the National Science Foundation-funded Research Coordination Network BASIN (Biogeosphere Atmosphere Stable Isotope Network), which provided significant financial and organizational support for the *Isoscapes 2008* meeting. An additional RCN that represented a key isoscapes "contingency" in the study of animal migration also provided financial support (MIGRATE). So, along with the other two editors of this book (Dawson and Tu), we designed a meeting that we believe accomplished our goals, bringing together individuals from a diverse set of disciplines (see Fig. 1) for substantive dialogs about isoscapes. The meeting was held in Santa Barbara, California in April 2008 and, in spite of the beautiful weather and very nearby beach, the sessions were well-attended and generated exciting dialogs about questions being asked, methodology, results, analytical approaches, and of course interpretations. Break-out discussions developed ideas that were incorporated in an article published in Eos (Bowen et al. 2009) and there were 81 contributions to poster sessions, some of which resulted in publications in a special issue of the Journal of Geochemical Exploration.

The chapters here were developed by our invited speakers and their co-authors from ideas presented at the meeting. The book as a whole is intended to serve as a reference for the current state of the science and highlight some of the exciting avenues of future work envisioned by the chapter authors. It is organized into three thematic sections encompassing isoscapes in current research: (1) gathering and using spatially explicit isotope data, (2) isotope mapping: theory and methods, and (3) multidisciplinary applications of isoscapes. In the first section there are six chapters that address the development, advances, and future promise of spatially explicit isotope data. These chapters primarily focus on global and regional isotope data collection, including that of small groups of investigators, national and international organizations, and post hoc approaches to integrating data across multiple, individual

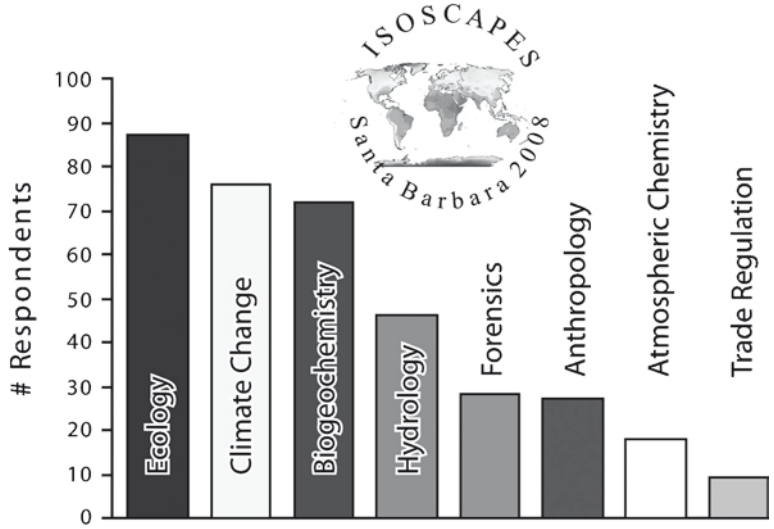

Fig. 1 Areas of research interest represented at the Isoscapes 2008 conference. Registrants (N = 124) were asked to indicate one or more primary areas of research interest

efforts. Atmospheric gases, precipitation and other surface waters are discussed, as are new approaches and methodologies for collecting isotope data using remote sensing instruments, laser spectroscopy, and plants as proxies. Section two is composed of chapters primarily on methodological and theoretical aspects of isoscapes modeling, including precipitation isoscapes at regional to global scales, plant carbon, hydrogen and oxygen isoscapes, nitrogen isoscapes of soils and plants and a discussion of statistical considerations important to inferring origins from these spatially explicit isotope predictions. Section three focuses on the wide array of questions addressed by researchers using isoscapes and highlights the diversity of insights that are possible. These include tracing the movements of animals across both terrestrial and aquatic environments in modern and paleoecological contexts, the information provided by isoscapes to archaeological investigations and modern forensic reconstruction efforts, improved understanding of large scale hydrologic systems, and the utility of plants as biomarkers of pollution. Together these sections offer case studies documenting the lifecycle of isoscapes, from the prerequisite and often fortuitous compilation of data, through quantitative, often multidisciplinary, data analysis, to application towards multiple problems in a range of scientific fields.

A Brief Isotope Primer

For those unfamiliar with isotope terminology and measurement approaches, we include here a very brief primer. Readers are also referred to books by Robert Criss (1999) and Zachary Sharp (2007) for more detailed information. Isotopes are elements

(or nuclides) with unique atomic masses – isotopes of a given element have the same number of protons, but have different numbers of neutrons. Stable isotopes are those that do not undergo radioactive decay, whereas radioactive isotopes are those that do decay with different half-lives and decay products. The light elements that are the primary focus of the book chapters presented here have more than one stable isotope. For example, carbon has two: ^{13}C and ^{12}C. The average abundances of the isotopes of elements discussed in this book are shown in Table 1.

Stable isotope abundances are expressed in a "difference" or delta (δ) notation relative to the rare to common isotope ratio of a standard:

$$\delta = \frac{R_{sample} - R_{standard}}{R_{standard}}, \quad (1)$$

where R is the molar ratio of the heavy (rare) to light (common) isotope of the sample and standard (e.g., the ratio of ^{13}C to ^{12}C). Delta values are quite small, and are usually reported in units of parts per thousand (per mil, ‰). Accepted standards used by the international community to allow traceability to internationally recognized scales

Table 1 Average abundances of stable isotopes and half-lives of radioactive isotopes important in an isoscapes context (Criss 1999; Fowler 1990). The *dashed line* separates the "light" isotopes from the "heavy" isotopes. Other "heavy" elements may also prove useful in the future as more efforts are directed at understanding their fractionations and abundances

Element	Isotope	Average abundance (atom fraction, %)	Half-life (years)
Hydrogen	^{1}H	99.985	
	^{2}H	0.015	
	^{3}H	–	12.3
Carbon	^{12}C	98.90	
	^{13}C	1.10	
	^{14}C	–	5,730
Nitrogen	^{15}N	99.63	
	^{14}N	0.37	
Oxygen	^{16}O	99.76	
	^{17}O	0.04	
	^{18}O	0.20	
Sulfur	^{32}S	95.02	
	^{33}S	0.75	
	^{34}S	4.21	
	^{36}S	0.02	
Rubidium	^{85}Rb	72	
	^{87}Rb	28	4.88×10^{10}
Strontium	^{84}Sr	0.6	
	^{86}Sr	10	
	^{87}Sr	7	
	^{88}Sr	83	

include (National Institutes of Standards and Technology-NIST) Vienna Standard Mean Ocean Water - VSMOW (NIST RM #8535) and Standard Light Antarctic Precipitation - SLAP (NIST RM #8537) for hydrogen and oxygen (SMOW scale), NBS 19 - limestone (NIST RM #8544) and L-SVEC - lithium carbonate (NIST RM #8545) for carbon (PDB scale), atmospheric air for nitrogen (on the AIR-N_2 scale), and IAEA-S-1 - silver sulfide (NIST RM #8554) for sulfur (on the VCDT scale). These materials can be obtained from the International Atomic Energy Agency (IAEA) or NIST and are used to calibrate laboratory reference materials that are then run with unknowns to allow data corrections (Werner and Brand 2001).

Changes in the isotopic composition of substances occurring as the result of a single process (e.g., evaporation), or sometimes, less satisfyingly, as the net result of a set of processes (e.g., cellulose formation), are expressed with fractionation factors. A fractionation factor is defined as:

$$\alpha_{A-B} = \frac{R_A}{R_B}, \tag{2}$$

where R_A and R_B are the isotope ratios of the two substances. Fractionations are also often expressed by simply subtracting the δ-value of one substance (e.g., that of the liquid) from the δ-value of its paired substance (e.g., that of the gas) as:

$$\Delta_{A-B} = \delta_A - \delta_B. \tag{3}$$

When the isotope ratio differences are small (e.g., <10‰) between substance A and substance B, then this so-called "big delta" is a reasonable approximation for α:

$$\Delta_{A-B} \approx 10^3 \ln \alpha_{A-B}. \tag{4}$$

Similarly, epsilon is defined as:

$$\varepsilon = (\alpha - 1)10^3, \tag{5}$$

is similar to Δ and also approximately equal to 10^3. ln α when the differences between A and B are relatively small. Sharp (2007) recommends against using ε since it is has a different definition in radiogenic isotope geochemistry.

Radioactive carbon isotope abundances are expressed in a similar fashion, with reference to an Oxalic Acid standard (OX1) but also removing mass-dependent fractionation and accounting for the radioactive decay of the Oxalic Acid standard since 1950. Since the introduction of additional ^{14}C into the atmosphere by atmospheric nuclear weapons testing, radioactive carbon isotopes can be expressed in the following manner:

$$\Delta^{14}C = \left[\frac{\left(\frac{^{14}C}{^{22}C} \right)_{sample(-25\%)}}{0.95 \times \left(\frac{^{14}C}{^{22}C} \right)_{OX_1(-19\%,1950)}} - 1 \right] \times 1000, \tag{6}$$

Most of the stable isotope ratio data discussed in this book will have come from analyses performed using isotope ratio mass spectrometers. These instruments are capable of measuring, at very high precision, the ratios of heavy to light isotopes in gases. They are often coupled to peripherals that generate and separate these gases from liquid and solid materials and then deliver these, using helium as a carrier gas, to the mass spectrometer (so-called continuous flow approaches; see Dawson and Brooks 2001 or Sharp 2007). The radioactive isotope of carbon (^{14}C) is often measured using accelerator mass spectrometers (AMS), with important offline preparation methodologies to ensure accurate measurements. The reader is referred to de Groot (2004, 2008) for extensive information on stable isotope methodology and Tuniz (2001) and references therein for additional information on accelerator mass spectrometry methodology.

TX, USA Jason B. West
IN, USA Gabriel J. Bowen
CA, USA Todd E. Dawson

References

Adar EM, Neuman SP (1988) Estimation of spatial recharge distribution using environmental isotopes and hydrochemical data. 2. Application to Aravaipa Valley in southern Arizona, USA. J Hydrol 97:279–302

Barnett-Johnson R, Ramos FC, Grimes CB, MacFarlane RB (2005) Validation of Sr isotopes in otoliths by laser ablation multicollector inductively coupled plasma mass spectrometry (LA-MC-ICPMS): opening avenues in fisheries science applications. Can J Fish Aquat Sci 62:2425–2430

Bowen GJ, West JB, Vaughn BH, Dawson TE, Ehleringer JR, Fogel ML, Hobson K, Hoogewerff J, Kendall C, Lai C-T, Miller CC, Noone D, Schwarcz H, Still CJ (2009) Isoscapes to address large-scale Earth science challenges. Eos, Trans, Am Geophys Union 90:109–116

Capo RC, Stewart BW, Chadwick OA (1998) Strontium isotopes as tracers of ecosystem processes: theory and methods. Geoderma 82:197–225

Clayton RN, Friedman I, Graf DL, Mayeda TK, Meents WF, Shimp NF (1966) Origin of saline formation waters. 1. Isotopic composition. J Geophys Res 71:3869.

Criss RE (1999) Principles of stable isotope distribution. Oxford University Press, New York

Dawson TE, Brooks PD (2001) Fundamentals of stable isotope chemistry and measurement. In: Unkovich M, McNeill L, Pate J, Gibbs J (eds) The application of stable isotope techniques to study biological processes and the functioning of ecosystems. Kluwer, Dordrecht

de Groot P (2004) Handbook of stable isotope analytical techniques, volume I. Elsevier, Amsterdam

de Groot P (2008) Handbook of stable isotope analytical techniques, volume II. Elsevier, Amsterdam

Farquhar GD, Lloyd J, Taylor JA, Flanagan LB, Syvertsen JP, Hubick KT, Wong SC, Ehleringer JR (1993) Vegetation effects on the isotope composition of oxygen in atmospheric CO_2. Nature 363:439–443

Fowler CMR (1990) The solid earth: an introduction to global geophysics. Cambridge University Press, Cambridge

Friedman I (1953) Deuterium content of natural waters and other substances. Geochim Cosmochim Acta 4:89–103

Goodchild ME (2003) Geographic information science and systems for environmental management. Ann Rev Env Res 28:493–519

Jensen ES (1991) Evaluation of automated-analysis of N-15 and total N in plant-material and soil. Plant Soil 133:83–92

Justice CO, Vermote E, Townshend JRG, Defries R, Roy DP, Hall DK, Salomonson VV, Privette JL, Riggs G, Strahler A, Lucht W, Myneni RB, Knyazikhin Y, Running SW, Nemani RR, Wan ZM, Huete AR, van Leeuwen W, Wolfe RE, Giglio L, Muller JP, Lewis P, Barnsley MJ (1998) The Moderate Resolution Imaging Spectroradiometer (MODIS): land remote sensing for global change research. IEEE Trans Geosci Remote Sens 36:1228–1249

Lis G, Wassenaar LI, Hendry MJ (2008) High-precision laser spectroscopy D/H and O-18/O-16 measurements of microliter natural water samples. Anal Chem 80:287–293

Marshall R, Whiteway J (1985) Automation of an interface between a nitrogen analyser and an isotope ratio mass spectrometer. Analyst 110:867–871

Martinelli LA, Devol AH, Victoria RL, Richey JE (1991) Stable carbon isotope variation in C_3 and C_4 plants along the Amazon River. Nature 353:57–59

Metzger J (1978) Schnelle Simultanbestimmung yon Stickstoff-15 und Gesamtstickstoff durch direkte Kopplung yon Massenspektrometer und automatischer Elementaranalyse. Fresenius Z Anal Chem 292:44–45

Njoku EG, Jackson TJ, Lakshmi V, Chan TK, Nghiem SV (2003) Soil moisture retrieval from AMSR-E. IEEE Trans Geosci Remote Sens 41:215–229

Preston T, Owens N (1983) Interfacing an automatic elemental analyser with an isotope ratio mass spectrometer: the potential for fully automated total nitrogen and nitrogen-15 analysis. Analyst 108:971–977

Rozanski K, Gonfiantini R, Araguasaraguas L (1991) Tritium in the global atmosphere – distribution patterns and recent trends. J Phys G: Nucl Part Phys 17:S523–S536

Sharp Z (2007) Principles of stable isotope geochemistry. Pearson Education, Upper Saddle River, NJ

Southon J, Santos G, Druffel-Rodriguez K, Druffel E, Trumbore S, Xu XM, Griffin S, Ali S, Mazon M (2004) The Keck Carbon Cycle AMS laboratory, University of California, Irvine: initial operation and a background surprise. Radiocarbon 46:41–49

Tuniz C (2001) Accelerator mass spectrometry: ultra-sensitive analysis for global science. Rad Phys Chem 61:317–322

Werner RA, Brand WA (2001) Referencing strategies and techniques in stable isotope analysis. Rapid Commun Mass Spectrom 15:501–519

Wölfli W (1987) Advances in accelerator mass spectrometry. Nucl Instr Methods Phys Res B: Beam Interact Mater Atoms 29:1–13

Zimmermann U, Cegla U (1973) Isotope content (D, O-18) of human blood - changes induced by change of location. Naturwissenschaften 60:243–246

Acknowledgments

We would like to thank all of the authors for their hard work and contributions to this exciting volume. Thanks also to the many reviewers who provided valuable feedback, improving the quality of the chapters. Many thanks to Tamara Welschot and Judith Terpos at Springer Science+Business Media for their work, support, encouragement, and patience during the entire process. Kathy Kincade is also thanked for her editorial assistance in the final stages of preparing the manuscript. Partial support from the National Science Foundation under Grant No. 0743543 to Bowen and West is gratefully acknowledged.

We would also like to thank all of the participants in the Isoscapes 2008 meeting for their enthusiasm and contributions to fascinating discussions that undoubtedly influenced authors' thinking about isoscapes in their work. The meeting was enriched by tutorials from Mike Goodchild and Phaedon Kyriakidis who are thanked for volunteering their time to make these contributions. Many thanks to Chris Still and Maria Murphy for providing guidance in all that Santa Barbara has to offer, and for a wide range of needed local support. Thanks to Kevin Simonin, Sara Bagusjas, and Park Williams who helped with meeting logistics and thanks to the Hotel Mar Monte for all of their help with the meeting venue. We would also like to thank Rebecca Hufft Kao, Michael Keller, and Hank Loescher at NEON, Inc. for their participation in Isoscapes 2008 and discussion of NEON in relation to spatial understanding of isotope variation. The meeting received support from two National Science Foundation Research Coordination Networks: BASIN (Lead PI: Todd Dawson; Grant No. 0743543) and MIGRATE (Lead PI: Jeff Kelly; Grant No. 0541740). Any opinions, findings, and conclusions or recommendations expressed in this material are those of the author(s) and do not necessarily reflect the views of the National Science Foundation.

Contents

Contributors

Pradeep K Aggarwal
Isotope Hydrology Section, International Atomic Energy Agency,
Vienna, Austria
P.Aggarwal@iaea.org

David Aurioles
Centro Interdisciplinario de Ciencias Marinas, Instituto Politécnico
Nacional, La Paz Baja California Sur, 23060 Mexico
daurioles@hotmail.com

Rachel Barnett-Johnson
Institute of Marine Sciences, University of California Santa Cruz,
100 Schaffer Road, Santa Cruz, CA 95060, USA
Barnett-Johnson@biology.ucsc.edu

Gabriel J. Bowen
Department of Earth and Atmospheric Sciences, Purdue Climate
Change Research Center, Purdue University, West Lafayette,
IN 47907, USA
gabe@purdue.edu

Thure E. Cerling
Department of Biology, University of Utah, 257 S 1400 E, Salt Lake City,
UT 84112, USA
thure.cerling@utah.edu

Lesley A. Chesson
IsoForensics Inc., 423 Wakara Way, Suite 205, Salt Lake City,
UT 84108, USA
lesley@isoforensics.com

Todd E. Dawson
Center for Stable Isotope Biogeochemistry, Department of Integrative Biology,
University of California, Berkeley, CA 94720, USA
tdawson@berkeley.edu

Paul Dostie
Mammoth Lakes Police Department, 568 Old Mammoth Road,
Mammoth Lakes, CA 93546, USA
pdostie@mammothlakespd.org

James R. Ehleringer
Department of Biology, University of Utah, Salt Lake City, UT, USA
ehleringer@biology.utah.edu
and
IsoForensics Inc., Salt Lake City, UT, USA
jim@isoforensics.com

Candice U. Evans
UCB 450 INSTAAR, University of Colorado, Boulder,
CO 80309, USA
Candice.evans@colorado.edu

Balázs M. Fekete
Global Water Center of the CUNY Environmental Crossroads Initiative,
The City College of New York at the City University of New York,
160 Convent Avenue, New York, NY 10031, USA
bfekete@ccny.cuny.edu

John J. Gibson
Alberta Research Council, University of Victoria, Vancouver Island
Technology Park, 3 - 4476 Markham St., Victoria, BC, Canada V8Z 7X8
jjgibson@uvic.ca

Brittany S. Graham
Department of Oceanography, University of Hawai'i, Honolulu, HI 96822, USA
Stable Isotopes in Nature Laboratory (SINLAB), Canadian Rivers Institute,
University of New Brunswick, Fredericton, NB, Canada E3B 5A3
grahamb@unb.ca

Nancy E. Grulke
Pacific Southwest Research Station, USDA Forest Service, Riverside, CA
ngrulke@fs.fed.us

Brent R. Helliker
Department of Biology, University of Pennsylvania, Philadelphia, PA
helliker@sas.upenn.edu

MaryKay Herzenach
Department of Ecology and Evolutionary Biology, University of Colorado,
Boulder, CO
marykay.herzenach@colorado.edu

Keith A. Hobson
Environment Canada, 11 Innovation Blvd., Saskatoon, SK, S7N 3H5, Canada
Keith.Hobson@ec.gc.ca

James W.C. White
CB 450 INSTAAR, University of Colorado, Boulder, CO 80309, USA
James.white@colorado.edu

Jocelyn Turnbull
National Oceanic and Atmospheric Administration, Earth System Research Lab,
325 Broadway, Boulder, CO, 80305-3337, USA
Jocelyn.Turnbull@noaa.gov

Carol Kendall
U. S. Geological Survey, 345 Middlefield Road, MS 434, Menlo Park, CA
ckendall@usgs.gov

Kenneth A. Masarie
National Oceanic and Atmospheric Administration, Earth System Research Lab,
325 Broadway, Boulder, CO 80305-3337, USA
Kenneth.Masarie@noaa.gov

Paul L. Koch
Dept. of Earth and Planetary Sciences, University of California,
Santa Cruz, CA 95064 USA
pkoch@pmc.ucsc.edu

Helen W. Kreuzer
Pacific Northwest National Laboratory
helen.kreuzer@pnl.gov

Kshitij M. Kulkarni
Isotope Hydrology Section, International Atomic Energy Agency,
Vienna, Austria, K.Kulkarni@iaea.org
Isotope Applications Division, Bhabha Atomic Research Centre, Trombay,
Mumbai 400085, India
km.kulu@gmail.com

Turker Kurttas
Isotope Hydrology Section, International Atomic Energy Agency,
Vienna, Austria
T.Kurttas@iaea.org

Steven W. Leavitt
Lab. of Tree-Ring Research, University of Arizona, Tucson, AZ 85721, USA
sleavitt@ltrr.arizona.edu

Liu Yu
The State Key Laboratory of Loess and Quaternary Geology,
The Institute of Earth Environment, Chinese Academy of Sciences,
Xian 710075, PR China, liuyu@loess.llqg.ac.cn

Fred J. Longstaffe
Department of Earth Sciences, University of Western Ontario,
London, Ontario, Canada, flongsta@uwo.ca

Araguás-Araguás Luis J
Isotope Hydrology Section, International Atomic Energy Agency, Vienna, Austria
L.Araguas@iaea.org

Stephen A. Macko
Department of Environmental Sciences, University of Virginia,
291 McCormick Road, Charlottesville, VA 22904, USA
Program in Geobiology and Low Temperature Geochemistry,
U. S. National Science Foundation, Arlington, VA 22230, USA
sam8f@virginia.edu, or smacko@nsf.gov

Manfred Groening
Isotope Hydrology Section, International Atomic Energy Agency, Vienna, Austria
M.Groening@iaea.org

Kelton W. McMahon
MIT-WHOI Joint Program in Biological Oceanography,
Woods Hole Oceanographic Institution, Woods Hole, MA 02543 USA
kmcmahon@whoi.edu

Knute J. Nadelhoffer
Department of Ecology and Evolutionary Biology, University of Michigan,
830 N. University, Ann Arbor, MI
knute@umich.edu

Brent Newman
Isotope Hydrology Section, International Atomic Energy Agency, Vienna, Austria
B.Newman@iaea.org

Seth D. Newsome
Carnegie Institution of Washington, Geophysical Laboratory,
Washington, DC 20015, USA
snewsome@ciw.edu

David Noone
Department of Atmospheric and Oceanic Sciences, and Cooperative
Institute for Research in Environmental Sciences, University of Colorado,
Boulder, CO
dcn@colorado.edu

Gregory S. Okin
Department of Geography, 1255 Bunche Hall, University of California,
Los Angeles, CA 90095, USA
okin@ucla.edu

Linda H. Pardo
Northern Research Station, USDA Forest Service, 705 Spear St.,
S. Burlington, VT 05403, USA
lpardo@fs.fed.us

Todd Park
Salt Lake County Sheriff's Office, 3365 S 900 W, Salt Lake City,
UT 84119, USA
tpark@slco.org

Diane E. Pataki
Department of Earth System Science, University of California, Irvine, CA
Department of Ecology and Evolutionary Biology, University of California,
Irvine, CA
dpataki@uci.edu

David Podlesak
Department of Biology, University of Utah, 257 S 1400 E,
Salt Lake City, UT 84112, USA
podlesak@biology.utah.edu

Rebecca L. Powell
Department of Geography, 2050 E. Iliff Avenue, University of Denver,
Denver, CO 80208, USA
rpowell8@du.edu

James T. Randerson
Department of Earth System Science, University of California,
Irvine, CA
jranders@uci.edu

Margaret J. Schoeninger
Department of Anthropology, University of California at San Diego,
La Jolla, CA 92093-0532, USA
mjschoen@ucsd.edu

Henry P. Schwarcz
School of Geography and Earth Sciences, McMaster University,
Hamilton, ON Canada L8S 3Z7
schwarcz@mcmaster.ca

Steven R. Silva
U. S. Geological Survey, 345 Middlefield Road, MS 434, Menlo Park, CA
srsilva@usgs.gov

Christopher J. Still
Department of Geography, Institute for Computational Earth System Science,
University of California Santa Barbara, Santa Barbara, CA 93106, USA
still@icess.ucsb.edu

Christophe Sturm
Bert Bolin Centre for Climate Research, Institute for Geology and Geochemistry,
Stockholm University, Stockholm, Sweden
Christophe.Sturm@geo.su.se

Alexandra H. Thompson
Department of Biology, University of Utah, 257 S 1400 E,
Salt Lake City, UT 84112
ahthompson@biology.utah.edu

Kerstin Treydte
Swiss Federal Research Institute WSL, CH-8903 Birmensdorf, Switzerland
kerstin.treydte@wsl.ch

Bruce H. Vaughn
UCB 450 INSTAAR, University of Colorado, Boulder, CO 80309, USA
bruce.vaughn@colorado.edu

Tomas Vitvar
Isotope Hydrology Section, International Atomic Energy Agency, Vienna, Austria
T.Vitvar@iaea.org

Lixin Wang
Department of Environmental Sciences, University of Virginia,
291 McCormick Road, Charlottesville, VA 22904, USA
Department of Civil and Environmental Engineering, Princeton University,
Princeton, NJ 08544, USA
lixinw@princeton.edu

Wenwen Wang
Department of Ecology and Evolutionary Biology, University of California,
Irvine, CA
wenwenw@uci.edu

Jason B. West
Texas AgriLife Research and Department of Ecosystem Science and
Management, Texas A&M University
jbwest@tamu.edu

Christine D. White
Department of Anthropology, University of Western Ontario,
London, Ontario, Canada
white2@uwo.ca

Michael B. Wunder
University of Colorado Denver, Department of Biology,
Campus Box 171, Denver, CO
michael.wunder@ucdenver.edu

Megan B. Young
U. S. Geological Survey, 345 Middlefield Road, MS 434, Menlo Park, CA
mbyoung@usgs.gov

Part I
Gathering and Using Spatially Explicit Isotope Data

Chapter 1
Global Network Measurements of Atmospheric Trace Gas Isotopes

Bruce H. Vaughn, Candice U. Evans, James W.C. White, Christopher J. Still, Kenneth A. Masarie, and Jocelyn Turnbull

1.1 Introduction

Human activities have been altering the environment in very visible ways for millennia, but only in the last century have we been able to detect significant changes in our global atmosphere. Numerous ice core records have documented the changing composition of the Earth's atmosphere, and the accompanying alterations in temperature and precipitation patterns (e.g., Indermühle et al. 1999; Flückiger et al. 2002; Spahni et al. 2005). Humans continue to play an ever-increasing role in driving environmental change, as documented by the four different assessments by the Intergovernmental Panel on Climate Change (IPCC). The 2007 IPCC assessment stated that continued greenhouse gas (GHG) emissions at or above current rates would cause further global warming, and induce many changes in the global climate system during the twenty-first century that would *very likely* be larger than those observed during the twentieth century (Solomon et al. 2007). Atmospheric monitoring programs with long-term direct measurements of GHGs and their isotopes in the lower troposphere provide critical observations that constrain global

B.H. Vaughn (✉) and C.U. Evans
UCB 450 INSTAAR, University of Colorado, Boulder, CO, 80309, USA
e-mails: bruce.vaughn@colorado.edu Candice.evans@colorado.edu

J.W. White
CB 450 INSTAAR, University of Colorado, Boulder, CO, 80309, USA
e-mail: James.white@colorado.edu

C.J. Still
Department of Geography, University of California Santa Barbara,
Santa Barbara, CA, 93106, USA
e-mail: still@icess.ucsb.edu

K.A. Masarie and J. Turnbull
National Oceanic and Atmospheric Administration, Earth System Research Lab,
325 Broadway, Boulder, CO, 80305-3337, USA
e-mails: Kenneth.Masarie@noaa.gov Jocelyn.Turnbull@noaa.gov

J.B. West et al. (eds.), *Isoscapes: Understanding Movement, Pattern, and Process on Earth Through Isotope Mapping*, DOI 10.1007/978-90-481-3354-3_1,

climate models to improve our understanding of biosphere/ocean processes that drive atmospheric changes. In this chapter we highlight several global measurement programs and outline critical elements necessary to operate these observational networks. Current consensus objectives and criteria for intercomparison and linking of atmospheric isotopic data sets from the global measurement community are presented along with some recent data products and results for isotopic models.

The awareness of these hugely consequential changes in our atmosphere began in part with the visionary and insightful work of Charles Keeling and his colleagues, who initiated measurements of atmospheric carbon dioxide, at Mauna Loa, Hawaii in 1958 (Keeling et al. 1976). His pioneering efforts uncovered both the steady increase in concentration and the seasonal cycle in CO_2, beginning the record on which we base much of our present understanding of the carbon cycle. Continuing to monitor the changing composition of the atmosphere on a global scale will become even more crucial as the climate continues to adjust in response to increases in population, energy consumption and fossil fuel emissions, as well as land cover changes.

Greenhouse gases, along with solar input and albedo, are key elements in the Earth's energy balance that drives the climate system. Therefore the Earth's response to climate forcing from relatively short-term perturbations in greenhouse gases is important. However the mean lifetime of anthropogenic CO_2 can be complex to assess accurately (Siegenthaler and Joos 1992), any peak is also accompanied by a long tail associated with the role of ocean sequestration of CO_2 into carbonates through deep-water formation (Stouffer and Manabe 2003). Estimates of lifetimes of atmospheric CO_2 range from a few hundred years to a much longer estimate of 30–35 kyr for the entire process, depending upon the model (Archer 2005). Given the potential for long lifetimes of fossil fuel carbon releases, it follows that the anthropogenic climate perturbation will likely interact with ice sheets, methane clathrate deposits, and alter normal glacial/interglacial climate dynamics (Siegenthaler and Joos 1992; Archer 2005; Caldeira and Wickett 2005). And, the carbon cycle will likely take a long time to completely stabilize and sequester the current fluxes of anthropogenic CO_2. Because of these consequences, global measurements of GHGs are crucial to our ability to understand, quantify, and predict the planet's response to the perturbation of the composition of our atmosphere. And because isotopes are ubiquitous indicators, integrators and recorders, they will undoubtedly continue to inform our understanding of environmental processes and global change.

Isotopes of atmospheric constituents contain a wealth of information about biosphere–atmosphere and ocean–atmosphere interactions, particularly when examined in combination with trace gas mixing ratios. For example, the isotopes of carbon ($\delta^{13}C$) in atmospheric CO_2 track changes in key parts of the terrestrial carbon cycle, including photosynthesis, respiration, and organic matter decomposition, as well as interaction with oceans during air–sea gas exchange. The isotopes of oxygen ($\delta^{18}O$) of CO_2 reflect many complex processes including linkages between terrestrial carbon and water cycles through H_2O/CO_2 oxygen isotope exchanges in leaf water and soil water. Small-scale studies that link direct isotopic measurements with models have shown progress in understanding mechanisms at the ecosystem level (Bowling et al. 2002; McDowell et al. 2008; Schaeffer et al. 2008). Large-

scale isotopic measurement networks record regional to meso-scale processes that may ultimately affect global-scale climate change. Global observations also constrain top-down models that suggest flux mechanisms, quantify sources and sinks of critical greenhouse gases, and partition them between terrestrial biosphere and oceanic model fluxes (e.g., Ciais et al. 1995; Fung et al. 1997; Rayner et al. 1999; Randerson et al. 1999, 2002a, b; Battle et al. 2000). Currently, the stable isotopes of atmospheric CO_2 and CH_4 make up the majority of isotope measurements. Lessons learned from maintaining these atmospheric observing networks and the challenges in assessing comparability among measurements made using independent methods, can be directly applied to ecosystem monitoring networks at any scale.

1.2 Isotopic Measurement Programs

Today there are numerous international atmospheric programs making valuable measurements of gas concentrations that continue to expand our understanding of the dynamic nature of the troposphere (Fig. 1.1). Most atmospheric isotope measurement networks currently in operation have utilized the infrastructure of these existing trace gas programs. Following the work initiated by Keeling in 1958,

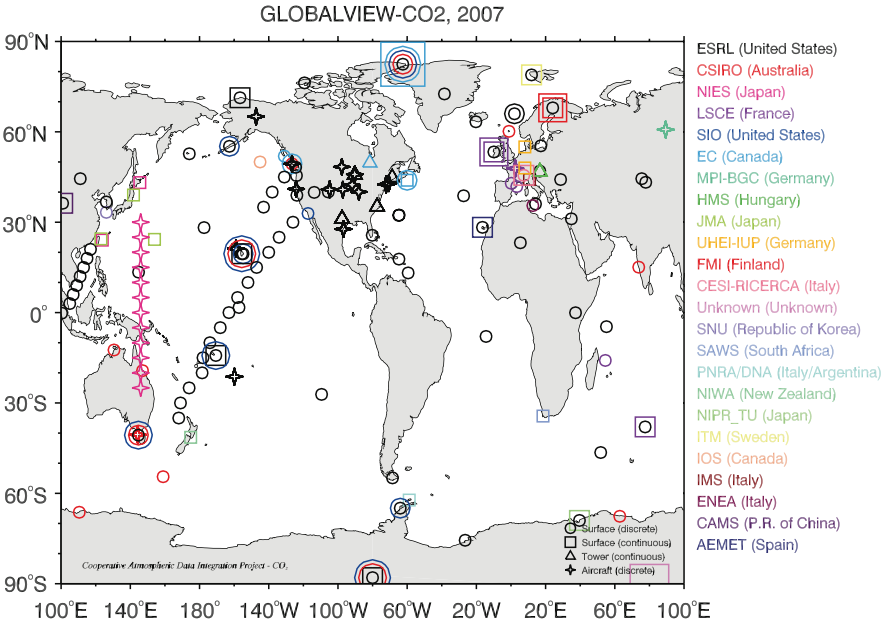

Fig. 1.1 Map of sampling sites for multiple laboratories that measure trace gas concentrations and contribute to GLOBALVIEW. A smaller subset of these labs also measure stable isotopes. Fig. 1.1, see Appendix 1, Color Section

researchers from Scripps Institute of Oceanography (SIO) joined with Willem Mook at the Centrum voor Isotopen Onderzeok (CIO) at the University of Groningen, The Netherlands, to make some of the first large-scale measurements of carbon and oxygen isotopes of atmospheric CO_2 in 1977. The network began with 10 sampling stations, along a rough latitudinal transect of the Pacific Ocean (Keeling et al. 1979; Keeling and Whorf 2005). This measurement program continues today with other sites around the globe.

The Commonwealth Scientific and Industrial Research Organization (CSIRO), Australia maintains an atmospheric monitoring network that began in 1976 with sampling at Çape Grim Australia, and at present data are available for four atmospheric trace gases at nine stationary sites and one moving platform (aircraft sampling over Cape Grim, Tasmania, and Bass Strait, during flights between the Australian continent and Tasmania). Measurements of $\delta^{13}C$ from CO_2 are made at each site, along with trace gas mixing ratios for CO_2 CH_4 CO, and H_2.

European researchers have been active participants in campaigns to measure trace gases and their isotopes. The CarboEurope program emerged as a group of European projects in the late 1990s, collaborating to understand and quantify the terrestrial carbon balance of Europe and the associated uncertainty at local, regional and continental scales. Since then, it has consolidated an interdisciplinary research community focused on ecosystems, the atmosphere, measurements, and models into the CarboEurope-IP, which expands on these earlier projects and allows for consistent gathering of data and integration of space and time scales (Sturm et al. 2005). In January 2004, over 60 research centers from 17 European countries joined forces for a 5-year European Union-funded continuation of CarboEurope-IP which addresses carbon cycle issues, and helps support a European network of measurement sites including 24 lower troposphere sites, seven tall tower sites, and four aircraft profile sites. It is a multi-scale and multi-method exercise, which goes beyond basic atmospheric measurements, and requires both methodological as well as technical integration. The new European Union Integrated Carbon Observation System (ICOS) will build on the CarboEurope framework with a longer-term vision and additional measurements. Measurements from these programs, including trace gases, $\delta^{13}C$, $\delta^{18}O$, and $\Delta^{14}C$ of CO_2, are rigorously intercompared, and the data will be available from a common website.

Perhaps the most extensive observing network for monitoring atmospheric trace gases, is the U.S. program operated by the United States National Oceanic and Atmospheric Administration (NOAA), Earth System Research Laboratory (ESRL), Global Monitoring Division (GMD) Carbon Cycle Greenhouse Gas (CCGG) cooperative air sampling network. This program, which began in 1967 at Niwot Ridge, Colorado today includes regular discrete samples from the four NOAA baseline observatories (Barrow, Alaska; Mauna Loa, Hawaii; American Samoa; South Pole, Antarctica), plus a network of over 50 cooperative fixed sites, several commercial ships, as well as a growing network of aircraft sampling programs and tall tower sampling sites in the United States. Air samples are collected approximately weekly from the globally distributed network of sites, and are analyzed in Boulder, Colorado by CCGG for mixing ratios of: CO_2, CH_4, CO, H_2, N_2O, and SF_6; these

same air samples are analyzed for the stable isotopes $\delta^{13}C$ and $\delta^{18}O$ of CO_2, $\delta^{13}C$ and δD of CH_4, and $\Delta^{14}C$ of CO_2 by the Institute of Arctic and Alpine Research, (INSTAAR) at the University of Colorado. Both the concentration and isotopic data are used to identify long-term trends, seasonal variability, and spatial distribution of carbon cycle gases. From this program, the largest of its kind, we can learn much about the organization, methodology, and analyses required of a global network to function successfully, and will be revisited in subsequent sections.

Measurements utilizing aircraft have helped define vertical profiles of trace gases in the atmosphere, potentially alleviating problems in interpreting surface observations, such as the rectifier effect, whereby daily and seasonal variability in vertical mixing is correlated with daily and seasonal variability in (for example) CO_2 fluxes, so that annual budgets based solely on surface measurements may be biased. These aircraft programs can help identify distinct air mass plumes, boundary layers, and large gradients over large distances. Programs that utilize commercial aircraft are growing both in technology and scope. Since December 2004, a consortium of eleven partners from seven European countries have supporting the efforts of the CARIBIC (Civil Aircraft for the Regular Investigation of the atmosphere Based on an Instrument Container) system, that involves the monthly deployment of an automated atmospheric chemistry observatory inside an air-freight-container onboard a Lufthansa Airlines Airbus A340–600 (Brenninkmeijer et al. 2007). Measurements of over 25 different atmospheric parameters are made either in-flight or in the lab, including isotopes of CO, CH_4 and CO_2.

The Japanese have also initiated a program to measure CO_2 from commercial aircraft that has yielded broad, long-range transects of tropospheric measurements never before obtained (Machida et al. 2007). Stable carbon isotopes are also being measured for CO_2 and CH_4, but have not yet been published.

The French MOZAIC (Measurements of OZone, water vapour, carbon monoxide and nitrogen oxides by in-service AIrbus aircraft, http://mozaic.aero.obs-mip.fr/web/) program has been funded by the European Commission from 1994 to February 2004 to use commercial aircraft for measuring vertical profiles of ozone and water vapor (Gierens et al. 1997; Clark et al. 2007). Currently, stable isotopes are not measured, but MOZAIC has established itself as a long-term sustainable European research infrastructure with potential to expand its measurement capabilities. Since 2006, it has transformed into the European initiative IAGOS-ERI (In-service Aircraft for a Global Observing System – European Research Infrastructure) adding more measurements.

There are also organizations, both national and international that serve to promote, facilitate, and orchestrate atmospheric isotope measurement efforts, including Ameriflux, BASIN, Euroflux, and others. In the United States, the North American Carbon Program is a recently formed overarching organization that is supported by multiple U.S. Federal agencies (i.e. NOAA, NIST, NASA, NSF, DOE, EPA, USDA) in an effort to enhance scientific understanding of North America's carbon cycling through measurements of carbon dioxide, methane, and carbon monoxide across North America and over adjacent ocean regions. A major thrust of the program is to make measurements from atop tall (~100–400 m) towers that

may otherwise be used for television or radio broadcasting. These towers allow for analyses of the vertical dimension to local sources and sinks over short timescales. Another NOAA program, MAGNETT (Measurements of Anthropogenic Gases and Natural Emissions from Tall Towers) began in 1992 and utilizes existing tall (>400 m) towers as sampling platforms for in-situ and flask sample analyses of atmospheric trace gases.

All of these ongoing, long-term observational networks and programs are essential to understanding atmospheric composition and how it relates to the dynamics of global climate change. Unfortunately, these programs struggle with obtaining long-term funding, necessary for projects that take the long view. Typically, funding is for a set of specific short term scientific objectives that address questions relevant to government agencies. Monitoring does not fit neatly within this structure. Another problem is the relatively short funding cycles that agencies operate within, usually one to a few years. Monitoring generally requires a longer-term commitment to yield the required information. As a result, there are limited global networks that are maintained at the levels necessary to capture large-scale, long-term signals in atmospheric dynamics, or that are able to insure their political survival for scientific funding.

An international community of CO_2 measurement experts have been working together for more than 25 years to improve measurement techniques and develop network comparison methods designed to better assess the comparability of measurements made by different laboratories. Every two years, the World Meteorological Organization (WMO) Global Atmospheric Watch (GAW), and the International Atomic Energy Agency (IAEA) bring this community together with the purpose of sharing information and results; evaluating measurement practices and programs; facilitating interaction and collaborations; and recommending procedures and actions to the entire atmospheric carbon cycle measurement community. They have made explicit recommendations regarding the level of network comparability for many trace species and isotopes required to meet current research topics and have developed several intercomparison activities designed to meet these recommendations. We will refer to the most recent set of recommendations from the WMO/IAEA CO_2 Experts meeting in Helsinki, September 2007, throughout this chapter in the appropriate sections. In addition, the WMO/GAW World Data Center for Greenhouse Gases (WDCGG) serves as a data archive center for atmospheric carbon cycle measurements, a topic that will be addressed in detail later.

1.3 Instrumentation

Traditionally, isotope ratio mass spectrometers have been the instrument used for measuring isotopic ratios in trace gases, but occasionally even the precision of these instruments can seem like a blunt tool for the task at hand. The current global growth rate and seasonal isotopic variations of atmospheric CO_2 are small and can

approach the detection limit of modern analytical techniques. Calculating fluxes with small uncertainty requires precise determinations of both the CO_2 mole fraction (ppm) and the $\delta^{13}C$ concentration. For example, fossil fuel emissions during the 1990s are estimated at 6.4 Gt C per year and increased to ~7.4 Gt C per year in 2000–2005, resulting in a yearly change of the CO_2 mixing ratio in the atmosphere during 1995–2005 of approximately 1.9 ppm per year and a $\delta^{13}C$ change of about −0.025‰ per year (Solomon et al. 2007). While CO_2 mixing ratio analyses typically can be made with a precision of 0.1 ppm or better, $\delta^{13}C$ precision for IRMS methods is near ±0.01‰ (1 std dev) at best (Trolier et al. 1996; Vaughn et al. 2004; Ghosh et al. 2005). High precision measurements have been predominantly performed using dual inlet mass spectrometry that requires relatively large whole air sample sizes of approximately 500 cc (Vaughn et al. 2004, describe the typical method in detail). However, continuous flow mass spectrometry methods that utilize a carrier gas to introduce a single peak for the sample integration have steadily progressed in the 1990s and early 2000s, and precision for these measurements is approaching that of the dual inlet technique, while consuming considerably less gas (Allison and Francey 1995). Because these are laboratory instruments, neither IRMS method realistically lends itself (yet) to in situ measurements, forcing measurement programs to focus on sample collection by means of large (1–3 L) glass flasks that are collected and stored for subsequent laboratory analyses. Flasks have the advantage that a number of other laboratory intensive measurements can be made on that same aliquot of air. The disadvantage is that they are limited in time to discrete event sampling.

More recently, advances have been made in alternatives to mass spectrometry, including a variety of laser-based methods that exploit the radiation absorption qualities of trace gases or specific isotopic species at various wavelengths. Tunable diode laser absorption spectroscopy (TDLAS) for stable isotope applications is becoming more common, particularly for field experiments, where isotopic signals can be large (Becker et al. 1992; Durry and Megie 1999; Bowling et al. 2003; McDowell et al. 2008). Likewise, cavity ring down spectroscopy (CRDS) has shown promise since its development in the 1980s (O'Keefe and Deacon 1988), and continues to improve in both its precision and application (Wheeler et al. 1998; Crosson et al. 2002). Instruments have been developed that can analyze $\delta^{13}C$ of CO_2 and CH_4, as well as $\delta^{18}O$ and δD of water vapor (Crosson et al. 2002; Lee et al. 2005). Advances have also been made in Fourier transform infrared (FTIR) spectroscopy to measure isotopes of atmospheric N_2O, and atmospheric CO_2 (e.g. Esler et al. 2000; Griffith et al. 2002). So far, laser-based isotope techniques for $\delta^{13}C$ fall short of the <0.01‰ precision goal of traditional mass spectrometry that is often required for long term atmospheric monitoring objectives, and hover in the ±0.3‰ range at best. But this number is probably far from static, and is bound to change in the future, as the technology continues to improve. Data from laboratory studies generally fare better than field studies, and in one study comparing flask-based IRMS to in situ laser-based measurements yielded reproducibility nearly ten times worse for laser measurements (Schaeffer et al. 2008). However, there are many field experiments and campaigns with large isotopic signals where laser-based

instruments offer the advantages of in situ capability, and since advances are still being made in the techniques, they remain an exciting prospect for the future development of the isotope measurement field.

Measuring the $\Delta^{14}C$ of CO_2 may be one of the best methods for quantifying fossil fuel CO_2 emissions (Levin et al. 2003a; Turnbull et al. 2006; Hsueh et al. 2007). Due to the very low abundance of ^{14}C (~1 in 10^{12} carbon atoms), current measurement precision is at best 2‰, but this is sufficient to detect recently added fossil fuel CO_2 concentrations of less than 1 ppm. Two distinct measurement methods are used. In the first method, conventional radioactive decay counting of ^{14}C is used. This method requires very large samples (the equivalent of 15 m^3 of whole air) to obtain sufficient precision, and to avoid collection and transportation of such large air samples, samples are collected by absorbing the CO_2 from air into sodium hydroxide over a period from days to weeks. The CO_2 is desorbed from the NaOH in the laboratory prior to ^{14}C analysis. In the second method, accelerator mass spectrometry (AMS) is used for the ^{14}C analysis, requiring vastly smaller sample sizes, currently as small as 2 L of whole air, and obtaining precision that is comparable to the decay counting method. The AMS method allows analysis of $^{14}CO_2$ in flask samples collected in many of the existing greenhouse gas sampling networks. Current research is focused on further improving the measurement precision and lowering the required sample size.

1.4 Data Reporting, Corrections and Standards

Because of the need for high precision, advances in the various corrections used for the mass spectrometric determinations are important, and have continued to evolve in the last several decades. The ^{17}O correction is a good example. This accounts for the well-established phenomenon that the ion current on the mass 45 Faraday cup is comprised of $^{13}C^{16}O_2^+$ as well as $^{12}C^{17}O^{16}O^+$, where the latter isobaric interference amounts to about 7% of the total ion current. If the oxygen isotopic signature between the sample and the reference gas is different, traditionally, the ^{17}O contribution to the m/z 45 ion current can be corrected for by measuring the $\delta^{18}O$ signature on m/z 46 and assume a constant law for the fractionation of ^{17}O and ^{18}O. Although this does not strictly apply, this is the standard procedure first used by Harmon Craig (1957), and is usually referred to as the 'Craig' correction. A number of improvements or alterations have been proposed in the literature, including the set of absolute ratios for the reference materials and the exponent of the fractionation law (Craig and Keeling 1963; Santrock et al. 1985; Mook and Jongsma 1987; Merritt and Hayes 1994; Brenninkmeijer and Röckmann 1998; Assonov and Brenninkmeijer 2003, 2006). Clearly, a consensus regarding the ^{17}O correction is needed for improving the accuracy of air-CO_2 $\delta^{13}C$ data, because the choice of a particular ^{17}O correction can produce a significant $\delta^{13}C$ shift of about 0.03‰ when, for example, moving from Craig /Allison to the Assonov correction. In 2005, the 13th WMO/IAEA meeting of CO_2 experts recommended adopting the Assonov and Brenninkmeijer (2003) parameter set and

to discontinue the use of any others. However, Kaiser (2008) critically re-evaluated many of the historic and recent isotope ratio corrections in detail, and suggested that to achieve the highest accuracy in the $^{13}C/^{12}C$ ratio, independent triple oxygen isotope measurements are required. Consensus in the measurement community is an ever-evolving process, and this debate will no doubt continue. The ISO lab at the Max Planck Institute, Jena has compiled a good summation of some of the methods, and offers different correction techniques and algorithms in a spreadsheet file (http://www.bgc-jena.mpg.de/service/iso_gas_lab/activities/index.shtml).

Another even larger adjustment to isotope ratio measurements is the N_2O correction. For isotopic analyses, CO_2 is typically extracted from atmospheric samples using cryogenic (liquid nitrogen) methods that also condense N_2O. When ionized in the mass spectrometer, the N_2O will contribute to the same *m/z* values as the CO_2 (masses 44, 45 and 46). Therefore to determine the correct $\delta^{13}C$ and $\delta^{18}O$ of CO_2, the raw isotopic data must be corrected for the N_2O contribution, which is typically about 0.22‰ and 0.33‰ for each isotope, respectively (Mook and van der Hoek 1983). However, though different techniques have been suggested, (Craig and Keeling 1963; Mook and van der Hoek 1983; Mook and Jongsma 1987; Ghosh and Brand 2004; Sirignano et al. 2004; and Assonov and Brenninkmeijer 2006), lack of awareness or consensus on methodology in the measurement community may be one of the reasons that laboratory intercomparisons remain difficult. Continuous flow methods for mass spectrometry typically isolate the CO_2 using chromatography, and are therefore free of N_2O, which offers a distinct advantage over cryogenic extraction methods, as there is no need for the N_2O correction.

Determinations of isotopic values for unknowns can be made with high confidence *relative* to another material; however, determining absolute isotopic concentrations is far more difficult. Different attempts have been made to tightly link the whole air-CO_2 carbon and oxygen isotopic scales to Vienna Pee Dee Belemnite (VPDB). The VPDB scale replaced the PDB scale in 1987 where VPDB was defined by assigning $\delta^{13}C$ VPDB = +1.95 and $\delta^{18}O$ VPDB = 2.2 (exactly) to the reference material NBS 19 (Coplen 1994, 1995, 1996). However, measurements of $\delta^{13}C$ of CO_2 extracted from whole air have much better long term reproducibility than measurements of $\delta^{13}C$ of CO_2 evolved from the reaction carbonate and 100% orthophosphoric acid (Ghosh et al. 2005). Laboratory intercomparison activities have helped illuminate this problem, and solutions to this issue are discussed below in the section on intercomparison activities.

Many of the issues described above, including scale and precision, are also true for $\delta^{13}C$ of methane. Issues of scale and laboratory intercomparison are more pronounced since far fewer measurements have been made and fewer labs are involved. Modern ambient concentrations are quite light (~−47‰ relative to VPDB), so a second standard that is lighter than VPDB is used, the IAEA reference material LSVEC. LSVEC is a lithium carbonate with a value set to −46.6‰ relative to VPDB (Coplen et al. 2006). In the case of ^{14}C, results are usually reported as $\Delta^{14}C$, which is analogous to $\delta^{13}C$, except that it is normalized to a standard $\delta^{13}C$ value, corrected for radioactive decay of ^{14}C between the time of collection and measurement, and reported according to the conventions described by Stuiver and Polach (1977).

1.5 Considerations for Flask Measurement Networks

1.5.1 Flasks

Whole air samples collected for trace gas analyses are usually sampled with the intent of representing the great mixing and integrating abilities of the atmosphere; therefore, consideration must be given to air collection methods that are free from anthropogenic contaminants. Water vapor collected along with atmospheric air should be minimized, as it can be problematic especially for analyses of $\delta^{18}O$ of CO_2 because of exchange with the water vapor and the CO_2 in the flask (Gemery et al. 1996). Care must also be taken to avoid introducing the sample into flask conditions that could adulterate the gas through leakage, interaction with the flask walls, or the elastomers used for sealing the flask. Most flask networks today use some type of elongated Pyrex glass flask with two Teflon seated glass valves, which facilitate flushing of the volume during sample collection. Stainless steel flasks have occasionally been used in the past, but have generally been abandoned in favor of less reactive glass versions, although for some species, such as halocarbons, steel flasks may be preferable. Flask volumes vary from 0.5 to 3.0 L. NOAA uses 2.5-L flasks, which allow for a variety of measurements to be made on a single parcel of air. Collection is often accomplished by pumping large amounts (>10 lpm for 10 min) of air through two flasks, connected in series. Collecting and analyzing flasks in pairs allows pair agreement to be used as one metric of a successful, unbiased measurement (Trolier et al. 1996). For example, the typical maximum pair difference criteria for the NOAA flask network for stable isotopes of CO_2 are 0.06‰ and 0.12‰ for $\delta^{13}C$ and $\delta^{18}O$ of CO_2, respectively.

1.5.2 Sites

Careful consideration must be given to site selection to meet the objectives of the network, and the biases of the sites selected must be identified. For example, some sites have access to air masses that integrate large sectors of open ocean air, and are referred to as marine boundary layer sites. Others may be more affected by local anthropogenic fluxes or dominated by local-to-regional ecosystem exchanges, and these need to be identified before data from these sites can be interpreted. Often sites have been chosen not for their ideal location, but because they were previously established, or a contact is available. From the outset, many of the global networks have attempted to obtain a latitudinal transect (Keeling et al., 1976; Masarie and Tans 1995). With time, networks have grown, gaining greater coverage over all latitudes, but some areas remain under-sampled, including those that are dominated by large regional signals, such as rain forests (Amazonia), or developed agricultural areas (American Midwest). Data extension techniques can sometimes be used to fill in geographical and temporal gaps in the records (Masarie and Tans 1995).

Measurements from tall towers and aircraft have helped to better constrain these areas, and to alleviate difficulties in assessing the vertical distribution of the trace gases and isotopes. Future international collaborations may help fill holes in areas where sampling is sparse or nonexistent. Some notable areas for better sampling include high latitude sites in the Arctic, Africa, South America, and Russia, where each area has its special concerns. For example, much of South America is dominated by local source/sink issues, and background air sampling is difficult; however, sampling efforts from towers in the Amazon basin will continue to help in this regard.

1.5.3 Data Management

Data management is a simple concept: organize and save atmospheric trace gas measurements made today so that we can evaluate their quality and explore their meaning at a later date. Yet a common pitfall among laboratories is the tendency to spend considerable effort developing the measurement technique while neglecting the development of a strategy for managing the observations that have been so carefully made. Data management is often an afterthought. In some instances the need for a data management strategy arises only after a data crisis occurs where, for example, precious data are lost, corrupted or confused with other data sets.

The analytical method, calibration system, and data management strategy are all fundamental components of an ongoing measurement program. If inadequate resources prevent establishing any one of these components, maintaining an ongoing program becomes a tenuous proposition. Failing to develop an essential component is more likely related to the environment in which a program is developed. Often we obtain a source of funding to develop a measurement technique where funding is typically for a fixed time period, supports temporary personnel, and periodic reports to the funding agency document progress. This process establishes an environment driven by short-term objectives: develop the technique, measure atmospheric samples, and interpret initial results. Managing the data is typically not among the short term objectives. However, if the technique is feasible and can be adapted to making ongoing measurements, there is often some urgency to begin as soon as possible. It is during this transition when the short-term project is converted into a long-term program where development of a data management strategy is often overlooked. All too often, the management tools (e.g., lab notebooks, text files, spreadsheets) used to meet the short-term objectives become, by default, the basis for the long-term strategy.

1.5.4 Flow of Data

Within an ongoing measurement program, the natural flow of information is from data in its most raw form (e.g., beam currents) to data in its most processed

form (e.g., averaged isotope ratios). Intermediate steps establish a hierarchical data structure. A tiered data structure is critical to an atmospheric trace gas data management strategy because it enables the lab to retroactively revise numbers at any level in the hierarchy and automatically propagate the changes to affected data at lower levels. In practice, the flow of information is more complicated and includes information about the observations and details on how to treat data produced using different methods. This supporting information or metadata must also be managed as it is critical in assessing the quality of the measurements. An ideal data management strategy must guarantee that at any time in the future, all data can be unambiguously reprocessed to exactly reproduce the current results.

Managing data requires a strategy that has at its core a database management system (DBMS). A DBMS is a collection of tables related to the measurement process. If tables are related to each other, e.g., by sharing one or more attributes (keys), the DBMS is called a "relational" DBMS or RDBMS. Attributes whose fields never change once assigned make suitable keys. Non-key data stored in a RDBMS typically exist in a single location and are not repeated in other tables. A well-constructed RDBMS makes few assumptions about how data are related or how they will be extracted from the database. "Queries" can be used to extract, append, remove, and alter data. RDBMS manufacturers recommend using a RDBMS when (1) data are dynamic; (2) the volume of data is large and increasing; (3) routine and automatic data updates are required; (4) queries may be initiated from external applications (e.g., C, Perl, PHP, IDL); (5) external applications are required to derive, process, and analyze data; (6) tables must relate; (7) many users will be accessing the same data; and (8) strategies for data exploration are many and varied.

An ongoing atmospheric trace gas measurement program, regardless of size, requires a data management strategy that includes some type of RDBMS. Working with a RDBMS does require an understanding of general data management concepts, the RDBMS architecture and a working knowledge of Standard Query Language (SQL), the language used by most RDBMSs. These prerequisites may present a barrier. Unfortunately, there are few acceptable alternatives. A spreadsheet application is not a RDBMS. Spreadsheet manufacturers recommend using a spreadsheet when (1) data are static; (2) the volume of data is small and fixed; and (3) the spreadsheet owner is the primary user of the data. These criteria are not consistent with an ongoing atmospheric trace gas measurement program. Nevertheless, many labs have, on occasion, opted to use a spreadsheet to "manage" observational data because it was readily available and easy to use. The spreadsheet works well initially, but in time it fails as a data management strategy. The price to disentangle from the spreadsheet and migrate to a proper RDBMS can be painfully high. The WMO document No. 150 entitled "Updated Guidelines for Atmospheric Trace Gas Data Management" (Masarie and Tans 2003) is intended to serve as a starting point for new and existing laboratories ready to develop a data management strategy. The document includes an introduction to general data management terms and concepts, a recipe for developing a strategy, and a discussion on selecting the RDBMS. Importantly, as an observing network evolves, so too must the data management strategy.

1.5.5 Intercomparison Activities

A critical component of collaboration between laboratories that seek to integrate data from measurement networks is on-going intercomparison programs designed to determine the level of comparability among independent measurements. These experiments have the potential to suggest causes when measurement differences occur. If the experiment includes weekly comparisons, problems can sometimes be identified shortly after they develop, serving as an important quality control exercise beneficial to participating laboratories. Historically, these experiments have taken several forms: the exchange of high pressure cylinders among labs for inter-calibration exercises, co-measurement of certain sampling sites, and flask intercomparison programs where labs routinely analyze the same sample flasks from a particular site.

CSIRO (with support from the IAEA) initiated an intercomparison experiment termed CLASSIC, in which a number of high-pressure cylinders of air were prepared and a suite of five were circulated among at least four international labs. Two small pure CO_2 cylinders were also circulated. The results of this intercomparison exercise, spanning measurements made over almost 4 years, were presented at the 11th IAEA/WMO meeting of CO_2 experts in Tokyo (Allison et al. 2002, 2003). Significant differences in the mean carbon and oxygen isotopic compositions reported by the different laboratories were observed. Differences in the reported values were up to ten times larger than the target precisions for merging data from different networks. The $\delta^{13}C$ as well as $\delta^{18}O$ data of pure CO_2 measured several years apart within a given laboratory showed poor consistency. The data for air-CO_2 were much more consistent than for pure CO_2, when the offsets are removed. Because of this, one clear conclusion from the CLASSIC experiment was that a reliable and long-lasting CO_2-in-air isotope ratio reference material was needed.

Intercomparison (ICP) exercises using methods that are closely related to those used for real atmospheric samples make a central contribution to an accurate international network of observations (Levin et al. 2007; Langenfelds et al. 2007). The NOAA/GMD facilitates on-going ICP exercises among several labs, including the United States (NOAA/INSTAAR); Australia (CSIRO); Canada (MSC); Germany (Max Planck Institute-Jena); and New Zealand (NIWA). Air from a single flask is measured in several labs, along with normal sampling at the chosen site for co-sampling. As a result, the long-term record allows direct comparison among labs, serving as a scale off-set indicator as well as an indicator of general reproducibility from that site. For example the record of CO_2-in-air isotopes measured at Cape Grim, Australia (Fig. 1.2) documents the 0.05‰ offset between two labs, which was created by a CSIRO scale change in mid-2005. Data are constantly updated to a web-based interface that allows each lab to track differences as a near real-time diagnostic of analytical performance.

NOAA/GMD has provided software support and guidance that facilitates these comparisons of measurements on a specific sample by two different laboratories,

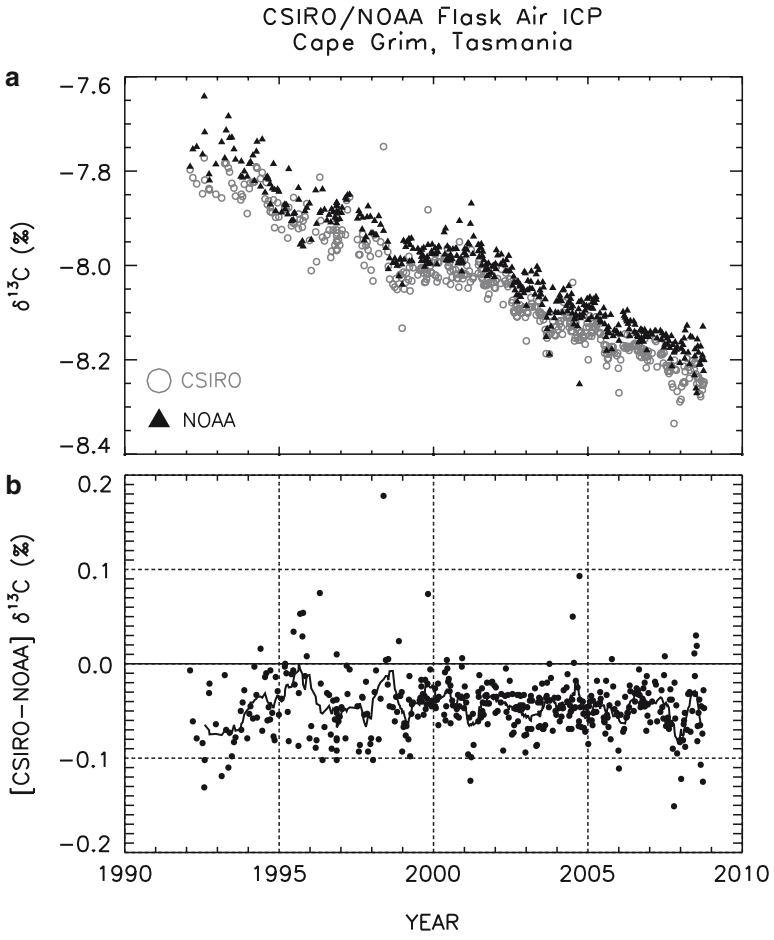

Fig. 1.2 Plots of $\delta^{13}C$ of atmospheric CO_2 collected from Cape Grim, Australia and measured by both CSIRO and NOAA/INSTAAR shown in (**a**). This Inter-Comparison activity (ICP) helps both labs identify analyses problems, and scale issues over time. The difference (CSIRO minus NOAA) is shown in (**b**)

but these ICP programs until recently have been only bi-lateral (Masarie et al. 2001). The European TACOS project initialized a multi-lateral so-called Sausage flask intercomparison program (Levin et al. 2003b, 2007). Today eight international laboratories participate in this project, all regularly analyzing the air filled into their regular network sample flasks from a large common source of well-mixed atmospheric air. This ICP, although not as frequent as the bi-lateral ICP's of weekly samples, has the advantage of being able to analyze results of all participating laboratories on the same sample over a short period; by this means, it is possible to more easily identify individual labs in error (Fig. 1.3).

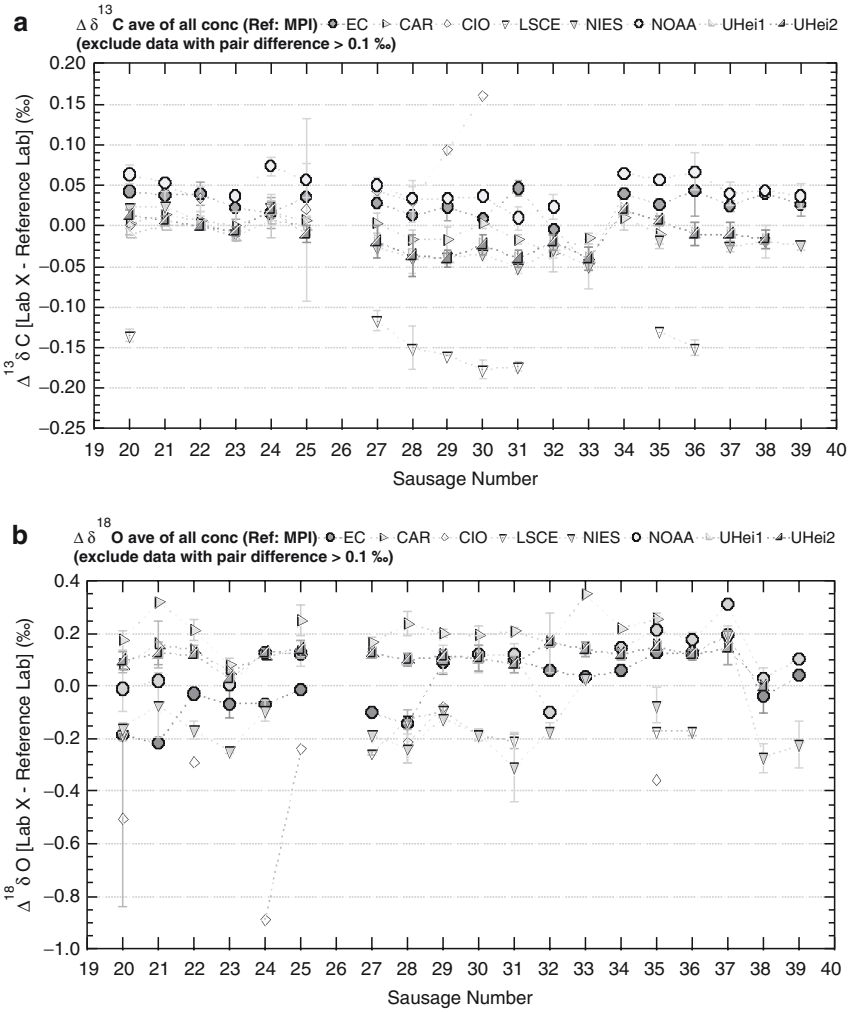

Fig. 1.3 Trends in laboratory inter-comparisons for seven labs measuring $\delta^{13}C$ and $\delta^{18}O$ in flasks filled with air from a single compressed air cylinder (*top* and *bottom* panels respectively). Data span in some cases up to 5 years. Dashed red lines indicate the target standard deviation for global sampling objectives, as defined by the WMO-IAEA CO2 Experts measurement group (Levin et al. 2007)

The majority of radiocarbon laboratories have carried out intercomparisons on various materials since the early 1990s (e.g., Boaretto et al. 2002) and a more recent intercomparison of $^{14}CO_2$ was initiated in 2007, as suggested by the 13th WMO/IAEA CO2 Experts meeting in Boulder, Colorado in 2005. Offsets between laboratories are less common with ^{14}C than with stable isotopes, in part due to the current measurement precision (2‰), and to the long history of intercomparison activities.

1.6 Some Examples of Isotopic Trace Gas Findings

1.6.1 ^{13}C of Atmospheric CO_2

Spatial and temporal variations of atmospheric CO_2 and its $^{13}C/^{12}C$ composition have received considerable attention from the carbon cycle community (e.g. Ciais et al. 1995; Fung et al. 1997; Rayner et al. 1999; Randerson et al. 2002a, b, c; Battle et al. 2000). Measurements from ongoing atmospheric trace gas networks fuel modeling efforts. A current "flying carpet" plot of $\delta^{13}C$ of CO_2 over time is shown in Fig. 1.4a. The overall trend is towards lower, or isotopically lighter values due to the addition to the atmosphere of isotopically light CO_2 from the burning of fossil fuels. The large seasonal cycles, particularly in the northern hemisphere, are the result of isotopic fractionation during photosynthesis. These features can be seen more clearly in an example site, Barrow, Alaska (Fig. 1.5). The utility of $\delta^{13}C$ analyses of atmospheric CO_2 is twofold. First, when combined with CO_2 concentration data, we can partition the atmospheric CO_2 sink into oceanic and terrestrial components. Second, where this partitioning is already highly constrained by a dense network of concentration analyses or in regions where ocean influences are small, changes in δ^{13} of CO_2 will reflect how plants are using CO_2 relative to their use of water.

Carbon fluxes can be partitioned between the ocean and land because short-term variations of atmospheric $\delta^{13}CO_2$ are caused largely by isotopic fractionation that occurs during net exchange of CO_2 with the terrestrial biosphere during photosynthesis, while net exchange of carbon with the oceans imparts very little signal to $\delta^{13}CO_2$ in the atmosphere (i.e. Ciais et al. 1995). Thus, after accounting for the latitudinal pattern of fossil fuel flux, we can use CO_2 concentration data to tell us the net flux to and from the atmosphere, and then use $\delta^{13}CO_2$ to separate that flux into the land and ocean components. This approach works best on relatively coarse time and space scales. As the $\delta^{13}CO_2$ is changing due to fossil fuel burning, the isotopic composition of CO_2 used in photosynthesis, that is the modern atmosphere, can be different than the CO_2 used in respiration, which is carbon from recent to decades or even centuries old pools. This isotopic disequilibrium can be quantified using carbon cycle models, but as time and space scales shrink, so does the confidence in these models.

The amplitude of the seasonal cycle can vary from year to year (and from site to site) primarily due to variations in the annual balance of net photosynthesis and respiration, and the degree of photosynthetic fractionation, which is controlled mainly by the efficiency of water use in plants. These factors also dominate in areas where CO_2 fluxes are more tightly constrained by dense sampling networks. The isotopic fractionation of CO_2 during photosynthesis is a balance of the enzymatic preference for ^{12}C during the carboxylation reaction and the slower diffusivity of $^{13}CO_2$ relative to $^{12}CO_2$ into the stomatal cavity. When stomata are more closed, water loss is constrained, and CO_2 utilization is very high. When stomata are open and water loss is high, the discrimination is much larger, over 20‰. The plant-water feedback is a key component of climate predictions for continental areas and one that $\delta^{13}CO_2$ will contribute to as dense, continental sampling networks become better established.

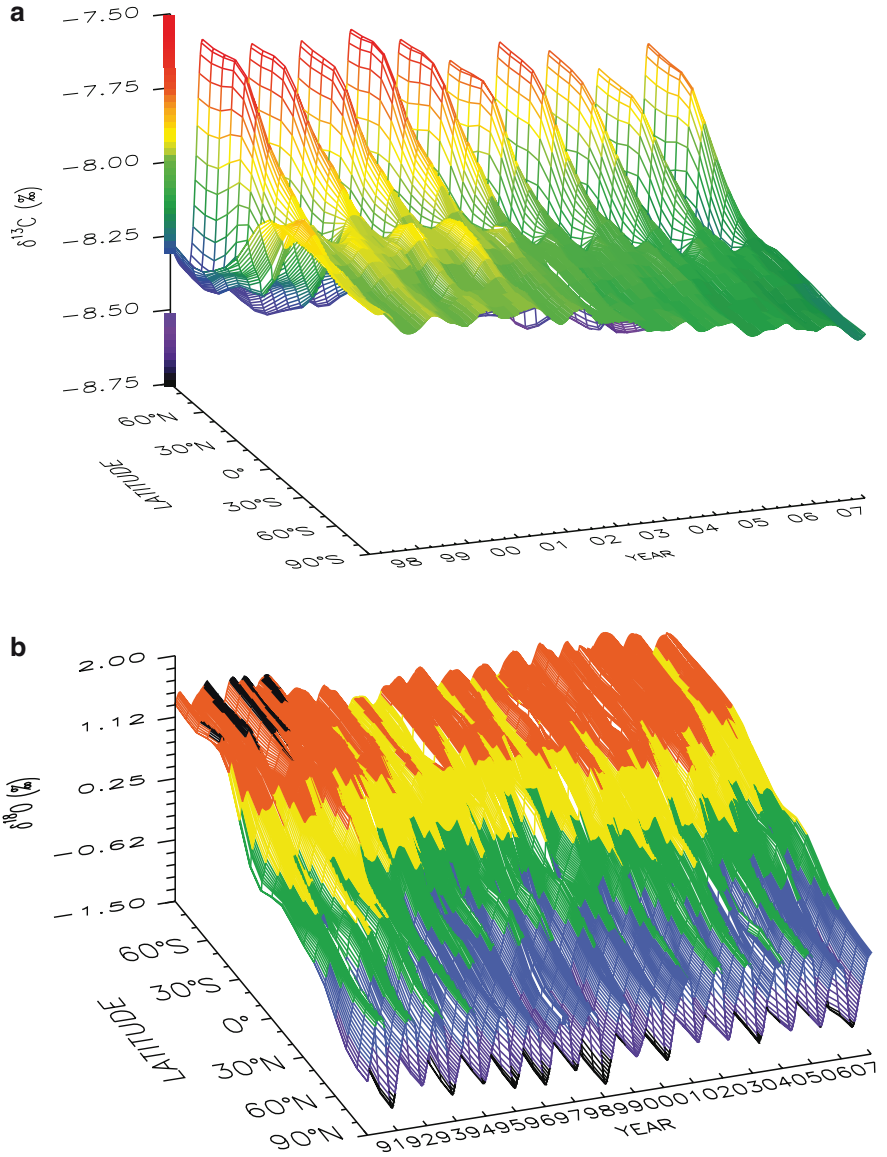

Fig. 1.4 (**a**) Surface plot of spatial δ^{13}C-CO_2 data from the NOAA/INSTAAR global flask network through time, created from 55 sites from south to north. (**b**) Surface plot of spatial δ^{18}O-CO_2 data from the NOAA/INSTAAR global flask network through time, created from 55 sites. Note the y-axis is reverse of the δ^{13}C-CO_2 plot, from north to south, in order to better display the large latitudinal gradient. Fig. 1.4, see Appendix 1, Color Section

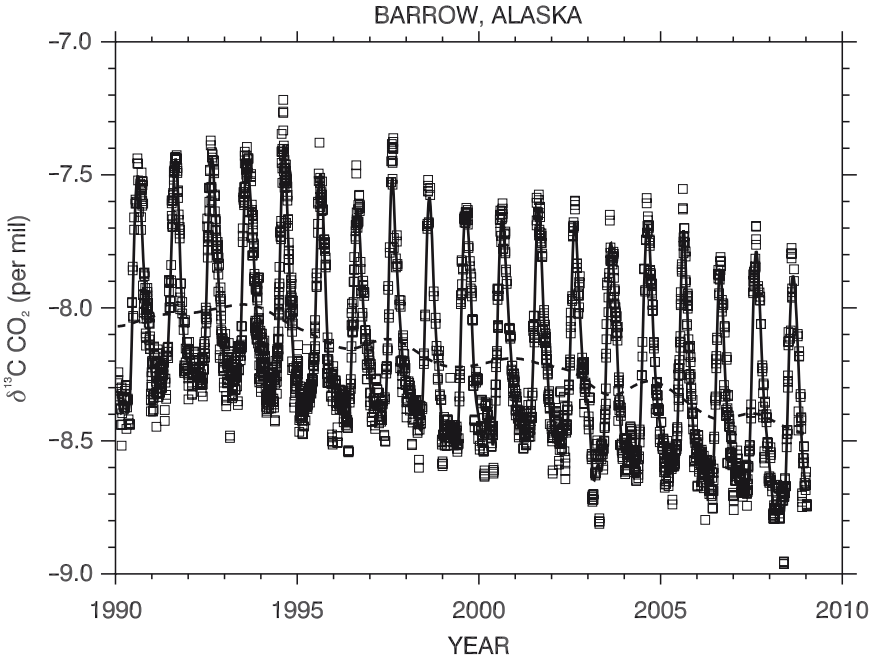

Fig. 1.5 $\delta^{13}C\text{-}CO_2$ measured from Barrow, Alaska, plotted with smoothed and long-term trend curves

1.6.2 ^{18}O of Atmospheric CO_2

Spatial and temporal variations of atmospheric $\delta^{18}O\text{-}CO_2$ are primarily influenced by four factors: air–sea exchange, biomass and fossil fuel burning, stratospheric reactions, and terrestrial carbon exchange (Ciais et al. 1997a, b; Cuntz et al. 2003a, b; Ciais et al. 2005). Various estimates have been made of the size of the $\delta^{18}O\text{-}CO_2$ fluxes and reservoirs (Yakir and Sternberg 2000). The dominant influence on the $\delta^{18}O\text{-}CO_2$ signature is the terrestrial biosphere, specifically the combined contribution of photosynthesis and respiration. These two processes display unique isotopic signatures resulting from oxygen isotopic exchange that occurs in distinct reservoirs: the water inside a leaf and soil water. Leaf and soil water $\delta^{18}O$ are in turn determined primarily by the $\delta^{18}O$ of precipitation (Welker 2000; Vachon et al. 2007) and water vapor and subsequent isotopic fractionations during evaporation and diffusion (Craig and Gordon 1965; Allison et al. 1983).

Substantial progress has been made in global simulations of $\delta^{18}O\text{–}CO_2$ and the processes that control it (e.g. Farquhar et al. 1993; Ciais et al. 1997a, b; Peylin et al. 1999; Cuntz et al. 2003a, b), yet basic aspects of its behavior as deduced from global atmospheric observation remain poorly understood. For example, state-of-the-art coupled global model simulations have difficulty capturing the observed phase shift between the detrended seasonal cycles of CO_2 and $\delta^{18}O\text{–}CO_2$ at high northern

latitudes (Cuntz et al. 2003a, b). However, a recent one-box atmosphere modeling study demonstrates that this shift is sensitive to boreal forest plant functional type composition and the isotope ratio of source water (Welp et al. 2006). Furthermore, global mean $\delta^{18}O\text{-}CO_2$ observations exhibit large, multi-year variations (Fig. 1.4b), and the same models fail to predict both the global mean value and its inter-annual variations. For example, the pronounced downward excursion in $\delta^{18}O\text{-}CO_2$ observed during the early and mid-1990s averaged roughly −0.1‰ per year for all extratropical, marine boundary layer stations, implying isotope fluxes of several hundred Pg C‰ per year. This excursion remains largely unexplained, although published hypotheses relate it to terrestrial carbon fluxes (Gillon and Yakir 2001; Stern et al. 2001; Ishizawa et al. 2002; Flanagan 2005).

Because $\delta^{18}O\text{-}CO_2$ is determined largely by exchanges of $C^{18}O$ between the atmosphere and terrestrial ecosystems during photosynthesis and respiration (Francey and Tans 1987; Friedli et al. 1987; Farquhar et al. 1993; Ciais et al. 1997a, b; Cuntz et al. 2003a, b), there is great interest in using spatial and temporal patterns in $\delta^{18}O\text{-}CO_2$ (Fig. 1.4a) to trace terrestrial ecosystem gross carbon fluxes, at regional (Riley et al. 2003; Ogee et al. 2004) and continental (Peylin et al. 1999) scales. It is tempting to ascribe the variations in $\delta^{18}O\text{–}CO_2$ such as the pronounced downward excursion in the 1990s to variations in terrestrial gross carbon fluxes that would not necessarily impact atmospheric CO_2 or its $^{13}C/^{12}C$ composition (e.g., Ishizawa et al. 2002). However, variations in the water cycle that impact the $\delta^{18}O$ value of leaf and soil water can also impact $\delta^{18}O\text{–}CO_2$, independent of carbon flux variations. Although either the carbon or the water cycle may drive $\delta^{18}O\text{–}CO_2$ variations, it is likely that the unexplained multi-year variations in $\delta^{18}O\text{–}CO_2$ result from perturbations to both cycles. In any case, observations of $\delta^{18}O\text{–}CO_2$ from the NOAA global trace gas network continue to challenge our understanding of the earth system and its response to global environmental change. For more discussion of oxygen and hydrogen isotopes in plants, leaf water and the biosphere, see West et al. (this volume).

1.6.3 ^{13}C of Atmospheric CH_4

Methane remains an important GHG with considerable radiative forcing (~0.5 W m^{-2}). It is well documented in ice cores that concentrations of global atmospheric methane have grown considerably since pre-industrial levels (Ferretti et al. 2005). However, for reasons not well understood, the growth rate slowed slightly at the beginning of 1994 and extended to the early 2000s, whereas recent (2007) methane measurements of CH_4 and $\delta^{13}C$ of CH_4 at Alert, Canada show an increase in the growth rate (Fig. 1.6). In general, large uncertainties in the budget of atmospheric methane have limited the accuracy of climate change model projections, and the high-latitude terrestrial biosphere remains a suspect for this uncertainty. For example, there are northern high-latitude thaw-lakes known to emit methane (Zimov et al. 1997), but the magnitude of these emissions remains uncertain because most methane is released through ebullition (bubbling), which is spatially and temporally

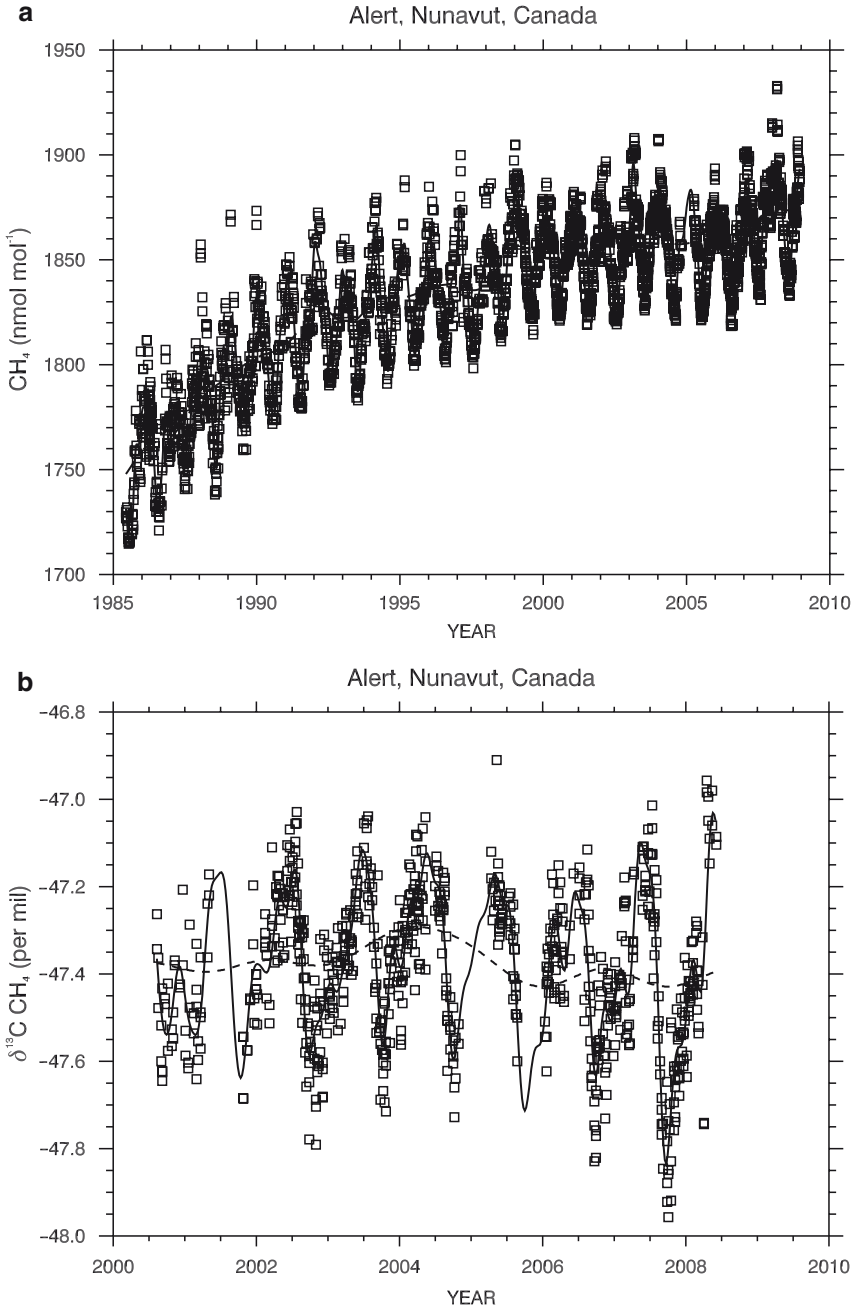

Fig. 1.6 Plot showing atmospheric concentration of methane and $\delta^{13}C$ of methane collected at Alert, Canada (N 82.45 W −62.52, 200 m.a.m.s.l.) showing changes in 2007

variable. Recently, a study by Walter et al. (2007) found that Northern Siberian thaw-lakes are a significantly larger source of atmospheric CH_4 than previously recognized, and that ebullition accounts for 95% of methane emissions from these lakes. The methane flux calculated by Walter et al. indicated that thaw lakes in their study region could be five times higher than previously estimated. Extrapolation to all thaw lakes in northern Siberia yields 3.8 Tg of methane per year, which increases present estimates of methane emissions from northern wetlands (<6–40 Tg per year) by between 10% and 63%. Using ^{14}C of CH_4, Walter et al. discovered that methane emitted from hot spots originated during the Pleistocene age (35,260–42,900 years), suggesting that this positive feedback to climate warming has led to the release of old carbon stocks previously stored in permafrost.

The measurements of Keppler et al. (2006) suggested terrestrial plants are a large global source of methane, causing great controversy surrounding the global methane budget, and leading to much misinterpretation by the news media. This led to intense speculation that methane emissions by plants could diminish or even outweigh the carbon storage effect of reforestation programs with important implications for the Kyoto Protocol, where such programs are to be used in national CO_2 reduction strategies. Controversy still continues, but no one is arguing that this mechanism would seriously undermine the climate benefits from reforestation. The fundamental problem still remaining is the large-scale global anthropogenic burning of fossil fuels.

1.6.4 ^{14}C of Atmospheric CO_2

^{14}C measurements, while more difficult than most stable isotope measurements, and thus less widely used, benefit from much larger leverage on carbon cycle exchange processes. ^{14}C is produced naturally in the upper atmosphere by interaction of nitrogen with cosmic rays, and this cosmogenic ^{14}C reacts to form $^{14}CO_2$, which is gradually taken up by all carbon reservoirs. It is radioactive (half-life of 5730 ± 40 years, Godwin 1962), so carbon reservoirs that exchange relatively rapidly with the atmosphere (the biosphere and oceans) have ^{14}C content close to that of the atmosphere. Fossil fuel CO_2, on the other hand, has been isolated from the atmosphere for millions of years, and contains no ^{14}C atoms. When this fossil fuel CO_2 is added to the atmosphere, the $\Delta^{14}C$ value of atmospheric CO_2 decreases (Suess 1955). A large pulse of anthropogenic ^{14}C was produced in the early 1960s by atmospheric nuclear weapons testing, almost doubling the atmospheric ^{14}C concentration. After the International Test Ban Treaty came into effect in 1963, this pulse of "bomb ^{14}C" was taken up into the biosphere and oceans, and the rate of uptake has been used to assess the rate of uptake and exchange of carbon in these reservoirs (e.g., Peacock 2004; Broecker et al. 1995; Trumbore 2006; Gaudinski et al. 2000). Recently, as the bomb ^{14}C has almost reached equilibrium in the atmosphere, the effect of fossil fuel CO_2 has again become the dominant driver of variability in $\Delta^{14}C$ of atmospheric CO_2. Several recent studies have demonstrated that measurements of $\Delta^{14}C$ of CO_2 provide the most reliable estimates of additions of fossil fuel CO_2 to the atmosphere

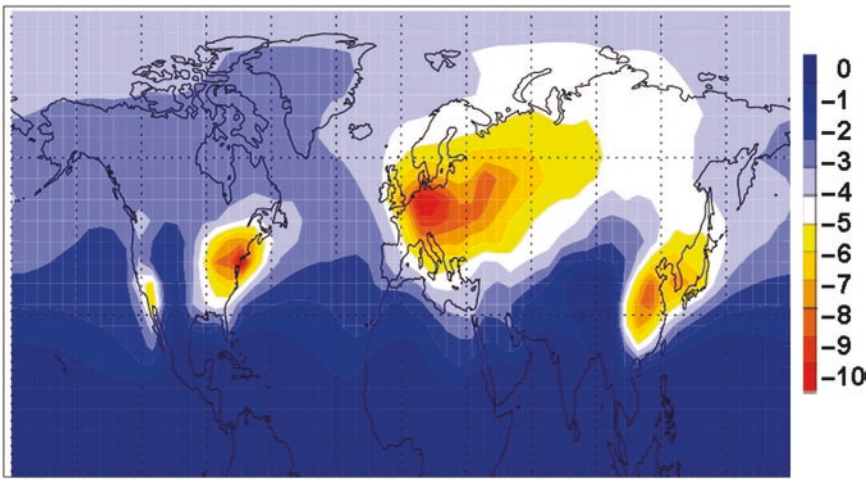

Fig. 1.7 Northern Hemisphere surface distribution of $\Delta^{14}C$ predicted by the TM5 model for 2004. Fig. 1.7, see Appendix 1, Color Section

(Hsueh et al. 2007; Turnbull et al. 2006; Levin et al. 2003a). This effect can be seen graphically in Fig. 1.7, which shows a modeled prediction of the northern hemisphere surface distribution of $\Delta^{14}C$ (Turnbull et al. 2009). The spatial pattern is strongly dominated by the effect of ^{14}C-free fossil fuel CO_2 emissions, which lower the atmospheric $\Delta^{14}C$ value. Furthermore, Levin and Karstens (2007) showed how weekly measurements of $\Delta^{14}C$ of CO_2 could be used in combination with high temporal resolution CO measurements to provide temporally varying estimates of fossil fuel CO_2 emissions; this methodology is currently being implemented at several European sites. To date, the $\Delta^{14}C$ method has been applied to quantification of fossil fuel CO_2 *concentrations* at individual sites, yet the ultimate goal is to use these atmospheric measurements to examine fossil fuel CO_2 *fluxes* from nations and regions, as an independent, objective method of validating the emissions reported by governments and industry (which are currently based solely on reporting of economic data). Atmospheric transport models will be needed to translate the measured fossil fuel CO_2 concentrations into estimates of the regional fluxes; initial results are promising (e.g., Levin and Rödenbeck 2007; Hsueh et al., 2007), and this is an area of ongoing research. For more discussion of the basis for the use of radiocarbon as a pollution tracer, and the relationships between radiocarbon and other isotope tracers in polluted environments, see Pataki et al. (this volume).

1.7 Conclusions and New Frontiers

Measuring changes in the Earth's atmosphere is important because it integrates and links oceanic and terrestrial processes at the very largest scales to long-term climate change. Isotopic measurements of atmospheric trace gases have proven to be

powerful tools that trace and record changes affecting the Earth's climate system. These measurements are also critical for assessing global climate models, and for quantifying sources and sinks of important greenhouse gases. For network measurements to be useful on a global scale, isotopic measurements from labs around the world must continue to be well calibrated against primary isotopic reference materials, and labs should continue to participate in flask/cylinder intercomparison exercises. Functional utility of large global networks is only possible if rigorous data protocols and true relational databases are employed, thus allowing for complete re-calculations if necessary for scale adjustments. Continued propagation of multi-point isotope scales is critical for merging of international databases.

The focus of large-scale network measurements has so far been on methane and carbon dioxide, and continues to hold promise for future studies. For example, as boreal forests and the Arctic begin to experience further warming, unknown amounts of carbon dioxide and methane locked in permafrost may be released into the atmosphere, ensuring that monitoring of fluxes with concentration measurements and isotopes in these areas will be critical in coming decades. Likewise, as global debates on energy solutions continue to include plans for hydrogen-based energy sources, there are research groups moving to obtain baseline measurements of atmospheric hydrogen isotopes, prior to any large-scale changes that may occur with hydrogen use. Issues affecting nitrogen cycling remain poorly understood on global scales, yet atmospheric levels of N_2O continue to grow. Isotopic investigations of nitrogen fluxes may shed light on processes not fully characterized or quantified at large scales. And, understanding N_2O and the nitrogen cycle may also help us better understand the role of the extremely reactive hydroxyl radical (OH)– otherwise known and the 'detergent of the atmosphere' that plays such a critical role in the oxidation of so many trace gas species. As the nations of the world move closer to policies to reduce carbon emissions and greenhouse gases, monitoring of atmospheric composition will become even more important, by constraining the emissions claims of various countries. Already, we are seeing movement by governments to sponsor more long-term monitoring of the atmosphere and ecosystems (e.g. the European ICOS program, and the U.S. National Ecological Observatory Network, or NEON). The lessons learned from today's networks and applied to these promising initiatives will make them even more valuable.

New and emerging technologies can change any field over time, and there are several recent developments that can easily be seen to show promise in the near future. For example, the laser-based optical measurements of isotopes and isotopologues have made considerable progress in recent years and continue to gain precision. Advances in signal processing, lasers, and gas handling have all contributed to better instrumentation. In the end, there may ultimately be hard physical laws that limit or prevent laser based methods from surpassing the precision obtained with conventional mass spectrometry; however, developments are ongoing and proceeding rapidly. One real value of laser-based technology is the potential for low cost, field-deployable instruments that can obtain continuous in situ data. Small cycloidal mass spectrometers represent another technology that may provide some of the advantages of IRMS and laser-based approaches as these new

mass spectrometers may be adaptable to field deployment, and they are capable already of the precision that can be obtained from standard isotope ratio mass spectrometry methods.

Measurements of atmospheric trace gas isotopes will continue to grow in order to expand our understanding and tracking of different gases in the atmosphere, and because of emerging technologies that will enable novel approaches, and perhaps deliver more precise, frequent measurements. This is critical to provide the increased density of measurements necessary to create improved isoscapes to drive models and better understand global climate change. Clearly, this is an exhilarating time for this rising and important field.

References

Allison CE, Francey RJ (1995) High precision stable isotope measurements of atmospheric trace gases. In: Reference and intercomparison materials for stable isotopes of light elements: proceedings of a consultants meeting, Vienna (IAEA-TECDOC-825). International Atomic Energy Agency, Vienna, Austria, pp 131–153

Allison CE, Francey RJ, Steele LP (2002) The International Atomic Energy Agency circulation of laboratory air standards for stable isotope comparisons: aims, preparation and preliminary results. In: Isotope aided studies of atmospheric carbon dioxide and other greenhouse gases Phase II (IAEA-TECDOC-1269). International Atomic Energy Agency, Vienna, Austria, pp 5–23

Allison CE, Francey RJ, White JWC, Vaughn BH, Wahlen M, Bollenbacher A, Nakazawa T (2003) What have we learnt about stable isotope measurements from the IAEA CLASSIC? In: Report of the eleventh WMO/IAEA meeting of experts on carbon dioxide concentration and related tracer measurement techniques, Tokyo, Japan, 25–28 September 2001, WMO/GAW Report No. 148, Geneva, pp 17–30

Allison GB, Barnes CJ, Hughes MW (1983) The distribution of deuterium and ^{18}O in dry soils (2). Exp J Hydrol 64:377–397

Archer D (2005) Fate of fossil fuel CO_2 in geologic time. J Geophys Res 110 (C9):C09S05.1-C09S05.6. DOI 10.1029/2004JC002625

Assonov SS, Brenninkmeijer CAM (2003) On the ^{17}O correction for CO_2 mass spectrometric isotopic analysis. Rapid Commun Mass Spectrom 17:1007–1016

Assonov SS, Brenninkmeijer CAM (2006) On the N_2O correction used for mass spectrometric analysis of atmospheric CO_2. Rapid Commun Mass Spectrom 20:1809–1819

Battle M, Bender ML, Tans PP, White JWC, Ellis JT, Conway TJ, Francey RJ (2000) Global carbon sinks and their variability inferred from atmospheric CO_2 and $\delta^{13}C$. Science 287:2467–2470

Becker JF, Sauket TB, Loewenstein M (1992) Stable isotope analysis using tunable diode laser spectroscopy. Appl Opt 31(12):1921–1927

Boaretto E et al (2002) Summary findings of the fourth international radiocarbon intercomparison (FIRI) (1998–2001). J Q Sci 17(7):633–637

Bowling DR, McDowell NG, Bond BJ, Law BE, Ehleringer JR (2002) ^{13}C content of ecosystem respiration is linked to precipitation and vapor pressure deficit. Oecologia 131(1):113–124

Bowling DR, Sargent SD, Tanner BD, Ehleringer JR (2003) Tunable diode laser absorption spectroscopy for stable isotope studies of ecosystem–atmosphere CO_2 exchange. Agric For Meteorol 118(1–2):1–19

Brenninkmeijer CAM, Röckmann T (1998) A rapid method for the preparation of O_2 from CO_2 for mass spectrometric measurement of $^{17}O/^{16}O$ ratios. Rapid Commun Mass Spectrom 12:479–483

Brenninkmeijer CAM et al (2007) The CARIBIC aircraft system for detailed, long-term, global-scale measurement trace gases and aerosol changing atmosphere. Int Glob Atmos Chem Newsl 37

Broecker WS, Sutherland D, Smethie W (1995) Oceanic radiocarbon: separation of natural and bomb components. Glob Biogeochem Cycles 9(2):263–288

Caldeira K, Wickett ME (2005) Ocean model predictions of chemistry changes from carbon dioxide emissions to the atmosphere and ocean. J Geophys Res 110(C9):C09S04.1-C09S04.12. DOI 10.1029/2004JC0026

Ciais P, Tans PP, White JWC, Trolier M, Francey RJ, Berry JA, Randall DR, Sellers PJ, Collatz JG, Schimel DS (1995) Partitioning of ocean and land uptake of CO_2 as inferred by $\delta^{13}C$ measurements from the NOAA climate monitoring and diagnostics laboratory global air sampling network. J Geophys Res 100:5051–70

Ciais P et al (1997a) A three-dimensional synthesis study of $\delta^{18}O$ in atmospheric CO_2. 1. Surface fluxes. J Geophys Res-Atmos 102:5857–5872

Ciais P et al. (1997b) A three-dimensional synthesis study of $\delta^{18}O$ in atmospheric CO_2 2. Simulations with the TM2 transport model. J Geophys Res-Atmos 102(D5):5873–5883

Ciais P et al (2005) Remarks on the use of ^{13}C and ^{18}O isotopes in atmospheric CO_2 to quantify biospheric carbon fluxes. In: Flanagan LB, Ehleringer JR, Pataki DE (eds) Stable isotopes and biosphere–atmosphere interactions: processes and biological controls. Elsevier Academic, San Diego, CA

Clark HL, Cathala ML, Teyssedre H, Cammas JP, Peuch VH (2007) Cross-tropopause fluxes of ozone using assimilation of MOZAIC observations in a global CTM. Tellus B 59(1):39–49

Coplen TB (1994) Reporting of stable carbon, hydrogen and oxygen isotopic abundances. Pure Appl Chem 66:273–276

Coplen TB (1995) Reporting of stable hydrogen, carbon, and oxygen isotopic abundances. Geothermics 24(5–6):707–712

Coplen TB (1996) New guidelines for reporting stable hydrogen, carbon, and oxygen isotope-ratio data. Geochim Cosmochim Acta 60(17):3359–3360

Coplen TB, Brand WA, Gehre M, Gröning M, Meijer HAJ, Toman B, Verkouteren RM (2006) New guidelines for $\delta^{13}C$ measurements. Anal Chem 78:2439–2441

Craig H (1957) Isotopic standards for carbon and oxygen and correction factors for mass-spectrometric analysis of carbon dioxide. Geochim Cosmochim Acta 12:133–149

Craig H, Gordon LI (1965) Isotopic oceanography; deuterium and oxygen 18 variations in the ocean and the marine atmosphere. In: Symposium on marine geochemistry, 1964, Narragansett Marine Laboratory, University of Rhode Island, Kingston, RI, pp 277–374

Craig H, Keeling CD (1963) The effect of atmospheric N_2O on the measured isotopic composition of atmospheric CO_2. Geochim Cosmochim Acta 27:549–551

Crosson ER, Ricci KN, Richman BA, Chilese FC, Owano TG, Provencal RA, Todd MW, Glasser J, Kachanov AA, Paldus BA (2002) Stable isotope ratios using cavity ring-down spectroscopy: determination of 13C/12C for carbon dioxide. Anal Chem 74:2003–2007

Cuntz M, Ciais P, Hoffmann G, Knorr W (2003a) A comprehensive global three-dimensional model of $\delta^{18}O$ in atmospheric CO_2: 1. Validation of surface processes. J Geophys Res-Atmos 108(D17):4527. DOI 10.1029/2002JD003153

Cuntz M et al. (2003b), A comprehensive global three-dimensional model of $\delta^{18}O$ in atmospheric CO_2: 2. Mapping the atmospheric signal. J Geophys Res-Atmos 108(D17):4528. DOI 10.1029/2002JD003154

Durry G, Megie G (1999) Atmospheric CH_4 and H_2O monitoring with near-infrared InGaAs laser diodes by the SDLA, a balloonborne spectrometer for tropospheric and stratospheric in situ measurements. Appl Opt 38(36):7342–7354

Esler MB, Griffith DWT, Turatti F, Wilson SR, Rahn T, Zhang H (2000) N_2O concentration and flux measurements and complete isotopic analysis by FTIR spectroscopy. Chemosphere – Global Change Sci 2(3–4):445–454

Farquhar GD, Lloyd J, Taylor JA, Flanagan LB, Syvertsen JP, Hubick KT, Wong SC, Ehleringer JR (1993) Vegetation effects on the isotope composition of oxygen in atmospheric CO_2. Nature 363:439–443

Ferretti DF, Miller JB, White JWC, Etheridge DM, Lassey KR, Lowe DC, MacFarling Meure CM, Dreier MF, Trudinger CM, van Ommen TD, Langenfelds RL (2005) Unexpected changes to the global methane budget over the past 2000 years. Science 309(5741):1714–1717

Flanagan LB (2005) Ecosystem CO_2 exchange and variation in the $\delta^{18}O$ of atmospheric CO_2. In: Flanagan LB, Ehleringer JR, Pataki DE (eds) Stable isotopes and biosphere–atmosphere interactions: processes and biological controls. Elsevier Academic, San Diego, CA, pp 171–181

Flückiger J, Monnin E, Stauffer B, Schwander J, Stocker TF, Chappellaz J, Raynaud D, Barnola JM (2002) High resolution Holocene N_2O ice core record and its relationship with CH_4 and CO_2. Glob Biogeochem Cycles 16(1):1010. doi:10.1029/2001GB001417

Francey RJ, Tans PP (1987) Latitudinal variation in oxygen-18 of atmospheric CO_2. Nature 327:495–497

Friedli H, Siegenthaler U, Rauber D, Oeschger H (1987) Measurements of concentration, $^{13}C/^{12}C$ and $^{18}O/^{16}O$ ratios of tropospheric carbon dioxide over Switzerland. Tellus 39B:80–88

Fung I, Field CB, Berry JA, Thompson MV, Randerson JT, Malmström CM, Vitousek PM, Collatz GJ, Sellers PJ, Randall DA, Denning AS, Badeck F, John J (1997) Carbon 13 exchanges between the atmosphere and biosphere. Glob Biogeochem Cycles 11:507–533. doi:10.1029/97GB01751

Gaudinski JB, Trumbore SE, Davidson EA, Zheng S (2000) Soil carbon cycling in a temperate forest: radiocarbon-based estimates of residence times, sequestration rates and partitioning of fluxes. Biogeochem 51:33–69

Gemery PA, Trolier M, White JWC (1996) Oxygen isotope exchange between carbon dioxide and water following atmospheric sampling using glass flasks. J Geophys Res 101(D9):14,415–14,420

Ghosh P, Brand W (2004) The effect of N_2O on the isotopic composition of air-CO_2 samples. Rapid Commun Mass Spectrom 18:1830–1838

Ghosh P, Patecki M, Rothe M, Brand WA (2005) Calcite-CO_2 mixed into CO_2-free air: a new CO_2-in-air stable isotope reference material for the VPDB scale. Rapid Commun Mass Spectrom 19(8):1097–1119

Gierens KM, Schumann U, Smit HG, Helten M, Zängl G (1997) Determination of humidity and temperature fluctuations based on MOZAIC data and parametrisation of persistent contrail coverage for general circulation models. Ann Geophys 15:1057–1066

Gillon J, Yakir D (2001) Influence of carbonic anhydrase activity in terrestrial vegetation on the ^{18}O content of atmospheric CO_2. Science 291:2584–2587

Godwin H (1962) Half-life of radiocarbon. Nature 195:984

Griffith DW, Leuning R, Denmead OT, Jamie IM (2002) Air-land exchanges of CO_2, CH_4 and N_2O measured by FTIR spectrometry and micrometeorological techniques. Atmos Environ 36(11):1833–1842

Hsueh DY, Krakauer NY, Randerson JT, Xu X, Trumbore SE, Southon JR (2007) Regional patterns of radiocarbon and fossil fuel-derived CO_2 in surface air across North America. Geophys Res Lett 34:L02816

Indermühle A, Stocker TF, Joos F, Fischer H, Smith HJ, Wahlen M, Deck B, Mastroianni D, Tschumi J, Blunier T, Meyer R, Stauffer B (1999) Holocene carbon-cycle dynamics based on CO_2 trapped in ice at Taylor Dome, Antarctica. Nature 398:121–126

Ishizawa M, Nakazawa T, Higuchi K (2002) A multi-box model study of the role of the biospheric metabolism in the recent decline of $\delta^{18}O$ in atmospheric CO_2. Tellus 54B:307–324

Kaiser J (2008) Reformulated ^{17}O correction of mass spectrometric stable isotope measurements in carbon dioxide and a critical appraisal of historic 'absolute' carbon and oxygen isotope ratios. Geochim Cosmochim Acta 72(5):1312–1334

Keeling CD, Whorf TP (2005) Atmospheric CO_2 records from sites in the SIO air sampling network. In: Trends: a compendium of data on global change. Carbon Dioxide Information Analysis Center, Oak Ridge National Laboratory, U.S. Department of Energy, Oak Ridge, TN

Keeling CD, Bacastow RB, Bainbridge AE, Ekdahl CA, Guenther PR, Waterman LS (1976) Atmospheric carbon dioxide variations at Mauna Loa Observatory, Hawaii. Tellus 28:538–551

Keeling CD, Mook WG, Tans PP (1979) Recent trends in the C-13-C-12 ratio of atmospheric carbon-dioxide. Nature 277(5692):121–123

Keppler F, Hamilton JTG, Bras M, Roeckmann T (2006) Methane emissions from terrestrial plants under aerobic conditions. Nature 439(7073):187–191

Langenfelds RL, Allison CE, Steele LP, Francey RJ, Neubert REM, Meijer HAJ, Machida T, Mukai H, Conway T, Vaughn B, Worthy D (2007) Report on Five Years of International Flask Intercomparison (Sausage ICP). IAEA 2007 report

Lee X, Sargent S, Smith R, Tanner B (2005) In situ measurement of the water vapor $^{18}O/^{16}O$ isotope ratio for atmospheric and ecological applications. J Atmos Oceanic Technol 22:555–565

Levin I, Karstens U (2007) Inferring high-resolution fossil fuel CO_2 records at continental sites from combined (CO2)-C-14 and CO observations. Tellus B-Chem Phys Meteor 59(2):245–250

Levin I, Rödenbeck C (2007) Can the envisaged reductions of fossil fuel CO_2 emissions be detected by atmospheric observations? Naturwissenschaften 95(3):203

Levin I, Kromer B, Schmidt M, Sartorius H (2003a) A novel approach for independent budgeting of fossil fuel CO_2 over Europe by $^{14}CO_2$ observations. Geophys Res Lett 30(23):2194

Levin I et al. (2003b) Eurosiberian Carbonflux – CO_2 Intercomparison. In Sasaki Toru (ed) Report of the 11th WMO/IAEA meeting of experts on carbon dioxide concentration and related tracer measurement techniques, Tokyo, Japan, 25–28 September 2001, WMO-Report No. 148

Levin I et al. (2007) Five years of international flask intercomparison (sausage flask ICP). 14th WMO/IAEA meeting of experts on carbon dioxide, other greenhouse gases, and related tracer measurement techniques, Helsinki, Finland, 10–13 September 2007

Machida T, Matsueda H, Sawa Y, Ikeda H, Kondo N, Yoshida O, Nakazawa T, Oka T (2007) Measurements of atmospheric CO_2 using commercial airliners. 14th WMO/IAEA meeting of experts on carbon dioxide, other greenhouse gases, and related tracer measurement techniques, Helsinki, Finland, 10–13 September 2007

Masarie KA, Tans PP (1995) Extension and integration of atmospheric carbon dioxide data into a globally consistent measurement record. J Geophys Res 100(D6):11593-11610

Masarie KA, Tans PP (2003) Updated guidelines for atmospheric trace gas data management. Global Atmospheric Watch Report Series No. 150, World Meteorological Organization, TD No. 1149, Geneva, 2003

Masarie KA, Langenfelds RL, Allison CE, Conway TJ, Dlugokencky EJ, Francey RJ, Novelli PC, Steele LP, Tans PP, Vaughn B, White JWC (2001) NOAA/CSIRO flask air intercomparison experiment: a strategy for directly assessing consistency among atmospheric measurements made by independent laboratories. J Geophys Res 106:20445

McDowell NG, Baldocchi D, Barbour J, Bickford C, Cuntz M, Hanson D, Knohl A, Powers H, Rahn T, Randerson J, Riley WJ, Still C, Walcroft A (2008) Understanding the stable isotope composition of biosphere-atmosphere CO_2 exchange. EOS Trans AGU 89(10):94–95

Merritt DM, Hayes JM (1994) Factors controlling precision and accuracy in isotope-ratio-monitoring mass spectrometry. Anal Chem 66(14):2336

Mook WG, Jongsma J (1987) Measurement of the N_2O correction for $^{13}C/^{12}C$ ratios of atmospheric CO_2 by removal of N_2O. Tellus 39B:96–99

Mook WG, van der Hoek S (1983) The N_2O correction in the carbon and oxygen isotopic analysis of atmospheric CO_2. Isotope Geosci 1:237–242

Ogee J et al. (2004) Partitioning net ecosystem carbon exchange into net assimilation and respiration with canopy-scale isotopic measurements: an error propagation analysis with (CO2)-C-13 and (COO)-O-18 data. Glob Biogeochem Cycles 18(2):GB2019

O'Keefe A, Deacon DAG (1988) Cavity ring-down optical spectrometer for absorption measurements using pulsed laser sources. Rev Sci Instrum 59:2544

Peacock S (2004) Debate over the ocean bomb radiocarbon sink: closing the gap. Glob Biogeochem Cycles 18(2):GB2022

Peylin P et al (1999) A 3-dimensional study of $\delta^{18}O$ in atmospheric CO_2: contribution of different land ecosystems. Tellus 51B:642–667

Randerson JT, Field CB, Fung IY, Tans PP (1999) Increases in early season ecosystem uptake explain recent changes in the seasonal cycle of atmospheric CO_2 at high northern latitudes. Geophys Res Lett 26:2765–2769

Randerson JT et al (2002a) Carbon isotope discrimination of arctic and boreal biomes inferred from remote atmospheric measurements and a biosphere-atmosphere model. Glob Biogeochem Cycles 16(3):1028

Randerson JT, Chapin FS III, Harden JW, Neff JC, Harmon ME (2002b) Net ecosystem production: a comprehensive measure of net carbon accumulation by ecosystems. Ecol Appl 12:937–947

Randerson JT et al (2002c) A possible covariance between terrestrial gross primary production and ^{13}C discrimination: consequences for the atmospheric ^{13}C budget and its response to ENSO. Glob Biogeochem Cycles 16:1136

Rayner PJ, Enting IG, Francey RJ, Langenfelds R (1999) Reconstructing the recent carbon cycle from atmospheric CO_2 $d^{13}C$ and O_2/N_2 observations. Tellus 51B:213–228

Riley WJ et al (2003) ^{18}O composition of CO_2 and H_2O ecosystem pools and fluxes in a tallgrass prairie: simulations and comparisons to measurements. Glob Change Biol 9:1567–1581

Santrock J, Studely SA, Hayes JM (1985) Isotopic analyses based on the mass spectrum of carbon dioxide. Anal Chem 57(7):1444–1448

Schaeffer SM, Miller JB, Vaughn BH, White JWC, Bowling DR (2008) Long-term field performance of a tunable diode laser absorption spectrometer for analysis of carbon isotopes of CO2 in forest air. Atmos Chem Phys Discuss 8:9531–9568

Siegenthaler U, Joos F (1992) Use of a simple model for studying oceanic tracer distributions and the global carbon cycle. Tellus B – Chem Phys Meteor 44B(3):186–207

Sirignano C, Neubert REM, Meijer HAJ (2004) N_2O influence on isotopic measurements of atmospheric CO_2. Rapid Commun Mass Spectrom 18:1839–1846

Solomon S, Qin D, Manning M, Chen Z, Marquis M, Avery KB, Tignor M, Miller HL (eds) (2007) Climate change 2007: the physical science basis. Contribution of working group I to the fourth assessment report of the intergovernmental panel on climate change. Cambridge University Press, Cambridge, UK

Spahni R, Chappellaz J, Stocker TF, Loulergue L, Hausammann G, Kawamura K, Flückiger J, Schwander J, Raynaud D, Masson-Delmotte V, Jouzel J (2005) Atmospheric methane and nitrous oxide of the late Pleistocene from Antarctic ice cores. Science 310:1317–1321

Stern LA, Amundson R, Baisden WT (2001) Influence of soils on oxygen isotope ratio of atmospheric CO_2. Glob Biogeochem Cycles 15:753–759

Stouffer RJ, Manabe S (2003) Equilibrium response of thermohaline circulation to large changes in atmospheric CO_2 concentration. Clim Dyn 20(7–8):759–773

Stuiver M, Polach HA (1977) Discussion; reporting of C-14 data. Radiocarbon 19(3):355–363

Sturm P, Leuenberger M, Schmidt M (2005) Atmospheric O_2, CO_2 and $\delta^{13}C$ observations from the remote sites Jungfraujoch, Switzerland, and Puy de Dôme, France. Geophys Res Lett 32:L17811

Suess HE (1955) Radiocarbon concentration in modern wood. Science 122:414–417

Trumbore SE (2006) Carbon respired by terrestrial ecosystems – recent progress and challenges. Glob Change Biol 12(2):141–153

Trolier M, White JWC, Tans PP, Masarie KA, Gemery PA (1996) Monitoring the isotopic composition of atmospheric CO_2: measurements from the NOAA global air sampling network. J Geophys Res 101(D20):25,897–25,916

Turnbull JC, Miller JB, Lehman SJ, Tans PP, Sparks RJ, Southon JR (2006) Comparison of $^{14}CO_2$, CO and SF_6 as tracers for determination of recently added fossil fuel CO_2 in the atmosphere and implications for biological CO_2 exchange. Geophys Res Lett 33:L01817

Turnbull JC, Miller JB, Lehman SJ, Hurst DF, Peters W, Tans PP, Southon JR, Montzka SA, Elkins JW, Mondeel DJ, Romashkin PA, Elansky NF, Shkorokhod A (2009) Spatial distribution of Δ14CO2 across Eurasia: measurements from the TROICA-8 expedition. Atmos Chem Phys 9:175–187

Vachon RW, White JWC, Gutmann E, Welker JM (2007) Amount-weighted annual isotopic ($\delta^{18}O$) values are affected by the seasonality of precipitation: a sensitivity study. Geophys Res Lett 34:L21707

Vaughn B, Ferretti D, Miller J, White JWC (2004) Stable isotope measurements of atmospheric CO_2 and CH_4. In: Handbook of stable isotope analytical techniques, vol 1. Elsiever, p 1248 Elsevier B.V. Sara Burgerhartstraat 25 Amsterdam, P.O. Box 211, 1000 AE, The Netherlands

Walter KM, Edwards ME, Grosse G, Zimov SA, Chapin FS III (2007) Thermokarst lakes as a source of atmospheric CH_4 during the last deglaciation. Science 318(5850):633

Welker JM (2000) Isotopic (18O) characteristics of weekly precipitation collected across the USA: An initial analysis with application to water source studies. Hydrol Process 14:1449–1464

Wheeler MD, Newman SM, Orr-Ewing AJ, Ashfold MNR (1998) Cavity ring-down spectroscopy. J Chem Soc Faraday Trans 94:337–351. doi:10.1039/a707686j

Welp LR, Randerson JT, Liu HP (2006) Seasonal exchange of CO2 and delta O-18-CO2 varies with postfire succession in boreal forest ecosystems. J Geophys Res-Biogeosci 111(G3):G03007

Yakir D, Sternberg LSL (2000) The use of stable isotopes to study ecosystem gas exchange. Oecologia 123(3):297–311

Zimov SA, Voropaev YV, Semiletov IP, Davidov SP, Prosiannikov SF, Chapin FS III, Chapin MC, Trumbore S, Tyler S (1997) North Siberian lakes: a methane source fueled by Pleistocene carbon. Science 277:800–802

Chapter 2
Global Hydrological Isotope Data and Data Networks

Pradeep K. Aggarwal, Luis J. Araguás-Araguás, Manfred Groening, Kshitij M. Kulkarni, Turker Kurttas, Brent D. Newman, and Tomas Vitvar

2.1 Introduction

Environmental isotopes in water and other substances have been extensively used for almost five decades to improve our understanding of hydrologic, climatologic, oceanographic processes as well as other environmental processes involving several geochemical cycles. In case of the water cycle, oxygen-18, deuterium, tritium and carbon-14, among other isotopes, are considered excellent tracers of the water molecule and dissolved salts, providing information on processes in the hydrosphere or residence time indicators in water systems. Environmental isotopes have been used in hydrological studies for addressing issues such as recharge processes, origin of water, groundwater dynamics, vulnerability to pollution and interconnections among different water bodies.

Most applications of environmental isotopes rely on the analysis of temporal and/or spatial variability of isotope ratios in the different components of the water cycle, particularly precipitation, surface water and groundwater. In this chapter, we review the current status of isotope databases, operation of the monitoring networks and compilation and dissemination of isotope data on the global scale. Most of the databases mentioned in the chapter are maintained and updated by the IAEA, but other global isotope data sets, compiled by national or international organizations, are also described.

P.K. Aggarwal, L.J. Araguás-Araguás, M. Groening, K.M. Kulkarni, T. Kurttas, B.D. Newman, and T. Vitvar
Isotope Hydrology Section, International Atomic Energy Agency, Vienna, Austria
e-mails: P.Aggarwal@iaea.org; L.Araguas@iaea.org; M.Groening@iaea.org; km.kulu@gmail.com; T.Kurttas@iaea.org; B.Newman@iaea.org; T.Vitvar@iaea.org

K.M. Kulkarni
Now at: Isotope Applications Division, Bhabha Atomic Research Centre, Trombay, Mumbai, 400085, India

J.B. West et al. (eds.), *Isoscapes: Understanding Movement, Pattern, and Process on Earth Through Isotope Mapping*, DOI 10.1007/978-90-481-3354-3_2,

2.2 A Brief Historical Note on Isotope Hydrology Datasets

Development of mass spectrometric techniques in late 1940s and early 1950s, allowing the precise measurement of isotope ratios in water samples (Nier 1947; McKinney et al. 1950) led to the initial efforts in collecting information on isotope variability in freshwaters on a global scale. A number of local and regional isotope hydrological studies were conducted during the 1950s (Dansgaard 1953, 1954; Friedman 1953) to characterize isotope variability in different types of waters and at different locations. However, it was not until 1961 that the first compilation of isotope composition in freshwaters on a global scale was published (Craig 1961). Also in 1961, the International Atomic Energy Agency, in cooperation with the World Meteorological Organization launched a worldwide survey to measure the isotope composition of precipitation that culminated in the Global Network of Isotopes in Precipitation (GNIP). Dansgaard (1964) published one of the classical papers in isotope hydrology, reviewing the early data gathered by the GNIP programme. One year later, Craig and Gordon (1965) also published a monograph analyzing the stable isotope composition of oceanic waters and marine atmosphere. Over the next decades, several national networks contributing their data to GNIP were established, consolidating GNIP as the main source of isotope data in atmospheric waters. In the early 1980s, the first compilation of isotope composition in recent snow, ice cores in Antarctica was published (Morgan 1982). Also in this period, the first compilation of systematic measurements of isotope composition of river waters from several continents was carried out by Mook (1982). Other important hydrological isotope databases not operated by the IAEA networks are the Global Seawater Oxygen-18 database (Schmidt et al. 1999), the USGS National Stream Quality Account Network, NASQAN (Coplen and Kendall 2000) and an extensive isotope data set from snow pits and ice cores in Antarctica (Masson-Delmotte et al. 2008).

Besides the isotope data provided by the GNIP, as a result of isotope hydrological and climatological studies in the following years, a large number of isotope data sets from surface waters and groundwaters were generated (e.g. Gat and Dansgaard 1972; Schoch-Fischer et al. 1984; Ingraham and Taylor 1986; Friedman et al. 1992; Davisson and Criss 1993; Criss and Davisson 1996; Kendall and Coplen 2001; Smith et al. 1992; Longinelli and Selmo 2003; Lachniet and Patterson 2002; Kurita et al. 2004; Aggarwal et al. 2007; Vachon et al. 2007). However, these isotope results were not compiled into a single database, and therefore they were not easily available and accessible for regional or continental studies. Only recently, the IAEA has embarked on the systematic collection of isotope data from surface waters and groundwaters obtained as part of hydrological studies mainly in Africa, Latin America, and Asia and the Pacific regions (Aggarwal et al. 2007; International Atomic Energy 2007, 2008).

Existing isotope data sets mainly include oxygen and hydrogen isotope ratios in precipitation and other water bodies, as well as tritium and carbon-14 in surface waters and groundwaters. In most cases, the compiled isotope and related hydrological/hydrogeochemical data have only been used for specific hydrological or

climatological applications. In recent years, geostatistical methods and geographic information system (GIS) tools are being used to map spatial and temporal variability of isotope composition (Birks et al. 2002; Bowen and Wilkinson 2002; Bowen and Revenaugh 2003; Dutton et al. 2005; Lykoudis and Argiriou 2007; Aggarwal et al. 2007). Online isotope maps are available at a number of web sites (e.g., www.waterisotopes.org and www.iaea.org/water). Availability of GIS and improved geostatistical tools are leading to the development of dedicated thematic layers in an integrated manner with other hydrological and ecological tools. Isotope maps showing different temporal and spatial distributions of isotopes in precipitation and other water types are also being produced (Bowen et al. 2007).

2.3 Global Network of Isotopes in Precipitation

As mentioned above, the IAEA, in cooperation with the World Meteorological Organization (WMO), has conducted since 1961 a worldwide survey of oxygen and hydrogen isotope composition in precipitation. Initially, the main interest of GNIP was the systematic monitoring of tritium fallout at a global scale as a consequence of the atmospheric thermonuclear tests carried out during the late 1950s and early 1960s. During the first years of operation, a total of 151 WMO meteorological stations, from 65 countries and territories, participated in the GNIP, reaching a maximum of about 220 active stations in 1963/1964. Reference WMO meteorological stations were selected to optimize geographical coverage and to ensure proper implementation of sampling protocols.

The first years of operation of this network provided adequate coverage of tritium fallout and enough stable isotope data to complete the first evaluation of the GNIP data (Dansgaard 1964). This led to identification of main factors controlling spatial variability of isotope ratios in precipitation on a global scale. After the ban on atmospheric thermonuclear tests in 1963, the focus for maintaining the GNIP shifted to temporal and spatial variations of stable isotopes in precipitation. This interest was mainly driven by applications in hydrology and palaeoclimatology in 1970s and 1980s.

After a revision of operational aspects of the GNIP in 1977, some stations were discontinued, mainly under the assumption that further tritium monitoring was not necessary. However, establishment of number of national networks and growing demand for isotope data in precipitation led to establishment or reactivation of existing/new stations in the following years, maintaining the number of active GNIP stations around 170–200 over the following decades.

Tritium and stable isotopes of water have been systematically used since the early 1960s in the field of isotope hydrology, within the scope of water resources inventory, planning and development. Even today this primary ‘hydrological’ objective remains the main driving factor for the operation of the network. In recent years, other disciplines have significantly increased interest in stable isotope data for: (i) providing input data to verify and further improve atmospheric circulation models,

(ii) studying climate change at different time scales, and (iii) ecological research. Disciplines and recent applications now routinely using stable isotope data, include archaeology, palaeontology, anthropology, landscape ecology, plant physiology, food webs, animal migrations, forensics and food authentication.

2.3.1 GNIP – Mode of Operation

Since the early stages of GNIP, the standard mode of operation was collection of aliquots representing monthly precipitation at participating stations. Standard tritium and stable isotope sampling protocols were sent to the IAEA/WMO stations. Generally two monthly composite samples are provided to the isotope laboratories; a 500-mL bottle for tritium analysis and a 50-mL bottle for stable isotopes. Isotope results and meteorological data are compiled, verified and uploaded into the GNIP database by staff of the Isotope Hydrology Section at the IAEA headquarters in Vienna. The participating stations in the GNIP programme provide basic meteorological data (monthly amount of precipitation, mean monthly air temperature and mean monthly water vapor pressure), and collect composite monthly rainfall samples for tritium, deuterium and oxygen-18 analyses.

Precipitation samples at the GNIP stations are collected in cooperation with the WMO, national meteorological services and national research institutes. The GNIP network contains data provided by the following types of stations: (i) reference WMO stations situated in climatically relevant locations, (ii) national networks composed of stations operated by national institutes/authorities; and (iii) affiliated stations resulting from various studies, often short-term in nature, set-up for scientific/research purposes by national research institutions. The IAEA/WMO stations are those where national institutes are performing monthly composite sampling of precipitation, compiling relevant meteorological parameters and shipment of samples to the IAEA laboratory for isotope analyses. The stations belonging to national networks report the results to the IAEA, generally once a year, for their incorporation into the GNIP database. About seventy laboratories from 40 countries have contributed isotope measurements to the GNIP programme. In recent years, only 30–40% of the collected precipitation samples are analysed at the IAEA's Isotope Hydrology Laboratory, while the remaining samples are measured in cooperating laboratories. Today, the following categories of isotope records of atmospheric waters are available in the GNIP database:

1. Regular IAEA/WMO stations collecting composite monthly samples, either official WMO stations, stations part of a national networks or sites selected as part of hydrological or scientific studies. About 900 GNIP stations, providing more than 120,000 monthly records are available in the main GNIP database.
2. Stations collecting precipitation samples with a time frequency different than the standard monthly format, ranging from fractions of a rain episode, to rain events with daily or weekly frequency. Detailed isotope, climatological or hydrological studies for about 125 stations with several sampling frequencies

(contributing about 20,000 records) have been added in the last few years to the GNIP database.
3. Stations, generally located in isotope laboratories or universities, collecting water vapor on the roof of the research buildings. Data from about ten sites (1,000 records) are available in the GNIP database.
4. GNIP–Antarctica, containing isotope data from surface snow pits and ice core samples from about 1,250 sites in Antarctica (Masson-Delmotte et al. 2008).

The IAEA provides logistical support for sampling and shipment of samples to/from the participating stations, as well as analytical support for isotope analysis and intercomparison exercises to ensure a consistent reporting of isotope composition. Compiled meteorological and isotope data from several sources are regularly uploaded into the GNIP database by the Isotope Hydrology Section of the IAEA. Raw isotope data and the statistical treatment in the early stages of the GNIP programme have been published by the IAEA (IAEA 1981, 1992). Since 1995 electronic access to the GNIP database has been provided from the IAEA's Water Resources Programme. Now the revised and updated database, as well as the statistical treatment of the isotope and meteorological data for each station, is available through the online application called Water Isotope System for Data Analysis, Visualization and Electronic Retrieval (WISER) accessible at the IAEA web site: http://www.iaea.org/water, (IAEA/WMO 2008).

GNIP and the other IAEA isotope networks operate on a voluntary basis and it is difficult to establish and maintain long-term sampling stations, especially in remote areas. To help with this problem the IAEA supplies interested parties with operational procedures and information on how to make inexpensive but effective precipitation samplers. In developing countries, the IAEA may also supply sample bottles and provision of analyses. The IAEA also helps countries design and implement national precipitation networks. Despite these efforts, maintaining effective global networks is still a challenge and improved methods for collecting multiple samples in remote areas, as well as more capacity to conduct isotope analyses are going to be required to improve the existing networks.

2.3.2 Deuterium and Oxygen-18 in Global Precipitation

The spatial and temporal distribution of deuterium and oxygen-18 composition in precipitation exhibits complex distribution patterns with spatial variability ranging from 10^2 to 10^7 m, and temporal scales from 10^2 to 10^{12} s. For example, intra-storm isotope variability in time and space is usually of the same magnitude as the seasonal isotopic range for many climatic conditions (Rindsberger et al. 1990; Celle-Jeanton et al. 2004). Differences in isotopic compositions of precipitation are the result of physical processes operating at different scales: (a) at the microscopic scale, kinetic and equilibrium fractionation processes during the phase change episodes shift isotope ratios, (b) at the macroscopic scale, isotope variability is a

consequence of Raleigh-type distillation processes in the atmosphere and mixing of water bodies with different isotope composition. Under equilibrium conditions, at 15ºC water vapor is ~10‰ more negative in $\delta^{18}O$ (and about 85‰ in $\delta^{2}H$) with respect to the isotopic composition of liquid water. Equilibrium isotope effects mainly depend on temperature, while kinetic fractionation in the water cycle is controlled by relative humidity and other factors.

The spatial coverage of the GNIP monitoring stations with an isotope record covering at least 1 year, as well as the GNIP-Antarctica sites described in Section 2.3.1, is shown in Fig. 2.1. Stations with at least one full year of isotope records are shown. The 900 regular GNIP stations and 1,250 Antarctic sites provide a reasonable spatial coverage at global and continental scales. However the geographical coverage and temporal distribution of active GNIP stations is not homogeneous. Some areas, like Western Europe show a relative high density of long-term stations, while others like Siberia or several areas in Africa show a few and mostly short-term stations. About 50% of the GNIP stations are located in the latitude belt 30–60ºN. Only 27% of the stations are located above 600 m a.s.l. (Fig. 2.2). One hundred and thirty five GNIP stations have a length of record above 200 monthly records, with the Vienna station approaching 600 monthly records.

The isotope and meteorological data gathered in the GNIP database has been reviewed in several occasions after the pioneering works of Craig and Dansgaard, (Yurtsever and Gat 1981; Gonfiantini 1985; Rozanski et al. 1993). All those reviews confirmed the basic findings reported in the pioneer papers. Global distribution patterns can be related to isotope fractionation processes occurring during evaporation and condensation in the water cycle, usually described as a Raleigh distillation process. More negative isotope values of precipitation are observed as the result of progressive fractionation during rainout of an air mass (Craig 1961; Craig and Gordon 1965; Gat 1996). Degree of rainout can generally be used to explain the so-called ‘isotope

Fig. 2.1 Geographical distribution of the meteorological stations belonging to the IAEA/WMO global network of isotopes in precipitation (GNIP) and the GNIP-Antarctica sites

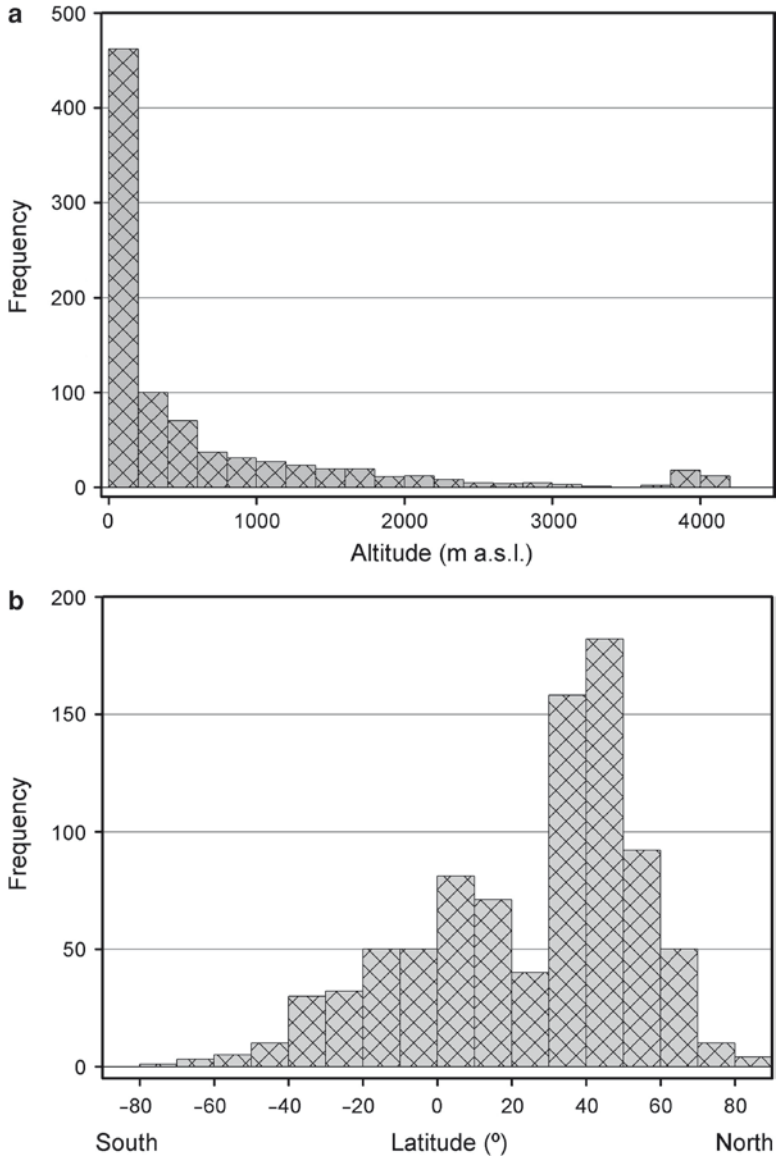

Fig. 2.2 Latitudinal and altitudinal frequency distributions of the GNIP stations

effects': latitudinal and altitudinal changes related to decreasing mean air temperature (Rozanski et al. 1992), progressive depletion of heavy isotope composition in precipitation as distance increases from the source area of the water vapor (also known as continentality effect), and amount effect, i.e., more negative isotope values of heavy rain events in tropical areas. Degree of rainout is generally controlled by the interaction between air masses and atmospheric circulation processes.

For hydrological applications, yearly and long-term means, weighted by the amount of precipitation, are usually calculated from the original records in the GNIP database. The weighted mean values are computed as follows:

$$\overline{\delta}_w = \frac{\sum_{i=1}^{n} P_i \cdot \delta_i}{\sum_{i=1}^{n} P_i} \tag{2.1}$$

where P_i and δ_i represent the monthly precipitation amount and its δ value, respectively. In case of tritium, the measured monthly tritium values, expressed in tritium units (T.U., equal to 0.118 Bq/L), are used instead of the δ values. Weighted mean values are generally representative isotopic fingerprints of recharging waters to aquifers and other water bodies.

The statistical analysis of the stable isotope data in the GNIP has confirmed the validity, using both arithmetic and weighted means, of the equation known as the Global Meteoric Water Line (GMWL), which represents, on a global scale, the linear relationship between the oxygen-18 and deuterium composition in precipitation and in other meteoric waters. Computation of the GMWL using the long-term isotope data for 650 stations, covering $\delta^{18}O$ range from +4 to –30‰, provides the following equation:

$$\delta^2H = 8.10\ \delta^{18}O + 11.1 \quad (n = 650;\ r^2 = 0.99) \tag{2.2}$$

The oxygen-18 vs. deuterium relationship for all long-term monthly means for the GNIP stations collecting precipitation samples on monthly samples is presented in Fig. 2.3. Minor variations in the slope and intercept of this equation are observed when comparing regression lines obtained from different geographical areas (Rozanski et al. 1993) or sampling periods (Gourcy et al. 2005).

For example, the regression line for snow and ice samples collected in Antarctica shows a slightly different equation, for $\delta^{18}O$ range of –10 to –60‰:

$$\delta^2H = 7.75\ \delta^{18}O - 4.8 \quad (n = 895;\ r^2 = 0.99) \tag{2.3}$$

If both GNIP and Antarctic $\delta^{18}O$ and δ^2H data are combined, the equation obtained is:

$$\delta^2H = 8.11\ \delta^{18}O + 10.0 \quad (n = 1545;\ r^2 = 0.99) \tag{2.4}$$

The relationship between isotope composition of precipitation and mean air temperature has been studied since the early days of isotope geochemistry because of its implications in reconstructions of paleoclimates. The corresponding long-term mean values of these two parameters obtained from the GNIP and Antarctic datasets are presented in Fig. 2.4.

The mean $\delta^{18}O$/temperature gradient for sampling sites in the Antarctic is 0.80‰ per degree Celsius whereas gradients of 0.67‰ per degree Celsius are obtained for the GNIP stations with mean annual temperature below 10ºC. The GNIP stations in mid- and tropical latitudes with mean annual temperature above 10ºC show a lower

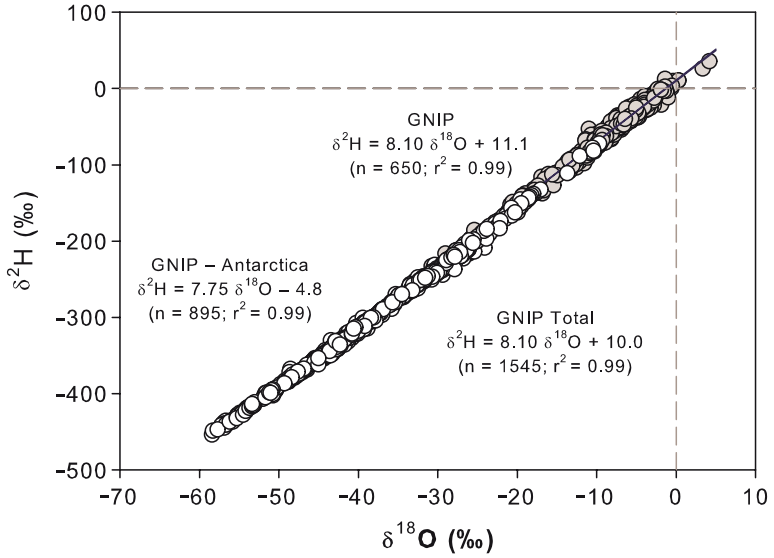

Fig. 2.3 Relationship between long-term deuterium vs. oxygen-18 annual means for GNIP stations collecting precipitation samples on monthly basis and for Antarctic snow

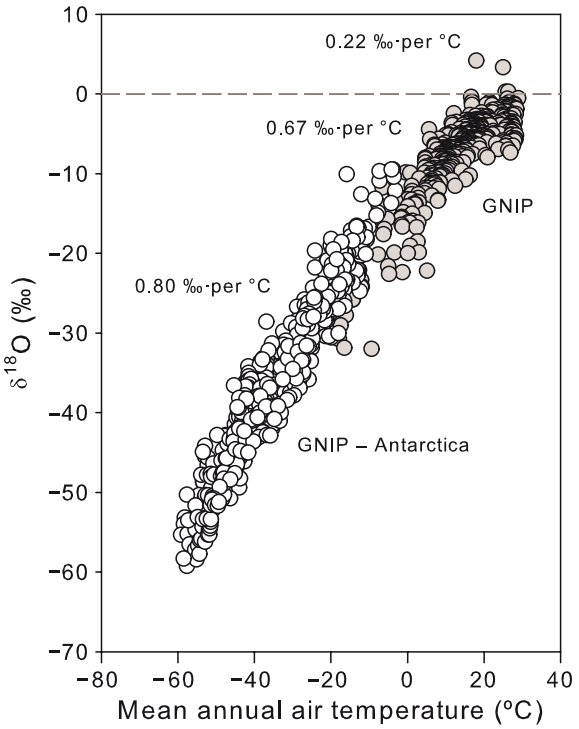

Fig. 2.4 Relationship between long-term mean annual air temperature and long-term mean $\delta^{18}O$ values in precipitation for the GNIP and the Antarctica data sets

slope of 0.22‰ per degree Celsius. The overall slope for all the GNIP stations is 0.50‰ per degree Celsius. Further details of the temporal and spatial variability of this gradient can be found in Rozanski et al. (1992).

The GNIP database, together with other complementary data sets, has been used to study the relationship between isotope composition in atmospheric waters and relevant climatic parameters such as temperature (discussed above), amount of precipitation or relative humidity. The interest for understanding such relationships under present conditions is to validate Atmospheric Global Circulation Models (AGCM) and to use isotope records preserved in paleoclimatic archives like lake sediments, speleothems, tree rings, ice cores, groundwater, etc. as proxy indicators of past climate changes (Hoffmann et al. 1998, 2000; Jouzel et al. 2000; Noone and Simmonds 2002; Sturm et al. 2005). A number of atmospheric global circulation models incorporate water isotopes with the aim of simulating present day spatial isotope distribution, and in this way, confirm our understanding and validate numerical models of atmospheric dynamics for the study of global climate change processes as well as paleoclimates.

The development and increased use of interpolation methods incorporated into GIS tools, such as regular kriging, multiple regression methods, optimal interpolation, etc. resulted in the development and publication of gridded maps (Bowen this volume). Examples of such global scale interpolations are presented in Fig. 2.5 or can be found at www.waterisotopes.org. This site provides access to global and

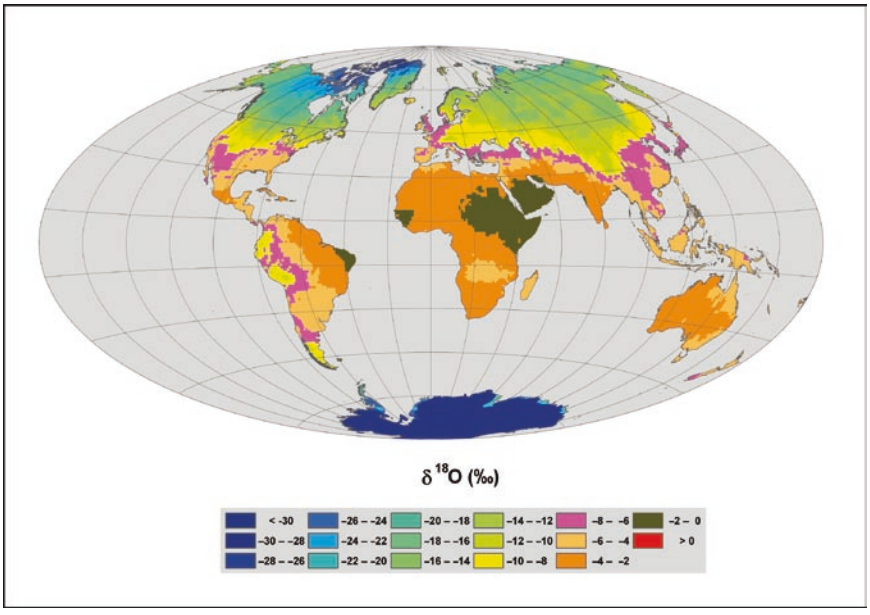

Fig. 2.5 Global interpolation map of oxygen-18 composition of precipitation (Modified from Aggarwal et al. 2007) Fig. 2.5, see Appendix 1, Color Section

continental isotope maps of mean annual δ^2H and $\delta^{18}O$ composition of precipitation, based on algorithms presented in Bowen and Revenaugh (2003).

2.3.3 *Tritium in Global Precipitation*

The GNIP database also provides the most complete and detailed chronicle of tritium composition in precipitation, going back to the early tritium measurements during the thermonuclear tests in early 1950s (Rozanski et al. 1991). The tritium compositions in precipitation for the reference GNIP stations in the northern and southern hemispheres from 1950 to 2002 are shown in Fig. 2.6. Ottawa, Canada has been considered the reference station in the northern hemisphere, while Kaitoke, New Zealand is considered to better represent the tritium chronicle in the southern hemisphere. Very often, the GNIP database has been used as the main or only source to estimate the input function of this tracer (Doney et al. 1992) into hydrological systems, mainly for groundwater and oceanographic investigations. Tritium has been used in the past as the main tracer for determining groundwater age of recent waters (up to 50 years). Lumped-parameter models were used to determine residence times of groundwater and large river basins, by comparing tritium concentrations in springs and shallow groundwaters with the known input function provided by the GNIP data (e.g. Maloszewski and Zuber 1996; Michel 1992).

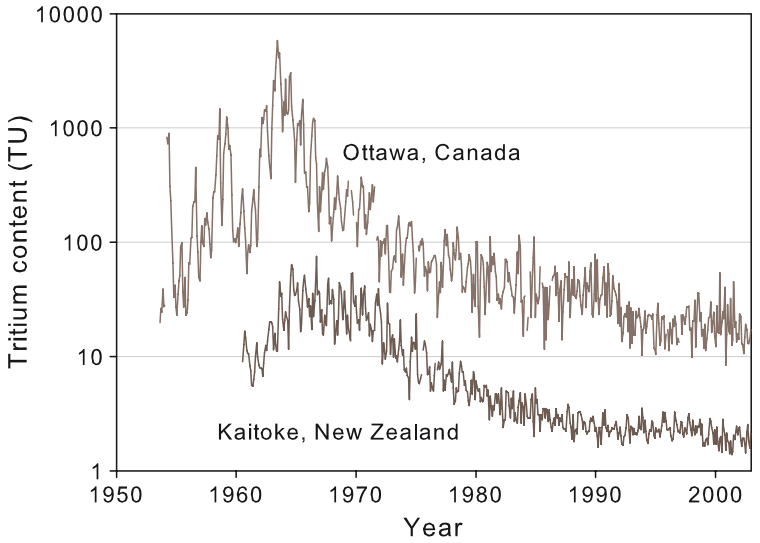

Fig. 2.6 Tritium compositions in precipitation for reference stations in the northern and southern hemispheres from 1950 to 2002

2.4 Global Network of Isotopes in Rivers (GNIR)

Rivers constitute an important freshwater resource and an essential link in the global hydrological cycle, returning a significant fraction of continental precipitation to the oceans. Rivers are also important integrators of climate and land use impacts within a basin. There is a basic need to improve our scientific understanding of hydrological processes in river basins and the ability to detect and predict impacts of climate change on water resources (Gibson et al. 2002). Special interest is given to the study of processes relevant to characterization of baseflow conditions in rivers, i.e., the interaction between groundwater and other contributions to river flows. The Water Resources Programme of the IAEA launched the GNIR in 2007 (Vitvar et al. 2007) to monitor isotope composition of runoff in large rivers. The GNIR programme supports sampling and isotope analysis of river discharge primarily at river mouths, and provides additional tracers for improved understanding of water dynamics in catchments and river basins. The programme represents a complimentary monitoring activity to the GNIP programme.

Many international efforts have extensively explored water and energy budget methods and modelling in river basins. A limited number of studies have mapped isotope distribution in river runoff and compared this to isotope distribution in precipitation (e.g. Dutton et al. 2005; Gibson et al., this volume). However, use of isotope tracer techniques has been limited due largely to the lack of availability of isotope data for the major hydrological components and fluxes of the continental hydrological cycle including river discharge. The GNIR is expected to provide additional tools to assess a number of hydrological aspects relevant to catchment hydrology. Coupled with measurement of isotopes in water sources, analysis of river discharge and other tracers are expected to provide a clearer focus on groundwater recharge/discharge processes, water balance, and snow and glacier melt water mixing. Contributions to the early stages of the GNIR have been provided by the participants of two IAEA Coordinated Research Projects: ‘Design criteria for a network to monitor isotope compositions of runoff in large rivers’ and ‘Isotopic Age and Composition of Stream Flow as Indicators of Groundwater Sustainability’. Additionally, the GNIR database includes tritium in large rivers, mainly in the USA (Michel et al. 2006). Some additional isotope data has also been provided by the NASQAN programme in the USA, (Coplen and Kendall 2000; Coplen and Huang 2000; Kendall and Coplen 2001). Recent contributions of ongoing isotope studies in rivers and data compilation efforts from published scientific papers are expected to result in more than 25,000 records in the GNIR database in the near future.

2.5 Moisture Isotopes in the Biosphere and Atmosphere (MIBA)

The Water Resources Programme of the IAEA launched the MIBA programme in 2004 to improve availability of isotope data for other water cycle components. The aim is to supplement the GNIP data for better integration of isotope applications

in the water and carbon cycles as well as in climate research. Field sites were selected in broadly defined global regions to sample water vapor, leaves, stems and soil moisture. Additional stations were created as part of a dedicated coordinated research project of the IAEA. Sampling sites were selected in more than ten countries. Participants sent plant and soil samples for water extraction and isotopic analyses to the designated laboratories. The IAEA and several other institutes provided isotopic analyses for participants who do not have the availability or capacity to perform the required extraction and/or analysis. Results of isotope analysis and related information are available through the IAEA's online WISER application.

As of early 2009, around 1,000 isotope records that relate to MIBA activities are available and the number is expected to reach to 5,000 in 2010. Isotope data from water vapor are relevant to partitioning of evaporation and evapotranspiration, a topic of major interest to ecohydrology and related fields. The importance of water recycling in the water cycle, even at continental scale, has been shown in several studies, (Salati et al. 1979). Similarly, isotope tracers in water vapor have been used to study interaction between the oceans and the atmosphere, where air masses with contrasting properties result in complex atmospheric circulation and weather patterns (Gat et al. 2003).

2.6 Isotope Composition of Surface Waters and Groundwaters (IAEA-TWIN)

In addition to the global monitoring programmes briefly described above, systematic compilation of isotope and related hydrological information obtained as part of IAEA activities in Member States, mainly from surface waters and groundwaters, was initiated in 2003. Isotope data generated as part of IAEA-supported projects has been compiled and processed from the original electronic and hard copy sources for the dedicated database called IAEA – Terrestrial Water Isotope Network, IAEA-TWIN. All samples are geo-referenced, using original field reports or scanned maps from the hydrological reports and/or publications. Metadata on the ultimate source of various data sets are also being included in the database. Some of the IAEA-TWIN information is available through WISER.

To date, about 25,000 records have been collected from studies in the African Member States and a similar number is expected to be gathered from isotope projects in the Asia and Pacific, and Latin America regions. Basic information on each project, such as location of the study area, background information of the project, a summary table and basic isotope plots, have been presented in the Isotope Hydrology Atlas – Africa (IAEA 2007) and – Asia and the Pacific (IAEA 2008). Similar atlases are being developed for Latin America as well as for Europe and the Middle East. For example, recent isotope mapping of groundwaters includes large regional scale maps showing carbon-14 distribution in deep groundwaters over large aquifers in Northern Africa (Aggarwal et al. 2007). The carbon-14 distribution map in Fig. 2.7 shows how extensive very old groundwater (> 10,000 years) is in the northern Africa region based on the predominance of groundwater

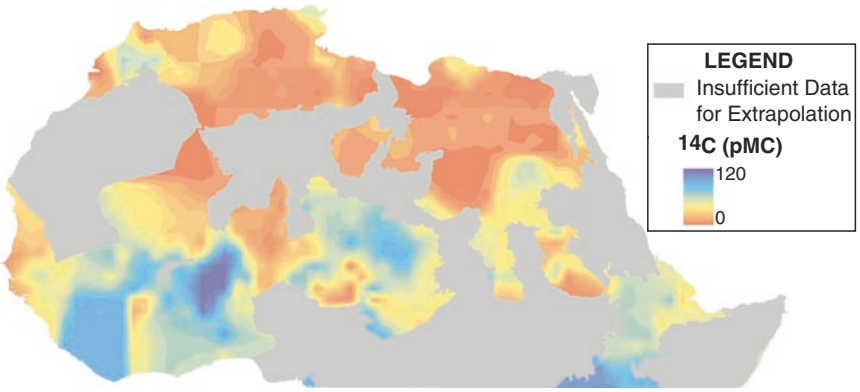

Fig. 2.7 Carbon-14 (percent of modern carbon) in deep groundwater of northern Africa (modified from Aggarwal et al. 2007) Fig. 2.7, see Appendix 1, Color Section

with little or no modern carbon (expressed as percent modern carbon, pMC) in dissolved carbon in groundwater.

2.7 Isotope Composition of Seawater

The NASA Goddard Institute for Space Studies hosts the Global Seawater Oxygen-18 Database (Schmidt et al. 1999) which contains a collection of over 22,000 seawater $\delta^{18}O$ values obtained since 1950. The complete database and interpolated gridded maps showing the spatial distribution of isotope composition are available from the NASA portal. Available information in this database includes $\delta^{18}O$ values ($\delta^{2}H$ if available) in seawater samples, salinity, water temperature, depth, geographical coordinates and date of sampling. Global gridded isotope distribution maps have been produced and incorporated into atmospheric circulation models to simulate sources of water vapor and for oceanographic studies (LeGrande and Schmidt. 2006).

2.8 Concluding Remarks

The need for global- and regional-scale isotope data continues to increase. This is not just because of an increased focus on problems at these large scales, but also because isotopes are being used in ways that extend far beyond the traditional hydrological applications. Despite the operational difficulties in running monitoring networks, global databases are growing, providing improved coverage in time and space to better map and visualize isotope distributions with increasing resolution.

The objective of this paper was to describe spatially-oriented isotope networks and databases that can be used for a variety of applications and provide a few examples of large scale visualization. The focus has been on the IAEA databases because of their uniqueness, large size, variety, and in the case of GNIP, decades of data collection from around the world. During the last 45 years, GNIP has produced a unique set of isotope data that still has significant potential to be exploited to study processes controlling the spatial and temporal variability of isotope composition in atmospheric waters on a global scale. The IAEA has made continuous pioneering efforts over five decades to strengthen the operation of GNIP in areas with poor coverage or sites highly relevant for climatological or hydrological research. The establishment of links to other international programmes, research groups and national isotope hydrology laboratories is expected to continue and grow to increase the number of global network stations in general and improve the quality and coverage of isotope monitoring efforts.

Similar network expansion efforts are required to enhance the two new IAEA networks/databases GNIR and MIBA. The GNIR already contains significant data sets on isotopes in rivers and should become a more powerful tool in the coming years as more data are collected and new stations are added. Its focus on rivers will be useful for studying impacts of land use change and climate variability particularly at the basin scale. Similarly, the MIBA network/database should expand and be increasingly useful for atmospheric and ecohydrological applications. The combination of isotope data from soil water, atmospheric water and plant water links important parts of the water cycle and can support studies related to both climate and plant water use among others. In addition, other non-IAEA isotope databases such as the Antarctic snow and ice database and the Global Seawater Oxygen-18 Database are available with unique sets of data applicable to many types of studies. Use of enhanced spatial and temporal analysis tools with isotope network data are powerful approaches for understanding complex processes at large scales. Thus, robust, spatially extensive isotope data sets from a variety of networks are needed to realize the potential for understanding complex, coupled processes and the links between different parts of the hydrological cycle.

Improved Internet access, increased availability of data analysis and visualization tools along with new analytical technologies, such as laser absorption based isotope spectrometers for liquid and vapor isotope analyses will also foster better global data sets and increased use of large scale isotope data. Ultimately, field deployable laser analyzers and automated precipitation samplers (e.g., Coplen et al. 2008) may greatly aid in building networks with better spatial coverage in the future.

References

Aggarwal PK, Alduchov O, Araguás-Araguás L, Dogramaci S, Katzlberger G, Kriz K, Kulkarni KM, Kurttas T, Newman BD, Pucher A (2007) New capabilities for studies using isotopes in the water cycle. EOS Trans AGU 88(49):537–538

Birks SJ, Gibson JJ, Gourcy L, Aggarwal PK, Edwards TWD (2002) Maps and animations offer new opportunities for studying the global water cycle. EOS Trans AGU 83(37):406

Bowen GJ (2010) Statistical and geostatistical mapping of precipitation water isotope ratios. In: JB West et al. (eds.), Isoscapes: Understanding movement, pattern, and process on Earth through isotope mapping, Springer Science.

Bowen GJ, Revenaugh J (2003) Interpolating the isotopic composition of modern meteoric precipitation. Water Resour Res 39(10):1299

Bowen GJ, Wilkinson BH (2002) Spatial distribution of $\delta^{18}O$ in meteoric precipitation. Geology 30(4):315–318

Bowen GJ, Ehleringer JR, Chesson LA, Stange E, Cerling TE (2007) Stable isotope ratios of tap water in the contiguous United States. Water Resour Res 43:W03419

Celle-Jeanton H, Gonfiantini R, Travi Y, Sol B (2004) Oxygen-18 variations of rainwater during precipitation: application of the Rayleigh model to selected rainfalls in Southern France. J Hydrol 289:165–177

Coplen TB, Huang R (2000) Stable hydrogen and oxygen isotope ratios for selected sites of the National Oceanic and Atmospheric Administration's Atmospheric Integrated Research Monitoring Network (AiRMoN). US Geological Survey Open File Report 00-279 Reston

Coplen TB, Kendall C (2000) Stable hydrogen and oxygen isotope ratios for selected sites of the US Geological Survey's NASQAN and Benchmark surface-water networks. US Geological Survey Open File Report 00-160 Reston

Coplen TB, Neiman PJ, White AB, Landwehr JM, Ralph FM, Dettinger MD (2008) Extreme changes in stable hydrogen isotopes and precipitation characteristics in a landfalling Pacific storm. Geophys Res Lett 35:L21808

Craig H (1961) Isotopic variations in meteoric waters. Science 133:1702–1703

Craig H, Gordon LI (1965) Deuterium and oxygen-18 variations in the ocean and the marine atmosphere. In: Tongiorgi E (ed) Stable isotopes in oceanographic studies and paleotemperatures. Lab di Geologia Nucleare, Pisa, pp 9–130

Criss RE, Davisson ML (1996) Isotopic imaging of surface water/groundwater interactions, Sacramento Valley, California. J Hydrol 178:205–222

Dansgaard W (1953) The abundance of ^{18}O in atmospheric water and water vapour. Tellus 5:461–469

Dansgaard W (1954) The ^{18}O abundance of fresh water. Geochim Cosmochim Acta 6:241–260

Dansgaard W (1964) Stable isotopes in precipitation. Tellus 16:438–468

Davisson ML, Criss RE (1993) Stable isotope imaging of a dynamic groundwater system in the southwestern Sacramento Valley, California, USA. J Hydrol 144:213–246

Doney SC, Glover DM, Jenkins WJ (1992) A model function of the global bomb tritium distribution in precipitation, 1960–1986. J Geophys Res 97(C4):5481–5492

Dutton A, Wilkinson BH, Welker JM, Bowen GJ, Lohmann KC (2005) Spatial distribution and seasonal variation in $^{18}O/^{16}O$ of modern precipitation and river water across the conterminous USA. Hydrol Process 19:4121–4146

Friedman I (1953) Deuterium content of natural waters and other substances. Geochim Cosmochim Acta 4:89–103

Friedman I, Smith GI, Gleason JD, Warden A, Harris JM (1992) Stable isotope composition of waters in southeastern California. 1 Modern precipitation. J Geophys Res 97(D5):5795–5812

Gibson JJ, Fekete BM, Bowen, GJ (2010) Stable isotopes in large scale hydrological applications In: JB West et al. (eds.), Isoscapes: Understanding movement, pattern, and process on Earth through isotope mapping, Springer Science.

Hoffmann G, Werner M, Heimann M (1998) Water isotope module of the ECHAM atmospheric general circulation model: a study on timescales from days to several years. J Geophys Res 103(D14):16,871–16,896

Hoffmann G, Jouzel J, Masson V (2000) Stable water isotopes in atmospheric general circulation models. Hydrol Process 14:1385–1406

Gat JR (1996) Oxygen and hydrogen isotopes in the hydrologic cycle. Annu Rev Earth Planet Sci 24:225–262

Gat JR, Dansgaard W (1972) Stable isotope survey of the freshwater occurrences in Israel and the northern Jordan rift valley. J Hydrol 16:177–212

Gat JR, Klein B, Kushnir Y, Roether W, Wernli H, Yam R, Shemesh A (2003) Isotope composition of air moisture over the Mediterranean Sea: an index of the air–sea interaction pattern. Tellus B Chem Phys Meteorol 55(5):953–965

Gibson JJ, Aggarwal PK, Hogan J, Kendall C, Martinelli LA, Stichler W, Rank D, Goni I, Choudry M, Gat JR, Bhattacharya S, Sugimoto A, Fekete B, Pietronino A, Maurer T, Panarello H, Stone D, Seyler P, Maurice-Bourgoin L, Herczeg A (2002) Isotope studies in large river basins: a new global research focus. EOS Trans AGU 83(52):613, 616–617

Gonfiantini R (1985) On the isotopic composition of precipitation in tropical stations. Acta Amaz 15:121–139

Gourcy L, Groening M, Aggarwal PK (2005) Stable oxygen and hydrogen isotopes. In: Aggarwal PK, Gat JR, Froehlich K (eds) Isotopes in the Water Cycle International Atomic Energy Agency. Springer, Dordrecht, pp 39–51

Ingraham NL, Taylor BE (1986) Hydrogen isotope study of large-scale meteoric water transport in northern California and Nevada. J Hydrol 85:183–197

International Atomic Energy Agency (1981) Statistical treatment of environmental isotope data in precipitation. Technical Reports Series No 206 IAEA, Vienna

International Atomic Energy Agency (1992) Statistical treatment of data on environmental isotopes in precipitation. Technical Reports Series No 331 IAEA, Vienna

International Atomic Energy Agency (2007) Atlas of isotope hydrology – Africa STI-PUB-1302 IAEA, Vienna

International Atomic Energy Agency (2008) Atlas of isotope hydrology – Asia and the Pacific STI-PUB-1364 IAEA, Vienna

International Atomic Energy Agency/World Meteorological Organization (2008) Global network of isotopes in precipitation. The GNIP Database. http://www.iaea.org/water Accessed date: May 2008

Jouzel J, Hoffmann G, Koster RD Masson V (2000) Water isotopes in precipitation: data/model comparison for present-day and past climates. Q Sci Rev 19:363–379

Kendall C, Coplen T (2001) Distribution of oxygen-18 and deuterium in river waters across the United States. Hydrol Process 15:1363–1393

Kurita N, Yoshida N, Inoue G, Chayanova EA (2004) Modern isotope climatology of Russia: a first assessment. J Geophys Res 109:D03102

Lachniet MS, Patterson WP (2002) Stable isotope values of Costa Rica surface waters. J Hydrol 260:135–150

LeGrande AN, Schmidt GA (2006) Global gridded data set of the oxygen isotopic composition in seawater. Geophys Res Lett 33:L12604

Longinelli A, Selmo E (2003) Isotopic composition of precipitation in Italy: a first overall map. J Hydrol 270:75–88

Lykoudis SP, Argiriou AA (2007) Gridded data set of the stable isotopic composition of precipitation over the Eastern and central Mediterranean. J Geophys Res 112:D18107

Maloszewski P, Zuber A (1996) Lumped parameter models for the interpretation of environmental tracer data. In: Manual on mathematical models in isotope hydrology IAEA TECDOC 910. International Atomic Energy Agency, Vienna, pp 9–58

Masson-Delmotte V, Hou S, Ekaykin A, Jouzel J, Aristarain A, Bernardo RT, Bromwhich D, Cattani O, Delmotte M, Falourd S, Frezzotti M, Gallée H, Genoni L, Isaksson E, Landais A, Helsen M, Hoffmann G, Lopez J, Morgan V, Motoyama H, Noone D, Oerter H, Petit JR, Royer A, Uemura R, Schmidt GA, Schlosser E, Simões JC, Steig E, Stenni B, Stievenard M, van den Broeke M, van de Wal R, van den Berg MJ, Vimeux F, White JWC (2008) A review of Antarctic surface snow isotopic composition: observations, atmospheric circulation and isotopic modelling. J Clim 21:3359–3387

McKinney CR, McCrea JM, Epstein S, Allen HA, Urey HC (1950) Improvements in mass spectrometers for the measurement of small differences in isotope abundances ratios. Rev Sci Instrum 21:724–756

Michel RL (1992) Residence times in river basins as determined by analysis of long-term tritium records. J Hydrol 130:367–378

Michel RL, Aggarwal PK, Kurttas T, Araguás-Araguás L, Kulkarni KM (2006) The use of tritium in river baseflow to understand long-term changes in water quality. EGU Conference, Vienna, April 2006

Mook WG (1982) The oxygen-18 content of rivers. Mitt Geol-Paläont Int Univ Hamburg SCOPE/ UNEP Sonderbrand 52:565–57

Morgan VI (1982) Antarctic ice sheet surface oxygen isotope values. J Glaciol 28(99):315–323

Nier AO (1947) A mass spectrometer for isotope and gas analysis. Rev Sci Instrum 18:398–411

Noone D, Simmonds I (2002) Associations between $\delta^{18}O$ of water and climate parameters in a simulation of atmospheric circulation for 1979–95. J Clim 15(22):3150–3169

Rindsberger M, Jaffe S, Rahamim S, Gat JR (1990) Patterns of the isotopic composition of precipitation in time and space: data from the Israeli storm water collection program. Tellus B Chem Phys Meteorol 42:263–271

Rozanski K, Gonfiantini R, Araguás-Araguás L (1991) Tritium in the global atmosphere: distribution patterns and recent trends. J Phy G: Nucl Part Phys 17:S523–S536

Rozanski K, Araguás-Araguás L, Gonfiantini R (1992) Relation between long-term trends of oxygen-18 isotope composition of precipitation and climate. Science 258:981–985

Rozanski K, Araguás-Araguás L, Gonfiantini R (1993) Isotopic patterns in modern global precipitation. In: Swart PK, Lohmann KL, McKenzie J, Savin S (eds) Climate change in continental isotopic records. Geophysical Monograph 78 American Geophysical Union, Washington DC, pp 1–37

Salati E, Dall'Olio A, Matsui E, Gat JR (1979) Recycling of water in the Amazon basin: an isotopic study. Water Resour Res 15(5):1250–1258

Schmidt GA, Bigg GR, Rohling EJ (1999) Global seawater oxygen-18 database. http://data.giss.nasa.gov/o18data Accessed date: May 2008

Schoch-Fischer H, Rozanski K, Jacob H, Sonntag C, Jouzel J, Östlund G, Geyh MA(1984) Hydrometeorological factors controlling the time variation of D, ^{18}O and ^{3}H in atmospheric water vapour and precipitation in the northern westwind belt. In: Isotope Hydrology 1983, International Atomic Energy Agency, Vienna, pp 3–31

Smith GI; Friedman I; Gleason JD, Warden A (1992) Stable isotope composition of waters in southeastern California: 2 groundwaters and their relation to modern precipitation. J Geophys Res 97(D5):5813–5823

Sturm K, Hoffmann G, Langmann B, Stichler W (2005) Simulation of $\delta^{18}O$ in precipitation by the regional circulation model REMOiso. Hydrol Process 19(17):3425–3444

Vachon RW, White JWC, Gutman E, Welker JM (2007) Amount-weighted annual isotopic ($\delta^{18}O$) values are affected by the seasonality of precipitation. A sensitivity study. Geophys Res Lett 34:L 21707

Vitvar T, Aggarwal PK, Herczeg AL (2007) Global Network is launched to monitor isotopes in rivers. Eos Trans AGU 88(33):325–326

Yurtsever Y, Gat JR (1981) Atmospheric waters. In: Gat JR, Gonfiantini R (eds) Stable isotope hydrology: deuterium and oxygen-18 in the water cycle. IAEA Technical Reports Series 210. International Atomic Energy Agency, Vienna, pp 103–142

Chapter 3
Remote Sensing of Nitrogen and Carbon Isotope Compositions in Terrestrial Ecosystems

Lixin Wang, Gregory S. Okin, and Stephen A. Macko

3.1 Introduction

Variations in stable isotope compositions have been frequently used to indicate the sources and the processes affecting stable isotope compositions of elements such as C and N in marine or terrestrial ecosystems as well as in the atmosphere. For example, $\delta^{15}N$ has been used to track origin of nitrate pollution (Kreitler 1979) and food-web dynamics (Shaner et al. 2007), to partition the atmospheric N_2O sources between nitrification and denitrification (Yoshida and Toyoda 2000), to assess ecosystem N cycling (Davidson et al. 2007; Wang et al. 2007a), and to indicate climatic variability (Rau et al. 2003). Measurements of $\delta^{13}C$ have been used to indicate plant water use efficiency (Farquhar et al. 1989), to partition source C in soils (Balesdent et al. 1987; Biggs et al. 2002; Bond et al. 1994), to constrain ecosystem respiration (Pataki et al. 2003), to indicate vegetation distribution (Still et al. 2003), to constrain CO_2 exchange between biosphere and atmosphere (Fung et al. 1997), and to indicate long-term climatic variability (Wilson and Norris 2001). Clearly, stable isotopes of C and N are powerful tools to either directly reveal or constrain

L. Wang and S.A. Macko
Department of Environmental Sciences, University of Virginia,
291 McCormick Road, Charlottesville, VA, 22904, USA
e-mail: lixinw@princeton.edu

G.S. Okin
Department of Geography, University of California, 1255 Bunche Hall,
Los Angeles, CA, 90095, USA
e-mail: okin@ucla.edu

L. Wang (✉)
Department of Civil and Environmental Engineering, Princeton University,
Princeton, NJ, 08544, USA

S.A. Macko
Also at Program in Geobiology and Low Temperature Geochemistry,
U. S. National Science Foundation, Arlington, VA, 22230, USA
e-mail: sam8f@virginia.edu

J.B. West et al. (eds.), *Isoscapes: Understanding Movement, Pattern, and Process on Earth Through Isotope Mapping*, DOI 10.1007/978-90-481-3354-3_3,

the ecological processes in ecosystems. On the other hand, with the exception of the recently developed tunable diode laser absorption spectroscopy (TDLAS) techniques for $^{13}C–CO_2$ measurements (Bowling et al. 2003; Griffis et al. 2005), technical and instrumental limitations commonly limit C and N isotope measurements in terrestrial ecosystems to spatially discrete and point-in-time sampling assessments. Continuous measurements of C and N isotopes, at larger spatial scales, could significantly improve understanding of biogeochemical cycling and the related ecological processes across multiple spatial and temporal scales.

A union of point isotope measurements with remote sensing is one possible way to achieve continuous large-scale examination of isotope compositions. Remote sensing is a powerful tool to identify ecosystem patterns and processes at larger scales (e.g., from landscape to global scale). Remote sensing techniques have been widely used to estimate plant biomass (e.g., Houghton 2005), forest structure (e.g., Hyde et al. 2006; Treuhaft et al. 2004), and canopy chemistry (e.g., Asner and Vitousek 2005; Curran et al. 1992). The joining of remote sensing and isotope measurement techniques will help to elucidate ecosystem processes at larger spatial scales with more detailed process information. The combination of these two techniques for use in ecological studies is, however, still at an exploratory stage, similar to the state of remotely-sensed canopy chemical composition in the late 1980s (Card et al. 1988; Peterson et al. 1988; Wessman et al. 1988). This is chiefly the result of a limitation in technology and the form of the sample on which measurements are made, e.g., remote sensing data do not yet have high enough spatial and spectral resolution to predict isotope composition. In this chapter, we describe the current state of methods to create spatial estimates of the stable isotope compositions of N and C, focusing on mechanisms, assumptions, applications and future directions.

3.2 Remote Sensing of Foliar N Isotope Composition

In terrestrial ecosystems, the ratio of the rare, but naturally occurring, ^{15}N isotope to the highly abundant ^{14}N isotope is an index of many processes occurring in soils, plants, and the atmosphere (Robinson 2001; Pardo and Nadelhoffer this volume). These analyses are powerful approaches that can be used to elucidate biogeochemical relationships.

Analyses of foliar N concentrations utilizing reflectance spectrometry can be as accurate as traditional wet-chemistry procedures and in fact, in many laboratories, near-infrared spectrometry has replaced wet chemistry as the standard analytical procedure for analysis of dried and ground leaves (Card et al. 1988; Peterson et al. 1988; Yoder and Pettigrew-Crosby 1995). Furthermore, Yoder and Pettigrew-Crosby (1995) showed that N concentrations could be determined from reflectance spectra of fresh leaves, in the laboratory, and possibly at canopy scales. Martin and Aber (1997) further demonstrated that foliar N concentrations could be estimated at canopy scales using satellite data. There exist close relationships between foliar $\delta^{15}N$ and foliar N contents (e.g., Hobbie et al. 2000; Pardo et al. 2006), and a recent

report indicates a relationship between foliar $\delta^{15}N$ and spectral reflectance (Wang et al. 2007b).

This topic is still in an exploratory stage with relatively few reports being available (e.g., Wang et al. 2007b). Presented here are examples containing both published and previously unpublished data, suggesting the feasibility of using high-resolution spectral data to estimate $\delta^{15}N$ in fresh leaves from leaf level to canopy level.

3.2.1 Leaf and Canopy Scale Using Field Spectra Data

Field spectral measurements paired to isotope determinations were carried out at two levels (leaf vs. canopy levels) to correlate datasets of foliar $\delta^{15}N$ and spectra. The detailed site description, field measurement, chemical analyses and data processing were reported in Wang et al. (2007b). In summary, leaf-level spectral reflectance was measured in Ghanzi, Botswana in March 2005 (21.65°S, 21.81°E). Leaf reflectance was measured with an ASD FieldSpec Pro FR portable spectroradiometer using a leaf contact probe with a halogen light source (ASD, Inc., Boulder, CO). Canopy-level reflectance was measured at the Blandy Experimental Farm (BEF) of northern Virginia (39°09′N, 78°06′W), USA in four successional fields using the same instrument with a 20° field of view. Stable N isotope analysis was performed on vegetation from these sites using a Micromass Optima Isotope Ratio Mass Spectrometer (IRMS) coupled to an elemental analyzer (EA) (GV/Micromass, Manchester, UK). Pearson correlation coefficients were calculated between foliar $\delta^{15}N$ and reflectance (R), between foliar $\delta^{15}N$ and first-difference spectra of log 1/R ((log 1/R)') at all wavelengths using SAS (v. 9.1), and correlograms were created based on Pearson correlation coefficients to easily visualize the results. Stepwise regressions (SAS v. 9.1) were performed to find the best predictors (e.g. the best wavelengths) of foliar $\delta^{15}N$ at both leaf and canopy levels. Wavelength selection was based on the correlograms, and only the wavelengths associated with significant peaks ($p < 0.05$) were used in the stepwise regression analysis.

The canopy reflectance spectra were significantly different between two successional stages in both succession series (Fig. 3.1a and b). The mean canopy reflectances in the early stage were significant higher than that in the middle stage in both series except in the near-infrared regions range (NIR: 800–1,350 nm) where the mean canopy reflectance was higher in the middle stages for successional series 1 (Fig. 3.1a and b). In both sets of the series, foliar $\delta^{15}N$ at the canopy level was significantly higher in the early stages than that in the middle successional field (Fig. 3.1c), presumably due to a less open system in the latter field (Wang et al. 2007d). In other words, the ratio of N input/output to within ecosystem N cycle in the early successional field is higher than that in the middle, with consequently higher losses of ^{14}N.

Correlograms provide a clear picture of the relationships between spectral reflectance and foliar $\delta^{15}N$. The regions marked with a black circle indicate values that may be useful for predicting foliar $\delta^{15}N$. These regions were chosen based on three

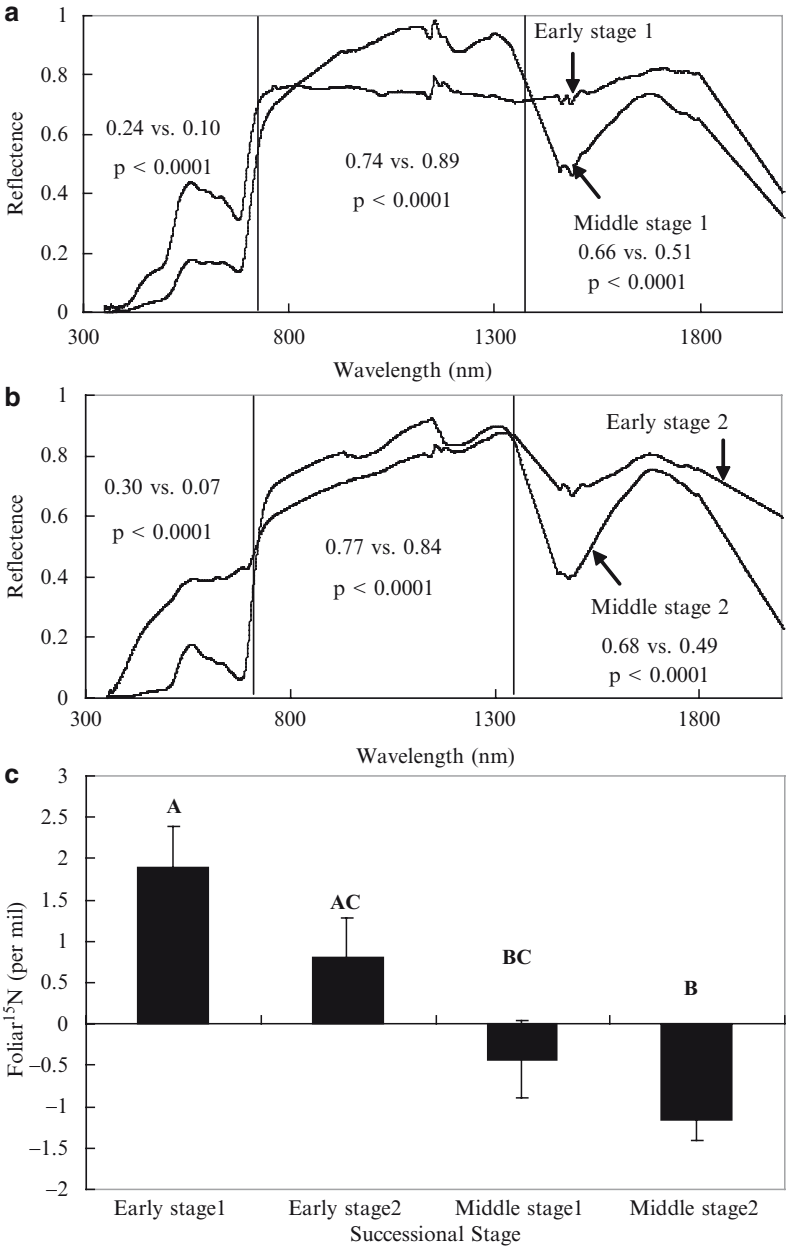

Fig. 3.1 The canopy reflectance spectra between early and middle succesional stages in succession series 1 (**a**) and succession series 2 (**b**). Numbers in each section are mean canopy reflectances in the visible range (450–700 nm), NIR range (800–1,350 nm) and >1,350 nm for early and middle succesional stages. (**c**) Canopy level foliar $\delta^{15}N$ in two successional stages of two sets of successional series (different capital letters indicate different mean values of foliar $\delta^{15}N$, e.g., any shared letters indicate no difference)

criteria: 1) correlation coefficients are statistically significant ($p < 0.05$), 2) the region is wide enough to be used in normal field and laboratory conditions (>15 nm) and 3) the regions do not fall in wavelength ranges where atmospheric water vapor or other factors might interfere with field or remote sensing-based spectroscopy. For instance, water vapor absorptions at ~940, ~1,140, 1,360–1,470 and 1,800–2,000 nm preclude the use of these regions in practical applications. In our case, significant noise >1,780 nm due to weak solar irradiance in this region also eliminates these regions from practical use for the spectroscopic estimation of $\delta^{15}N$.

At the leaf scale, two broad regions were observed in which the correlation between R and foliar $\delta^{15}N$ are significant (λ = 481–523 and 564–703 nm, $|r|$ = 0.71–0.86) (Fig. 3.2a). At the canopy scale, the strong relationship between R and foliar $\delta^{15}N$ appears at several ranges including both visible and near-infrared (VNIR) regions ($|r|$ = 0.60–0.80) (Fig. 3.2b). Although VNIR wavelength regions exhibit very high correlations, the use of R to estimate foliar $\delta^{15}N$ may not always be practical for remote sensing applications. This is due to the fact that variable lighting conditions can cause significant changes in the overall reflected brightness. The use of R to estimate $\delta^{15}N$ should be limited to cases where lighting conditions and geometry can be controlled (e.g., a leaf-contact probe or laboratory conditions) or where R is empirically found to be advantageous.

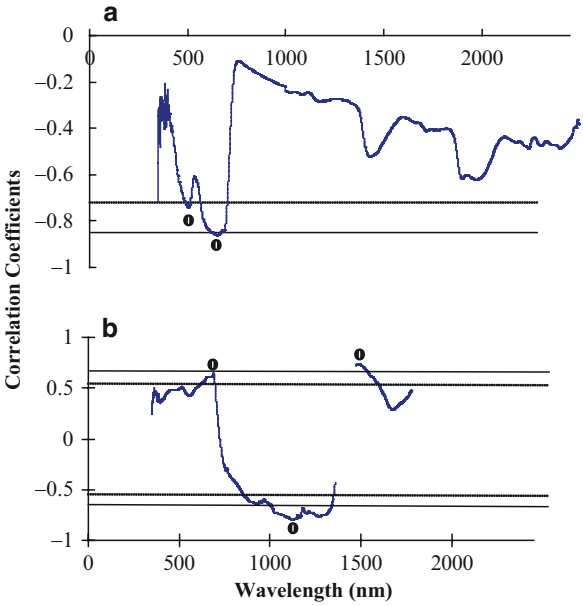

Fig. 3.2 Correlation coefficients between leaf-level reflectance (**a**) or canopy-level reflectance (**b**) and foliar $\delta^{15}N$. Dash horizontal bars indicate the area of significance, $p < 0.05$; *solid horizontal bars* indicate the area of significance, $p < 0.01$, the regions marked with a *black circle* indicate regions that may be useful for predicting foliar $\delta^{15}N$. The ranges of wavelength for *black circle* regions from left to right for (**a**) are λ = 483–517 and 617–703 nm, for (**b**) are λ = 670–694, 1,098–1,319 and 1,480–1,522 nm (Modified from Wang et al. 2007b)

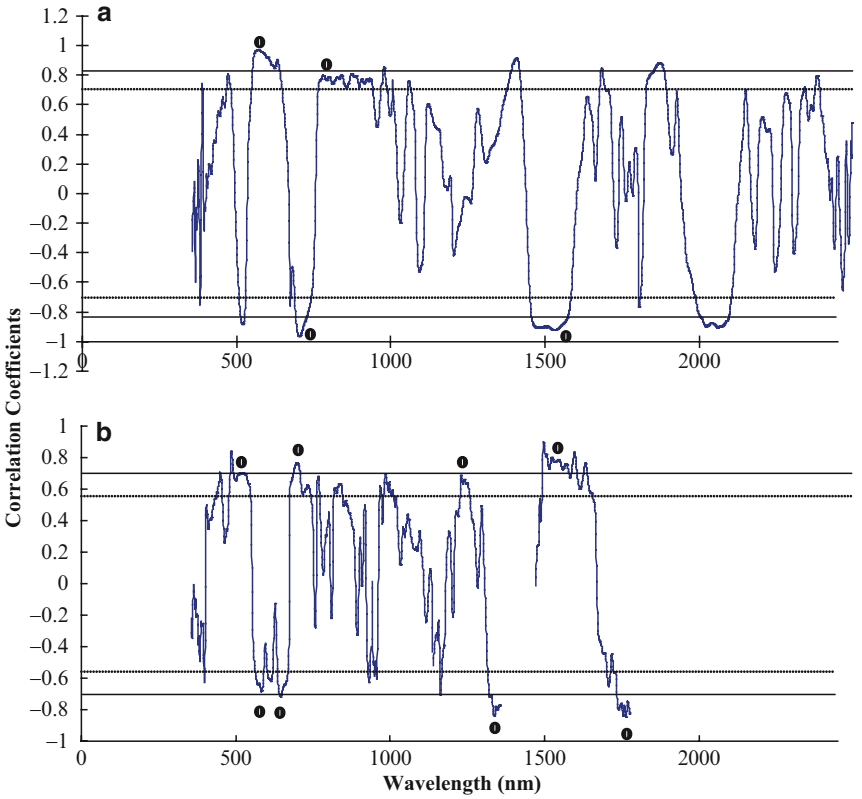

Fig. 3.3 Correlation coefficients between leaf-level first difference of log 1/R (log 1/R)' (**a**) or canopy-level (log 1/R)' and foliar $\delta^{15}N$. *Dash*, *solid horizontal bars* and *black circles* have the same meaning as in Fig. 3.2. The ranges of wavelength for *black circle* regions from left to right for (**a**) are λ = 587–637, 690–745, 798–940 and 1,504–1,573 nm. For (**b**) are λ = 517–535, 580–590, 639–661, 693–708, 1,249–1,254, 1,345–1,358, 1,509–1,604 and 1,760–1,778 nm (Modified from Wang et al. 2007b)

With the first-difference transformation [(log 1/R)'], there are several narrow regions in the VNIR that appear to be useful for the estimation of $\delta^{15}N$ (leaf level: Fig. 3.3a; canopy-level: Fig. 3.3b). First-difference spectra highlight regions where the spectral reflectance changes due to variations in absorption or scattering in the foliage. The (log 1/R)' spectra therefore tend to highlight the edges of absorption features, such as those due to chlorophyll. At both the leaf and canopy levels, significant correlations between foliar $\delta^{15}N$ and (log 1/R)' at ~600 and ~700 nm were found. These wavelengths occur at the edge of chlorophyll absorptions and most likely arise from variable widths of chlorophyll absorption bands in samples with different ^{15}N abundances. The underlying relationship between foliar $\delta^{15}N$ and spectral reflectance data may therefore rely on the different reflectance between chlorophylls (a and b) and other leaf components. Because first-difference spectra ((log 1/R)') are less sensitive to lighting conditions, it may be more practical for

Table 3.1 Stepwise multiple regression results to predict foliar $\delta^{15}N$ at both leaf level and canopy level (Modified from Wang et al. 2007b)

		λ (nm)	Partial R^2	Cumulative R^2	p
Leaf level	R	619	0.46		0.06
		695	0.36	0.82	0.02
	Log (1/R)'	603	0.46		0.07
		704	0.46	0.92	0.004
Canopy level	R	1,135	0.63	0.63	0.004
	Log (1/R)'	702	0.67		0.0006
		639	0.09	0.76	0.08

At the leaf level, regressions for R, were performed with λ = 483–517 nm, 617–703 nm; regressions for Log (1/R)', were performed with λ = 587–637 nm, 690–745 nm, 798–846 nm, 904–940 nm and 1504–1573 nm. At the canopy level, regressions for R, were performed with λ = 670–694 nm, 1,098–1,136 nm, 1,261–1,319 nm and 1,480–1,522 nm; regressions for Log (1/R)', were performed with λ = 517–535 nm, 639–661 nm, 693–708 nm, 932–934 nm and 1,249–1,254 nm. Please refer to the text for detailed explanation of the choice of bands.

remote sensing-based determinations of $\delta^{15}N$ than R. In this way, this finding concerning ^{15}N abundances follows those of Martin and Aber (1997) for N concentration. Based on (log 1/R)' stepwise regressions results, at leaf scales, the best predictors for foliar $\delta^{15}N$ are at λ = 603 and 704 nm; at the canopy scale, the best predictor for foliar $\delta^{15}N$ is λ = 702 nm (Table 3.1).

Both visible and NIR wavelengths have been used to estimate foliar N (Martin and Aber 1997; Yoder and Pettigrew-Crosby 1995). Because of the close relationship between foliar N concentration and foliar ^{15}N abundance, it is not surprising that there are strong correlations between foliar $\delta^{15}N$ and spectral data in the VNIR at the leaf scale and canopy scales. The R exhibits correlograms with wider regions of significance than those of (log 1/R)'. However, the first-difference (derivative) spectra are probably more robust predictors than the simple reflectance spectra. Environmental factors such as brightness and shading can influence total reflectance, whereas the shape of the reflectance curve, as characterized by the first-difference curve is more conservative (i.e., is less impacted by environmental or analytical conditions). Traditionally first-difference spectra have been used to resolve fine-scale spectra from background noise (Wessman et al. 1988; Yoder and Pettigrew-Crosby 1995). In the current study, (log 1/R)' shows a stronger correlation with foliar $\delta^{15}N$ than R, and occurs over narrower wavelength regions. In stepwise regressions, (log 1/R)' predictors generated higher R^2 values (R^2 = 0.76 and 0.92 respectively) than R predictors at both leaf scale and canopy scale (Table 3.1).

As shown in this example, there is a strong relationship between foliar $\delta^{15}N$ and leaf reflectance at both leaf and canopy scales. The underlying relationship between foliar $\delta^{15}N$ and spectral reflectance is not fully understood, it may rely on the different reflectance between chlorophylls (a and b) and other leaf components. Spectral analysis of foliar $\delta^{15}N$, by its non-destructive and continuous nature, is a promising tool to detect terrestrial foliar $\delta^{15}N$ spatial patterns and dynamics using airborne or satellite-borne sensors through ground validation processes.

3.2.2 Laboratory Assessment of Leaf $\delta^{15}N$ Using Spectra Data

To assess whether the observed $\delta^{15}N$-spectra relationship could be actually used in the laboratory routinely to predict foliar $\delta^{15}N$, a customized system was designed (Fig. 3.4a) and used to test this idea. The foliar specimens included a variety of samples (e.g., African grasses, temperate trees, and temperate herbaceous species, 22 samples in total) with the $\delta^{15}N$ values being published previously (Wang et al. 2009a; Wang et al. 2009b). The spectral measurements were carried out in a completely darkened room with a full-spectrum halogen light being the only light source for foliar samples. The sample holder was black fitting tightly into the light tube. The spectroradiometer instrument and halogen light used in this setup were as identical to that used in the field. The instrument parameter settings and operational procedures (e.g., white reference reading and optimizing) were the same as in the field except that the integration time was set to 100 Hz instead of 10 Hz (Wang et al. 2007b) to reduce the noise. Correlograms revealed a highly significant correlation between spectral reflectance and foliar $\delta^{15}N$ ($r = 0.87$, $p < 0.01$) at wavelength of 400–420 nm. Half the 22 randomly-selected samples were chosen to calibrate the relationship between spectral reflectance and foliar $\delta^{15}N$ at a wavelength of 420 nm (Fig. 3.4b). Foliar $\delta^{15}N$ values were calculated using remaining samples and the established regression parameters. The finding was that 83% of the variance of predicted foliar $\delta^{15}N$ values could be explained by the measured foliar $\delta^{15}N$ values (Fig. 3.4c) although the predicted values differed from the "true" values (measured $\delta^{15}N$ values). This laboratory prediction experiment provides the possibility to measure foliar $\delta^{15}N$ values based on spectra data in the laboratory, but more rigorous tests with samples from more diverse $\delta^{15}N$ ranges are clearly needed to further refine the prediction equations.

3.2.3 Mechanisms

The underlying mechanisms of the relationships between $\delta^{15}N$ and spectra data are not fully understood. The observed relationships are presumably the result of two known relationships. The first is between N content and foliar reflectance, which has already been shown to exist in many ecosystems across different scales (Asner and Vitousek 2005; Card et al. 1988; Curran et al. 2001; Martin and Aber 1997; Yoder and Pettigrew-Crosby 1995). The second is likely based on the correlation between $\delta^{15}N$ and N content. The linear relationship between $\delta^{15}N$ and N content has been observed in some ecosystems, for example, a primary succession site at Alaska, US (e.g., Hobbie et al. 2000), but whether such linear relationships exist in other types of ecosystems and at larger spatial scales is not known. We reviewed literature data from a number of published datasets that contained both foliar $\delta^{15}N$ and foliar N content data, encompassing sites from four continents and including literally all biomes. After excluding the N fixing plants, which show no relationship between foliar $\delta^{15}N$ and foliar N content (Hobbie et al. 2000; Hogberg 1997), we observed a significant linear relationship between foliar $\delta^{15}N$ and foliar N in all the regions, with R^2 ranging from 0.13 to 0.46 (Fig. 3.5a–f). When all the available data from all the regions were combined, foliar N content explained 12% of the variation in foliar $\delta^{15}N$ (Fig. 3.5g).

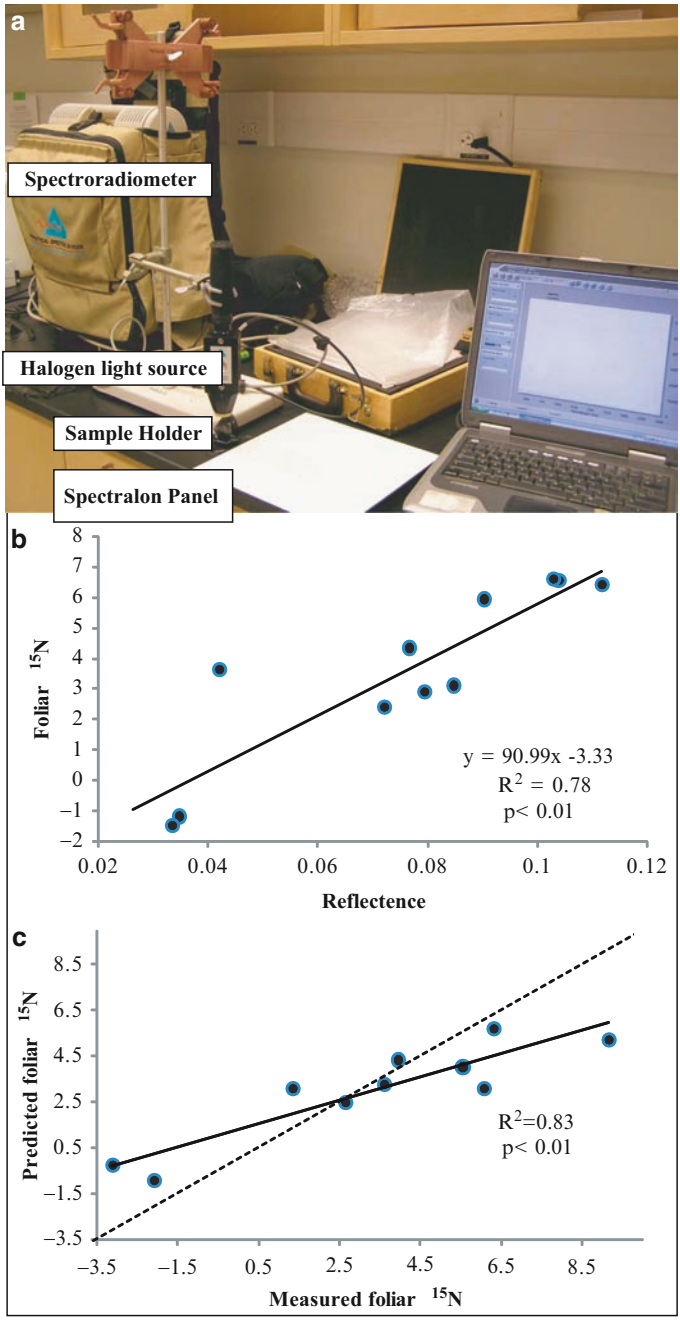

Fig. 3.4 The setup and results from the laboratory spectroscopy experiment, showing (**a**) the customized setup for spectra analysis in the laboratory. (**b**) The calibration regression between foliar spectra data (420 nm, reflectance was calculated as the ratio of the reflected radiance of the leaf to the reflected radiance of a Spectralon panel) and ^{15}N data. (**c**) The predictions of foliar ^{15}N from independent validation samples versus the measured values. The *dotted line* is one to one line, which shows the agreement/departure between the predicted values and measured values. Fig. 3.4, see Appendix 1, Color Section

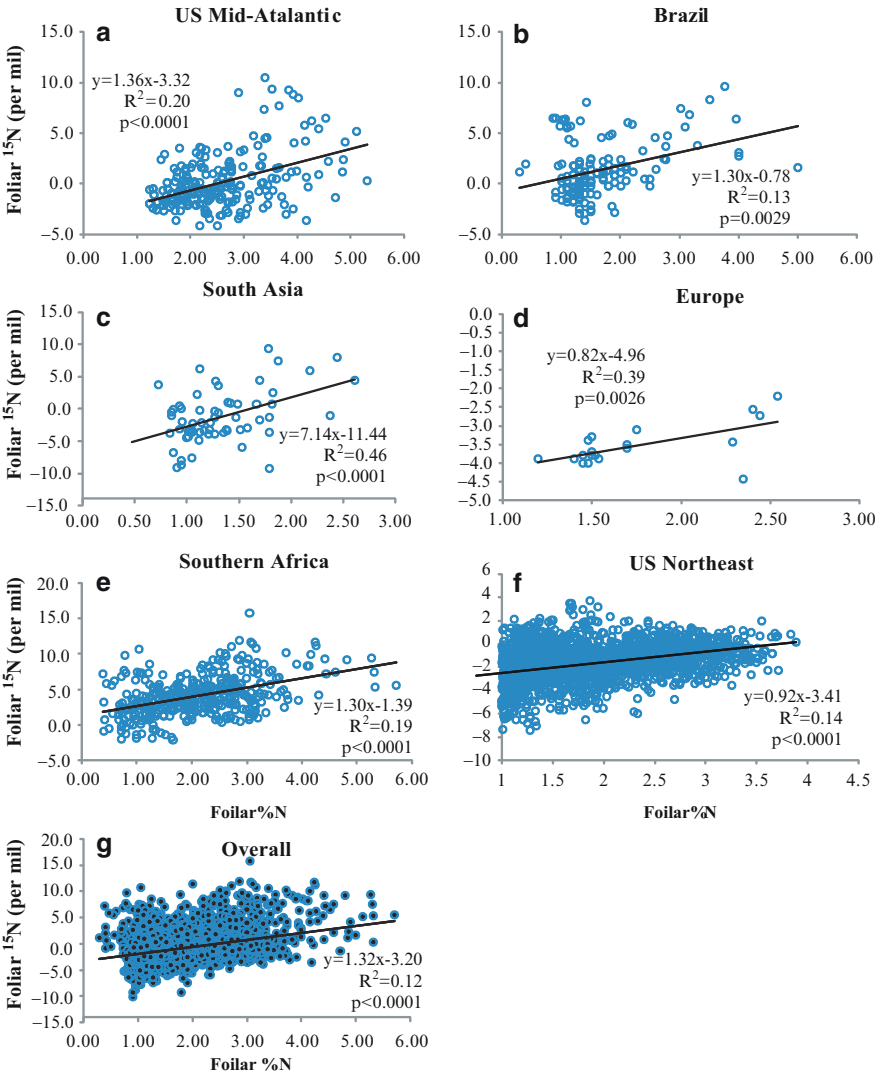

Fig. 3.5 The relationships between foliar $\delta^{15}N$ and foliar %N (excluding the nitrogen-fixing species) across different regions. Data are from (**a**) the US Mid-Atlantic succession fields and forests (Martinelli et al. 1999; Wang et al. 2007a), (**b**) the Brazilian savannas and rainforests (Bustamante et al. 2004; Martinelli et al. 1999), (**c**) the Asian forests and marshes (Martinelli et al. 1999; Tateno et al. 2003; Zhou et al. 2006), (**d**) European forests (Koerner et al. 1999; Martinelli et al. 1999), (**e**) the southern African savannas and woodlands (Aranibar and Macko 2005; Hogberg 1986, 1990, 1997; Hogberg and Alexander 1995; Schulze et al. 1991; Wang et al. 2009b) (**f**) the US Northeast forests (Pardo et al. 2006) and (**g**) the overall dataset. Fig. 3.5, see Appendix 1, Color Section

These results support the existence of a linear relationship between foliar $\delta^{15}N$ and foliar N content in natural vegetations globally. This linear relationship, in combination with known relationships between foliar N content and foliar reflectance, likely serves as a basis for the observed relationship between foliar $\delta^{15}N$ and spectral reflectance.

3.2.4 Future Directions

Obviously, many more observations from a diverse array of ecosystems are needed to test the robustness and generality of the $\delta^{15}N$-reflectance relationships. In addition, the underlying mechanisms between the observed relationship of $\delta^{15}N$ and spectra data need further explanation. Owing to the fact that the relationship between $\delta^{15}N$ and foliar reflectance is strongest in the visible portion of the spectrum, the underlying relationship between N content and spectral reflectance data may rely on the variations of reflectance of different leaf pigments such as chlorophylls (a and b), carotenoids and anthocyanins. It is reasonable to speculate that variations of $\delta^{15}N$ in these leaf pigments and their different spectral reflectance may be also responsible for the $\delta^{15}N$–spectra relationships. In addition, there is evidence that $\delta^{15}N$ of chlorophyll and whole organic matter are linearly correlated (Kennicutt et al. 1992; Sachs 1997) and chlorins are enriched in ^{15}N compared with whole leaf components (Sachs 1997). Chlorophylls (magnesium-containing chlorins) play an important role in leaf reflectance at visible bands. We expect that higher leaf chlorophyll concentrations will lead to higher foliar $\delta^{15}N$ and higher leaf reflectance. There are still open issues, such as the effects of waxy cuticles and trichome density of fresh leaves (Levizou et al. 2005) on spectral reflectance in the visible and effects of canopy geometry, leaf turgidity, and water contents on $\delta^{15}N$ estimation. These issues need to be better resolved to improve the application of remote sensing to foliar $\delta^{15}N$ analysis. In particular, the existence of significant relationships between N isotope composition and spectral reflectance of powdered foliar samples would be strong evidence that leaf and canopy structure are not the main origin of the observed relationship between N isotope composition and spectral reflectance.

3.3 Remote Sensing and C Isotope Composition Prediction

Soil organic matter (SOM) is one of the largest and most dynamic reservoirs of C in the global cycle of carbon. The amount of C stored in SOM is about twice that stored in the biosphere and atmosphere combined (Schlesinger 1997). $\delta^{13}C$ is a very powerful tool in the study of soil C cycling and $\delta^{13}C$ is probably the best way to partition C source between C_3 and C_4 vegetation based on the discovery of distinct C isotope signatures for these two vegetation types in early 1970s (O'Leary 1981; Smith and Epstein 1971). To our knowledge, there are no direct measurements of the vegetation or soil $\delta^{13}C$ values using remotely sensed data, although indirect relationships between of remote sensing data and $\delta^{13}C$ values have been reported. For example, Guo and Xie (2006) correlated MODIS-derived NDVI (Normalized Difference Vegetation Index) data to field measured vegetation $\delta^{13}C$ data in the Tibetan plateau. They found that NDVI and precipitation have the same trends with foliar $\delta^{13}C$ values. Such use of remotely sensed data treats $\delta^{13}C$ values as proxies, and does not focus on predicting the $\delta^{13}C$ itself.

In practice, quantification of the relationship between vegetation structure and $\delta^{13}C$ distribution (e.g., Biggs et al. 2002), might allow the use of remote sensing techniques to predict the spatial distribution of $\delta^{13}C$ through the quantitative relationship between remotely-sensed vegetation parameters and $\delta^{13}C$ distribution. Illustrated here is one such possibility using a case study from southern African savanna ecosystems. First we quantitatively evaluated the soil $\delta^{13}C$ distribution using geostatistical techniques and related this distribution to vegetation structure. Then soil $\delta^{13}C$ values were predicted from high spatial resolution IKONOS satellite products using the calculated ground relationships between vegetation structure and $\delta^{13}C$ values.

3.3.1 Geostatistical Analysis of Soil $\delta^{13}C$ Distribution on Ground

Geostatistical analysis was used to quantify the spatial variation of soil $\delta^{13}C$ at each site. A semivariogram (SV hereafter) is a plot of a series of semivariance values (γ) against the corresponding lag distances (h). The semivariance γ at each h is defined as:

$$\gamma(h) = \frac{1}{2N(h)} \sum_{i=1}^{N(h)} [z(i) - z(i+h)]^2 \tag{3.1}$$

where $N(h)$ is the number of sample pairs separated by the lag distance h. The $Z(i)$ is a measured value at location i and $Z(i + h)$ is a measured value at location $i + h$. There are several commonly used SV models. The model selection is generally based on fitted model shape. A spherical model was chosen to facilitate the comparison of parameters between variables and because this model has been shown in many cases to be adequate for soil data (Schlesinger et al. 1996; Su et al. 2006; Wang et al. 2007c). The most important SV parameters derived from geostatistical analysis for our purpose is range (A_o), which indicates the distance of spatial autocorrelation between pairs of data (Brooker 1991; Li and Reynolds 1995; Wang et al. 2007c).

Field work was conducted at sites along the Kalahari Transect (KT), one of a set of IGBP (International Geosphere–Biosphere Programme) "megatransects" identified for global change studies (Koch et al. 1995; Scholes et al. 2002; Shugart et al. 2004). The soil substrate along the entire KT is relatively homogenous, being covered by the Kalahari sands. The physical and hydraulic parameters such as soil texture (>96% of sand) and bulk density (around 1.4–1.5 g cm^{-3}) do not have significant variations along the KT (Wang et al. 2007d). The KT thus provides an ideal setting to investigate changes in ecosystem dynamics, vegetation composition and structure, and C or nutrient cycles along a gradient of precipitation while minimizing confounding effects of soil heterogeneity. We expect that precipitation-induced effects on the localized spatial pattern of vegetation (i.e., more patchy vegetation at drier sites) would have corresponding effects on the localized spatial patterns of soil $\delta^{13}C$. Two sites along the KT in Botswana with different climate conditions were chosen to quantify the soil $\delta^{13}C$ spatial patterns (Fig. 3.6). The two sites represent locations near the extremes for mean annual precipitation (MAP).

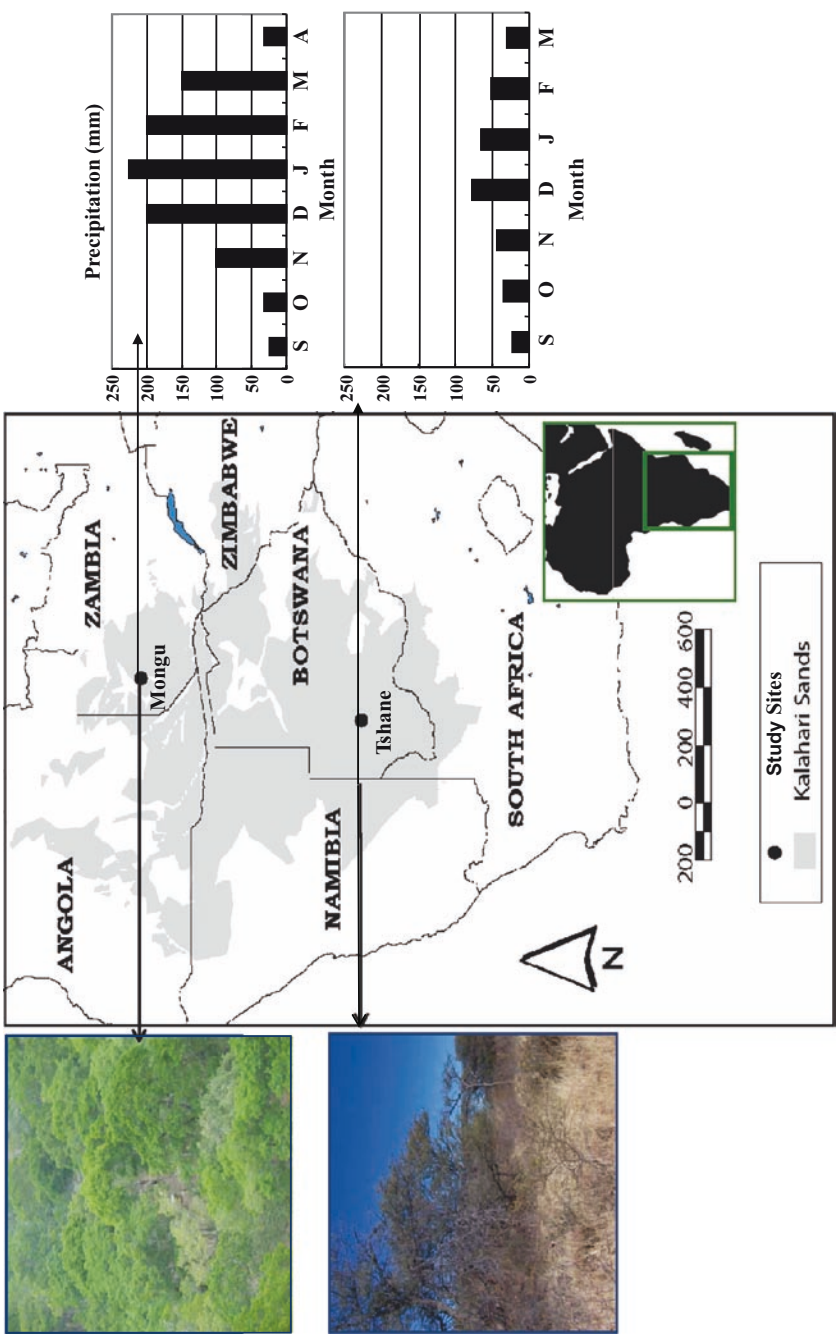

Fig. 3.6 Sampling locations, rainfall characteristics and field photos of the sites along the Kalahari Transect. The column charts are the mean annual monthly precipitation data (1961–1990) of the two sampling locations from Shugart et al. (2004). Fig. 3.6, see Appendix 1, Color Section

Tshane is at the dry end of the Transect (~365 mm MAP) and Mongu is at the wet end of the Transect (~900 mm MAP) (Shugart et al. 2004). The vegetation in Mongu is woodland savanna dominated by tree species such as *Brachystegia spiciformis* Benth and the common grass species are *Eragrostis* spp. The vegetation in Tshane is open savanna dominated by *Acacia* species such as *A. luederizii* Engl. and *A. mellifera* Benth, the dominant grass species are *Eragrostis lehmanniana* and *Schmidtia pappophoroides*. A 300-m transect oriented N–S was set up at each site. Surface soil samples (5-cm depth) were randomly collected along the 300 m transect: 271 samples were collected and analyzed from the Mongu (wet) site and 296 samples were collected and analyzed from the Tshane (dry) site. The sampling locations were selected by the generation of random numbers prior to fieldwork.

The SVs were constructed using the jackknife method presented by Shafer and Varljen (1990) and discussed Huisman et al. (2003). All SVs were fit to the spherical model using a non-linear least squares fit employing the Levenberg–Marquardt algorithm, which combines the steepest descent and inverse-Hessian function fitting methods (Press et al. 1992). The uncertainties (95% confidence limits) were determined using the variance-covariance method of Pardo-Iguzquiza and Dowd (2001). Because the sill of the semivariograms of $\delta^{13}C$ at Tshane demonstrated periodicity, a hole effect model (2) was also used to better fit these data following (Ma and Jones 2001):

$$\gamma(h) = V\,[1 - \exp(-3h/A_o)\cos(bh)] \qquad h \geq 0 \tag{3.2}$$

where V is the sill of the semivariogram plot, h is lag distance, A_o is the effective range, $b = 2\pi/\lambda$ is the angular frequency, and λ is the wavelength of the periodicity.

There appear to be spatial patterns for soil $\delta^{13}C$ at both Tshane and Mongu but the range of autocorrelation is much larger at Tshane than at Mongu (Table 3.2; Fig. 3.7). At Tshane, the range of autocorrelation of soil $\delta^{13}C$ is 9.66 m (Table 3.2). The excellent fit provided by the hole-effect model ($R^2 = 0.932$ for $\delta^{13}C$) to the Tshane SVs underscores the strong spatial structuring of $\delta^{13}C$ at this site (Fig. 3.7c). At Mongu, the range of autocorrelation of $\delta^{13}C$ is 5.04 m (Table 3.2). These results generally support the expectation that spatial patterns of soil $\delta^{13}C$ would exist at both ends of the rainfall gradient and the spatial patterns would be stronger at the dry end. The SVs of $\delta^{13}C$ at Tshane showed a clear periodic pattern (Fig. 3.7a), which was successfully modeled using the hole effect equation (Eq. 3.2) with a wavelength (λ) of 18 m for both $\delta^{13}C$ and %C (Fig. 3.7c). The hole-effect behavior

Table 3.2 Ground measured soil $\delta^{13}C$ range (m) for spherical models of variograms from both sites. "M" denotes the mean jackknife estimate. "L" and "U" denote the lower and upper bounds of the 95% confidence estimates, respectively

Location	Range (m)		
	M	L	U
Tshane	9.66	9.42	9.90
Mongu	5.04	4.59	5.49

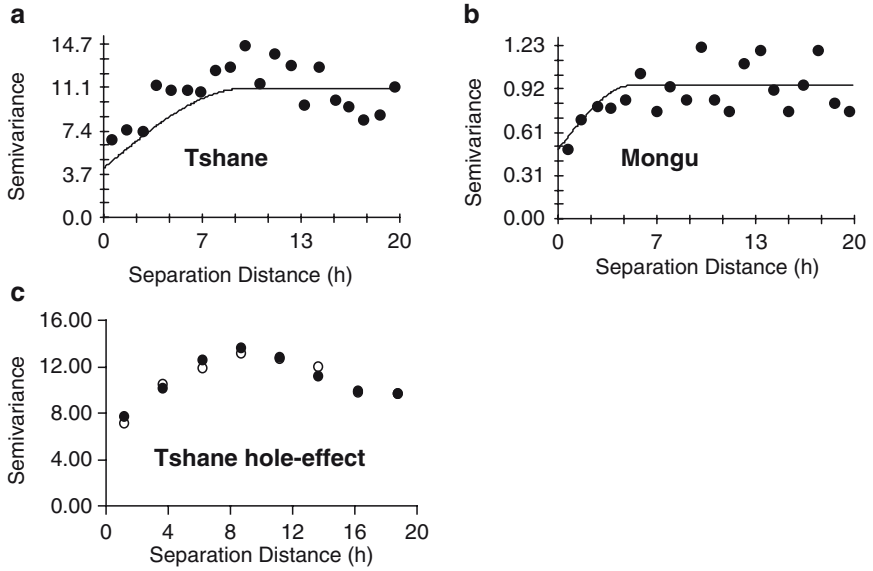

Fig. 3.7 Semivariograms of $\delta^{13}C$ at Tshane (**a**) and Mongu (**b**) using spherical models, and semivariograms of $\delta^{13}C$ (**c**) at Tshane using hole-effect model. For (**c**), the *open circles* are actual data points and the *filled circles* are the modeled data points, and the $R^2 = 0.932$

in Tshane also suggests a higher soil C heterogeneity at the dry end of the KT since hole-effect model generally represents the existence of multiple hierarchies in spatial patterns (Ma and Jones 2001).

Through the geostatistical analysis and published woody-plant spacing distance at the corresponding locations (~6–10 m at Tshane and ~2–5 m at Mongu, (Caylor 2003)), the results showed that the spatial distributions of soil $\delta^{13}C$ are strongly influenced by tree distributions at both ends of the transect, providing a strong base to using high-resolution satellite data to infer ground soil $\delta^{13}C$ through vegetation structure characterization.

3.3.2 Soil $\delta^{13}C$ Prediction Using Satellite Data

The IKONOS satellite product is used because it is among the highest spatial resolution (1 m for panchromatic data) available from commercially available satellite data. Such spatial resolution is well above the observed tree crown size (~6–10 m at Tshane, Caylor 2003) and soil $\delta^{13}C$ autocorrelation ranges (Table 3.2) in these African savanna ecosystems. The IKONOS image of Tshane site (Fig. 3.8a) was classified to highlight the location of trees using ENVI software (ITT Visual Information Solutions, Boulder, CO). The unsupervised classification option was used to produce two classes of data, "trees" and "not trees" (Fig. 3.8b). The "not

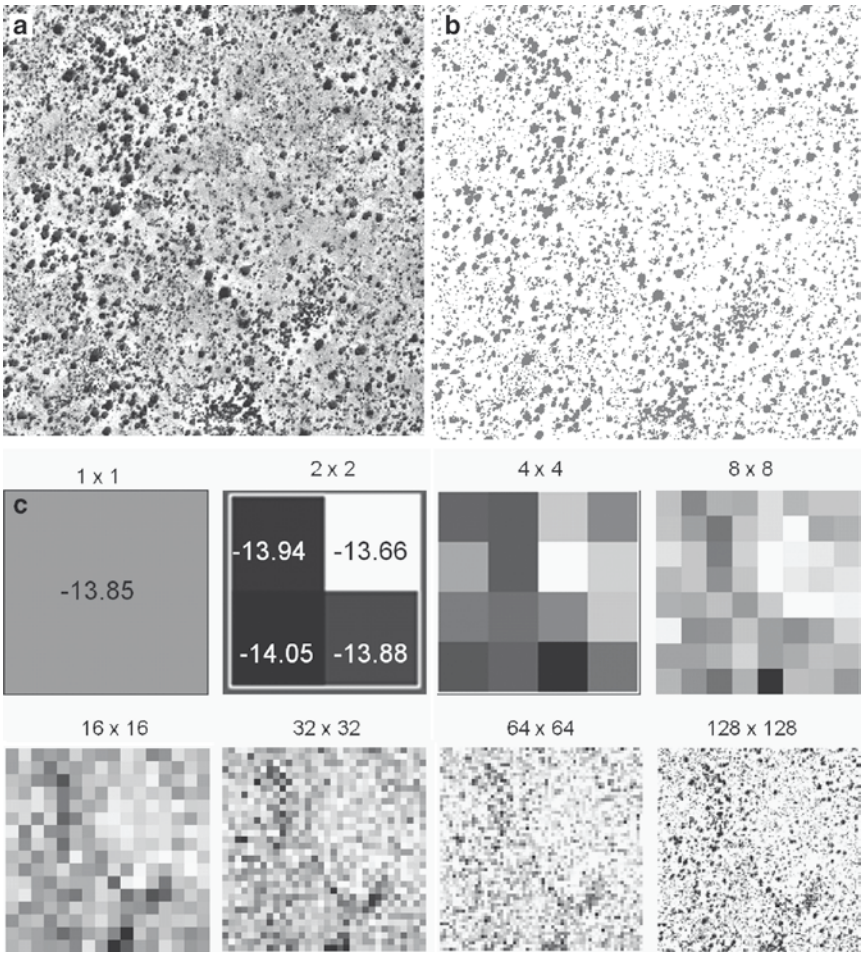

Fig. 3.8 The IKONOS satellite image of Tshane site (**a**), the classified tree distributions in Tshane based on the IKONOS image (the *shade/dark areas* are trees) (**b**), and the soil $\delta^{13}C$ distribution map based on classification at different resolutions (the *shade/dark areas* are soil patches with more depleted soil $\delta^{13}C$)

trees" class consisted of bare soil and soil–grass mixtures in the tree interspaces. The classified data were transformed so that tree-filled pixels were given a value of 1 and pixels without trees were given a value of 0. The classified data were averaged at different spatial scales. Fractional cover thus obtained at these different spatial aggregations were used as inputs to a simple isotope mixing model using the known soil $\delta^{13}C$ values under and between canopies, to generate soil $\delta^{13}C$ distribution maps at different spatial scales (Fig. 3.8c). Geostatistical block kriging would provide a slight improvement to these estimates, especially at the finest spatial scales. Nonetheless, the current results show a promising future to predict the soil

$\delta^{13}C$ distributions from space for ecosystems whose interactions of soil $\delta^{13}C$ distribution and vegetation spatial pattern can be quantified.

3.4 Summary

A union of remote sensing technique and stable isotope measurements holds promise to allow for spatially continuous estimates of isotope compositions, thus providing unprecedented information into the patterns and processes within the Earth's ecosystems. To date, however, the combination of isotope and remote sensing techniques is still in the exploratory stage. Two examples, one utilizing high spectral resolution remote sensing and the other employing high spatial resolution remote sensing, suggest the possibility of the integration of remote sensing and isotope methods. Experimental results have shown that there is a strong correlation between foliar $\delta^{15}N$ and spectral reflectance in certain visible and near-infrared wavelengths. Stepwise regression showed that the first-difference of the log1/R [(log 1/R)'] could explain 76–92% of the variation in foliar $\delta^{15}N$, providing the most reliable correlations with foliar $\delta^{15}N$ at bands near 600 and 700 nm. The relationships between remote sensing and foliar $\delta^{15}N$ are correlative and further work must be done to discover the causal reasons behind these correlations. The potential use of high-resolution remote sensing to scale up vegetation-$\delta^{13}C$ relationships is also suggested. Although limitations still exist, because of the non-destructive and continuous nature, remote sensing is a promising tool to expand measurements of terrestrial $\delta^{15}N$ and $\delta^{13}C$ spatial patterns and dynamics.

Acknowledgements The project was supported by NASA-IDS2 (NNG-04-GM71G) and a research fund from the Blandy Experimental Farm of University of Virginia. We are grateful for field assistance and earlier contributions from Paolo D'Odorico, Kelly Caylor, Howie Epstein and Jin Wang. We thank Dr. Linda Pardo from USDA Forest Service for providing raw data of her published work. Lixin Wang thanks Dr. Gengsuo Jia and Dr. Domingo Alcaraz for the technical support of ENVI. The clarity of this chapter greatly benefited from the comments provided by Dr. Brenden E. McNeil and one anonymous reviewer. This manuscript is based in part on IR/D support by the National Science Foundation, to SAM while working at the Foundation. Any opinion, finding, and conclusions or recommendations expressed in this material are those of the authors and do not necessarily reflect the views of the National Science Foundation.

References

Aranibar JN, Macko SA (2005) SAFARI 2000 plant and soil C and N Isotopes, Southern Africa, 1995–2000. Oak Ridge National Laboratory Distributed Active Archive Center, Oak Ridge, TN

Asner GP, Vitousek PM (2005) Remote analysis of biological invasion and biogeochemical change. PNAS 102:4383–4386

Balesdent J, Mariotti A, Guillet B (1987) Natural ^{13}C abundances as a tracer for studies of soil organic matter dynamics. Soil Biol Biochem 19:25–30

Biggs TH, Quade J, Webb RH (2002) $\delta^{13}C$ values of soil organic matter in semiarid grassland with mesquite (Prosopis) encroachment in southeastern Arizona. Geoderma 110:109–130

Bond WJ, Stock WD, Hoffman MT (1994) Has the Karoo spread? A test for desertification using carbon isotopes from soils. S Afr J Sci 90:391–397

Bowling DR, SS D, TB D, EJ R (2003) Tunable diode laser absorption spectroscopy for stable isotope studies of ecosystem-atmosphere CO_2 exchange. Agric For Meteorol 118:1–19

Brooker PI (1991) A geostatistical primer. World Scientific Publishing, Singapore

Bustamante MMC et al (2004) ^{15}N natural abundance in woody plants and soils of central Brazilian savannas (cerrado). Ecol Appl 14:200–213

Card DH, Peterson DL, Matson PA, Aber JD (1988) Prediction of leaf chemistry by the use of visible and near infrared reflectance spectroscopy. Remote Sens Environ 26:123–147

Caylor KK (2003) The structure and function of Kalahari transect vegetation. Ph.D. dissertation, University of Virginia, Charlottesville, VA

Curran PJ, Dungan JL, Macler BA, Plummer SE, Peterson DL (1992) Reflectance spectroscopy of fresh whole leaves for the estimation of chemical concentration. Remote Sens Environ 39:153–166

Curran PJ, Dungan JL, Peterson DL (2001) Estimating the foliar biochemical concentration of leaves with reflectance spectrometry: testing the Kokaly and Clark methodologies. Remote Sens Environ 76:349–359

Davidson EA et al (2007) Recuperation of nitrogen cycling in Amazonian forests following agricultural abandonment. Nature 447:995–998

Farquhar G, Ehleringer J, Hubick K (1989) Carbon isotope discrimination and photosynthesis. Ann Rev Plant Physiol Mol Biol 40:503–537

Fung I et al (1997) Carbon 13 exchanges between the atmosphere and biosphere. Global Biogeochem Cycles 11:507–534

Griffis TJ, Lee X, Baker JM, Sargent S, King JY (2005) Feasibility of quantifying ecosystem-atmosphere $C^{18}O^{16}O$ exchange using laser spectroscopy and the flux-gradient method. Agric For Meteorol 135:44–60

Guo G, Xie G (2006) The relationship between plant stable carbon isotope composition, precipitation and satellite data, Tibet Plateau, China. Quatern Int 144:68–71

Hobbie EA, Macko SA, Williams M (2000) Correlations between foliar $\delta^{15}N$ and nitrogen concentrations may indicate plant-mycorrhizal interactions. Oecologia 122:273–283

Hogberg P (1986) Nitrogen fixation and nutrient relations in savanna woodland trees (Tanzania). J Appl Ecol 23:675–688

Hogberg P (1990) ^{15}N natural abundance as a possible marker of the ectomycorrhizal habit of trees in mixed African woodlands. New Phytol 115:483–486

Hogberg P (1997) ^{15}N natural abundance in soil-plant systems. New Phytol 137:179–203

Hogberg P, Alexander I (1995) Role of root symbioses in African woodland and forest: evidence from ^{15}N abundance and foliar analysis. J Ecol 83:217–224

Houghton RA (2005) Aboveground forest biomass and the global carbon balance. Global Change Biol 11:945–958

Huisman JA, Snepvangers JJJC, Bouten W, Heuvelink GBM (2003) Monitoring temporal development of spatial soil water content variation: comparison of ground penetrating radar and time domain reflectometry. Vadose Zone J 2:519–529

Hyde P, Dubayah R, Walker W, Blair JB, Hofton M, Hunsaker C (2006) Mapping forest structure for wildlife habitat analysis using multi-sensor (LiDAR, SAR/InSAR, ETM plus, Quickbird) synergy. Remote Sens Environ 102:63–73

Kennicutt MCI, Bidigare RR, Macko SA, Keeney-Kennicutt WL (1992) The stable isotopic composition of photosynthetic pigments and related biochemicals. Chemical Geology 101: 235–245

Koch GW, Scholes RJ, Steffen WL, Vitousek PM, Walker BH (1995) The IGBP terrestrial transects: science plan, report No. 36. International Geosphere–Biosphere Programme, Stockholm

Koerner W, Dambrine E, Dupouey JL, Benoît M (1999) $\delta^{15}N$ of forest soil and understorey vegetation reflect the former agricultural land use. Oecologia 121:421–425

Kreitler C (1979) Nitrogen isotope ratio studies of soils and groundwater nitrate from alluvial fan aquifers in Texas. J Hydrol 42:147–170

Levizou E, Drilias P, Psaras GK, Maneras Y (2005) Nondestructive assessment of leaf chemisty and physiology through spectral reflectance measurements may be misleading hen changes in trichome density co-occur. New Phytol 165:463–472
Li HR, Reynolds JF (1995) On the quantification of spatial heterogeneity. Oikos 73:280–284
Ma YZ, Jones TA (2001) Teacher's aide Modeling hole-effect variograms of lithology-indicator variables. Math Geol 33:631–648
Martin ME, Aber JD (1997) High spectral resolution remote sensing of forest canopy ligin, nitrogen and ecosystem process. Ecol Appl 7:431–443
Martinelli LA et al (1999) Nitrogen stable isotopic composition of leaves and soil: tropical versus temperate forests. Biogeochemistry 46:45–65
O'Leary MH (1981) Carbon isotope fractionation in plants. Phytochemistry 20:553–567
Pardo-Iguzquiza E, Dowd P (2001) Variance-covariance matrix of the experimental variogram: assessing variogram uncertainty. Math Geol 33:397–419
Pardo LH et al (2006) Regional assessment of N saturation using foliar and root $\delta^{15}N$. Biogeochemistry 80:143–171
Pataki DE et al (2003) The application and interpretation of Keeling plots in terrestrial carbon cycle research. Global Biogeochem Cycles 17:1022. doi:1010.1029/2001GB001850
Peterson DL et al (1988) Remote sensing of forest canopy and leaf biochemical contents. Remote Sens Environ 24:85–108
Press WH, Teukolsky SA, Vetterling WT, Flannery BP (1992) Numerical recipes in C: the art of scientific computing, 2nd edn. Cambridge University Press, Cambridge
Rau GH, Ohman MD, Pierrot-Bults A (2003) Linking nitrogen dynamics to climate variability off central California: a 51 year record based on $^{15}N/^{14}N$ in CalCOFI zooplankton. Deep Sea Res II: Topical Stud Oceanogr 50:2431–2447
Robinson D (2001) $\delta^{15}N$ as an integrator of the nitrogen cycle. Trends Ecol Evol 16:153–162
Sachs P (1997) Nitrogen isotopes in Chlorophyll and the origin of Eastern Mediterranean sapropels. PhD dissertation, Massachusetts Institute of Technology, Cambridge, MA, USA
Schlesinger WH (1997) Biogeochemistry: an analysis of global change, 2nd edn. Academic, New York
Schlesinger WH, Raikes JA, Hartley AE, Cross AF (1996) On the spatial pattern of soil nutrients in desert ecosystems. Ecology 77:364–374
Scholes RJ, Dowty PR, Caylor K, Parsons DAB, Frost PGH, Shugart HH (2002) Trends in savanna structure and composition along an aridity gradient in the Kalahari. J Veg Sci 13:419–428
Schulze E-D, Gebauer G, Ziegler H, Lange OL (1991) Estimates of nitrogen fixation by trees on an aridity gradient in Namibia. Oecologia 88:451–455
Shafer JM, Varljen MD (1990) Approximation of confidence-limits on sample semivariograms from single realizations of spatially correlated random-fields. Water Resour Res 26:1787–1802
Shaner P-J, Michael B, Stephen M (2007) Giving-up density and dietary shifts in the white-footed mouse, *peromyscus leucopus*. Ecology 88:87–95
Shugart HH et al (2004) The SAFARI 2000-Kalahari transect wet season campaign of year 2000. Global Change Biol 10:273–280
Smith BN, Epstein S (1971) Two categories of $^{13}C/^{12}C$ ratios for higher plants. Plant Physiol 47:380–384
Still C, Berry J, Collatz G, DeFries R (2003) Global distribution of C-3 and C-4 vegetation: carbon cycle implications. Global Biogeochem Cycles 17:1006. doi:1010.1029/2001GB001807
Su Y, Li Y, Zhao H (2006) Soil properties and their spatial pattern in a degraded sandy grassland under post-grazing restoration, Inner Mongolia, northern China. Biogeochemistry 79:297–314
Tateno R et al (2003) Use of foliar N-15 and C-13 abundance to evaluate effects of microbiotic crust on nitrogen and water utilization in *Pinus massoniana* in deteriorated pine stands of south China. Ecol Res 18:279–286
Treuhaft RN, Law BE, Asner GP (2004) Forest attributes from radar Interferometric structure and its fusion with optical remote sensing. BioScience 54:561–571

Wang L, Shaner P-JL, Macko S (2007a) Foliar $\delta^{15}N$ patterns along successional gradients at plant community and species levels. Geophys Res Lett 34:L16403. doi:16410.11029/12007GL030722

Wang L, Okin GS, Wang J, Epstein H, Macko SA (2007b) Predicting leaf and canopy ^{15}N compositions from reflectance spectra. Geophys Res Lett 34:L02401. doi:02410.01029/02006GL028506

Wang L, Mou PP, Huang J, Wang J (2007c) Spatial variation of nitrogen availability in a subtropical evergreen broadleaved forest of southwestern China. Plant Soil 295:137–150

Wang L, D'Odorico P, Ringrose S, Coetzee S, Macko S (2007d) Biogeochemistry of Kalahari sands. J Arid Environ 71:259–279. doi:210.1016/j.jaridenv.2007.1003.1016

Wang L, D'Odorico P, Ries L, Caylor K, Macko S (2009a) Combined effects of soil moisture and nitrogen availability variations on grass productivity in African savannas. Plant and Soil doi 10.1007/s11104-009-0085-z

Wang L, D'Odorico P, Ries L, Macko S (2009b) Patterns and implications of plant-soil δ13C and δ15N values in African savanna ecosystems. Quaternary Research doi:10.1016/j.yqres.2008.11.

Wessman CA, Aber JD, Peterson DL, Melillo JM (1988) Foliar analysis using near infrared reflectance spectroscopy. Can J For Res 18:6–11

Wilson P, Norris R (2001) Warm tropical ocean surface and global anoxia during the mid-Cretaceous period. Nature 412:425–429

Yoder B, Pettigrew-Crosby R (1995) Predicting nitrogen and chlorophyll content and concentrations from reflectance spectra (400–2500 nm) at leaf and canopy scales. Remote Sens Environ 53:199–211

Yoshida N, Toyoda S (2000) Constraining the atmospheric N_2O budget from intramolecular site preference in N_2O isotopomers. Nature 405:330–334

Zhou J, Wu Y, Zhang J, Kang Q, Liu Z (2006) Carbon and nitrogen composition and stable isotope as potential indicators of source and fate of organic matter in the salt marsh of the Changjiang Estuary, China. Chemosphere 65:310–317

Chapter 4
Novel Approaches for Monitoring of Water Vapor Isotope Ratios: Plants, Lasers and Satellites

Brent R. Helliker and David Noone

4.1 Introduction

Water vapor is central to understanding the water balance in the terrestrial biosphere, surface landscapes and in the atmosphere. As such measurements of the isotopic composition of atmospheric vapor are highly desirable. In the past measurements of water vapor isotopes has been particularly laborious, and consequently sparse. Here we discuss new methods that are emerging that will make water vapor isotope measurement a more practical endeavor, and thereby facilitate better mapping of the spatial and temporal variations. To date the interest in water vapor isotope measurements has been in the context of understanding processes governing hydrologic balance at local scales since spatially distributed measurements, such as those available for precipitation, have been unavailable. Emerging measurement techniques have changed this landscape, and the potential to construct empirically based isoscapes of water vapor isotopes has arrived.

The methods examined here lend themselves to developing new comprehensive isotopic datasets. Specifically, plant material that preserves the isotopic composition represents archive of the water vapor isotopic history, which can be exploited to infer spatial gradients of the isotopic composition. Using plants to provide samples gives a time integrated proxy measurement, and avoids some of the technical limitations that arise when collecting vapor samples. Similarly, direct measurements using optical approaches remove the need to capture samples completely. In situ laser-based spectroscopy provides a method that simplifies the measurement of the vapor phase; however the observational detail is obtained in time domain

B.R. Helliker (✉)
Department of Biology, University of Pennsylvania, Philadelphia, PA
e-mail: helliker@sas.upenn.edu

D. Noone
Department of Atmospheric and Oceanic Sciences, Cooperative Institute for Research in Environmental Sciences, University of Colorado, Boulder, CO
e-mail: dcn@colorado.edu

J.B. West et al. (eds.), *Isoscapes: Understanding Movement, Pattern, and Process on Earth Through Isotope Mapping*, DOI 10.1007/978-90-481-3354-3_4,

though continuous operation and spatial mapping will require deployment of sensor arrays. Measurement of spatial distributions of water vapor isotopes in the mid-troposphere is obtained though satellite-remote sensing, yet there remain questions on the ability to measure the isotopic composition in the boundary layer and at the surface from space. In this chapter, our aims are to outline the importance of spatially resolving the isotope ratio of atmospheric water vapor, to describe both the plant-based and the optical approaches, and discuss the strength and weaknesses of these new measurement methods.

4.2 Water Vapor Isotopes and Measurement Challenges

The isotope ratio of atmospheric water vapor is controlled by many exchange mechanisms that reflect the isotope ratio of water in biological water pools (i.e. plant stems and leaves), soils, open water bodies, precipitation and air mass movement from the local scales up to general circulation (Craig and Gordon 1965; Ehleringer et al. 2002; Gat 1996; Yakir and Sternberg 2000; Noone 2008). Many of these processes are understood in detail and can be accounted for in comprehensive models (Noone and Sturm 2008, this volume). Recent attention has been drawn to the study of the isotope ratio of atmospheric water vapor, particularly in an attempt to partition the fluxes of surface evaporation from plant transpiration, to enhance our understanding of precipitation processes and to balance hydrological budgets at the basin-scale (Helliker et al. 2002; Williams et al. 2004; Yakir and Wang 1996; Yepez et al. 2003). In addition to these efforts, regular measurements of water vapor isotope ratios can significantly enhance our understanding of a wide range of topics from leaf-scale isotope studies (Farquhar and Cernusak 2005; Roden and Ehleringer 1999) to climate reconstruction through isotopes in tree rings to global-scale estimates of productivity (Brunel et al. 1992; Ciais et al. 1997; Farquhar et al. 1993).

Improved estimates of either spatial averages or variation in water vapor isotopes will lead to a substantial improvement in applications of stable water isotopes to understanding life and earth processes and function. Yet in many applications of stable isotopes, the isotope ratio of water vapor is either not measured or measured infrequently. In these cases, one common procedure to estimate near surface water vapor isotope ratios is to assume a temperature-based equilibrium with the isotope ratio of precipitation, which is more readily measurable (IAEA/WMO 2006; Agarwaal et al. this volume). While there are a variety of plausible choices as to what precipitation inputs and what temperature should be used to arrive at an assumed equilibrium value (e.g., mean annual temperature and mean annual precipitation or growing season temperature and growing season precipitation or some combination thereof) the existence of a robust relationship is neither guaranteed nor unambiguous. While the equilibrium approach is often necessary in the lieu of little real data availability, it should be approached with caution as the isotope ratio of precipitation can vary seasonally and can be substantially different from the isotope ratio of water entering plant roots. As such, any simple estimation approach is difficult to defend.

An alternative is to use estimates from global and regional dynamical models that also simulate isotopes (Ciais et al. 1997; Riley et al. 2003; Buenning et al. 2007; Noone and Sturm 2008, this volume), although there remains question as to the quantitative reliability of such models for accurately constraining estimate of, for instance, $CO^{18}O$ (Buenning and Noone 2008).

The potential offset between the isotope ratio of plant root water and any equilibrium assumption of water vapor isotopes can lead to large errors in the interpretation of the $\delta^{18}O$ of CO_2, O_2 and the $\delta^{18}O$ and D/H of plant organic material. For an example with $\delta^{18}O$, an error of 2‰ in water-vapor $\delta^{18}O$ translates into an error of about 1.5‰ in leaf-water $\delta^{18}O$ under global estimates for evaporative enrichment (e.g., Craig and Gordon 1965; Ciais et al 1997). A consistent 1.5‰ error in leaf-water $\delta^{18}O$ results in an approximate 10% error in the calculated photosynthetic effect on the $\delta^{18}O$ of atmospheric CO_2, this is significant considering global estimates for average leaf water range from 4‰ to 8‰. A 1.5‰ error in leaf-water $\delta^{18}O$ results in a 1‰ error in the $\delta^{18}O$ of tree-ring cellulose, equivalent to 10–66% of observed tree-ring $\delta^{18}O$ signals (Poussart and Schrag 2005; Verheyden et al. 2004; Evans and Schrag 2004). Many of these uncertainties are minimized if the isotopic composition of vapor was indeed known.

While the importance of stable isotopic measurements of atmospheric water vapor to the above applications is without doubt, so too is the fact that there is a paucity of measurements. The reason for this is, in part, due to current methods of obtaining atmospheric water vapor samples for isotopic analysis. Reliable methods to collect atmospheric water vapor exist, but the logistical constraints inherent to these methods either limit widespread use in field-based sampling campaigns or severely limit spatial or temporal coverage. There are four primary methods in common use for ground-based sampling atmospheric water vapor: cryogenic condensation traps, trapping with Peltier coolers, chemical capturing with molecular sieves, and vapor collection with vacuum flasks. However, each of these methods is not without their limitations.

To ensure accurate isotopic analysis via trapping liquid samples for subsequent standard isotope ratio mass spectrometric analysis, nearly complete removal of all water molecules from the air needs to be achieved. Water-condensing traps that are cooled below −70°C have been used successfully in numerous studies (Blaga and Blaga 1977; Helliker et al. 2002; Huebner et al. 1978; Yakir and Wang 1996; Yepez et al. 2003; Sharp 2007) and the efficiency of this method is not questioned. However, this method requires a continuous supply of dry ice or liquid nitrogen, which raises problems for field work and for long sampling periods. Additionally, the flow rate of air through cyrogenic traps is often unacceptably high (>1 L/min) resulting in fractionation or direct loss of ice crystals. Further, with the use of very cold cryogens, CO_2 and explosive O_2 can condense, which yields practical constraints at very low temperature. The Peltier method produces a minimum temperature of about −50°C, which avoids condensing some other gasses. However, this temperature is not low enough to quantitatively trap water vapor below the working precision of an isotope ratio mass spectrometer and leads to enrichment of heavy isotopes in the sampled water (Schoch-Fischer et al. 1983). Corrections for this enrichment

require precise measurements of flow rate, condenser temperature, ambient temperature and ambient humidity during the period of sampling. These ancillary measurements propagate error through to the determination of the final isotope ratio. Molecular sieves have been shown to precisely and accurately capture water vapor isotope ratios and can potentially be deployed to gain large spatial coverage (Han et al. 2006). But the molecular sieve method needs further testing for a variety of potential problems, including: long and short-term storage of samples on the molecular sieve, recovery of samples from saturated versus unsaturated states and tests to determine if exchange occurs when moist air continues to be drawn through a saturated column. Also, a modular system of field sampling and laboratory extraction from the molecular sieve columns must be developed for the method to be fully field-deployable. A method to directly analyze small amounts of water vapor that has been captured in very dry and clean vacuum flasks has been successful for measuring HDO abundance, but cannot be used to measure ^{18}O in such low volumes (Strong et al. 2007). This method avoids some of the problems associated with trapping the vapor in liquid forms, but there remains a requirement to ensure there is no condensation within the flask (Sharp 2007)

With a clear need to obtain water vapor isotope data, new techniques have emerged in recent years that complement the existing direct collection sampling. Specifically, optical methods using laser-based spectroscopy allow direct in situ measurement. While there are specific challenges in using these new instruments, their strength is in avoiding the need to collect samples for later laboratory analysis. Similarly, high-resolution emission spectrometers that are able to discern individual water isotoplogue emission lines from the background atmospheric emission, and are beginning to find homes on space based platforms, which enables global-scale monitoring of the isotopic composition of atmospheric water. So too the advance in understanding of the linkage between the isotopic composition of vapor and the isotopic composition of plant material yields novel opportunities to estimate water vapor isotopes from natural archives. These emerging techniques provide valuable new capabilities to map the spatial and temporal distribution of water vapor isotopes, but like more traditional sampling techniques, have their limitations.

4.3 Motivation for Plant-Based Proxies

Plants can operate as bio-recorders of water vapor isotopes if a few environmental and physiological requirements are met. The necessary environmental condition is that of relative humidity being near or greater than 90%, which drives leaf water isotopes to be reasonably close to equilibrium with the isotopes of atmospheric vapor. The physiological patterns necessary for plants to act as bio-recorders are that plants must lose water during periods that satisfy the environmental conditions above – this would most likely be at night. To the best of our knowledge, the only plants that satisfy these conditions are epiphytic plants with Crassulacean acid metabolism (CAM).

CAM photosynthesis is characterized by nocturnal assimilation of CO_2 and, consequently, nocturnal water loss. The CO_2 that is assimilated at night is converted to malic acid and stored within cell vacuoles. Upon the next day's light, the malic acid is decarboxylated and the liberated CO_2 is used, along with incident sunlight, in the normal photosynthetic carbon reduction cycle to produce simple carbohydrates that are the building blocks for all plant organic material. Through the diel cycle there is tight control over the leaf pores, or stomata, of CAM plants so that during the day little water or CO_2 is lost from inside the plant. Therefore CAM photosynthesis represents a physiological mechanism to maximize CO_2 gain while minimizing water loss. The cost of this mechanism is twofold: first, there is a chemical-energy cost to storing CO_2 as malic acid and second, there is a restricted amount of CO_2 that can be stored as malic acid, thus the growth rate of CAM plants is limited in comparison to plants that assimilate CO_2 only during the day (Martin 1994).

The eco-physiological significance of CAM photosynthesis is that it allows for survival in areas that are typified by low water availability and high solar radiation inputs – explicitly including desert biomes and functionally including the epiphytic lifeform. An epiphyte is a non-parasitic plant that grows on another plant (known as the porophyte) for support and has no continuous source of water. Examples of epiphytes include the symbiotic organisms known as lichens and higher plants such as bromeliads and orchids. Lichens are active only immediately after a rain event, whereas epiphytic bromeliads and orchids with the CAM pathway are capable of maintaining physiological activity long after the rains have passed. Fortunately, the distributional constraints for ephiphytic CAM plants mirror the environmental conditions required for them to act as bio-recorders of water vapor isotopes.

The physical requirements for a plant to act as a recorder of water vapor isotopes are best described (following Helliker and Griffiths 2007), by starting with the standard Fick's law approach to estimate net transpiration from a plant (E, μmol m^{-2} s^{-1}),

$$E = g\,(w_i - w_a) \tag{4.1}$$

where g is stomatal conductance (mol m^{-2} s^{-1}) and w_i and w_a are the mole fractions of water vapor in the substomatal cavity and ambient air, respectively. Thus, net diffusion of water from the leaf is characterized by the difference of two real, one-way fluxes of water vapor from the leaf to the atmosphere (gw_i) and from the atmosphere into the leaf (gw_a).

Following Craig and Gordon (1965), the flux of heavy water molecules out of the leaf can be written as

$$R_E E = \frac{g}{\alpha_K}\left(\frac{R_L}{\alpha_e} w_i - R_a w_a\right) \tag{4.2}$$

where R is the molar isotope ratio of transpiration (E), leaf water (L) and water vapor (a), α_e is the temperature dependent equilibrium fractionation factor, and α_K is a balance of the ratio of diffusivities of light to heavy water molecules through the stomata and through the leaf boundary layer (Farquhar and Lloyd 1993; Farquhar and Cernusak 2005; Flanagan et al. 1991).

By rearranging Eq. 4.2 to solve for R_L and relating the water vapor mole fractions to leaf-based relative humidity where $h = w_a/w_i$ we arrive at,

$$R_L = \alpha_e \left[\alpha_K R_E (1 - h) + R_a h\right]. \tag{4.3}$$

For an epiphyte, tissue water content is recharged by each precipitation event, either rainfall or dewfall. The gross flux of water from the plant, gw_i, is drawn from a finite and small volume of water. Whereas the gross flux of water into the plant from the atmosphere, gw_a, is a finite but dramatically larger volume of water. Therefore, over time the volume of water within the epiphyte is exchanged by atmospheric water vapor. From Eq. 4.3 it can be seen that as w_a increases relative to w_i (i.e., as h increases), the isotope ratio of water remaining in the plant becomes dominated by atmospheric water vapor.

Under constant or nearly constant environmental conditions with h near unity, the isotope ratio of water vapor exiting (R_E) the leaf approaches that remaining in the leaf (R_L) and we can write:

$$R_L \approx \frac{\alpha_e R_a h}{1 - \alpha_e \alpha_K (1 - h)} \tag{4.4}$$

In the limit when $h = 1$, the denominator vanishes and the isotopic enrichment in a steadily evaporating CAM epiphyte is equal to the isotope composition of atmospheric water vapor, corrected for the equilibrium fractionation factor,

$$R_{L=} \alpha_e R_a \tag{4.5}$$

As such, the main limitation in existing trapping based vapor sampling methods can be avoided by simply collecting the entire water sample that is enclosed in the leaf material of an appropriate candidate species. The water can be obtained from the leaf using traditional vacuum extraction methods, then analyses using traditional isotope mass spectrometry. Once known, Eq. 4.5 can be applied to estimate the water vapor isotopes for the time over which the leaf recently transpired. Similarly, to the degree to which this water is used in cellulose production, the isotopic composition of cellulose can be used to develop a history of isotopic composition. This in turn holds potential for developing records of isotopic composition that extend beyond the modern era.

4.4 Application of Plant Proxy Estimates

Tillandsia usneoides (Spanish Moss) is an ideal candidate organism for testing the efficacy of a plant-water-vapor-isotope proxy. *T. usneoides* is a subtropical to tropical epiphyte that ranges from coastal Virginia, USA through the tropics to Argentina. The distribution is determined by high nocturnal relative humidity (Garth 1964) and it is a constitutive CAM plant. The plant achieves a net gain of water solely

from rain or dewfall by absorption through a heavy cover of modified, hygroscopic trichomes. The trichomes also directly adsorb atmospheric water vapor as a function of *h*, however the water potential gradients from the trichomes to cellular water mitigates use of this water for plant metabolism (Martin and Schmitt 1989). The plant hangs from the branches of trees and grows as a series of ramets that, while physically connected, are isolated in terms of CO_2 assimilation and metabolite translocation (Martin 1982). The epiphytic lifeform and the isolation of each ramet allows for *T. usneoides* to be modelled, in terms of water loss, as an evaporating cup that slowly loses water during a high humidity night and is refilled infrequently with each precipitation event. *T. usneoides* exhibits slow growth rates of about 1 cm/month and new ramets are produced at the tip of a given strand (Martin 1980). Therefore, the growth of *T. usneoides* strands can be viewed as analogous to a tree ring recording growth environment from year to year. The results discussed here may hold true for other species of epiphytic plants with CAM photosynthesis within and outside of the western hemisphere. Therefore, our approach can potentially be expanded to tropical and subtropical regions throughout the world.

To test the controls of water vapor on leaf water we placed strands of *T. usneoides* in a climate-controlled chamber that was fed water vapor and air from a 23 L temperature-controlled "water tower." Using the water-tower setup a constant water vapor $\delta^{18}O$ for several weeks with $h = 0.97$ and temperature = 27.5°C could be maintained (Fig. 4.1). In contrast to most studies of isotopic enrichment in leaf water during evaporation, leaf water $\delta^{18}O$ in *T. usneoides* became depleted during transpiration. The large gross flux of water into the leaves replaced the initial leaf water by water vapor that entered the leaf and condensed. After a period of about 4 days, leaf water $\delta^{18}O$ was in equilibrium with observed water vapor $\delta^{18}O$. This was a similar period of turnover time that we observed in a previous study (Helliker and Griffiths 2007). This slow leaf-water turnover time in *T. usneoides* acts as a buffer against rapid, short-term changes in water vapor isotopes that have been observed in field studies (Helliker et al. 2002, Lai et al. 2006) and suggest that *T. usneoides* leaf water will act as a long-term integrator of water vapor isotopes.

On August 2, 2007 a large-scale sampling effort for *T. usneoides* leaf water was conducted as a first step to characterize regional variation in atmospheric water vapor. The samples were collected within a couple of hours either side of solar noon by volunteers at various colleges and universities. Figure 4.2 shows the mean leaf-water $\delta^{18}O$ for each sample site and the reconstructed water-vapor $\delta^{18}O$. While a preliminary effort, it is clear that there is a regional coherence of water vapor $\delta^{18}O$ as reconstructed by leaf water. Values around the Gulf Coast of Texas were constantly relatively high and water vapor $\delta^{18}O$ values decreased towards the eastern Gulf states. There were marked differences across the Florida peninsula with the east coast sample sites being more ^{18}O-enriched than the Gulf Coast sites.

With a view to extending this analysis approach, we note that leaf-water isotopes are recorded in leaf cellulose and the analysis of *T. usneoides* cellulose $\delta^{18}O$ along with basic climate data allows for the reconstruction of water vapor $\delta^{18}O$ from herbarium specimens. To demonstrate this, the $\delta^{18}O$ of bulk organic material was determined on samples obtained from Miami, Florida in September of 2005 and

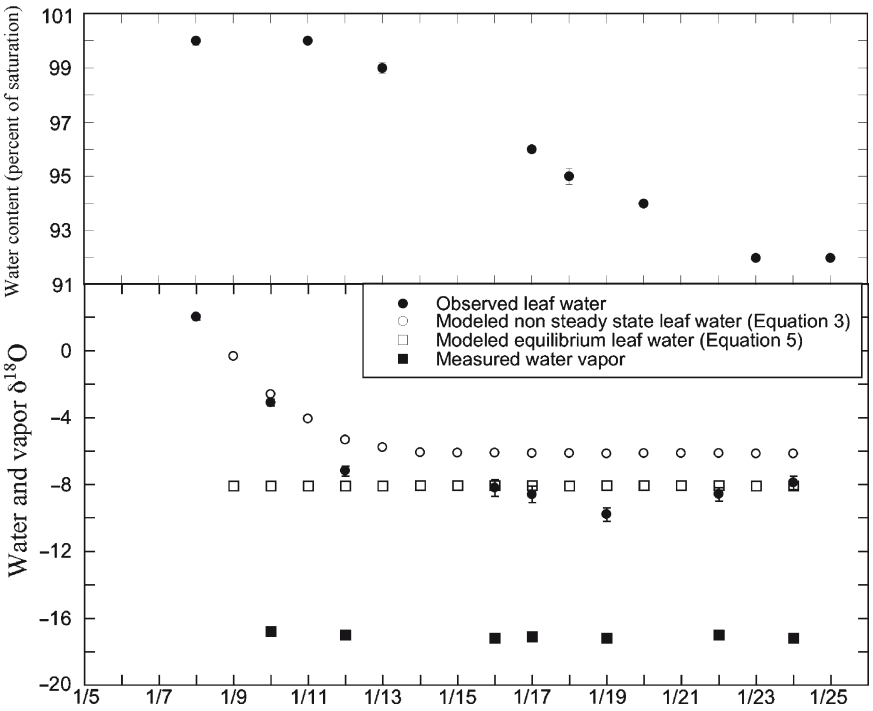

Fig. 4.1 Observed leaf water loss and $\delta^{18}O$ for *T. usneoides*. Panel (**a**), water loss as a percent of full saturation. Panel (**b**), changes in the $\delta^{18}O$ through time. The day/night *h* was 94/98%, respectively and water loss was determined by weighing the individual strands. n = 5 for each day

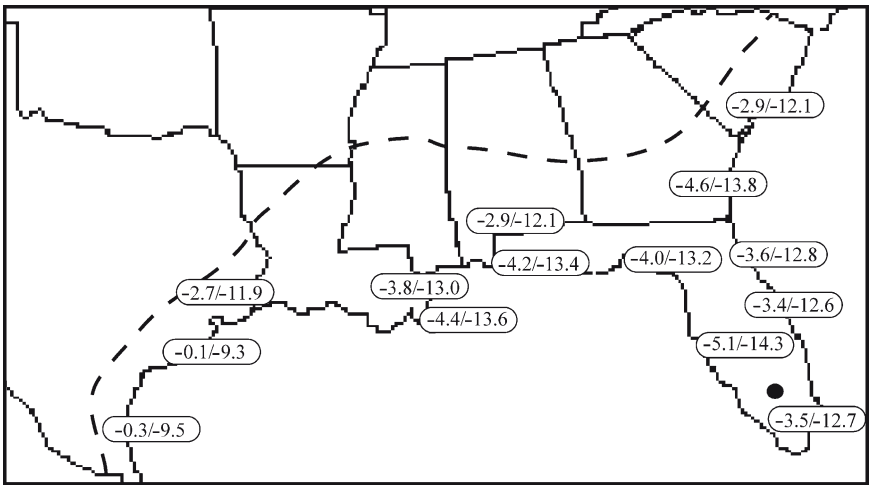

Fig. 4.2 Observed leaf water $\delta^{18}O$ (the first number) and reconstructed water vapor $\delta^{18}O$ (the second number) for August 2, 2007. All samples were taken within 2 h of solar noon during a coordinated survey. The *dashed line* is the fall line for *T. usneoides* distribution in the US. The *black dot* is a field site where mean, measured water vapor $\delta^{18}O$ was −12.0 ± 0.8 from 9–13 Aug 2007

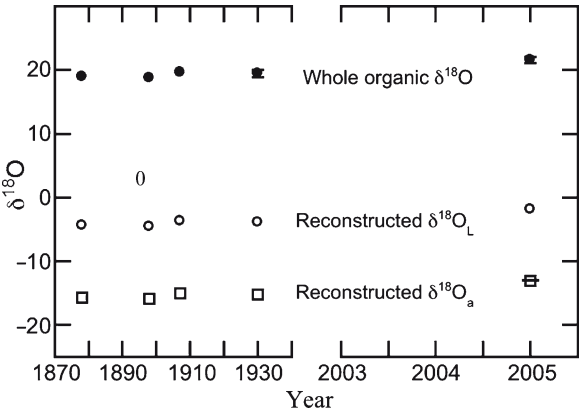

Fig. 4.3 Reconstructed leaf water ($\delta^{18}O_L$) and water vapor ($\delta^{18}O_a$) $\delta^{18}O$ in Miami, FL. Leaf water and water vapor $\delta^{18}O$ were calculated from whole-leaf $\delta^{18}O$ of *T. usneoides* of fresh material sampled in September of 2005 and herbarium specimens sampled from 1878 to 1930. See text for details of the calculations. The *horizontal dash* for 2005 is the calculated modern equilibrium value for $\delta^{18}O_a$ using the 30-year mean annual temperature in Miami of 23.3°C and surface water $\delta^{18}O = -3.5‰$. n = 2 for 1930, n = 5 for 2005, n = 1 for all other years, *error bars* represent one standard error mean (Reprinted from Helliker and Griffiths (2007) with permission from Blackwell Scientific)

compared to herbarium specimens which were originally collected in Miami in the late nineteenth and early twentieth centuries (Fig 4.3). Miami is a good location to examine our approach because of the availability of herbarium specimens and Miami is near the southern tip of an oceanic peninsula that has little variation in mean temperature and $\delta^{18}O$ of precipitation compared to continental regions (Bowen and Revenaugh 2003). Therefore, we would expect that water vapor $\delta^{18}O$ is near equilibrium with precipitation $\delta^{18}O$ throughout the growing season.

We first reconstructed leaf-water $\delta^{18}O$ values by using a leaf-water-to-bulk-leaf fractionation factor of 23.4‰. Bulk material of *T. usneoides* has a large lignin component and it was assumed that bulk organic offset of *T. usneoides* strands to leaf cellulose was similar to that of whole wood versus α-cellulose obtained by a weighted average of published fractionation factors (Barbour et al. 2001; Ferrio and Voltas 2005). The $\delta^{18}O$ water vapor was estimated using the reconstructed leaf water $\delta^{18}O$ using the equilibrium offset, as before. To obtain mean values of h we used mean annual nocturnal relative humidity from the Miami area for the years 2001–2005. The same value for h was used for the herbarium specimens due to a lack of temperature and humidity records for the period spanning 1878 to 1930. While this assumption introduces a large uncertainty when one considers the role of h in Eq. 4.3, one should note that the selection of *T. usneoides* was motivated by its distribution in regions with very high and constant humidity. Given this, the observed bulk organic $\delta^{18}O$ and calculated leaf water and water vapor $\delta^{18}O$ were nearly constant from 1878 to 1930 (average water vapor $\delta^{18}O = -15.5 \pm 0.25‰$). Contemporary $\delta^{18}O$ values in Miami were higher than the average values from the past by 2.3‰. The 2005 value for water vapor $\delta^{18}O$ (−13.1 ± 0.5‰) was similar to what would be expected by water vapor $\delta^{18}O$ being, on average, in equilibrium with

the $\delta^{18}O$ of annual rainfall at the mean annual temperature (−13‰). It is worth noting that this reconstructed value from Miami in 2005, the leaf water value obtained in the survey sampling for Miami 2 years later (−12.7 ± 0.3‰; Fig. 4.3) and the average measured water vapor from a field experiment near Miami a week after the survey sampling (−12.0 ± 0.8‰) are all similar.

T. usneoides records water vapor $\delta^{18}O$ of nocturnal periods while the majority of plants (and hence isoscape applications) will be affected by daytime values of water vapor $\delta^{18}O$. Any systematic offset between nocturnal and diurnal $\delta^{18}O_a$ would lessen the importance of reconstructing water vapor $\delta^{18}O$ via *T. usneoides*. In recent direct observations water vapor $\delta^{18}O$ at a Florida field site there has been no clear diel pattern. In general, changes in observed water vapor $\delta^{18}O_a$ in Florida seem to be governed more by synoptic-scale weather patterns than diel cycles. This observation is consistent with observations of $\delta^{18}O_a$ in a New England forest, but contrary to those of a forest site in the Pacific Northwest (Lai et al. 2006; Lee et al. 2006). Additionally, precipitation inputs have an immediate effect on *T. usneoides* leaf water $\delta^{18}O$, but these effects are short-lived and do not appear to change the long-term control of water vapor $\delta^{18}O$ on leaf water $\delta^{18}O$. In lab and field experiments, any measurable effect of the precipitation water on leaf water $\delta^{18}O$ is typically gone within 2 days. However, carbon is being assimilated during the periods following a precipitation event while leaf water $\delta^{18}O$ approaches equilibrium with water vapor $\delta^{18}O$. Therefore, through future research we must gain a better understanding of the relationship between precipitation and leaf water $\delta^{18}O$ to more accurately reconstruct water vapor $\delta^{18}O$ through leaf water and plant organic material.

The tropical epiphytic CAM plant *T. usneoides* offers a means to reconstruct past and present water vapor isotopic signals. In the future, we hope to develop an Isoscape of water vapor $\delta^{18}O$ across the entire southeastern US coastal plain. Further, there are similar plants throughout the tropical Americas for which reconstructions of water vapor isotopes can potentially be made. While little knowledge is available of epiphytic CAM plants in African or Pacific tropical systems, the same ecological niche exists in these biomes so there is certainly potential that similar plants exist and we can expand the spatial extent of water vapor reconstruction beyond the Americas. Continued examination of herbarium material will extend this analysis to allow for the temporal reconstruction of isotopic ratios of water vapor for a large portion of the terrestrial biosphere through a period of rapid climate change during the past century. However there remains a need to validate the plant-derived samples with a direct field measurement in modern environments before these proxies can be used with confidence.

4.5 Direct Measurement by Optical Methods

While collecting physical samples for later laboratory analysis has had success in many cases, the issues associated with capturing liquids from the vapor phase without fractionation and the intricacies associated with proxy sampling leave great

potential for direct in situ measurement of water vapor isotopes. Spectrometric isotopic analysis (with isotope ratio mass spectrometers) in a laboratory setting is highly precise and is in common use, but is not presently a field portable technology. Similarly, it is particularly laborious to develop time series data with traditional sampling or proxy methods since each individual measurement needs lengthy collection, preparation and transport to a laboratory. On the other hand, laser-based spectroscopic analyzers can be deployed in a field setting, run in an almost continuous sampling mode and thereby offer substantial potential to improved measurement density.

Estimation of isotopic abundance from either absorption or emission spectroscopy entails measuring some fraction of the spectrum at sufficiently high resolution to be able to quantitatively identify individual spectroscopic line features associated with the isotopologues of interest. Figure 4.4 shows a section of the infrared absorption spectrum of a gas in which water isotopologues are found. Given accurate measurement of a spectrum, the line features (peak shape and size) can be mapped to the concentration of each isotopologue identified in the spectrum, and the isotope ratio constructed. This is typically performed using an estimation approach in which the concentration is found as a best fit between the measured spectrum and a spectrum based on physical considerations in light of known uncertainties. Alternatively, the concentration estimate can simply be made by finding the integral of a specific line feature as a function of frequency, and again using the physical expectation to map the integrated quantity back to the of number of molecules of the species within the gas sample.

While a number of different optical configurations are possible, two variations of the spectroscopic approach have emerged as useful in developing commercial

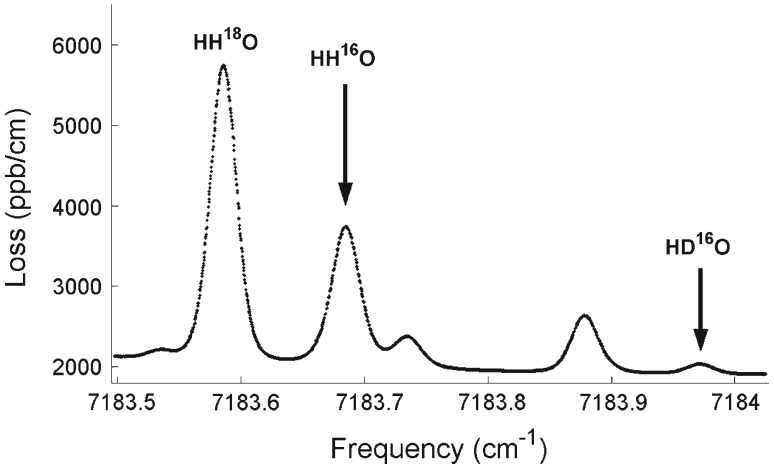

Fig. 4.4 An example section of the infrared ring-down spectrum showing the signature of water isotopologues measured by a Picarro G1102-I Water Vapor Isotope Analyzer in the region scanned by a tunable diode laser as part of the CRDS measurement. The shape and size of each line feature is related to the number of molecules in the sample. (P. Gupta, 2009, personal communication)

field-deployable instruments, and both of which use Tunable Diode Lasers (TDL) to accurately probe a small region of the spectrum. Integrated Cavity Output Spectroscopy (ICOS; Baer et al. 2002) illuminates the sample gas and directly measure the absorption spectrum from light that leaks from optical cell. The second approach is Wavelength Scanning – Cavity Ring-Down Spectroscopy (WS-CRDS; Crosson 2008) in which the optical cavity is filled with a pulse of light and the measurement is of the decay in light intensity as a function of time when the laser is switched off. While there are some technical advantages for either method, both approaches are fast enough that in field applications, measurements can be made in a near continuous manner with measurements made every few seconds. It has been shown that the precision and accuracy of these types of instruments now rivals that of the laboratory based isotope ratio mass spectrometers. Gupta et al. (2009) reports the precision on continuous (12 s) samples to be 0.17‰ for $\delta^{18}O$ and 1.1 ‰ for δD even at very low water vapor concentrations.

Figure 4.5 shows an example of a time series of hourly $\delta^{18}O$ and deuterium excess data measured over a 10-day period in New Haven (L. Welp and X. Lee, 2008, personal communication) using a direct absorption method as described by Wen et al. (2008), which yields a measurement precision around 0.07‰ for $\delta^{18}O$ and 1.1‰ for δD and an absolute accuracy of 1.2‰ for $\delta^{18}O$ and 1.1‰ for δD for hourly average data. The figure shows clear diurnal variability that is tied to the daily transpiration cycle and boundary layer activity at the measurment site in New Haven, Connecticut. Both longer term weather-scale variability, and higher

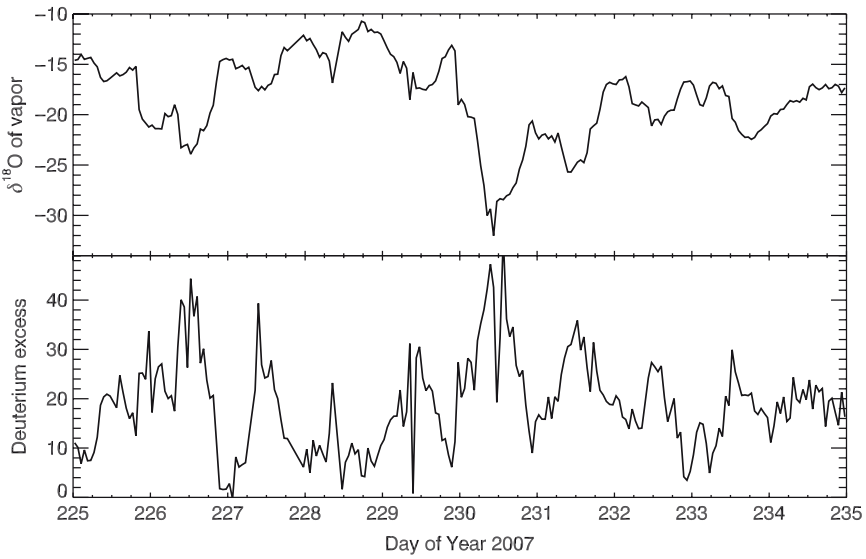

Fig. 4.5 Example of an hourly time series of $\delta^{18}O$ (*upper panel*) and deuterium excess (*lower panel*) measured via infrared absorption spectroscopy between measured 13–23 August 2007 in New Haven (L. Welp and X. Lee, 2008, personal communication)

frequency variability associated with local conditions are also seen. Rain occurred on 17 August (day 229) and 20–21 August (day 232–233) and likely linked to the lower $\delta^{18}O$ values measured at those times because of both local recycling by evaporation of fallen water and that the rain is associated with arrival of different prevailing air masses. Being able to examine this fine scale structure in the time domain as a function of meteorological controls is not readily possible from traditional methods and is a clear advance provided by optical systems.

The ability to use a network of such instruments to map spatial variations in water vapor isotopes is of great interest in the future but to date is lacking. On the other hand, the scientific benefit for surrendering spatial detail is in the advantages offered by what is learned from the structure found the temporal domain. Time series data lend themselves to improving understanding of the controlling processes and the ability to resolve isotope variability from the order of seconds, upwards though the diurnal cycle, weather timescales, the annual cycle and beyond, cannot be understated.

Until the recent appearance of commercial analyzers, the use of laser-based instruments has been the domain of specialist research groups. For instance, there have been applications that focused on upper tropospheric water with high frequency measurements needed for fast moving high altitude aircraft (Webster and Heymsfield 2003; Hanisco et al. 2007), and specialist surface studies are beginning to appear (e.g., Welp et al. 2008). With the availability of commercial analyzers in 2007 and 2008, wider use of such instruments is likely, and there is great potential for continuous in situ instruments to revolutionize water isotope science. At this early stage of their availability, care is needed to demonstrate the accuracy of laser-based measurements relative to exiting sample collection and mass spectrometer methods. While decades of experience with mass spectrometry has lead to many refinements in laboratory practices that allow reliability in measurements, there remains a number of technical issues that can scientifically degrade performance of optical analyzers if not kept in check. For instance the polar nature of the water molecules provides special concern in continuous flow systems since the water can "stick" to sample inlet tubes and surfaces with the optical cavity. Sticking can lead to an isotopic fractionation and degrade the precision of the instrument. Further, the use of multiple passes of the laser though the sample cavity requires high quality and well calibrated optical components such as mirrors. Similarly, the most accurate measurements require accurate and well calibrated lasers that can be precisely tuned. Nonetheless, while obtaining lasers of appropriate quality remains a particular technological issue, gaining confidence in the measurements from existing instruments remains a scientific endeavor and indeed there remains some question as to how such systems can be reliably calibrated against known liquid standards.

Due to their fledgling status, laser-based instruments are presently not being used to provide information on spatial gradients at any scale, although the opportunity certainly exists. An ideal platform for monitorial global scale spatial distributions is provided by satellites. The use of high resolution space-borne spectrometers to obtain the spectra of natural emission of infrared radiation from satellite can be used

to estimate the isotopic composition. Due to the temperature of the atmosphere, radiative emission is mostly in the infrared, but the specific frequencies at which radiation is emitted depends on the abundance of each nuclide in the mixture of gases in the atmosphere at any time. Of interest, all water vapor isotopologues emit radiation that leads to specific spectral features that can be measured by precise space-based spectrometers. To date, four Fourier transform infrared spectrometers have been flown and provided demonstration of the methodology. The Interferometric Monitor for Greenhouse-gasses (IMG) instrument on the Japanese Advanced Earth Observing System spacecraft operated for nine months at the end of 1996 and 1997. Zakharov et al. (2004) used these data to estimate the total column mean HDO abundance and demonstrated that the latitudinal gradient could be recovered. The Michelson Interferometer for Passive Atmospheric Sounding (MIPAS) was flown on the Envisat satellite and operated at high resolution between 2002 and 2004. This limb scanning instrument was used to retrieve HDO from 6 km upwards to the top of the mesosphere, and is most reliable in the stratosphere (Payne et al. 2007). The Tropospheric Emission Spectrometer (TES) on NASA's Aura spacecraft was launched in 2004, and continues to recover spectra from which global maps of HDO can be constructed at approximately 5 × 5 degree resolution every two days from observations taken at local 2 a.m. and 2 p.m. as an operational product from that mission (Worden et al. 2006, 2007). Because of the accuracy and operational nature, these results are a remarkable leap in the ability to monitor naturally occurring isotopes. The Infrared Atmospheric Sounding Interferometer (IASI) instrument on Eumetsat has similar optical characteristics to TES, and while isotope retrievals have been done in an experimental capacity (Herbin et al. 2007) they have not been obtained in an operational manner. IMG, TES and IASI are all downward looking instruments and recover the isotopic composition in the lower-mid troposphere above the boundary layer.

Figure 4.6 shows a climatology of the TES HDO measurements for the layer between 800 and 500 hPa based on measurements between December 2004 and February 2008. Many aspects of the large scale spatial structure of the free troposphereic δD distribution emerge, including a latitude effect, continental-oceanic contrasts, and both enriching and depleting influences of convective activity. Analysis of the data show that the large scale atmospheric hydrology can be directly inferred from the isotopes (Brown et al. 2008; Noone 2008). It is important to recognize that satellite derived data are not for vapor at the surface but in the free troposphere and as such do not necessarily match the isotopic composition of boundary layer vapor or precipitation which are governed by different sets of processes. Also, while the spectroscopic methodology used by space-based sensors is fundamentally similar to in situ instruments, they are less precise because of measurement and retrieval uncertainty. As a case in point, TES obtains δD with a precision of 10‰, compared to the in situ instruments at around 1‰, and traditional mass spectrometry of around 0.2‰. Similarly, is it more difficult to estimate $\delta^{18}O$ since the $H_2{}^{18}O$ lines are less well separated from the H_2O lines even though the abundance of $H_2{}^{18}O$ molecules is greater, and contain little information beyond that provided by δD. Even so, the ability of space platforms to provide spatial context and make regular

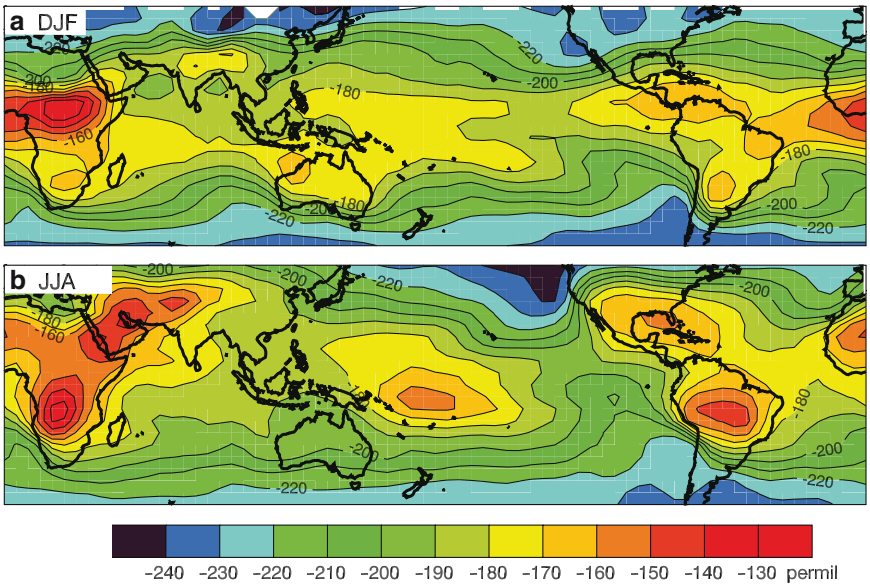

Fig. 4.6 DJF and JJA mean δD for the atmosphere between 800 and 500 hPa derived from the infrared spectra measured by the NASA Tropospheric Emission Spectrometer on the Aura spacecraft. Observations were taken between December 2004 and February 2008. Contour interval is 10‰ and the data are most reliable between 30°N and 30°S. Fig. 4.6, see Appendix 1, Color Section

isotopic measurements of otherwise unobserved parts of the atmosphere leads them to hold observational advantages that compliment in situ measurements.

4.6 Final Remarks

There is now a range of measurement techniques available that will greatly advance the ability to map the spatial and temporal distributions of water vapor isotopes near the surface and in the free atmosphere. These new methods are not without their limitations, but provide new strengths that complement existing techniques. To this end, new measurements provide opportunities to pose new scientific problems in the realm of isotope hydrological studies. Importantly, since water vapor abundance is a measure of the atmospheric state (as compared to precipitation, which is a flux) better constraint on theoretical models and explanations of water exchange can be investigated in a more integrated manner. Also, with a wider range of water vapor isotope measurements that span from the stratosphere, though the troposphere, and to the surface, the pathways of water movement in the atmosphere and surface hydrological systems can be better understood. Given improved understanding, more detailed mapping of water vapor isotopes will allow better constraint on developing secondary isoscapes, for instance, leaf water isotopes.

References

Baer DS, Paul JB, Gupta M, O'Keefe A (2002) Sensitive absorption measurements in the near-infrared region using off-axis integrated-cavity-output spectroscopy. Appl Phys B . doi:10.1007/s00340-002-0971-z

Barbour MM, Andrews TJ, Farquhar GD (2001) Correlations between oxygen isotope ratios of wood constituents of Quercus and Pinus samples from around the world. Austr J Plant Physiol 28:335–348

Blaga LM, Blaga L (1977) Angaben ueber die Konzentration von Deuterium in atmosphaerischenWasserdampf. Isotopenpraxis 13:113

Bowen G, Revenaugh J (2003) Interpolating the isotopic composition of modern meteoric precipitation. Water Resour Res 39:1299

Brown D, Worden J and Noone D (2008) Comparison of atmospheric hydrology over convective continental regions using water vapor isotope measurements from space. J Geophys Res 113. doi: 10.1029/2007JD009676

Brunel JP, Simpson HJ, Herczeg AL, Whitehead R, Walker GR (1992) Stable isotope composition of water vapor as an indicator of transpiration fluxes from rice crops. Water Resour Res 28:1407–1416

Buenning N and Noone D (2008) The role of local and non-local processes in the seasonal cycle and interannual variability of the isotopic composition of precipitation deduced through observations and models. J Geophys Res (submitted June 2008)

Buenning N et al. (2007) Modeling interannual variability of $\delta^{18}O$ of atmospheric CO2 and its dependence on humidity and isotope hydrology. In: Cote J (ed) Research activities in atmospheric and oceanic modelling. Report No. 36, World Meteorological Organization, 4-03, Geneva

Ciais P et al (1997) A three-dimensional synthesis study of $\delta^{18}O$ in atmospheric CO_2 1. Surface fluxes. J Geophys Res 102:5857–5872

Craig H, Gordon LI (1965) Deuterium and oxygen 18 variations in the ocean and marine atmosphere. In: Tongiorigi E (ed) Stable isotopes in oceanographic studies and paleotemperatures. Consiglio Nazionale Delle Ricerche Laboratorio di Geologia Nucleare, Pisa, pp 9–130

Crosson ER (2008) A cavity ring-down analyzer for measuring atmospheric levels of methane, carbon dioxide, and water vapor. Appl Phys B 92(3):403–408

Ehleringer JR et al (2002) Stable isotopes and carbon cycle processes in forests and grasslands. Plant Biol 4:181–189

Evans MN, Schrag DP (2004) A stable isotope-based approach to tropical dendroclimatology. Geochim Cosmochim Acta 68:3295–3305

Farquhar GD, Cernusak LA (2005) On the isotopic composition of leaf water in the non-steady state. Funct Plant Biol 32:293–303

Farquhar GD, Lloyd J (1993) Carbon and oxygen isotope effects in the exchange of carbon dioxide between terrestrial plants and the atmosphere. In: Ehleringer JR, Hall AE, Farquhar GD (eds) Stable isotopes and plant carbon/water relations. Academic, San Diego, CA, pp 47–70

Farquhar GD et al (1993) Vegetation effects on the isotopic composition of oxygen in atmospheric CO_2. Nature 363:439–443

Ferrio JP, Voltas J (2005) Carbon and oxygen isotope ratios in wood constituents of *Pinus halepensis* as indicators of precipitation, temperature and vapour pressure deficit. Tellus B 57:164–173

Flanagan LB, Comstock JP, Ehleringer JR (1991) Comparison of modeled and observed environmental influences on the stable oxygen and hydrogen isotope composition of leaf water in *Phaseolus vulgaris* L. Plant Physiol 96:588–596

Garth RE (1964) Ecology of Spanish Moss (*Tillandsia usneoides*): its growth and distribution. Ecology 45:470–481

Gat JR (1996) Oxygen and hydrogen isotopes in the hydrologic cycle. Annu Rev Earth Planet Sci 24:225–262

Gupta P, Noone D, Sweeney C, Vaughn B, Crosson E (2009) A new age in isotope hydrology: demonstration of autonomous and continuous laboratory-class measurements of water vapor isotopologues in remote field deployments. Rapid Commun Mass Spectrom (submitted 15 January 2009)

Han LF, Groning M, Aggarwal P, Helliker BR (2006) Reliable determination of oxygen and hydrogen isotope ratios in atmospheric water vapour adsorbed on 3A molecular sieve. Rapid Commun Mass Spectrom 20:3612–3618

Hanisco TF et al (2007) Observations of deep convective influence on stratospheric water vapor and its isotopic composition. Geophys Res Lett 34:L04814

Helliker BR, Griffiths H (2007) Toward a plant-based proxy for the isotope ratio of atmospheric water vapor. Glob Change Biol 13:723–733

Helliker BR, Roden JR, Cook C, Ehleringer JR (2002) A rapid and precise method for sampling and determining the oxygen isotope ration of atmospheric water vapor. Rapid Commun Mass Spectrom 16:929–932

Herbin H et al (2007) Global distributions of water vapour isotopologues retrieved from IMG/ADEOS data. Atmos Chem Phys Disc 7:4857–4888

Huebner H, Kowski P, Hermichen W-D, Richter W, Schuetze H (1978) Regional and temporal variations of deuterium in the precipitation and atmospheric moisture of Central Europe. In: Isotope hydrology 1978, vol I. IAEA, Vienna

IAEA/WMO (2006). Global Network of Isotopes in Precipitation. The GNIP Database. http://isohis.iaea.org January 1, 2009.

Lai CT, Ehleringer JR, Bond BJ, KTP U (2006) Contributions of evaporation, isotopic non-steady state transpiration and atmospheric mixing on the delta O-18 of water vapour in Pacific Northwest coniferous forests. Plant Cell Environ 29:77–94

Lee X, Smith R, Williams J (2006) Water vapor 18O/16O isotope ratio in surface air in New England, USA. Tellus B 58:293–304

Martin CE (1980) Field and laboratory studies of crassulacean acid metabolism in the epiphyte *Tillandsia usneoides*. Dissertation, Duke University, Durham, NC

Martin CE (1982) Translocation of nocturnally fixed 14C in the Crassulacean acid metabolism epiphyte *Tillandsia usneoides* L. Bot Gaz 143:1–4

Martin CE (1994) Physiological ecology of the Bromeliaceae. Bot Rev 60:1–82

Martin CE, Schmitt AK (1989) Unusual water relations in the CAM atmospheric epiphyte *Tillandsia usneoides* L. (Bromeliaceae). Bot Gaz 150:1–8

Noone D (2008) An isotopic evaluation of the factors controlling low humidity air in the troposphere. J Clim (submitted June 2008)

Noone D, Sturm C (2008) Comprehensive dynamical models of global and regional water isotope distributions. In: West J, Bowen G, Dawson T, Tu K (eds) Isoscapes: understanding movement, pattern, and process on Earth through isotope mapping. Springer, this volume.

Payne VH et al (2007) A global view of the deuterium content of upper tropospheric/stratospheric water vapour from satellite measurements. Q J Roy Meteor Soc 133(627):1459–1471

Poussart PF, Schrag DP (2005) Seasonally resolved stable isotope chronologies from northern Thailand deciduous trees. Earth Planet Sci Lett 235:752–765

Riley WJ, Still CJ, Helliker BR, Ribas-Carbo M, Berry JA (2003) O-18 composition of CO2 and H2O ecosystem pools and fluxes in a tallgrass prairie: simulations and comparisons to measurements. Glob Change Biol 9:1567–1581

Roden JS, Ehleringer JR (1999) Observations of hydrogen and oxygen isotopes in leaf water confirm the Craig–Gordon model under wide-ranging environmental conditions. Plant Physiol 120:1165–1173

Schoch-Fischer H et al. (1983) Hydrometeorological factors controlling the time variation of D, 18O and 3H in atmospheric water vapour and precipitation in the northwestern westwind belt. In: Isotope hydrology. IAEA, Vienna, pp 3–30

Sharp Z (2007) Principles of STABLE ISOTOPE GEOCHEMISTRY. Prentice-Hall, Upper Saddle River, NJ

Strong M, Sharp ZD, Gutzler DS (2007) Diagnosing moisture transport using D/H ratios of water vapor. Geophys Res Lett 34:L03404. doi:10.1029/2006GL028307

Verheyden A, Helle G, Schleser GH, Dehairs F, Beeckman H, Koedam N (2004) Annual cyclicity in high-resolution stable carbon and oxygen isotope ratios in the wood of the mangrove tree *Rhizophora mucronata*. Plant Cell Environ 27:1525–1536

Webster CR, Heymsfield AJ (2003) Water isotope ratios D/H, O-18/O-16, O-17/O-16 in and out of clouds map dehydration pathways. Science 302:1742–1745

Welp LR et al. (2008) $\delta^{18}O$ of water vapor, evapotranspiration and the sites of leaf evaporation in a soybean canopy. Plant Cell Environ 31:1214–1218

Wen X et al (2008) Continuous measurement of water vapor D/H and $^{18}O/^{16}O$ isotope ratios in the atmosphere. J Hydrol 349:489–500

Williams DG et al (2004) Evapotranspiration components determined by stable isotope, sap flow and eddy covariance techniques. Agr For Meteor 125:241–258

Worden JR et al. (2006) TES observations of the tropospheric HDO/H2O ratio: retrieval approach and characterization. J Geophys Res 111(D16):D16309. doi: 10.1029/2005JD006606.

Worden JR, Noone D, Bowman K (2007) Importance of rain evaporation and continental convection in the tropical water cycle. Nature 445:528–532. doi:10.1038/nature05508

Yakir D, Sternberg LSL (2000) The use of stable isotopes to study ecosystem gas exchange. Oecologia 123:297–311

Yakir D, Wang XF (1996) Fluxes of CO_2 and water between terrestrial vegetation and the atmosphere estimated from isotope measurements. Nature 380:515–517

Yepez EA, Williams DG, Scott RL, Lin G (2003) Partitioning overstory and understory evapotranspiration in a semiarid savanna woodland from the isotopic composition of water vapor. Agr For Meteor 119:53–68

Zakharov VI et al (2004) Latitudinal distribution of the deuterium to hydrogen ratio in the atmospheric water vapor retrieved from IMG/ADEOS data. Geophys Res Lett 31:L12104. doi:10.1029/2004GL019433

Chapter 5
Applications of Stable Isotopes for Regional to National-Scale Water Quality and Environmental Monitoring Programs

Carol Kendall, Megan B. Young, and Steven R. Silva

5.1 Introduction

Isotope studies conducted over large spatial and/or temporal scales can provide powerful insights into natural ecosystem functions and the effects of anthropogenic disturbances. Large-scale field campaigns require considerable monetary and personnel resources, and it is therefore advantageous to combine isotope studies with existing monitoring programs. This approach leverages existing field sampling resources to provide large sets of isotope samples, and the isotope data can, in turn, provide valuable information for the monitoring programs. Isotope studies can also be useful during the planning stages of large-scale monitoring programs, because high-resolution isotope sampling can provide strong indications of locations that will be critical to monitoring efforts. For example, locations exhibiting unusually high rates of biogeochemical cycling or elevated pollution levels usually have distinctive isotopic compositions that are suggestive or diagnostic of the reactions and pollution sources. Furthermore, combining isotope measurements with other physical and chemical analyses may reveal important inputs or processes that could not be identified with concentration analyses alone.

In this chapter, we will discuss how isotope measurements have been successfully integrated into several regional and national-scale monitoring programs, and provide suggestions for using this approach. We will show how data from these studies have revealed spatial and temporal patterns in the stable isotopes of nutrients, organic matter, and water using isotope contour maps (isoscapes). These broad isotope patterns can be used to indicate sources, track important biogeochemical processes, and assess ecosystem health. This chapter will focus on developing and interpreting watershed and river isoscapes.

C. Kendall (✉), M.B. Young, and S.R. Silva
U.S. Geological Survey, 345 Middlefield Road, MS 434, Menlo Park, CA 94025 USA
e-mail: ckendall@usgs.gov; mbyoung@usgs.gov; srsilva@usgs.gov

J.B. West et al. (eds.), *Isoscapes: Understanding Movement, Pattern, and Process on Earth Through Isotope Mapping*, DOI 10.1007/978-90-481-3354-3_5,

5.2 Isotopes and Monitoring Programs

The different components of the world – atmosphere, hydrosphere, and biosphere – are constantly changing in response to both natural and anthropogenic processes. These changes, at the local, regional, national, and global scales, can have significant repercussions on the inhabitants, the environment, and the economy. Hence, there is an increasing need for cross-disciplinary integrated science to provide the information necessary to make regulatory decisions. The main purpose of many monitoring programs is to determine the status of a resource and to detect changes in that resource. One example is the USGS National Stream Quality Accounting Network (NASQAN).The basic premise of this and many river-based water quality monitoring programs is that rivers reflect the landscape through which they flow. More precisely, the chemistry of a water sample collected at one location reflects a complex combination of transport, mixing, biogeochemical processes, and human activities in the watershed upstream of the sampling point. Hence, by measuring the amounts and types of chemicals and sediments at sites in state and national-scale networks, these monitoring programs seek to provide the data needed to characterize the watersheds, to determine sources of these materials, and to assess the effects of various human and natural influences on the observed measurements. The National Atmospheric Deposition Program (NADP) is another example of a status-and-trends network, but focused on precipitation rather than rivers.

Other environmental monitoring programs are implemented for more site-specific reasons, usually related to deteriorations in ecosystem health that can have severe economic consequences. Examples include eutrophication, acidification of stream and lakes, and toxic spills. Accurate identification of sources and a thorough understanding of processes are needed for effective regulation and mitigation.

5.2.1 Tracers of Hot Spots and Hot Moments in Watersheds

High resolution isotope studies can be very useful for designing large-scale monitoring programs because isotopes can often be used to identify sites of critical importance within a given system. In recent years there has been increased understanding of the role that small spatial areas or short time periods can play in determining conditions throughout the larger system. According to the original definition in McClain et al. (2003), hot spots are patches that show disproportionately high reaction rates relative to the surrounding matrix, and hot moments are short periods of time that exhibit disproportionately high reaction rates relative to longer intervening time periods. However, these terms are commonly used for places and times where some type of disturbance, often anthropogenic, has resulted in abrupt changes in composition.

Since reaction rates at hot spots may be many times larger than reaction rates in other parts of the system, these locations need to be identified and included in monitoring programs in order to better characterize ecosystem function. However, identifying hot

spots may be difficult, and fixed-site monitoring locations are often chosen without consideration of the possible existence of hot spots. How do we find these critical hot spots? Although remote sensing methods (Chapter 3: Wang et al. 2009). Can identify certain types of hot spots, perhaps the easiest and cheapest approach for looking for hot spots in a river is to conduct a downstream synoptic (transect) sampling of the river, dragging some kind of fast-responding instrument to measure such parameters as temperature, conductivity, nitrate concentration, etc. Given the low cost of such sensors, synoptic cruises can provide critical siting information for subsequent monitoring at a small cost relative to the cost of typical monitoring networks. Illustrations in Vaccaro and Maloy (2006) provide good examples of the usefulness of this kind of approach.

Another approach is to collect discrete samples for more comprehensive characterization of hot spots and hot moments. Isotopes can be more effective at identifying hot spots and hot moments than concentrations alone because isotopic ratios may change even when concentrations don't, thereby allowing identification of hot spots and moments that otherwise would not be apparent. Furthermore, many processes that cause hot spots and hot moments leave distinguishable isotopic signatures, especially in $\delta^{13}C$, $\delta^{15}N$, and $\delta^{34}S$.

There are a wide variety of stable isotopic tools that are useful for studies related to (1) nutrient and organic matter sources, particularly investigations focused on anthropogenic disturbances, (2) biogeochemical processes in aquatic environments, and (3) ecosystem function or health. These isotope tools, and examples of their applications to environmental studies, are listed in Table 5.1.

5.2.2 Sampling Strategies Used by Monitoring Programs

Most state and national river monitoring programs (e.g., the USGS NASQAN program) have emphasized the importance of sampling at fixed sites, at fixed-time (or discharge-weighted) intervals for estimation of hydrological and solute budgets. Unfortunately, sites and sampling intervals that are appropriate for water and solute budgets may inadequately assess the variability in important biogeochemical and anthropogenic processes and inputs that can occur at distributed positions along a river reach. Studies of ecosystem health (e.g., EMAP, EPA's Environmental Monitoring and Assessment Program), on the other hand, are usually conducted using synoptics, where sample locations are chosen using statistics-based distributions of sites; this sampling design improves the chance of having a sampling site detect any hot spots present. These kinds of synoptics are usually duplicated (but using a different grid of sites) during different seasons or years, to improve assessments of controlling variables.

Another useful approach is to conduct longitudinal transects of chemistry and hydrology along a stream reach. These longitudinal transects may be truly Lagrangian (i.e., following a specific parcel of water downstream), pseudo-Lagrangian (sites are sampled in downstream order but not within a single water parcel), or synoptic (sites are sampled at roughly the same time, within a designated time-scale – which could be a day, week, or season).

Table 5.1 Description of several useful stable isotope tracers and what information they provide for water quality and environmental monitoring programs

Tracer type	Interpretive value
Water $\delta^{18}O$ and $\delta^{2}H$	Ideal conservative tracer of water sources and mixing; useful for quantifying flow contributions from different tributaries and groundwater; sensitive indicator of evaporation
Nitrate $\delta^{18}O$, $\delta^{15}N$, and $\Delta^{17}O$	Quantify nitrate from different sources (fertilizer, wastewater, wetlands, atmospheric deposition, etc.); role in the production of algae and degree of recycling; evidence for denitrification, assimilation, and nitrification
Particulate organic matter (POM) $\delta^{15}N$, $\delta^{13}C$, and $\delta^{34}S$	Information on sources of POM; information about the source of the C, N, and S – and the biogeochemical reactions that cycle the elements – even after incorporation into algal biomass; quantify algal vs terrestrial contributions to biomass
Dissolved organic matter (DOM) $\delta^{15}N$, $\delta^{13}C$, and $\delta^{34}S$	Information on sources of DOM; information about the source of the C, N, and S – and the biogeochemical reactions that cycle the elements – even after incorporation into biomass; quantify algal vs terrestrial contributions to biomass; evidence for degradation of organic matter
Dissolved inorganic carbon (DIC) $\delta^{13}C$	Information on sources of DIC, evidence for in situ algal productivity, evidence for degradation of organic matter, degree of gas exchange with atmosphere, nitrification
Dissolved oxygen (DO) gas $\delta^{18}O$	Information about the ratio of productivity to respiration in the water column, source of the O_2, degree of gas exchange with atmosphere, biological oxygen demand (BOD) mechanism
Sulfate $\delta^{34}S$, $\delta^{18}O$, and $\Delta^{17}O$	Quantify sulfate from different sources (soil, wastewater, wetlands, atmosphere, etc.), source of algae, and extent recycling
Phosphate $\delta^{18}O$	Quantify phosphate from different sources; information about the extent of algal production, recycling of material within the river reach, and P limitation
Biota (algae, invertebrates, fish) $\delta^{15}N$, $\delta^{13}C$, $\delta^{34}S$, $\delta^{2}H$, and $\delta^{18}O$	Information on geographic origin of biota; information about the source of the C, N, and S – and the biogeochemical reactions that cycle the elements – even after incorporation into biomass; quantify algal vs terrestrial contributions to biomass; trophic structure; food chain base

One main benefit of doing preliminary synoptics of a river is to locate potential hot spots/moments of human or other disturbances before selecting river sampling sites for routine monitoring. Another benefit of regional synoptics and longitudinal transects is spatial data density (compared to the normal fixed-site networks). Such datasets are obvious candidates for plotting using Google Earth, LiDAR, or other base maps with different colored symbols for different compositions. Such isoscapes are easy to prepare and can be valuable tools for assessing possible linkages between the locations of hot spots and landscape features such as waste lagoons or tile drains (Vaccaro and Maloy 2006). Communicating the results of isotope measurements to local stakeholders can be challenging, and strong graphical presentation techniques

can provide a bridge between scientists, stakeholders, and regulators, conveying isotope results in ways that are accessible to everyone involved. In particular, this kind of detailed information and effective graphic can be extremely useful in getting local stakeholders interested in the inputs and/or processes that are causing the changes in the river near their own homes and farms.

5.2.3 *Benefits of Piggybacking Isotopic Sampling on Monitoring Programs*

There are many benefits to the scientist of including isotope studies as part of national and state monitoring programs. One main benefit is the savings in cost. A large percent of the expense of a monitoring program is the manpower required for collecting the water-quality samples. For minimal additional time and manpower at the field site, additional water can be collected at the same time for eventual isotope analyses, and such samples archived pending future funding and interest.

Large monitoring programs are often willing to collect splits of samples for other scientists at the same time they are collecting samples for their own purposes, and then archive the samples until the accumulated set is sent to the isotope laboratory. Examples include the water, nitrate, and POM (particulate organic matter) isotope samples collected at NASQAN sites (Kendall and Coplen 2001; Battaglin et al. 2001; Kendall et al. 2001); and periphyton, mosquitofish, and sediment composites collected at EPA REMAP (Regional EMAP) sites in Florida (Kendall et al. 1997). Sometimes it is possible to retrieve valuable samples that would otherwise be discarded by the programs. For example, the study of temporal and spatial variability in the POM sources at major US rivers (Kendall et al. 2001) originated with our learning that the NASQAN program filtered water samples for pesticide analyses with glass fiber filters, and then discarded the filters. We approached the head of the program and requested that the field workers instead save the filters, archive them frozen until a year's worth of samples were collected, and then ship them to the USGS Menlo Park isotope lab (Kendall et al. 2001).

Some national programs archive several years worth of extra sample material, and will provide splits of samples upon request. For example, splits of NADP rain samples were obtained and analyzed for water isotopes (e.g., Welker 2000) and nitrate isotopes (e.g., Elliott et al. 2007; Kendall et al. 2007), and the data have been presented as isoscapes. EPA's CASTNET (Clean Air Status and Trends Network) program archives dry deposition samples; samples for sites in the NE USA were obtained, analyzed for nitrate $\delta^{15}N$ and $\delta^{18}O$, and isoscapes presented (Elliott et al. in press).

Other major benefits of piggybacking on large monitoring programs include the fact that these samples are commonly collected using more rigorous protocols than individual scientists are likely to afford. For example, samples collected at NASQAN sites are depth and width-integrated, whereas almost all river samples collected by other programs and individual scientists are near-shore grab samples. Also, these programs typically analyze the samples for a very comprehensive list of constituents, and rapidly make the data available to the public. Hence, they provide large amounts

of chemical and hydrological data about the same samples and sites as your sample splits that you don't have to pay for. And because your isotope data are on the samples collected by the monitoring program, your data and science add value to the programs and enhance the usefulness of the monitoring programs to society. Funding agencies (e.g., NSF) commonly favor research that piggybacks on major monitoring programs because it leverages scarce resources.

There are several less obvious benefits of the large sets of data made possible by measuring isotope ratios of samples collected by monitoring programs. One is that large-scale patterns may become apparent which otherwise would have been obscured by minor sources of variability in studies at smaller temporal or spatial scales, or with fewer samples. Another benefit is that the number of large-scale isotope studies is still relatively limited, and many research groups focus only on their own sample collection programs. Hence, your results are likely to be considered novel and easily publishable. Also, the large-scale sets of samples made possible by national monitoring programs (e.g., EMAP, NASQAN, NADP) are obvious candidates for use in detecting and assessing environmental changes.

Table 5.2 lists our recommended sampling scheme for piggybacking isotope measurements onto monitoring programs concerned with nutrient-related issues. Each time that chemistry samples are collected, we suggest that you consider collecting and archiving splits of samples for isotopic analysis. These abbreviated instructions are based on the analytical methods used in our lab; other labs may have other requirements. A good set of collection guidelines are posted at: http://isotopes.usgs.gov/Instructions.htm.

The list in Table 5.2 includes only a subset of the isotope tools described in Table 5.1. The shorter list was prepared based on our experience with many riverine studies. We find that the first three sample types in the list are especially easy to collect, prepare, and archive – and have always proved useful for nutrient-related studies, especially rivers with low dissolved oxygen problems. POM samples, in particular, provide "good bang for the buck" in that they are very easy and cheap to collect and archive, cheap to analyze for isotopes, and provide semi-quantitative information

Table 5.2 Suggestions for collection and archiving isotope samples for river nutrient studies

Isotope	Recommendations
Nitrate $\delta^{15}N$, $\delta^{18}O$, $\Delta^{17}O$	Collect 20–50 mL, filter (0.2 μm), and freeze. Alternatively, samples can be preserved by adding reagent-grade NaOH or KOH to pH greater than 10–11.
POM $\delta^{13}C$, $\delta^{15}N$, $\delta^{34}S$	Collect 1–2 L of water. Filter through a flat, pre-combusted, 0.7 μm glass fiber filter, and freeze the filters.
Water $\delta^{18}O$, $\delta^{2}H$	Collect and archive 10–25 mL of water at room temperature. The filtrate from the POM samples can be used for water samples.
DOC $\delta^{13}C$	Collect, and filter (0.2 μm) 40 mL into well-cleaned glass bottles containing 50 μL of 85% reagent grade phosphoric acid. Store chilled.
Sulfate $\delta^{34}S$ and $\delta^{18}O$	Collect, filter (0.7 μm), and archive 10–100 mL at room temperature. The filtrate from the POM samples can be used for sulfate samples.
DOM $\delta^{13}C$, $\delta^{15}N$, $\delta^{34}S$	Collect 100–1,000 mL, filter (0.2 μm), and freeze and/or acidify to pH ~ 2. The filtrate from the POM samples can be used for DOM samples.

about the percent of the POM that is algal-derived, sources of nutrients to the water column, and biogeochemical processes – all critical information for nutrient-impacted rivers. Since large amounts of water have to be filtered at monitoring sites for other chemical samples anyway, and if a flat filter is used instead of a cartridge filter, the POM isotopes samples are essentially a "free" byproduct of the filtration process.

5.3 Causes of Spatial and Temporal Isotope Patterns in Watersheds

Isotopes are a potentially powerful complement to monitoring and assessment programs aimed at quantifying and mitigating alterations to ecosystems from human activities because different physical and biogeochemical processes in landscapes often create distinctive isotopic signatures. In particular, isotopic techniques have proved useful for tracing sources and sinks of various pollutants in large river basins, wetlands, and airsheds. This section presents an overview of the causes of spatial patterns in $\delta^{13}C$, $\delta^{15}N$, and $\delta^{34}S$ in watersheds, primarily in rivers. For more information about tracing sources of organic matter and nitrate, see Finlay and Kendall (2007) and Kendall et al. (2007), respectively. The fundamental processes controlling the distributions of water isotopes are not summarized here because they are thoroughly covered in several chapters in this book and others (e.g., Kendall and McDonnell 1998).

Figure 5.1 shows how several main biogeochemical processes in the water column affect the $\delta^{13}C$ of DIC and the $\delta^{15}N$ of nitrate, and subsequently the $\delta^{13}C$ and $\delta^{15}N$ of algae growing in the water column. For example, assimilation (uptake) of C and N by growing algae causes progressive increases in the $\delta^{13}C$ and $\delta^{15}N$ of the residual dissolved species, and in the newly grown algae. Hence, a large algal bloom in a river is likely to create an isotopic hot spot, observable in both the $\delta^{13}C$ and $\delta^{15}N$ of dissolved species and of algae. Since several recent publications have found that a large percent of the seston (POM) in large rivers in the USA is derived from primary productivity in the water column (e.g., Kendall et al. 2001; Kratzer et al. 2004; Volkmar and Dahlgren 2006), an easy way to look for such hot spots is collect and analyze POM samples for $\delta^{13}C$ and $\delta^{15}N$ as proxies for algae.

5.3.1 Longitudinal Spatial Patterns in $\delta^{13}C$

The relative contributions of organic carbon from terrestrial and aquatic sources vary systematically in rivers, depending on river size (Vannote et al. 1980). Terrestrial sources dominate in small streams because shading by overhanging trees limits algal photosynthesis. As streams widen, algal contributions progressively increase and usually dominate unless turbidity reduces light penetration and hence limits in-stream productivity. Downstream changes in biogeochemical processes can also produce

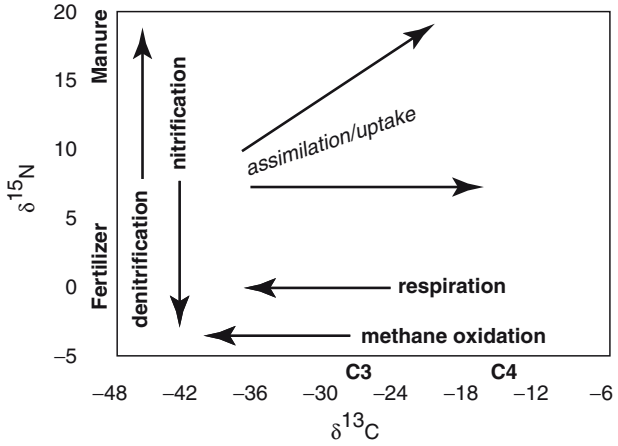

Fig. 5.1 Conceptual model showing the main biogeochemical processes that control the $\delta^{13}C$ of DIC and the $\delta^{15}N$ of nitrate, and consequently the $\delta^{13}C$ and $\delta^{15}N$ of aquatic plants and POM in the water column. The arrows indicate the usual effect of an increased amount of the specified process on $\delta^{13}C$ and $\delta^{15}N$. For example, increased amounts of nitrate formed by nitrification probably cause decreases in $\delta^{15}N$ (but usually minimal effect on $\delta^{13}C$); increased amounts of respiration probably cause decreases in the $\delta^{13}C$. The approximate $\delta^{13}C$ and $\delta^{15}N$ values of important C and N sources are also shown (e.g., for C3 and C4 plants and nitrate from fertilizer and manure, respectively)

longitudinal changes in the $\delta^{13}C$ of DIC, algae, and biota. Important biogeochemical factors include longitudinal patterns in DIC concentrations; changes in isotope fractionation due to declining DIC and increasing algal growth rates; and higher DIC-$\delta^{13}C$ due to uptake of DIC, exchange with atmospheric CO_2, and degassing.

Longitudinal gradients in DIC-$\delta^{13}C$ and consequently algal $\delta^{13}C$ in streams can also be produced by the physical and anthropogenic factors in the watershed. Examples of important physical factors include changes in water velocity due to successive pools and riffles (Finlay et al. 2002), springs or groundwater upwelling zones (Finlay 2004), variable percentages of water in the stream derived from groundwater vs soil water with watershed scale (Bullen and Kendall 1998), and junctions with other water bodies (e.g., rivers, lakes, impoundments, estuaries) that contribute nutrients and cause algal blooms. Mixing of river and wetlands waters with marine water in estuaries will also produce a strong longitudinal gradient in $\delta^{13}C$ because marine DIC typically has a higher $\delta^{13}C$ value than DIC in rivers.

5.3.2 Anthropogenic and Other Spatial and Temporal Effects on $\delta^{15}N$

The $\delta^{15}N$ of plants reflects the $\delta^{15}N$ of available elemental sources in the atmosphere, soil, and aquatic environment as well as a whole host of environmental conditions. There is considerable literature on using the $\delta^{15}N$ of algae, terrestrial

plants, and animals as "proxies" for the isotopic compositions of nitrate and/or ammonium (especially related to sewage) – and hence for sources and land uses that are specific to the N source. This use of isotopes to explain spatial distributions of sources and/or biogeochemical processes is sometimes called "isotope biomonitoring". Some good examples include: Harrington et al. (1998), Koerner et al. (1999), Hebert and Wassenaar (2001), Saurer et al. (2004), Anderson and Cabana (2005, 2006), and Kohzu et al. (2008).

Longitudinal changes in NO_3 concentrations and $\delta^{15}N$, due to changes in sources or cycling of NO_3, often result in similar spatial patterns in algal $\delta^{15}N$. Potential causes of longitudinal gradients or abrupt changes in $\delta^{15}N$ of NO_3 and POM in streams include anthropogenic effects (e.g. fertilizer, animal waste, emissions from power plants), proximity to the ocean (e.g., marine-derived nutrients), redox chemistry (e.g., denitrification, nitrification of ammonium), and uptake of nitrate by algae. In particular, the $\delta^{15}N$ of nitrate, algae, POM, and biota can be affected by inputs of water from waste water treatment plants (WWTPs) in urban areas, or confined animal feeding operations (CAFOs) and agricultural runoff in farming areas.

5.3.3 Anthropogenic and Other Spatial Effects on $\delta^{34}S$

There is much less known about spatial distributions in the $\delta^{34}S$ of riverine sulfate and biota. Three main potential causes of spatial gradients in $\delta^{34}S$ in streams and wetlands are proximity to the ocean, bedrock geology, and redox chemistry. Agricultural inputs such as S fumigants and fertilizers (Bates et al. 2002, Hinckley et al. 2008) may also be important in agricultural rivers. $\delta^{34}S$ values are an effective tracer of organic matter at the land–ocean margin (Connolly et al. 2003) because ^{34}S-enriched sulfate can be transported up to hundreds of kilometers inland. For example, the $\delta^{34}S$ of marine sulfate and vegetation near the ocean is ~+20‰ but decreases to +6‰ over ~100 km (Wadleigh et al. 1996; Wadleigh and Blake 1999). Geology may influence $\delta^{34}S$ where rivers cross geologic units with large concentrations of sulfide minerals. Oxidation of the sulfide minerals can decrease the $\delta^{34}S$ of riverine sulfate, and presumably aquatic plants, as observed in the McKenzie River system (Hitchon and Krouse 1972). Last, reducing conditions typical of wetlands, bogs, and the deep waters of some lakes lead to low $\delta^{34}S$ values because sulfate reduction produces H_2S with low $\delta^{34}S$, which may be assimilated into plants (Nriagu et al. 1991).

5.4 Isotopes, Isolation, Isotropy, and Isoscapes

Whether or not a particular set of spatially (or temporally) distributed data can be validly presented as a contoured isotope map (isoscape) involves a number of considerations (see Wunder 2009 this volume). Among the important factors to consider are how isolated the sampling sites are (in time and space), whether the

sites are connected by some mechanism, and the degree of geographic anisotropy. In other words, how isotropic (similar in all directions) are the landscape and data, in terms of sources and processes. Spatial patterns of isotopic compositions in some environments (e.g., lakes and airmasses) are relatively easy to present as contour maps because the media are well connected and "relatively isotropic". Isotropic, in this context, means that the media mix similarly in all directions. Hence, the data define a myriad of compositional gradients in various directions and the compositions of adjacent samples are generally related by some process and/or by the mixing of sources, supporting the use of gridding and contouring algorithms.

Rivers are characterized by linear connections of water, water-column constituents, and biota because of the unidirectional (downstream) flow of water. Other examples of linearly connected systems include roads, atmospheric rivers, and perhaps migration paths. There are two main kinds of river datasets, each with their own special challenges for preparing valid isoscapes. The first type of dataset is comprised of many isolated sites in hydrologically separate watersheds (e.g., the normal fixed-site networks of most river monitoring programs). Construction of isoscapes using such datasets makes implicit assumptions about the connectivity of these isolated rivers that may not be supported by the data, or supported equivalently for the isotopic compositions of different constituents (e.g., the water $\delta^{18}O$ values may be spatially connected but nitrate $\delta^{15}N$ values probably aren't). The second type of dataset is comprised of several linearly connected sites along a single river reach (e.g., from samples collected along a downstream transect).

One main complication for modeling riverine data is the heterogeneity of watersheds. The isotopic compositions of nitrate, algae, and other constituents from different isolated rivers – or successive downstream sites along a single river – can be affected by a wide range of sources and processes that occur at unpredictable locations along the river reach (Section 5.3). Examples of sources include groundwater, overland flow, and tributaries; examples of processes within the river include algal uptake, nitrification, and evaporation. However, the main challenge to preparing isoscapes for longitudinal river data is that transport is unidirectional – that the effects of spatially distributed sources to the river and processes within the river only mix downstream. In a strict sense, the validity of gradational (or contoured) presentations of the data depends on whether downstream changes in isotopic composition are due mainly to source-mixing during transport or fractionating processes.

Since the river water only flows downstream, mixing of sources (e.g., the input of water from a tributary or groundwater into the main river channel) can only influence sites downstream of the source locations. Therefore – to give an example relevant to the discussion below – the $\delta^{15}N$ value of POM or NO_3 at one location cannot influence the $\delta^{15}N$ values of upstream sites and, hence, should not be used to interpolate the values of intermediate upstream locations. In contrast, if a main control on the POM-$\delta^{15}N$ values is some process (e.g., uptake of nitrate by algae) that produces a predictable downstream trend in $\delta^{15}N$ values (e.g., $\delta^{15}N$ decreases as more algae with low-$\delta^{15}N$ grows in the river, or $\delta^{15}N$ increases because algal uptake is significantly reducing nitrate concentration and thus increasing the $\delta^{15}N$

of the residual nitrate), then downstream changes in POM-$\delta^{15}N$ values would be expected to be gradational. However, in many river studies, the temporal and spatial changes in sources and processes are unknown (and were probably major reason for the study). Hence, contour plots developed using simple interpolation protocols can be an appropriate and useful means for investigating processes and sources, and developing hypotheses.

5.5 Developing Isoscapes from Riverine Data

This section focuses on how to prepare isoscapes for riverine data, using examples from several studies generated while piggybacking isotope sampling on routine monitoring programs. As discussed in Section 5.2, water quality monitoring programs are of two general types: fixed-site studies with isolated samples on separate rivers, and longitudinal synoptics with multiple, linearly-connected samples on the same reach of river. The section is intended to (1) illustrate the wide range of useful applications of isotopes for monitoring programs at local to regional to national scales, and (2) provide a basis for discussions of the relative merits of different approaches for preparing isoscapes and evaluating the spatial and temporal variability

5.5.1 Isoscapes of Regional to National-Scale Riverine Studies

Preparation of regional to national-scale isoscapes of average $\delta^{18}O$ and $\delta^{2}H$ values of a large set of generally unconnected rivers, each sampled at a single integrator location (i.e., the normal "fixed-site" protocol of large monitoring programs), presents a number of challenges. These challenges and several empirical approaches for dealing with them are discussed in great detail in Kendall and Coplen (2001), and will be briefly summarized here to illustrate some of the issues to consider when preparing isoscapes of datasets with potential connectivity and heterogeneity problems.

The Kendall and Coplen (2001) study piggybacked on USGS water quality monitoring programs whereby depth and width-integrated samples were collected from 391 selected sites within the NASQAN and Hydrologic Benchmark Network (HBN) programs, and sent to the USGS stable isotope lab in Reston VA for analysis (Coplen and Kendall 2000). Each site was sampled bimonthly to quarterly (depending on site and season – the networks generally use discharge-based sampling protocols) for 2.5 to 3 years intervals during the years 1984–1987, with an average of 12 samples per site (range 2–35 samples). Drainage areas ranged in size from 6 km^2 to almost 3 million km^2 (i.e., the Mississippi River at Arkansas City). Thus, this was a very heterogeneous isotope dataset compared to the precipitation studies discussed by Bowen 2009 (this volume), where all samples are volume-weighted monthly samples.

One major issue that had to be resolved was whether the $\delta^{18}O$ and $\delta^{2}H$ values of this diverse collection of rivers were sufficiently similar to ambient rain that interpolating δ values from unconnected watersheds was valid. These plots were the first detailed map of meteoric (or meteoric-derived) waters in the USA, and the first detailed and rigorous maps of river δ values ever attempted. These rivers had unknown contributions from local groundwater, lake water, and irrigation returnflow, and some had dams and other human disturbances. Furthermore, evaporative effects might have caused the isotopic compositions of rivers in arid regions to be less "connected" to each other and to precipitation than in more humid environments. Hence, it was not known whether the river isotope patterns would be spatially coherent.

However, comparison of the river $\delta^{18}O$ and $\delta^{2}H$ values with the sparse precipitation isotope data available at the time – plus evaluation of the correlations of the river $\delta^{18}O$ and $\delta^{2}H$ values with temperature, precipitation amount, latitude, etc. – showed that the river data showed patterns very similar to precipitation (Fig. 5.2), providing support for contouring data from samples in geographically unconnected watersheds (Kendall and Coplen 2001). Other challenges included (1) whether the "instantaneous" river sample data should be discharge-weighted before averaging; (2) should sites with small and non-representative datasets, or ones where the δ values were unlikely to resemble those of the original precipitation, be excluded to eliminate artifacts; and (3) what should be the size-cutoff for "too large" drainage areas.

Ultimately, only the simplest and most defendable site selection criterion, drainage area, was used for excluding data for the $\delta^{18}O$ and $\delta^{2}H$ plots because thorough investigation of various possible criteria showed that only exclusion of basins >130,000 km^2 (27 sites) made any significant difference in the positions of the contour lines. Several conclusions can be drawn from the insensitivity of the contours to the various site selection criteria evaluated: (1) the kriging parameters were chosen appropriately to minimize artifacts caused by anomalous single-site compositions, (2) there were sufficient sampling points to make an adequate assessment of major spatial patterns, and (3) that the spatial patterns were coherent and robust. This study concluded that water isotopes can be successfully contoured between river basins because the river samples mainly derive their isotope patterns from large-scale atmospheric processes.

Other kinds of isotope data (e.g., NO_3, DIC, SO_4, POM, DOM isotopes) from regional to national-scale river studies are less likely to show the same kind of continuity (connectivity) between watersheds or basins as water isotopes. Two main factors are responsible for the lower expectations for spatial continuity of such "biogeochemical" isotopes, as opposed to "hydrological" isotopes like O and H: (1) major C, N, and S sources of dissolved inorganic species and organic matter are generally local, with variable relations to sources in adjacent watersheds; and, (2) variation in biogeochemical processes within and between watersheds probably has a stronger effect on isotopic compositions than does geographic proximity. However, while the C, N, and S isotope ratios of riverine materials are generally only minimally connected via the atmosphere, compared to the O and H isotopes of riverine materials, we anticipate that future large-scale river studies will deliver some surprises with regard to the role of anthropogenic

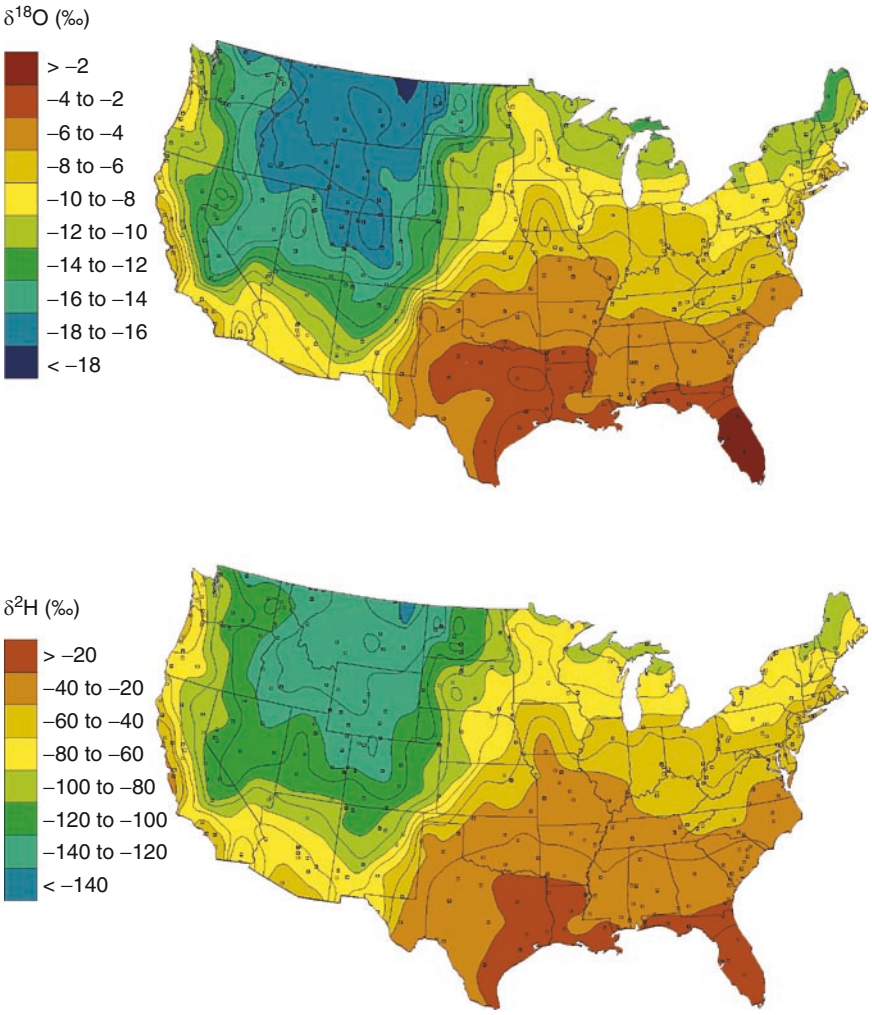

Fig. 5.2 Spatial distributions of discharge-weighted average water-$\delta^{18}O$ values for ~400 USGS NASQAN river sites, sampled 1984–1987; almost 5,000 samples were analyzed (Modified from Kendall and Coplen 2001). Fig. 5.2, see Appendix 1, Color Section

processes in controlling large-scale spatial patterns in isotopic compositions in geographically isolated rivers.

Human activities over the last century have had major effects on regional to global scale C budgets (via increased CO_2 emissions), N budgets (via anthropogenic NOx emissions and fertilizers), and S budgets (via SOx emissions). Many of the coherent spatial isoscapes of $\delta^{13}C$, $\delta^{15}N$, and $\delta^{34}S$ values of biological materials in terrestrial and marine environments presented in the various chapters in the book are a consequence of the impact of human activities on biota isotopes.

Hence, it is not too hard to imagine that the connectivity of diverse river sites via the atmosphere or via persistent land-based human activities (agriculture, urbanization) may ultimately supercede the effects of local differences in elemental sources, human activities, hydrology, and aquatic processes in controlling the distributions of $\delta^{13}C$, $\delta^{15}N$, and $\delta^{34}S$ of constituents in rivers. Coherent spatial patterns in $\delta^{13}C$, $\delta^{15}N$, and $\delta^{34}S$ in riverine systems are probably more likely for large sets of data collected at the regional to global scale, or for datasets that compare isotope values collected over decades to centuries.

5.5.2 Isoscapes for Longitudinal Riverine Studies

The rest of this section will be devoted to a discussion of several types of river-delta-estuary isoscapes prepared using data from the San Joaquin River (SJR), its delta, and the northern San Francisco Bay. This study was a direct result of recommendations from a group of local stakeholders that there was a need for more detailed information about sources of nutrients and organic matter in the SJR basin (that might be contributing to low dissolved oxygen levels downstream) than could be accomplished with a few river synoptics or with data from the single USGS NASQAN site on the SJR (at Vernalis). Consequently, the state of California (CA) funded a 3 year fixed-site study that included the collection of land-based grab samples and physical data from six mainstem sites and 15 tributaries draining into the SJR, at weekly to twice-monthly intervals (Stringfellow et al. 2008). With funding from the state, we piggybacked on this river monitoring program and obtained splits of all samples for isotope analyses (Table 5.2). In order to follow the nutrients and organic matter through the entire estuary, we also piggybacked on routine fixed-site water quality programs in the Delta (conducted by the CA DWR, Department of Water Resources) and in the northern San Francisco Bay (conducted by the USGS). For these two programs, our piggybacking was literal – we rode along on the routine cruises and collected boat-based grab samples ourselves at ~30 sites.

5.5.2.1 Example: San Joaquin River POM Isoscapes

Unlike most other regional datasets discussed in this book, the spatial data from river synoptic studies are narrow (i.e., they define a very thin geographic band on a map), whereas the temporal data are broad (i.e., twice-weekly to monthly data collected over 2–3 years in the SJR). Bivariate plots of δ values vs locations are the obvious way to present the spatial changes in rivers. For example, Fig. 5.3a shows the spatial changes in $\delta^{15}N$ of POM at 35 mainstem sites on the SJR, for boat-based samples collected during a 5-day downstream synoptic in August 2007. Samples from all significant tributaries (~30 sites) along this reach of river were also collected and analyzed, but the data were omitted from Fig. 5.3a for the sake of clarity.

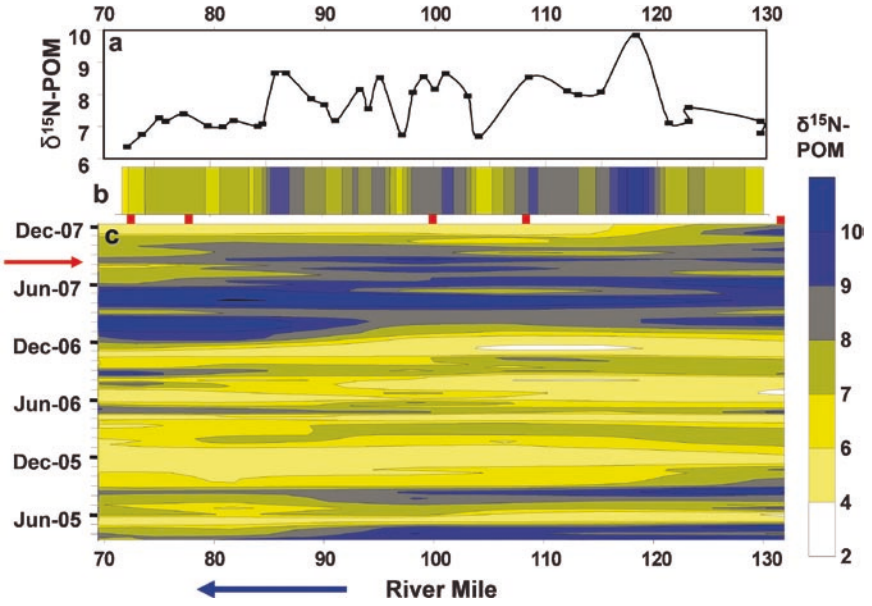

Fig. 5.3 Comparison of three different approaches for plotting $\delta^{15}N$ data for riverine POM samples from a 60 mile reach of the San Joaquin River. The lower the river mile number, the further downstream the location. The spatial distributions of $\delta^{15}N$ values from a boat synoptic in August 2007 are presented in two manners: (**a**) as a typical bivariate plot ($\delta^{15}N$ vs river mile), and (**b**) as gradational changes in color within a thin "band" representing the river channel. The spatial and temporal distributions of $\delta^{15}N$ values from five fixed-location monitoring sites (locations shown with *red bars* at the top of Fig. 5.3c) sampled ~ 75 times March 2005–December 2007 are shown in (**c**). The date of the August 2007 synoptic is shown with a *red arrow* to the left of the panel. Fig. 5.3, see Appendix 1, Color Section

There are several other ways to present the data in Fig. 5.3a as gradational changes in $\delta^{15}N$. Figure 5.3b, which shows the spatial relations as a band of color, was easy to prepare. Similar "band" or "ribbon" plots using other isotope data from the same sites and dates (e.g., the corresponding water $\delta^{18}O$ and $\delta^{2}H$, nitrate $\delta^{15}N$ and $\delta^{13}C$, DOC $\delta^{13}C$, and POM $\delta^{13}C$ and C:N data) could be stacked vertically, to facilitate comparisons. Both types of plots convey the main points about downstream trends approximately equally well: that $\delta^{15}N$ values are initially low, they increase to their maximum values at about river mile (RM) 118, and then oscillate between low and moderately high values downstream until about RM 84, when the values then gradually decrease to values lower than the initial $\delta^{15}N$ values.

The spatial trends for this single transect can be compared with the isoscape prepared from data from six "fixed-sites" (only five shown) sampled during 75 transects March 2005 to December 2007 (Fig. 5.3c). This isoscape shows the temporal and spatial distributions of POM-$\delta^{15}N$ using data for ~400 samples collected weekly to twice-monthly. The POM is predominantly (>75%) algal in origin, with lower percentages during the winter because of larger contributions of terrestrial-derived material from major tributaries draining the Sierra Nevada Mountains, and

higher percentages during the summer due to larger contributions of algae from upstream tributaries and in-stream productivity. The year 2007 was much drier than 2006, and resulted in significantly higher $\delta^{15}N$ values.

In general, POM-$\delta^{15}N$ values during July–September 2007 on Fig. 5.3c showed similar ranges of values to those of Fig. 5.3b, with a slight decrease in values starting downstream of ~RM 90. However, the main difference between the perspectives to be gained from the two isoscapes is that Fig. 5.3c suggests a consistency in the $\delta^{15}N$ values downstream whereas Fig. 5.3b clearly shows that some mechanism is causing rapid oscillations. In short, based on this single comparison of intensively sampled synoptic vs fixed-site data, sampling at only six sites captured the main spatial trend (decreasing $\delta^{15}N$ values after RM 118) but failed to capture the oscillatory nature of POM-$\delta^{15}N$ values in the river along this reach. Given that >30 tributaries along this reach had measurable flow during August, it is not unreasonable to suppose that POM inputs from the tributaries might be the cause of some of the oscillations.

Plotting the data from Fig. 5.3a on some sort of base map as a series of different colored dots (e.g., Fig. 5.4), or as a thin ribbon with gradational changes in color, is much more effective in illustrating linkages of the isoscape to physical landscape features. For example, if a sudden change in POM-$\delta^{15}N$ in the river is noted just downstream of a tributary marked on the map, then one can hypothesize that inputs from the tributary helped cause the change. Linking changes at mainstem sites to inputs from the tributaries can be facilitated by also plotting the isotopic compositions of the tributaries on the map. Plotting the data on a LiDAR or Google Earth map might be even more effective.

On Fig. 5.4, POM-$\delta^{15}N$ values of tributary samples (grab samples collected slightly upstream of their confluences with the SJR) are plotted as colored rectangles using the same color choices as for mainstem sites. Many of the rectangles appear to be located at about the same location as the mainstem site. However, the mainstem samples were always collected just upstream of a significant tributary, so that the mainstem compositions were not unduly affected by unmixed point sources.

Rectangles were chosen for tributary symbols because they were not equant (like the mainstem symbols) and, by placing them on either side of the river, their shapes effectively indicate whether the tributary enters the river on the east or west side. There are distinct differences in sediments and land uses on different sides of the SJR, so knowing the geographic source of the tributary is important for the interpretation of the data.

It is interesting to note that the tributary samples almost always have lower POM-$\delta^{15}N$ values than mainstem samples immediately upstream. Hence, if POM loads from the tributaries were high enough (which they rarely are, except for the major tributaries: the Merced, Tuolumne, and the Stanislaus, labeled on Fig. 5.4), these inputs could cause sudden decreases in the mainstem POM-$\delta^{15}N$ values. Careful inspection of Fig. 5.3 shows that mainstem $\delta^{15}N$ values drop slightly near the confluences with Tuolumne River (RM 84) and the Stanislaus (RM 75), perhaps because of dilution by low-$\delta^{15}N$ POM from these rivers. However, the mainstem $\delta^{15}N$ values increase sharply near the confluence of the Merced River (RM 118),

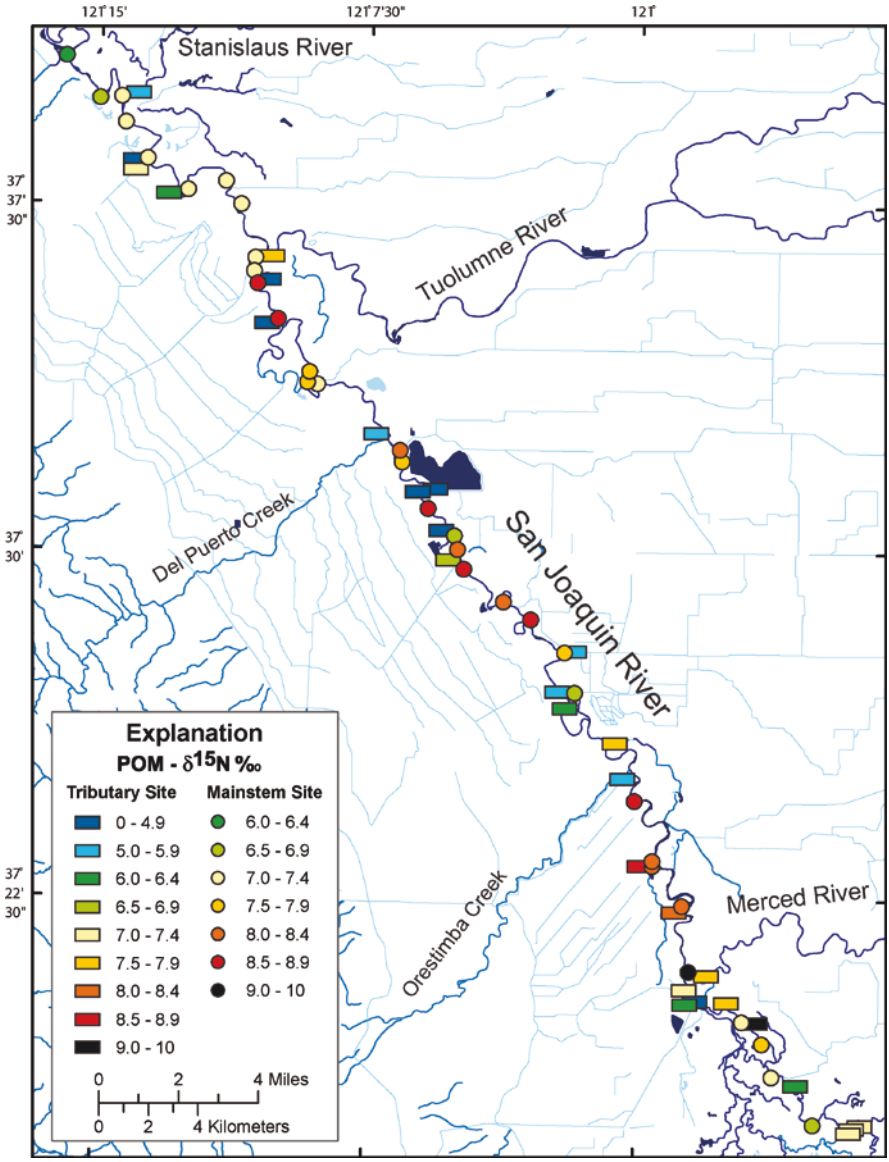

Fig. 5.4 Spatial distribution of POM-$\delta^{15}N$ values in the San Joaquin River collected during a synoptic in August 2007, plotted as a series of colored dots on a base map; these are the same data shown in Fig. 5.3a and b. $\delta^{15}N$ values for samples collected at the mouths of tributaries are plotted as *colored rectangles*. The positions of the rectangles relative to the San Joaquin River show whether the tributaries drain into the river from the E or W side. Fig. 5.4, see Appendix 1, Color Section

and stay high for several miles downstream. Since the POM from the Merced has significantly lower $\delta^{15}N$ values than downstream mainstem sites, addition of POM from the Merced cannot explain the high mainstem $\delta^{15}N$ values. Based on field observations and lab measurements, the likely cause of the high $\delta^{15}N$ values of POM (which, as always during the summer and fall, is almost entirely algal in origin) is an intense algal bloom caused by the input of clear water from the Merced into the high nutrient San Joaquin River (Kendall et al. 2008, unpublished).

Per discussions earlier, if mixing with POM from tributaries is the main cause of downstream changes in the $\delta^{15}N$ of POM, then contour plots Fig. 5.3b and c can be misleading because data from below the tributary were used to calculate compositions upstream of the tributary. Isoscapes like Fig. 5.4, that don't make implicit and possibly unwarranted assumptions about the connectivity of the isotopic compositions, are a very effective means for evaluating the causes of spatial changes observed during longitudinal synoptics of rivers, in specific for changes due to inputs from tributaries.

5.5.2.2 Example: Nitrate Isoscapes Along the River-Estuary Continuum

Figure 5.5 shows the spatial and temporal distributions of the nitrate $\delta^{15}N$ and $\delta^{18}O$ values from ~18 months of samples collected from ~ 35 sites distributed along the entire 170 miles of the river-estuary system, which extends from the current headwaters of the San Joaquin River in agricultural return waters in the Central Valley, through the delta of the San Joaquin and Sacramento Rivers, and across the northern San Francisco Bay to where the estuary drains into the Pacific Ocean. These transects show large ranges in nitrate $\delta^{15}N$ (~16‰) and $\delta^{18}O$ (~25‰). A detailed interpretation of these fascinating isoscapes is beyond the scope of this chapter, but a few observations are merited.

The nitrate $\delta^{15}N$ values upstream of ~RM 56 show spatial and temporal patterns roughly similar to those of POM-$\delta^{15}N$ (Fig. 5.3c). One prominent feature is the abrupt decrease in nitrate $\delta^{15}N$ at ~ RM 30, which is probably a result of tidal and pumping-induced mixing with water from the Sacramento River within the delta. The hot spots of high $\delta^{15}N$ values around RM 40 reflect excess nutrients derived from a nearby WWTP, the resulting massive algal blooms, and the consequent isotope fractionations caused by assimilation and nitrification. Downstream of this location, $\delta^{15}N$ values eventually increase because of mixing with higher-$\delta^{15}N$ marine-dominated waters (Kendall et al. 2008, unpublished).

The spatial patterns in nitrate $\delta^{18}O$ and $\delta^{15}N$ are very different (Fig. 5.5). First, spatial and temporal changes in $\delta^{15}N$ appear gradual and smooth, whereas $\delta^{18}O$ values appear temporally and spatially erratic, with frequent small oscillations in value. Some of the difference may be a result of two to three time higher analytical uncertainty of $\delta^{18}O$ compared to $\delta^{15}N$. $\delta^{18}O$ values decrease abruptly at about ~RM 30, at the same place as the $\delta^{15}N$ values decrease, and probably for the same reason: mixing.

The lack of correlation of $\delta^{15}N$ and $\delta^{18}O$ patterns suggests that these isotopes are "decoupled". Wankel et al. (2006) studied spatial changes in nitrate isotopes in the Bay, observed decoupled responses of $\delta^{15}N$ and $\delta^{18}O$ values, and explained the decoupling as the effect of N cycling (especially nitrification) in the Bay.

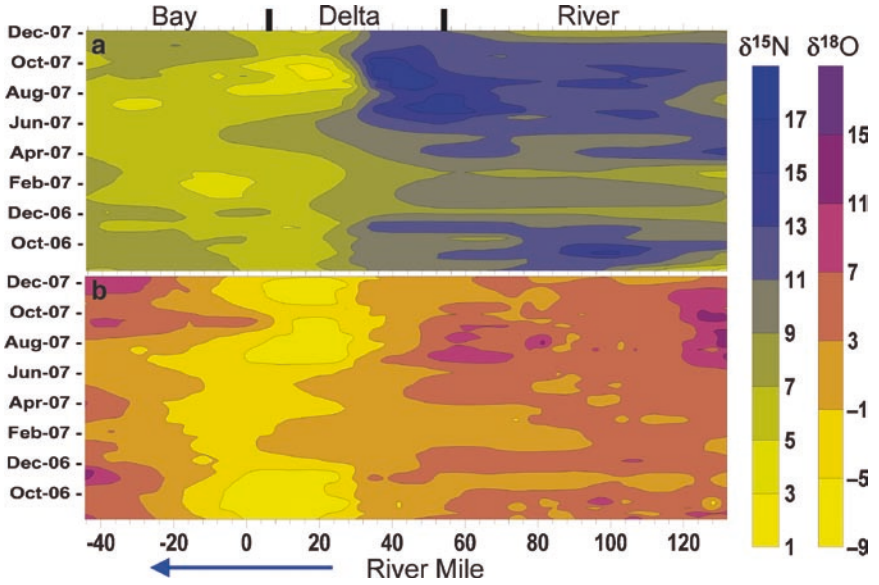

Fig. 5.5 Spatial and temporal distributions of nitrate $\delta^{15}N$ values (**a**) and nitrate $\delta^{18}O$ values (**b**) from 170 miles of river, extending from the headwaters of the San Joaquin River in agricultural return waters in the Central Valley, through the delta of the San Joaquin and Sacramento Rivers, and across the northern San Francisco Bay to where the estuary drains into the Pacific Ocean. The river miles are measured from where the river converges with the larger Sacramento River (=0). This plot reflects data from ~1,200 samples collected August 2006–December 2007). Fig. 5.5, see Appendix 1, Color Section

Nitrate samples derived from many of the tributaries to the SJR are also labeled with the distinctive isotopic signatures of nitrification, as are many samples collected near the Stockton WWTP (Kendall et al. 2008, unpublished). Therefore, nitrate derived from nitrification of ammonium is a major contributor to nitrate in the SJR, and there appears to be significant amounts of nitrate derived from nitrification in the delta associated with Sacramento River water.

Space limitations preclude further discussion of the use of isotopes as indicators of ecosystem processes, functions, and health in aquatic environments. This topic is discussed in several recent books focused on ecological applications of isotopes: Fry (2006), Michener and Lajtha (2007), Hobson and Wassenaar (2008), and Nagata and Miyajima (2008; in Japanese, with some figures labeled in English).

5.6 Conclusions

The incorporation of stable isotope techniques into regional and national water quality and environmental monitoring programs provides many benefits to both the programs and the investigators. Isotopes are a potentially powerful complement to monitoring and assessment programs aimed at quantifying and mitigating alterations

to ecosystems from human activities for many reasons. Locations exhibiting unusually high rates of biogeochemical cycling or elevated pollution levels usually have distinctive isotopic compositions that are suggestive or diagnostic of the reactions and pollution sources. Isotopes can be more effective at identifying hot spots and hot moments than concentrations alone because isotopic ratios may change even when concentrations don't. Hence, isotopes facilitate the identification of hot spots and moments that otherwise would not be apparent, thereby providing a valuable addition to standard chemical and hydrological mass balance methods.

Watersheds are characterized by spatial gradients, patchiness at all scales (Vannote et al. 1980), and temporal variability. In many studies at large scales, isotope hydrologists and biogeochemists have found that stable isotope data – collected at the appropriate temporal and spatial scale – usefully integrate the natural patterns of this organized world. With the increasing automation of isotope techniques, it is becoming ever easier to acquire the large sets of isotope data that make it easy to see the environmental patterns beyond the noise. Isoscapes provide a useful means for illustrating the nature of the temporal and spatial variations in isotopic composition at the landscape scale, and for generating hypotheses about causes of the patterns. Hence, isoscapes are effective tools for identifying large-scale environmental patterns and changes which may be critical to understanding ecosystem function and regulating existing or future anthropogenic impacts. They can also provide invaluable information about the sources of various contaminants impacting human use of water supplies in the basin.

Isotope techniques are especially valuable for tracing sources of nitrate and organic matter in rivers, as illustrated by several examples of how isotope measurements have been successfully integrated into regional and national-scale monitoring programs. To the investigator, perhaps the main advantage of piggybacking onto large-scale monitoring programs to obtain splits of samples is that the large sets of samples made possible by national monitoring programs are obvious candidates for use in detecting and assessing environmental changes. Other benefits include leveraging of resources by the savings in collection costs, that samples are commonly collected using more rigorous protocols than individual scientists are likely to afford, and that the program provides a comprehensive set of environmental data associated with the samples at no additional cost. This chapter provides suggestions of which isotope tools are especially useful for nutrient-related studies, guidelines on how to collect and archive samples for isotopic analysis, examples of their applications to environmental studies, and a discussion of how to prepare isoscapes using data from river synoptics and networks.

The development of isoscapes for different kinds of riverine isotope data poses several challenges, among which are the linear and unidirectional flow of water, the heterogeneity of sources and processes within rivers and watersheds, and the lack of geographic connectivity of isolated sampling sites in large regional studies. River datasets can be complicated because river-related data have explicit spatial and temporal relations. Even in cases where the spatial relations among river sampling points might remain constant (as in fixed-site monitoring programs), the temporal relations do not (e.g., temporal changes in flow and nutrient levels from different

point sources). There is a need for guidelines for how to incorporate spatial and temporal isotope data for river studies (for different isotopes, site types, and tributaries) into a GIS context, so that the combined dataset can be used for spatial/temporal modeling of water and constituent budgets, and the development and testing of remediation strategies.

Large-scale regional and national monitoring programs present an excellent opportunity for the development of new isotope studies aimed at examining broad patterns that are usually obscured by spatial and/or temporal variability in smaller-scale studies. Although this chapter focused on the integration of isotope techniques into large-scale river and watershed studies, there are many other opportunities for isotope researchers and isoscapes to bring new insights into other types of large-scale monitoring programs, including those focused on atmospheric deposition (e.g., NADP) and ecosystem health (e.g., EMAP). As more studies demonstrate the value of isotopes in large-scale monitoring programs, we hope to see these analyses eventually incorporated into routine monitoring plans.

References

Anderson C, Cabana G (2005) Delta N-15 in riverine food webs: effects of N inputs from agricultural watersheds. Can J Fish Aquat Sci 62:333–340

Anderson C, Cabana G (2006) Does $\delta^{15}N$ in river food webs reflect the intensity and origin of N loads from the watershed? Sci Total Environ 367:968–978

Bates AL, Orem WH, Harvey JW, Spiker EC (2002) Tracing sources of sulfur in the Florida Everglades. J Environ Qual 31:287–299

Battaglin WA et al (2001) Chemical and isotopic evidence of nitrogen transformation in the Mississippi River, 1997–98. Hydrol Process 15:1285–1300

Bowen GJ (2009) Statistical and geostatistical mapping of precipitation water isotope ratios. In: West JB, Bowen GJ, Dawson T, Tu KP (eds) Isoscapes: understanding movement, pattern, and process on Earth through isotope mapping. Springer, Berlin

Bullen TD, Kendall C (1998) Tracing of weathering reactions and water flowpaths: a multi-isotope approach. In: Kendall C, McDonnell JJ (eds) Isotope tracers in catchment hydrology. Elsevier Science, Amsterdam

Connolly RM, Guest MA, Melville AJ, Oakes JM (2003) Sulfur stable isotopes separate producers in marine food-web analysis. Oecologia 138:161–167

Coplen TB, Kendall C (2000) Stable hydrogen and oxygen isotope ratios for selected sites of the US Geological Survey's NASQAN and Benchmark surface-water networks. US Geol Surv Open-File Rep 00-160; 424

Elliott EM et al (2007) Nitrogen isotopes as indicators of NOx source contributions to atmospheric nitrate deposition across the midwestern and northeastern United States. Environ Sci Technol 41:7661–7667

Elliott EM et al. (2009) Dual nitrate isotopes in actively and passively collected dry deposition: utility for partitioning NOx sources, understanding reaction pathways, and comparison with isotopes in wet nitrate deposition. J Geophy Res-Biogeosciences (in press)

Finlay JC (2004) Patterns and controls of lotic algal stable carbon isotope ratios. Limnol Oceanogr 49:850–861

Finlay JC, Kendall C (2007) Stable isotope tracing of temporal and spatial variability in organic matter sources to freshwater ecosystems. In: Michener RH, Lajtha K (eds) Stable isotopes in ecology and environmental science, 2nd edn. Blackwell Publishing, p. 283–333

Finlay JC, Khandwala S, Power ME (2002) Spatial scales of carbon flow in a river food web. Ecology 83:1845–1859

Fry B (2006) Stable isotope ecology. Springer, New York

Harrington RR et al (1998) ^{15}N enrichment in agricultural catchments: field patterns and applications to tracking Atlantic salmon (*Salmo salar*). Chem Geol 147:281–294

Hebert CE, Wassenaar LI (2001) Stable nitrogen isotopes in waterfowl feathers reflect agricultural land use in western Canada. Environ Sci Technol 35:3482–3487

Hinckley ES, Kendall C, Loague K (2008) Not all water becomes wine: sulfur inputs as an opportune tracer of hydrochemical losses from vineyards. Water Resour Res 44:W00401. doi:10.1029/2007WR006672

Hitchon B, Krouse HR (1972) Hydrogeochemistry of the surface waters of the Mackenzie River drainage basin, Canada – III Stable isotopes of oxygen, carbon and sulphur. Geochim Cosmochim Acta 36:1337–1357

Hobson KA, Wassenaar LI (eds) (2008) Tracking animal migration with stable isotopes. Academic, Boston, MA

Kendall C, Coplen TB (2001) Distribution of oxygen-18 and deuterium in river waters across the United States. Hydrol Process 15:1363–1393

Kendall C, McDonnell JJ (eds) (1998) Isotope tracers in catchment hydrology. Elsevier Science Publishers p. 839

Kendall C, Stober QJ, Meyer P, Silva SR (1997) Spatial distributions of isotopic compositions of Gambusia and periphyton at REMAP marsh sites in the Everglades. [abs], in USGS Program on the South Florida Ecosystem. In: Proceedings of the technical symposium in Ft Lauderdale, Florida, August 25–27, 1997. USGS Open-File Report 97-385, pp 44–45

Kendall C, Silva SR, Kelly VJ (2001) Carbon and nitrogen isotopic compositions of particulate organic matter in four large river systems across the United States. Hydrol Proc 15:1301–1346

Kendall C, Elliott EM, Wankel SD (2007) Tracing anthropogenic inputs of nitrogen to ecosystems. In: Michener RH, Lajtha K (eds) Stable isotopes in ecology and environmental science, 2nd edn. Blackwell Publishing, p. 375–449

Kendall C, Young MB, Silva SR (2008) Determination of sources of organic matter and nutrients in the San Joaquin River. USGS Open File Report (unpublished)

Koerner W, Dambrine E, Dupouey JL, Benoit M (1999) Delta N-15 of forest soil and understorey vegetation reflect the former agricultural land use. Oecologia 121:421–425

Kohzu A et al (2008) Use of stable nitrogen isotope signatures of riparian macrophytes as an indicator of anthropogenic N inputs to river ecosystems. Environ Sci Technol 42(21):7837–7841. doi:10.1021/es801113k

Kratzer CR et al. (2004) Sources and transport of nutrients, organic carbon, and chlorophyll-a in the San Joaquin River upstream of Vernalis, California, during summer and fall, 2000 and 2001. USGS WRI 03-4127. 124 p. http://waterusgsgov/pubs/wri/wri034127/2/2009

McClain ME et al (2003) Biogeochemical hot spots and hot moments at the interface of terrestrial and aquatic ecosystems. Ecosystems 6:301–312

Michener RH, Lajtha K (eds) (2007) Stable isotopes in ecology and environmental science, 2nd edn. Blackwell Publishers, p. 592

Nagata T, Miyajima T (eds) (2008) Stable isotopes in environmental assessment of watersheds – progress towards an integrated approach. Kyoto University Press, 476 p (Japanese language)

Nriagu JO et al. (1991) Hydrosphere. In: Krouse HR, Grinenko V (eds) Stable isotopes: natural and anthropogenic sulphur in the environment. SCOPE 43, Wiley, Chichester

Saurer M et al (2004) First detection of nitrogen from NOx in tree rings: a 15N/14N study near a motorway. Atmos Environ 38:2779–2787

Stringfellow WT et al. (2008) San Joaquin River Up-Stream DO TMDL Project, ERP-02D-P63, 2321 p. http://www.eerp-pacific.org/2/2009

Vaccaro JJ, Maloy KJ (2006) A thermal profile method to identify potential ground-water discharge areas and preferred Salmonid habitats for long river reaches. USGS Scientific Investigations Report 2006–5136

Vannote RL et al (1980) The river continuum concept. Can J Fish Aquat Sci 37:130–137
Volkmar EC, Dahlgren RA (2006) Biological oxygen demand dynamics in the Lower San Joaquin River, California. Environ Sci Technol 40:5653–5660
Wadleigh MA, Blake DM (1999) Tracing sources of atmospheric sulphur using epiphytic lichens. Environ Pollut 106:265–271
Wadleigh MA, Schwarcz HP, Kramer JR (1996) Isotopic evidence for the origin of sulphate in coastal rain. Tellus 48B:44–59
Wang L, Okin GS, Macko SA (2009) Remote sensing of nitrogen and carbon isotope compositions in terrestrial ecosystems. In: West JB, Bowen GJ, Dawson T, Tu KP (eds) Isoscapes: understanding movement, pattern, and process on Earth through isotope mapping. Springer, Berlin
Wankel SD, Kendall C, Francis CA, Paytan A (2006) Nitrogen sources and cycling in the San Francisco Bay Estuary: a nitrate dual isotopic composition approach. Limnol Oceanogr 51(4):1654–1664
Welker JM (2000) Isotopic ($\delta^{18}O$) characteristics of weekly precipitation collected across the USA: an initial analysis with application to water source studies. Hydrol Process 14:1449–1464
Wunder MB (2009) Using isoscapes to model probability surfaces for determining geographic origins. In: West JB, Bowen GJ, Dawson T, Tu KP (eds) Isoscapes: understanding movement, pattern, and process on Earth through isotope mapping. Springer, Berlin

Chapter 6
Environment in Time and Space: Opportunities from Tree-Ring Isotope Networks

Steven W. Leavitt, Kerstin Treydte, and Liu Yu

6.1 Introduction

Light stable isotopes of plant organic matter are imprinted with a broad set of environmental effects contributing to the isotopic composition of precipitation and CO_2 available to the plant, and associated with subsequent biological mediation through the plant's role in evaporation, diffusion through stomata, photosynthesis and respiration. The most common strategies in studies investigating isotopes in plant matter are either to identify the strongest environmental signal in the plant isotope composition by empirical testing or to account for all factors influencing the isotope composition in more mechanistic analysis using available plant isotope fractionation models (e.g., Farquhar et al. 1982; Edwards and Fritz 1986; Roden et al. 1999). Additionally, it may often be useful to determine how the environmental variable of interest varies across a region or perhaps even how it has varied through time. The annual growth rings of trees provide an opportunity to meet all of these prospective objectives in isotopic studies with plants.

The most powerful feature of tree rings is that they can be individually dated to the exact year because regional climate can impose year-to-year variability in secondary xylem growth of trees. Methods of "crossdating" are used to match these patterns of wide and narrow rings among tree-ring series from the same tree and

S.W. Leavitt (✉)
Lab. of Tree-Ring Research, University of Arizona, Tucson, AZ, 85721, USA
e-mail: sleavitt@ltrr.arizona.edu

K. Treydte
Swiss Federal Research Institute WSL, CH-8903, Birmensdorf, Switzerland
e-mail: kerstin.treydte@wsl.ch

L. Yu
The State Key Laboratory of Loess and Quaternary Geology,
The Institute of Earth Environment, Chinese Academy of Sciences,
Xian 710075, PR China
e-mail: liuyu@loess.llqg.ac.cn

J.B. West et al. (eds.), *Isoscapes: Understanding Movement, Pattern, and Process on Earth Through Isotope Mapping*, DOI 10.1007/978-90-481-3354-3_6,

among trees at a site (Stokes and Smiley 1968; Fritts 1976; Schweingruber 1987). Crossdating thus provides confidence that contemporaneous rings are being analyzed in several trees when mean and variance of isotope composition are being quantified for a given year. It is also possible to identify features within tree rings that permit analysis at sub-annual scales, such as earlywood cells frequently formed in spring and early summer, and latewood cells formed in late summer (Fritts 1976). Another useful attribute of the growth rings is that they integrate isotopic signals from around the tree crown and may smooth out some of the high intra-crown variability associated with microenvironments (Leavitt and Long 1986). Most of the existing chronologies based on traditional tree-ring parameters such as tree-ring width or maximum latewood density are in temperate regions where ring boundaries are easily distinguishable because of the sharp contrast between growing season and winter dormant period (Schweingruber 1996). Depending on site history, tree species and available historic/fossil material, such chronologies can easily cover centuries or even more than a millennium back in time (e.g., Buentgen et al. 2006; Esper et al. 2007). In some cases they can even be much longer when living trees are supplemented with wood from historical structures and subfossil wood, such as the bristlecone pine chronology from the White Mts. of California (8,600 years, Ferguson and Graybill 1983) and German oak and pine (>12,000 years, Becker 1979; Friedrich et al. 2004).

Living trees are present throughout six of seven continents, and even the seventh continent Antarctica has fossil remains of trees millions of years old (Francis 1986). This extensive distribution has already been frequently used for regional to hemispheric climate reconstructions from ring width and maximum density networks (e.g., Briffa et al. 2002; Cook et al. 2004; Esper et al. 2002; Frank and Esper 2005). However, it offers many additional opportunities to develop large networks in which isotopic composition can be measured through time and therefore can provide added value beyond the reconstruction of traditional and single environmental parameters alone. Because isotopic differences are seen among tree species at a site (e.g., Stuiver and Braziunas 1987; Marshall and Monserud 1996, 2006; Saurer et al. 1997), it may nevertheless be preferable to develop a network with a single species, and several tree species are particularly widespread and their distribution covers millions of hectares. For example, *Pinus sylvestris* occurs over about 30° of latitude and 140° of longitude in Europe and Asia. *Pinus ponderosa* in North America ranges over 25° of latitude and 25° of longitude. Other examples of widespread species include *Pinus halepensis* in the Mediterranean region, *Picea glauca* in N. America, *Larix sibirica* and *Larix decidua* in Eurasia, various *Quercus* spp. in N. America, Eurasia and Africa, *Betula* spp. in N. America and Eurasia, *Prosopis* spp. in N. America, S. America, Africa, and *Pinus tabulaeformis* in N. Asia.

The isotopic composition in tree rings has been related to numerous environmental parameters (summary of models and relationships in McCarroll and Loader 2004), with growing examples of isotope data providing environmental information distinct from or stronger than that provided by ring-width analysis alone (e.g., Treydte et al. 2006). For example, $\delta^{13}C$ has been associated with temperature (Liu et al. 1996, 2002; Treydte et al. 2009) and light (McCarroll et al. 2003), and with various moisture

variables including precipitation (Gagen et al. 2006; Liu et al. 2004b), relative humidity (Saurer and Siegenthaler 1989; Hemming et al. 1998; Edwards et al. 2000), soil moisture (Dupouey et al. 1993), and drought (Leavitt and Long 1989a) through effects on stomatal conductance. The $\delta^{18}O$ and $\delta^{2}H$ values have primarily been associated with precipitation amount (Liu et al. 2004a, b, 2008; Treydte et al. 2006), relative humidity (Wright and Leavitt 2006), isotopic composition of precipitation (Robertson et al. 2001), and temperature (Burk and Stuiver 1981) through evaporation from the leaf and water-line influences, although some questions have been raised about the extent to which $\delta^{18}O$ and $\delta^{2}H$ values follow the same forcing (e.g., Waterhouse et al. 2002). Undoubtedly many of these environmental parameters are influencing isotope composition simultaneously, but reconstructions are most effective when a single parameter is dominant.

Thus tree-ring isotope networks may provide a multitude of useful spatial and temporal environmental data. Additionally, the isotope measurements in such network modes may provide more fundamental ecophysiological information in time and space such as C_i/C_a (intercellular to atmospheric [CO_2] ratio), A/g (photosynthetic rate/stomatal conductance rate), or intrinsic water-use efficiency (iWUE). However, it is worth noting that pollution (e.g., Martin and Sutherland 1990; Sakata and Suzuki 2000; Savard et al. 2005) and other disturbances might also influence tree physiology and tree-ring isotopes, and would normally be avoided unless networks were being developed to identify or quantify those disturbance effects (Savard et al. 2004; McDowell et al. 2003; Bukata and Kyser 2005). Furthermore, because many of these environmental parameters can possibly influence isotope composition simultaneously, the exactness of interpretation in terms of climate signals can also be limited and needs to be overcome by careful site selection (e.g., one environmental variable being dominant such as drought) or even by the application of multivariate models.

Several tree-ring isotope networks have already been developed. In a northern latitude $\delta^{13}C$ (whole wood) network of 26 sites including *Pinus*, *Larix* and *Picea* species extending from Scandinavia to Siberia (60–72°N, 11–168°E), Saurer et al. (2004) found a mean increase of iWUE of 19% from the 1861–1890 period to the 1961–1990 period. The same network was used to demonstrate the strong correlation of tree-ring $\delta^{18}O$ with precipitation $\delta^{18}O$, and to reveal a decline in $\delta^{18}O$ during the twentieth century despite increasing temperatures (Saurer et al. 2002). This was interpreted as possibly a result of increasing contribution of winter precipitation to the moisture used by the trees. These studies used five trees per site to ensure a site-representative isotopic value. Data from a network of five *Pinus sylvestris* sites (cellulose in four trees per site) spanning 10° of latitude in central Siberia along the Yenisei River also suggested an increase in iWUE over the twentieth century (Arneth et al. 2002). Other recent examples of tree-ring isotope networks include *Sabina* and *Picea* in the Qilian Mts. China (Liu et al. 2007a), *Pinus* and *Picea* in the U.S. Midwest (Leavitt 2007), and *Pinus ponderosa* in the U.S. Southwest (Leavitt et al. 2002).

This paper examines tree-ring isotope networks in various stages of development on three continents in greater detail to illustrate the methodologies, findings, successes and limitations of this approach.

6.2 Examples of Networks Around the World

6.2.1 Pinyon Pine in the U.S. Southwest

Development of early tree-ring $\delta^{13}C$ chronologies with dendrochronologically dated wood in the American Southwest utilized trees of the widespread pinyon pine group (Leavitt and Long 1988). Leavitt and Long (1988, 1989c) collected tree rings from 14 sites in six Southwestern states (Fig. 6.1) as part of an early systematic effort to quantify changes in atmospheric $\delta^{13}C$. Pinyon pine was chosen in part because of its widespread distribution, but also because of its typical occurrence in open-canopy woodlands thereby reducing the potential for biasing the signal in background air with ^{13}C-depleted, locally respired soil CO_2. For tree-ring studies a large number of trees are usually sampled (usually 15–20, but sometimes even more than 60), but because tree-ring chronologies had already been developed at these sites for earlier non-isotope studies, eight to ten trees were sampled for the isotope study. From these eight to ten trees, the "best" four trees, based on comparable age, comparable ring sizes, fewest missing rings, least distortion by branch scars, etc., were used to produce the site isotopic chronology. Initial testing with pinyon pine indicated four trees could accurately represent the isotope chronology of trees at a site (Leavitt and Long 1984).

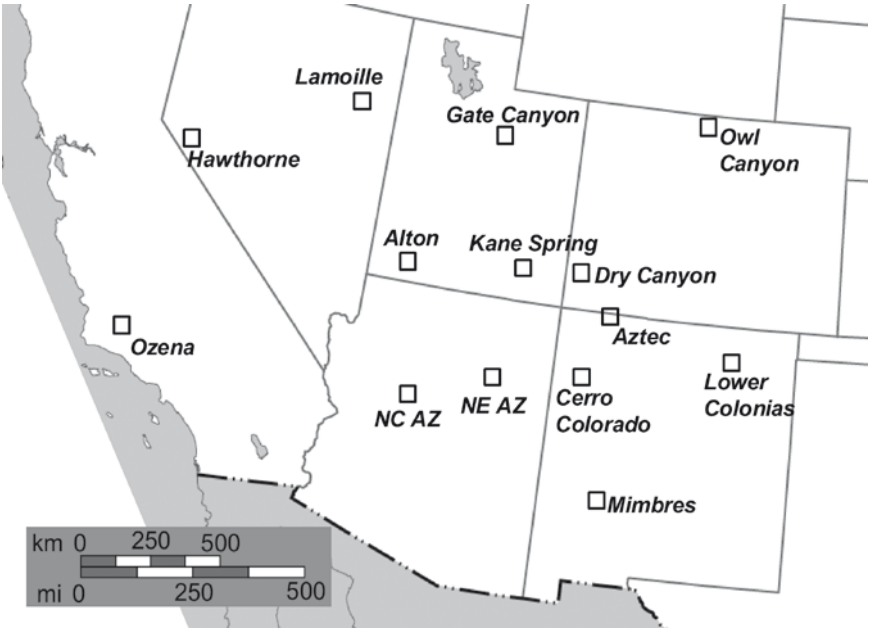

Fig. 6.1 Network of pinyon pine sites in the U.S. Southwest (from left clockwise, states are California, Nevada, Utah, Colorado, New Mexico and Arizona)

Because the primary goal of the study was related to quantifying long-term trends in $\delta^{13}C$ of atmospheric CO_2, the isotopic analysis was conducted on sequences of pentads (5-year ring groups 1800–1804, 1805–1809, etc). Analysis of ring pentads provides *de facto* smoothing of the isotope record because individual annual extreme values are suppressed, but it also reduces potential carryover effects of photosynthates fixed in 1 year but used in the latewood of the next ring (Helle and Schleser 2004; Kagawa et al. 2006). Furthermore, in an effort to reduce time and expense, the pentads from all trees were pooled prior to milling and chemical pretreatment. However, to estimate inter-tree isotope variability, every 50th year the pentads of each tree were analyzed separately, e.g., 1800–1804, 1850–1854, etc. (Leavitt and Long 1989b). To assure capture of an isotopic signal laid down in the year of ring formation and unaffected by mobility of chemical compounds in the wood, the holocellulose component of the tree rings was chemically isolated for analysis.

Common signals were being captured particularly well in the high-frequency domain of the isotope chronologies, in some cases among sites well over 500 km apart (Fig. 6.2). This indicates the presence of regional forcing in the tree-ring isotope composition, subsequently identified as a pervasive relationship with moisture: higher $\delta^{13}C$ values associated with moisture deficiency and lower $\delta^{13}C$ values associated with moisture excess (Leavitt and Long 1989a). The dryness/wetness conditions from each site's isotope chronology were assessed as deviations (calculated as ratios) from the long-term smoothed isotope trend. The algorithm also converts the higher-than-trend $\delta^{13}C$ values during dry pentads to negative values and lower-than-trend $\delta^{13}C$ values to positive values, generally from about −6 to +6, with values of 0 indicating the measured $\delta^{13}C$ value is the same as that of the smoothing curve. This range of isotope "drought indices" is therefore similar to that calculated instrumentally for the Palmer Drought Severity Index (PDSI) (Palmer 1965), which uses temperature and precipitation to estimate moisture conditions at a site as deviations from the long-term moisture average. Increasing PDSI negative values (−1 to −6) indicate dryness (drought), increasing positive values (+1 to +6) represent increasing moisture above normal, and values near 0 are considered to be normal moisture conditions.

Using the isotope network, maps have been developed presenting drought patterns in the Southwest based on isotope composition (Fig. 6.3). The isotope drought maps generally compare well with the instrumentally derived PDSI maps, which is highly promising given that the tree-ring records are from single sites, whereas PDSI is often tabulated on the basis of state climate subdivisions, a composite of many individual climate stations. Furthermore, the isotope maps can be thought of as representing leaf-level physiological response to many environmental parameters, but moisture effects appear to be dominant in this region. At the turn of the most recent century, the network was resampled to update the isotopic composition of all sites up to 1999, and the rings from 1985 to 1999 were individually analyzed to characterize the isotopic variability in the network on the annual timescale (Leavitt et al. 2007).

The 1740–1744 map depicts a pentad showing prevalent drought conditions in the eastern part of the network but near-normal or above normal moisture in the center and western sector (Fig. 6.3a). The drought index maps developed from more recent analysis for 1998 and 1999 (Fig. 6.3b) indicate excess moisture conditions

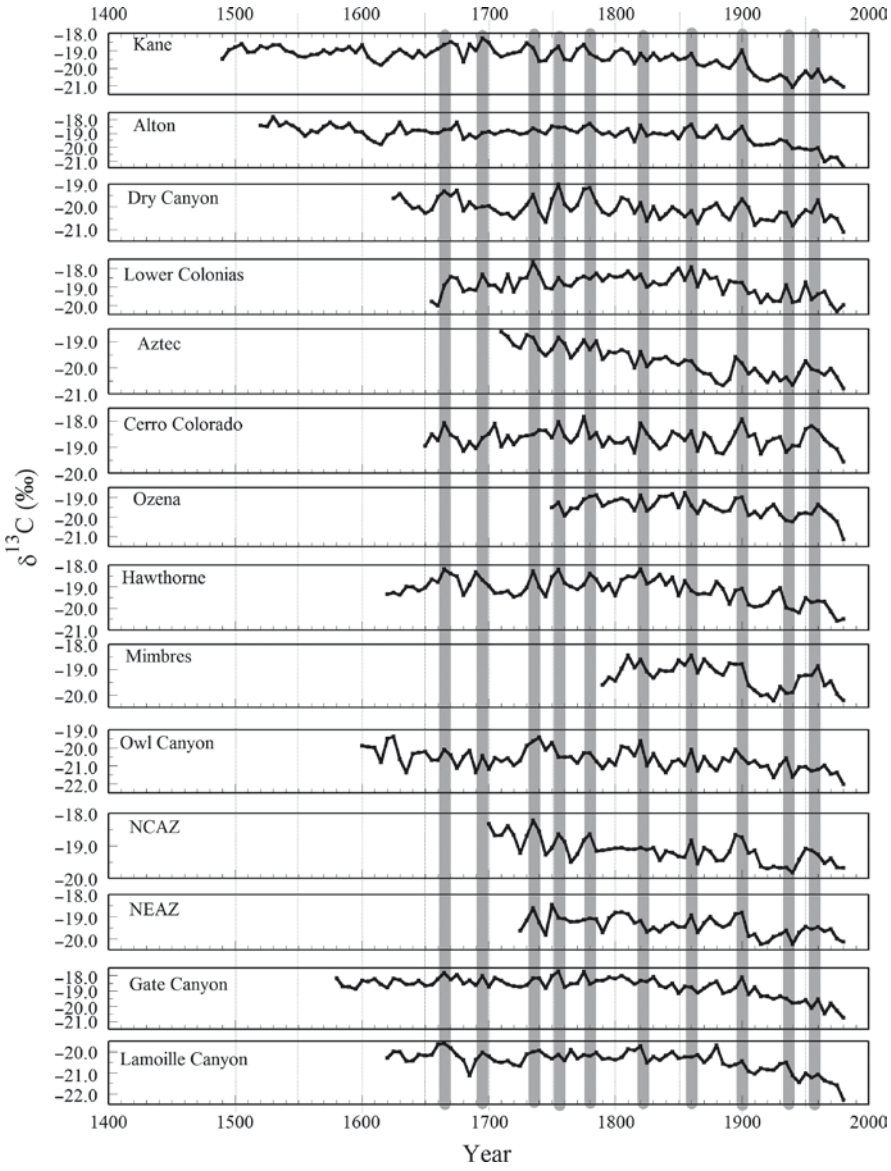

Fig. 6.2 $\delta^{13}C$ chronologies of holocellulose from pinyon pine tree-ring pentads around the U.S. Southwest. Shaded vertical bars link temporally coherent isotopic signatures among many of the sites

throughout much of the network in the 1998 growing season preceded by above-normal winter-spring moisture during the 1997–1998 "El Niño of the Century", but normal or below normal moisture throughout the network in the 1999 growing season preceded by below-normal winter-spring moisture from the strong 1998–1999 La Niña event. The full set of maps back to 1700 is available at NOAA World Data Center Paleoclimatology web site (http://www.ncdc.noaa.gov/paleo/treering/isotope/).

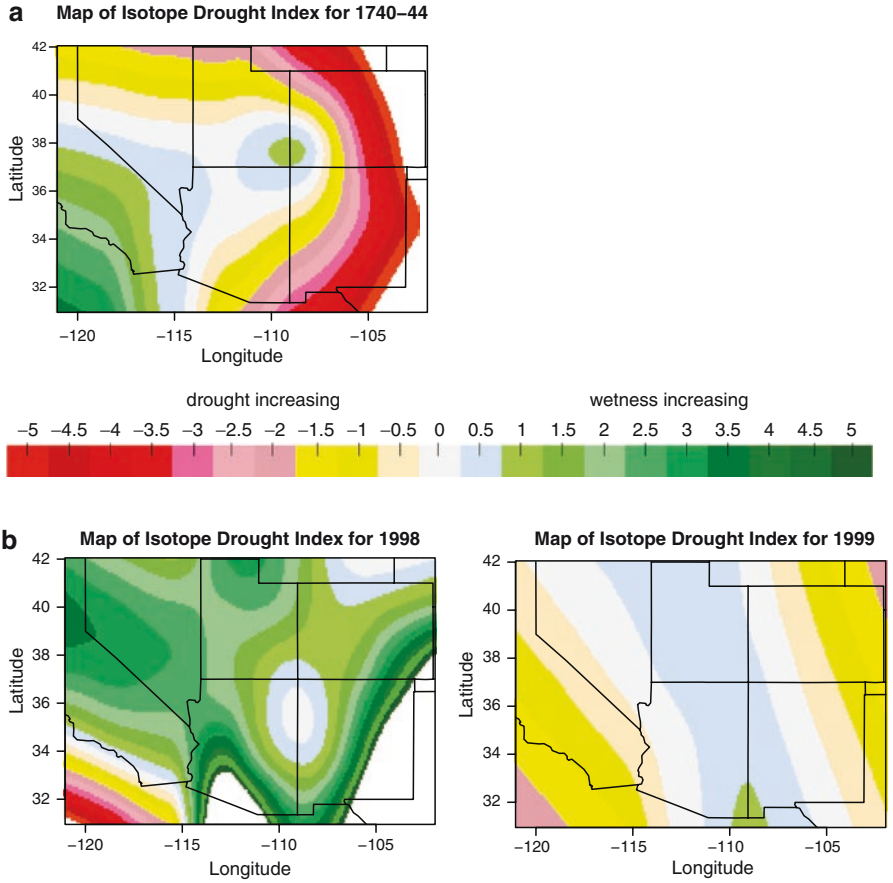

Fig. 6.3 Map of isotope "drought indices" from the initial pentad chronologies developed by Leavitt and Long (1989a) for 1740–44 (**a**) and for the more recently developed annual chronologies (Leavitt et al., 2007) for 1998 and 1999 (**b**). Maps of drought indices for 1998 when the Southwest had above-normal El Niño winter-spring precipitation prior to the 1998 growing season, and for the year 1999 when the Southwest had below-normal La Niña winter-spring prior precipitation. Outside the field of 14 sites, the high gradients of index change for 1740–44 and 1998 are extrapolations of trends within the network and may not be real; also the contouring is set to plot indices at an interval of 0.5 and only from −5 to +5. Fig. 6.3, see Appendix 1, Color Section

6.2.2 *China Tree-Ring Isotope Network – Example of Work in Progress*

An abundance of recently published individual tree-ring $\delta^{13}C$ and $\delta^{18}O$ studies around China collectively constitutes a *de facto* isotope network over about 15° of latitude and over 30° of longitude containing eight sites (Fig. 6.4). Although the fact that the isotope chronologies were developed independently by different study groups in China and the sites are spread over a wide range of climatic conditions

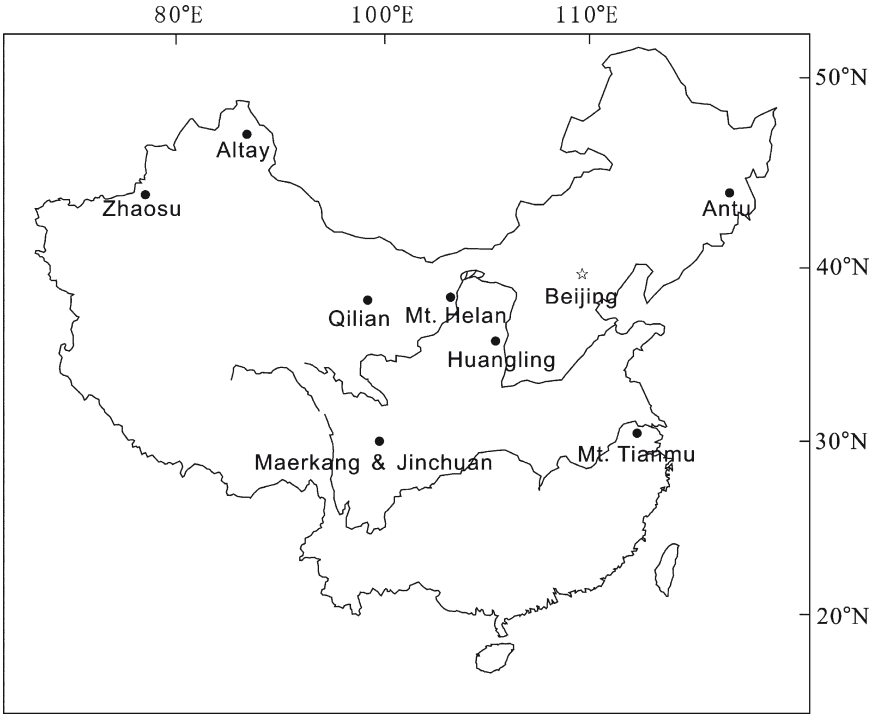

Fig. 6.4 Map of locations of tree-ring isotope chronologies in China

(westerlies to monsoonal climate), the results we highlight are roughly based on similar approaches and highlight the network potential. Generally, in all of these studies two increment cores from each of 20–60 trees were collected for crossdating to establish the ring-width chronology, and a third core was collected from 10 to 20 trees among the total for analysis of stable isotope composition. Usually four to ten cores (but in all cases at least two) with wider rings and fewer missing rings were then chosen and pooled for stable isotope analysis. The isotope series we selected here for presentation all represent cellulose analysis.

Although this collection of isotope studies has yet to be synthesized into a comprehensive ensemble depicting regional environment, examination of the available isotope chronologies demonstrates potential with respect to providing a variety of environmental information and investigation of relationships at different frequencies. Perhaps the most consistent and dramatic low-frequency feature of almost all tree-ring $\delta^{13}C$ series, regardless of region, is the generally decreasing trend since 1850–1900 (Fig. 6.5). At least part of this is attributable to input of ^{13}C-depleted CO_2 to the atmosphere from combustion of fossil fuel and land-use change. Other effects (e.g., climate), however, must be responsible for features such as the pre-1800 decline in trees at the Mt. Tianmu site and the rising then declining pattern in the twentieth century at the Maerkang and Jinchuan sites.

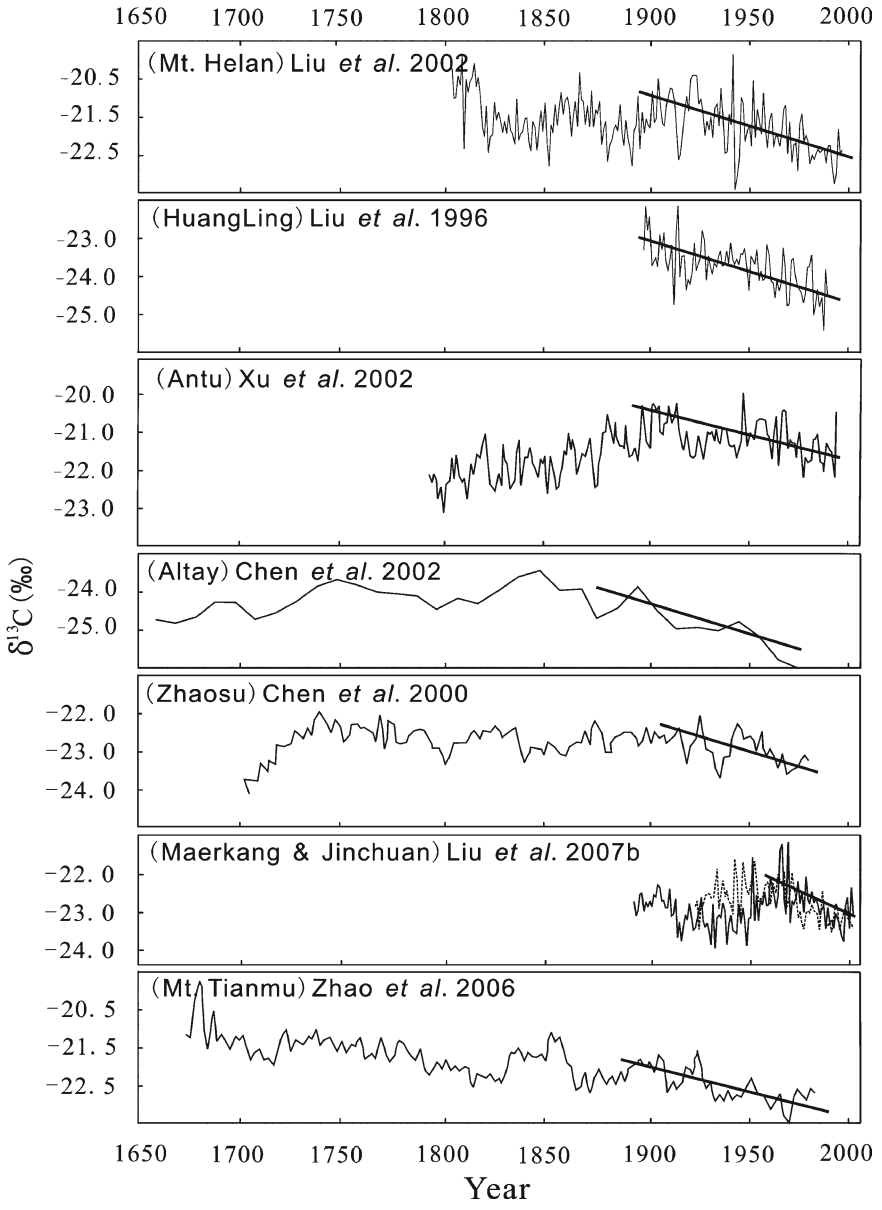

Fig. 6.5 Tree-ring $\delta^{13}C$ series from Chinese sites showing decline of recent decades. Species= *Pinus tabulaeformis* at Mt. Helan and Huangling, *Pinus koraiensis* at Antu, *Larix sibirica* at Altay, *Pinus schrenkiana* at Zhaosu, *Tsuga chinensis* (*solid line*) at Maerkang and *Pinus dendata* (*dashed line*) at Jinchuan, and *Cryptomeria fortunei* at Mt. Tianmu

Pinus tabulaeformis is one of the most widespread conifer species in China, commonly growing for hundreds of years and widely used in dendroclimatological studies. Liu and others studied the tree-ring α-cellulose $\delta^{13}C$ records at two sites, Huangling and Mt. Helan (Figs. 6.4 and 6.5) in north-central China, the results revealing that the discrimination ($\Delta^{13}C \approx \delta^{13}C_{air} - \delta^{13}C_{plant}$ and inversely correlated to $\delta^{13}C$) of *Pinus tabulaeformis* tree-ring cellulose correlated negatively with temperature variations (Liu et al. 1996, 2002), and positively with the total precipitation from February to July back to 1804 using linear regression ($R^2 = 0.415$, $R_{adj}^2 = 0.394$, $F = 19.88$, $P < 0.0001$), with best chronology replication for AD 1845–1991 (Liu et al. 2004b). The reconstruction shows annual to decadal wetness/dryness fluctuations. The $\delta^{18}O$ in tree-ring cellulose in the same areas correlated positively with the annual precipitation, especially with East Asian summer monsoon precipitation from May to August (Liu et al. 2004a; Liu et al. 2008). This correlation may be attributed to precipitation amount effects because precipitation amount is inversely related to precipitation $\delta^{18}O$ (Liu et al. 2004a). The $\delta^{18}O$ and $\delta^{13}C$ series from the Helan Mountain region show opposite trends in the low frequency, but no significant statistical correlation (Liu et al. 2008). The study at Mt. Helan demonstrates great potential for both $\delta^{18}O$ and $\delta^{13}C$ in tree rings with respect to providing long records of the East Asian summer monsoon variations in the past.

In Antu (Figs. 6.4 and 6.5), Jilin Province of northeastern China, the stable carbon and oxygen isotopic composition of *Pinus koraiensis* tree-ring cellulose was also investigated (Xu et al. 2002, 2003). This area in the westerly belt of the Northern Hemisphere is moist and cold, belonging to the mild temperate climate type. The $\Delta^{13}C$ series positively correlated with the combined climate index of temperature and humidity (TH) from May to August, whereas the $\delta^{18}O$ record was negatively correlated with the same index (Xu et al. 2002), and $\delta^{13}C$ was found to be significantly negatively correlated with mean low-cloud amount from May to July (Xu et al. 2003). The TH index from May to August in the last 200 years was reconstructed based on the regression equations between isotopic composition ($\Delta^{13}C$ and $\delta^{18}O$) and climatic parameters. Quasi-11-, 4-, and 2-year periods were detected in $\delta^{13}C$ and $\delta^{18}O$ series by power spectrum analysis.

In Xinjiang Province, western China, two tree-ring $\delta^{13}C$ series were reported (Zhaosu and Altay, Figs. 6.4 and 6.5). A clear relationship exists between the $\Delta^{13}C$ of *Pinus schrenkiana* and precipitation and relative humidity. Meanwhile, based on the functional relationship between $\Delta^{13}C$ and precipitation from previous June to current May, a 295-year precipitation series was reconstructed for Zhaosu region (Chen et al. 2000). Another 450-year tree-ring $\delta^{13}C$ chronology was developed from *Larix sibirica* in the Altay Region. Using the available temperature coefficient of tree-ring $\delta^{13}C$ (0.13–0.48‰°C^{-1}), a decrease of 0.67–2.46°C in the seventeenth century was reconstructed (Chen et al. 2002).

Elsewhere in western China, *Sabina przewalskii* and *Picea crassifolia* representing different tree functional types, can be found extensively. The relationship between iWUE and [CO_2] at the Maerkang and Jinchuan sites (Fig. 6.4) reveals that the *Picea* is more sensitive than the *Sabina przewalskii* to increasing [CO_2], suggesting a species-specific adaptation to long-term environmental changes (Liu et al. 2007a).

Correlations between the high-frequency variations in stable-carbon isotope discrimination and climate indicate similar intra-site responses to climate in both species, although the response strengths are different (Liu et al. 2007a).

In the temperate-moist region of China, the tree-ring $\delta^{13}C$ analysis of different tree species showed an inconsistent relationship between the raw $\delta^{13}C$ series in hemlock (*Tsuga chinensis*) and alpine pine (*Pinus densata*) in Maerkang (Fig. 6.5, solid line) and Jinchuan (Fig. 6.5, dashed line) (Liu et al. 2007b). However, after removing the low-frequency effects of declining atmospheric $\delta^{13}C$ of CO_2, the high-frequency (year-to-year) inter-series correlation of $\Delta^{13}C$ was high, indicating that $\Delta^{13}C$ of the two tree species was controlled by common environmental conditions. However, in this temperate-moist region, the $\Delta^{13}C$ was not controlled by a dominant single climatic parameter, so the optimal multiple-regression functions explained just 38.5% of the total variance. Therefore, the potential for using $\delta^{13}C$ alone to identify clear, reliable climatic signals from two species is limited.

In southeastern China, Zhao et al. (2006) determined the $\delta^{13}C$ annual series of three *Cryptomeria fortunei* trees in the West Tianmu Mountain (Figs. 6.4 and 6.5). During the period 1837–1982, the correlations among the three $\delta^{13}C$ series were significant, with $r_{12} = 0.47$, $r_{13} = 0.65$ and $r_{23} = 0.52$ ($p < 0.001$, $n = 146$), respectively. After removing the high frequencies from the original $\delta^{13}C$ series by using a polynomial function model, a significant correlation was observed among the three trees at low frequencies, with the correlation coefficient varying from 0.95 to 0.998. This suggested that high-frequency variations record climatic variations, whereas low-frequency trends reflect the variations related to the declining $\delta^{13}C$ values of atmospheric CO_2.

Although tree-ring isotope study areas in China are currently limited, they encompass most of the country and the number of new studies is increasing rapidly. Based on this evaluation of the available studies, we can see great potential especially in northern arid to semiarid regions of China for further studies of regional to large-scale climatic variations utilizing the tree-ring isotope chronologies presented above in more systematic network approaches.

6.2.3 European Isotope Network

Our final example presents a recently published isotope network of European tree ring chronologies (Treydte et al. 2007). Sixteen European isotope laboratories collaborated in the ISONET project (coordinator: G. Schleser, Research Centre Juelich, Germany) developing the first large-scale network of $\delta^{13}C$ and $\delta^{18}O$ from oak (*Q. petrea, Q. robur*), pine (*Pinus leucodermis, P. nigra, P. uncinata, P. sylvestris*) and cedar (*Cedrus atlantica*) tree rings, covering 23 sites from Finland to Morocco (33°–69°N/5°W–31°E) (Fig. 6.6a) (Treydte et al. 2007). The sampling design considered not only ecologically "extreme" sites, with a single climate factor predominantly determining tree growth, as required for ring width and wood density analyses (Frank and Esper 2005), but also temperate regions with diffuse

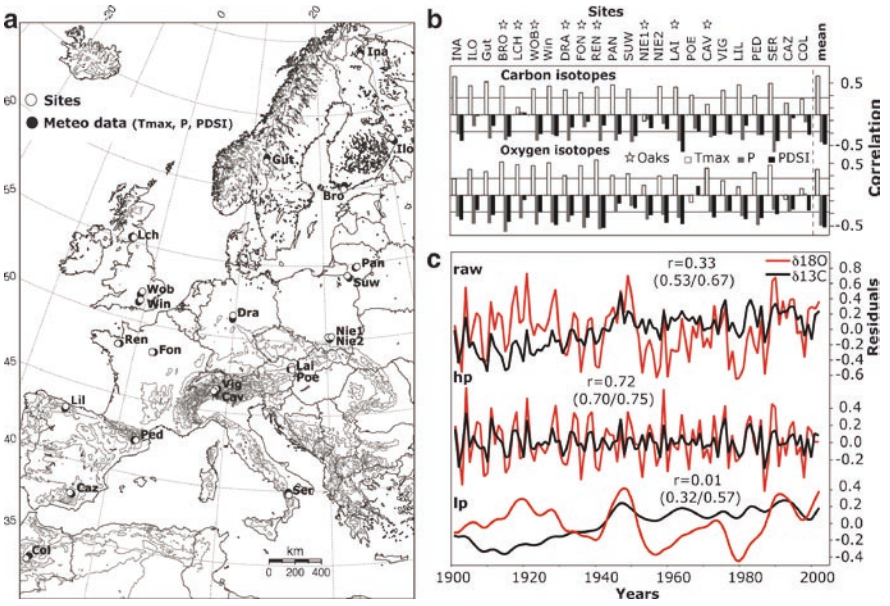

Fig. 6.6 (**a**) European tree sites and corresponding meteorological grid cells for the twentieth century with codes indicating site names; (**b**) site dependent June–August climate correlations of 'raw' carbon and oxygen isotope chronologies, with sites being latitudinally arranged (for detailed site information see Treydte et al. 2007); stars indicate oak sites (other sites are pine, and cedar in Morocco); 'mean' are correlations between mean isotope records averaged over all sites and mean meteorological data averaged over corresponding grid cells; lines are $p < 0.01$ significance levels; (**c**) 'European' carbon and oxygen isotope chronologies (each calculated by averaging site chronologies); 'raw' = residuals from 1901–1998 means, hp = high-pass filtered data; lp = low-pass filtered data; r = Pearson's correlation coefficient; numbers in brackets are r-values for the early AD 1901–1951 and the recent AD 1952–2002 period, respectively (from Treydte et al. 2007). Fig. 6.6, see Appendix 1, Color Section

climate signals recorded in the 'traditional' tree-ring parameters ring width and maximum latewood density. This strategy enabled expanding climatic reconstructions into regions not yet well covered. Climate variability is addressed on intra-annual to century timescales to allow understanding both, high-frequency variations including the exploration of seasonality signals and extreme events, and longer-term trends including source water/air mass changes and baseline variability across Europe.

At every site, ring widths were measured with 0.01 mm resolution and crossdated following standard procedures (Fritts 1976). At least four dominant trees per site (two cores per tree) were selected for isotope analysis, a number proven to be satisfactory to develop a population-representative isotope site record (Leavitt and Long 1984; McCarroll and Loader 2004; Gagen et al. 2004; Treydte et al. 2001, 2006). Criteria for sample selection were low numbers of missing rings and regular ring boundaries. Tree rings were separated year-by-year, and for oak only latewood was considered. For the majority of sites tree rings grown in the same year were pooled (Leavitt and

Long 1984; Treydte et al. 2001) prior to cellulose extraction and analysis (Boettger et al. 2007) to facilitate the development of this large network.

Raw $\delta^{13}C$ measurements were normalized to a pre-industrial atmospheric $\delta^{13}C$ base value of −6.4‰ using the tables in McCarroll and Loader (2004) derived from Francey et al. (1999). Signal strength analyses were conducted on high-pass and low-pass filtered data using cubic smoothing splines with 50% frequency-response cut-off at 10 years (Cook and Peters 1981).

Correlation between isotope ratios and climate variables was calculated using an updated version of the 0.5° × 0.5° gridded meteorological data set TS 2.1 of the Climate Research Unit (CRU, Norwich/UK). This grid provides homogenized monthly data of a large number of meteorological variables for the full twentieth century (1901–2002) (Mitchell and Jones 2005). Mean, minimum and maximum temperatures, precipitation, wet day frequencies and vapor pressure were tested, but here we present only results from the two variables leading to highest correlations, namely maximum temperatures and precipitation. Moreover a newly developed European 0.5° × 0.5° grid of monthly resolved Palmer Drought Severity Index data that are available for the same period (van der Schrier et al. 2006; Wells et al. 2004) was also tested. At every site, the closest grid cell was chosen and in cases of similar distance to the site, all relevant grid cells were tested and finally the one providing best results was used. It should be noted that in some cases correlations using single weather station records reveal higher correlation values, because artificial grid cells might sometimes not ideally represent local site conditions. To achieve best homogeneity in terms of data use and treatment when running analyses over the whole network, however, single cases of lower correlation were accepted as long as they did not contradict site internal results.

Despite different sources and fractionation processes driving C and O isotope values in tree rings, surprisingly strong similarities in the response of $\delta^{13}C$ and $\delta^{18}O$ networks to summer climate conditions were found. On a site basis, the strongest responses of both isotope parameters are found with climate variables for the year of tree-ring formation, displaying highest correlations with the summer months. Correlation signs of combined June–August (JJA) maximum temperature (positive), precipitation (negative) and PDSI (negative), respectively, are common at the majority of sites, despite the broad climatic and ecological range (Fig. 6.6b). Interestingly, signals are not only robust between sites but also between isotope parameters. Obviously they are linked through effects at the leaf level, mediated through variation in stomatal conductance caused by the combined effect of varying temperature and precipitation conditions.

Previous-year conditions do not have a strong effect on either carbon or oxygen isotope values. This finding was somewhat expected for the latewood cellulose from oak, but interestingly also holds for pine (whole ring cellulose) and, thus does not indicate substantial carry-over effects in conifers from remobilized reserves from previous summer (Kagawa et al. 2006; Helle and Schleser 2004).

A grand mean over all site records and a comparison with corresponding instrumental data provides an indication of the common climatic variance emphasized by combining numerous sites ("mean" in Fig. 6.6b). Notably the temperature signal in

the $\delta^{13}C$ network (r = 0.61) and the PDSI signal in the $\delta^{18}O$ network (r = −0.51) are higher than most individual site correlations. Comparisons of the 'European' $\delta^{13}C$ and $\delta^{18}O$ chronologies indicate strong and temporally robust similarity in the higher frequency domain. Discrepancies, however, can be found in the longer-term trends with increasing $\delta^{13}C$, particularly in the first half of the twentieth century, and more decadal variation in $\delta^{18}O$ (Fig. 6.6c) suggesting possible connection to cyclic modes of European precipitation/moisture.

To identify spatial and/or ecological coherence within the isotope networks, principal component analysis (PCA) was applied. The first five PCs containing 56% of the variance in the $\delta^{13}C$ and 57% of the variance in the $\delta^{18}O$ network were retained and subjected to Varimax Rotation (Richman 1986). Interestingly, the rotated principal components (RPC) of the $\delta^{18}O$ network are independent from species and allow the identification of four regional subsets: northern and eastern Central Europe, Scandinavia and the western Mediterranean. The identified sub-groups are identical for the RPCs derived from high pass filtered $\delta^{18}O$ records, and hence are robust over different frequencies. In contrast, RPC patterns of the $\delta^{13}C$ chronologies are much more diffuse and timescale dependent (not shown), a result that we attribute to more site-specific variance and/or complex long-term behavior of this parameter.

Comparison of the most relevant PCs with European climate field data (Fig. 6.7) revealed strongest influences of all climate variables during JJA on RPC1 (northern central Europe) and 3 (Scandinavia), and slightly shifted maximum temperature response seasons for RPC2 (eastern Europe) and 4 (Mediterranean). Generally, the spatial distribution of the highest loading sites nicely corresponds with the highest climate correlation patterns (see the colors in Fig. 6.7), which verifies the distinct regional climate modes being captured by each of the RPCs.

Altogether, temperatures yield the highest correlations and spatially the most homogenous patterns, which can be explained by the spatial homogeneity of this variable itself. Precipitation signals are patchier, but particularly for RPC1 correspond more closely to the region covered by the relevant tree sites. The PDSI patterns, especially for RPC1 and RPC3, cover the broadest areas, and appear relatively homogenous. This homogeneity is, however, partly affected by the coarser resolution of the PDSI grid and increased dependency of individual grid cells caused by the inclusion of temperature and soil type information (Dai et al. 2004).

The retrieved west–east and north–south gradients and the close association of tree-ring $\delta^{18}O$ with precipitation and temperature regimes support the theory of isotopic fractionation as a function of air mass sourcing (temperature of condensation) and air mass trajectory (Rozanski et al. 1993). The less distinct regional patterns in the $\delta^{13}C$ network, which are also wavelength dependent, as well as the discrepancies between $\delta^{13}C$ and $\delta^{18}O$ records in the low-frequency domain, are, however, not yet understood. It is possible that they are related to more local climatic and/or ecological conditions and trends, but could also result from long-term biases within the isotope records through individual age-related trends, site-dependent varying physiological response to increasing CO_2, or currently unexplainable noise (Treydte et al. 2001, 2006). Once the problem of differing long-term trends is solved, the approach of combining both isotopes may yield relationships that are less influenced by physiological disturbances, thereby further enhancing the climate signal.

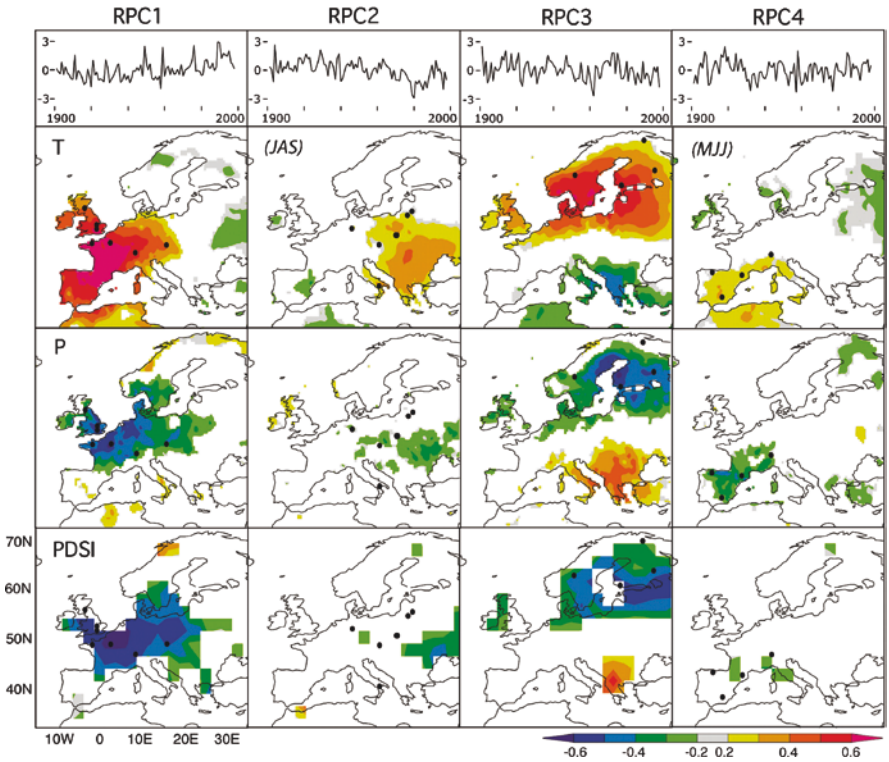

Fig. 6.7 Maps of sites with highest loading on varimax-rotated principal components, for the first four of five retained $\delta^{18}O$ chronology factors (RPC1-4) and corresponding spatial correlation fields maps for temperature (T), precipitation (P) and PDSI, calculated via the KMNI climate explorer (http://climexp.knmi.nl). Dots are sites with highest loadings at the corresponding RPCs (time series shown in the upper panel). Correlations were calculated with seasonal means of June to August (JJA), if not noted differently (JAS = July to September, MJJ = May to June). All calculations are based on the 1901–1998 common period (from Treydte et al. 2007). Fig. 6.7, see Appendix 1, Color Section

Based on the results described and such novel approaches, further studies will concentrate on reconstructing local to European scale climate variability over the past 400 years and at additional sites even over the past millennium, including multi-proxy approaches.

6.3 Discussion and Conclusions

The overall development of tree-ring isotope networks, like many other types of isotope networks (e.g., precipitation, stream hydrology), is still in its early stages. The examples presented here range from a conceptually and logistically advanced European network carefully designed at the outset for reconstruction of climate across the region over hundreds of years and sampled by a large consortium of

research groups, to the emerging (and expanding) China tree-ring network that is largely represented by independent development of isotope series for the specific studies by different groups. The U.S. Southwest network is somewhat intermediate in that it was the outcome of well-organized initial study by one research group examining a question of long-term isotopic trends, which was then re-focused to address regional climate.

These studies above are exclusively based on $\delta^{13}C$ and $\delta^{18}O$, but illustrate the bounty of information they contain related to moisture and temperature. Furthermore, linked together through stomatal pathways of CO_2 uptake and H_2O evaporation from leaves, the two isotope parameters often seem to exhibit surprisingly strong common high-frequency variation as was systematically demonstrated for the first time with the European approach. This fact particularly allows the identification of periods with environmental conditions most strongly influencing variations in stomatal conductance. Low-frequency variations, however, are often significantly different between both isotope parameters and might allow the identification of specific plant physiological processes related to increasing atmospheric CO_2 concentration (Treydte et al. 2009; McCarroll et al. 2009) and/or periods with independent response to different environmental variables (e.g., temperature, precipitation, changes in source water conditions/availability). Furthermore, when the isotope ratios contain stronger or different climate signals than obtained from reconstructions using ring widths or maximum latewood densities (e.g., Robertson et al. 1997, 2001), they can be combined with ring widths and densities in multi-parameter approaches, often incorporating mathematical methods such as EOF (empirical orthogonal function), to infer past climate parameters more accurately (Gagen et al. 2004, 2006; Kirdyanov et al. 2008; McCarroll et al., 2003; Robertson et al. 1997, 2001).

The isotopes of carbon and oxygen are also the easiest to analyze given the current state of chemical pretreatment options and mass-spectrometry. δ^2H analysis, however, is still often absent in such isotope studies and sometimes regarded as unlikely to contain any information beyond that from $\delta^{18}O$ because in principle the two isotopes in water generally follow similar pathways from the atmosphere to tree-ring cellulose. Yet, more and more evidence suggests that tree-ring δ^2H contains additional physiological and environmental signals not inherent in tree-ring $\delta^{18}O$, which are currently not yet fully understood (Waterhouse et al. 2002; M. Leuenberger, personal communication 2008), but perhaps related to more complex biosynthetic and enzymatic functions controlling isotopic fractionation for hydrogen. Promising new research suggests there may be separable climate and physiological signals in δ^2H of tree-ring cellulose (Augusti et al. 2006, 2008).

Many elements are considered in properly developing formal isotope networks (Table 6.1). Site selection, species selection and dating will commonly be at the forefront of all studies. With respect to site selection, inadvertent biasing of tree-ring isotope composition by effects of air pollution on physiology can be avoided by careful choice of sites. More generally, any sites where soil pH and nutrient (or toxin) concentrations vary in time regardless of source, could bias tree-ring isotope series. Local spatial heterogeneity as it affects isotopic fractionation, e.g., depth to water table or depth of soil zone, could also induce incongruous isotope records among

Table 6.1 Considerations for tree-ring isotope networks from modern trees

Consideration	Importance	Reason	How to accomplish
Site selection	High	Optimizes the strength of the environmental/ecophysiologic signal	Select locations where the parameter of interest is particularly dominant
Avoidance of pollution (if pollution is not the environmental parameter being investigated)	High	Pollution may negatively or positively bias metabolic performance of plants, including physiology related to isotope fractionation, e.g., stomatal conductance	Sites can be located distant from point sources of pollution and cities; sometimes air quality data may be available to better insure avoidance of this affect
Avoidance of other anthropogenic effects	High	Human disturbance, e.g., forest clearing and grazing, may influence growth and physiology related to isotope fractionation	Sites with known disturbance should be avoided
Dendrochronological dating	High	Ensures exact dates of isotope values compared within and between trees	Select species/location for which dating is likely
Number of trees at each site	High	Ensures isotopic value is representative of site	Analyze isotopes of three to six trees/site; number should be proved using EPS (McCarroll and Loader 2004) and inter-series correlation
Tree species	Potentially high	Using a single species could avoid physiological differences that affect isotopes among species	Select single widespread species and use for climate calibration and reconstruction
Environmental/ecophysiologic parameter of interest	High	Project questions are related to a specific parameter	Select species and location where the parameter of interest is particularly dominant
"Juvenile" or age-related effects	High (at least for carbon and hydrogen)	Early period of growth may be different than when the tree is mature, so isotopic composition in early rings may be anomalously more or less depleted because of non-climatic effects on fractionation; also general "age effects" might result from changing physiology as tree ages	Careful trend analyses to identify the length of the juvenile period; potentially statistical de-trending; isotope values from innermost rings might be excluded (Treydte et al. 2006; Gagen et al. 2007); rings of similar cambial age might be analyzed and compared to avoid general "age effects" (e.g., Marshall and Monserud 2006)

(continued)

Table 6.1 (continued)

Consideration	Importance	Reason	How to accomplish
Portion of ring to be analyzed (also relevant to "time-lag" effects)	Potentially high	Storage effects may result in significant time lag between photosynthesis and when the isotopic composition is incorporated into rings; therefore besides the more typical analysis of whole rings, other options might be preferred such as only earlywood, only latewood, or perhaps even latewood of one year + earlywood from the next	Separate rings according to scheme that works best for project goals; account for autocorrelation in the time series (Monserud and Marshall 2001)
Pooling then analysis and isotope chronology development OR separate development of chronologies from each tree and then averaging	High	Can save time and resources if rings from several trees are pooled prior to analysis, but statistical assessment of reconstructions is less certain if pooled.	Will probably depend on project goals, but at least some separate analysis of trees is needed to quantitatively assess inter-tree variability
Chemical pretreatment	Mixed	Ensures confidence that isotopic value represents the year of interest; analysis of single compound may reduce some uncertainties	Cellulose has long been advocated, but in recent years whole wood or whole wood with extractives removed by organic solvents have been advocated as producing effectively equivalent results, at least for $\delta^{13}C$, but probably not $\delta^{18}O$ (Battipaglia et al. 2008); with sub-fossil wood, however, cellulose may not be an option

trees at a site. However, such spatial variability is usually not visually evident, so sampling multiple trees will at least help to develop an inclusive isotopic record representing the common population signal at the site.

The goals and resources of a project in many cases will determine choices related to other considerations, such as pooling, chemical pretreatment and portion of the ring to be analyzed. Additionally, a number of other factors may need to be considered in project planning, data analysis or interpretation of results as related to age-related effects during both early and late stages of growth, timing of the environmental conditions that produce the isotopic signal relative to the time at which the isotopes are incorporated into the tree ring (e.g., storage effects), the possible influence of increasing atmospheric CO_2 concentration on isotope fractionation (McCarroll et al. 2009; Treydte et al. 2009), and methods of standardization to remove trends in the records. Standardization may also be important because of differences in average isotope composition among species, at least for carbon isotopes (e.g., Stuiver and Braziunas 1987).

In the end, besides serving as basic networks to provide slices of regional moisture and temperature conditions through time, the findings in these networks may contribute to broader questions such as the history of atmospheric circulation patterns (e.g., the Asian monsoon), the regional accumulation of biomass through time, and sensitivities of species to different past climate conditions to better forecast future performance under global climate change. If the challenging problems related to dating can be overcome, in the future data from lowland tropical forests on four continents might eventually be enlisted into tree-ring isotope networks. Given many widely distributed tree species around the globe, these networks are likely to proliferate either as part of a focused effort or an assemblage of independent studies that can be combined into a network. As an example for ongoing studies that point in such directions mentioned above, we want to mention a new European tree-ring isotope network initiative with 1,000-year chronologies, that is already underway as part of the Millennium European climate project (http://geography.swansea.ac.uk/millennium/index.htm).

Finally, for such purposes a public domain database of available tree-ring isotope series would be particularly useful, much like the current International Tree-Ring Data Bank (ITRDB 2009) of ring-width data. This might eventually lead to global tree-ring isotope networks, the closest to reality of which is the growing number of studies finding $\delta^{13}C$ trends over the last 200 years consistent with an increase in intrinsic water-use efficiency as atmospheric CO_2 concentrations rise (e.g., Feng 1999; Saurer et al. 2004; Waterhouse et al. 2004).

References

Arneth A, Lloyd J, Šantrůčková H, Bird M, Grigoryev S, Kalaschnikov YN, Gleixner G, Schulze E-D (2002) Response of central Siberian Scots pine to soil water deficit and long-term trends in atmospheric CO_2 concentration. Global Biogeoch Cycles 16(1):1005. doi:10.1029/2000GB001374

Augusti A, Betson TR, Schleucher J (2006) Hydrogen exchange during cellulose synthesis distinguishes climatic and biochemical isotope fractionations in tree rings. New Phytol 172:490–499

Augusti A, Betson TR, Schleucher J (2008) Deriving correlated climate and physiological signals from deuterium isotopomers in tree rings. Chem Geol 252:1–8

Battipaglia G, Jaeggi M, Saurer M, Siegwolf RTW, Cotrufo MF (2008) Climatic sensitivity of $\delta^{18}O$ in the wood and cellulose of tree rings: results from a mixed stand of *Acer pseudoplatanus* L. and *Fagus sylvatica* L. Palaeogeogr Palaeoclimatol Palaeoecol 261:193–202

Becker B (1979) Holocene tree-ring series from southern central Europe for archaeological dating, radiocarbon calibration, and stable isotope analysis. In: Berger R, Suess HE (eds) Radiocarbon dating. University of California Press, Berkeley, CA

Boettger T, Haupt M, Knöller K, Weise SM, Waterhouse JS, Rinne KT, Loader NJ, Sonninen, E Jungner H, Masson-Delmotte V, Stievenard M, Guillemin M-T, Pierre M, Pazdur A, Leuenberger M, Filot M, Saurer M, Reynolds CE, Helle G, Schleser GH (2007) Wood cellulose preparation methods and mass spectrometric analyses of $\delta^{13}C$, $\delta^{18}O$, and nonexchangeable $\delta^{2}H$ values in cellulose, sugar, and starch: an interlaboratory comparison. Anal Chem 79:4603–4612

Briffa KR, Osborn TJ, Schweingruber FH, Jones PD, Shiyatov SG, Vaganov EA (2002) Tree-ring width and density data around the Northern Hemisphere: part 2, spatio-temporal variability and associated climate patterns. Holocene 12:759–789

Buentgen U, Frank DC, Nievergelt D, Esper J (2006) Summer temperature variations in the European Alps, A.D. 755–2004. J Clim 19:5606–5623

Bukata AR, Kyser TK (2005) Response of the nitrogen isotopic composition of tree-rings following tree-clearing and land-use change. Environ Sci Technol 39:7777–7783

Burk RL, Stuiver M (1981) Oxygen isotope ratios in trees reflect mean annual temperature and humidity. Science 211:1417–1419

Chen T, Qin D, Li J, Ren J, Liu X, Sun W (2000) Study on climatic significance of fir tree-ring $\delta^{13}C$ from Zhaosu country of Xinjiang region, China. J Glaciol Geocryol 22(4):347–352

Chen T, Qin D, Liu X, Li J, Ren J, Sun W (2002) Tree-ring $\delta^{13}C$ records in the Little Ice Age in Altay prefecture of Xinjiang region. J Glaciol Geocryol 24(1):83–86

Cook ER, Peters K (1981) The smoothing spline: a new approach to standardizing forest interior tree-ring width series for dendroclimatic studies. Tree-Ring Bull 41:45–53

Cook ER, Woodhouse C, Eakin CM, Meko DM, Stahle DW (2004) Long-term aridity changes in the western United States. Science 306:1015–1018

Dai A, Trenberth KE, Qian T (2004) A global data set of Palmer Drought Severity Index for 1870–2002: relationship with soil moisture and effects of surface warming. J Hydrometeorol 5:1117–1130

Dupouey J-L, Leavitt S, Choisnel E, Jourdain S (1993) Modelling carbon isotope fractionation in tree rings based on effective evapotranspiration and soil water status. Plant Cell Environ 16:939–947

Edwards TWD, Fritz P (1986) Assessing meteoric water composition and relative humidity from ^{18}O and ^{2}H in wood cellulose: paleoclimatic implications for southern Ontario, Canada. Appl Geochem 1:715–723

Edwards TWD, Graf W, Trimborn P, Stichler W, Lipp J, Payer HD (2000) $\delta^{13}C$ response surface resolves humidity and temperature signals in trees. Geochim Cosmochim Acta 64:161–167

Esper J, Cook ER, Schweingruber FH (2002) Low-frequency signals in long tree-ring chronologies for reconstructing of past temperature variability. Science 295:2250–2253

Esper J, Frank DC, Büntgen U, Verstege A, Luterbacher J, Xoplaki E (2007) Long-term drought severity variations in Morocco. Geophys Res Lett 34, doi: 10.1029/2007GL030844

Farquhar GD, O'Leary MH, Berry JA (1982) On the relationship between carbon isotope discrimination and intercellular carbon dioxide concentration in leaves. Aust J Plant Physiol 9:121–137

Feng X (1999) Trends in intrinsic water-use efficiency of natural trees for the past 100–200 years: a response to atmospheric CO2 concentration. Geochim Cosmochim Acta 63:1891–1903

Ferguson CW, Graybill DA (1983) Dendrochronology of bristlecone pine: a progress report. Radiocarbon 24:287–288

Francis JE (1986) Growth rings in Cretaceous and Tertiary wood from Antarctica and their palaeoclimatic implications. Palaeontology 29(4):665–684

Francey RJ, Allison CE, Etheridge DM, Trudinger CM, Enting IG, Leuenberger M, Langenfelds RL, Michel E, Steele LP (1999) A 1000-year high precision record of $\delta^{13}C$ in atmospheric CO_2. Tellus 51B:170–193

Frank D, Esper J (2005) Temperature reconstructions and comparisons with instrumental data from a tree-ring network for the European Alps. Int J Climatol 25:1437–1454

Friedrich M, Remmele S, Kromer B, Hofmann J, Spurk M, Kaiser KF, Orcel C, Küppers M (2004) The 12,460-year Hohenheim oak and pine tree-ring chronology from central Europe—a unique annual record for radiocarbon calibration and paleoenvironment reconstructions. Radiocarbon 46:1111–1122

Fritts HC (1976) Tree rings and climate. Academic, New York

Gagen M, McCarroll D, Edouard JL (2004) Latewood width, maximum density, and stable carbon isotope ratios of pine as climate indicators in a dry subalpine environment, French Alps. Arct Antarct Alp Res 36:166–171

Gagen M, McCarroll D, Edouard J-L (2006) Combining ring width, density, and stable carbon isotope proxies to enhance the climate signal in tree-rings: an example from the southern French Alps. Clim Change 78:363–379

Gagen M, McCarroll D, Loader NJ, Robertson I, Jalkanen R, Anchukaitis KJ (2007) Exorcising the 'segment length curse': summer temperature reconstruction since AD 1640 using non-detrended stable carbon isotope ratios from pine trees in northern Finland. Holocene 17:435–446

Helle G, Schleser GH (2004) Beyond CO_2-fixation by Rubisco – an interpretation of $^{13}C/^{12}C$ variations in tree rings from novel intra-seasonal studies on broad-leaf trees. Plant Cell Environ 27:367–380

Hemming DL, Switsur VR, Waterhouse JS, Heaton THE, Carter AHC (1998) Climate variation and the stable carbon isotope composition of tree ring cellulose: an intercomparison of *Quercus robur, Fagus sylvatica* and *Pinus silvestris*. Tellus 50B:25–33

ITRDB, International Tree-Ring Data Bank (2009) IGBP PAGES/World Data Center for Paleoclimatology. NOAA/NCDC Paleoclimatology Program, Boulder, Colorado, USA. http://www.ncdc.noaa.gov/paleo/treering.html Jan. 20, 2009

Kagawa A, Sugimoto A, Maximov TC (2006) Seasonal course of translocation, storage, and remobilization of ^{13}C pulse-labeled photoassimilate in naturally growing *Larix gmelinii* saplings. New Phytol 171:793–804

Kirdyanov AV, Treydte K, Nikolaev A, Helle G, Schleser GH (2008) Climate signals in tree-ring width, density and $\delta^{13}C$ from larches in Eastern Siberia. Chem Geol . doi:10.1016/j.chemgeo.2008.01.023

Leavitt SW (2007) Regional expression of the 1988 U.S. Midwest drought in seasonal $\delta^{13}C$ of tree rings. J Geophys Res-Atmos 112, D06107, doi:10.1029/2006JD007081

Leavitt SW, Long A (1984) Sampling strategy for stable carbon isotope analysis of tree rings in pine. Nature 311:145–147

Leavitt SW, Long A (1986) Stable-carbon isotope variability in tree foliage and wood. Ecology 67:1002–1010

Leavitt SW, Long A (1988) Stable carbon isotope chronologies from trees in the southwestern United States. Global Biogeochem Cycles 2:189–198

Leavitt SW, Long A (1989a) Drought indicated in carbon-13/carbon-12 ratios of southwestern tree rings. Water Resour Bull 25:341–347

Leavitt SW, Long A (1989b) Intertree variability of $\delta^{13}C$ in tree rings. In: Rundel PW, Ehleringer JR, Nagy KA (eds) Stable isotopes in ecological research. Springer-Verlag, New York, Chapter 7

Leavitt SW, Long A (1989c) The atmospheric $\delta^{13}C$ record as derived from 56 pinyon trees at 14 sites in the southwestern U.S. Radiocarbon 31:469–474

Leavitt SW, Wright WE, Long A (2002) Spatial expression of ENSO, drought and summer monsoon in seasonal $\delta^{13}C$ of ponderosa pine tree rings in southern Arizona and New Mexico. J Geophys Res 107 (D18) 4349, doi:10.1029/2001JD001312

Leavitt SW, Chase TN, Rajagopalan B, Lee E, Lawrence PJ, Woodhouse CA (2007) Southwestern U.S. drought maps from pinyon tree-ring carbon isotopes. Eos Tran Am Geophys Union 88(4):39–40

Liu W, Feng X, Liu Y, Zhang Q, An Z (2004a) $\delta^{18}O$ values of tree rings as a proxy of monsoon precipitation in arid Northwest China. Chem Geol 206:73–80

Liu X, Shao X, Liang E, Zhao L, Chen T, Qin D, Ren J (2007a) Species-dependent responses of juniper and spruce to increasing CO_2 concentration and to climate in semi-arid and arid areas of northwestern China. Plant Ecol 193:195–209

Liu X, Shao X, Wang L, Zhao L, Wu P, Chen T, Qin D, Ren J (2007b) Climatic significance of the stable carbon isotope composition of tree-ring cellulose: comparison of Chinese hemlock (*Tsuga chinensis* Pritz) and alpine pine (*Pinus densata* Mast) in a temperate-moist region of China. Sci China Ser D 50(7):1076–1085

Liu Y, Leavitt S, Wu X, Hughes M (1996) Stable carbon isotope in tree rings from Huangling, China, and climatic variation. Sci China Ser D 39(2):152–161

Liu Y, Ma L, Cai Q, An Z, Liu W, Gao L (2002) Reconstruction of summer temperature (June-August) at Mt. Helan, China, from tree-ring stable carbon isotope values since AD 1890. Sci China Ser D 45(12):1127–1136

Liu Y, Ma L, Leavitt S, Cai Q, Liu W (2004b) Seasonal precipitation reconstruction from tree-ring stable carbon isotopes for Mt. Helan, China since AD 1800. Glob Planet Change 41:229–239

Liu Y, Cai Q, Liu W, Yang Y, Sun J, Song H, Li X (2008) Monsoon precipitation variation recorded by tree-ring $\delta^{18}O$ in arid Northwest China since 1878 AD. Chem Geol . doi:10.1016/j.chemgeo.2008.01.024

Marshall JD, Monserud RA (1996) Homeostatic gas-exchange parameters inferred from $^{13}C/^{12}C$ in tree rings of conifers. Oecologia 105:13–21

Marshall JD, Monserud RA (2006) Co-occurring species differ in tree-ring $\delta^{18}O$ trends. Tree Physiol 26:1055–1066

Martin B, Sutherland EK (1990) Air pollution in the past recorded in width and stable carbon isotope composition of annual growth rings of Douglas-fir. Plant Cell Environ 13:839–844

McCarroll D, Loader NJ (2004) Stable isotopes in tree rings. Q Sci Rev 23:771–801

McCarroll D, Jalkanen R, Hicks S, Tuovinen M, Gagen M, Pawellek F, Eckstein D, Schmitt U, Autio J, Heikkinen O (2003) Mulitproxy dendroclimatology: a pilot study in northern Finland. Holocene 13:829–838

McCarroll D, Gagen MH, Loader NJ, Robertson I, Anchukaitis KJ, Los S, Young GHF, Jalkanen R, Kirchhefer A, Waterhouse JS (2009) Correction of tree ring stable carbon isotope chronologies for changes in the carbon dioxide content of the atmosphere. Geochim Cosmochim Acta 73:1539–1547

McDowell NG, Brooks JR, Fitzgerald SA, Bond BJ (2003) Carbon isotope discrimination and growth response of old *Pinus ponderosa* trees to stand density reductions. Plant Cell Environ 26:631–644

Mitchell TD, Jones PD (2005) An improved method of constructing a database of monthly climate observations and associated high-resolution grids. Int J Climatol 25:693–712

Monserud RA, Marshall JD (2001) Time-series analysis of $\delta^{13}C$ from tree rings. I. Time trends and autocorrelation. Tree Physiol 21:1087–1102

Palmer WC (1965) Meteorological drought. Research Paper No. 45, US Weather Bureau (NOAA Library and Information Services Division, Washington, DC 20852)

Richman MB (1986) Rotation of principal components. J Clim 6:293–335

Robertson I, Rolfe J, Switsur VR, Carter AHC, Hall MA, Barker AC, Waterhouse JS (1997) Signal strength and climate relationships in $^{13}C/^{12}C$ ratios of tree ring cellulose from oak in southwest Finland. Geophys Res Lett 24:1487–1490

Robertson I, Waterhouse JS, Barker AC, Carter AHC, Switsur VR (2001) Oxygen isotope ratios of oak in east England: implications for reconstructing the isotopic composition of precipitation. Earth Planet Sci Lett 191:21–31

Roden JS, Lin G, Ehleringer JR (1999) A mechanistic model for interpretation of hydrogen and oxygen isotope ratios in tree ring cellulose. Geochim Cosmochim Acta 64:21–35

Rozanski K, Arguas-Arguas L, Gonfiantini R (1993) Isotopic patterns in modern global precipitation. In: Swart PK et al. (eds) Climate change in continental isotopic records. Geophys Monogr 78:1–36

Sakata M, Suzuki K (2000) Evaluating causes for the decline of Japanese fir (*Abies firma*) forests based on $\delta^{13}C$ records of annual growth rings. Environ Sci Technol 33:373–376

Saurer M, Siegenthaler U (1989) $^{13}C/^{12}C$ ratios in tree are sensitive to relative humidity. Dendrochronologia 7:9–13

Saurer M, Aellen K, Siegwolf R (1997) Correlating $\delta^{13}C$ and $\delta^{18}O$ in cellulose of trees. Plant Cell Environ 20:1543–1550

Saurer M, Schweingruber F, Vaganov EA, Shiyatov SG, Siegwolf R (2002) Spatial and temporal oxygen isotope trends at the northern tree-line in Eurasia. Geophys Res Lett 29. doi:10.1029/2001GL013739

Saurer M, Siegwolf RTW, Schweingruber FH (2004) Carbon isotope discrimination indicates improving water-use efficiency of trees in northern Eurasia over the last 100 years. Glob Chang Biol 10:2109–2120

Savard MM, Begin C, Parent M, Smirnoff A, Marion J (2004) Effects of smelter sulfur dioxide emissions: a spatiotemporal perspective using carbon isotopes in tree rings. J Environ Qual 33:13–25

Savard MM, Bégin C, Smirnoff A, Marion J, Sharp Z, Parent M (2005) Fractionation change of hydrogen isotopes in trees due to atmospheric pollutants. Geochim Cosmochim Acta 69:3723–3731

Schweingruber FH (1987) Tree rings: basic applications to dendrochronology. D. Reidel (Kluwer), Dordrecht, The Netherlands

Schweingruber FH (1996) Tree rings and environment – dendroecology. Haupt, Frankfurt, Germany

Stokes MA, Smiley TL (1968) An introduction to tree-ring dating. University of Chicago Press, Chicago, IL

Stuiver M, Braziunas TF (1987) Tree cellulose $^{13}C/^{12}C$ isotope ratios and climate change. Nature 328:58–60

Treydte K, Schleser GH, Schweingruber FH, Winiger M (2001) The climatic significance of $\delta^{13}C$ in subalpine spruce (Lötschental, Swiss Alps) – a case study with respect to altitude, exposure and soil moisture. Tellus 53B:593–611

Treydte K, Schleser GH, Helle G, Frank D, Winiger M, Haug G, Esper J (2006) The 20th century was the wettest period in northern Pakistan over the past millennium. Nature 44:1179–1182

Treydte K, Frank D, Esper J, Andreu L, Bednarz Z, Berninger F, Boettger T, D'Alessandro CM, Etien N, Filot M, Grabner M, Guillemin MT, Gutierrez E, Haupt M, Helle G, Hilasvuori E, Jungner H, Kalela-Brundin M, Krapiec M, Leuenberger M, Loader NJ, Masson-Delmotte V, Pazdur A, Pawelczyk S, Pierre M, Planells O, Pukiene R, Reynolds-Henne CE, Rinne KT, Saracino A, Saurer M, Sonninen E, Stievenard M, Switsur VR, Szczepanek M, Szychowska-Krapiec E, Todaro L, Waterhouse JS, Weigl M, Schleser GH (2007) Signal strength and climate calibration of a European tree-ring isotope network. Geophys Res Lett 34. doi:10.1029/2007GL031106

Treydte, K, Frank, DC, Saurer, M, Helle, G, Schleser, GH, Esper J (2009) Impact of climate and CO_2 on a millennium-long tree-ring carbon isotope record. Geochim Cosmochim Acta 73:4635–4647

Van der Schrier G, Briffa KR, Jones PD, Osborn TJ (2006) Summer moisture variability across Europe. J Clim 19:2818–2834

Wells N, Goddard S, Hayes MJ (2004) A self-calibrating Palmer drought severity index. J Clim 17:2335–2351

Waterhouse JS, Switsur VR, Barker AC, Carter AHC, Robertson I (2002) Oxygen and hydrogen isotope ratios in tree rings: how well do models predict observed values? Earth Planet Sci Lett 201:421–430

Waterhouse JS, Switsur VR, Barker AC, Carter AHC, Hemming DL, Loader NJ, Robertson I (2004) Northern European trees show a progressive diminishing response to increasing atmospheric carbon dioxide concentrations. Quat Sci Rev 23:771–801

Wright WE, Leavitt SW (2006) Boundary layer humidity reconstruction for a semiarid location from tree ring cellulose $\delta^{18}O$. Geophys Res Lett 111:D18105. doi:10.1029/2005JD006806

Xu H, Hong Y, Zhu Y, Liu G (2002) Information on climate change recorded in $\delta^{13}C$ and $\delta^{18}O$ series of *Pinus Koraiensis* tree ring cellulose in Antu area. Geol-Geochem 30(2):59–65

Xu H, Hong Y, Zhu Y, Liu G (2003) Information about low cloud amount recorded in $\delta^{13}C$ series of tree ring cellulose of *Pinus Koraiensis* in Antu area, Jilin. Chin J Geochem 22(1):30–37

Zhao X, Wang J, Qian J, Zeng Z (2006) Differences of $\delta^{13}C$ annual series among *Cryptomeria fortunei* tree rings at Tianmu Mountain. Chin J ApplEcol 17(3):362–367

Part II
Isotope Mapping: Theory and Methods

Chapter 7
Statistical and Geostatistical Mapping of Precipitation Water Isotope Ratios

Gabriel J. Bowen

7.1 Introduction

The partitioning of the stable isotopes of hydrogen (^{1}H, ^{2}H) and oxygen (^{16}O, ^{17}O, ^{18}O) during phase-change reactions in the water cycle creates one of the simplest, most profound examples of global-scale patterning in natural spatial isotopic distributions. Air is charged with water vapor of relatively uniform isotopic composition as it passes over the low- and mid-latitude oceans. As this air is transported northward and across the continents by the atmospheric circulation it loses water to condensation and rainout, preferentially stripping the heavy isotopes (here we will consider ^{2}H and ^{18}O) from the remaining pool of vapor. This process progresses as airmasses cool and their specific humidity decreases, and at each condensation event the isotopic composition of the precipitation formed ($\delta^{2}H_{p}$, $\delta^{18}O_{p}$) reflects the declining relative abundance of the heavy isotopes in the residual atmospheric vapor pool. Because this process is directional, and because the atmospheric circulation is patterned, $\delta^{2}H_{p}$ and $\delta^{18}O_{p}$ values exhibit strong, consistent spatial variation at regional to global scales.

These spatial patterns have been found to be relevant to fields ranging from paleoclimatology to forensics, and form the foundation of many applications described throughout this volume. Study of spatial precipitation (and vapor) isotope distributions has lead to improved understanding of large-scale water cycle dynamics and surface-atmosphere vapor fluxes, both in the present (e.g., Salati et al. 1979; Gat et al. 2003; Worden et al. 2007; Noone and Sturm this volume) and in Earth's history (e.g., Ufnar et al. 2004; Schmidt et al. 2007). Spatial variations in precipitation isotope ratios are a source of natural tracers for surface hydrology studies, allowing partitioning of water sources in large-scale hydrological studies (Fekete et al. 2006; Bowen et al. 2007; Fekete and Gibson this volume). As water interacts with and

G.J. Bowen (✉)
Department of Earth and Atmospheric Sciences, Purdue Climate Change Research Center, Purdue University, West Lafayette, IN 47907, USA
e-mail: gabe@purdue.edu

J.B. West et al. (eds.), *Isoscapes: Understanding Movement, Pattern, and Process on Earth Through Isotope Mapping*, DOI 10.1007/978-90-481-3354-3_7,

is incorporated in biological, geological, and man-made materials its isotopic composition is reflected in these materials, which, if they are subsequently chemically inert, means that they can often be attributed to a geographic source based on variations in water isotopic compositions among locations. Such applications are of interest in ecology, anthropology, and forensic science (Hobson et al., Schwarcz et al., Ehleringer et al. this volume).

The lengthy record of research on spatial precipitation isotope ratio distributions has involved a wide range of approaches, ranging from simple analysis of point-based data to full-fledged GCM modeling incorporating water isotope tracers. The goal of this chapter is to provide an introduction and review of an approach of intermediate complexity: the generation and analysis of precipitation water isotope 'isoscapes' using geostatistical and hybrid geostatistical/regression methods. The application of geostatistics, which describes the spatial autocorrelation of data and provides tools for predicting data values based on this autocorrelation, to the study of δ^2H_p and $\delta^{18}O_p$ values has been productive largely because of (1) the mechanisms within the water cycle that lead to strong, continuous spatial variation in these values, and (2) the existence of large datasets documenting the spatial distribution of precipitation isotope ratios. We will examine each of these factors in more detail before turning our attention to various examples of the use of geostatistics in the study of precipitation isotope ratios, example applications of these methods and the resultant isotope maps, and future directions and opportunities in this area.

7.2 Precipitation Isotope Systematics

The primary driver of spatial patterns in the isotopic composition of precipitation is the progressive rainout process described above, which is commonly modeled as a Rayleigh process:

$$R_v = R_0 f^{(\alpha - 1)}. \tag{7.1}$$

Here R_v is the isotopic ratio ($^2H/^1H$ or $^{18}O/^{16}O$) of residual atmospheric vapor at some point in time, R_0 is the initial isotope ratio of the vapor when the air mass was last 'replenished' with moisture, f is the fraction of vapor remaining, and α is the temperature-dependent fractionation factor between condensation and vapor (such that at any point in time, $R_p = R_v \times \alpha$). For atmospheric precipitation, changes in f are driven by changes in airmass temperature and pressure via their effect on saturation vapor pressure, whether driven by frontal, convective, or orographic processes. Together, these processes lead to robust patterns of heavy isotope depletion with increasing latitude, altitude, continentality, and, in tropical areas of strong convection, precipitation amount (Dansgaard 1964).

The systematics governing real-world precipitation isotopic compositions are somewhat more complex, however, than represented by the simple Rayleigh model. First, the concept of the 'starting point' for the process is imprecise because at most

places on Earth there is a continuous replenishment of water from the land or ocean surface via evapotranspiration. As a result, precipitation isotope ratios in most parts of the world do not trend towards infinitely low values as airmasses dry to completion, but rather stabilize as precipitable moisture decreases and the back-flux of water from the surface to the atmosphere comes into balance with precipitation rate (Ingraham and Taylor 1991). Second, the Rayleigh process describes an ideal, isolated 'parcel' of air that does not exist in the real world, where mixing through turbulent dispersion and eddies is ubiquitous. Where lateral mixing is strong, the efficiency of the Rayleigh process (and thus the spatial isotopic gradient) is reduced (Hendricks et al. 2000). Third, real world precipitation, unlike the ideal product of a Rayleigh process, continues to interact with atmospheric vapor after its condensation. Partial evaporation of falling droplets below cloud base and isotopic exchange with vapor act to influence the isotopic composition of precipitation reaching the land surface, which may be subtly or widely different that of condensation formed in the cloud (Lee and Fung 2007).

With the exception of precipitation that has experienced significant post-condensation evaporation or isotope exchange below cloud base and some solid-phase precipitation (Jouzel and Merlivat 1984), precipitation water isotopes are usually fractionated relative to those in the source vapor according to the equilibrium fractionation factors for the vapor-liquid or vapor-solid phase change. Because the proportional change in δ^2H and $\delta^{18}O$ values during equilibrium fractionation is ~8:1, in most cases precipitation has a deuterium excess value ($d = \delta^2H - \delta^{18}O \times 8$; Dansgaard 1964) similar to that atmospheric vapor. The global mean d value of meteoric precipitation is approximately +10‰, and is set by non-equilibrium fractionation processes associated with evaporation of water from the sea surface (Craig and Gordon 1965). Deviations of precipitation and vapor d values from the global mean can be related to the relative humidity of vapor source regions, 'recycling' of water through evaporation from the land surface, and below-cloud evaporation of falling raindrops (Merlivat and Jouzel 1979; Gat et al. 1994, 2003).

7.3 Precipitation Isotope Data

Precipitation isotope ratio data were among the first stable isotope data to be collected systematically by a large-scale (in this case global) network, and thus it is not surprising that work on spatial δ^2H_p and $\delta^{18}O_p$ distributions has a long history. The Global Network for Isotopes in Precipitation (GNIP) program (Aggarwal et al. this volume) has provided the foundation for most of this work. In recent years several complimentary, semi-autonomous national and regional networks have developed, which now provide ongoing coverage for parts of Canada, the USA, Siberia, New Zealand, and Australia (e.g., Welker 2000; Kurita et al. 2004; Gibson et al. 2005). In addition to these coordinated, network-based, data collection programs, numerous research groups have independently accumulated data sets on precipitation isotope ratios, either for specific research initiatives or as informal

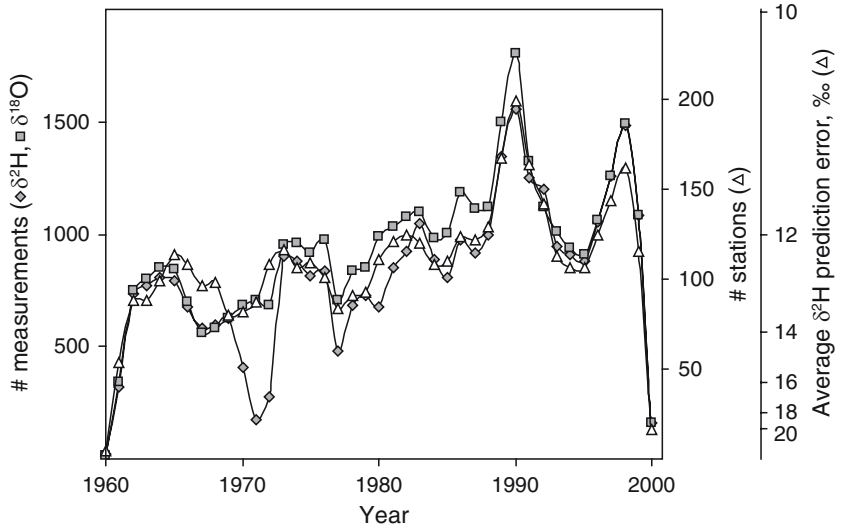

Fig. 7.1 Number of precipitation isotope ratio measurements and monitoring stations per year in the author's compilation of GNIP and literature data. The decline in records during 1999 and 2000 is an artifact reflecting that not all GNIP data for these years had been entered in the database at the time the compilation was produced. The right-hand axis gives estimated δ^2H_p prediction error for the method of Bowen and Revenaugh (2003), which scales with number of stations

monitoring projects. Although some of these data appear in the literature in some form (e.g., Jacob and Sonntag 1991; Friedman et al. 2002; Burnett et al. 2004; Peng et al. 2004), many such records remain unpublished.

The GNIP database (IAEA/WMO 2004), containing monthly integrated precipitation δ^2H and $\delta^{18}O$ values, is an indispensible resource for work on large-scale precipitation isotope ratio patterns. Thorough statistical reviews of the data have been produced at several points during the program's history (e.g., IAEA 1992; Rozanski et al. 1993), and provide good entry points for researchers interested in the data from this program. The GNIP data and documentation can be accessed through the IAEA's isotope hydrology website (www.iaea.org/water). The number of isotope ratio measurements in the database is enormous (Fig. 7.1; see also Aggarwal et al. this volume), and both spatial and temporal coverage of the data are relatively good for some parts of the world, most notably continental Europe.

Although I will not provide a comprehensive review of the GNIP data, one limitation that should be introduced here given its relevance to mapping applications is the significant unevenness of the data in space and time. After its initiation in 1959 the network rapidly grew to nearly 100 stations, and has operated at or above that level for most of the time since (Fig. 7.1). In order to achieve widespread spatial sampling, however, stations have frequently been added and dropped from the network throughout its history, and not all stations were in continuous operation throughout their time in-network (Fig. 7.2). As a result, only a small number of

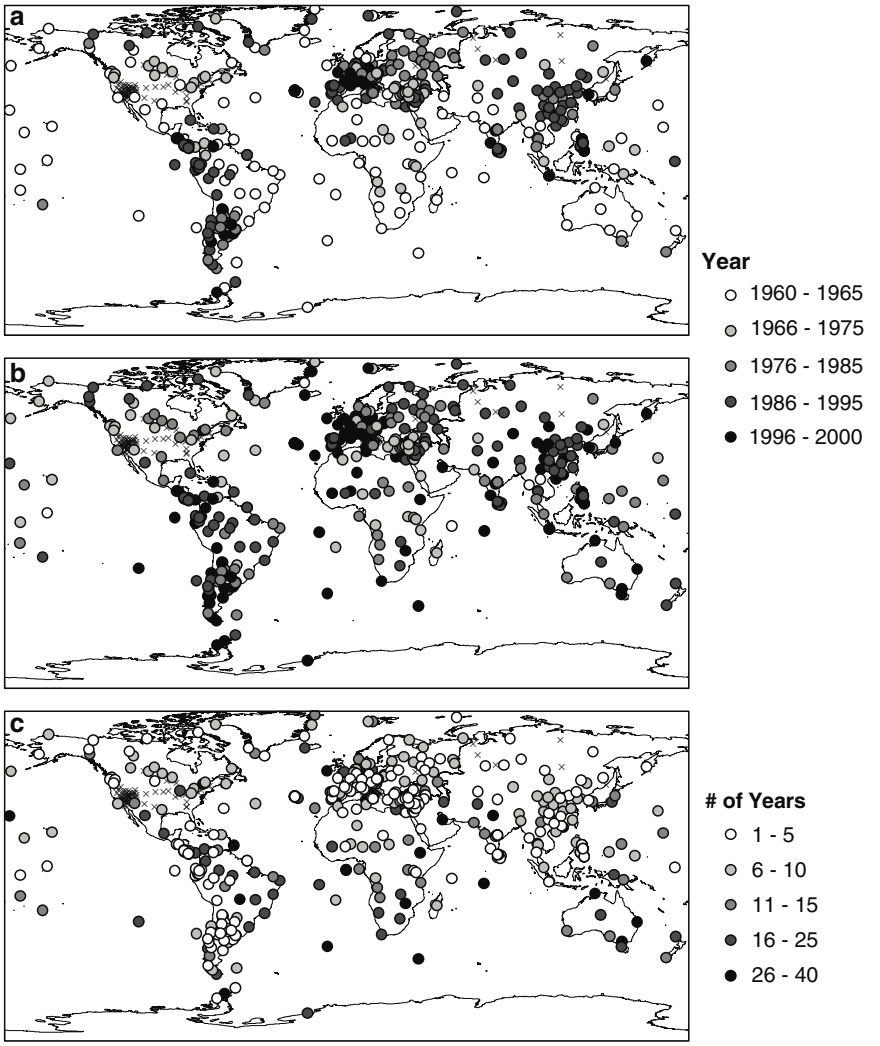

Fig. 7.2 Spatial distribution of precipitation isotope ratio monitoring stations and periods of record for GNIP stations. First (**a**) and last (**b**) years in which one or more complete monthly precipitation records exist (δ^2H or $\delta^{18}O$ value and precipitation amount). (**c**) Number of years with one or more complete monthly records. In all panels, ×'s represent non-GNIP sites from which the author has complied annual average precipitation isotope ratio records based on published or unpublished monitoring data

stations have long-term records spanning a large part of the 40+ year program: according to my calculations based on data for 461 GNIP stations through the year 2000, the average station had 9.25 years with one or more complete monthly records (δ^2H or $\delta^{18}O$ value plus precipitation amount), and the median number of

years with one or more records was 6. Only two stations (Vienna and Bet Dagan) had 39 or more years of record. In addition to limited temporal continuity, the dataset also has limited spatial density for short-term windows of time. Bowen and Revenaugh (2003), for example, found that annual average δ^2H values could be calculated at 50 or more stations for <10% of all 12-consecutive-month windows between 1960 and 2000. Because the accuracy and precision of geostatistical estimation is closely linked to data density (Fig. 7.1), these inconsistencies in data availability significantly complicate efforts to evaluate long-term trends in isotope distributions and draw comparisons between spatial patterns for different years.

Nonetheless, the GNIP provides one of the most comprehensive, global stable isotope datasets for any natural system, and has enabled many applications built on spatial analysis. To date, the most common approach to addressing the spatiotemporal heterogeneity of the data has been to deal with long-term average values rather than data for specific months or years, thus greatly increasing the spatial sampling density by integrating data across time. Monthly data are usually averaged with weighting by the amount of precipitation (e.g., Bowen and Wilkinson 2002), giving a measure of the net isotope flux to the land surface, but some studies have used un-weighted averages (Dutton et al. 2005). Clearly the details of data reduction should be carefully considered as they could potentially introduce random or systematic error within the reduced dataset, for example through use of short station records derived from climatologically unusual time periods (random) or as the result of integrating data representing different parts of the long-term trend in twentieth century climate (systematic). Data aggregation is advantageous in many ways, and often necessary, but the potential pitfalls of this approach should be kept in mind, particularly given the characteristics of currently available datasets as described above.

There are a large and growing number of non-GNIP records in the literature, and use of non-GNIP records can greatly improve data coverage for many studies of spatial water isotope distributions (Fig. 7.2). Compiling and integrating this data, however, often involves serious challenges. Precipitation is a dynamic and continuous hydrological flux, but precipitation isotope ratio measurements are made on discrete samples representing the integration of some part of this flux. As a result, choices must be made in each monitoring effort about the method and duration of sample integration, and examples can be found in the literature of studies where samples were integrated over event- and sub-event timescales, weeks, months, quarters, and semi-annual time intervals. Data compilation, therefore, commonly requires significant efforts to aggregate (or disaggregate) sample values to a common sampling interval required by the study, as well as decisions regarding how comparisons among samples representing physically-defined (e.g., storm system) and arbitrary (e.g., week) intervals will be handled. All of this becomes much more difficult where records are incomplete, in terms of either the continuity of isotopic data or the availability of ancillary (e.g., precipitation amount) data. Given the challenges associated with this work, the community could benefit greatly if workers routinely made their carefully conducted and well-documented data compilations publically available in formats that allowed their convenient re-use.

7.4 Geostatistical Modeling of Precipitation Isotope Ratios

Geostatistical methods enable the prediction of variable values at un-monitored sites based on the premise, either assumed or inferred from data, that values at nearby sites will be more closely related than those at sites widely separated in space. This premise of spatial autocorrelation is valid for a wide diversity of systems and implicitly underlies many basic data-display and data-analysis activities (e.g., contouring). These methods represent a geographic translation of regression analysis, wherein geographic location is taken to be an independent predictor variable for a quantity of interest. Dependent variable values at un-monitored sites are predicted as weighted averages of the observations from surrounding stations. The volume by Cressie (1993) provides a comprehensive review of basic geostatistical tools and methods.

Because the processes that underlie variation in isotopes ratios of precipitation are spatially continuous (i.e. discrete boundaries are rare in the atmosphere!), the premise of spatial autocorrelation should be valid for large-scale patterns of δ^2H_p and $\delta^{18}O_p$. This can be observed empirically by calculating the sample semivariance (γ):

$$\gamma(h) = \frac{1}{2n}\sum_{i=1}^{n}[Z(xi) - Z(xi+h)]^2 \tag{7.2}$$

where h is a distance or range of distances between points (typically given in arc degrees for global datasets), n is the number of points in the data set separated by h, and Z(x) is the observed isotopic value at a monitoring site. In the case of $\delta^{18}O_p$, for example, there is a strong tendency for values from closely spaced stations to be more similar, and hence have a smaller semivariance, than those for more widely separated sites (Fig. 7.3).

All interpolation is inherently subjective at some level, involving choices about which model is most appropriate for a given data set, how the model should be parameterized, and what parameter values should be used (comparable to the choice of model form, independent variables, and regression type in standard linear regression analysis). The class of geostatistical methods known as Kriging, however, reduces the subjectivity of interpolation by allowing the practitioner to use the observed spatial autocorrelation to derive the model weights to be used in interpolation. Sample semivariance is first calculated for a range of values of h, plotted as a sample semivariogram (Fig. 7.3) and used to fit a semivariogram model that describes the weights to be used in prediction at un-monitored sites. In this case, selection of the form of the semivariogram model is still a somewhat subjective process, but the sample semivariogram determines the model parameters based on goodness-of-fit between the modeled and observed semivariance.

The semivariogram model parameters also provide a powerful means of quantifying the spatial structure of the observational data. Basic isotropic variogram models typically include three parameters: the nugget, representing residual local variance not described by the model (e.g., measurement error, temporal variation);

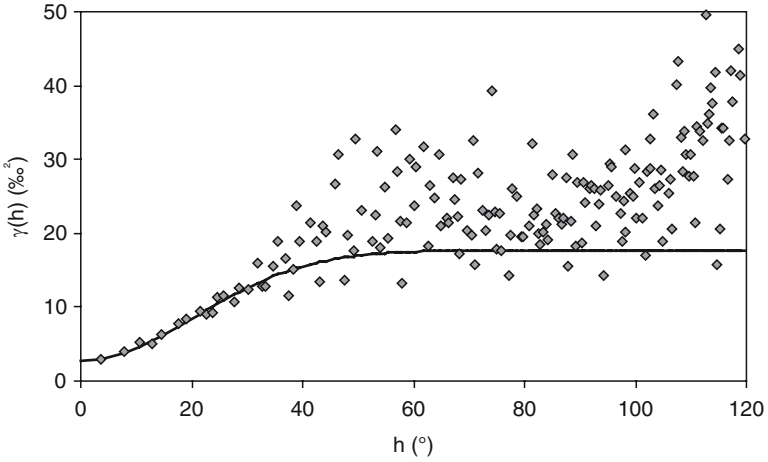

Fig. 7.3 Semivariogram for global mean annual $\delta^{18}O_p$ values. h = lag distance (angle between sites); γ(h) = semivariance. Dark line represents the Gaussian semivariogram model $\gamma(h) = 15.0 \times \exp(-(h^2/29.0^2)) + 2.8$

the sill, representing the total variance; and the range, representing the rate at which similarity between values decreases with distance. The ratio of the nugget and sill values, by analogy with the coefficient of determination, provides an approximate estimate of the fraction of the total variance that can be explained in terms of spatial autocorrelation. A Gaussian semivariogram model for global $\delta^{18}O_p$ values, for example, gives nugget and sill values of 2.8 and 15.0, implying that ~81% of the global variance in $\delta^{18}O_p$ values can be described in terms of geographic location alone (Fig. 7.3). The range value for this semivariogram model (29.0°) implies that the covariance of $\delta^{18}O_p$ values for stations separated by this distance is only 0.31, and the relatedness of these values falls to <5% within 49°. These values can clearly be related with the length scales of atmospheric processes controlling $\delta^{18}O_p$ distributions: for example the Hadley circulation and zonal width of the continents define maximum length-scales over which one would expect strong relatedness between precipitation isotope ratio values.

A number of statistical and geostatistical approaches have been applied to produce maps of precipitation isotope ratio distributions. In the following sections we will examine the historical trajectory of this work and compare data products produced using different methodologies.

7.4.1 Contour and Pure Geostatistical Maps

Recognition of the strong spatial patterning of precipitation isotope ratios emerged within the first few years of the GNIP program, and led to the generation of early maps showing the primary, large-scale features of this distribution. The earliest

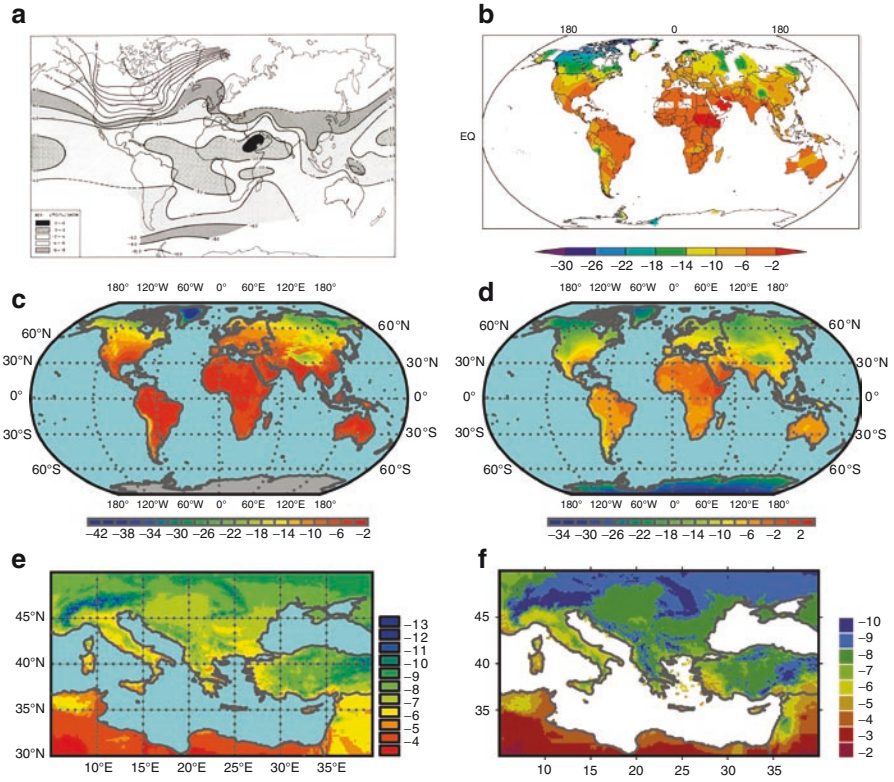

Fig. 7.4 Global and regional maps of mean annual $\delta^{18}O_p$ values. (**a**) An early contour map based on the GNIP station data (Yurtsever and Gat 1981). (**b**) Interpolated map generated by Cressman objective analysis (IAEA 2001; Birks et al. 2002). (**c**) A regression-model based map using the parameterization of Farquhar et al. (1993) in terms of mean annual temperature, precipitation amount, and elevation. Calculations were based on publically available gridded climate (New et al. 1999) and topographic data (U. S. National Geophysical Data Center 1998). (**d**) A hybrid geostatistical/regression map parameterized in terms of latitude and elevation, with interpolation by inverse distance weighting (http://waterisotopes.org; modified from Bowen and Revenaugh 2003). (**e**) Close-up of $\delta^{18}O_p$ values for the Mediterranean region from the map shown in panel **d**. (**f**) Regional map of $\delta^{18}O_p$ for the Mediterranean region based on a hybrid geostatistical/regression approach parameterized in terms of temperature and vapor pressure, with interpolation by ordinary Kriging with an exponential semivariogram model (Modified from Lykoudis and Argiriou 2007). Fig. 7.4, see Appendix 1, Color Section

maps, produced during the 1960s and 1970s, were primarily hand-contoured interpretations of the station data, but depicted features such as the strong zonal δ^2H_p and $\delta^{18}O_p$ gradients over North America, relatively high values over the North Atlantic due to vapor recharge from the Gulf Stream, and very high values over East Africa and the Arabian Peninsula (Fig. 7.4a). These illustrations did a reasonable job of displaying the first-order spatial distributions and motivated a great deal of work focused on understanding the mechanisms underlying these patterns,

but were highly generalized interpretations of the data with limited documentation and traceability.

In subsequent decades more quantitative methods have been applied by many researchers to produce interpolated depictions and point-estimates of the GNIP data. The most notable such effort led to the production of a comprehensive series of long-term average monthly and annual δ^2H, $\delta^{18}O$, and *d* maps that has been made web-accessible (IAEA 2001; Birks et al. 2002). These products were produced from GNIP data using the method of 'Cressman objective analysis' (Cressman 1959). Briefly, isotopic values (δ) are predicted at grid cell locations *x* based on an initial guess of the isotopic value and a series of correction factors ($C_{x,k}$):

$$C_{x,k} = \frac{\sum_{i=1}^{n_k}\left[\left(\delta_i - p_{i,k-1}\right)\frac{r_k^2 - D_{xi}^2}{r_k^2 + D_{xi}^2}\right]}{n_k}, \tag{7.3}$$

where $p_{i,k-1}$ is the predicted value at measurement station *i* at the previous step, r_k is a radius of influence, D_{xi} is the distance between the grid cell and a measurement site, and n_k is the number of measurement sites within the current radius of influence. The procedure proceeds sequentially, adjusting the predicted value at a grid cell based on the mismatch between data and predictions at surrounding measurement sites within progressively smaller spheres of influence. Although the method is traceable in the sense of having a clear mathematical formulation, there are several important aspects of the procedure that should be noted. First, it is a space-only method, meaning that the information it incorporates is limited to the location and observed δ_p values at the measurement sites. As a result, predicted values will be forced to vary smoothly between data points (as is the case with all pure spatial interpolation methods). Second, in contrast to what might be implied by the name, the method is highly subjective (the term 'objective analysis' appears to derive from contemporary jargon for data gridding procedures; Cressman 1959). The practitioner of this method must choose a series of spheres of influence with little to no theoretical basis for this decision, and the formulation of the method a priori specifies the incremental correction procedure and the form of the spatial weighting function, which may or may not be appropriate for any particular dataset.

The resulting products provide a more rigorous depiction of the large-scale patterns of precipitation isotope ratio variation, and may improve the representation of some features such as the east/west asymmetry of δ_p values across North America (Fig. 7.4b), presenting new opportunities for data exploration. Like the earlier contour maps, however, the relatively smooth weighting functions used here fail to capture many of the finer details of the distribution such as orographic effects. These products are also limited in their ability to predict values at sites that are not in close proximity to monitoring stations, and the Cressman method does not allow for analytical estimates of prediction error. As a result, the use of these and other space-only interpolated δ_p grids in quantitative analysis should be approached with caution.

7.4.2 Empirical Models

Farquhar et al. (1993) were among the first to create a global map of precipitation isotope ratios using ancillary (i.e. other than spatial position) variables. In order to estimate the transfer of ^{18}O from leaf water to atmospheric CO_2 these authors developed a regression model relating long-term mean annual $\delta^{18}O_p$ values to climatological variables. A re-assessment of their parameterization fitted to data from 558 GNIP and non-GNIP continental stations gives the following relationship:

$$\delta^{18}O_p = 0.587(T) - 0.00993(T)^2 + 1.152(P) - 0.339(P)^2 - 0.054\left(\sqrt{A}\right) - 13.3, \quad (7.4)$$

where T is mean annual temperature (°C), P is annual precipitation (m), and A is altitude (m). This relationship describes approximately 72% of the total variance in global $\delta^{18}O_p$ values and has a standard error of 2.2‰. Note that this formulation predicts decreases in $\delta^{18}O_p$ with decreasing temperature (below ~25°C), increasing altitude, and increasing precipitation amount (above ~2 m/year), consistent with observed patterns in global δ_p data sets (Dansgaard 1964; Rozanski et al. 1993). These patterns are clearly depicted in the resulting map of $\delta^{18}O_p$ values, which appears broadly similar to those produced using contouring but includes predictions for sites far from monitoring stations as well as fine-scale variation related to topography (Fig. 7.4c). Other parameterizations can be derived using these and other climatological and geographic parameters that explain similar or slightly larger amounts of the total $\delta^{18}O_p$ variance (Lykoudis and Argiriou 2007).

Given that space-only interpolation can explain a similar or larger proportion of the spatial δ_p variability (e.g., 82% for $\delta^{18}O_p$), it seems valid to question why a regression-based model with inferior overall performance should be considered for precipitation isotope ratio mapping. At least two concrete reasons can be highlighted. First, the regression model attempts to derive explicit relationships between isotopic values and parameters that have understood, mechanistic relationships with δ_p values. To the extent that these ancillary parameters are better sampled (e.g., known at more places or more accurately than δ_p values) they provide basis for extrapolating precipitation isotope ratio variation to unmonitored locations. For example, most GNIP-based space-only maps do not attempt to depict δ_p values for Siberia due to the absence of monitoring sites there (Fig. 7.4a and b). If the relationship described by Eq. 7.4 is global and robust, however, it should allow us to make reasonable predictions of $\delta^{18}O_p$ values for this region (Fig. 7.4b). Second, the regression statistics for this relationship provide simple, quantitative estimates of uncertainty, enabling reporting of the confidence of predicted values. Nontheless, the regression method does fail to capitalize on the strong spatial autocorrelation in δ_p values. In places where the climate parameters used are decoupled, to some extent, from atmospheric circulation, it fails to capture elements of the spatial δ_p pattern: for example the low δ_p values in the northern interior of Asia, high values in East Africa and Arabia, and the northeast/southwest δ_p gradient across Amazonia.

7.4.3 Coupling Regression and Geostatistics

In order to capitalize on the strengths of both the regression and geostatistical approaches, Bowen and Wilkinson (2002) introduced a hybrid procedure that involved: (1) fitting a regression model for δ_p, (2) calculating regression model predictions for each gridcell, (3) calculating the residuals from the regression model at all monitoring sites, (4) geostatistical interpolation of the residuals, and (5) summation of regression model and interpolated residual values. The hybrid method, in effect, takes advantage of the power of the regression model to describe large-scale patterns and extrapolate based on semi-mechanistic parameterizations, while turning to geostatistics to describe finer-scale regional variation related to circulation patterns and other processes not adequately reflected by the ancillary variables. The transformation of the data into regression model residuals also validates one of the theoretical assumptions of most geostatistical interpolation methods: that the data distribution has a stationary mean (i.e. in the absence of any other information the mean value would be a good estimate everywhere in the prediction domain). This assumption is clearly violated by global δ_p datasets, and although other methodological variants exist for dealing with non-stationary means most do not allow for the incorporation of non-geographic variables, such as elevation, in prediction.

In their analysis, Bowen and Wilkinson (2002) used a simple polynomial function of latitude and altitude to represent global, temperature-driven patterns in the $\Delta^{18}O_p$ distribution:

$$p_x = -0.0051(L)^2 + 0.1805(L) - 0.002(A), \tag{7.5}$$

where L is the absolute value of latitude. This function described 76% of the $\delta^{18}O_p$ variance in their 232-station dataset (64% in the current version of the author's expanded dataset), and in comparison with Eq. 7.4 there is a clear similarity in form between the δ_p/temperature and δ_p/latitude relationships. The residuals from this model were interpolated using an inverse distance model of the form:

$$C_x = \frac{\sum_{i=1}^{n} (\delta_i - p_i) e^{(-D_{xi}/\beta)}}{\sum_{i=1}^{n} e^{(-D_{xi}/\beta)}}, \tag{7.6}$$

in which C_x is the residual correction for a grid-cell regression model prediction, n is the number of monitoring station data, and β is a weighting parameter. Despite encompassing only a small fraction of the total $\delta^{18}O_p$ variance, the distribution of C_x values is highly spatially coherent (Figs 7.5 and 7.6). For the expanded dataset of 558 $\delta^{18}O_p$ stations, spatial autocorrelation describes up to ~80% of the residual variance (Fig. 7.5). When summed with the regression model predictions, then, the hybrid geostatistical/regression approach represents ~92% of the total global δ_p variance.

Precipitation isotope ratio maps generated using the hybrid approach depict the fine-scale variation and global trends seen in the regression model products while

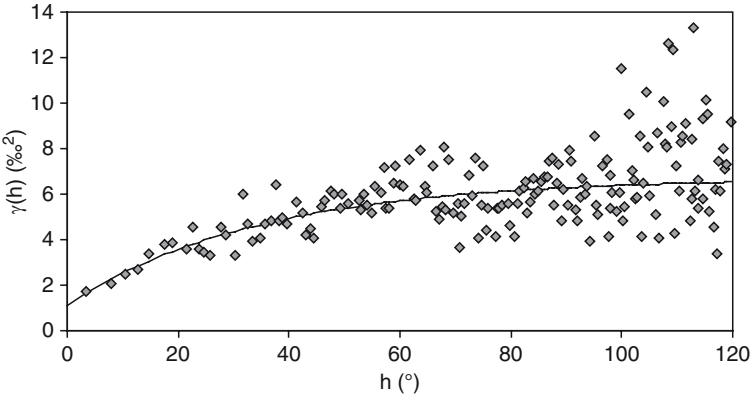

Fig. 7.5 Semivariogram of $\delta^{18}O_p$ residuals (C_x) from a latitude/altitude regression model. *Dark line* represents the exponential semivariogram model $\gamma(h) = 5.6 \times (1 - \exp(-(h/34.8)) + 1.1$

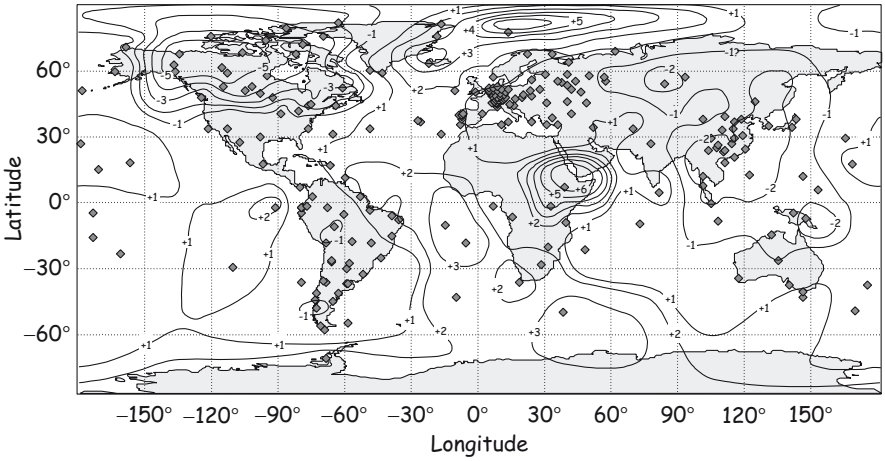

Fig. 7.6 Model residuals from a latitude/altitude regression model for $\delta^{18}O_p$ interpolated using an inverse distance method with exponential weighting (Reprinted from Bowen and Wilkinson 2002)

also faithfully representing regional effects captured by the geostatistical methods (Fig. 7.4d). Patterns related to orographic effects, for example, are more realistically represented than in the geostatistical maps, where if they are represented at all they appear as bullseye patterns divorced from the geography of the underlying physical process. The hybrid maps also capture patterns such as the east/west asymmetry of North American δ_p values and high $\delta^{18}O$ values in east Africa and Arabia that are anomalous in the context of the regression models. Regression model residual maps show the distribution of such patterns, many of which can be attributed to climatological mechanisms such as extreme reduction of airmass vapor content over the Northern Hemisphere continents and recharge of atmospheric vapor by warm oceanic western boundary currents.

The stepwise procedure introduced by Bowen and Wilkinson (2002) was refined by Bowen and Revenaugh (2003), who applied a gradient search method to fit the regression model and interpolation weighting parameter β in a single step. This improvement offered two major benefits. First, it allowed for simultaneous optimization of all model parameters, allowing tradeoffs between the regression- and interpolation-model predictions to be balanced. Second, once the regression model parameterization and weighting function were chosen, the process of fitting the model and generating gridded predictions could be automated. As a result of this second advance, quantitative, spatially-distributed, error estimates for the entire hybrid procedure could be generated through cross-validation ('leave one out'; Fig. 7.7). In addition to providing estimates of uncertainty for use in quantitative applications of precipitation isotope ratio maps, the error estimates show where δ_p values are most poorly known and additional monitoring might be most useful (see Section 7.6). Bowen and Revenaugh (2003) further used cross-validation and jackknifing ('leave many out') to examine the influence of data density on prediction uncertainty (Fig. 7.1) and to demonstrate that the hybrid geostatistical/regression approach produced δ_p estimates at un-monitored sites that were ~10–15% more accurate, on average than those derived from pure geostatistical methods. These map products have been made accessible in several forms through the WaterIsotopes.org website (http://waterisotopes.org), including GIS grid files and the Online Isotopes in Precipitation Calculator, an interactive tool providing point estimates of precipitation isotopic composition (and confidence limits) for user-specified locations.

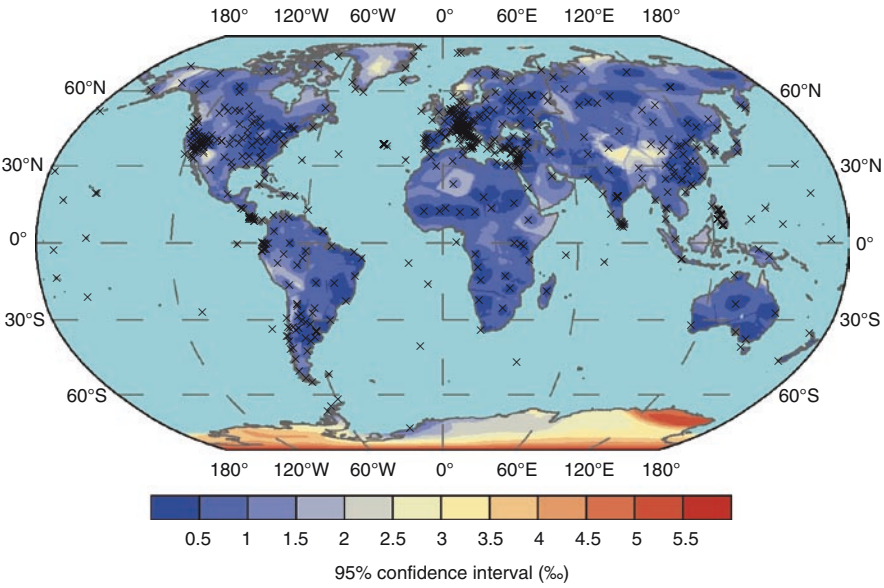

Fig. 7.7 Ninety-five percent confidence intervals for hybrid geostatistical/regression map shown in Fig. 7.4d (http://waterisotopes.org; modified from Bowen and Revenaugh 2003). Data station locations are shown by X's, see Appendix 1, Color Section

The hybrid approach can be applied to any reasonable regression model parameterization and geostatistical interpolation method, and a number of subsequent regional and global studies have extended on the approach by incorporating climatological variables and alternate geostatistical methods such as Kriging (Meehan et al. 2004; Lykoudis and Argiriou 2007; van der Veer et al. in press). In its general form, however, the approach introduced by Bowen and Wilkinson (2002) remains the current standard for quantitative, rigorous mapping of precipitation isotope ratio distributions. Nonetheless, the accuracy of the method remains limited in some regions, and given the widespread interest in the scientific, commercial, and regulatory application of δ_p maps there is a need for continued improvement. One avenue of work that seems particularly promising is the development of new model parameterizations incorporating atmospheric variables, such as surface pressure or wind direction, that reflect the atmospheric circulation. Because the current hybrid models represent spatial patterns uniquely related to the geometry and direction of circulation through geostatistical interpolation, the representation of these patterns is strongly dependent on data density. As a result, isotopic patterns related to effects such as rain shadows and circulation system boundaries are only represented where adequate data exist to document them. The development of models incorporating relevant ancillary variables could significantly improve the representation of these patterns, and by linking the hybrid geostatistical/regression approach to dynamic atmospheric variables may improve attempts to generate maps representing δ_p values for discrete time intervals.

7.4.4 Parameterizations for Regional and Sub-annual Models

With the exception of the Cressman-method map series developed by the IAEA, the work we have discussed thusfar was focused exclusively on mapping the global, long-term, annual average δ_p values of precipitation. Several studies have now applied the hybrid method to generate maps of regional and monthly or seasonal δ_p distributions, and this work has shown that for these targeted applications adjustments in regression model parameterization can often produce significant improvements in prediction accuracy. There has been significant interest in the generation of sub-annual maps for ecological applications, based on the premise that the water entering ecosystems is biased towards precipitation that fell during parts of the year where climate is conducive to plant growth. At the global scale, Bowen et al. (2005) used the hybrid geostatistical/regression method to map long-term monthly average δ_p values using monthly GNIP data. They found that the approximate hemispheric symmetry that characterizes the annual data broke down for monthly data due to the N–S shift in the zonally averaged position of the intertropical convergence zone (ITCZ, Fig. 7.8). As a result, the use of *L*, the absolute value of latitude, as a regression model parameter does not make sense for monthly data, and the authors introduced a derived parameter describing the climatological ‘effective latitude’ of a site during a given month based on a rescaling of

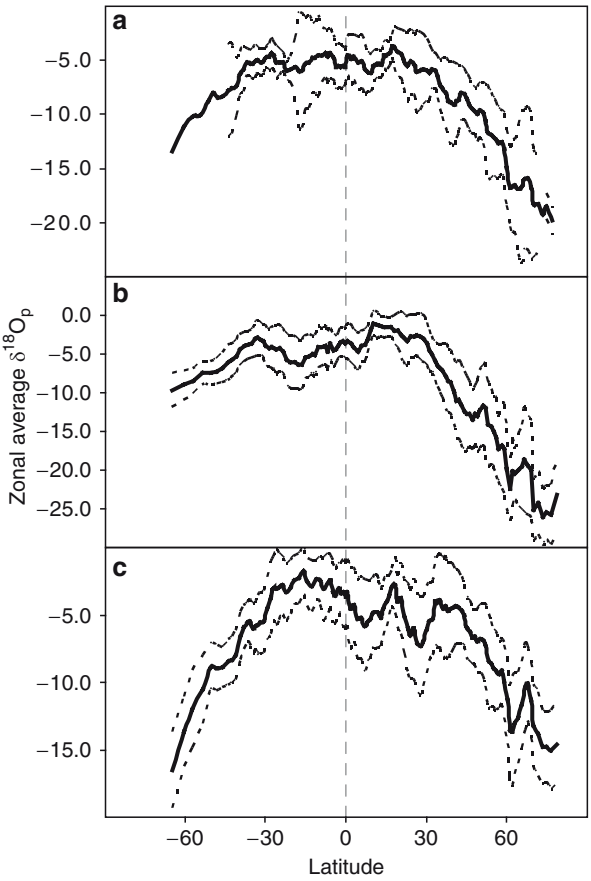

Fig. 7.8 Zonal long-term average $\delta^{18}O_p$ values from a compilation of GNIP and non-GNIP data (±1 standard devaiation). The plane of approximate symmetry for the zonal distributions, located near the equator for mean annual values (**a**) shifts from ca. 5°S in January (**b**) to ca. 18°N in July (**c**) due to the N–S migration of the intertropical convergence zone (Bowen et al. 2005). Long-term mean annual average and raw monthly observations were averaged in 1° bins and zonal profiles smoothed using a 5-point running average

L between the hemispheric pole and the approximate zonal position of the ITCZ in a given month (Bowen et al. 2005). The revised parameterization was implemented in a hybrid model to generate monthly average δ_p maps and precipitation-amount weighted growing season δ_p grids, which are also available at http://waterisotopes.org.

A number of studies focusing on regional δ_p mapping have shown that parameters and parameter values can be optimized for regional isotope/climate or isotope/geography relations that may differ somewhat from the global relationships. Dutton et al. (2005) used the hybrid model to create a regional, mean annual $\delta^{18}O_p$ map based on data from the contiguous USA and found that δ_p/latitude and δ_p/altitude slopes for this region were somewhat higher than for the global dataset.

Meehan et al. (2004) developed a regional, growing-season δ^2H_p map for North America that is now widely used by avian ecologists. Although the regression parameter values for this map were not published and it is unclear how the regression coefficients differ from those of other studies, the patterns and values shown in the final product are not widely different from those depicted by global analysis.

A more exhaustive analysis of climatological and geographic parameterizations for regional δ_p values in the Mediterranean region demonstrated that the choice of parameterization had a significant effect on the quality of regression-model predictions, with r^2 values ranging from 0.68 to 0.84 for models of mean annual δ^2H_p values and from 0.61 to 0.83 for mean annual $\delta^{18}O_p$ values (Lykoudis and Argiriou 2007). Models based on latitude and altitude alone performed relatively well in most cases examined, though incorporation of climatological parameters such as temperature generally improved prediction. The regional maps produced in this analysis are similar to those from global analysis in most respects (Fig. 7.4e and f), though local differences, for example along the eastern Mediterranean coast, likely reflect the improved ability of the geostatistical interpolation to resolve fine-scale details in regional analyses. Interestingly, Lykoudis and Argiriou (2007) also noted that regression models were much more accurate predictors of cool-season precipitation δ_p values than warm-season values, a finding that seems to be emphasized by recent work showing that global mean-annual δ_p is more closely related to cool-season temperature than mean-annual or warm-season temperature (van der Veer 2009).

7.5 Applications

Precipitation isotope ratio maps are now widely used as source of δ_p estimates for studies in which H and O stable isotopes are used to trace geographic movement of water, organisms, or products (Fekete et al. 2006; Bowen et al. 2007; Ehleringer et al., Gibson et al., Hobson et al., Schwarcz et al. this volume). Analysis of the spatial distribution of δ_p in gridded datasets can also represent a powerful approach to the study of water transport dynamics in the atmosphere and surface/atmosphere water fluxes. Early examples include studies that used spatial δ_p and vapor isotope ratio distributions to quantify water recycling from the land surface over Amazonia and eastern North America (Salati et al. 1979; Gat et al. 1994, 2003). As datasets documenting the isotopic composition of atmospheric and meteoric water expand and methods for the spatial analysis of water isotope distributions improve, there is great potential to extend upon this work and use new approaches to generate improved understanding of the water cycle (e.g., Worden et al. 2007).

Because δ_p and d_p values evolve in a continuous manner as airmasses lose water as precipitation, are recharged with vapor, and mix, the spatial patterns of these values can reveal patterns of connectivity in the atmospheric water cycle. By mapping relationships between intra-annual variability in precipitation isotope ratios and climate variables, for example, Bowen (2008) recognized regions of the subtropics where seasonal δ_p variability was amplified relative to that which should have

resulted from changes in the local intensity of rainout, and hypothesized that these reflected the seasonal, high-level advection of ^{2}H- and ^{18}O-depleted moisture to these areas from lower-latitude regions influenced by deep tropical convection. This seasonal pattern and connectivity is also apparent, for example, in the expression of the ITCZ in zonal δ_p profiles (e.g., Fig. 7.8c), where δ_p values are relatively high in the areas of strongest convergence and decrease outward. In addition to the outward advection of low-δ_p vapor (e.g., Lawrence et al. 2004), this pattern may reflect the importance of post-condensation isotope exchange between falling rain and lower-level vapor in the rising (high-δ_p) and falling limb (low-δ_p) of the Hadley cell. A similar but less pronounced pattern is centered on the Arctic polar front (Fig. 7.8c), and may reflect similar climatological processes.

The zonal pattern of deuterium excess values is also strongly structured, and Bowen and Revenaugh (2003) noted the similarity between this pattern and that of tropospheric relative humidity over the oceans (Fig. 7.9). Given the strong

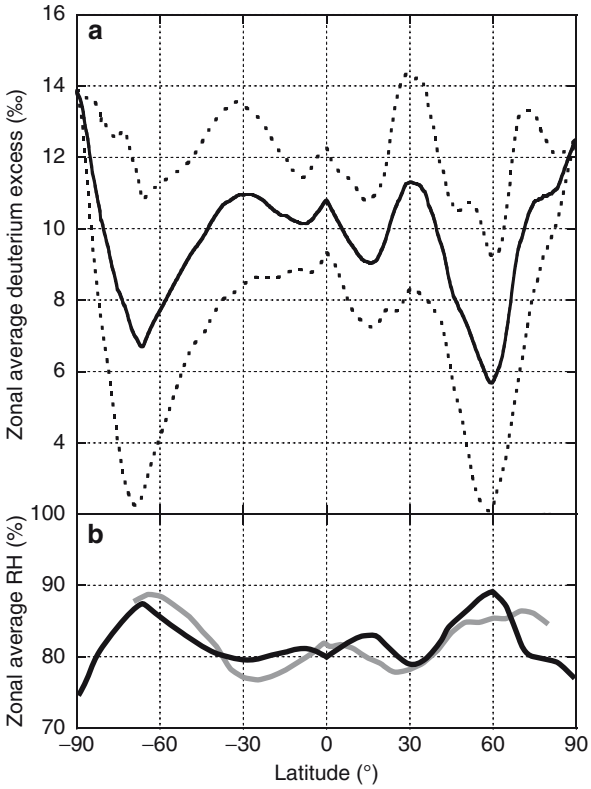

Fig. 7.9 Deuterium excess values (**a**) of precipitation (zonal averages ±1 standard deviation of gridded values from a hybrid geostatistical/regression model) and tropospheric humidity (RH; **b**) for oceanic regions. In (**b**), the *grey line* gives observed climatological values (Peixoto and Oort, 1996) and the *black line* indicates the expected vapor-source RH values based on zonal mean *d* and the model of Merlivat and Jouzel (1979) (Modified from Bowen and Revenaugh 2003)

relationship between *d* values of evaporating vapor and the relative humidity of the atmosphere into which evaporation occurs, and the fact that *d* is largely conservative during the rainout process, the global pattern of *d* values in precipitation can be related to the spatial structure of vapor source locations and vapor transport. Comparison of the observed zonal distribution of surface atmosphere humidity over oceanic regions with the modeled values of RH for vapor sources (based on the model of Merlivat and Jouzel 1979, using an average friction velocity of 20 cm/s and wind speed of 6.1 m/s at 10 m height) suggests that although the patterns are similar, the *d*-inferred source RH values are skewed poleward by 10–15° throughout the tropics and the southern mid-latitudes (Fig. 7.9b). This suggests that the global *d* distribution may be a sensitive indicator of the pattern and length scale of poleward vapor and heat transport.

7.6 Temporal Resolution and the Way Forward

The isotopic composition of precipitation is documented by a large number of globally distributed data, and this has allowed detailed investigation of the patterns and mechanisms of spatial variation in δ_p values. Precipitation isotope ratio maps produced using statistical and geostatistical methods have played an important role in the identification and characterization of meaningful and useful patterns of δ_p variation. A wide range of methods have been applied, and depending on the intended application each may have its merits. Awareness of the limitations of particular methods, however, is important, particularly where the resulting products are to be applied in quantitative analysis. Ideally all such products should be accompanied by robust estimates of prediction error, though this is not possible or practical with many of the methods that have been applied thusfar.

Maps of global and regional δ_p distribution carry information on the dynamics of the atmospheric water cycle and surface-atmosphere water flux, and they have found widespread use as templates for geographic source reconstructions. The pace of application development has increased significantly as new maps have been developed and the distribution of isoscapes through websites like the IAEA map site and WaterIsotopes.org has increased the availability of these products. Considering the requirements of these applications, one of the most critical limitations of the current generation of statistical and geostatistical tools for δ_p mapping is their inability to provide accurate, time-explicit maps. Such products would allow spatial precipitation water isotope distributions to be used to more closely probe the spatiotemporal dynamics of atmospheric water transport, monitor and identify changes in hydroclimate, and reconstruct material origins with reference to both space and time.

This shortcoming is tied to the limited and uneven distribution of available precipitation isotope data in time: for example, Bowen and Revenaugh (2003) found that even with a sample network of 50 stations (a larger number than are available for most years during the history of the GNIP program) prediction error increased by ~70% over that attainable with a composite dataset of long-term

annual average values. Although data collection at the global scale is an arduous task and may preclude the establishment of a traditional surface-collected data network with significantly increased spatiotemporal coverage and evenness, developing technologies for sample collection and analysis and even the remote measurement of vapor isotope ratios may enable more comprehensive sampling of global water isotope distributions in the future (Helliker and Noone this volume). Error estimates from geostatistical mapping analyses (e.g., Figs. 7.1 and 7.7) can also provide a guide for future investments in ground-based monitoring. In fact, many of the regions that these analysis highlight as significant areas of uncertainty (e.g., Antarctica, and Siberia) have been the focus of recent sampling programs leading to improved data coverage (Kurita et al. 2004; Masson-Delmotte et al. 2008). Other areas where additional sampling could help to constrain regional map patterns include the Tibetan Plateau, north and east Africa, and the Andes. It is critical, however, to recognize that without sustained monitoring of precipitation across existing sites and coordination with existing programs (particularly in terms of sampling strategies such as temporal integration) this additional data will do little to increase our ability to generate time-explicit precipitation isoscapes or assess trends in spatial patterns.

The limited ability of these methods to produce time-explicit isoscapes is also, however, related to the model parameterizations in use, which relegate representation of many of the dynamic features of the δ_p distribution (e.g., those tied to the trajectory and interaction of circulation systems) to geostatistical interpolation. As parameterizations are developed that enhance the ability of regression models to represent dynamic features of the δ_p distributions and improve the assimilation of monitoring data for geostatistical residual correction, the need for extensive data collections will be reduced. Such work is ongoing, for example leveraging the circulation model results of the Stable Water Isotope INtercomparison Group (SWING; http://people.su.se/~cstur/SWING2/), and should lead to a new generation of dynamical maps and web-based mapping and analysis tools (http://isomap.org). The resulting products will fit somewhere between isotope-enabled circulation-model simulations and the early contour maps of water isotope distributions, capturing the dynamic effects of climate on the stable water isotopes and doing so using transparent methods that leverage and respect the data in hand.

References

Birks SJ, Gibson JJ, Gourcy L, Aggarwal PK and Edwards TWD (2002) Maps and animations offer new opportunities for studying the global water cycle. Eos Trans. AGU (electronic supplement) 83. http://www.agu.org/eos_elec/020082e.html

Bowen GJ (2008) Spatial analysis of the intra-annual variation of precipitation isotope ratios and its climatological corollaries. J Geophys Res 113:D05113. doi:10.1029/2007JD009295

Bowen GJ, Ehleringer JR, Chesson LA, Stange E, Cerling TE (2007) Stable isotope ratios of tap water in the contiguous USA. Water Resour Res 43:W03419. doi:10.1029/2006wr005186

Bowen GJ, Revenaugh J (2003) Interpolating the isotopic composition of modern meteoric precipitation. Water Resour Res 39:1299. doi:10.1029/2003WR002086

Bowen GJ, Wassenaar LI, Hobson KA (2005) Global application of stable hydrogen and oxygen isotopes to wildlife forensics. Oecologia 143:337–348. doi:10.1007/s00442-004-1813-y

Bowen GJ, Wilkinson B (2002) Spatial distribution of $\delta^{18}O$ in meteoric precipitation. Geology 30:315–318

Burnett AW, Mullins HT, Patterson WP (2004) Relationship between atmospheric circulation and winter precipitation $\delta^{18}O$ in central New York State. Geophys Res Lett 31:L22209. doi:10.1029/2004GL021089: 1–4

Craig H, Gordon LI (1965) Deuterium and oxygen-18 variations in the ocean and the marine atmosphere. In: Tongiorgi E (ed) Proceedings of a conference on stable isotopes in oceanographic studies and paleotemperatures. Spoleto, Italy

Cressie NAC (1993) Statistics for spatial data. Wiley, New York, p 900 pp

Cressman GP (1959) An operative objective analysis system. Mon Weather Rev 87:367–374

Dansgaard W (1964) Stable isotopes in precipitation. Tellus 16:436–468

Dutton A, Wilkinson BH, Welker JM, Bowen GJ, Lohmann KC (2005) Spatial distribution and seasonal variation in $^{18}O/^{16}O$ of modern precipitation and river water across the conterminous United States. Hydrol Process 19:4121–4146. doi:10.1002/hyp. 5876

Farquhar GD et al (1993) Vegetation effects on the isotope composition of oxygen in atmospheric CO_2. Nature 363:439–443

Fekete BM, Gibson JJ, Aggarwal P, Vorosmarty CJ (2006) Application of isotope tracers in continental scale hydrological modeling. J Hydrol 330:444–456. doi:10.1016/j.jhydrol.2006.04.029

Friedman I, Smith GI, Johnson CA, Moscati RJ (2002) Stable isotope compositions of waters in the Great Basin, United States – 2. Modern precipitation. J Geophys Res 107:4401. doi:10.1029/2001JD000566

Gat JR, Bowser CJ, Kendall C (1994) The contribution of evaporation from the Great Lakes to the continental atmosphere; estimate based on stable isotope data. Geophys Res Lett 21:557–560

Gat JR et al (2003) Isotope composition of air moisture over the Mediterranean Sea: an index of the air–sea interaction pattern. Tellus 55B:953–965

Gibson JJ et al (2005) Progress in isotope tracer hydrology in Canada. Hydrolog Process 19:303–327

Hendricks MB, DePaolo DJ, Cohen RC (2000) Space and time variation of $\delta^{18}O$ and δD in precipitation: can paleotemperature be estimated from ice cores? Global Biogeochem Cycles 14:851–861

IAEA (1992) Statistical treatment of data on environmental isotopes in precipitation. IAEA, Vienna, p 781 pp

IAEA (2001) GNIP Maps and Animations. http://isohis.iaea.org

IAEA/WMO (2004) Global network for isotopes in precipitation, the GNIP database. http://www-naweb.iaea.org/napc/ih/GNIP/IHS_GNIP.html

Ingraham NL, Taylor BE (1991) Light stable isotope systematics of large-scale hydrologic regimes in California and Nevada. Water Resour Res 27:77–90

Jacob H, Sonntag C (1991) An 8-year record of the seasonal variation of ^{2}H and ^{18}O in atmospheric water vapour and precipitation at Heidelberg, Germany. Tellus 43B:291–300

Jouzel J, Merlivat L (1984) Deuterium and oxygen 18 in precipitation: modelling of the isotopic effects during snow formation. J Geophys Res 89:11749–11757

Kurita N, Yoshida N, Inoue G, Chayanova EA (2004) Modern isotope climatology of Russia: a first assessment. J Geophys Res 109:D03102. doi:10.1029/2003JD003404

Lawrence JR et al. (2004) Stable isotopic composition of water vapor in the tropics. J Geophys Res 109. DOI 10.1029/2003JD004046

Lee J-E, Fung I (2007) "Amount effect" of water isotopes and quantitative analysis of post-condensation processes. Hydrol Process . doi:10.1002/hyp. 6637

Lykoudis SP, Argiriou AA (2007) Gridded data set of the stable isotopic composition of precipitation over the eastern and central Mediterranean. J Geophys Res 112:D18107. doi:10.1029/2007JD008472

Masson-Delmotte V et al (2008) A review of Antarctic surface snow isotopic composition: observations, atmospheric circulation, and isotopic modeling. J Clim 21:3359–3387. doi:10.1175/2007JCLI2139.1

Meehan TD, Giermakowski JT, Cryan PM (2004) GIS-based model of stable hydrogen isotope ratios in North American growing-season precipitation for use in animal movement studies. Isot Environ Health Stud 40:291–300

Merlivat L, Jouzel J (1979) Global climatic interpretation of the deuterium-oxygen 18 relationship for precipitation. J Geophys Res 84:5029–5033

New M, Hulme M, Jones P (1999) Representing twentieth-century space-time climate variability. Part I: development of a 1961–90 mean monthly terrestrial climatology. J Clim 12:829–856

Peixoto JP, Oort AH (1996) The climatology of relative humidity in the atmosphere. J Clim 9:3443–3463

Peng H, Mayer B, Harris S, Krouse HR (2004) A 10-year record of stable isotope ratios of hydrogen and oxygen in precipitation at Calgary, Alberta, Canada. Chem Phys Meteorol 56:147–159. doi:10.1111/j.1600-0889.2004.00094.x

Rozanski K, Araguás-Araguás L and Gonfiantini R (1993) Isotopic patterns in modern global precipitation. In: Swart PK, Lohmann KC, McKenzie J, Savin S (eds) Climate change in continental isotopic records. Geophysical Monograph 78. American Geophysical Union, Washington, D.C., pp 1–36

Salati E, Dall'Olio A, Matsui E, Gat JR (1979) Recycling of water in the Amazon Basin: an isotopic study. Water Resour Res 15:1250–1258

Schmidt GA, LeGrande AN, Hoffmann G (2007) Water isotope expressions of intrinsic and forced variability in a coupled ocean-atmosphere model. J Geophys Res 112:D10103. doi:10.1029/2006JD007781

U. S. National Geophysical Data Center (1998) ETOPO-5 five minute gridded world elevation. NGDC, Boulder, Colorado, USA. http://www.ngdc.noaa.gov/mgg/global/etopo5.HTML

Ufnar DF, González LA, Ludvigson GA, Brenner RL, Witzke BJ (2004) Evidence for increased latent heat transport during the Cretaceous (Albian) greenhouse warming. Geology 32:1049–1052. doi:10.1130/G20828.1

van der Veer, G., et al. (2009), Spatial interpolation of the deuterium and oxygen-18 composition of global precipitation using temperature as ancillary variable, *Journal of Geochemical Exploration*, 101(2): 175–184. doi:10.1016/j.gexplo.2008.06.008.

Welker JM (2000) Isotopic ($\delta^{18}O$) characteristics of weekly precipitation collected across the USA: an initial analysis with application to water source studies. Hydrol Process 14:1449–1464

Worden J, Noone D, Bowman K (2007) Importance of rain evaporation and continental convection in the tropical water cycle. Nature 445:528–532. doi:10.1038/nature05508

Yurtsever Y and Gat JR (1981) Atmospheric waters. In: Gat JR, Gonfiantini R (eds) Stable isotope hydrology: deuterium and oxygen-18 in the water cycle. International Atomic Energy Agency, Vienna, pp 103–142

Chapter 8
Approaches to Plant Hydrogen and Oxygen Isoscapes Generation

Jason B. West, Helen W. Kreuzer, and James R. Ehleringer

8.1 Introduction

The hydrogen and oxygen stable isotope ratios (δ^2H and $\delta^{18}O$) of plant water, the organic molecules that make up plant tissues and the gases produced during plant metabolism all record important aspects of a plant's growth environment and physiological activity at various spatial and temporal scales. These environmental signals are also modulated by morphological and other differences between species, including their responses to environmental variation. As such, stable isotope ratios are important tools for improved understanding in plant ecology and beyond (West et al. 2006). The connections between these isotopic records in plants and spatially-varying processes have been evident for decades. Recent efforts are expanding our mechanistic understanding (e.g., Barbour et al. 2007; Cuntz et al. 2007; Ripullone et al. 2008; Shu et al. 2008) and significant technological developments continue to provide the potential to significantly accelerate advances in understanding (e.g., Lis et al. 2008; Peters and Yakir 2008; Vendramini and Sternberg 2007). Among others, these advances will stimulate a significant increase in sampling intensity and model sophistication, allowing the generation of highly useful and data rich plant hydrogen and oxygen isoscapes and insights in a wide variety of fields (Helliker and Richter 2008; Kahmen et al. 2008).

J.B. West (✉)
Texas AgriLife Research and Department of Ecosystem Science and Management, Texas A&M University System, College Station, TX
e-mail: jbwest@tamu.edu

H.W. Kreuzer
Pacific Northwest National Laboratory, Richland, Washington
e-mail: helen.kreuzer@pnl.gov

J.R. Ehleringer
Department of Biology, University of Utah, Salt Lake CityUtah,
e-mail: ehleringer@biology.utah.edu

J.B. West et al. (eds.), *Isoscapes: Understanding Movement, Pattern, and Process on Earth Through Isotope Mapping*, DOI 10.1007/978-90-481-3354-3_8,

The focus for this chapter is on spatial variation in plant hydrogen and oxygen isotopes, with an emphasis on continental to global scales and the utility of isoscapes to improving understanding of a variety of processes. The central research areas in which plant δ^2H and $\delta^{18}O$ isoscapes are likely to continue to yield significant insights are: (1) biosphere–atmosphere interactions, (2) past continental climate, and (3) forensic applications. The role of plant δ^2H and $\delta^{18}O$ isoscapes in these three central research areas will form the focus of this chapter, with an attempt to identify common themes and approaches across disciplines rather than to treat these comprehensively. It should also be noted that many aspects of the use of plant δ^2H and $\delta^{18}O$ in primarily non-spatial contexts have been reviewed elsewhere (e.g., Barbour 2007; Dawson et al. 2002; Ehleringer et al. 2002; Pataki et al. 2003; Yakir and Sternberg 2000).

In order to provide a mechanistic context for the generation and application of isoscapes to spatial problems, the major models of leaf water and cellulose δ^2H and $\delta^{18}O$ will be outlined first and existing efforts to utilize these models to make spatially explicit predictions will be described.

8.2 Leaf Water Isoscapes

Attempts to model large-scale spatial variability in leaf water $\delta^{18}O$ were first motivated by a desire to understand its effect on the isotopic composition of atmospheric gases, specifically atmospheric oxygen $\delta^{18}O$ (Farquhar et al. 1993; Gillon and Yakir 2001) and the $\delta^{18}O$ of CO_2 (Peylin et al. 1999). Leaf water may also be thought of as the fundamental starting point for plant H & O isoscapes, linking plant H & O isoscapes to meteoric, surface, and sub-surface waters, as well as plant organic compounds and their connection to the rest of the biosphere. In general, the isotopic composition of xylem water prior to entering the leaf will be very similar to the isotopic composition of plant source water, as there is generally no fractionation with root uptake (White et al. 1985), with this source water being derived ultimately from precipitation. This is true also only in the case that there is not evaporation from the stems being sampled (Dawson and Ehleringer 1993). There are two primary classes of models that describe the isotopic composition of leaf water: steady-state and non-steady-state and a range of approaches to modeling both, including a set of approaches to understanding within-leaf heterogeneity (e.g., Gan et al. 2003; Helliker and Ehleringer 2000; Ogee et al. 2007; Yakir et al. 1994). In this section, we discuss briefly the primary models that form the basis for describing leaf water isotope ratios and the current state of leaf water H & O isoscapes.

Leaf water isotope ratios have been modeled using modified open water body analogs (the Craig–Gordon model, Flanagan et al. 1991; Roden and Ehleringer 1999). A formulation of the steady-state leaf water isotope ratio, which includes diffusion through the leaf boundary layer, is:

$$R_e = \alpha^* \left[\alpha_k R_S \left(\frac{e_i - e_s}{e_i} \right) + \alpha_{kb} R_S \left(\frac{e_s - e_a}{e_i} \right) + R_A \left(\frac{e_a}{e_i} \right) \right] \tag{8.1}$$

where R_e is the isotope ratio of evaporatively-enriched leaf water (at the site of evaporation), R_S is the isotope ratio of the source water, R_A is the isotope ratio of the atmospheric water vapor, e_i is internal leaf vapor pressure, e_s is the leaf surface vapor pressure, and e_a is atmospheric vapor pressure. The equilibrium fractionation (α*) is described as:

$$\alpha^* = \frac{R_L}{R_V} = e^{\left(\frac{a}{T^2} - \frac{b}{T} - c \right)} \tag{8.2}$$

where e here is Euler's number, R_L is the liquid water isotope ratio ($^2H/^1H$ or $^{18}O/^{16}O$), R_V is the water vapor isotope ratio, and T is temperature in degrees Kelvin, and a & b are constants (Majoube 1971). Values for the constants are: a = 1,137, b = 0.4156, c = 0.0020667 for oxygen and a = 24,844, b = 76.248, and c = 0.052612 for hydrogen. The effect of diffusion is described by α_k and is estimated as 1.032 for oxygen and 1.0164 for hydrogen, with boundary layer diffusion estimated by $\alpha_k^{2/3}$ (Cappa et al. 2003). Observed leaf water isotope ratios are often less enriched than those predicted by C-G formulations, although monocot leaves yield a special case of greater enrichment not treated here (Helliker and Ehleringer 2000; Ogee et al. 2007). Modifications to account for this discrepancy recognize multiple pools within the leaf (Gan et al. 2002), as well as the incorporation of a Péclet effect (opposing effects of convection of water towards the site of evaporation and diffusion of the heavier isotopologues away from the site of evaporation; Barbour et al. 2000):

$$\wp = \frac{LE}{CD} \tag{8.3}$$

where L is the effective path length between the site of evaporation and the un-enriched source water, E is the evaporation rate (mol m^{-2} s^{-1}), C is the molar density of water (55.5×10^3 mol m^{-3}), and D is the diffusivity of the $H_2{}^{18}O$ in water (2.66×10^{-9} m^2 s^{-1}).

Non-steady state models of leaf water oxygen isotope ratios explicitly include the dynamic nature of changing leaf water isotope ratios as conditions change (Dongmann et al. 1974; Lai et al. 2006). A formulation that describes the non-steady leaf water $\delta^{18}O$ is:

$$\delta_{en}(t) = \delta_e(t) - [\delta_e(t) - \delta_{en}(t-1)] \exp\left(\frac{-\delta t}{\tau \zeta} \right) \tag{8.4}$$

where $\delta_{en}(t)$ and $\delta_{en}(t-1)$ represent non-steady state oxygen isotope ratios of leaf water at the sites of evaporation at time t and t − 1, respectively, and $\delta_e(t)$ is the leaf water $\delta^{18}O$ at steady state, predicted by Eq. 8.3. τ and ζ describe the turnover times and fractionations, which are dependent on leaf water volume, transpiration and relative humidity (Bariac et al. 1994; Cuntz et al. 2003). Further developments and improvements in modeling the isotopic composition of leaf water continue in this active area of research (Cuntz et al. 2007) and as our understanding of the controls on leaf water isotopic composition grows so will the sophistication of leaf water H & O isoscapes and their potential utility to a range of questions.

Global leaf water oxygen isoscapes have been produced based primarily on these models and with the goal of understanding the isotopic composition of atmospheric gases, (e.g., Ciais et al. 1997; Farquhar et al. 1993). Although clearly useful for specific research questions, these model outputs are not readily accessible across the scientific disciplines that could benefit from them. This is in spite of their potential utility to a number of researchers in diverse fields. Following the development of high resolution climate and precipitation isotope data layers, an approach that takes advantage of Geographic Information System tools was developed to generate global, continuous leaf water δ^2H and $\delta^{18}O$ isoscapes (West et al. 2008). These isoscapes were generated using a steady-state modeling approach similar to that described above, with input drivers that included global precipitation isoscapes (http://waterisotopes.org, also see Bowen this volume) and continuous climate grids from, in this case, the Climate Research Unit (http://www.cru.uea.ac.uk). The annual average (unweighted) leaf water isoscapes for the sites of evaporation from this work are shown in Fig. 8.1. These annual average isoscapes as well as the monthly isoscapes generated directly by the models are available now as GIS raster data layers (http://isoscapes.org), along with the model code and data layers used as inputs from the author, and will soon be available through a web-based modeling interface called "IsoMAP." In addition to the steady-state Craig–Gordon output, other leaf water isoscapes were generated using a two-pool model for bulk leaf water and an additional output incorporating a Péclet effect. Clearly a large range of model structures and parameters could be envisioned and potentially appropriate for a specific question, making the GIS platform a productive avenue for streamlining modeling efforts and sharing among researchers. Certain assumptions were necessary for the generation of these isoscapes and should be noted. Among the most important were: (1) the model(s) accurately described the controls on long-term, average leaf water enrichment (across species), (2) long-term, average plant source water was approximated well by the annual average precipitation isoscapes, (3) long-term, average environmental conditions affecting leaf water isotope enrichment were approximated well by the long-term average climate grids, and (4) vapor was in isotopic equilibrium with plant source water (average precipitation). Adjustments of stomatal conductance and leaf temperature were also made (see West et al. 2008 for more information). Although these assumptions are difficult to test at global scales and

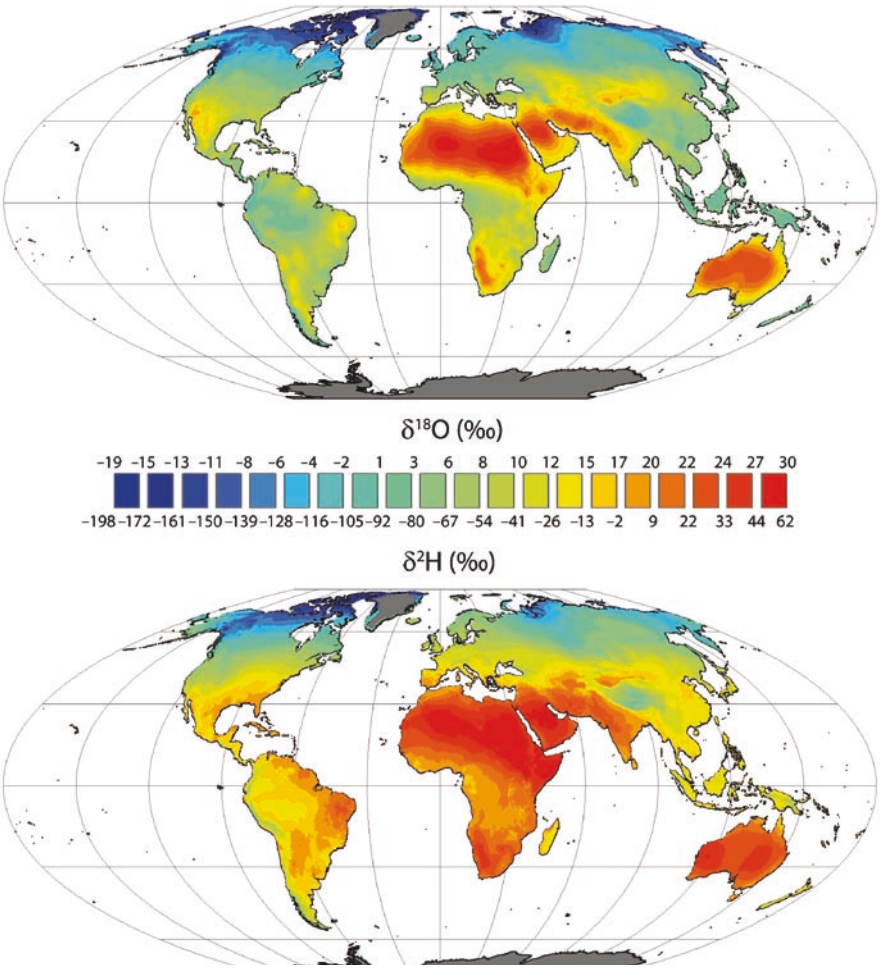

Fig. 8.1 Global mean annual average leaf water $\delta^{18}O$ and $\delta^{2}H$ isoscapes for the sites of evaporation within leaves (Eq. 8.1; reproduced with permission from West et al. 2008; see Appendix 1, Color Section)

are certainly incorrect at small scales in particular cases, the long-term average leaf water $\delta^{18}O$ isoscape produced values were quite comparable to measured average values and prior modeled latitudinal variation (West et al. 2008), suggesting that at a global scale, the modeling approach yielded leaf water isoscapes that approximated reasonably well the true long term average values. The advantage of the GIS approach using mechanistic models is that it is scalable to the objective and available data layers and can be interfaced with other spatially explicit data that could be relevant.

8.3 Modern Biosphere–Atmosphere Interactions

The integration of plant hydrogen and oxygen isoscapes into biosphere–atmosphere modeling and research is in its infancy. This is due in part to significant uncertainties in key variables and data limitations imposed by the labor and time intensive nature of stable isotope analysis of relevant components. However, we know that terrestrial vegetation has a significant impact on the hydrogen and oxygen isotopic composition of atmospheric gases, varies across space and time (Vaughn et al. this volume), and this impact is the result of a range of biological and biophysical processes (Cuntz et al. 2003; Farquhar et al. 1993; Hoffmann et al. 2004; Lee et al. 2007). In addition to the dominant role of soils and anthropogenic influences, biomass burning also has important consequences for the stable isotope ratios of CH_4 and H_2 globally, but with this component likely dominated by the fractionations associated with combustion, rather than spatial variation in the vegetation δ^2H (Gerst and Quay 2001; Yamada et al. 2006). Improved interpretation of the observed spatiotemporal variation in atmospheric gas δ^2H and $\delta^{18}O$ will develop in part through better understanding of the spatiotemporal variation in vegetation. That is, better vegetation H & O isoscapes will yield better understanding of coupled carbon and water cycle processes, especially at regional to global scales. The development of improved isoscapes follows in part improved mechanistic understanding of the relationships between vegetation, incoming radiation and climate. Exciting advances in this area are being made, for example in understanding the complex influences of clouds on plant physiology and therefore on the exchange of $CO^{18}O$ and CO_2 between vegetation and the atmosphere through intensive measurement and modeling efforts (Still et al. in press). New approaches to partitioning the transpiration and evaporation fluxes from the biosphere to the atmosphere based on the isotopic composition of precipitation and river stable isotopes in closed hydrologic basins are also being pursued (Ferguson and Veizer 2007). Here, if spatially explicit direct estimates of transpiration fluxes across these watersheds could be developed, this would provide an independent test of these indirect estimates. Although several unknowns remain, plant hydrogen and oxygen isoscapes hold significant promise in this area by contributing to improved understanding of the coupled carbon–water dynamics of the biosphere.

8.4 Inferring Past Environments

Understanding the controls on spatiotemporal variation in plant δ^2H and $\delta^{18}O$ values is also critical to interpreting a wide range of proxies for past environments (Feng and Epstein 1996; Feng et al. 2007; Hou et al. 2008; Loader and Hemming 2004; Miller et al. 2006, also see Leavitt et al. this volume). Because the isotopic composition of plant compounds have the potential to record climate (e.g., the

oxygen isotope ratios of cellulose extracted from tree rings (Epstein et al. 1977; Gray and Thompson 1977), significant experimentation and modeling has been done to address fractionation associated with photosynthesis and post-photosynthesis biochemical reactions. Interest in spatial variation of the δ^2H & $\delta^{18}O$ of the organic components of plants has been focused primarily on bulk cellulose as a potential recorder of temperature (Gray and Thompson 1977), but has since expanded to other exciting potential proxies such as n-alkanoic acids from leaf waxes and compounds derived from cellulose that might be better recorders (phenylglucosazone; Hou et al. 2008; Sternberg et al. 2007). The fractionations associated with cellulose synthesis have been modeled as an essentially two-step process: photosynthetic formation of sucrose in isotopically-enriched leaf water followed by cellulose formation, either in the leaf or in the stem where the water environment is assumed to be similar to that of the plant source water. Fractionation factors for hydrogen and oxygen have been estimated as $\varepsilon = -171‰$ and $+27‰$ (Yakir and Deniro 1990) for the effects of photosynthesis (note that Estep and Hoering 1981 estimated a range from $-120‰$ to $-100‰$ for hydrogen). The subsequent formation of cellulose (so-called heterotrophic fractionation) has been estimated as $\varepsilon = +158‰$ for hydrogen and $+27‰$ for oxygen (Roden and Ehleringer 2000), again with other observations being similar (e.g., Luo and Sternberg 1992 estimated it to range from ranging from $+144‰$ to $+166‰$). These models group or "black box" a number of biochemical processes and make implicit or explicit assumptions that, if incorrect, could have significant consequences for interpretations of the isotopic composition of cellulose. For example, recent work on the $\delta^{18}O$ and δ^2H of cellulose argues that, contrary to one of these assumptions, there are position-specific effects, calling into question efforts to interpret bulk cellulose $\delta^{18}O$ in terms of source water and climate influences only (Augusti et al. 2008; Sternberg et al. 2006). An additional, central assumption used to interpret cellulose $\delta^{18}O$ records in tree rings is that leaf temperature is coupled to atmospheric temperature. A recent paper reports striking constancy of leaf temperature across a wide range of environments, suggesting homestasis in leaf temperature and only weak coupling with ambient temperatures (Helliker and Richter 2008). Continued efforts here promise to improve and refine models of isotopic fractionations in plants during metabolism, thus yielding greater accuracy in developing plant organic matter isoscapes. The isotopic compositions of several other plant compounds have recently been analyzed and described (e.g., leaf waxes, Sachse et al. 2004; Smith and Freeman 2006) and hold promise as additional proxies as our understanding of these plant-based archives improves.

A recent report provides an excellent example of the utility of spatially explicit sampling and analysis of modern wood cellulose $\delta^{18}O$ to improve the interpretation of cellulose $\delta^{18}O$ in the context of reconstructing paleoenvironmental conditions (Richter et al. 2008). Samples here were collected both across a wide range of environments and from several species in one area. Comparisons were made between the cellulose $\delta^{18}O$ and climate variables (temperature and relative humidity) and precipitation $\delta^{18}O$. As expected, strong correlations between precipitation and climate variables were observed. However, variation was observed across species

and the significant correlation with relative humidity limits the potential to interpret cellulose $\delta^{18}O$ simply in terms of temperature. Clearly large, distributed sampling networks and the development of improved cellulose isoscapes that reflect the drivers of spatiotemporal variability in cellulose or other plant compound $\delta^{2}H$ and $\delta^{18}O$ would significantly improve our ability to interpret these proxies (Hemming et al. 2007; Williams et al. 2007).

In addition to archives preserved in organic plant material, atmospheric gases trapped in ice cores have been studied for decades as rich stores of past atmospheric and environmental conditions. Much of the isotopic information in these cores is related to the activities of the biosphere, including that of vegetation. As discussed above, a significant effect of vegetation on the isotopic composition of atmospheric gases is the effect of leaf water $\delta^{18}O$ on atmospheric oxygen $\delta^{18}O$, which is enriched above ocean water and therefore results in a significant enrichment of atmospheric O_2. This effect remains relatively poorly constrained because of the incomplete understanding of the spatiotemporal variation in leaf water $\delta^{18}O$, thus limiting inferences that can be drawn from atmospheric O_2 $\delta^{18}O$ trapped in ice cores. The difference between ocean water $\delta^{18}O$ and atmospheric oxygen is +23.8‰ and largely reflects photosynthesis and respiration in the marine and terrestrial biospheres, as well as other more minor influences. The magnitude of this "Dole effect" has remained surprisingly constant over approximately 130,000 years (Bender et al. 1994), with some more rapid variations reported recently from ice cores (Landais et al. 2007). Understanding these variations depends on an understanding of the primary controls on atmospheric oxygen $\delta^{18}O$, and leaf water $\delta^{18}O$ is an important factor here. Although great strides are being made in improving our understanding of the controls on leaf water $\delta^{18}O$, this remains an important area of research, especially as it relates to what controls variation in leaf water $\delta^{18}O$ at a range of spatiotemporal scales. Again, large sampling networks, continued efforts to understand and model the mechanistic controls, and further work on generating leaf water isoscapes and integrating them into larger modeling efforts promise to significantly improve the interpretability of these archives.

8.5 Forensic Applications

Hydrogen and oxygen isotope ratios of plant organic materials have shown significant utility for a wide array of research and applications related to human activities. These include archaeological trade routes and social interactions, modern criminal forensic reconstructions and investigations, and food and trade security and verification (Aramendia et al. 2007; DeNiro et al. 1988; Kelly et al. 2005; Keppler et al. 2007; Stern et al. 2006, 2008). Across all three categories, the utility of hydrogen and oxygen isotope ratios have been recognized as potential recorders of geographic origin and initial efforts at generating isoscapes for use in these fields are

ongoing. Two examples are described here demonstrating both the potential utility of plant H and O isoscapes and two different approaches to their generation with the intention that future work will further enhance the accuracy and utility of the models and isoscapes generated. We describe the methodological aspects in some detail to illustrate the range of questions, data, and decisions related to the generation of these isoscapes.

8.5.1 Cellulose Isoscapes – Counterfeit Money Tracking

As part of an effort to develop a tool for tracking sources of counterfeit money (the paper of which is composed largely of cotton cellulose) global cellulose isoscapes have been developed (Ehleringer 2009 unpublished). These cellulose isoscapes could also be utilized for forming expectations about spatial variability of cellulose isotope ratios, or in an inverse fashion to infer climate from cellulose isotopic compositions of spatial gradients. Just as in the leaf water example above, a GIS approach was taken. Monthly climate normal grids (WMO normal period of 1961–1990) produced at 10' resolution over the Earth's land surface for air temperature and relative humidity (CRU CL 2.0; http://www.cru.uea.ac.uk) were used. In order to produce a "cotton growing season" climate grid, each month's grid was masked with a "binary grid" produced from the monthly temperature grids. These binary grids were produced by replacing each grid cell with a "1" if the monthly average temperature was at least 16°C, or a "0" if that grid cell value was less than 16°C (null values remained null). Both the temperature and relative humidity monthly grids were then multiplied by their respective "binary grids" and then divided by the annual sum of binary grids. This produced an estimate of cotton growing season climate for each grid cell. This method results in some grid cells that have non-zero climate values based on as little as 1 month of climate. Clearly cotton is not grown in regions where the average monthly temperature rises above 16°C for only 1 or 2 months. These cells are eliminated from the final prediction map based on a raster of cotton growing regions described below.

Amount-weighted growing season precipitation isotope grids were also produced in a similar fashion. We began with monthly precipitation isoscapes estimated using modified published methods and at 10' resolution (Bowen this volume). Each monthly isotope grid was then multiplied by its respective binary 16°C grid described above. In addition, average monthly total precipitation grids were multiplied by their respective binary 16°C grids to produce approximate cotton growing season grids. Each month's growing season isotope grid (δgs_i, where i = month number) was then multiplied by its respective growing season precipitation amount grid (Pgs_i). These 12 monthly grids were then summed and divided by the sum of the 12 monthly precipitation amount grids to give an amount-weighted growing season precipitation isotope grid ($\delta_{gs\text{-}wtd}$). These input layers were then used to calculate cotton boll cellulose $\delta^{18}O$ at each raster grid cell using the

model described by Roden et al. (2000). Note that, as described previously, several of the characteristics of this model are the subject of active, current investigation and debate. As such, the predictions from the model should be taken as an initial attempt at a global cellulose isoscape, limited by available data and model uncertainties. In order to make cotton boll $\delta^{18}O$ predictions only for locations in which it is likely that cotton is grown, an additional raster layer was used to mask these "raw" predictions of cotton boll cellulose. Leff et al. (2004) employed satellite, agricultural census, and other data to produce global datasets of major crop producing regions. These datasets are available as 5' resolution global grids where each grid cell has a value that represents the fraction of that area covered by a given crop. The 5' grids made available by the authors were averaged to our 10' resolution using nearest neighbor resampling. Non-zero cells were assigned a value of one, and the cells with a value of zero retained that value. This resulted in a binary raster where each grid cell with a 1 represented a non-zero probability of having cotton growing within that cell. This binary grid was then multiplied by the above cotton boll cellulose $\delta^{18}O$ grids. This eliminated predictions for regions that are unlikely to produce cotton, but it may be thought of as a conservative elimination since it includes all cells that Leff et al. estimated contained any cotton production.

The resulting global $\delta^{18}O$ range covers approximately 36‰ (see Fig. 8.2). The highest predicted values in the world were for areas of Africa and the Middle East, whereas some of the lowest values predicted were for areas such as the eastern region of China and North Korea. Values predicted for the United States exhibited a mean of 29‰, with a low of 25‰, and a few isolated values reaching as high as 39‰. Comparisons with a small, poorly-constrained global collection of cotton fiber and currencies revealed reasonable overlap between data and model predictions. Of the 11 fiber samples obtained from nine countries, ten of the $\delta^{18}O$ values fell within the predicted ranges for those countries (Ehleringer 2009 unpublished). Although evaluation of the cotton isoscape is currently limited by comparison with "authentics," the reasonable agreement at a large scale was encouraging. It is possible that isoscapes targeted at perhaps phenylglucosazone or other compounds along with a greater intensity of data for authentics could yield better predictive isoscapes. At present these cellulose isoscapes are useful for general targeting of efforts, in conjunction with additional information.

8.5.2 Plant Lipid Isoscapes – Ricin Source Tracking

Although leaf water and cellulose have been the most extensively modeled, other plant components, such as lipids, have the potential to yield important information about plant environments (Jia et al. 2008; Jones et al. 2008; Smith and Freeman 2006; Sternberg 1988; Xia et al. 2008). Motivation for understanding the drivers of geographic variation in plant lipids also includes their potential use in forensic reconstruction or intelligence. An example is provided by the oil derived from

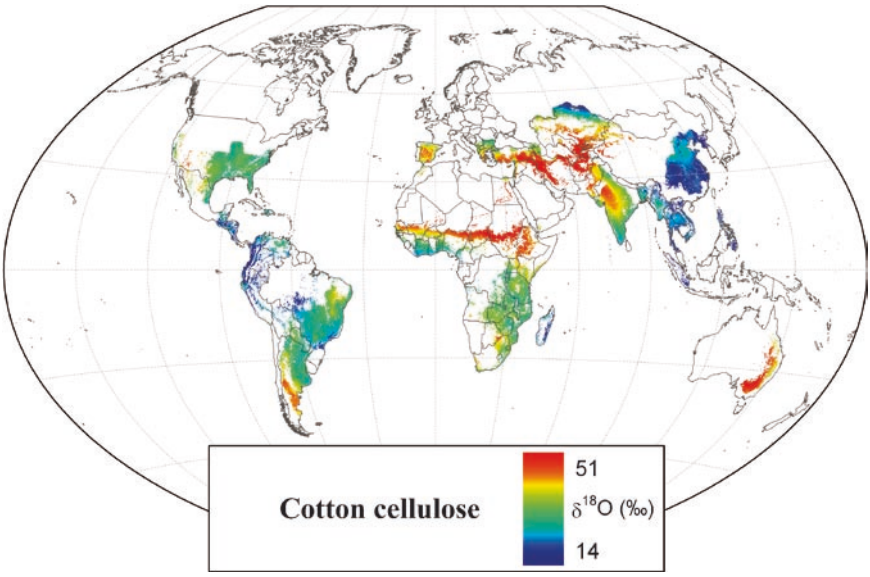

Fig. 8.2 Cotton $\delta^{18}O$ isoscape produced using a steady-state leaf water model (see Fig. 7.1), published fractionation factors for cellulose and masked for climate limitations and mapped agricultural production of cotton (see text for details; see Appendix 1, Color Section)

Castor Bean (*Ricinus communis*) seeds. From a forensics standpoint, the growth location of castor bean seeds used to make ricin (a deadly poison) is important. The simplest component of the castor bean seed is arguably castor oil. It is primarily ricinoleate (McKeon et al. 2000) and therefore from a compositional standpoint, should be relatively simple to model its isotopic composition, relative to the ricin itself, for example. In addition, the δ^2H of plant lipids is well correlated with plant source water isotopic composition. From a controlled experiment with known source water isotopic composition, a castor oil fractionation factor of $\alpha = 0.875$ was estimated (Ehleringer 2009 unpublished), a value that compares well to a previous model of lipid fractionation of $\alpha = 0.870$ (Sternberg 1988). With this experimentally derived model of castor oil, global castor oil hydrogen isoscape could be constructed, assuming that the source water is accurately estimated, the model is complete and there is no retention of the leaf water δ^2H in the castor oil (i.e., all, or nearly all of the hydrogen atoms exchange with the seed water that is close to the source water δ^2H). Part of the outcome of this exercise is to determine the potential magnitudes of the effect of these uncertainties on global-scale modeling of plant lipids. The model shown above was executed using annual average precipitation values from the Bowen precipitation δ^2H isoscape to yield the castor oil δ^2H isoscape (Fig. 8.3). Individual predictions from the isoscape were then compared with measured values from plants grown at many locations around the world.

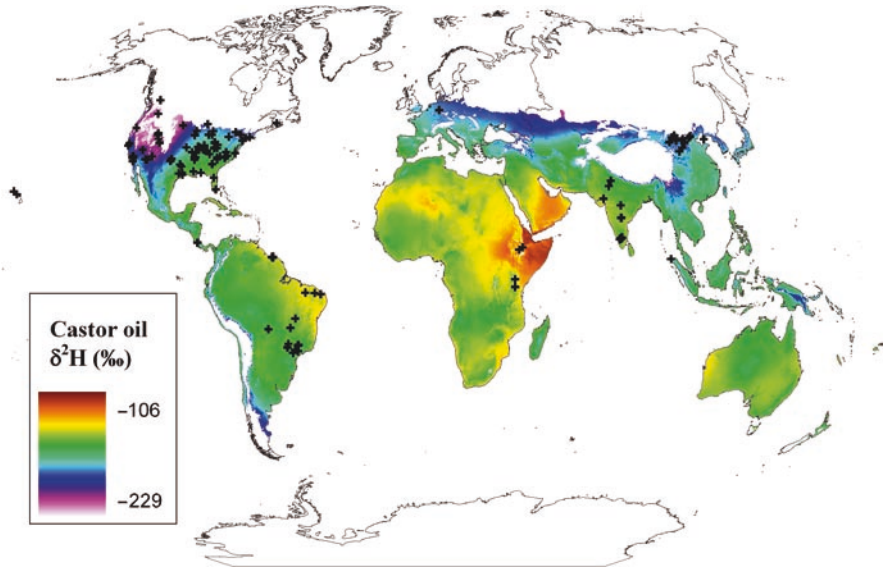

Fig. 8.3 Source water δ^2H and predicted castor oil δ^2H (‰) based on an experimentally-derived fractionation factor (see text). Lanud areas in *white* have mean annual temperatures below 7°C and are therefore unlikely to be regions where castor beans are grown. Continents are outlined in *black*. Locations of plants sampled and for which the δ^2H of extracted castor oil was determined are shown as *black crosses* (see Appendix 1, Color Section)

All measured values fell close to the 1:1 line suggesting that the very simplistic model predicts the observed castor oil δ^2H reasonably well, but does not capture the local and perhaps regional variability (Fig. 8.4). In evaluating the scatter around the 1:1 line of the model, it is important to understand the potential sources of variation. For the locations of the castor oil samples, the average 95% confidence interval for the modeled precipitation δ^2H was 6‰ (Bowen this volume), with a minimum of 1‰ and a maximum of 11‰. This suggests that some of the variation observed in Fig. 8.4 is likely due to precipitation model inaccuracies. Also, plant source water can vary from long term average annual precipitation and this potential source of variation is not well constrained here. Further, even under controlled conditions castor oil δ^2H exhibits substantial variability (potentially as much as ±10‰), contributing to uncertainty about the model itself (Ehleringer 2009 unpublished). In addition, no mechanisms for physiological effects were incorporated into the model.

Although modeled castor oil δ^2H values occur above and below the 1:1 line, a greater proportion of them fall above the line, suggesting a general over-prediction of castor oil δ^2H by this simple model. In addition, a large part of this group is composed entirely of tropical samples. This suggests that either the model does not perform well in the tropics, or that the map predictions for tropical precipitation consistently overestimate the actual castor bean source water δ^2H. Although Bowen & Revenaugh point out that their model does generally account for the tropical

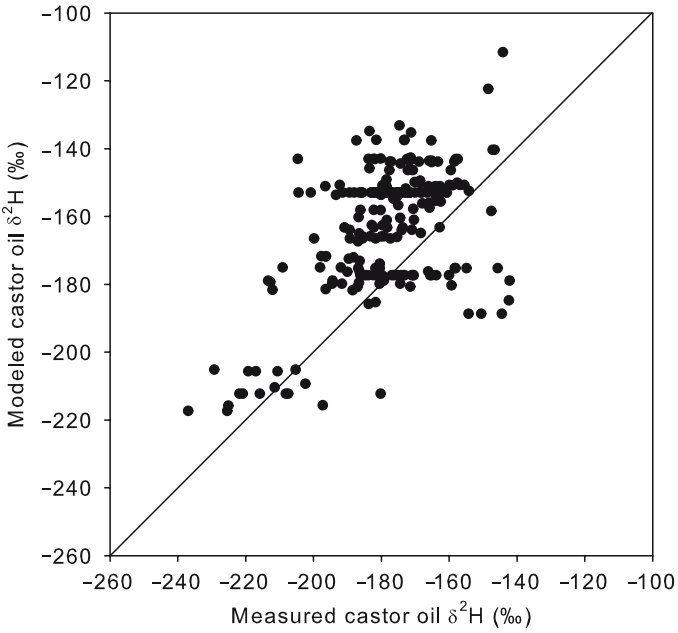

Fig. 8.4 Measured versus predicted castor oil δ^2H (‰). *Open circles* are samples from the temperate zone and the closed triangles are tropical samples (within 23.5° of the equator). The diagonal line is the 1:1 line

"rainout effect," due to the somewhat poor data sampling density in the tropics, there might remain some consistent inaccuracies in the model predictions for that part of the globe. In addition, there was no provision for the effects of either evaporative enrichment of seed water or retention of the leaf water signal in the castor oil, both of which could increase its δ^2H value. Since the fractionation factor was estimated in a relatively dry environment (Salt Lake City, Utah), this might also have resulted in enrichment bias in the model.

This example demonstrates the promise and current challenges associated with plant isoscapes. Clearly there is a record of global spatial variation in this plant organic material and a simple model captures this variation reasonably well. However, there are also obviously important effects not incorporated in this particular model, including accounting for potential effects of evaporative enrichment.

8.6 Frontiers

Networks of observations of plant H & O isotope ratios are only recently being assembled (Hemming et al. 2007, Agarwaal et al. this volume) and are not yet able to supply the distributed data necessary to directly test large-scale spatial

predictions of plant stable isotope ratios. However, individual efforts at data collection and model application are improving our understanding and ability to test and develop models and descriptions of spatial variability in plant H & O isotope ratios. These efforts should be encouraged and supported. In addition, there are a number of large-scale enterprises underway that include distributed sampling and stable isotope analysis, including the National Ecological Observatory Network (NEON) in the USA and more commerce or forensics oriented initiatives (e.g., TRACE, http://www.trace.eu.org/; Kelly et al. 2005; Rossmann et al. 1999). Nascent efforts such as the IAEA-sponsored Moisture Isotopes in the Biosphere and Atmosphere (MIBA) should be encouraged and expanded to begin to describe the large-scale variability in plant stable isotopes and to include where possible measurements of the isotope ratios of atmospheric water vapor. These large, spatially explicit databases of plant or plant-derived materials continue to be populated and expanded to more species or products and are of obvious utility for geo-sourcing these materials.

Efforts to improve underlying models are also ongoing and should be enhanced and expanded, given the significant potential insights to be gained by improving our understanding of the spatio-temporal variability of plant hydrogen and oxygen isotope ratios. The technological capacity to collect and efficiently analyze large, spatially explicit databases is now available and should also be actively exploited. It will be critical that workers across disciplines share data, models, and model products, including isoscapes using available and forthcoming cyberinfrastructure. In addition to ongoing model improvements and distributed data collection, cross-disciplinary interaction will be critical to rapid advancements in the utilization of the information recorded in the spatiotemporal variation of plant hydrogen and oxygen stable isotopes. It is likely that efforts targeted at specific objectives (e.g., wine provenancing; West et al. 2007) can yield insights into other areas (e.g., wines as climate archives; Ingraham and Caldwell 1999). Two important frontiers can therefore be identified: (1) improve our mechanistic understanding and models of plant stable isotope ratios, including leaf water and plant organic components, and (2) develop and improve distributed data collection networks. It will be important to make progress on both fronts to enhance our understanding of these “recorders” of the biochemical and biophysical processes with which plants interact.

References

Aramendia MA et al (2007) Oxygen-18 measurement of Andalusian olive oils by continuous flow pyrolysis/isotope ratio mass spectrometry. Rapid Commun Mass Spectrom 21:487–496

Augusti A, Betson TR, Schleucher J (2008) Deriving correlated climate and physiological signals from deuterium isotopomers in tree rings. Chem Geol 252:1–8

Barbour MM (2007) Stable oxygen isotope composition of plant tissue: a review. Funct Plant Biol 34:83–94

Barbour MM, Farquhar GD, Hanson DT, Bickford CP, Powers H, McDowell NG (2007) A new measurement technique reveals temporal variation in delta O-18 of leaf-respired CO2. Plant Cell Environ 30:456–468

Barbour MM, Schuur U, Henry BK, Wong SC, Farquhar GD (2000) Variation in the oxygen isotope ratio of phloem sap sucrose from castor bean. Evidence in support of the Péclet Effect. Plant Phys 123:671–679

Bariac T, Gonzalezdunia J, Katerji N, Bethenod O, Bertolini JM, Mariotti A (1994) Spatial variation of the isotopic composition of water (O-18, H-2) in the soil-plant-atmosphere system. 2. Assessment under field conditions. Chem Geol 115:317–333

Bender M, Sowers T, Labeyrie L (1994) The Dole effect and its variations during the last 130,000 years as measured in the Vostok ice core. Global Biogeochem Cycles 8:363–376

Cappa CD, Hendricks MB, DePaolo DJ, Cohen RC (2003) Isotopic fractionation of water during evaporation. J Geophys Res – Atmos 108(D16), Art.No. 4525

Ciais P et al (1997) A three-dimensional synthesis study of delta O-18 in atmospheric CO2. 1. Surface fluxes. J Geophys Res – Atmos 102:5857–5872

Cuntz M, Ciais P, Hoffmann G, Knorr W (2003) A comprehensive global three-dimensional model of δ18O in atmospheric CO2: 1. Validation of surface processes. J Geophys Res 108(D17), Art. No. 4527

Cuntz M, Ogee J, Farquhar GD, Peylin P, Cernusak LA (2007) Modelling advection and diffusion of water isotopologues in leaves. Plant Cell Environ 30:892–909

Dawson TE, Ehleringer JR (1993) Isotopic enrichment of water in the "woody" tissues of plants: implications for plant water source, water uptake, and other studies which use the stable isotopic composition of cellulose. Geochim Cosmochim Acta 57:3487–3492

Dawson TE, Mambelli S, Plamboeck AH, Templer PH, Tu KP (2002) Stable isotopes in plant ecology. Annu Rev Ecol Syst 33:507–559

DeNiro MJ, Sternberg LD, Marino BD, Druzik JR (1988) Relation between D/H ratios and 18O/16O ratios in cellulose from linen and maize-implications for paleoclimatology and from sindonology. Geochim Cosmochim Acta 52:2189–2196

Dongmann G, Nurnberg HW, Forstel H, Wagener K (1974) On the enrichment of $H_2^{18}O$ in the leaves of transpiring plants. Radiat Environ Biophys 11:41–52

Ehleringer JR et al (2002) Stable isotopes and carbon cycle processes in forests and grasslands. Plant Biol 4:181–189

Epstein S, Thompson P, Yapp CJ (1977) Oxygen and hydrogen isotopic ratios in plant cellulose. Science 198:1209–1215

Estep MF, Hoering TC (1981) Stable hydrogen isotope fractionations during autotrophic and mixotrophic growth of microalgae. Plant Physiol 67:474–477

Farquhar GD et al (1993) Vegetation effects on the isotope composition of oxygen in atmospheric CO_2. Nature 363:439–443

Feng XH, Epstein S (1996) Climatic trends from isotopic records of tree rings: the past 100–200 years. Clim Change 33:551–562

Feng XH, Reddington AL, Faiia AM, Posmentier ES, Shu Y, Xu XM (2007) The changes in North American atmospheric circulation patterns indicated by wood cellulose. Geology 35:163–166

Ferguson PR, Veizer J (2007) Coupling of water and carbon fluxes via the terrestrial biosphere and its significance to the Earth's climate system. J Geophys Res – Atmos 112:17

Flanagan LB, Comstock JP, Ehleringer JR (1991) Comparison of modeled and observed environmental influences on the stable oxygen and hydrogen isotope composition of leaf water in *Phaseolus-vulgaris* L. Plant Physiol 96:588–596

Gan KS, Wong SC, Yong JWH, Farquhar GD (2002) O-18 spatial patterns of vein xylem water, leaf water, and dry matter in cotton leaves. Plant Physiol 130:1008–1021

Gan KS, Wong SC, Yong JWH, Farquhar GD (2003) Evaluation of models of leaf water O-18 enrichment using measurements of spatial patterns of vein xylem water, leaf water and dry matter in maize leaves. Plant Cell Environ 26:1479–1495

Gerst S, Quay P (2001) Deuterium component of the global molecular hydrogen cycle. J Geophys Res – Atmos 106:5021–5031

Gillon J, Yakir D (2001) Influence of carbonic anhydrase activity in terrestrial vegetation on the O-18 content of atmospheric CO2. Science 291:2584–2587

Gray J, Thompson P (1977) Climatic information from O-18/O-16 analysis of cellulose, lignin and whole wood from tree rings. Nature 270:708–709
Helliker BR, Ehleringer JR (2000) Establishing a grassland signature in veins: O-18 in the leaf water of C-3 and C-4 grasses. Proc Natl Acad Sci U S A 97:7894–7898
Helliker BR, Richter SL (2008) Subtropical to boreal convergence of tree-leaf temperatures. Nature 454:511–U516
Hemming D et al (2007) The future of large-scale stable isotope networks. In: Dawson T, Siegwolf R (eds) Stable isotopes as indicators of ecological change. Academic, London
Hoffmann G et al. (2004) A model of the Earth's Dole effect. Global Biogeochemical Cycles 18. GB1008. doi:10.1029/2003GB002059
Hou JZ, D'Andrea WJ, Huang YS (2008) Can sedimentary leaf waxes record D/H ratios of continental precipitation? Field, model, and experimental assessments. Geochim Cosmochim Acta 72:3503–3517
Ingraham NL, Caldwell EA (1999) Influence of weather on the stable isotopic ratios of wines: tools for weather/climate reconstruction? J Geophys Res – Atmos 104:2185–2194
Jia GD, Wei K, Chen FJ, Peng PA (2008) Soil n-alkane delta D vs. altitude gradients along Mount Gongga, China. Geochim Cosmochim Acta 72:5165–5174
Jones AA, Sessions AL, Campbell BJ, Li C, Valentine DL (2008) D/H ratios of fatty acids from marine particulate organic matter in the California Borderland Basins. Geochemistry 39:485–500
Kahmen A et al (2008) Effects of environmental parameters, leaf physiological properties and leaf water relations on leaf water delta O-18 enrichment in different Eucalyptus species. Plant Cell Environ 31:738–751
Kelly S, Heaton K, Hoogewerff J (2005) Tracing the geographical origin of food: the application of multi-element and multi-isotope analysis. Trends Food Sci Technol 16:555–567
Keppler F et al (2007) Stable hydrogen isotope ratios of lignin methoxyl groups as a paleoclimate proxy and constraint of the geographical origin of wood. New Phytol 176:600–609
Lai C-T, Ehleringer JR, Bond BJ, Paw UKT (2006) Contributions of evaporation, isotopic non-steady state transpiration and atmospheric mixing on the 18O of water vapour in Pacific Northwest coniferous forests. Plant, Cell Environ 29:77–94
Landais A et al (2007) Millenial scale variations of the isotopic composition of atmospheric oxygen over Marine Isotopic Stage 4. Earth Planet Sci Lett 258:101–113
Lee XH, Kim K, Smith R (2007) Temporal variations of the O-18/O-16 signal of the whole-canopy transpiration in a temperate forest. Global Biogeochem Cycles 21:12
Leff B, Ramankutty N, Foley JA (2004) Geographic distribution of major crops across the world. Global Biochemical Cycles 18. GB1009. doi:10.1029/2003GB002108
Lis G, Wassenaar LI, Hendry MJ (2008) High-precision laser spectroscopy D/H and O-18/O-16 measurements of microliter natural water samples. Anal Chem 80:287–293
Loader NJ, Hemming DL (2004) The stable isotope analysis of pollen as an indicator of terrestrial palaeoenvironmental change: a review of progress and recent developments. Quat Sci Rev 23:893–900
Luo YH, Sternberg LDL (1992) Hydrogen and oxygen isotopic fractionation during heterotrophic cellulose synthesis. J Exp Bot 43:47–50
Majoube M (1971) Oxygen-18 and deuterium fractionation between water and steam. J Chim Phys Phys-Chim Biol 68:1423–1436
McKeon TA, Chen GQ, Lin JT (2000) Biochemical aspects of castor oil biosynthesis. Biochem Soc Trans 28:972–974
Miller DL, Mora CI, Grissino-Mayer HD, Mock CJ, Uhle ME, Sharp Z (2006) Tree-ring isotope records of tropical cyclone activity. Proc Natl Acad Sci U S A 103:14294–14297
Ogee J, Cuntz M, Peylin P, Bariac T (2007) Non-steady-state, non-uniform transpiration rate and leaf anatomy effects on the progressive stable isotope enrichment of leaf water along monocot leaves. Plant Cell Environ 30:367–387
Pataki DE et al (2003) Tracing changes in ecosystem function under elevated carbon dioxide conditions. BioScience 53:805–818

Peters LI, Yakir D (2008) A direct and rapid leaf water extraction method for isotopic analysis. Rapid Commun Mass Spectrom 22:2929–2936

Peylin P, Ciais P, Denning A, Tans P, Berry J, White J (1999) A 3-dimensional study of d18O in atmospheric CO2: contribution of different land ecosystems. Tellus B 51:642–667

Richter SL, Johnson AH, Dranoff MM, Taylor KD (2008) Continental-scale patterns in modern wood cellulose delta O-18: implications for interpreting paleo-wood cellulose delta O-18. Geochim Cosmochim Acta 72:2735–2743

Ripullone F et al (2008) Environmental effects on oxygen isotope enrichment of leaf water in cotton leaves. Plant Physiol 146:729–736

Roden JS, Ehleringer JR (1999) Observations of hydrogen and oxygen isotopes in leaf water confirm the Craig–Gordon model under wide-ranging environmental conditions. Plant Physiol 120:1165–1173

Roden JS, Ehleringer JR (2000) Hydrogen and oxygen isotope ratios of tree ring cellulose for field-grown riparian trees. Oecologia 123:481–489

Roden JS, Lin GG, Ehleringer JR (2000) A mechanistic model for interpretation of hydrogen and oxygen isotope ratios in tree-ring cellulose. Geochim Cosmochim Acta 64:21–35

Rossmann A, Reniero F, Moussa I, Schmidt HL, Versini G, Merle MH (1999) Stable oxygen isotope content of water of EU data-bank wines from Italy, France and Germany. Zeitschrift Fur Lebensmittel-Untersuchung Und-Forschung a – Food Res Technol 208:400–407

Sachse D, Radke J, Gleixner G (2004) Hydrogen isotope ratios of recent lacustrine sedimentary n-alkanes record modern climate variability. Geochim Cosmochim Acta 68:4877–4889

Shu Y, Feng XH, Posmentier ES, Sonder LJ, Faiia AM, Yakir D (2008) Isotopic studies of leaf water. Part 1: a physically based two-dimensional model for pine needles. Geochim Cosmochim Acta 72:5175–5188

Smith FA, Freeman KH (2006) Influence of physiology and climate on delta D of leaf wax n-alkanes from C-3 and C-4 grasses. Geochim Cosmochim Acta 70:1172–1187

Stern B, Clelland SJ, Nordby CC, Urem-Kotsou D (2006) Bulk stable light isotopic ratios in archaeological birch bark tars. Appl Geochem 21:1668–1673

Stern B, Moore CDL, Heron C, Pollard AM (2008) Bulk stable light isotopic ratios in recent and archaeological resins: towards detecting the transport of resins in antiquity? Archaeometry 50:351–370

Sternberg L, Pinzon MC, Anderson WT, Jahren AH (2006) Variation in oxygen isotope fractionation during cellulose synthesis: intramolecular and biosynthetic effects. Plant Cell Environ 29:1881–1889

Sternberg LDL, Pinzon MC, Vendramini PF, Anderson WT, Jahren AH, Beuning K (2007) Oxygen isotope ratios of cellulose-derived phenylglucosazone: an improved paleoclimate indicator of environmental water and relative humidity. Geochim Cosmochim Acta 71:2463–2473

Sternberg LdSL (1988) D/H ratios of environmental water recorded by D/H ratios of plant lipids. Nature 333:59–61

Still C J, Riley WJ, Biraud SC, Noone DC, Buenning NH, Randerson JT, Torn MS, Welker J, White JWC, Vachon R, Farquhar GD, Berry JA (2009) Influence of clouds and diffuse radiation on ecosystem-atmosphere CO2 and (COO)-O-18 exchanges. J Geophys Res-Biogeosciences 114:17

Vendramini PF, Sternberg L (2007) A faster plant stem-water extraction method. Rapid Commun Mass Spectrom 21:164–168

West JB, Bowen GJ, Cerling TE, Ehleringer JR (2006) Stable isotopes as one of nature's ecological recorders. Trends Ecol Evol 21:408–414

West JB, Ehleringer JR, Cerling TE (2007) Geography and vintage predicted by a novel GIS model of wine delta O-18. J Agric Food Chem 55:7075–7083

West JB, Sobek A, Ehleringer JR (2008) A simplified GIS approach to modeling global leaf water isoscapes. PLoS ONE 3:e2447

White JWC, Cook ER, Lawrence JR, Broecker WS (1985) The D/H ratios of sap in trees: implications for water sources and tree ring D/H ratios. Geochim Cosmochim Acta 49:237–246

Williams D, Evans R, West J, Ehleringer J (2007) Applications of stable isotope measurements for early-warning detection of ecological change. In: Dawson T, Siegwolf R (eds) Stable isotopes as indicators of ecological change. Academic, London

Xia ZH et al (2008) Hydrogen isotope ratios of terrigenous n-alkanes in lacustrine surface sediment of the Tibetan Plateau record the precipitation signal. Geochem J 42:331–338

Yakir D, Deniro MJ (1990) Oxygen and hydrogen isotope fractionation during cellulose metabolism in *Lemna-gibba* L. Plant Physiol 93:325–332

Yakir D, Sternberg LDL (2000) The use of stable isotopes to study ecosystem gas exchange. Oecologia 123:297–311

Yakir D, Berry JA, Giles L, Osmond CB (1994) Isotopic heterogeneity of water in transpiring leaves – identification of the component that controls the delta-O-18 of atmospheric O-2 and CO2. Plant Cell Environ 17:73–80

Yamada K, Ozaki Y, Nakagawa F, Sudo S, Tsuruta H, Yoshida N (2006) Hydrogen and carbon isotopic measurements of methane from agricultural combustion: implications for isotopic signatures of global biomass burning sources. J Geophys Res – Atmos 111:12

Chapter 9
Continental-Scale Distributions of Vegetation Stable Carbon Isotope Ratios

Christopher J. Still and Rebecca L. Powell

9.1 Introduction

All terrestrial higher plants preferentially assimilate $^{12}CO_2$ relative to $^{13}CO_2$ during photosynthesis as a result of physical and biological isotope fractionation processes, with much larger overall ^{13}C fractionation by plants using the C_3 photosynthetic pathway (approximate range of 14–27‰) compared to plants using the C_4 pathway (approximate range of 3–6‰). Fractionation against $^{13}CO_2$ in both C_3 and C_4 plants includes kinetic and equilibrium isotope effects during the processes of gaseous diffusion of CO_2 along concentration gradients from the atmosphere to the sub-stomatal intercellular spaces, subsequent hydration and diffusion to the site of carboxylation in the chloroplast, and ultimately CO_2 fixation by the Rubisco enzyme (Farquhar et al. 1989). The key differences between C_3 and C_4 plants in photosynthetic ^{13}C fractionation are described in detail elsewhere (Farquhar 1983; Farquhar et al. 1982, 1989), but the lower fractionation by C_4 plants is primarily the result of a negative isotope fractionation during hydration of CO_2 at equilibrium, combined with a reduced effective fractionation by Rubisco, as the bundle sheath cells approximate a closed compartment. As a result of these differences, C_4 plants have considerably more enriched $\delta^{13}C$ values compared to C_3 plants; for example, a survey of grasses by Cerling et al. (1997) reported mean C_3 and C_4 plant $\delta^{13}C$ values of −26.7‰ and −12.2‰, respectively.

C.J. Still (✉)
Department of Geography, Institute for Computational Earth System Science, University of California Santa Barbara, Santa Barbara, CA, 93106, USA
e-mail: cstill@geog.ucsb.edu

R.L. Powell
Department of Geography, University of Denver, 2050 E. Iliff Avenue, Denver, CO, 80208, USA
e-mail: rpowell8@du.edu

J.B. West et al. (eds.), *Isoscapes: Understanding Movement, Pattern, and Process on Earth Through Isotope Mapping*, DOI 10.1007/978-90-481-3354-3_9,

Thus, to capture first-order terrestrial $\delta^{13}C$ variations at regional-to-continental scales, it is essential to first predict spatial variations in the relative abundances of C_3 and C_4 plants. Plant photosynthetic pathway is a basic physiological and ecological distinction in tropical and subtropical savannas, as well as in many temperate grasslands. The photosynthetic pathway is also necessary for plant functional type mapping for simulating biosphere–atmosphere exchanges and for understanding the response of vegetation to global change because of the different functional responses of C_3 and C_4 plants to nitrogen, radiation, temperature, and CO_2 (Still et al. 2003). In addition to the well-known differences imposed by rising atmospheric CO_2 on photosynthesis (e.g., Poorter 1993; Wand et al. 1999; Ainsworth and Long 2005), C_3 and C_4 plants are expected to respond differentially to climate change (Sage and Kubien 2003). This is because C_4 plants typically have higher photosynthetic rates at high temperatures and under high light conditions (Collatz et al. 1992; Long 1999); C_4 plants also have higher water-use efficiency than do comparable, co-occurring C_3 plants (e.g., Pearcy and Ehleringer 1984; Farquhar et al. 1989; Ehleringer and Monson 1993; Sage and Monson 1999 and references therein).

Numerous studies have examined the environmental factors that determine the C_3/C_4 composition of vegetation at a variety of scales, with the underlying goal of determining the physiological and ecological controls that underlie these factors (Teeri and Stowe 1976; Ehleringer 1978; Tieszen et al. 1979; Monson et al. 1983; Paruelo and Lauenroth 1996; Epstein et al. 1997; Ehleringer et al. 1997; Collatz et al. 1998; Long 1999; Sage et al. 1999). A comprehensive review of these environmental factors finds that the principal determinants of C_4 success are growing season temperature and availability of moderate to high light levels (Sage et al. 1999). Indeed, C_4 plants often dominate high light and high temperature environments like grassland and savannas (Long 1999; Sage et al. 1999). The temperature effect is a direct function of C_4 physiology, as discussed below, whereas the high light requirement reflects the restriction of the C_4 syndrome to low-stature, largely herbaceous ecosystems with no large forest overstory, such as grasslands and savannas.

The C_4 pathway concentrates CO_2 around the carboxylating enzyme, Rubisco, resulting in CO_2 levels as much as an order of magnitude above those in ambient air (Jenkins et al. 1989; von Caemmerer and Furbank 2003). This concentrating mechanism effectively eliminates photorespiratory losses, but it requires at least two additional ATP molecules for each CO_2 molecule fixed by Rubisco (Larcher 2003), an energetic expense that is compensated for at high light levels. Photosynthesis in unstressed C_4 plants with ample nutrient and water availability does not saturate at high light levels, unlike the typical light saturation for C_3 plants in similar circumstances (Collatz et al. 1991, 1992).

A pioneering physiological explanation for a temperature control on C_3/C_4 distributions was that quantum yield differences between these pathways drove ecological sorting (Ehleringer 1978). The quantum yield is the ratio of moles of CO_2 assimilated to moles of photosynthetically active radiation absorbed by a leaf during conditions when low light limits photosynthesis (Ehleringer and Björkman

1977; Collatz et al. 1998). A higher quantum yield should translate to a higher efficiency of light utilization, and thus a higher capacity for growth and reproduction, particularly if most carbon gain occurs under light-limited conditions (Collatz et al. 1998; Still et al. 2003). The quantum yield in C_3 plants decreases sharply with increasing temperature, whereas the quantum yield of C_4 plants is relatively constant across a range of temperatures as a result of the CO_2-concentrating mechanism (Ehleringer and Björkman 1977; Ehleringer and Pearcy 1983; Collatz et al. 1998; Long 1999). The 'crossover temperature' is the temperature at which the C_3 quantum yield equals the C_4 quantum yield (Ehleringer et al. 1997; Collatz et al. 1998); measured crossover temperatures vary from 16°C to 24°C (Ehleringer et al. 1997). The quantum yield is likely a proxy for the underlying physiological determinant of C_3 and C_4 ecological success. As discussed by Sage and Kubien (2003), the quantum yield in C_3 plants is directly proportional to photorespiratory inhibition, which occurs at all light levels. Indeed, the modeled crossover temperature for both light-limited and light-saturated (i.e., Rubisco-limited) photosynthesis also falls within this range (Collatz et al. 1998; Still et al. 2003). Photorespiration increases sharply with leaf temperature, along with the direct substrate limitation of Rubisco. These combined effects are likely the fundamental mechanism influencing C_3/C_4 distributions (Sage and Kubien 2003).

While quantum yield differences are probably not the ultimate cause of C_3/C_4 ecological sorting, the predicted crossover temperature correlates fairly well with growing season temperatures and observed C_3 and C_4 spatial gradients (Ehleringer 1978; Ehleringer et al. 1997; Collatz et al. 1998). Importantly, the crossover temperature does not predict the fraction of plants that use either the C_3 or C_4 pathway – it merely predicts which type should predominate as a function of temperature. Based on these considerations, Collatz et al. (1998) developed the following C_4 bioclimatic criteria for grasses: a minimum monthly mean temperature of 22°C and precipitation of at least 25 mm in that same month. The precipitation constraint was added to screen regions that meet the monthly temperature constraint, but do not receive enough precipitation to support plant growth in that month. In practice, this filters non-vegetated desert areas like the Sahara desert, and also Mediterranean climate regions that receive rainfall in cool winter months. These criteria were adopted by Still et al. (2003) in producing the first global distribution of C_3/C_4 vegetation fractions.

The other important component needed to predict C_3/C_4 fractions is a continuous representation of the distribution of vegetation growth forms (i.e., herbaceous or woody vegetation) on the land surface (e.g., DeFries et al. 1995), as the C_4 pathway is largely restricted to herbaceous growth forms like grasses and sedges (Teeri and Stowe 1976; Teeri et al. 1980). Although woody C_4 dicots exist and are important in some ecosystems (Stowe and Teeri 1978; Caldwell et al. 1977; Ehleringer et al. 1997), the herbaceous growth form is where C_4 photosynthesis is most successful and abundant in terms of total cover, biomass, or productivity. In areas with sufficient precipitation, even if the C_4 temperature criteria is satisfied, trees can outcompete and shade grasses, and the abundance of C_4 plants is correspondingly

reduced. Thus, using growth form distributions allows us to avoid prescribing an upper limit on precipitation for predicting C_4 climates.

Because large areas of the earth's surface are mosaics of natural and managed vegetation (i.e., croplands), crop-type fractional cover maps must also be incorporated in predicted C_3/C_4 distributions. This is because the planting of crop types does not always follow the bioclimatic criteria used to predict C_3 and C_4 dominance in natural vegetation. For example, C_4 corn (maize) is one of the top three agricultural crops in the world, but is often planted outside of C_4 climate zones; conversely, C_3 crops such as soybeans can be planted in areas that once were covered by C_4 grasses, as often occurs in the savannas of Brazil (Leff et al. 2004).

In the following sections, we describe our methods for producing a C_3/C_4 distribution on the continent of Africa. We then predict a $\delta^{13}C$ distribution for this continent and highlight potential applications of this isoscape. We focus on Africa because it contains large areas of C_4-dominated savanna and grassland, it exhibits striking climatic and vegetation gradients, and it is potentially very useful for studies of bird migration between Europe and Africa that rely on the spatial distribution of stable isotopes.

9.2 Methods

The C_3/C_4 composition of vegetation was predicted following the methodology developed by Still et al. (2003), but using next-generation, finer resolution vegetation cover fraction (VCF) fields, a different climate dataset, and an updated dataset of crop distributions. The algorithm first identifies potential C_4 vegetation cover by identifying herbaceous vegetation that is located in the C_4 climate zone; all other vegetation (i.e., woody vegetation in the C_4 climate zone and all vegetation in the C_3 climate zone) is assumed to utilize the C_3 photosynthetic pathway. The algorithm then integrates data on crop type fractional coverage to account for managed agroecosystems that may violate the natural climate constraints. Finally, the $\delta^{13}C$ content of vegetation is estimated from the relative abundance of C_3 and C_4 vegetation in each land grid cell and known end-member $\delta^{13}C$ values for each pathway. The algorithm we applied to spatially integrate climate, vegetation life form, and crop type datasets is summarized in Fig. 9.1 and is detailed below.

A climate mask of regions considered favorable to C_4 vegetation was generated from a 30-year (1961–1990) mean monthly terrestrial climatology (New et al. 1999, 2000). Each half-degree grid cell that satisfied the two C_4 bioclimatic constraints (mean monthly temperature $\geq 22°$ and mean monthly precipitation > 25 mm) for at least 1 month of the year is presented in the upper left corner of Fig. 9.1. In fact, many of these grid cells actually satisfied these simultaneous climate constraints for more than 1 month.

Vegetation growth form fields were taken from the MODIS Vegetation Continuous Fields (VCF) product for the year 2001 (Hansen et al. 2003a). The VCF product estimates mean annual percent cover of herbaceous, tree, and bare soil for each

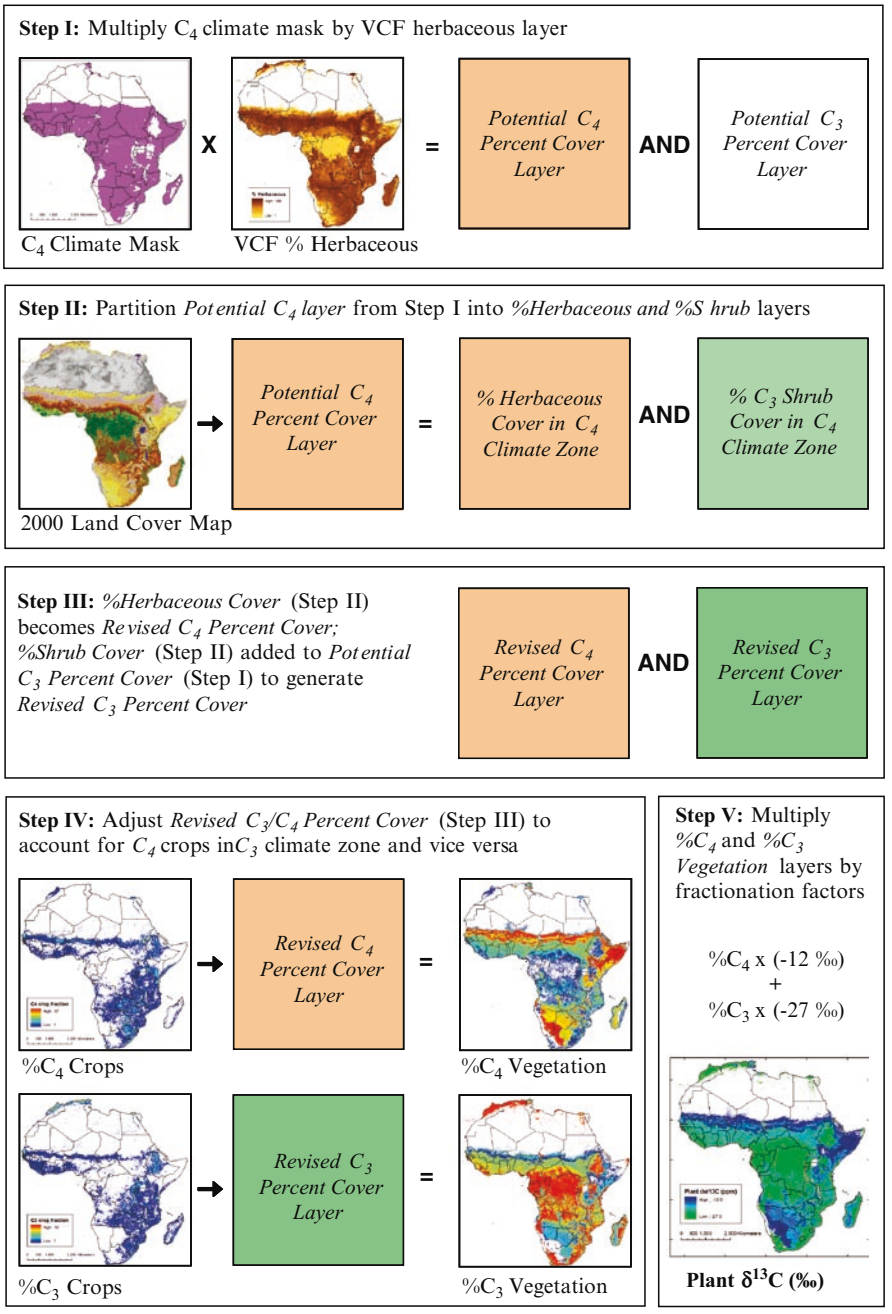

Fig. 9.1 Algorithm to predict vegetation C_3/C_4 composition and $\delta^{13}C$ (‰) content.
Fig. 9.1, see Appendix 1, Color Section

500-m grid cell. Percent-cover estimates are generated by an automated regression tree algorithm using the seven MODIS land bands, 68 metrics derived from annual MODIS-composited data, and the Normalized Difference Vegetation Index (NDVI) as input. Training data are derived from a global sample of fine-resolution Landsat data (Hansen et al. 2003b). We aggregated the MODIS VCF data to 1-km resolution, and conducted all further processing at this resolution. The VCF percent herbaceous layer was overlaid on the C_4 climate mask layer to generate a *Potential C_4 Percent Cover* layer. All other vegetation was assumed to be *Potential C_3 Percent Cover* (Fig. 9.1, Step I).

The MODIS VCF vegetation products correspond to tree and non-tree vegetation layers, rather than the percent woody and percent herbaceous cover layers that are needed to accurately derive Percent C_3 and Percent C_4 vegetation cover. Specifically, the MODIS VCF percent tree layer represents the percent canopy cover per pixel, where crown cover = canopy cover + within crown skylight (Hansen et al. 2003b). The impact of this subtle distinction is twofold. First, the per-pixel percent tree crown *cover* is on average underestimated. Second, the VCF percent herbaceous layer includes *all* vegetation below 5 m in height (Hansen et al. 2003b), meaning that the 'herbaceous' layer also includes most woody shrubs. (Although C_4 shrubs do exist and are ecologically important in certain arid regions (Caldwell et al. 1977; Sage et al. 1999), we have no simple, robust way to partition C_3 and C_4 shrubs in our mapping approach. For the purpose of predicting C_3 and C_4 fractions at continental to global scales for applications in isotope mapping and carbon cycle modeling, we feel that this error is negligible. However, future efforts will attempt to address this issue.

In an attempt to address these two issues, which would impact our predicted C_3/C_4 distribution, the Potential C_4 Percent Cover layer was partitioned into shrub and herbaceous layers using the 1-km Global Land Cover Map 2000 (GLC 2000) (Mayaux et al. 2003; Fig. 9.1, Step II). The GLC 2000 is primarily derived from the VEGETATION sensor on board the Système Pour l'Observation de la Terre (SPOT-4) satellite. A combination of automated classification algorithms and visual interpretation by regional experts was applied to the spectral and seasonal properties of vegetation cover to classify every land pixel on the African continent as one of 27 categories. Each land-cover class is defined in terms of a minimum and/or maximum percent cover for tree, shrub, and herbaceous vegetation (Mayaux et al. 2004).

The Potential C_4 Percent Cover layer was partitioned into shrub and herbaceous layers based on the following rules: For pixels assigned to GLC classes consisting only of shrub and tree cover (e.g., 'closed evergreen forest'), the corresponding Potential C_4 Percent Cover value was reassigned to the shrub percent cover layer. For pixels assigned to GLC classes consisting only of herbaceous and tree cover (e.g., 'open grassland'), the corresponding Potential C_4 Percent Cover value was retained as herbaceous percent cover. The remaining pixels in the Potential C_4 Percent Cover – associated with GLC classes that included mixtures of shrub and herbaceous cover – were assumed to be equally divided between shrub and herbaceous layers, subject to the constraints imposed by the GLC 2000 classes.

For example, the 'degraded evergreen lowland forest' class was defined as 0–60% herbaceous cover, 0–60% shrub cover, and 40–70% tree cover. Therefore, the Potential C_4 Percent Cover for pixels corresponding to this class was partitioned such that the new herbaceous and shrub layers were each 50% of the original Potential C_4 Percent Cover values. The shrub layer (i.e., what was removed from the original herbaceous layer) was next added to the Potential C_3 Percent Cover layer, resulting in a Revised C_3 Percent Cover layer. The herbaceous cover in C_4 climates that remained after partitioning became the Revised C_4 Percent Cover layer (Fig. 9.1, Step III).

The distributions of herbaceous C_3 and C_4 crops were generated from a global dataset of 18 major crop types (Leff et al. 2004), which characterizes the global geographic distribution of crop types using a combination of satellite data and agricultural census data. The C_4 crops identified in this dataset (corn, sorghum, millet, and sugar cane) were used to calculate the C_4 crop fraction (i.e., fraction of crop area that is C_4) for each grid cell; all other (C_3) crops were used to calculate the C_3 crop fraction. Subsequently, the Revised C_3 and Revised C_4 Percent Cover layers were adjusted to account for C_3 crops planted in the C_4 climate zone and C_4 crops planted in the C_3 climate zone. The algorithm applied to integrate the crop type data and Percent C_3 and Percent C_4 layers is shown in Fig. 9.1, Step IV and resulted in Final C_3 and C_4 Percent Cover layers.

The C_3 and C_4 Percent Cover layers were converted to C_3 and C_4 Percent Vegetation layers (i.e., the percent of the vegetation in a given grid cell using either the C_3 or C_4 photosynthetic pathway; this is different from the percentage cover of each pathway in a grid cell when the percent cover of bare soil is non-zero), so that each 1-km grid cell was assigned the proportion of vegetation associated with each photosynthetic pathway (Fig. 9.1, Step IV). Areas bordering on desert, such as the Horn of Africa or the northern fringe of the Sahel, may have low total vegetation cover, yet can have a large C_4 vegetation fraction. Finally, the distribution of vegetation $\delta^{13}C$ was estimated from the C_3 and C_4 Percent Vegetation layers, assuming constant values of −27‰ and −12‰ for C_3 and C_4 organic matter, respectively (Fig. 9.1, Step V).

9.3 Results and Discussion

The predicted distributions for each photosynthetic pathway are presented in Fig. 9.2. Comparison of Fig. 9.3a and b highlights the difference in predicted C_4 percentages before and after applying the shrub correction; the potential overestimation of C_4 percentage cover in the original data (Fig. 9.3b) is striking. C_4 vegetation dominates the savanna and grassland regions, particularly in the Sahel region sandwiched between the Sahara Desert and the Congo rain forest, the horn of East Africa, and the arid regions south of the Congo rain forest and east of the Namib Desert in Southern Africa. C_3 vegetation cover is greatest in the lowland moist tropical forests of the Congo Basin, in the cooler high-elevation regions of Ethiopia

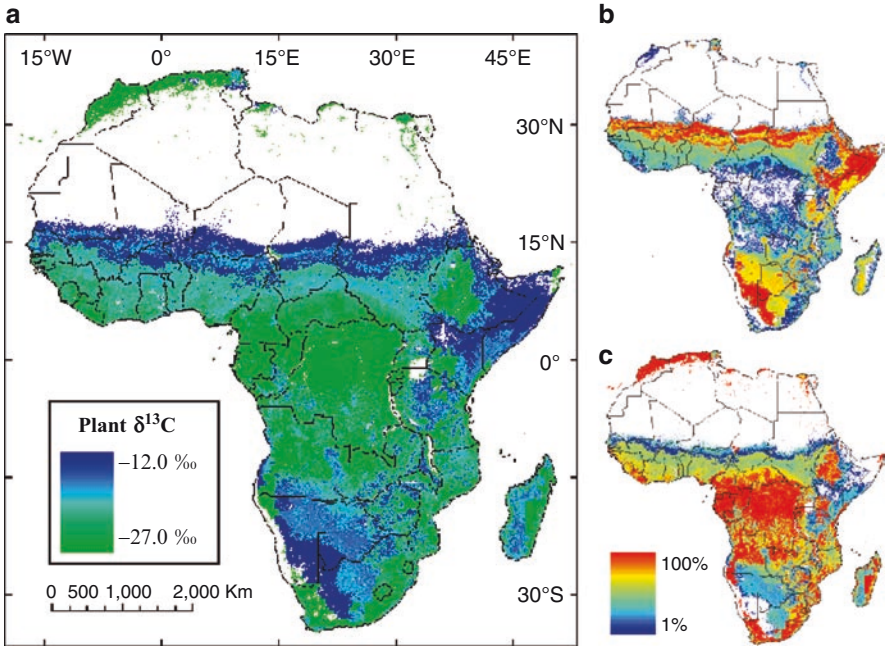

Fig. 9.2 (**a**) Stable carbon isotopic distribution for the African continent, (**b**) percentage of vegetation that uses the C_4 pathway, and (**c**) percentage of vegetation that uses the C_3 pathway. Fig. 9.2, see Appendix 1, Color Section

that remain below the crossover temperature threshold, and in Mediterranean climate regions of north Africa and the Cape region of South Africa that receive cool-season precipitation. Madagascar is predicted to contain a sharp C_3/C_4 longitudinal gradient that follows from the increase in precipitation from west to east across the island (Fig. 9.2b and c).

We define Sub-Saharan Africa as the portion of the continent south of 17° N latitude. Excluding Madagascar, the total area of Sub-Saharan Africa covered by C_3 vegetation is predicted to be 9.8 million square kilometre, or approximately 49% of the total dry land surface, while the total area covered by C_4 vegetation is 6.3 million square kilometre, or approximately 31% or the land surface (Table 9.1). The remainder of the land surface (approximately 20% of the total area) is unvegetated. The total area of Madagascar covered by C_3 vegetation is 340,000 km^2, approximately 58% of the land surface, and C_4 vegetation covers 200,000 km^2, approximately 33% of the surface. Approximately 10% of Madagascar's dry land surface is unvegetated (Table 9.1).

The impact of each adjustment made to the VCF percent herbaceous layer (i.e., Fig. 9.1, Steps II–IV) on final predicted C_3 and C_4 vegetation cover is quantified in Table 9.2. If no adjustment is made to account for crop types planted outside of their climatic zone ('no crop correction' in Table 9.2), the total areal estimates for C_3 and C_4 vegetation cover vary by less than 1% of the total land-surface area.

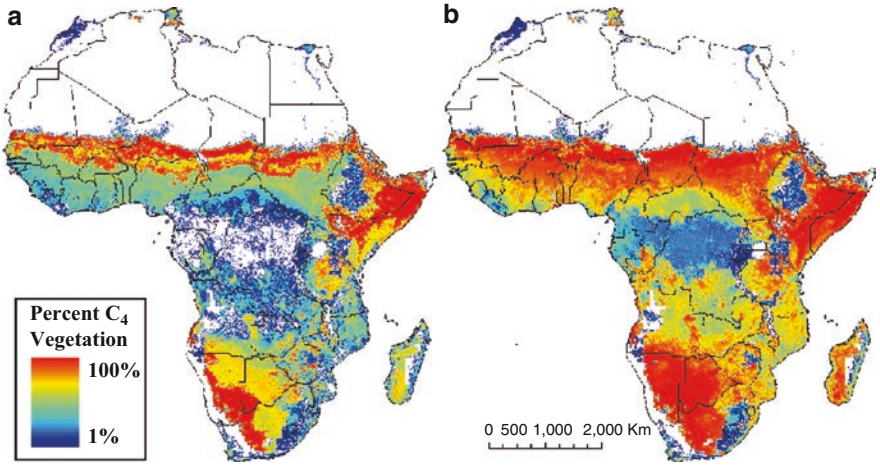

Fig. 9.3 (**a**) C_4 percent of vegetation with land-cover correction to partition shrubs and herbaceous cover. (**b**) C_4 percent of vegetation produced using the MODIS VCF herbaceous layer without land-cover correction. Fig. 9.3, see Appendix 1, Color Section

Table 9.1 Summary of cover for C_3 and C_4 vegetation for sub-Saharan Africa and Madagascar. Areal measurements include dry land surface only

	Area (10^6 km^2)	Woody cover (% area)	Herb cover (% area)	C_3 vegetation (10^6 km^2)	C_4 vegetation (10^6 km^2)	C_3 vegetation (% area)	C_4 vegetation (% area)
Sub-Saharan Africa[a]	20.0	44	36	9.8	6.3	49	31
Madagascar	0.59	49	42	0.34	0.20	58	33

[a] Excluding Madagascar

Table 9.2 Summary of 'corrections' applied to predict C_3/C_4 vegetation percentages. Numbers are reported for Sub-Saharan Africa only

	C_3 vegetation (10^6 km^2)	C_4 vegetation (10^6 km^2)	C_3 vegetation (% area)	C_4 vegetation (% area)
No crop or land-cover corrections	5.4	10.6	27	53
Crop correction only	5.6	10.5	28	53
Land-cover correction only	9.7	6.5	48	33
Land-cover and crop corrections	9.8	6.3	49	31

However, if the percent herbaceous layer is not adjusted to account for the presence of shrubs and other low-stature (<5-m height) woody vegetation, the predicted area of C_3 and C_4 vegetation shifts dramatically ('no land-cover correction' in Table 9.2). If no land-cover correction is applied to the herbaceous layer, C_4 vegetation is predicted to dominate sub-Saharan Africa (53% of land surface area), while C_3 vegetation covers

only 28% of the land surface. Thus, accounting for the distribution of agricultural crops has a relatively small effect on the predicted distribution of C_3 and C_4 vegetation on regional-to-continental scales, but failing to account for shrubs and other woody vegetation in the percent 'herbaceous' layer of the VCF product results in a gross overestimation of herbaceous land cover, and in turn, of C_4 vegetation cover.

The African vegetation $\delta^{13}C$ spatial patterns directly follow from the C_3/C_4 patterns (Fig. 9.2a). The predicted mean $\delta^{13}C$ value of all sub-Saharan vegetation biomass (excluding Madagascar and non-vegetated areas) is −21.4‰ (Fig. 9.2). This follows directly from our prediction that approximately 61% of sub-Saharan vegetation uses the C_3 pathway, and the remainder uses the C_4 pathway (we assume the percentage of vegetation using the CAM pathway is negligible in these calculations). While the algorithm we applied to predict the distribution of C_4 vegetation relied on a temperature threshold to sort C_3/C_4 vegetation, regional precipitation gradients also impact the relative abundance of each photosynthetic pathway and thus of vegetation carbon isotopic composition. Figure 9.4 plots zonally averaged mean vegetation $\delta^{13}C$ as a function of latitude (excluding Madagascar); mean annual precipitation (MAP) is also plotted by latitude in this figure. Not surprisingly, a strong relationship between these quantities emerges: increases in MAP are associated with decreases in vegetation $\delta^{13}C$. This is driven by the increase in (C_3) tree cover with precipitation, or conversely, the increase in (C_4) herbaceous cover with decreasing precipitation and decreasing overall vegetation cover. The relationship becomes blurred at the lowest latitudes (i.e., below 20° S), where rainfall regimes vary longitudinally more than latitudinally. Examination of Fig. 9.2a shows that latitudes between 15° S and 30° S also contain a great deal of longitudinal $\delta^{13}C$ variation driven by gradients in woody and herbaceous cover, and the relationship with MAP weakens.

At present, there is no way to directly derive the stable carbon isotope composition of vegetation from remotely sensed imagery, and efforts to link remotely

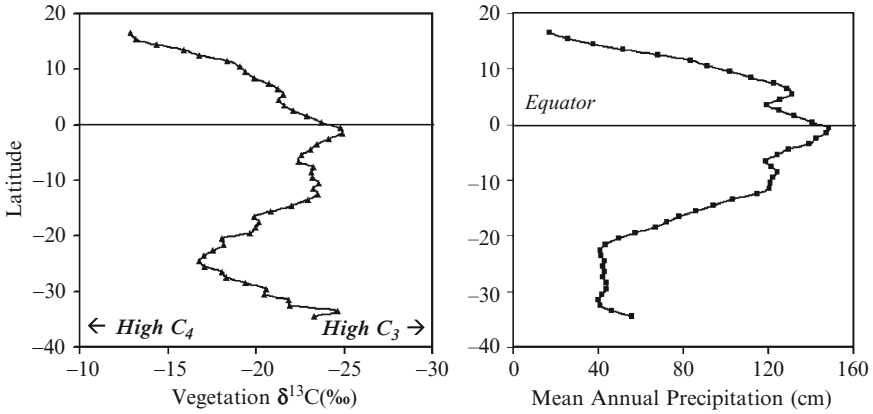

Fig. 9.4 (**a**) $\delta^{13}C$ of vegetation (‰) and (**b**) mean annual precipitation (cm) in sub-Saharan Africa averaged over 1° bands of latitude (from 17° N to 35° S). Mean $\delta^{13}C$ values do not include non-vegetated pixels. Madagascar is not included in these calculations

sensed parameters to plant $\delta^{13}C$ content remain preliminary but promising (Wang et al. this volume). The methodology we present in this chapter, therefore, relies on the integration of numerous datasets based on the functional and structural characteristics of C_3 and C_4 plants. Each dataset included in our analysis has a different spatial resolution, and each dataset is associated with its own set of errors. Here, we have not attempted to quantify the propagation of error associated with integrating multiple datasets; however, we have highlighted two large sources of uncertainty.

First, the 'herbaceous' layer of the VCF dataset is more aptly described as a 'non-tree' layer and must be adjusted to predict the distribution of C_3 and C_4 vegetation. Partitioning the VCF 'herbaceous' layer into 'woody' (i.e., shrub) and true 'herbaceous' (i.e., grasses and forbs) growth forms inherently introduces some uncertainty. Second, the crop-type layer effectively 'smears' agricultural census data from national and sub-national units across a spatially explicit global cropland dataset (Leff et al. 2004; Ramankutty and Foley 1998); therefore, while each aggregate percentage crop type holds for the political unit, the percent crop type cover for any given location is an approximation. The authors of this layer caution that the spatial distribution of crops should be used at regional or global scales, not for fine-scale analysis (Ramankutty and Foley 1998).

Despite these sources of uncertainty, we argue that our modeled C_3/C_4 distribution can be used to accurately predict the carbon isotopic composition of the vegetation at continental scales. Future improvements to this product would ideally generate C_3/C_4 and $\delta^{13}C$ layers that could be used at a much finer spatial scale than the current version. Such improvements would potentially include the following:

1. Generation of new vegetation layers that optimize the mapping of herbaceous and woody life forms, thereby improving these data layers for the purpose of mapping C_3/C_4 vegetation; this would eliminate the current land-cover correction step to account for shrubs (Fig. 9.1, Step II).
2. Investigation of the potential of preliminary studies that predict the relative composition of C_3/C_4 vegetation (Foody and Dash 2007) or the $\delta^{13}C$ content of vegetation directly (Wang et al. this volume), based on quantitative relationships between those variables and parameters derived directly from remote sensing imagery.
3. Generation of new crop type layers at finer spatial resolution, based on remotely sensed properties alone (i.e., without relying on census data). While the correction for crop types planted outside their photosynthetic region does not significantly impact regional-to-continental scale analyses (Table 9.2), a more accurate depiction of crop types would be important for finer-scale, sub-regional analyses, where croplands might cover a more significant portion of the study area.

9.4 Conclusions

Maps of the abundance and distribution of C_3 and C_4 plants provide the first and most important step in creating a landscape $\delta^{13}C$ distribution. The Africa $\delta^{13}C$ distribution has the potential to significantly improve our efforts to understand animal

migration and sources of insect pests and pathogens in Africa and elsewhere. For $\delta^{13}C$ values, animal tissues represent baseline food web values and these can be linked with reasonable confidence to our plant carbon isotope maps using known isotopic fractionation factors between plants and animal tissues (Hobson et al. this volume). Continental-scale C_3/C_4 and $\delta^{13}C$ isoscapes are also useful for a variety of carbon cycle applications. For example, previous $\delta^{13}C$ vegetation distributions (based on the C_3/C_4 maps of Still et al. 2003) were used to predict the carbon isotope composition of biomass burning emissions (Randerson et al. 2005), and the $\delta^{13}C$ distribution of terrestrial ecosystems is required for three-dimensional atmospheric inversion studies that infer land and ocean carbon fluxes (Rayner et al. 1999; Suits et al. 2005).

The values for C_3 plant tissue $\delta^{13}C$ can vary several per mil in space and time due to differences in isotope fractionation, whereas the values for C_4 plants are fairly constant (Farquhar et al. 1989; Cerling et al. 1997). Future efforts will include variable C_3 isotope fractionation values predicted by global biosphere models (e.g., Randerson et al. 2002; Suits et al. 2005), as well as an extension of this C_3/C_4 mapping approach to other continents. Since C_4 plants are found in regions subject to large climate variability, frequent fires, and intensive grazing and agricultural activity, interannual productivity and cover variations are expected to be large. Future work will quantify seasonal and interannual variations in the productivity and cover of C_3 and C_4 vegetation and permit the creation of dynamic $\delta^{13}C$ distributions, which are ultimately more useful than the static isoscape presented here.

The C_3/C_4 composition of the terrestrial biosphere is likely to be changing on decadal timescales as a result of global changes such as land-cover change, CO_2 fertilization, and climate change (Sage and Kubien 2003). Anthropogenic land-cover changes in many tropical regions typically exchange one pathway with another, such as cutting a C_3 tropical forest and replacing it with C_4 pasture grasses. Because our algorithm treats pasture as native grasslands, this would have important implications for the predicted $\delta^{13}C$ isoscapes, as well as modeling terrestrial-atmospheric ^{13}C cycling (e.g., Townsend et al. 2002; Scholze et al. 2008). Another widespread land-cover change phenomenon, woody encroachment of C_3 shrubs into C_4 grasslands (Archer et al. 1995), also affects C_3/C_4 distributions and will continue to do so for the near future.

Rising CO_2 and accompanying temperature increases should have counteracting effects on C_3 and C_4 photosynthetic performance (Ehleringer et al. 1997; Collatz et al. 1998; Koch et al. 2004), and thus, on future distributions and abundances of these plant types. The predictions of Collatz et al. (1998) for doubled CO_2 levels are sobering for the future distribution and abundance of C_4 vegetation. That study forecasts large changes in the fraction of the land surface suitable for C_4 dominance: increased CO_2 will reduce photorespiration in C_3 plants and increase the crossover temperature for quantum yields, and thus decrease the land surface area where C_4 plants should be favored over C_3 plants of similar stature. Ehleringer et al. (1997) reach similar conclusions, predicting a quantum yield crossover temperature under doubled CO_2 conditions of close to 30°. However, as discussed in Still et al. (2003), differences in quantum yields between C_3 and C_4 plants are unlikely to

capture all of the physiological factors that underlie the differing competitive success of these plant types in natural settings.

The predictions of these studies are buttressed by experimental work examining the response of C_4 species to enhanced CO_2 using the FACE technique. A meta-analysis of FACE studies by Ainsworth and Long (2005) shows that C_3 species have higher photosynthetic rates and dry matter production in response to elevated CO_2, whereas C_4 species are much less responsive. Future experiments using the FACE technique combined with warming manipulations will help resolve the variable response of C_3 and C_4 plants as predicted by models.

Ultimately, any changes in regional C_3/C_4 balances driven by factors such as climate variability, fires, land-cover change, and CO_2 fertilization, will obviously alter future $\delta^{13}C$ distributions. Importantly, changes in C_3/C_4 cover and productivity over the past few centuries would also affect our interpretation of studies that use historical and museum tissue $\delta^{13}C$ data to infer past animal migration and migratory connectivity.

Acknowledgements This work was supported by a NASA New Investigator Program award to CJ Still. We thank the anonymous reviewers for their helpful and constructive comments.

References

Archer S, Schimel DS, Holland EA (1995) Mechanisms of shrubland expansion: land use, climate or CO_2? Clim Change 29:91–99

Ainsworth EA, Long SP (2005) What have we learned from 15 years of free-air CO_2 enrichment (FACE)? A meta-analytic review of the responses of photosynthesis, canopy properties and plant production to rising CO_2. New Phytol 165(2):351–371

Caldwell MM, White RS, Moore TR, Camp LB (1977) Carbon balance, productivity, and water use of cold winter desert shrub communities dominated by C_3 and C_4 species. Oecologia 29:275–300

Cerling TE, Harris JM, MacFadden BJ et al (1997) Global vegetation change through the Miocene/Pliocene boundary. Nature 389:153–158

Collatz GJ, Ball JT, Grivet C, Berry JA (1991) Physiological and environmental regulation of stomatal conductance, photosynthesis and transpiration: a model that includes a laminar boundary layer. Agric For Meteorol 54:107–136

Collatz GJ, Ribas-Carbo M, Berry JA (1992) Coupled photosynthesis-stomatal conductance model for leaves of C_4 plants. Austr J Plant Physiol 19:519–538

Collatz GJ, Berry JA, Clark JS (1998) Effects of climate and atmospheric CO_2 partial pressure on the global distribution of C_4 grasses: present, past, and future. Oecologia 114:441–454

DeFries RS, Field CB, Fung I et al (1995) Mapping the land surface for global atmosphere–biosphere models: toward continuous distributions of vegetation's functional properties. J Geophys Res-Atmos 100:2867–2882

Ehleringer JR (1978) Implications of quantum yield differences to the distributions of C_3 and C_4 grasses. Oecologia 31:255–267

Ehleringer JR, Björkman O (1977) Quantum yields for CO_2 uptake in C_3 and C_4 plants: dependence on temperature, CO_2 and O_2 concentrations. Plant Physiol 59:86–90

Ehleringer JR, Monson RK (1993) Evolutionary and ecological aspects of photosynthetic pathway variation. Annu Rev Ecol Syst 24:411–439

Ehleringer JR, Pearcy RW (1983) Variation in quantum yield for CO_2 uptake among C_3 and C_4 plants. Plant Physiol 73:555–559

Ehleringer JR, Cerling TE, Helliker BR (1997) C_4 photosynthesis, atmospheric CO_2, and climate. Oecologia 112:285–299

Epstein HE, Lauenroth WK, Burke IC, Coffin DP (1997) Productivity patterns of C_3 and C_4 functional types in the U.S. Great Plains. Ecology 78:722–731

Farquhar GD (1983) On the nature of carbon isotope discrimination in C_4 species. Austr J Plant Physiol 10:205–26

Farquhar GD, O'Leary MH, Berry JA (1982) On the relationship between carbon isotope discrimination and intercellular carbon dioxide concentration in leaves. Austr J Plant Physiol 9:121–137

Farquhar GD, Ehleringer JR, Hubick KT (1989) Carbon isotope discrimination and photosynthesis. Annu Rev Plant Physiol Plant Mol Biol 40:503–537

Foody GM, Dash J (2007) Discriminating and mapping the C_3 and C_4 composition of grasslands in the northern Great Plains, USA. Ecol Inform 2:89–93

Hansen M, DeFries R, Townshed JR et al (2003a) Vegetation continuous fields MOD 44B, 2001 percent tree cover, collection 3. University of Maryland, College Park, MD 2001

Hansen MC, DeFries RS, Townshend JRG et al. (2003b) Global percent tree cover at a spatial resolution of 500 meters: first results of the MODIS vegetation continuous fields algorithm. Earth Interactions 7: Paper No. 10

Jenkins CLD, Furbank RT, Hatch MD (1989) Mechanisms of C_4 photosynthesis: a model describing the inorganic carbon pool in bundle sheath cells. Plant Physiol 91:1372–1381

Koch PL, Diffenbaugh NS, Hoppe KA (2004) The effects of late quaternary climate and pCO_2 change on C_4 plant abundance in the south-central United States. Palaeogeogr Palaeoclimatol Palaeoecol 207:331–357

Larcher W (2003) Physiological plant ecology, 4th edn. Springer, Berlin

Leff B, Ramankutty N, Foley JA (2004) Geographic distribution of major crops across the world. Global Biogeochem Cycles 18:GB1009. doi:10.1029/2003GB002108

Long SP (1999) Environmental responses. In: Sage RF, Monson RK (eds) C_4 plant biology. Academic, New York

Mayaux P, Bartholomé E, Cabral A et al (2003) The land cover map for Africa in the Year 2000. GLC2000 database, European Commission Joint Research Centre. http://www-gem.jrc.it/glc2000

Mayaux P, Bartholomé E, Fritz S, Belward A (2004) A new land-cover map of Africa for the year 2000. J Biogeogr 31:861–877

Monson RK, Littlejohn RO, Williams GJ (1983) Photosynthetic adaptation to temperature in four species from the Colorado shortgrass steppe: a physiological model for coexistence. Oecologia 58:43–51

New M, Hulme M, Jones P (1999) Representing twentieth-century space-time climate variability. Part I: development of a 1961–90 mean monthly terrestrial climatology. J Clim 12:829–856

New M, Hulme M, Jones P (2000) Representing twentieth-century space-time climate variability. Part II: development of 1901–1996 monthly grids of terrestrial surface climate. J Clim 13:2217–2238

Paruelo JM, Lauenroth WK (1996) Relative abundance of plant functional types in grasslands and shrublands of North America. Ecol Appl 6:1212–1224

Pearcy RW, Ehleringer JR (1984) Comparative ecophysiology of C_3 and C_4 plants. Plant Cell Environ 7:1–13

Poorter H (1993) Interspecific variation in the growth response of plants to an elevated CO_2 concentration. Vegetation 104(105):77–97

Ramankutty N, Foley JA (1998) Characterizing patterns of global land use: an analysis of global croplands data. Global Biogeochem Cycles 12:667–685

Randerson JT, Collatz GJ, Fessenden JE et al (2002) A possible global covariance between terrestrial gross primary production and ^{13}C discrimination: consequences for the atmospheric ^{13}C budget and its response to ENSO. Global Biogeochem Cycles 16:1136

Randerson, JT, van der Werf GR, Collatz GJ et al. (2005) Fire emissions from C_3 and C_4 vegetation and their influence on interannual variability of atmospheric CO_2 and $d^{13}CO_2$. Global Biogeochem Cycles 19:GB2019. doi:10.1029/2004GB002366

Rayner PJ, Enting IG, Francey RJ, Langenfelds R (1999) Reconstructing the recent carbon cycle from atmospheric CO_2, $\delta^{13}C$ and O_2/N_2 observations. Tellus B Chem Phys Meteorol 51:213–232

Sage RF, Kubien DS (2003) Quo vadis C_4? An ecophysiological perspective on global change and the future of C_4 plants. Photosynth Res 77:209–225

Sage RF, Monson RK (eds) (1999) C_4 plant biology. Academic, New York

Sage RF, Wedin DA, Li M (1999) The biogeography of C_4 photosynthesis: patterns and controlling factors. In: Sage RF, Monson RK (eds) C_4 plant biology. Academic, New York

Scholze M, Ciais P, Heimann M (2008) Modeling terrestrial ^{13}C cycling: climate, land use and fire. Global Biogeochem Cycles 22:GB1009. doi:10.1029/2006GB002899

Still CJ, Berry JA, Collatz GJ, DeFries RS (2003) The global distribution of C_3 and C_4 vegetation: carbon cycle implications. Global Biogeochem Cycles 17:GB1006. doi:10.1029/2001GB001807

Stowe LG, Teeri JA (1978) The geographic distribution of C_4 species of the dicotyledonae in relation to climate. Am Nat 112:609–623

Suits NS, Denning AS, Berry JA et al. (2005) Simulation of carbon isotope discrimination of the terrestrial biosphere. Global Biogeochem Cycles 19:GB1017. doi:10.1029/2003GB002141

Teeri JA, Stowe LG (1976) Climatic patterns and the distribution of C_4 grasses in North America. Oecologia 23:1–12

Teeri JA, Stowe LG, Livingstone DA (1980) The distribution of C_4 species of the Cyperaceae in North America in relation to climate. Oecologia 47:307–310

Tieszen LL, Senyimba MM, Imbamba SK et al (1979) The distribution of C_3 and C_4 grasses along and altitudinal and moisture gradient in Kenya. Oecologia 37:337–350

Townsend A, Asner GP, White JWC, Tans PP (2002) Land use effects on atmospheric ^{13}C imply a sizable terrestrial sink in tropical latitudes. Geophys Res Lett 29:1426

von Caemmerer S, Furbank RT (2003) The C_4 pathway: an efficient CO_2 pump. Photosynth Res 77:191–207

Wand SJE, Midgley GF, Jones MH et al (1999) Responses of wild C_4 and C_3 grass (Poaceae) species to elevated atmospheric CO_2 concentration: a meta-analytic test of current theories and perceptions. Global Change Biol 5:723–741

Chapter 10
Comprehensive Dynamical Models of Global and Regional Water Isotope Distributions

David Noone and Christophe Sturm

10.1 Introduction

Unlike statistical maps of water isotope distributions, the isotope distributions that emerge from numerical simulations with comprehensive mechanistic models reflect an ability to quantify and resolve the underlying physical and chemical processes which control the budgets of water and water isotopologues. A comprehensive model accounts for all processes which are determined to be, or likely to be, of significant influence on the budgets (e.g., transpiration, cloud formation and rain, oxidation of various chemical agents). Dynamical models, such as weather and climate models, are particularly advantageous for isotope studies because the often non-linear and non-local influences of transport processes can be accounted for in simulation. The final isotope distribution emerges from numerical integration of the budget equation, yet the result holds advantages over statistical maps because the mechanistic cause of the distribution can be determined quantitatively by examining additional diagnostics on all the contributions of each of the controlling processes computed by the model. In this way comprehensive dynamical models of water isotopologues can provide maps of isotope concentration that complement those obtained by statistical methods. Here we provide a basis for understanding how water isotope distribution can be simulated by incorporating isotope fractionation schemes into the water cycles of weather and climate models.

Comprehensive models can be distinguished from simpler models that appear frequently in isotope studies. Simple models such as those of trajectory and box

D. Noone (✉)
Department of Atmospheric and Oceanic Sciences, Cooperative Institute for Research in Environmental Sciences, University of Colorado, Boulder, CO
e-mail: dcn@colorado.edu

C. Sturm
Bert Bolin Centre for Climate Research, Institute for Geology and Geochemistry, Stockholm University, Stockholm, Sweden
e-mail: Christophe.Sturm@geo.su.se

J.B. West et al. (eds.), *Isoscapes: Understanding Movement, Pattern, and Process on Earth Through Isotope Mapping*, DOI 10.1007/978-90-481-3354-3_10,

budget-types (which includes Rayleigh models and simple mixing models) are extremely valuable at providing first order descriptions of water isotope distributions. However, they are limited in three important regards: (1) they often need appropriate initial conditions to be provided, (2) they require gross simplification of cloud and other exchange processes, and (3) they seldom account for mixing and transport of air masses in any detail. More comprehensive isotope models, such as those provided through modification of atmospheric general circulation models (GCMs) or regional meteorological models to include isotope tracers, can overcome some of these problems. To illustrate this, the basis of isotope tracking schemes as employed in comprehensive dynamical models is described and some examples of the use of such models in both reproducing climatological distributions and in informing process studies are discussed. Since the underpinning of comprehensive models is numerically evaluating the processes which contribute to the budgets, we describe in some detail the basic budget constraints and how account is made of the pertinent exchange processes. While models exist which can resolve exchanges at molecular scales and motions at turbulent scales, and some of these have been tasked with modeling isotopes, we focus here on dynamical models with grid resolution in the range 20–500 km.

10.2 Development and Uses of Comprehensive Isotope Models

In the early 1980s the Laboratoire de Météorologie Dynamique (LMD) atmospheric GCM was fitted with water isotope tracers with the technique obtaining notoriety with the seminal paper published in Nature (Joussaume et al. 1984). This work demonstrated that a global model with even modest representation of the atmospheric water cycle can reproduce the bulk features of the global and seasonal variations in isotopic composition in precipitation. Shortly after, J. Jouzel spent sabbatical time in New York and working with the modeling group at the Goddard Institute for Space Sciences developed an isotope scheme in that group's global model (Jouzel et al. 1991, 1987). Initially, early studies focused on testing the validity of water isotopes as climate proxies. Indeed Joussaume's early work included simulating dust concentrations such that results could also validate proxy reconstructions from ice core dust records (Joussaume 1993; Joussaume and Jouzel 1993). The interest in using comprehensive models to simulate isotope distributions in precipitation and vapor has continued to grow with numerous models now having isotopic tracers (Table 10.1). Intriguingly, the development of isotope schemes in models has often been the result of doctoral studies (Hoffmann 1995; Joussaume 1983; Lee 2005; Noone 2001; Risi et al. 2008; Sturm 2005; Werner and Heimann 2002).

While initially ice core records were of interest, and the validation of the so-called isotope-temperature slope, the community's attention quickly moved to other aspects of the isotope hydrology. Research areas include the monsoons (Hoffmann and Heimann 1997; Sturm et al. 2007a, b), tropical corals (Brown et al. 2006; Charles et al. 2001; Cole et al. 1999), atmospheric transport processes

Table 10.1 Historical account of isotope models, in almost chronological order. Other models reported to have isotope scheme being developed are the HadGem, UKMO, ACCESS and WRF (D. Noone, 2007, 2008, personal communication). Generation number in parentheses indicates the model is close to being classed at the higher level

Model	Reference	Domain	Type/resolution	Generation
LMD	Joussaume et al. (1984), Joussaume and Jouzel (1993)	Global	Finite difference	1 (2)
GISS 2'	Jouzel et al. (1987, 1991)	Global	Finite difference, 8 × 10 degree	1 (2)
Cloud model	Gedzelman and Arnold (1994), Lawrence et al. (1998)	Cloud scale	Two dimensional, 100 m	1 (3)
ECHAM 3	Hoffmann et al. (1998)	Global	Spectral/semi-Lagrangian T21/T42	2
ECHAM 4	Werner et al. (2001)	Global	Spectral/semi-LagrangianT63/106	2
MUGCM	Noone and Simmonds (2002b)	Global	Spectral/semi-Lagrangian R21/R31	1 (2)
GENESIS	Mathieu et al.(2002)	Global	Spectral/semi-Lagrangian T31	2
CCM3	Noone (2003)	Global	Spectral/semi-Lagrangian T42	2
ICM	Yoshimura et al. (2003)	Global 2d	Finite difference, offline, 1.25 degree	(1)
GISS E	Schmidt et al. (2005)	Global	Finite difference/quadratic moments, 4 × 5, 2 × 2.5	2 (3)
REMO	Sturm (2005)	Regional	Finite difference45, 10 km	2
CAM3	Noone (2003, 2006, in prep)	Global	Finite volume4 × 5, 2 × 2.5	3
DARMA	Smith et al. (2006)	Cloud scale	100 m	4
CAM2	Lee et al. (2007)	Global	Spectral/semi-Lagrangian T42	2
CCSR/NIES	Numaguti (1999), Kurita in prep	Global	Spectral/semi-Lagrangian T42	2
GSM	Yoshimura et al. (2008)	Global	Spectral T62	2
RSM	K. Yoshimura personnel communication, 2008	Regional	Spectral, 10–50 km	2
ECHAM 5	M, Werner personnel communication, 2008	Global	To be finalized	2 or 3
LMD4	Bony et al. (2008)	Global	To be finalized	2 or 3

(Noone and Simmonds 2002a; Vuille et al. 2003) and cloud processes (Lee et al. 2007; Schmidt et al. 2005). Still, because of the great experience with isotopes in the paleoclimate community, many of the published studies using water isotopes in comprehensive dynamical models have focused on examining past climate. There has been less attention given to using dynamical models of water isotopes to describe modern climate change, although the studies of Hoffmann et al. (2000), Schmidt et al. (2007) and Yoshimura et al. (2008) stand as exceptions.

The non-isotope modeling community often sees the utility isotopes as informing the construction of more accurate cloud microphysical packages for non-isotopic models, yet there has been little work in this area. Part of the reason for the lack of engagement is that there is rarely a perceived clear advantage in considering isotopic exchange, and in part that existing isotope models in fact only poorly constrain the detailed microphysics used in modern dynamical models. This is in part due to lack of an adequate amount of isotopic data for validation. Nonetheless a number of studies with comprehensive dynamical isotope models have informed understating of cloud processes in the underlying hydrology. As a case in point, Schmidt et al. (2005) aimed to explain the impact on the isotope distribution from different assumptions about cumulous clouds in the context of explaining the aircraft observations of Webster and Heymsfield (2003). Similarly, Bony and Risi (2008) used a parameterized model of convection (in an off-line configuration rather than coupled to a dynamical model) to explain the role of cloud microphysics in setting the isotopic composition of the tropics. So too, Lee et al. (2007) and Risi et al. (2008) targeted the impact of post condensation processes on the isotopic composition of precipitation. These studies demonstrate the utility in reconsidering the simulated hydrology by examining the impact on the isotopic results. To do so, however, requires an isotopic scheme that is designed and implemented with this as its objectives.

10.3 Isotopic Budgets in Comprehensive Models

While diagnostics on the isotopic composition of precipitation or evaporation are often the focus of modeling studies, the state variable of interest in atmospheric models is the water vapor abundance. Usually this is quantified by mass mixing ratio or specific humidity (q).[1] Modern climate models also include state variables for cloud liquid and ice and land surface components of global and regional models track the amount of water in soil, snow and sea ice. The isotopic composition of all these and any other state variables must be tracked to develop a comprehensive closed isotope scheme.

[1]Strictly the isotope ratio is the mole ratio of heavy to light isotopes, so one should use volume mixing ratio, which differs only by a constant (ratio of molecular weight of air and the vapor).

The water cycle in a dynamical model stems from the prediction of water vapor mixing ratio (q), and is described by the evaluation of the tendency equation:

$$\frac{\partial q}{\partial t} = \underset{(1)}{-\mathbf{V}\cdot\nabla q} \quad \underset{(2)}{+D\nabla_h^2 q} \quad \underset{(3)}{+\frac{\partial}{\partial p}\left(\overline{\omega' q'}\right)} \quad +E \quad -C \quad +S. \tag{10.1}$$

The first three terms on the right (numbered 1–3) warrant discussion. The three-dimensional wind field is $\mathbf{V}$, and the first term on the right ($-\mathbf{V}\cdot\nabla q$) is the large-scale advective transport in a coordinate system (e.g., x, y, p, where p is pressure and the velocity in the vertical is ω). Here, "large-scale" can be defined as that which can be resolved by the model, and is a function of the model resolution. Horizontal transport by smaller scale motions is expressed in the characteristic form of horizontal diffusion (i.e., $D\nabla_h^2 q$) with some, generally non-linear, effective eddy diffusion coefficient D. The third term on the right captures vertical transports due to small scale processes, and is expressed mathematically as associated with the Reynolds stress $\omega' q'$. Such processes are not resolved in models, yet the effects of the processes are important. As such they are accounted for through "parameterization," which aims to estimate the effects of small scale processes on the large-scale quantities using only large-scale information. Should the vertical transport be associated with (dry) turbulent motions the third term takes the meaning of turbulent flux, such as one finds most strongly in the boundary layer. On the other hand, if the turbulence occurs in concert with condensation, this term captures transport in the region of convective clouds, in which there may be water entrained at their base and detrained at some higher altitude. Accounting for both boundary layer turbulence and moist convection is a topic great interest in dynamical modeling, and a complex subject in its own right. It is appropriate to note here, however, that the sum of these three numbered terms in Eq. 10.1 capture the total transport and mixing of air masses, and it is the explicit evaluation of them which is a unique element of dynamical models.

Beyond transport, the water budget has both active sources and sinks. The primary source of water in the atmosphere is evaporation and evapo-transpiration at the surface and evaporation of falling hydrometeors, E. Loss of water is via condensation, C. The additional term, S, accounts for sources or sinks which are associated with other processes, and can include the water source associated with methane oxidation in the stratosphere (e.g., McCarthy et al. 2004), mass independent isotopic exchange in the region of the ozone layer (e.g., Yung and Miller 1997), and radioactive decay, in the case of, say, ^{19}O or ^{3}H.

A comprehensive model for simulation of isotopic composition stems from writing down an analog of the atmosphere budget (Eq. 10.1) for isotopologues and considering their changes relative to the most abundant nuclide. The challenge in developing an isotope model is seen by noting that where condensation and evaporation occur, it does so with both kinetic and equilibrium fractionation, and the additional sources typically have different isotopic signatures. Thus the terms E, C

and S need special attention because it is the isotopic variation in these which give rise to isotope distributions. The transport processes themselves do not impose fractionation (since there is no phase change), but the details of transport are fundamental in setting the spatial and temporal distributions. However, since the key strength of comprehensive models is in accounting for transport and mixing processes, they warrant further examination.

10.4 Transport Processes and Numerical Solution

10.4.1 Diagnostic Water Tracers

Before examining the details of isotopic calculations, it is useful to consider the more abstract idea of water tracers. The use of non-fractionating water tracers is greatly advantageous in diagnosing water transport pathways in the atmosphere, and tracking specific water origins (Bosilovich and Schubert 2002; Koster et al. 1986, 1993; Noone and Simmonds 2002a). Indeed the desire to use isotopes in diagnostic studies often stems from their ability to naturally tag water sources. Water tracers can be defined by duplicating the water budget equation, (Eq. 10.1), such that within the model "tracer water" follows the usual "prognostic water" exactly. The difference between tracer water and prognostic water is only that the latter influences the diabatic heating, and the former is purely a slave to the prognostically computed quantity. At a coding level this is easily (but often tediously) achieved by replicating lines of code for the tracer water whenever the prognostic water variable is modified. Denoted with subscript i, the tracer water budget is

$$\frac{\partial q_i}{\partial t} = -\mathbf{V}\cdot\nabla q_i + D\nabla_h^2 q_i + \frac{\partial}{\partial p}\left(\overline{\omega' q_i'}\right) + R_E E - R_C C + R_S S, \tag{10.2}$$

which conserves the tracer proportion during transport, and the ratio of tracer to total (prognostic) water is given via the source terms and the ratios R_E, R_C and R_S.

In the absence of the source S (or taking $R_S = 1$), should one be interested in tagging the water that originates from some geographical location defined as those model grid points (X,Y) and time (T), a useful choice is $R_c = q_i/q$, and an evaporative source mask can be defined such that

$$R_E = \begin{cases} 1 & \forall (x,y,t) \in (X,Y,T) \\ 0 & \text{otherwise} \end{cases}. \tag{10.3}$$

Figure 10.1 shows a case where the region of interest is defined as southern South America, and the quantity plotted is the fraction of total precipitation that results from evapotranspiration in that region. Values over the region itself give the recycling rate (i.e., the fraction of rain which came from local evapotranspiration). Values are high downstream and to the west in the southern midlatitudes and near

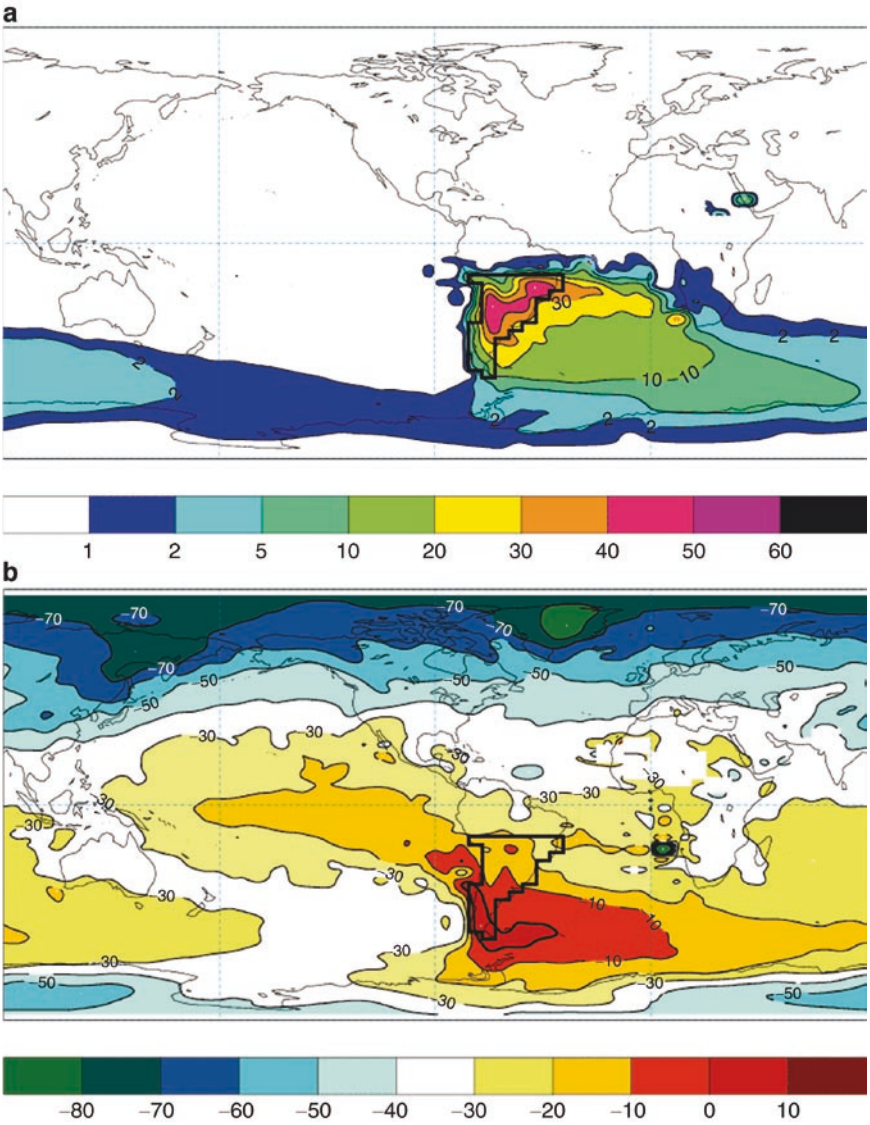

Fig. 10.1 (**a**) Percentage of precipitation that originated from evapotranspiration over a region in South America (shown as *bold box*) deduced using a non-fractionating water tracking scheme in the MUGCM, and (**b**) the isotopic composition of that water (Adapted from Noone and Simmonds 2002a). Fig. 10.1, see Appendix 1, Color Section

the equator to the east where the source water is entrained into the tropical easterlies. The source in this case was defined without a time constraint, but the methodology can be adapted to track water from, say, a given month. More elaborate source mask functions of $R_E = f(x,y,t)$ that are smooth have some numerical advantages because numerical transport of step-like anomalies is almost always problematic. Rather than considering surface sources, one can tag other water sources, such as the evaporation of ice crystals, water of stratosphere origin, water that has experience super-saturation, or any other specific condition that is of interest.

The tagging methodology is a required first step in building an isotope scheme, and indeed developing the code infrastructure to correctly tag the water, generate appropriate flux statistics comparable to, say, precipitation and evaporation, and handle archiving of model results, accounts for most of the effort in building an isotope scheme in comprehensive models. This is unlike the simpler task of tagging air masses, since the partitioning of water tracers changes during each instance of existing hydrological exchange. That is, one must account for the known (calculated) terms E, C and S in a hydrologic tracer scheme, while these are not present in gas-phase tracer schemes in which only transport is needed.

The difference between a tagging scheme and an isotope scheme is simply that the ratios R_E, R_C and R_S are modified by physically based fractionation, and i is a particular isotopologue rather than a generic tracer. In practice one can have a tagged-isotope scheme such that that isotopic composition of water from some specified source is tracked (e.g., Noone and Simmonds 2002b). Figure 10.1b shows the $\delta^{18}O$ of the water that originated from South America in a climate simulation. Notice the depletion away from the source region, and that the resulting pattern in some ways resembles the rainout that one expects from Rayleigh distillation. In this case, however, the distillation is combined with large-scale and turbulent mixing processes which ensures the simulation result is strictly (and quantifiably) non-Rayleigh. Such results provide significant diagnostic capabilities for understanding the final isotope distributions beyond simple attribution to different origins.

10.4.2 Numerical Issues for Transport Processes

Even though there is no fractionation associated with large-scale advection or during (dry) turbulent exchange, some care is needed in a numerical implementation. Because water vapor abundance changes by at least four orders of magnitude in nature, any numerical scheme must be able to resolve this range, plus three more orders of magnitude if one is interested in deviations there order of 1‰. This is a significant numerical challenge. Jouzel et al. (1987) found that the advection scheme used in the GISS model of the time was unable to conserve isotope ratios which introduced an isotopic fractionation. Artificial fractionation during transport is a purely numerical issue, but is clearly non-trivial and persists even in recent isotope schemes (Yoshimura et al. 2008). Noone and Simmonds (2002b) found that the treatment of water vapor transport via spectral methods was inadequate to preserved

the isotope ratio in very low temperature regions such as Antarctic and the upper troposphere, and lead them to replace their spectral advection scheme with the semi-Lagrangian scheme of Williamson and Rasch (1989). The spectral method, while appealing for resolving sharp gradients in dynamic fields (i.e., cold fronts), is remarkably poor at conserving covariance between two tracers (such as H_2O and any other isotopologue) in the region of such gradients. While the semi-Lagrangian scheme better preserves tracer-tracer correlations, it is not conservative, and the addition of mass fixers to ensure global conservation introduces a non-physical component to the transport. This is usually small compared to the dominant physical signal, at least in the lower troposphere where the lifetime of water is reasonably short. Prather (1986) developed a highly accurate numerical scheme based on the describing the sub-grid scale structure with quadratic moments, and which has been found to preserve isotope ratios adequately in the GISS model (Schmidt et al. 2005). A numerical scheme that is expressly designed to preserve tracer-tracer correlations was developed by Lin and Rood (1996) and guarantees the isotope ratio R will be preserved under advection of q and q_i independently. However, in all cases, more complicated schemes require more numerical operations and faster computers, and thus the ultimate choice is a practical compromise.

Part of the result stems from the choice of the state variable. The most physically meaningful choice is the isotope mass mixing ratio (or number density), such that the isotope budget perfectly mirrors the underlying water cycle given by Eq. 10.1, but another choice is the isotope ratio itself. Transforming Eq. 10.1 into a budget equation for the ratio R is straightforward, and given R and q, the source and sink terms can still be included as influences on q_i as needed. One can obtain the numerical benefits of using R in transport, by writing the isotope mass flux as the sum of a "base state" component, plus an "isotope flux" by appealing to the product rule:

$$\mathbf{V}\cdot\nabla q_i = R\left(\mathbf{V}\cdot\nabla q\right) + q\left(\mathbf{V}\cdot\nabla R\right). \tag{10.4}$$

While algebraically the same, the small differences that project onto numerical uncertainties provide substantial differences in the resulting δ values.[2] Jouzel et al. (1987) found a solution to the transport problem in the GISS model by using a scheme like Eq. 10.4, and considered the isotope advection relative to the advection

[2]Consider the inequality that results from simplest one-dimensional centered finite difference approximation to Eq. (10.4):

$$\frac{u}{2\Delta x}\left(q_i^+ - q_i^-\right) \neq \frac{u}{2\Delta x}\left[\frac{q_i}{q}\left(q^+ - q^-\right) + q\left(\frac{q_i^+}{q^+} - \frac{q_i^-}{q^-}\right)\right]$$

where the subscripts + and – denote values evaluated as some position $x + \Delta x$ and $x - \Delta x$, and values without subscripts are evaluated at position x. The error that leads to the inequality is a result of the order of the finite approximation, and the size of the error can be as large as the isotope variations of interest in cases where the changes in q are large relative to q.

of water. Improvements from such an approach are greatest for the least accurate schemes, and indeed the advantage in Lin and Rood's (1996) finite-volume scheme is trivial. Treatment of non-resolved fluxes by diffusion is subject to similar artifacts (particularly in boundary layer schemes that parameterize "non-local" transport), and these also can be overcome by recognizing no numerical scheme is perfect and designing a scheme in which the numerical precision is better than that needed for a given magnitude physical signal is the main requirement. The precision needed for isotopes is three orders of magnitude greater than for non-isotope applications because the physical signal of interest is measured in units of per mil.

10.5 Exchange Processes and Fractionation

10.5.1 Land and Ocean Water Sources

Craig and Gordon (1965) suggested a model for the evaporative flux of isotopes from both open water and through vegetation. These ideas persist to today and are considered both robust and applicable for modeling isotopic exchange in many instances. They posit that, following a Fickian transport process, one can express evaporation as a flux associated with mixing between ambient air and a reservoir of vapor that is in thermodynamic equilibrium with open water (say, ocean). This is a special case of a more general description of water mass mixing (Noone 2009). As such, the evaporative flux can be written:

$$\begin{aligned} E &= \rho c(q_s - q) \\ E_i &= \rho \eta c(R_s q_s - q_i) \end{aligned} \tag{10.5}$$

where c is an exchange coefficient (or, conductance), q_s is the saturation mixing ratio at the source temperature T_s, and ρ is the density of dry air. The two terms E and E_i can immediately be combined to give an expression for the isotope ratio of the flux R_E.

The isotopic flux E_i, depends on the isotopic composition of the source vapor R_s. Over the ocean this can be taken as $R_s = R_{ocean}/\alpha_e$, where α_e is the equilibrium fractionation factor which depends on the surface temperature (T_s). Figure 10.2a shows the annual mean $\delta^{18}O$ of precipitation simulated by a model in which only the surface fluxes fractionate (no fractionation is applied during condensation). Noone (2009) demonstrated that a mixing processes, such as evaporation and evapotranspiration, tends toward a steady state value set as the weighted mean of all source waters, which in this case is dominated by the infinite ocean source. As such the vapor tends toward the flux-weighted mean value of vapor in equilibrium with the ocean. Notice that the equilibrium fractionation factor is weakly temperature

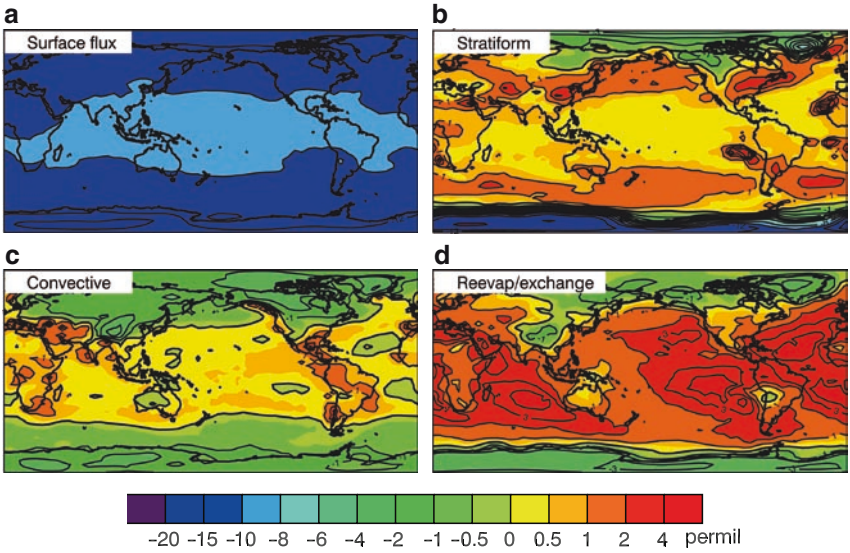

Fig. 10.2 Global model simulation of annual mean $\delta^{18}O$ in precipitation (‰) in a global isotope model with (**a**) fractionation only associated with surface evaporative sources and dew/frost sinks, (**b**) as in (**a**) but with fractionation also associated with stratiform condensation), (**c**) as in (**a**) but with fractionation also associated with convective condensation, and d) the influence of fractionation during exchange as raindrops fall from clouds. Panels (**b**) and (**c**) are differences relative to (**a**), and panel (**d**) is a difference relative to a control simulation that has all fractionations, and is shown in Fig. 10.4b. To the degree to which the model results are linear, the (weighted) sum of all four components composes the total isotope signal. Fig. 10.2, see Appendix 1, Color Section

dependant over the range 0–35°C that spans the global SST distribution, and gives rise to the spatial variation seen in the figure. Given the global mass weighted mean value of precipitation from this simulation of $\delta^{18}O = -10.05‰$, one finds the mean temperature of evaporation is 289 K, which corresponds with ocean surface temperature in the region of the extratropics and mid-latitudes. The rate at which the model approaches this steady state value is a function of the surface exchange coefficient (c), the kinetic fractionation efficiency (η), the strength of turbulence in the boundary layer, and large scale mixing by small and large-scale motions, and is on the order of months.

At steady state, Craig and Gordon (1965) showed that the isotopic composition of the water flux from plants must equal the isotopic composition of the soil water (Helliker and Noone 2009, this volume), and so $R_s = R_{soil}$ and there is no apparent fractionation. Dongmann et al. (1974) relaxed the steady state assumption and showed that Craig and Gordon's simpler model is often quite satisfactory in the time-mean. A non-steady state assumption has subsequently been used in a sophisticated process model by Noone et al. (2002) and Still et al. (2009), who again find for long-term statistics the steady-state assumption is quite valid, and only when one is interested in variations on, say, diurnal time-scales does one need to account for non-steady conditions.

The factor η in Eq. 10.5 accounts for the slightly differing conductance of isotopologues compared to normal water, and is slightly less than one. This arises because the total flux is composed of both transport by molecular diffusion and by turbulent eddy motions. While the transport by turbulence has no fractionation, the diffusive component for the different isotopologues introduces kinetic fractionation. Merlivat and Jouzel (1979) studied the influence of this kinetic effect as a function of the turbulent strength, and showed a clear transition as a function of the Richardson number (and thus, friction velocity), or near-surface wind speed (η here is equivalent to their $1 - k_{mol}$). Their parameterized theory is in common use for oceanic fluxes in global models, although there remains some question as to the value of some parameters (Cappa et al. 2003).

An alternate, but equivalent, approach was taken by Riley et al. (2002), who explicitly wrote down the isotopic conductances associated with both turbulent and diffusive fluxes in the case of transpiration and evaporation from soils. The advantage of Riley's scheme stems from the knowledge of both the molecular and turbulent components in the underlying model (Bonan 1994; Bonan et al. 1997). That is, the physics that controls the isotopic kinetic effect are represented explicitly. Because the fractionation is tied more directly to the model physics this is a more satisfying approach than introducing an additional parameterization.

10.5.2 Elementary Cloud Processes in Comprehensive Models

Within a modeled hydrologic cycle condensation and evaporation is parameterized depending on a number of large scale variables, including temperature and humidity. The humidity of an air mass changes due to variation in the moisture and temperature fields because of any number of the dynamic or thermodynamic influences simulated, and condensation can occur when vapor reaches some fraction of the saturation value. If the condensation is slow, then it can be considered thermodynamically reversible (as in a reversible moist adiabatic process, Noone 2009), and one can assume the formation of cloud liquid droplets occurs at isotopic equilibrium (i.e., a closed system). On the other hand if condensation is fast, to larger drops or the condensate is ice, the molecules composing the hydrometeors are effectively separated from the vapor and an open-system (Rayleigh) assumption is more reasonable. The first implementations of isotope tracers in a global models used this physical reasoning to model isotopic fractionation that accompanies rain formation by stratiform cloud as a closed process, and formation of ice condensate and either ice or liquid condensate from convective cloud as a Rayleigh process. We will refer here to isotope schemes of this type as "first generation" isotope schemes for the treatment of cloud processes. While the concepts are borrowed from simpler box/trajectory models, such a fractionation scheme can be fitted to comprehensive dynamical models.

Precipitation formed under a closed-system assumption in a discrete spatial model provides a finite estimate of the (continuous) Rayleigh process, and as such any model that uses this assumption will ultimately represent a distribution that approximates a Raleigh distillation. On the other hand, the choice of using a Rayleigh processes to model convective condensation is akin to suggesting a timescale separation between the processes which operate within clouds and those associated with the large-scale flow, and is an assumption that is implicit to all large scale models that do not track the evolution of cloud liquid and ice. Indeed prognosis of cloud liquid is required in high resolution models to explicitly account for sub-Rayleigh behavior if there is cloud liquid retained. This has been demonstrated analytically by Noone (2009) for the case of the two-phase model given by Merlivat and Jouzel (1979). On the other hand, the correct sub-Rayleigh behavior is implicit in low resolution dynamical models as a resolution artifact.

Given these considerations, one can envisage the simplest (but still comprehensive) isotope model in which one has an H_2O tracer, along with HDO and $H_2{}^{18}O$ tracers. There is some surface source, say given by Eq. 10.5, and the resulting water is subject to transport by non-fractionating large-scale motion, turbulent boundary layer motion, and by convective updrafts and downdrafts. A check is made at each time step for each grid box to see if the tracer water has exceeded saturation at the environmental temperature. If so, an adjustment (Δq_i) is made as either an open or closed isotope exchange such that

$$\begin{aligned} \Delta q &= \min(h_c q_s(T) - q, 0) \le 0 \\ \Delta q_i &= \begin{cases} q_i \left[\dfrac{1}{\alpha\left(1 - F^{-1}\right)} - 1 \right]^{-1} & T > T_{freeze} \text{ and small drops} \\ q_i \left(F^{\alpha} - 1\right) & T < T_{freeze} \text{ or large drops.} \end{cases} \end{aligned} \tag{10.6}$$

The fraction of vapor remaining after the adjustment (final/initial), F, is given by

$$F = \frac{h_c q_s}{q} = 1 + \frac{\Delta q}{q} \le 1 \tag{10.7}$$

where h_c is some critical relative humidity (often taken as 80% for a grid-cell mean), and the freezing temperature, T_{freeze}, could be taken below 0°C where supercooled liquid exists. In practice some care is needed to ensure that the solution of Eq. 10.6 avoids division by zero errors when F becomes small. Choice of the fractionation factor as the equilibrium value when condensation is to liquid is robust since this is assumed to be a slow process. During formation of ice condensate, the diffusivity slows the transport of vapor onto growing ice crystals, and this limitation is greater for the heavier isotopologues. Specifically, while there is a preference for the heavy nuclides to condense, the strength of this preference is reduced through the kinetic limitation. Jouzel and Merlivat (1984) introduced a parameterization

for the kinetic effect as a function of supersaturation of the vapor in the presence of ice, which remains in common use in isotope models.

Figure 10.2b shows a model simulation for the case where fractionation during condensation is applied only during stratiform condensation as by Eq. 10.6. Notice that in the tropics the influence enriches the precipitation relative to the original vapor because the condensation temperature is lower than the (surface) evaporation temperature and thus fractionation is more efficient. The removal of heavy isotopes at midlatitudes gives rise to the latitude effect, as seen in the greater depletion at higher latitudes and particularly over Antarctica and Greenland. Indeed, with fractionation in only stratiform cloud there is evidence for the latitude, altitude and continental effects noted by Dansgaard (1964). The impact of fractionation associated with convection is seen in Fig. 10.2c to mainly influence the spatial structure in the tropics and over land, where a large fraction of the total precipitation is associated with convective storms. At high latitudes a depleting influence is again seen because of condensation upstream, with subsequent transport of the remaining depleted vapor toward the poles. Indeed the globally integrated influences of fractionation during condensation is small (+0.66‰ for stratiform, and +0.18‰ for convective), and non-zero only because of non-linearity introduced by transport. As such, the importance of fractionation during condensation is best seen as affecting the spatial distribution, while the strength of fractionation associated with the surface fluxes, sets the mean. Notice that combining these two condensation terms, a spatial pattern emerges that is consistent with a spatial view of Dansgaard's empirical amount effect since the tropical regions where precipitation totals are higher are more depleted than the higher (subtropical) latitudes.

10.5.3 More Advanced Isotope Cloud Physics

First generation cloud schemes need not be tied all that closely to the underlying physical model yet can provide satisfying results for many applications. A second generation cloud isotope scheme incorporates more explicit treatment of hydrological exchanges within convective clouds, rather than simply applying a single bulk fractionation to capture the entire behavior of the cloud. Specifically, modern atmospheric GCMs represent the transport with the region of convection via convective updrafts and downdrafts. As indicated in Table 10.1, most isotope models presently in use can be described as of this type since they account in some way for convective scale transport. Accounting for fractionation within clouds is more complicated, but there are some simple bulk assumptions about isotopic exchange that can be made. For instance, in updrafts, rapid condensation ensures the environment is near-saturated with respect to the in-cloud temperature giving motivation for a Rayleigh distillation. Similarly, the existence of downdrafts is associated with evaporation of rain, and one might assume that these regions are also (near) saturated, and so isotopically close to equilibrium with liquid drops.

Within a region of convective clouds one can write the tendency associated with convection as

$$\left(\frac{\partial q}{\partial t}\right)_{convective} = \frac{\partial\left(w'q'\right)}{\partial p} \approx \frac{\partial}{\partial p}\left[w_u\left(q - q_u\right)\right] \tag{10.8}$$

where the subscript u indicates quantities in the updraft region, and an elementary mass balance for the in-cloud vapor can be written as

$$\frac{\partial q_u}{\partial t} = \frac{\partial\left(mq_u\right)}{\partial p} - C + \gamma q - \mu q_u = 0. \tag{10.9}$$

The budget equation of updraft water is assumed at steady state, which is justified by noting the timescale separation between convection (less than 1 h) and the resolved large-scale motion (order of a day). The rate at which water vapor from outside the plume is entrained is γ, μ is the rate of detrainment of the plume material, and m is the vertical mass flux. The mass flux is related to the updraft velocity ω_u through knowing the fraction of the grid box covered by updrafts. From conservation considerations, m, $\gamma$and μ are related (consider the case with C = 0 and q_u = q = 1). An isotopic version of Eq. 10.8 follows by assuming the vertical profile in q_u satisfies a Rayleigh profile, and so isotopic composition of condensation is set via equilibrium with the vapor (with a kinetic effect if the condensation is to ice). Because the convective mass flux, m, is found as part of the underlying convective parameterization, this is a reasonably convenient form. This approach can easily be adapted for models that track cloud liquid and ice in addition to large-scale vapor. Similarly, an expression analogous to Eq. 10.9 but for downdrafts can be written upon assuming that downdrafts are saturated, and one writes the isotopic composition of the downdraft as that in (or close to) equilibrium with precipitation falling in the downdraft region if liquid or resulting from non-fractionating sublimation if the precipitation is frozen.

Such second generation schemes begin to address issues surrounding the isotopic partitioning in the region of clouds. While this added complexity may not have a substantial influence on the simulated isotopic composition of precipitation, the microphysical and isotopic assumptions greatly influence the simulation of the isotopic composition of mid and upper troposphere water vapor. Schemes of even this complexity are not easily employed in models simpler than comprehensive dynamical models.

Third generation cloud isotope schemes are beginning to appear and represent the state of the art. They differ in their design by specifically fitting isotope physics to the more detailed cloud processes within modern atmospheric models. This is motivated in part by a desire to understand the isotopic exchange within clouds, rather than the isotopic composition that results from clouds in some average sense. To this end, the development of third generation models is facilitated by more detailed bulk microphysical schemes being used in modern climate and Earth-system models.

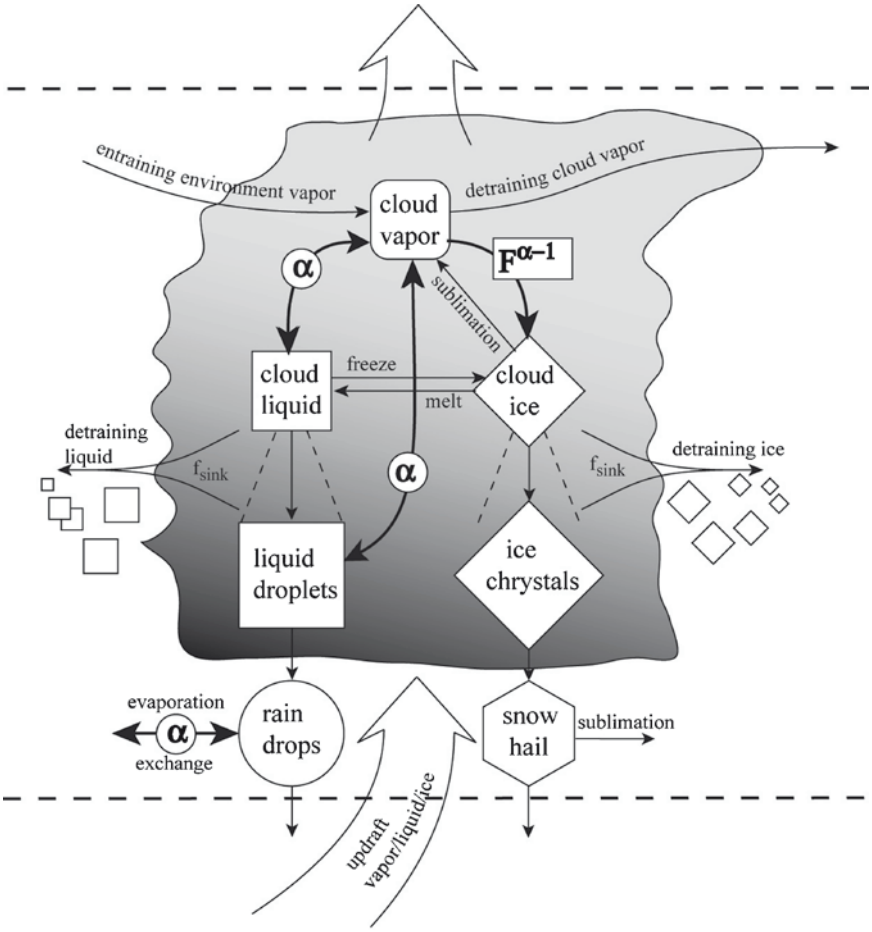

Fig. 10.3 Schematic depiction of the third-generation isotope scheme describing the cloud microphysics for isotopes used in CAM3 (adapted from Noone 2003). Detailed exchanges between in-cloud properties and the environment, the accounting for multiple microphysical moments, and inclusion of transport processes differentiates this scheme from first and second generation schemes. Because on non-linearity in the budget equations for the set of moments, such schemes usually need to be integrated numerically

Figure 10.3 shows a schematic example of a third-generation isotope cloud model and depicts the multiple exchanges between different microphysical moments that are explicitly (or implicitly) accounted for in the underlying non-isotopic cloud model. This scheme treats both grid-average and in-cloud vapor, cloud liquid, cloud ice, liquid drops (rain) and ice precipitation (a combination of snow, grauple and hail). Transport processes include the mixing between grid-scale and in-cloud properties

via entrainment and detrainment, and updraft and downdraft fluxes as expressed in Eq. 10.8. Such models share some similarities with the cloud models of Federer et al. (1982), Gedzelman and Arnold (1994), Lawrence et al. (1998), Bony and Risi (2008), and the mixed-phase cloud model of Ciais and Jouzel (1994). The computational demand of third-generation scheme is much greater since the isotopic (bulk) microphysics needs to be solved via numerical integration over each dynamical model time step to be accurate, which contrasts with second-generation schemes in which the bulk exchanges can be directly computed via integral expressions of the required adjustment, as, for instance, given by Eq. 10.6. It is this numerical requirement and the complexity of web of exchanges within clouds that separates second and third generation schemes.

Fourth generation cloud isotope schemes can be foreseen as those in which the microphysical exchanges (such as diffusional particle growth and coalescence processes) are resolved and isotopic exchanges can be computed directly, rather than resorting to the bulk microphysics used in third generation schemes. An example of such a scheme was used at cloud resolving scales with a detailed microphysical scheme by Smith et al. (2006). Such schemes will place constraints on the underlying assumed microphysics, which themselves are not well known, since both equilibrium and kinetic isotopic exchanges are resolved from first principles rather than derived from assumptions surrounding bulk microphysics. The practical issue of applying explicit microphysical schemes in large-scale models remains a challenge for the non-isotopic modeling community, and is an area where isotope constraints may be particularly informative.

10.5.4 Post Condensation Exchange

Although the cloud processes control the primary removal of water from the free atmosphere, Jouzel (1986) noted that the time taken for liquid drops to equilibrate with the environment through which they fall is usually comparable, and often shorter than, the time required to fall. The effect results from two drop-size dependant features: (1) small drops fall slowly, and (2) small drops equilibrate quickly. As such, sufficiently small rain drops will equilibrate with vapor near the ground, and the isotopic composition of liquid precipitation will closely resemble the isotopic composition of near surface (boundary layer) vapor. Stewart (1975) noticed this effect and explained the tendency toward the equilibrium as a mixing process.

The exchange mechanism has been used to explain the amount effect that Dansgaard observed (Bony and Risi 2008; Lee and Fung 2008; Noone 2009; Rozanski et al. 1993; Stewart 1975; Worden et al. 2007). Because the sub-cloud layer is sub-saturated (by definition), isotopic exchange is usually accompanied by a net evaporation of the falling rain, and exchange provides a net recycling of molecules between the condensate and the free atmospheric vapor (Noone 2009; Worden et al. 2007). In this way, the isotopic composition provides a metric of the efficiency with which water is removed from the atmosphere as precipitation.

While the solid matrix of ice precipitation prohibits any equilibration, large rain drops associated heavy rain events will undergo partial equilibration. Hoffmann et al. (1998) suggested that in a comprehensive model rain under convective clouds experiences 45% equilibration, while stratiform cloud (with assumed smaller drops and lower rainfall rates) almost completely equilibrate (95% equilibration). Lee et al. (2008) used a parameterization of the drop size distribution to allow this rate to be calculated within the model based on the modeled precipitation rates. Figure 10.2d shows the impact of allowing isotopic equilibration using a similar physically based scheme on the final precipitation. Notice that at high latitudes where the precipitation is largely ice, and in the tropics where the raindrops are typically large and associated with convection, the partial equilibration has limited influence. Generally the influence is to enrich the precipitation (the globally integrated enrichment is +1.45‰ for $\delta^{18}O$) and is largest in the subtropical regions where the sub-cloud relative humidity is low. With enriched precipitation the remaining tropospheric vapor is consequently more depleted. The depleting influence at high latitudes thus results from transport of vapor that has undergone this depleting influence at lower latitudes.

The isotopic composition of all but the heaviest rain is set through isotopic exchange as it falls from clouds, and because the vapor near the surface is tied to ocean water via the exchange coefficient c in Eq. 10.5, only in regions that are far from equilibrium should the precipitation deviate much from that set by exchange at the ocean surface. It is for this reason that atmospheric models, in which the strength exchange process can be tuned, can simulate the isotopic composition of precipitation over the ocean and moist continental regions with high fidelity. Doing so, however, does not suggest that these models accurately simulate the atmospheric hydrology and clouds processes in detail.

10.6 Interpretive Utility and Reproducibility

All models can be used with either the goal of reproducing some set of data, or be used to test the importance of some specific physics or processes being modeled. Illustrating the case of reproduction, Fig. 10.4 shows the annual mean $\delta^{18}O$ composition in precipitation from the three global isotope models that participated in the first Stable Water-isotope Intercomparison Group (SWING) experiment, compared to the observationally based map of Buenning and Noone (in review). It shows that many of the spatial features are reproduced, including the dominant latitude, altitude, continental and amount effects. However, there are also substantial model errors. While the three models all fit GNIP-based map with a root mean squared error around 2‰, errors the order of 2‰ can often be too large for applications. Closer examination of Fig. 10.4 reveals that many of the regions with largest model error are associated with regions where the underlying hydrology is less robust, and tied to deficiencies in the simulation of large scale transport, problems with cloud physics and poor representation of surface hydrology.

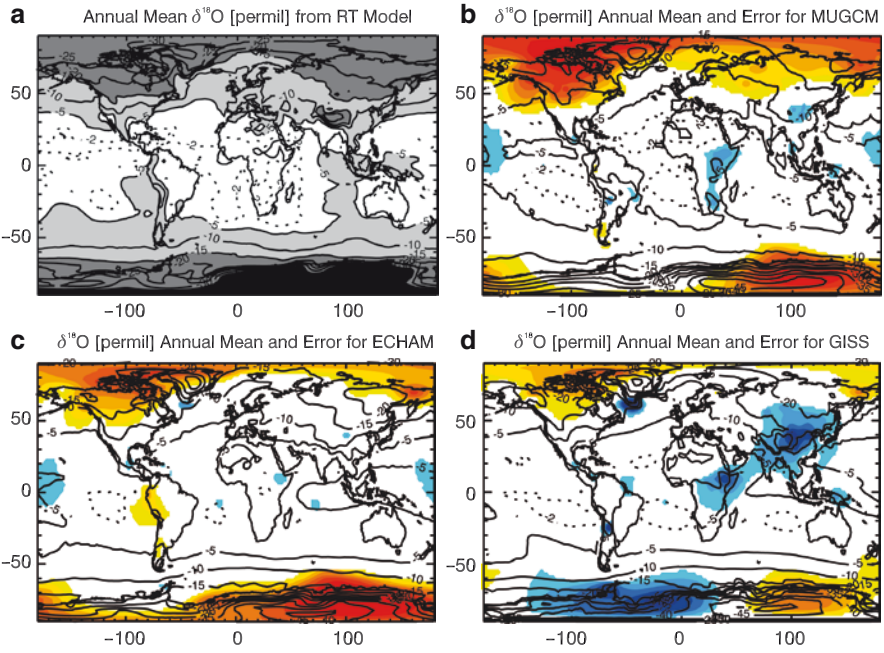

Fig. 10.4 Simulations of $\delta^{18}O$ in precipitation from three atmospheric models (MUGCM, ECHAM and GISS) participating in the first Stable Water-isotope Intercomparison Group (SWING) experiment, and from the observationally based regression model of Buenning and Noone (in review). Contour interval is 4‰ with extra contours at −2‰ and 0‰. Shading in panels (**b**–**d**) show where the models deviate from the GNIP data by more than 1‰. (*red* positive and *blue* negative) with gradations of 1‰ (Courtesy N. Buenning 2008). Fig. 10.4, see Appendix 1, Color Section

The deuterium excess simulation (Fig. 10.5) is even more problematic because of the less precise knowledge of kinetic effects. Similarly, many of the environmental conditions that give rise to kinetic effects are not modeled by the underlying hydrologic scheme (such as supersaturation, or the partitioning of molecular and turbulent transport during evaporation), and thus ultimately not well accounted for. To this end, mapping isotope distributions with comprehensive models is ultimately limited by both the robustness of the underlying model hydrology and the strength of the assumptions about the isotopic physics. Because the isotope physics in all but fourth generation schemes use bulk microphysical implementations of the isotope exchange, there is some uncertainty in the degree to which any errors in the final isotope fields are associated with the isotope scheme versus other errors in the underlying hydrological or climate simulation. Usually, isotope studies attribute much of the error to the underlying model with the assumption that the uncertainty in the isotope physics is much smaller than other model problems, but this has never been well quantified.

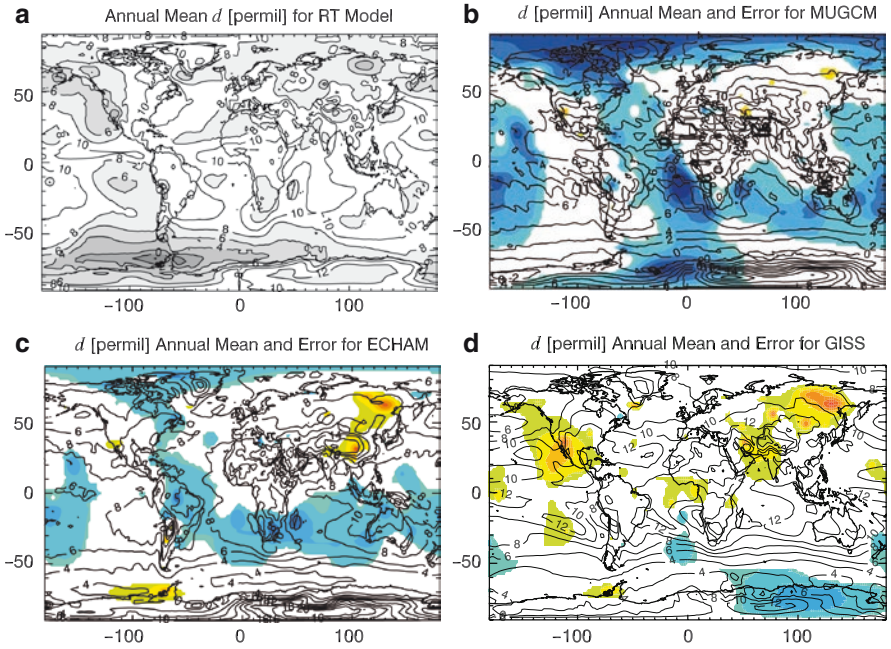

Fig. 10.5 As in Fig. 10.4 but for deuterium excess in precipitation. Contour interval is 1‰. Light shading in panels (**b**–**d**) show where the models deviate from the observations by less than −2‰, and dark shading shows where there differ by more than +2‰ with gradations of 1‰ (Courtesy N. Buenning 2008). Fig. 10.5, see Appendix 1, Color Section

10.7 Discussion and Outlook

While the advantages of comprehensive models are substantial, they are of course subject to a different set of limitations experienced by simpler models. Specifically, the simulation quality reflects both the detail to which the contributing processes are understood and the accuracy with which those processes are represented numerically. In part because of computational demand, no single aspect of these comprehensive models (clouds, land surface exchange, transport, etc.) is the most detailed available. This naturally places limits on the type of science questions that can be explored with such models. On the other hand, models of any complexity can be configured to provide meaningful results for some science application, and the choice to use comprehensive dynamical models of isotopes must stem from a need to account for combinations of processes or variability not well captured by simpler models. While the maps that result from comprehensive dynamical isotope models are useful in their own right for follow-on studies, a valuable use of isotopic models is in diagnosing the behavior of various processes. Indeed the most

powerful use of these models is in the ability to probe the mechanisms responsible for the true isotope distributions.

Being based on some underlying dynamical model, any biases in simulated climate variables (temperature, boundary layer dynamics, etc.) are reflected in the simulated isotopic distribution. The agreement between observations and simulations increases when some aspects of the simulation can be constrained. Recent interest has arisen in using isotopic models in which the large-scale meteorology is prescribed (say, nudged, Noone 2006; Yoshimura et al. 2008) and it is found that the simulated isotopic variability is remarkably robust on both daily and longer time scales. While this is a reminder that many aspects of the isotopic variability are associated with the large-scale transport pathways, it also suggests that constrained simulations are helpful in understanding the impact of synoptic circulation variability and organized patterns of variability (e.g., El Niño Southern Oscillation or North Atlantic Oscillation) on some observed isotopic record.

Comprehensive models lend themselves to hypothesis testing via sensitivity tests which can inform as to which types of mechanisms one should expect to influence a given set of measurements. This capability is at least of equal importance as the ability of comprehensive models to reproduce known isotopic distributions. While global scale models are especially useful in providing climatological understanding of isotope distributions, they are often not able to match isotope observed distributions because of the need to use relatively course resolution. This is of particular concern when the isotopic composition depends on geographic structures (topography, vegetation classification, coastlines) which are not well captured by relatively low resolution global models. Increasing the spatial resolution has several advantages, but it comes at a high cost in terms of computational burden. One option is therefore to use regional circulation models (RCM) for high resolution isotope studies over some region of interest (Sturm et al. 2005, 2007a). While the gap between the resolution of RCMs and global models has narrowed, many regional models now can be configured to run just short of resolving individual clouds and have other benefits.

Simulating isotopes within comprehensive dynamical models is a task which is limited by appropriate datasets for validation and testing. The International Atomic Energy Agency's GNIP remains a gold standard for testing global and regional models, but as argued here, these data do not provide a rigorous test of isotopic exchanges associated with cloud processes. Indeed even if the precipitation isotopes are simulated accurately, it is not a guarantee that the atmospheric water vapor isotopes are also simulated reliably because of post condensation exchange. Very few observations of the isotopic composition of water vapor exist, yet since this is the state variable in isotope models (as compared to the precipitation, which is a by-product flux), direct evaluation of the vapor phase is highly desirable. Complementing traditional water vapor collection and analysis methods, new observational techniques (including in situ and satellite based observations, (Helliker and Noone 2009, this volume) are poised to allow more detailed testing of specific isotope physics and hydrologic balances within comprehensive models, and will likely foster significant model improvements. The need for increased rigor in validation is particularly warranted as

the scope of scientific investigations to which comprehensive isotope models are being applied expands. Similarly, with greater validation effort comes increased confidence in the spatially and temporally resolved isotopic distributions that are simulated, and thus increased capacity to use the outputs from comprehensive dynamical isotope models as input to subsequent applications and isoscaping.

References

Bonan GB (1994) Comparison of 2 land-surface process models using prescribed forcings. J Geophys Res-Atmos 99:25803–25818

Bonan GB, Davis KJ, Baldocchi D, Fitzjarrald D, Neumann H (1997) Comparison of the NCAR LSM1 land surface model with BOREAS aspen and jack pine tower fluxes. J Geophys Res-Atmos 102:29065–29075

Bony S, Risi C, Vimeux F 2008, Influence of convective processes on the isotopic composition ($\delta^{18}O$ and δD) of precipitation and water vapor in the tropics: 1. Radiative-convective equilibrium and Tropical Ocean-Global Atmosphere-Coupled Ocean Ocean-Atmosphere Response Experiment (TOGA-COARE) simulations, J. Geophys Res. doi:10.1029/2008JD009942

Bosilovich MG, Schubert SD (2002) Water vapor tracers as diagnostics of the regional hydrologic cycle. J Hydrometeorol 3:149–165

Brown J, Simmonds I, Noone D (2006) Modeling delta O-18 in tropical precipitation and the surface ocean for present-day climate. J Geophys Res-Atmos 111:D05105. doi:10.1029/2004JD005611

Buenning N, Noone D 2009: An evaluation of annual mean and seasonal timing of local and non-local processes controlling the isotopic composition of precipitation from observations and comprehensive models. Journal of Geophysical Research-Atmospheres, Submitted, May, 2009

Cappa CD, Hendricks MB, DePaolo DJ, Cohen RC (2003) Isotopic fractionation of water during evaporation. J Geophys Res-Atmos 108:4525. doi:4510.1029/2003JD003597

Charles CD, Rind D, Healy R, Webb R (2001) Tropical cooling and the isotopic composition of precipitation in general circulation model simulations of the ice age climate. Clim Dyn 17:489–502

Ciais P, Jouzel J (1994) Deuterium and oxygen 18 in precipitation: an isotopic model including mixed cloud processes. J. Geophys Res 99:19783–16803

Cole JE, Rind D, Webb RS, Jouzel J, Healy R (1999) Climatic controls on interannual variability of precipitation $\delta^{18}O$: simulated influence of temperature, precipitation amount, and vapor source region. J Geophys Res 104:14223–14235

Craig H, Gordon LI (1965) Deuterium and oxygen-18 variations in the ocean and marine atmosphere. In: Tongiorgi E (ed) Proceedings of conference on stable isotopes in oceanic studies and paleotemperatures. Laboratory of Geology and Nuclear Science, Spoleto, Italy, pp 9–130

Dansgaard W (1964) Stable isotopes in precipitation. Tellus 16:436–468

Dongmann G, Nürnberg HW, Förstel H, Wagener K (1974) On the enrichment of $H_2{}^{18}O$ in the leaves of transpiring plants. Radiat Environ Biophys 11:41–52

Federer B, Brichet N, Jouzel J (1982) Stable isotopes in hailstones. Part I: the isotopic cloud model. J Atmos Sci 39:1323–1336

Gedzelman SD, Arnold R (1994) Modeling the isotopic composition of precipitation. J. Geophys Res 99:10455–10471

Helliker B, Noone D (2009) Novel approaches to monitoring of water vapor isotope ratios: plants, satellites and lasers. In: West, J.B.; Bowen, G.J.; Dawson, T.E.; Tu, K.P. (Eds.) 2010, ISBN: 978-90-481-3353-6. Isoscapes: understanding movement, pattern, and process on Earth through isotope mapping. Springer, Berlin

Hoffmann G (1995) Wasserisotope im allgemeinen Zirkulationsmodell ECHAM. Universitat Hamburg, Hamburg

Hoffmann G, Heimann M (1997) Water isotope modeling in the Asian monsoon region. Quart Int 37:115–128
Hoffmann G, Jouzel J, Masson V (2000) Stable water isotopes in atmospheric general circulation models. Hydol Process 14:1385–1406
Hoffmann G, Werner M, Heimann M (1998) Water isotope module of the ECHAM atmospheric general circulation model: a study on timescales from days to several years. J Geophys Res 103:16871–16896
Joussaume S (1983) Modèlisation des cycles des especes isotopiques de l'eau et des aerosols d'origine de'esertique dans un modele de circulation generale de l'atmosphere. Univeristy of Paris, Paris, France
Joussaume S (1993) Paleoclimate tracers: an investigation using an atmospheric general circulation model and ice age conditions. 1. Desert dust. J Geophys Res 98:2767–2805
Joussaume S, Jouzel J (1993) Paleoclimatic tracers: an investigation using an atmospheric general circulation model under ice age conditions. 2. Water isotopes. J Geophys Res 98:2807–2830
Joussaume S, Jouzel J, Sadourny R (1984) A general circulation model of water isotope cycles in the atmosphere. Nature 311:24–29
Jouzel J (1986) Isotopes in cloud physics: multistep and multistage processes. In: Fritz P, Frontes JC (eds) Handbook of environmental isotope geochemistry, vol.2, The terrestrial environment B. Elsevier, New York, pp 61–112
Jouzel J, Koster RD, Suozzo RJ, Russel GL, White JW, Broecker WS (1991) Simulations of the HDO and $H_2{}^{18}O$ atmospheric cycles using the NASA GISS general circulation model: sensitivity experiments for present day conditions. J Geophys Res 96:7495–7507
Jouzel J, Merlivat L (1984) Deuterium and oxygen 18 in precipitation, modelling of the isotopic effects during snow formation. J Geophys Res 89:11749–11757
Jouzel J, Russell GL, Suozzo RJ, Koster RF, White JWC, Broecker WS (1987) Simulation of the HDO and $H_2{}^{18}O$ atmospheric cycles using the NASA GISS general circulation model: the seasonal cycle for present-day conditions. J Geophys Res 92:14739–14760
Koster R, Jouzel J, Suozzo R, Russell G (1986) Global sources of local precipitation as determined by the NASA/GISS GCM. Geophys Res Lett 13:121–124
Koster RD, DPd V, Jouzel J (1993) Continental water recycling and $H_2{}^{18}O$ concentrations. Geophys Res Lett 20:2215–2218
Lawrence JR, Gedzelman SD, Zhang X, Arnold R (1998) Stable isotope ratios of rain and vapor in 1995 hurricanes. J Geophys Res 103:11381–11400
Lee JE (2005) Atmospheric water: perspectives from isotopes and the NCAR climate model. University of California, Berkeley, CA, p 162
Lee JE, Fung I (2008) "Amount effect" of water isotopes and quantitative analysis of post-condensation processes. Hydrol Process 22:1–8
Lee JE, Fung I, DePaolo DJ, Henning CC (2007) Analysis of the global distribution of water isotopes using the NCAR atmospheric general circulation model. J Geophys Res-Atmos 112:D16306. doi:16310.11029/12006JD007657
Lin SJ, Rood RB (1996) Multidimensional flux-form semi-Lagrangian transport schemes. Mon Weather Rev 124:2046–2070
Mathieu R, Pollard D, Cole JE, White JWC, Webb RS, Thompson SL (2002) Simulation of stable water isotope variations by the GENESIS GCM for present-day conditions. J Geophys Res 107. doi:10.1029/2001JD900255
McCarthy MC et al (2004) The hydrogen isotopic composition of water vapor entering the stratosphere inferred from high-precision measurements of δ D-CH_4 and δ D-H_2. J Geophys Res-Atmos 109:D07304. doi:07310.01029/02003JD004003
Merlivat L, Jouzel J (1979) Global climatic interpretation of the deuterium-oxygen-18 relationship for precipitation. J Geophys Res 84:5029–5033
Numaguti, A. (1999), Origin and recycling processes of precipitating water over the Eurasian continent: Experiments using an atmospheric general circulation model, J. Geophys. Res., 104, 19571972

Noone D (2003) Water isotopes in CCSM for studying water cycles in the climate system. Eighth annual CCSM workshop, Breckenridge, CO

Noone D (2006) Isotopic composition of water vapor modeled by constraining global climate simulations with reanalyes. In: Cote J (ed) Research activities in atmospheric and oceanic modelling. World Meteorological Organization, pp 2–37

Noone D (2009) An isotopic evaluation of the factors controlling low humidity air in the troposphere. J Clim (in review, June 2008)

Noone D, Simmonds I (2002a) Annular variations in moisture transport mechanisms and the abundance of $\delta^{18}O$ in Antarctic snow. J Geophys Res-Atmos 107:4742. doi:4710.1029/2002JD002262

Noone D, Simmonds I (2002b) Associations between δ O-18 of water and climate parameters in a simulation of atmospheric circulation for 1979–95. J Clim 15:3150–3169

Noone D, Still C, Riley W (2002) A global biophysical model of ^{18}O in terrestrial water and CO_2 fluxes. In: Ritchie H (ed) Research activities in atmospheric and oceanic modelling. World Meteorological Organization, pp 4.19–14.20

Noone DC (2001) A physical assessment of variability and climate signals in Antarctic precipitation and the stable water isotope record. Ph.D. thesis, School of Earth Sciences, University of Melbourne, Parkville, Victoria, Australia, p 404

Prather M (1986) Numerical advection by conservation of second-order moments. J Geophys Res 91:6671–6681

Riley WJ, Still CJ, Torn MS, Berry JA (2002) A mechanistic model of ($H_2{}^{18}O$) and ($C^{18}OO$) fluxes between ecosystems and the atmosphere: model description and sensitivity analyses. Global Biogeochem Cycles 16:1095. doi:1010.1029/2002GB001878

Risi C, Bony S, Vimeux F (2008) Influence of convective processes on the isotopic composition ($\delta^{18}O$ and δD) of precipitation and atmospheric water in the tropics 2. physical interpretation of the amount effect. J Geophys Res 113, D19309, doi:10.1029/2008ID009943

Rozanski K, Araguas-Araguas L, Gonfiantini R (1993) Isotopic patterns in modern global precipitation. In: Swart PK, Lohmann KC, McKenzie J, Savin S (eds) Climate change in continental isotopic records. Geophysical Monograph Series. No. 78, American Geophysical Union, Washington, pp 1–63

Schmidt GA, Hoffmann G, Shindell DT, Hu Y (2005) Modelling atmospheric stable water isotopes and the potential for constraining cloud processes and stratosphere–troposphere water exchange. J Geophys Res 110:D21314. doi:21310.21029/22005JD005790

Schmidt GA, LeGrande AN, Hoffmann G (2007) Water isotope expressions of intrinsic and forced variability in a coupled ocean-atmosphere model. J Geophys Res-Atmos 112, D10103. doi:10.1029/2006JD007781

Smith JA, Ackerman AS, Jensen EJ, Toon OB (2006) Role of deep convection in establishing the isotopic composition of water vapor in the tropical transition layer. Geophys Res Lett 33:L06812. doi:06810.01029/02005GL024078

Stewart MK (1975) Stable isotope fractionation due to evaporation and isotopic exchange of falling waterdrops: applications to atmospheric processes and evaporation of lakes. J Geophys Res 80:1133–1146

Still CJ, Riley WJ, Birand SC, Noone D, Buenning NH, Randerson JT, Torn MS, Welker J, White JWC, Vachon R, Farquhar GD, Berry JA (2009) The influence of clouds and diffuse radiation on ecosystem-atmosphere CO_2 and $C_{18}OO$ exchanges. Journal of Geophysycal Research-Biogeosciences, 114, G01018, doi:10.1029/2008JG000675

Sturm C, Langmann B, Hoffmann G, Stichler W (2005) Stable water isotopes in precipitation: a regional circulation modelling approach. Hydrol Process 19:doi: 10.1002/hyp5979

Sturm C, Hoffmann G, Langmann B (2007a) Simulation of the stable water isotopes in precipitation over South America: comparing regional to global circulation models. J Clim 20:3730–3750

Sturm C, Vimeux F, Krinner G (2007b) Intraseasonal variability in South America recorded in stable water isotopes. J Geophys Res-Atmos 112:D20118. doi:20110.21029/22006JD008298

Sturm K (2005) Regional modelling of the stable water isotope cycle. Université Joseph Fourier, Grenoble

Vuille M et al. (2003) Modeling delta O-18 in precipitation over the tropical Americas: 2. Simulation of the stable isotope signal in Andean ice cores. J Geophys Res-Atmos 108. doi:10.1029/2001JD002039

Webster CR, Heymsfield AJ (2003) Water isotope ratios D/H, $^{18}O/^{16}$, $^{17}O/^{16}O$ in and out of clouds map dehydration pathways. Science 302:1742–1745

Werner M, Heimann M (2002) Modeling interannual variability of water isotopes in Greenland and Antarctica. J Geophys Res-Atmos 107:4001. doi:4010.1029/2001JD900253

Werner M, Heimann M, Hoffmann G (2001) Isotopic composition and origin of polar precipitation in present and glacial climate simulations. Tellus 53B:53–71

Williamson DL, Rasch PJ (1989) Two-dimensional semi-Lagrangian transport with shape preserving interpolation. Mon Weather Rev 117:102–129

Worden J, Noone D, Bowman K (2007) Importance of rain evaporation and continental convection in the tropical water cycle. Nature 445:528–532

Yoshimura, K., T. Oki, N. Ohte, and S. Kanae, 2003: A quantitative analysis of short-term ^{18}O variability with a Rayleigh-type isotope circulation model. J. Geophys. Res., 108(D20), 4647, doi:10.1029/2003JD003477

Yoshimura K, Kanamitsu M, Noone D, Oki T (2008) Historical isotope simulation using reanalysis atmospheric data. J Geophys Res 113:D19108. doi:10.1029/2008JD010074

Yung YL, Miller CE (1997) Isotopic fractionation of stratospheric nitrous oxide. Science 278:1778–1780

Chapter 11
Using Nitrogen Isotope Ratios to Assess Terrestrial Ecosystems at Regional and Global Scales

Linda H. Pardo and Knute J. Nadelhoffer

11.1 Introduction

Advances in instrumentation, particularly continuous flow mass spectrometry, have made accurate and highly precise measurements of nitrogen (N) isotopes feasible across broad geographical scales. As ^{15}N natural abundance measurements are made at more and more sites across diverse ecosystem types, it is now possible to compile resulting datasets and to compare patterns across ecosystems at regional and even global scales. Such data syntheses have enormous potential for identifying broad and underlying patterns in ^{15}N which, in turn, may provide insights into patterns of and controls on N cycling across ecosystems. Some challenges, however, must be overcome if this potential is to be fully realized. Syntheses of N isotope datasets, therefore, must be interpreted with an understanding of ways in which various biotic and abiotic factors can influence ^{15}N natural abundances in plant tissues and soils. In this chapter, we discuss (1) previous uses of N isotopes, (2) factors contributing to variation at small scales which can complicate interpretation of N isotope data at regional to global scales, (3) issues to consider in collecting and synthesizing data at large scales, (4) results of regional and global scale studies, (5) gaps in knowledge and potential future applications.

L.H. Pardo (✉)
Northern Research Station, USDA Forest Service, 705 Spear St, S. Burlington, VT, 05403, USA
e-mail: lpardo@fs.fed.us

K.J. Nadelhoffer
Department of Ecology and Evolutionary Biology, University of Michigan, 830 N. University, Ann Arbor, MI, 48109-1048, USA
e-mail: knute@umich.edu

J.B. West et al. (eds.), *Isoscapes: Understanding Movement, Pattern, and Process on Earth Through Isotope Mapping*, DOI 10.1007/978-90-481-3354-3_11,

11.2 Background on N Cycling and ^{15}N

The N cycle has many internal and external fluxes (Fig. 11.1; Table 11.1). Its complexity has limited the development of mechanistic N cycling models that are broadly applicable; in particular, detailed process-based models capable of explaining spatial (and temporal) patterns of ^{15}N natural abundance have not yet been developed.

Isotopic fractionation occurs during physical, enzymatic, and other biological processes discriminating against the heavier ^{15}N and in favor of the lighter ^{14}N when chemical bonds are broken. Therefore, ^{15}N:^{14}N ratios of reaction products are typically lower than ratios of substrates, leading to higher ^{15}N:^{14}N, or *^{15}N enrichment,* of residual substrates in relation to *^{15}N depletion* of products (Mariotti et al. 1981; Shearer and Kohl 1986, Robinson 2001). For example, microbial discrimination during N mineralization produces ^{15}N-depleted ammonium and causes a direct enrichment of the residual soil organic nitrogen in ^{15}N (Létolle 1980). Nitrification (Fig. 11.1, Table 11.1; flux *b*) produces ^{15}N-depleted nitrate and ^{15}N-enriched (relative to nitrate) ammonium (Handley and Raven 1992). Other strongly fractionating processes include denitrification (*c*) and ammonia volatilization (*B1*) (Hübner 1986). When the depleted product is removed from the system (via leachate (*C*), gaseous losses (*B*), etc.), the residual N pools (soil, vegetation, and inorganic N pools – NH_4^+ and NO_3^-) become enriched in ^{15}N. For example, following nitrification, if ^{15}N-enriched ammonium is retained in the soil and ^{15}N-depleted nitrate is leached from the ecosystem, the net effect of nitrification is to enrich the soil in ^{15}N (Shearer and Kohl 1986; Nadelhoffer and Fry 1994; Högberg 1997). Denitrification leads to similar enrichment in the remaining N pools at sites where it is significant (Piccolo et al. 1994).

Nitrogen transformations, internal fluxes, inputs, and outputs can influence soil and plant $\delta^{15}N$ values (Table 11.1). However, $\delta^{15}N$ values of pools and isotopic fractionation factors both vary widely and are often poorly characterized or uncertain. Fractionation may be expressed as the result of a single enzymatic reaction or as the integrated result of sequential reactions (Evans 2007; Sutka et al. 2008). When several reactions in sequence are considered together, the resulting fractionation factors can be large (Perez et al. 2006; Sutka et al. 2008). Because it is difficult to measure fractionation factors, the observed discrimination is often reported, that is $\delta^{15}N_{substrate} - \delta^{15}N_{product}$ (Table 11.1). For certain processes (ammonification and NH_3 volatilization), a narrow range of fractionation factors has been reported. In contrast, observed discrimination varies widely for processes such as denitrification and nitrification, (Table 11.1). The variation in observed discrimination occurs, in part, as a function of which organism transforms the N and of the availability and $\delta^{15}N$ of the substrate and, in part, because it can be difficult to distinguish in the field whether a single reaction or a sequence of reactions has occurred (Evans 2007).

The combined effects of N isotope discrimination associated with these processes over time lead to variations in the isotopic signatures of ecosystem N pools. For example, foliar $\delta^{15}N$ is typically depleted relative to soil ^{15}N because N available for plant uptake has lower ^{15}N:^{14}N ratios than the source soil organic matter pools due to isotopic discrimination during mineralization and nitrification (Nadelhoffer and Fry 1994; Högberg 1997; Pardo et al. 2007). Soil $\delta^{15}N$ often

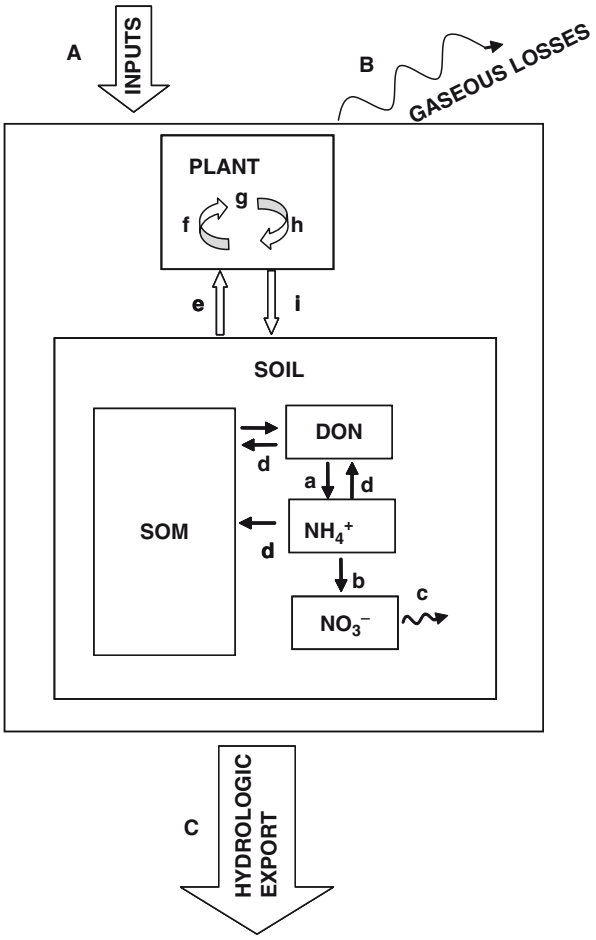

Fig. 11.1 Schematic of the nitrogen cycle. Letters identifying external and internal fluxes and ecosystem pools correspond to Table 11.1. Inputs (A) include atmospheric deposition (A1) and N fixation (A2). Outputs (B and C) include gaseous losses (B) via NH_3 volatilization (B1) and loss of denitrification products, NO, N_2O, N_2 (B2) and hydrologic leaching (C) which is composed of NO_3^- leaching (C1) and DON leaching (C2). Internal fluxes in soil include ammonification (a), nitrification (b), denitrification (c), immobilization (d) of inorganic N (d1) and organic N (d2). Internal fluxes involving plants include uptake (e) which can occur by plants associated with N fixers (e5), ericoid mycorrhizal fungi (e2), arbuscular mycorrhizal fungi (e3), ectomycorrhizal fungi (e4) and non-mycorrhizal plants (e1); within-plant transport (f); assimilation (g); retranslocation (h); and litterfall (i), above and belowground. Pools include plants, soil, and soil solution. The magnitude of the various pools and fluxes varies considerably across ecosystems

increases with depth such that surface organic horizons are depleted in ^{15}N relative to underlying mineral soil (Mariotti et al. 1980; Nadelhoffer and Fry 1988; Pardo et al. 2002; Evans 2007). Ecosystem pool $\delta^{15}N$ values are integrative measures of N pool dynamics, as they are influenced by the transformations and fractionations

Table 11.1 Observed discrimination ($\delta^{15}N_{substrate} - \delta^{15}N_{product}$) for N transformations and their effects on soil and plant $\delta^{15}N$

External fluxes			Discrimination (‰)	Reference	Effect on soil $\delta^{15}N$	Effect on plant $\delta^{15}N$
A	1	Deposition	n/a	–	Deposition can affect soil directly when the deposition is isotopically distinct and represents a significant annual input; changes in $\delta^{15}N$ would typically be most marked in surface soils or shallow soils	Deposition can affect plant tissue measurably when the deposition is isotopically distinct and represents a significant portion of plant N uptake
A	2	N fixation	0–2	Shearer and Kohl (1986)	Should cause soil $\delta^{15}N$ to move toward 0	Should cause plant $\delta^{15}N$ to move toward 0
B	1	NH_3 volatilization	38–40	Kreitler (1975), Mizutani et al. (1985), Högberg (1997)	Direct effect is to enrich soil; deposition of ^{15}N-depleted NH_4^+ (produced from volatilized NH_3) may lower surface soils $\delta^{15}N$	NH_3 with low $\delta^{15}N$ can lead to deposition of NH_4^+ with low $\delta^{15}N$, which causes plant $\delta^{15}N$ to be lower
B	2	Gaseous loss of denitrification products (NO, N_2O, N_2)	n/a	–	Losses of ^{15}N-depleted compounds should enrich soil solution and particulate N in ^{15}N	Losses of ^{15}N-depleted compounds should enrich the soil solution pool and lead to enrichment of the plant ^{15}N pool
C	1	NO_3^- leaching	n/a	–	Losses of ^{15}N-depleted NO_3^- should enrich soil solution and particulate N in ^{15}N	Losses of ^{15}N-depleted compounds should enrich the soil solution pool and lead to enrichment of the plant ^{15}N pool
C	2	DON leaching	n/a	–	If DON has the same $\delta^{15}N$ as soil, loss of DON will not alter the soil $\delta^{15}N$. If DON is enriched relative to soil, DON loss would lower soil $\delta^{15}N$; if DON were depleted relative to soil, DON loss would enrich soil $\delta^{15}N$	DON loss can affect plants directly if they utilize DON for nutrition either if the remaining DON has a different $\delta^{15}N$ or if plants switch to a different N source with a different $\delta^{15}N$. Loss of DON may also affect plants indirectly by altering soil $\delta^{15}N$ and hence the future $\delta^{15}N$ of soil solution (see entry to left)

–					
Internal fluxes					
Soils					
a	Ammonification	~0 to <5	Högberg (1997)	May enrich SOM N	Excluding further transformations of NH_4^+ (which could alter the NH_4^+ $\delta^{15}N$), ammonification should not alter plant $\delta^{15}N$ regardless of whether the plants take up NH_4^+, NO_3^-, or DON
b	Nitrification	5–112[a]	Delwiche and Steyn (1970), Yoshida et al. (1984), Yoshida (1988), Wada and Ueda (1996), Barford et al. (1999), Perez et al. (2006)	No direct effect on soil; should enrich NH_4^+ pool (if the NH_4^+ pool is not wholly consumed) which could lead to enrichment of soil N	If nitrification is high and ^{15}N –depleted N is lost from the system (NO_3^- leaching or denitrification), ammonium should become enriched and plants that take up ammonium should become enriched. If nitrate is not exported from the system, there will be no net enrichment of the system, but plants that take up more NH_4^+ than NO_3^- may become enriched under circumstances when a significant portion of the NH_4^+ pool is consumed and N uptake of NH_4^+ follows the nitrification. Under other circumstances, plant $\delta^{15}N$ should not be altered by nitrification. Plants that take up nitrate should be depleted relative to plants that take up NH_4^+

(continued)

Table 11.1 (continued)

External fluxes		Discrimination (‰)	Reference	Effect on soil $\delta^{15}N$	Effect on plant $\delta^{15}N$
c	Denitrification	11–75[a]	Olleros (1983), Yoshida (1988), Böttcher et al. (1990), Wada and Ueda (1996), Barford et al. (1999), Ueda et al. (1999); Perez et al. (2006), Sutka et al. (2008)	Effect on soil is indirect enrichment; should enrich NO_3^- pool (if the NO_3^- pool is not wholly consumed) which could lead to enrichment of soil N	Denitrification should lead to higher plant $\delta^{15}N$ if the plants take up nitrate and a significant portion of the nitrate pool is consumed by the denitrification
d	Immobilization	0	–	none or it may depend on the $\delta^{15}N$ of what was immobilized	n/a
Plant					
e 1	Uptake, non-mycorrhizal	0	Högberg (1997)	n/a	Assumed not to fractionate, therefore uptake of a constant N source should lead to a constant and similar $\delta^{15}N$ in the plant compared to the source. If the source $\delta^{15}N$ changes or if the plant switches to a different N source, the plant $\delta^{15}N$ should change accordingly
e 2	Ericoid mycorrhizal	Higher	Michelsen et al. (1998)	n/a	Highly depleting
e 3	AM mycorrhizal	Low	Michelsen et al. (1998)	n/a	Slightly depleting
e 4	Ectomycorrhizal	High	Hobbie and Hobbie (2006)	n/a	Moderately depleting

f	Within-plant transport	0–2		No direct effect	No effect on total plant $\delta^{15}N$; if ^{15}N-depleted N is transported, the tissue from which the N moved may become enriched, the tissue to which the N moved may become depleted. Note that in plants, roots may be enriched or depleted relative to shoots
g	Assimilation	~0	Hübner (1986), Högberg (1997)	No direct effect	Unknown, assumed to be negligible
h	Retranslocation	0–2		No direct effect	No effect on total plant $\delta^{15}N$; if ^{15}N-depleted N is translocated, the tissue from which the N moved may become enriched, the tissue to which the N moved may or may not become depleted
i	Litterfall, above and belowground			If litter is depleted relative to soil, as it often is, litterfall will decrease surface soil $\delta^{15}N$	If litter is slightly enriched relative to green tissue because ^{15}N-depleted N was retranslocated away, litterfall may cause a net depletion of the plant. If litterfall has a $\delta^{15}N$ not distinguishable from that of the plant, there will be no net effect on plant $\delta^{15}N$

[a] Fractionation varies widely for nitrification and denitrification. These values include the observed discrimination on the production of N_2O, NO, and N_2 during denitrification (including fungal denitrification) and nitrification (Perez et al. 2006; Sutka et al. 2008).

associated with all fluxes into and out of the pool. When N pool gains or losses are dominated by a single process, for example nitrification or denitrification, the system is constrained enough that it is possible to discern the record of the flux in the residual plant or soil N pool (e.g., Houlton et al. 2007). Under more complex conditions, it may be difficult to resolve the processes leading to patterns of $\delta^{15}N$ in ecosystem N pools.

Mass balance calculations (Amundson et al. 2003; Houlton et al. 2006) show that the mass-weighted $\delta^{15}N$ value of an entire ecosystem, or of a large ecosystem pool such as total plant or soil profile N, is solely a function of $\delta^{15}N$ values of the inputs and outputs of the system. However, this offers less guidance than it might appear to for mapping plant or soil $\delta^{15}N$ at large scales. First, because the plant and soil $\delta^{15}N$ comprise many separate pools with distinct isotopic signatures, determining the integrated $\delta^{15}N$ of the ecosystem is neither trivial nor necessarily valuable; in a well-mixed system, such as a stream, for example, this measurement and, therefore, the mass balance would be useful. Furthermore, what determines the $\delta^{15}N$ of exports from the system is complex: it is a function of the N transformations, their associated fractionations, the size of pools and fluxes of all the pools and fluxes through which the N exiting the system passes. Thus, the mathematically simple mass balance may generate an unsolvable equation. On the other hand, maps of N isotope measurements of particular ecosystem components (e.g. foliage, N deposition, or drainage water), if interpreted appropriately, could be used to evaluate patterns of N cycling, sources of N inputs, magnitudes of N losses, processes responsible for N export, and various perturbations of ecosystems.

11.3 Uses of N Isotopes

Nitrogen isotopes in terrestrial ecosystems have typically been used in two ways: first, to identify the relative importance of N sources, and second, to record N cycling patterns. For example, ^{15}N (which comprises 0.3663 atom % of atmospheric N, with the remaining 99.6337 being ^{14}N) natural abundance measurements have been used to identify sources and magnitudes of sewage or fertilizer inputs to surface waters (Kohl et al. 1971; Heaton 1986; Costanzo et al. 2001). Much early ^{15}N natural abundance work was concerned with quantifying N inputs to terrestrial ecosystems through N fixation (Virginia et al. 1989; Shearer and Kohl 1989; Vitousek et al. 1989). More recent work has examined the ^{15}N of atmospheric N deposition (Koopmans et al. 1998; Bauer et al. 2000; Elliott et al. 2007) and related that to measurements in the terrestrial ecosystem (Koopmans et al. 1998; Bauer et al. 2000). Other work has used the dual isotope method, ^{15}N and ^{18}O in nitrate, to evaluate sources of streamwater nitrate—to determine whether it comes directly from deposition or is produced microbially via the oxidation of ammonium within the ecosystem (Durka et al. 1994; Kendall et al. 1996; Burns and Kendall 2002; Pardo et al. 2004).

^{15}N natural abundance measurements have also been used to assess influences of past patterns of N cycling, typically the dominance of a particular nitrogen transformation (or flux), or changes over time of a single or several fluxes. Nitrogen isotopes have been used to examine patterns in terrestrial ecosystem pools such as soils, foliage, and other plant tissues including roots and wood, which do not lend themselves easily to large scale analyses because of the difficulty in collecting representative samples. Some of the clearest patterns in plant or soil $\delta^{15}N$ have been observed in response to disturbance when a single N transformation (or several, for example nitrification and denitrification, which have the same enriching effect on N that remains in the system) dominates other fluxes. For example, Piccolo et al. (1996) suggested that the very high soil $\delta^{15}N$ of up to 23‰ below 1-m depth at a wet site in the Brazilian Amazon Basin along a forest-to-pasture chronosequence was caused by high levels of denitrification combined with nitrification and solution nitrate loss. Forest cutting at several sites has lead to $\delta^{15}N$ increases in upper organic horizons (Pardo et al. 2002; Sah and Ilvesniemi 2007) which were attributed to the increased nitrification induced by cutting and the subsequent loss of depleted nitrate (Pardo et al. 2002). Boeckx et al. (2005) proposed that the form of N loss (nitrate or dissolved organic N, DON) will influence both $\delta^{15}N$ and %N of soils. This model may be useful for relating N dynamics and $\delta^{15}N$ values in tropical and temperate ecosystems.

Plant tissues are often considered more responsive to disturbance than soils (Johanisson and Högberg 1994; Pardo et al. 2002), likely because plant pools are typically smaller than bulk soil pools, and because much of the N in foliage and fine roots is derived from small and rapidly cycling fractions of soil N. For example, following clear-cut induced nitrification and nitrate loss in New Hampshire, USA, foliar $\delta^{15}N$ increased by about 3‰, while soil organic horizons increased by only about 1‰ (Pardo et al. 2002). Fertilization-induced nitrate losses can also lead to significant increases in foliar $\delta^{15}N$, as reported for a long-term fertilization of a Scots pine stand in Sweden (Högberg and Johannisson 1993). Finally, foliar $\delta^{15}N$ has been used in forests to evaluate the extent of N saturation (Emmett et al. 1998b, Pardo et al. 2006b, 2007).

Another important application of ^{15}N natural abundance has been to discern differences in resources used by different species and life forms in N-limited boreal and tundra ecosystems (Chapin et al. 1993; Nadelhoffer et al. 1996; Näsholm et al. 1998; McKane et al. 2002).

11.4 Factors Causing Variation in ^{15}N Signatures in Terrestrial Ecosystems

The nitrogen cycle is complex, with many fluxes entering and exiting an ecosystem as well as numerous internal transformations of N occurring at various time scales. Measurements of stable N isotopes offer the possibility of integrating all of the past

N transformations into a single measure. Several factors, however, can complicate efforts to explain N cycling using ^{15}N natural abundances at the local and, thus, at larger scales. These include: (1) prior land-use, which may leave long-lasting (decades to centuries) legacies on soil and hence plant $\delta^{15}N$; (2) variability in $\delta^{15}N$ by species within a given site, which can mask patterns across sites; (3) mycorrhizal associations, which may fractionate strongly under certain conditions; and (4) effects of climate, especially precipitation regime, which may influence the value of and temporal variability in plant $\delta^{15}N$. In some cases, these factors lead to systematic variation which can reveal patterns across a broad scale, and in some cases, they lead to significant, but as yet unexplained variation which obscures larger-scale patterns. In order for mapping to be successful, within-site heterogeneity must be considerably smaller than between-site variation in the parameter to be mapped.

11.4.1 Land-Use History in the Short-Term and Long Term

One of the more challenging of these complicating factors is prior land use, because of the duration of the effects of disturbance. Human settlement and cultivation may affect N cycling and isotopic composition for decades or centuries. Studies in France demonstrated the effect of Roman settlements that had been reforested for centuries on soil N cycling, species richness, and soil $\delta^{15}N$; the latter was about 1.5‰ higher at the center of the settlement than elsewhere in the settlement (Dupouey et al. 2002; Dambrine et al. 2007). A study of a village site in Greenland last inhabited in the early to mid eighteenth century detected a strong signal with an enrichment of plants (from marine mammal debris) of 10–16‰; at a nearby Norse settlement dating from two to three centuries earlier, similar levels of plant enrichment were reported (Commisso and Nelson 2006). The effects of past cultivation and manure application also persist; soil $\delta^{15}N$ remained elevated by ~4‰ for more than 60 years in previously cultivated sites that had been reforested since at least 1936, compared to ancient forest (continuous forest cover since at least the early 1800s; Koerner et al. 1999). Shifts from pasture to forest in New England were also associated with changes in plant and soil $\delta^{15}N$ (Compton et al. 2007). Based on a chronosequence of pasture to forest conversions, plant $\delta^{15}N$ decreased after 60 years of reforestation, while soil $\delta^{15}N$ increased with time over 120 years (Compton et al. 2007), revealing a divergence of plant and soil $\delta^{15}N$ values. Wang et al. (2007) report similar declines in foliar $\delta^{15}N$ of herbaceous and woody plants; 5‰ over 85 years across a chronosequence of previously cultivated sites in Virginia and 4‰ across a successional gradient in Glacier Bay, Alaska (Hobbie et al. 1998). However, in the Virginia study (Wang et al. 2007), soil $\delta^{15}N$ decreased over time in parallel with plant $\delta^{15}N$.

Fire may also impact $\delta^{15}N$ values in soils and plants. Severe fire often causes foliar and surface soil $\delta^{15}N$ to increase rapidly because of the removal of ^{15}N-depleted organic matter and subsequent disturbance-induced high nitrification and nitrate loss (M. Mack, personal communication 2005; Stephan and Kavanaugh

2005; Smithwick et al. 2005). The legacy of fire may be quite variable, however. For example, at Cone Pond Watershed, NH, a severe forest fire several years after a hurricane (ca. 1820; Buso et al. 1984) appears to have depleted the soil N pool so that the nitrogen cycling rate (net nitrification) and foliar $\delta^{15}N$ are still detectably lower in burned compared to unburned areas of the watershed (Hornbeck and Lawrence 1996, Pardo et al. 2007).

While these patterns provide insight into the specific controls on N cycling, for example, a divergence of plant and soil $\delta^{15}N$ or differences in $\delta^{15}N$ for different size fractions within a horizon (Compton et al. 2007; Koerner et al. 1999), they also present a challenge in interpreting $\delta^{15}N$, especially at larger spatial scales. The importance of identifying prior land use and its legacy is paramount, however, and is often difficult. In some cases, other observations give information about prior land-use, such as the presence of charcoal or an Ap horizon (or plow layer) in the soil (Compton et al. 2007).

11.4.2 Species Composition

Although external disturbances and fluxes can have strong impacts on $\delta^{15}N$ values of ecosystem pools, differences in $\delta^{15}N$ among species and, therefore, species composition are also important. Individual species often have distinct isotopic signatures (Nadelhoffer et al. 1996; Michelsen et al. 1998; Miller and Bowman 2002; Pardo et al. 2006b). Differences between species in $\delta^{15}N$ may be caused by factors including the $\delta^{15}N$ and form of N taken up, the relative rates of N cycling and loss, the extent and type of mycorrhizal association, rooting depth, and N transformations and transport within plants. In some cases, a regional scale analysis may facilitate interpretation of the patterns observed. For example, Pardo et al. (2002) reported a strong species pattern over 10 years at a single site. Several other studies showed a similar pattern of foliar $\delta^{15}N$, with values for American beech being consistently 1–2‰ greater than sugar maple values. Finally, a regional analysis, from Ontario to Maine, confirmed this same pattern (Pardo et al. 2006a, b). Because of the scale of the analysis, it became clear that the controlling factors had to be fundamental, physiological properties of the two species and not characteristics of the sites. In contrast to these systematic differences in $\delta^{15}N$ among species, in some cases, $\delta^{15}N$ values of different plant species are similar within a plot, based on plot characteristics including N cycling rates (Pardo et al. 2007) or within a site, based on the $\delta^{15}N$ of the dominant available N source (Houlton et al. 2007). At a site in New Hampshire, $\delta^{15}N$ of all species in a plot increased in concert across plots moving from conifer dominated to hardwood dominated, suggesting that species composition – presumably via differences in N cycling patterns – can control the $\delta^{15}N$ of all species present at a site (Pardo et al. 2007). In a study in Hawai'i, Houlton et al. (2007) reported that plant $\delta^{15}N$ of several species tracked solution $\delta^{15}N$ for the dominant form of inorganic N available in soil solution across a NO_3^- to NH_4^+ transition affected by increasing precipitation. In an instance where it is known that

plants are all utilizing the same N source – and perhaps future research will allow better prediction of those circumstances – plotting plant $\delta^{15}N$ should create a $\delta^{15}N$ map of the dominant available N form. A more general approach to minimizing the variation due to species differences is to utilize a single species across broad geographic scales.

Future research should elucidate the controls on species $\delta^{15}N$ patterns, $\delta^{15}N$ values of plant available N forms (i.e. NH_4^+, NO_3^-, and DON), relationships between the $\delta^{15}N$ of plant available N and plant $\delta^{15}N$ values (i.e., whether/when there is fractionation on uptake and within-plant transport), and the relative importance of species composition versus site characteristics for controlling plant $\delta^{15}N$.

11.4.3 Ectomycorrhizal Fungi

The impact of ectomycorrhizal fungi on plant tissue $\delta^{15}N$ must be taken into account when interpreting plant N isotopes (Högberg et al. 1996; Högberg 1997; Hobbie et al. 1999; Evans 2001). For example, ectomycorrhizal fungi have been reported to be enriched 12‰ relative to their host plants (Hobbie and Hobbie 2006). Typically, plants with ectomycorrhizal (EM) associations have foliage which is depleted in ^{15}N compared to those with arbuscular mycorrhizal (AM) associations, which, in turn, are depleted relative to plants without ectomycorrhizal or arbuscular mycorrhizal associations (Michelsen et al. 1998; Schmidt and Stewart 2003); ericoid plants have been reported to have the lowest $\delta^{15}N$ values in a given ecosystem (Nadelhoffer et al. 1996; Michelsen et al. 1998). In some cases, however, no such pattern is reported, rather, the EM species, beech, has a higher foliar $\delta^{15}N$ than the AM species, sugar maple (Pardo et al. 2006a, b) Many studies evaluating the relationship between ectomycorrhizal colonization and $\delta^{15}N$ have been conducted in N-limited ecosystems. For N-rich systems, however, the patterns may be different. Therefore, the interpretation of $\delta^{15}N$ data of plants with ectomycorrhizal association may vary with ecosystem type and condition. Further research on the extent of N nutrition provided by mycorrhizal fungi across ecosystems varying in N availability is needed to address this.

A global survey of saprotrophic and EM fungi (Mayor et al. 2009) has confirmed a strong separation using ^{15}N and ^{13}C isotopes between the two groups. The fact that the separation is observed at the global scale confirms that individual groups may have characteristic signatures. While the saprotroph/ectomycorrhizal "divide" (Henn and Chapela 2001) does not lend itself to mapping – the differences in ^{13}C and ^{15}N occur within sites as well as between–these patterns may form the basis of a comparative measure that could be mapped. For example, the difference between EM fungi and host plant foliage or the difference between foliage of plants with different mycorrhizal associations could be a measure that would provide information about N cycling, N saturation, and proportional dependence of host plants on ectomycorrhizal fungi.

11.4.4 Climate/Precipitation

Differences in N cycling caused by differences in climate (temperature and precipitation regime) can be notable across climate gradients and between temperate and tropical ecosystems (e.g. LeBauer and Treseder 2008). Those systematic variations that lead to coherent spatial patterns are discussed below (Section 11.7). This section will focus on the variations that are difficult to control for when synthesizing data (or sometimes even in site selection) and, therefore, contribute more significantly to noise than to discernible pattern. Interpretation of patterns across precipitation regimes may be complicated by confounding factors including plant species differences, prior land use, the seasonality and year-to-year variation in precipitation, and indirect climatic factors such as the inhibition (or enhancement) of microbial activity. For example, the impact of grazing (Schulze et al. 1998, 1999; Austin and Sala 1999; Evans 2007) may obfuscate the primary drivers of $\delta^{15}N$ variations. Similarly, soil $\delta^{15}N$ values >20‰ reported at a site in Brazil were attributed to a precipitation regime (shorter dry season; Piccolo et al. 1996) that increased denitrification further over already elevated levels across the region (Piccolo et al. 1994). Aranibar et al. (2004) report that the pattern of decreasing plant and soil $\delta^{15}N$ with precipitation in the Kalahari sands was more marked during wet years, because the $\delta^{15}N$ at dry sites increased during wet years; they attribute this increase in $\delta^{15}N$ to increased microbial activity (relative to dry years) resulting from increased water availability. In general, higher levels of microbial activity, N fixation, and denitrification were reported at the wet end of the precipitation gradient (Schulze et al. 1998; Aranibar et al. 2004), which may further complicate interpretation of $\delta^{15}N$ patterns along precipitation gradients. Increasing understanding of the specific mechanisms driving $\delta^{15}N$ patterns should facilitate interpretation of $\delta^{15}N$ patterns across large gradients.

The factors which lead to spatial heterogeneity in soil N cycling patterns may lead to heterogeneity in soil and plant $\delta^{15}N$. It is essential in mapping $\delta^{15}N$ at larger scales to consider the uncertainty in measurements at all scales.

11.5 Scaling Up: Issues to Consider

Working at large scales presents a set of challenges associated with minimizing unexplained variations. This is especially important for regional or global studies, which are likely to be syntheses of data collected from many separate studies. Analytical quality control is critical to any large scale analysis, particularly when multiple data sets are compiled. One useful tool for facilitating comparisons of samples analyzed on different instruments is an internal calibration standard for use across different laboratories. Ideally, the material used for calibration standards would resemble the tissue analyzed (rather than being a standard salt, for example, which might combust more easily than the samples). Pardo et al. (2006b) report the mean of NIST 1515 apple leaves and use these means to normalize data analyzed

in different labs (e.g. sample $\delta^{15}N$ values from Lab 2 would be corrected by subtracting the difference in apple leaf mean $\delta^{15}N$ of Lab 2 – Lab 1). NIST apple leaves, however, are not certified for ^{15}N; it would be extremely valuable to have a widely available and affordable standard that could be used to facilitate large-scale comparisons.

Variances of datasets from different studies may differ due to differences in sampling methods and in analytical precision and accuracy. Although it may be desirable to combine differing datasets in the interest of broadening spatial coverage, doing so could obscure actual patterns in ^{15}N abundances. Attention should be paid, therefore, to the level of uncertainty of the measurements and the magnitude of difference between datasets. Appropriate analytical quality control will improve the success of large-scale comparisons. In particular, (1) standard reference materials must be used to correct for instrument drift and to cross-calibrate among different laboratories and instruments, (2) sample masses must be sufficient to allow for accurate ^{15}N determinations, and (3) subsets of samples should be run in triplicate to characterize analytical precision.

Representative sampling also provides challenges across scales; for regional scale analysis, sampling must be representative at the site scale, for global analysis at the regional scale. Depending on the research question, representative sampling could mean characterizing the arithmetic site mean on an annual scale, for example. Or, it could mean an area-weighted, seasonal mean by ecosystem type. Large-scale surveys may be based on a single grab sample, of foliage and soil, for example. Foliage may be a good representation of the ecosystem (depending on the variability of foliar $\delta^{15}N$ over space and time within a site), whereas soil samples used to assess N cycling may include such high spatial or temporal heterogeneity that they serve as only coarse estimates of a representative mean.

In surveys where it is not feasible to use a more intensive sampling scheme, it may be helpful to quantify the uncertainty introduced by the sampling method. When analyzing large datasets, it may be possible to choose the scale at which the data are aggregated – the plot scale, for example, or the site scale. This may depend, in part, on the scale of data available across the dataset, and it may depend, in part, on the scale of the explanatory variables; obviously, the $\delta^{15}N$ data must be aggregated at the same scale as the explanatory variable (i.e., using site scale nitrification measurements will not elucidate patterns in $\delta^{15}N$ at the plot scale). Further, the scale of aggregation must be appropriate for the question. The temporal scale of measurements must also be considered. In a large-scale regional assessment, foliar $\delta^{15}N$ was more strongly correlated to yearlong *in situ* measurements of nitrification than to one-time lab incubations (Pardo et al. 2006b), presumably because the latter were more variable in terms of time of year of sampling and specific climatic conditions (temperature and soil moisture) than the former. The timing of the measurements can also introduce errors; comparing $\delta^{15}N$ measurements collected in different years or relating $\delta^{15}N$ measurements collected in one year to other parameters measured in a different year may also reduce the ability to discern patterns.

One effective way of reducing the importance of sampling and analytical method for parameters which are measured using many variations on a method is to normalize

those measures in some way. For example, the use of percent nitrification (or %nitrification = (net nitrification/net N mineralization) × 100) facilitates comparisons between studies using different methods of homogenizing, incubating and extracting soil samples (e.g., Goodale and Aber 2001; Pardo et al. 2006b). The *enrichment factor* (ε), defined as $\varepsilon = \delta^{15}N_{foliar} - \delta^{15}N_{mineral\ soil}$, is a method of normalizing foliar $\delta^{15}N$ values for the spatial heterogeneity in mineral soil $\delta^{15}N$ values. The enrichment factor has been useful in identifying strong relationships with N deposition, litterfall N, and measures of soil N cycling in some studies (Garten 1993; Garten and Van Miegroet 1994; Emmett et al. 1998b); in other studies, no relationship was observed (Pardo et al. 2006b).

11.6 Regional Scale Plant and Soil ^{15}N Analyses

Regional-scale analyses can be useful for testing hypotheses about important drivers in ecosystems. Large-scale analysis can reveal overall trends, while highlighting ecosystems that depart from the general pattern. For example, in the NITREX study, which evaluated N cycling across an N deposition gradient in Europe, the enrichment factor was related to N inputs in throughfall as hypothesized, except at one site (Fig. 11.2; Emmett et al. 1998b). The prior land use at this site included plowing and had led to significantly increased N cycling rates compared to the other (non-plowed) sites, partially decoupling N inputs from internal N cycling. The relationship between the enrichment factor and litterfall N, which is a measure of internal N cycling, was found to be robust across all sites. In this case, the regional analysis identified a departure from the original hypothesis.

A larger scale analysis evaluating patterns in foliar $\delta^{15}N$ at sites in North America, South America and Europe (Pardo et al. 2006b) found that local measures of N cycling (%nitrification, soil C:N) were more strongly correlated with foliar $\delta^{15}N$ than the regional driver of N deposition (Fig. 11.3). This finding has implications for the development of isoscapes for ^{15}N of terrestrial plants; the most meaningful maps will be made at the scale of the factors that determine the plant $\delta^{15}N$. However, our present understanding of which factors are most important in determining plant ^{15}N may be insufficient to allow us to properly choose which species or sites to include when attempting to develop reliable and useful isoscapes. For example, the way in which the form of N uptake (NO_3^- v. NH_4^+) influences plant $\delta^{15}N$ may vary. Kahmen et al. (2008) observed an increase in $\delta^{15}N$ with increasing NO_3^-:NH_4^+ uptake ratio across 18 grassland sites in Germany, while two other studies report the opposite pattern (Miller and Bowman 2002; Falkengren-Grerup et al. 2004).

As a worst case, the spatial heterogeneity of site characteristics could lead to enough variation in plant ^{15}N that the utility of mapping plant ^{15}N at regional or global scales is compromised. Isotope maps are most meaningful when the parameter mapped is well-mixed and representative of a larger spatial area; neither of these is true for ^{15}N in plants. As soils change less rapidly than plants, they may be slightly less problematic. Nonetheless, in many regions, soil heterogeneity is high

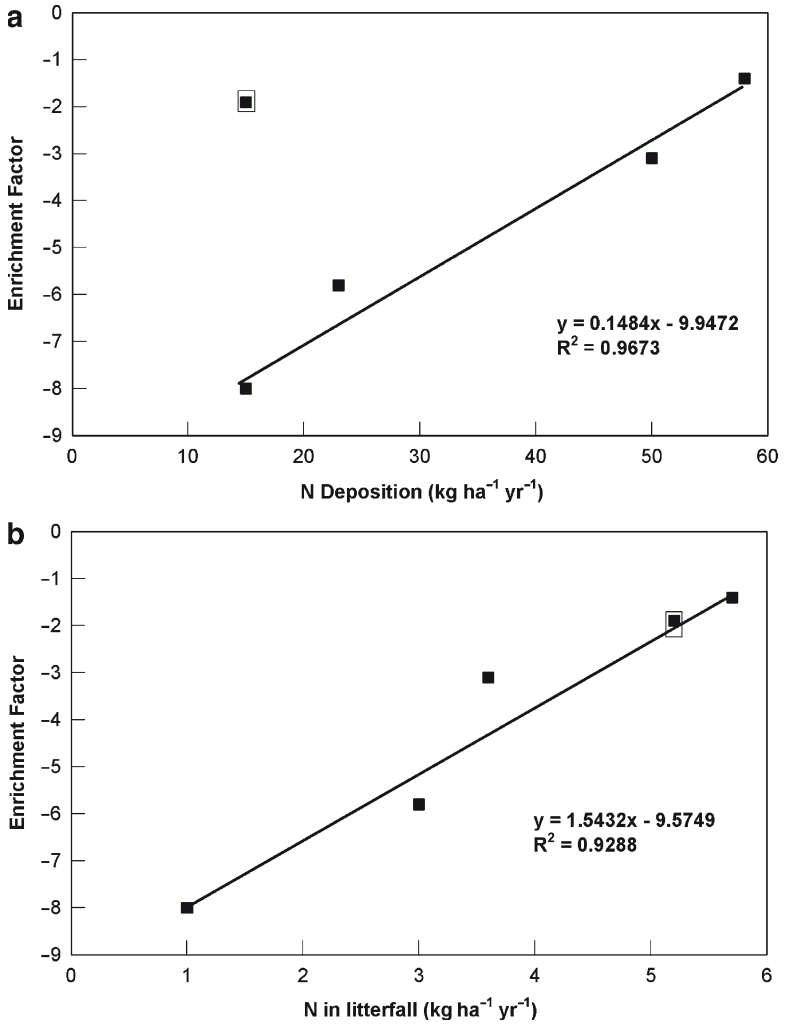

Fig. 11.2 The relationship between the enrichment factor and (**a**) annual nitrogen flux in throughfall and (**b**) litterfall N flux in the NITREX study. The anomalous site, Aber, is boxed (From Emmett et al. 1998b. Modified by permission of Elsevier)

even at small scales (Bell and Lechowicz 1994; Webster 2000). It is not known exactly how much the ^{15}N natural abundance varies with different soil types, but given the known differences in $\delta^{15}N$ between different horizons and the large variation in the thickness of different horizons, it is easy to imagine that the total soil profile $\delta^{15}N$ would vary spatially as well.

In order to make N isotope maps that reflect patterns of N cycling or responses of N processes to disturbance, further research linking plant and soil $\delta^{15}N$ with $\delta^{15}N$ of available N and with N transformations that vary in systematic ways across geographic and environmental gradients is necessary.

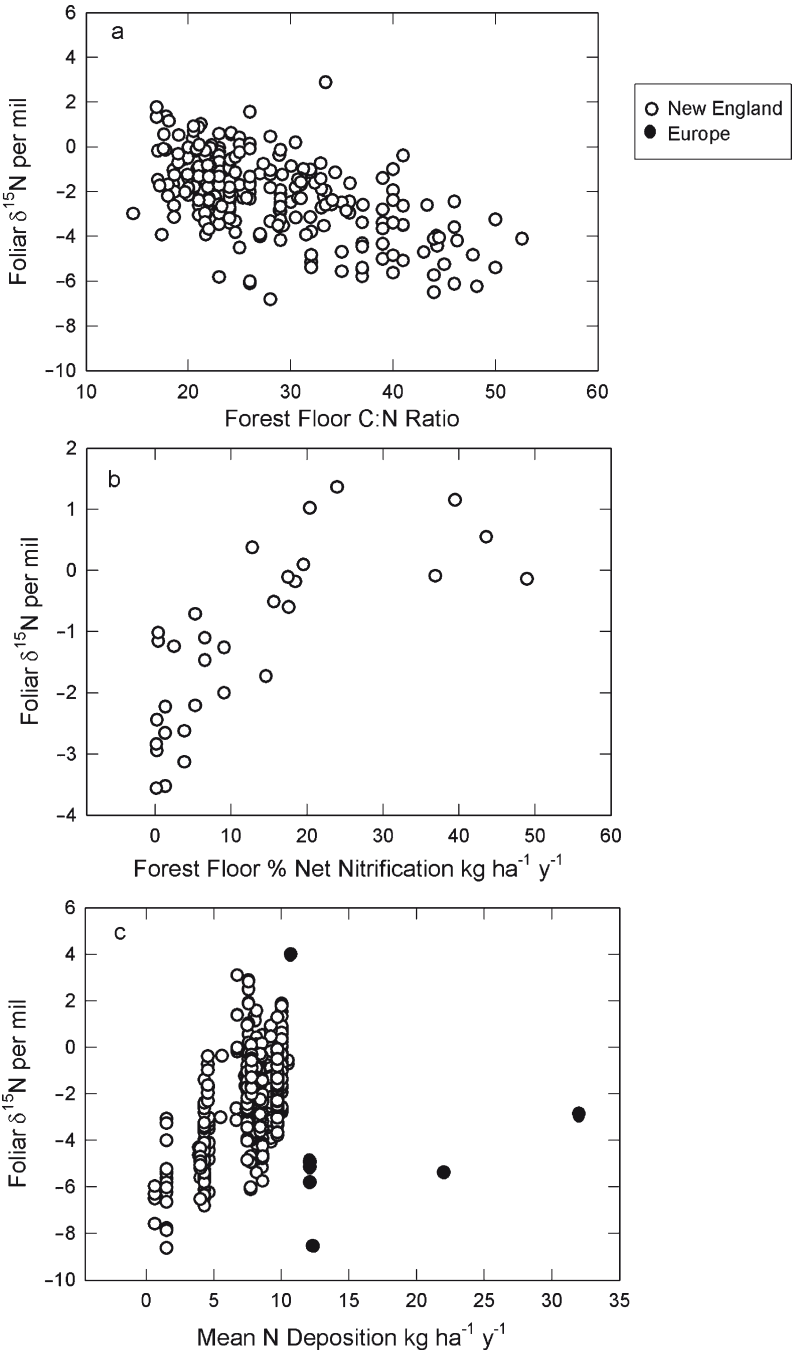

Fig. 11.3 Foliar $\delta^{15}N$ as a function of (**a**) forest floor C:N, (**b**) forest floor nitrification/mineralization for one-year buried bag incubations (kg ha^{-1} y^{-1}), and (**c**) N deposition. Sites in Europe are shown in filled symbols (After Pardo et al. 2006b)

11.7 Global Scale Plant and Soil ^{15}N Analyses

The previous decade has seen a number of global scale syntheses relating plant and soil ^{15}N values to broad climatic factors such as precipitation and temperature. Handley et al. (1999) found plant $\delta^{15}N$ to be negatively correlated to mean annual rainfall, although there was substantial variability associated with this pattern (Fig. 11.4). They attribute this relationship to differences along the dry to wet continuum, proposing that N losses relative to pool sizes are greater at drier sites and, because the N lost (via volatilization, denitrification, and leaching) is typically depleted in ^{15}N, this leads to ^{15}N-enrichment of soil and plants in the drier sites. In their analysis, the organic N cycle is more closed in cold, wet ecosystems than in hot, dry ecosystems, so there is less transfer of organic N to mineral pools which can subsequently be exported from the ecosystem. They note that this relationship may not hold at the landscape scale, where local wet spots can have higher foliar $\delta^{15}N$ than surrounding drier areas. This pattern is likely due to increased microbial activity (nitrification and/or denitrification) combined with increased solution and gaseous N losses in wetter spots. In a regional scale analysis, Pardo et al. (2006b) found a positive correlation between foliar $\delta^{15}N$ and mean annual precipitation (MAP), in contrast to the negative relationship reported at the global scale by Handley et al. (1999). Presumably the smaller range of MAP observed in the northeastern U.S. (1,000–1,700 mm; Pardo et al. 2006b) did not allow the opposite pattern (decreasing $\delta^{15}N$ with precipitation) to emerge as it did across a range of

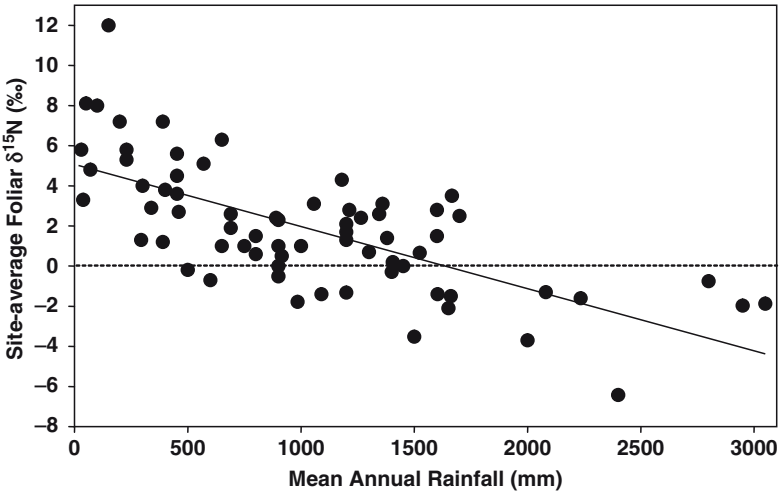

Fig. 11.4 Foliar $\delta^{15}N$ as a function of rainfall at 97 sites across a rainfall gradient. Data include only leaves or shoots of natural vegetation in ecosystems where soil is the major N source (After Handley et al. 1999. Copyright CSIRO 1999. Reproduced with permission from the "Aust J Plant Physiol" 26(2): 185–199. Published by CSIRO PUBLISHING, Melbourne Australia – http://www.publish.csiro.au/nid/103/issue/182.htm)

precipitation from 20–3,000 mm (Handley et al. 1999). These results suggest that the spatial scale of analysis has an impact on which patterns are discernible based on which drivers dominate at the study scale.

A complicating factor in using plant $\delta^{15}N$ across large regions is that there can be considerable variation in plant $\delta^{15}N$ within a site, based on different nutritional strategies of different species. In instances where plants use the same N source (e.g. Houlton et al. 2007), regional assessments will be more successful. For this reason, studies along a precipitation, age, and N and P availability gradient in Hawai'i (Austin and Vitousek 1998; Schuur and Matson 2001) provide a useful tool in understanding the effects of precipitation. They observed a strong pattern of declining plant and soil $\delta^{15}N$ with precipitation at sites dominated by the same species (*Metrosideros poymorpha*) across the deposition gradient. Attempts to extrapolate such patterns to larger regions and across varying ecosystems may reveal discernible patterns if the ecosystems are selected to have certain commonalities. In a broad synthesis, however, it can be more difficult to observe and interpret patterns, because of variations across life forms, ecosystem types, and other factors (e.g., Craine, et al. 2009). Further data compilations (including diverse ecosystems, geographic regions, and plant species) would help refine understanding of the robustness of broad-scale $\delta^{15}N$ patterns with precipitation. These comparisons are most likely to be useful if $\delta^{15}N$ data are accompanied by other measurements and if these measures are made in ways that allow for direct comparisons.

A comparison of tropical and temperate forest foliar $\delta^{15}N$ also focuses on the relative "openness" of the ecosystems. Martinelli et al. (1999) interpret the higher foliar $\delta^{15}N$ values they observed in tropical forests as evidence that these ecosystems are more open, that they have proportionately higher losses (and inputs) relative to internal N cycling in comparison to temperate forests. As with any large-scale isotope synthesis study, the selection of the study sites included in the analysis was based on where data from previous studies were available, rather than on a systematic selection of either a range of representative ecosystems or a subset of relatively similar ecosystems of temperate and tropical forests. Thus, the data included may not represent the range of values (excluding "extreme" ecosystems) that typify tropical and temperate forests. For example, the range of foliar $\delta^{15}N$ values observed in temperate forests in the northeastern U.S. extends above an upper value +3‰ (Pardo et al. 2006b), higher than any temperate values reported by Martinelli et al. (1999). Nonetheless, the fact that, for these particular sites, the foliar %N values were similar, while the tropical foliar $\delta^{15}N$ values were significantly higher than temperate, confirms that $\delta^{15}N$ is a useful tool and more refined at evaluating N cycling dynamics than %N alone.

In compiling plant and soil $\delta^{15}N$ data from the two previous global studies (Handley et al. 1999; Martinelli et al. 1999) in addition to new data, Amundson et al. (2003) found $\delta^{15}N$ in plant and soils to decrease with MAP and increase with mean annual temperature (MAT). They created the only global ^{15}N isotope map currently available for soil $\delta^{15}N$ and enrichment factor (Fig. 11.5). This map provides a baseline for assessing global patterns of soil $\delta^{15}N$ and enrichment factor. However, it also illustrates some challenges of mapping $\delta^{15}N$ at large scales.

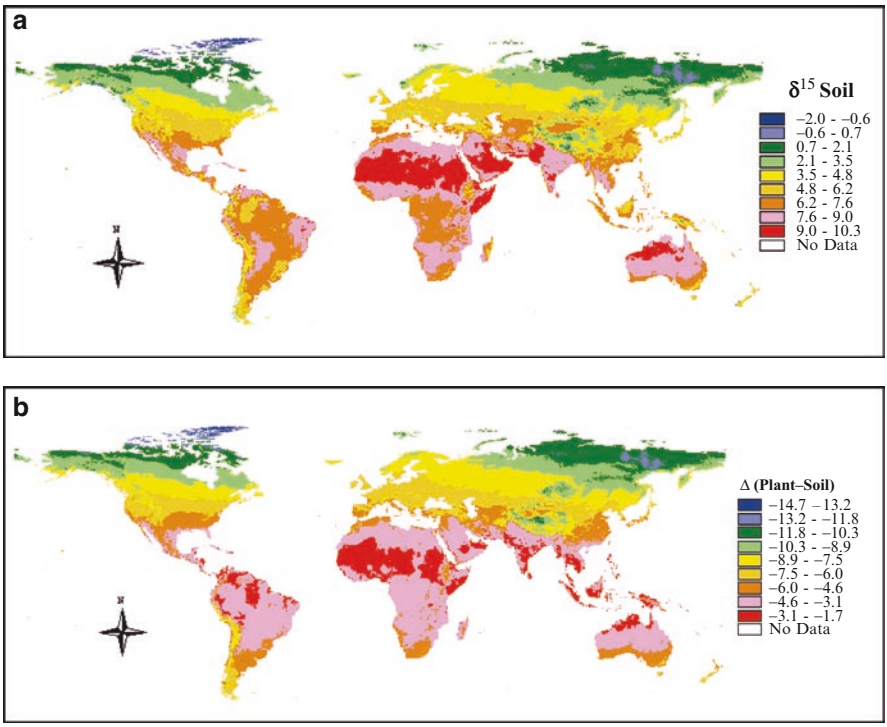

Fig. 11.5 (**a**) Estimated geographical distribution of soil $\delta^{15}N$ values to 50 cm and (**b**) estimated geographical trends in $\Delta\delta^{15}N_{plant\text{-}soil}$ (From Amundson et al. 2003. Copyright (2003) American Geophysical Union. Reproduced by permission of American Geophysical Union). Fig. 11.5, see Appendix 1, Color Section

The regression used to relate soil $\delta^{15}N$ to MAT and MAP explained considerably less than half of the variance (the highest $r^2 = 0.39$, $p < 0.1$, for soil $\delta^{15}N$ to 50 cm depth). Moreover, some biomes (e.g. arctic tundra, boreal forest) for which $\delta^{15}N$ values are predicted were not included in model development (or were represented by very few data points). As such, considerable uncertainty in model projections exists. They also present data indicating that factors such as soil parent material, topography, soil age, and cultivation may drive as much variation in $\delta^{15}N$ as predicted by the model used to generate their map (see Fig. 3 in Amundson et al. 2003).

Therefore, while the Amundson et al. (2003) map is a useful starting point for global analyses, the geographic gaps in data used for model development, the weak predictions (as indicated by low r^2 values of underlying regressions), and local drivers of plant and soil $\delta^{15}N$ values, which may obfuscate or override effects of MAT and MAP, limit its usefulness as a predictive tool. This is evident, for example, for the northeastern U.S., where soil and foliar $\delta^{15}N$ data are abundant (Pardo et al. 2006b); mineral soil $\delta^{15}N$ has been reported to be >7‰ (Nadelhoffer et al. 1995, 1999; Pardo et al. 2002, 2007) compared to the 3.5–4.8‰ mapped (Amundson et al. 2003). Similarly, a much broader range of enrichment factor values (−11 to 1‰)

has been reported for the northeastern U.S. (Pardo et al. 2006b, 2007, unpublished data) than the range (−8.9 to −7.5‰) mapped (Amundson et al. 2003). The global soil $\delta^{15}N$ map is useful for demonstrating broad general trends, such as higher $\delta^{15}N$ values in tropical than temperate soils. However, many of the questions about N cycling in forest ecosystems focus on refining understanding of the controls on N retention and loss, and thus must often be addressed at fairly small scales, as the controls on plant/soil/microbial interactions often vary at small spatial and temporal scales. A more detailed global ^{15}N map that includes many species and ecosystem types may, therefore, be useful for identifying gross trends, gaps in the data, or identifying regional and local factors driving differences in ^{15}N abundances. To address more mechanistic questions (e.g., about N cycling dynamics and the relative importance of different drivers of N cycling), it might be necessary to limit such comparisons to single or small ranges of species and ecosystems types with known land use histories. Attempts to relate plant or even soil $\delta^{15}N$ to regulating mechanisms at fine resolutions in large scale ^{15}N isotope maps are challenging, because of the local and regional variations discussed above (e.g., soil heterogeneity on the local scale, and variation in N deposition across regions). An N isotope map of a single species with a well-known nutritional strategy might be used to identify changes in form of available N, in other measures of internal N cycling, or to indicate prior disturbance, for example.

11.8 Mapping Precipitation $\delta^{15}N$

In contrast to the potentially large variability observed in plant and soil $\delta^{15}N$, precipitation $\delta^{15}N$ values appear to vary less over space and may have characteristic source-based signatures (Koopmans et al. 1998; Pearson et al. 2000). In some cases, precipitation $\delta^{15}N$ may influence foliar $\delta^{15}N$ (Koopmans et al. 1998). A pattern of increasing foliar $\delta^{15}N$ with increasing N deposition followed different trajectories comparing sites in Europe and North America (Fig. 11.3c; Pardo et al. 2006b). The European sites were strongly influenced by highly depleted ^{15}N in NH_4^+ from NH_3 volatilized from liquid manure at high N deposition sites (Koopmans et al. 1998; Bauer et al. 2000), resulting in lower absolute values of foliar $\delta^{15}N$ at a given deposition rate. This result demonstrates the usefulness of a large-scale analysis for identifying dominant factors controlling plant ^{15}N in different systems. However, it also shows that caution must be used when comparing sites in regions affected by different deposition sources.

Precipitation, itself, may be most amenable to ^{15}N isotope maps. Values of $\delta^{15}N$ in precipitation nitrate have distinct spatial and temporal patterns (Elliott et al. 2007). In the northeastern U.S., a pattern of increasing $\delta^{15}N$ with increasing NO_x emissions trending southwest was reported; higher winter time $\delta^{15}N$ in precipitation nitrate was also reported (Fig. 11.6; Elliott et al. 2007). The authors attribute the higher $\delta^{15}N$ values to increased power plant contributions (closer proximity power plants, increased power use in winter), however, they were not able to test their

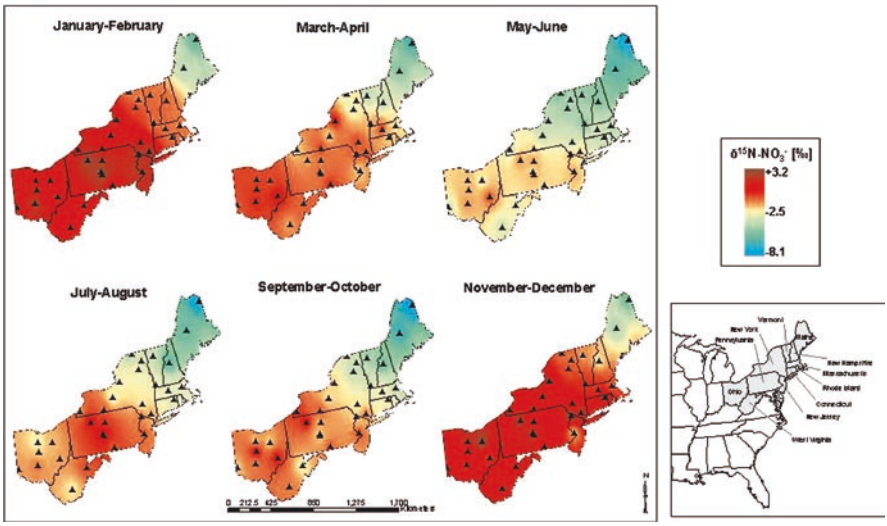

Fig. 11.6 Bimonthly, volume-weighted $\delta^{15}N$ values of precipitation NO_3^- at 30 sites in the northeastern U.S. (From Elliott et al. 2007). Fig. 11.6, see Appendix 1, Color Section

hypothesis, as their study did not include measurements of source $\delta^{15}N$. It would be most effective to evaluate the $\delta^{15}N$ of different sources of nitrate either by measuring the sources directly or sampling precipitation by events in order to capture storms dominated by power plant derived versus vehicular nitrate sources. One good test of this could be conducted in Los Angeles, where N inputs are high (Michalski et al. 2004), but come primarily from vehicles. Low nitrate $\delta^{15}N$ values in LA precipitation would be consistent with the hypothesis that power plant NO_x causes higher $\delta^{15}N$ in NO_3^-. High nitrate $\delta^{15}N$ values, on the other hand, would suggest that other factors, perhaps transformations that occur in the atmosphere (Dentener and Crutzen 1993, Johnston et al. 1995; Krankowsky et al. 1995), contribute to the $\delta^{15}N$ signature of nitrate in deposition.

Translating the systematic variation in precipitation nitrate $\delta^{15}N$ to measurements of plants in terrestrial systems remains difficult in the U.S. for several reasons. First, atmospheric inputs via NH_4^+ and forms other than bulk nitrate are not insignificant, especially at certain sites, and there is little information about $\delta^{15}N$ of NH_4^+ inputs. A number of studies (Heaton et al. 1997; Pearson et al. 2000) have reported lower $\delta^{15}N$ for NH_4^+ than for NO_3^-. If this is the case in the northeastern U.S., it could dampen the trend of increasing $\delta^{15}N$ with increasing N deposition. Second, studies have shown that most nitrate deposited on forest ecosystems in the Northeast and in the Rockies is processed microbially before it reaches streams (Kendall et al. 1996; Burns and Kendall 2002; Pardo et al. 2004; Hales et al. 2007), which may suggest that little nitrate deposition would be taken up by plant roots without first being transformed by microbes. Finally, the magnitude of the microbially produced nitrate relative to N deposition at many sites in the U.S., for example

in the Northeast, is such that microbially produced nitrate is likely to be at least an order of magnitude more abundant than nitrate deposition inputs. At the European sites impacted by ^{15}N-depleted NH_4^+ deposition, deposition rates were >50 N ha^{-1} $year^{-1}$ (Emmett et al. 1998a; Koopmans et al. 1998; Pardo et al. 2006b), so the ratio of deposition to microbially produced nitrate would have been significantly higher. Nonetheless, the intriguing correlation between $\delta^{15}N$ in foliage and in precipitation NO_3^- needs to be explored and further explained.

An important next step in mapping precipitation $\delta^{15}N$ would be to characterize the isotopic signature of NH_4^+. A second step would be to characterize the isotopic signature of deposition inputs from different sources (power plants, vehicle tailpipes, agriculture). A site with elevated deposition with a characteristic N source (only power plants or only vehicles) and the potential for canopy uptake would be ideal to test the potential to measure deposition signal in foliage – an example of such a site might be the San Bernardino Mountains in southern California, where deposition of N exceeds 70 kg ha^{-1} $year^{-1}$ (Fenn et al. 2003). Another tool that could be used to map deposition $\delta^{15}N$ would be to measure the $\delta^{15}N$ of organisms other than vascular plants, such as bryophytes or non-N fixing lichens.

In contrast to vascular plants, bryophytes and non-N fixing lichens use precipitation as their sole N source and thus can be used as an integrated indicator of $\delta^{15}N$ of total precipitation N. This approach has been used to map %N and $\delta^{15}N$ using data from 220 sites in Austria (Zechmeister et al. 2008). Although it is not simple to extract total N deposition patterns from the moss $\delta^{15}N$ values, further studies, including more extensive information on $\delta^{15}N$ of different sources of N, would be useful. Mosses have also been used to distinguish depleted $\delta^{15}N$ deposition values originating in sewage NH_x–N in an urban area from more enriched values at less polluted sites in southwestern China (Liu et al. 2008)

11.9 Future Research Directions

In addition to the issues of scale, site characteristics and spatial heterogeneity, fundamental questions remain regarding how various processes and factors are expressed in plant N isotope signatures. One of the outcomes of analyzing data at the global scale is to identify limitations in our understanding of ^{15}N dynamics. Reciprocally, working at the global scale may force these questions to be addressed. For example, it is often assumed that plants do not fractionate on uptake and therefore that the plant $\delta^{15}N$ is a reflection of the $\delta^{15}N$ of plant-available N. Studies have clearly demonstrated, however, that fractionation on uptake occurs under some conditions (Yoneyama et al. 2001; Kolb and Evans 2003) and that fractionation during plant transport may be a function of water availability (Handley et al. 1999). The goal, then, of this area of research must be to identify the conditions under which fractionation on uptake and within-plant transport will occur. Another assumption is that inorganic N $\delta^{15}N$ increases with depth in soil with particulate organic $\delta^{15}N$. There are few data to confirm or refute this pattern; Koba et al. (1998)

report an increase in inorganic N $\delta^{15}N$ with depth in a forest soil, while Ledgard et al. (1984) report no increase in inorganic N $\delta^{15}N$ with increasing soil depth and $\delta^{15}N$ under pasture. In some ecosystems, dissolved organic N is available and may play a significant role in plant nutrition, which adds another complicating factor that can affect plant $\delta^{15}N$. Refining understanding of when and how mycorrhizal fungi affect plant $\delta^{15}N$, especially in N-rich ecosystems, and identifying the factors that control species differences are critical for making large scale comparisons.

Dual isotopic techniques should also be further developed. ^{15}N and ^{18}O in NO_3^- in solution may be useful in identifying sources and pathways of nitrate in an ecosystem, while ^{15}N and ^{13}C in plants have the potential to link information about nutrient dynamics to water status (Farquhar et al. 1989).

11.10 Summary

One of the challenges in large scale analysis is the selection of representative data – poorly selected data may mask extant patterns or may falsely suggest that patterns exist. One of the advantages in developing large-scale isotope maps is that, once they are sufficiently populated with reliable data, patterns may become evident and the range of variability well characterized. The critical need in ^{15}N isotope mapping is to better link mechanistic controls of N transformations and associated fractionation with plant and soil $\delta^{15}N$ values. Because of the complexity of the N cycle, dynamic modeling is a necessary next step for identifying the dominant controlling fluxes and factors. Once it is possible to evaluate the potential drivers quantitatively, it will be feasible to better assess and interpret large-scale data sets. One potentially powerful tool is the use of remote sensing to estimate foliar $\delta^{15}N$ (Wang et al. this volume). The development of such a tool would, in itself, represent a significant advance in understanding ^{15}N patterns and the relationships of these patterns to N cycling across scales of space and time. Development of robust, empirically grounded models would require more and better data on: (1) $\delta^{15}N$ values in plant-available NH_4^+, NO_3^-, and DON; (2) relationships between $\delta^{15}N$ in NH_4^+ and NO_3^- and nitrification rate, as measured in the field; and (3) relationships between soil available $\delta^{15}N$ and plant $\delta^{15}N$.

References

Amundson R, Austin AT, Schuur AG et al (2003) Global patterns of the isotopic composition of soil and plant nitrogen. Global Biogeochem Cycles 17:1031

Aranibar JN, Otter L, Macko SA et al (2004) Nitrogen cycling in the plant-soil system along a precipitation gradient in the Kalahari sands. Global Change Biol 10:359–373

Austin AT, Sala OE (1999) Foliar $\delta^{15}N$ is negatively correlated with rainfall along the IGBP transect in Australia. Aust J Plant Physiol 26:293–295

Austin AT, Vitousek PM (1998) Nutrient dynamics on a precipitation gradient in Hawai'i. Oecologia 113:519–529

Barford CC, Montoya JP, Altabet MA et al (1999) Steady-state nitrogen isotope effects of N_2 and N_2O production in *Paracoccus denitrificans*. Appl Environ Microbiol 65:989–994

Bauer GA, Gebauer G, Harrison AF et al (2000) Biotic and abiotic controls over ecosystem cycling of stable natural nitrogen, carbon and sulphur isotopes. In: Schulze E-D (ed) Carbon and nitrogen cycling in European Forest ecosystems. Springer, Berlin, pp 189–214

Bell G, Lechowicz MJ (1994) Spatial heterogeneity at small scales and how plants respond to it. In: Caldwell MM and Pearcy RW (eds) Exploitation of environmental heterogeneity by plants: ecophysiological processes above- and belowground. Academic, San Diego, CA, pp 391–414

Böttcher J, Strebel O, Voerkelius S et al (1990) Using isotope fractionation of nitrate nitrogen and nitrate oxygen for evaluation of microbial denitrification in a sandy aquifer. J Hydrol 114: 413–424

Boeckx P, Paulino L, Oyarzún C et al (2005) Soil $\delta^{15}N$ patterns in old-growth forests of southern Chile as integrator for N-cycling. Isotopes Environ Health Stud 41(3):249–259

Burns DA, Kendall C (2002) Analysis of sources of ^{15}N and ^{18}O to differentiate NO_3^- sources in runoff at two watersheds in the Catskill Mountains of New York. Water Resour Res 38:1051–1062

Buso DC, Martin CW, Hornbeck JW (1984) Potential for acidification of six remote ponds in the White Mountains of New Hampshire. Water Resources Research Center, Durham, New Hampshire, Research Report No 62

Chapin FS III, Moilanen L, Kielland K (1993) Preferential use of organic nitrogen for growth by a non-mycorrhizal arctic sedge. Nature 361:150–153

Commisso RG, Nelson DE (2006) Modern plant $\delta^{15}N$ values reflect ancient human activity. J Archeol Sci 33:1167–1176

Compton JE, Hooker TD, Perakis SS (2007) Ecosystem N distribution and $\delta^{15}N$ during a century of forest regrowth after agricultural abandonment. Ecosystems 10:1197–1208

Costanzo SD, O'Donohue MJ, Dennison WC et al (2001) A new approach for detecting and mapping sewage impacts. Mar Pollut Bull 42:149–156

Craine JM, Elmore AJ, Aidar MPM (2009) Global patterns of foliar nitrogen isotopes and their relationships with climate, mycorrhizal fungi, foliar nutrient concentrations, and nitrogen availability. New Phytologist 183: 980–992. doi 10.1111/j.1469-8137.2009.02917.x

Dambrine E, Dupouey JL, Laut L (2007) Present forest biodiversity patterns in France related to former Roman agriculture. Ecology 88:1430–1439

Delwiche CC, Steyn PL (1970) Nitrogen isotope fractionation in soils and microbial reactions. Environ Sci Technol 4:929–935

Dentener FJ, Crutzen PJ (1993) Reaction of N_2O_5 on tropospheric aerosols: impact on the global distributions of NO_x, O_3, and OH. J Geophys Res 98(D4):7149–7163

Dupouey JL, Dambrine E, Laffite JD et al (2002) Irreversible impact of past land use on forest soils and biodiversity. Ecology 83:2978–2984

Durka W, Schulze ED, Gebauer G et al (1994) Effects of forest decline on uptake and leaching of deposited nitrate determined from ^{15}N and ^{18}O measurements. Nature 372:765–767

Elliott EM, Kendall C, Wankel SD (2007) Nitrogen isotopes as indicators of NO_x source contributions to atmospheric nitrate deposition across the midwestern and northeastern United States. Environ Sci Tech 41:7661–7667

Emmett BA, Boxman D, Bredemeier M et al (1998a) Predicting the effects of atmospheric nitrogen deposition in conifer stands: evidence from the NITREX ecosystem scale experiments. Ecosystems 1:352–360

Emmett BA, Kjønaas OJ, Gundersen P et al (1998b) Natural abundance of ^{15}N in forests across a nitrogen deposition gradient. For Ecol Manag 101:9–18

Evans D (2001) Physiological mechanisms influencing plant nitrogen isotope composition. Trends Plant Sci 6:121–127

Evans RD (2007) Soil nitrogen isotope composition. In: Lajtha K, Michener RH (eds) Stable isotopes in ecology and environmental science, 2nd edn. Blackwell, Oxford, pp 83–98

Falkengren-Grerup U, Michelsen A, Olsson MO et al (2004) Plant nitrate use in deciduous woodland: the relationship between leaf N, ^{15}N natural abundance of forbs and soil N mineralization Soil Biol Biochem 36:1885–1891

Farquhar GD, Hubick KT, Condon AG, et al. (1989) Carbon isotope discrimination and water-use efficiency. In: Rundel PW, Ehleringer JR, Nagy KA (eds) Stable isotopes in ecological research. Springer, Berlin/Heidelberg/New York, pp 21–46

Fenn ME, Haueber R, Tonnensen GS et al (2003) Nitrogen emission, deposition, and monitoring in the western United States. Bioscience 53:391–403

Garten CT Jr (1993) Variation in foliar ^{15}N abundance and the availability of soil nitrogen on the Walker Branch Watershed. Ecology 74:2098–2113

Garten CT Jr, Van Miegroet H (1994) Relationships between soil nitrogen dynamics and natural ^{15}N abundance in plant foliage from the Great Smoky Mountains National Park. Can J For Res 74:1636–1645

Goodale CL, Aber JD (2001) The long-term effects of land-use history on nitrogen cycling in northern hardwood forests. Ecol Appl 11:253–267

Hales HC, Ross DS, Lini A (2007) Isotopic signature of nitrate in two contrasting watersheds of Brush Brook, Vermont, USA. Biogeochemistry 84:51–66

Handley LL, Raven JA (1992) The use of natural abundance of nitrogen isotopes in plant physiology and ecology. Plant Cell Environ 15:965–85

Handley LL, Austin AT, Robinson D et al (1999) The ^{15}N natural abundance ($\delta^{15}N$) of ecosystem samples reflects measures of water availability. Aust J Plant Physiol 26:185–199

Heaton THE (1986) Isotopic studies of nitrogen pollution in the hydrosphere and atmosphere: a review. Chem Geol 59:87–102

Heaton THE, Spiro B, Madeline S, Robertson C (1997) Potential canopy influences on the isotopic composition of nitrogen and sulphur in atmospheric deposition. Oecologia 109: 600–607

Henn MR, Chapela IH (2001) Ecophysiology of ^{13}C and ^{15}N isotopic fractionation in forest fungi and the roots of the saprotrophic-mycorrhizal divide. Oecologia 128:480–487

Hobbie EA, Macko SA, Shugart HH (1998) Patterns in N dynamics and N isotopes during primary succession in Glacier Bay, Alaska. Chem Geol 152:3–11

Hobbie EA, Macko SA, Shugart HH (1999) Insights into nitrogen and carbon dynamics of ectomycorrhizal and saprotrophic fungi from isotopic evidence. Oecologia 118:353–360

Hobbie JE, Hobbie EA (2006) ^{15}N in symbiotic fungi and plants estimates nitrogen and carbon flux rates in arctic tundra. Ecology 87:816–822

Högberg P (1997) ^{15}N natural abundance in soil-plant systems. New Phytol 137:179–203

Högberg P, Johannisson C (1993) ^{15}N abundance of forests is correlated with losses of nitrogen. Plant Soil 157:147–150

Högberg P, Högbom L, Schinkel H et al (1996) ^{15}N abundance of surface soils, roots and mycorrhizas in profiles of European forest soils. Oecologia 108:207–214

Hornbeck JW, Lawrence GB (1996) Eastern forest fires can have long-term impacts on nitrogen cycling. In: Proceedings of the (1996) Society of American Foresters Convention, Albuquerque, NM

Houlton BZ, Sigman DM, Hedin LO (2006) Isotopic evidence for large gaseous nitrogen losses from tropical rainforests. Proc Natl Acad Sci U S A 103:8745–9750

Houlton BZ, Sigman DM, Schuur EAG et al (2007) A climate-driven switch in plant nitrogen acquisition within tropical forest communities. Proc Natl Acad Sci U S A 104:8902–8906

Hübner H (1986) Isotope effects of nitrogen in soil and the biosphere. In: Fritz P, Fontes JC (eds) Handbook of environmental and isotope chemistry Vol 2b, The Terrestrial Environment. Elsevier, Amsterdam, pp 361–425

Johanisson C, Högberg P (1994) ^{15}N abundance of soils and plants along an experimentally induced forest nitrogen supply gradient. Oecologia 97:322–325

Johnston JC, Cliff SS, Thiemens MH (1995) Measurement of multioxygen isotopic (delta18O and delta17O) fractionation factors in the stratospheric sink reactions of nitrous oxide. J Geophys Res 100(D8):16,801–16,804

Kahmen A, Wanek W, Buchmann N (2008) Foliar delta N-15 values characterize soil N cycling and reflect nitrate or ammonium preference of plants along a temperate grassland gradient. Oecologia 156:861–870

Kendall C, Silva SR, Change CCY et al. (1996) Use of the delta 18-O and delta 15-N of nitrate to determine sources of nitrate in early spring runoff in forested catchments. In: Isotopes in Resource Management International Atomic Energy Agency Symposium 1, pp 167–176

Kolb KJ, Evans RD (2003) Influence of nitrogen source and concentration on nitrogen isotopic discrimination in two barley genotypes (*Hordeum vulgare* L.). Plant Cell Environ 26:1431–1440

Koba K, Tokuchi N, Yoshioka T et al (1998) Natural abundance of nitrogen-15 in a forest soil. Soil Sci Soc Am J 62:778–781

Koerner W, Dambrine E, Dupouey JL et al (1999) $\delta^{15}N$ of forest soil and understorey vegetation reflect the former agricultural land use. Oecologia 121:421–425

Kohl DH, Shearer GB, Commoner B (1971) Fertilizer nitrogen: contribution to nitrate in surface water in a corn belt watershed. Science 174:1331–1334

Koopmans CJ, Tietema A, Verstraten JM (1998) Effects of reduced N deposition on litter decomposition and N cycling in two N saturated forests in the Netherlands. Soil Bio Biochem 30:141–151

Krankowsky D, Bartecki F, Klees GG et al (1995) Measurement of heavy isotope enrichment in tropospheric ozone. Geophy Res Lett 22:1713–1716

Kreitler CW (1975) Determining the source of nitrate in ground water by nitrogen isotope studies. Report of investigations No. 83, Bureau of Economic Geology, University of Texas at Austin

LeBauer DS, Treseder KK (2008) Nitrogen limitation of net primary productivity in terrestrial ecosystems is globally distributed. Ecology 89:371–379

Ledgard SF, Freney JR, Simpson JR (1984) Variations in natural enrichment of ^{15}N in the profiles of some Australian pasture soils. Aust J Soil Res 22:155–164

Létolle R (1980) Nitrogen-15 in the natural environment. In: Fritz P, Fontes JC (eds) Handbook of environmental and isotope chemistry. Elsevier, Amsterdam, pp 407–433

Liu X-Y, Xiao H-Y, Liu C-Q et al (2008) Stable carbon and nitrogen isotopes of the moss *Haplocladium microphyllum* in an urban and a background area (SW China): the role of environmental conditions and atmospheric nitrogen deposition. Atmos Environ 42:5413–5423

Mariotti A, Germon JC, Hubert P et al (1981) Experimental determination of nitrogen kinetic isotope fractionations: some principles; illustration for denitrification and nitrification processes. Plant Soil 62:413–430

Mariotti A, Pierre D, Vedy JC et al (1980) The abundance of natural nitrogen-15 in the organic matter of soils along an altitudinal gradient. Catena 7:293–300

Martinelli LA, Piccolo MC, Townsend AR et al (1999) Nitrogen stable isotopic composition of leaves and soil: tropical versus temperate forests. Biogeochemistry 46(1–3):45–65

Mayor JR, Schuur EAG, Henkel TW (2009) Elucidating the nutritional dynamics of fungi using stable isotopes. Ecol Lett 12:171–183. doi:10.1111/j.1461-0248.2008.01265.x

McKane RB, Johnson LC, Shaver GR et al (2002) Resource-based niches provide a basis for plant species diversity and dominance in arctic tundra. Nature 415(6867):68–71

Michalski G, Meixner T, Fenn M et al (2004) Tracing atmospheric nitrate deposition in a complex semiarid ecosystem using $\Delta^{17}O$. Environ Sci Tech 38:2175–2181

Michelsen A, Quarmby C, Sleep D et al (1998) Vascular plant ^{15}N natural abundance in health and forest tundra ecosystems is closely correlated with presence and type of mycorrhizal fungi in roots. Oecologia 115:406–418

Miller AE, Bowman WD (2002) Variation in nitrogen-15 natural abundance and nitrogen uptake traits among co-occurring alpine species: do species partition nitrogen form? Oecologia 130:609–616

Mizutani H, Kabaya Y, Wada E (1985) Ammonia volatilization and high $^{15}N/^{14}N$ ratio in a penguin rookery in Antarctica. Geochem J 19:323–327

Nadelhoffer KJ, Fry B (1988) Controls on natural nitrogen-15 and carbon-13 abundances in forest soil organic matter. Soil Sci Soc Am J 52:1633–1640

Nadelhoffer KJ, Fry B (1994) Nitrogen isotope studies in forest ecosystems. In: Lajtha K, Michener RH (eds) Stable isotopes in ecology and environmental science. Blackwell, Cambridge, pp 22–44

Nadelhoffer KJ, Downs MR, Fry B et al (1995) The fate of ^{15}N-labelled nitrate additions to a northern hardwood forest in eastern Maine, USA. Oecologia 103:292–301

Nadelhoffer KJ, Shaver G, Fry B et al (1996) ^{15}N natural abundances and N use by tundra plants. Oecologia 107:386–394

Nadelhoffer KJ, Downs MR, Fry B (1999) Sinks for ^{15}N-enriched additions to an oak forest and a red pine plantation. Ecol Appl 9:72–86

Näsholm T, Eklblad A, Nordin A et al (1998) Boreal forest plants take up organic nitrogen. Nature 392:914–916

Olleros (1983) Kinetische Isotopeneffekte der Arginase-und Nitratereduktasse-Reaktion; ein Beitrag zur Aufklärung der entsprechenden Reaktionsmechanismen. Diss Tech Univ München Weihenstephan, 158 p

Pardo LH, Hemond HF, Montoya JP et al (2002) Response of the natural abundance of ^{15}N in forest soils and foliage to high nitrate loss following clear-cutting. Can J For Res 32:1126–1136

Pardo LH, Kendall C, Pett-Ridge J et al (2004) Evaluating the source of streamwater nitrate using $\delta^{15}N$ and $\delta^{18}O$ in nitrate in two watersheds in New Hampshire, USA. Hydrol Process 18:2699–2712

Pardo LH, Templer PH, Fahey TJ (2006a) Species differences in root and foliar $\delta^{15}N$: causes and implications. In: Proceedings ecological society of America annual meeting abstracts, 91st annual meeting of the ecological society of America, Memphis, TN, 9–11 August 2006

Pardo LH, Templer PH, Goodale CL et al (2006b) Regional assessment of N saturation using foliar and root $\delta^{15}N$. Biogeochemistry 80:143–171

Pardo LH, Hemond HF, Montoya JP et al (2007) Natural abundance ^{15}N in soil and litter across a nitrate-output gradient in New Hampshire. For Ecol Manag 251:217–230

Pearson J, Wells DM, Seller KJ, Bennett A, Soares A, Woodall J, Ingrouille MJ (2000) Traffic exposure increases natural ^{15}N and heavy metal concentrations in mosses. New Phytol 147: 317–326

Perez T, Garcia-Montiel D, Trumbore S et al (2006) Nitrous oxide nitrification and denitrification ^{15}N enrichment factors from Amazon forest soils. Ecol Appl 16:2153–2167

Piccolo M, Neill C, Mellilo JM et al (1996) ^{15}N natural abundance in forest and pasture soils of the Brazilian Amazon Basin. Plant Soil 182:249–258

Piccolo MC, Neill C, Cerri C (1994) Natural abundance of ^{15}N in soils along forest-to-pasture chronosequences in the western Brazilian Amazon Basin. Oecologia 99:112–117

Robinson D (2001) $\delta^{15}N$ as an integrator of the nitrogen cycle. Trends Ecol Evol 16:153–162

Sah SP, Ilvesniemi H (2007) Interspecific variation and impact of clear-cutting on natural ^{15}N abundance and N concentration in the needle-to-soil continuum of a boreal conifer forest. Plant Soil Environ 53:329–339

Schmidt S, Stewart GR (2003) δ15N values of tropical savanna and monsoon forest species reflect root specializations and soil nitrogen status. Oecologia 134:569–577

Schulze E-D, Farquhar GD, Miller JM et al (1999) Interpretation of increased foliar $\delta^{15}N$ in woody species along a rainfall gradient in northern Australia. Aust J Plant Physiol 26:296–298

Schulze ED, Williams RJ, Farquhar GD et al (1998) Carbon and nitrogen isotope discrimination and nitrogen nutrition of trees along a rainfall gradient in northern Australia. Aust J Plant Physiol 25:413–425

Schuur EAG, Matson PA (2001) Net primary productivity and nutrient cycling across a mesic to wet precipitation gradient in Hawaiian montane forest. Oecologia 128:431–442

Shearer G, Kohl D (1986) N_2 fixation in field settings, estimations based on natural ^{15}N abundance. Aust J Plant Physiol 13:699–757

Shearer G, Kohl D (1989) Estimates of N_2 fixation in ecosystems: the need for and basis of the ^{15}N method. In: Rundel PW, Ehleringer JR , Nagy KA (eds) Stable isotopes in ecological research, Springer, New York, pp 342–374

Smithwick EAH, Turner MG, Mack MC et al (2005) Postfire soil N cycling in northern conifer forests affected by severe, stand-replacing wildfires. Ecosystems 8:163–181

Stephan K, Kavanaugh K (2005) Fire effects on nitrogen dynamics in headwater systems. In: Proceedings of the 90th annual meeting of the ecological society of America. Montreal, Canada

Sutka RL, Adams GC, Ostrom NE et al (2008) Isotopologue fractionation during N_2O production by fungal denitrification. Rapid Comm Mass Spectrom 22:3989–3996

Ueda S, Go S-C, Suwa Y et al. (1999) Stable isotope fingerprint of N_2O produced by ammonium oxidation under laboratory and field conditions. In: International workshop on the atmospheric N2O budget: an analysis of the state of our understanding of sources and sinks of atmospheric N_2O. National Institute of Agro-Environmental Sciences, Tsukuba, Japan

Virginia RA, Jarrell WM, Rundel PW et al. (1989) The use of variation in the natural abundance of ^{15}N to assess symbiotic nitrogen fixation by woody plants. In: Rundel PW, Ehleringer JR , Nagy KA (eds) Stable isotopes in ecological research, Springer, New York, pp 345–394

Vitousek PM, Shearer G, Kohl DH (1989) Foliar ^{15}N natural abundance in Hawaiian rainforest: patterns and possible mechanisms. Oecologia 78:383–388

Wada E, Ueda S (1996) Carbon, nitrogen, and oxygen isotope ratios of CH_4 and N_2O on soil ecosystems. In: Boutton TW, Yamasaki S-I (eds) Mass spectrometry of soils. Marcel Dekker, New York, pp 177–204

Wang L, Shaner P-JL, Macko S (2007) Foliar $\delta^{15}N$ patterns along successional gradients at plant community and species levels. Geophys Res Lett 34:L16404

Webster R (2000) Is soil variation random? Geoderma 97:149–163

Yoneyama T, Matsumaru T, Usui K et al (2001) Discrimination of nitrogen isotopes during absorption of ammonium and nitrate at different nitrogen concentrations by rice (*Oryza sativa* L.) plants. Plant Cell Environ 24:133–139

Yoshida N (1988) ^{15}N-depleted N_2O as a product of nitrification. Nature 335:528–529

Yoshida N, Hattori A, Saino T et al (1984) $^{15}N/^{14}N$ ratio of dissolved N_2O in the eastern tropical Pacific Ocean. Nature 307:442–444

Zechmeister HG, Richter A, Smidt S et al (2008) Total nitrogen content and $\delta^{15}N$ signatures in moss tissue: indicative values for nitrogen deposition patterns and source allocation on a nationwide scale. Environ Sci Technol 42:8661–8667

Chapter 12
Using Isoscapes to Model Probability Surfaces for Determining Geographic Origins

Michael B. Wunder

12.1 Introduction and Background

A common goal for studies using isoscapes is to determine geographic areas in which organic material was developed, particularly in studies of wildlife or human forensics. For example, studying animal migration by direct observation is difficult and expensive for any species, and is impossible for many small species and for questions involving archaic systems. The use of stable isotope tracers, however, has proven useful for inferring geographic origins and spatial connections for a range of species or materials and a variety of temporal extents. Examples include estimating single-season movement patterns of songbirds (Norris et al. 2004), reconstructing geographic histories for modern butterflies (Wassenaar and Hobson 1998), prehistoric humans (Muller et al. 2003; Sharp et al. 2003) and historic human trade routes (Giuliani et al 2000), as well as forensic work to determine recent human movement (Fraser et al. 2006), or the origin of illicit substances such as drugs or explosives (Ehleringer et al. 2000; Benson et al. 2006).

The availability of isoscapes has generated much excitement about potential GIS-based analyses to determine geographic origins in studies of wildlife or human forensics. However, there are some misconceptions in the literature about the nature of isoscapes and isotope-based geographic assignments. Most significantly, many studies fail to recognize that GIS-based information in isoscapes is not really data at all, but rather is a set of expectations from the isoscape model. That is, values in isoscape grids are predicted values from a model; they describe a general pattern, and for the most part disregard the degree to which observed data are scattered about that pattern. A secondary and less pervasive misconception is that some isoscapes are universal in application. An isoscape that can be effectively applied

M.B. Wunder (✉)
Department of Biology, University of Colorado Denver, Campus Box 171, Denver, CO, 80217-3364
e-mail: michael.wunder@ucdenver.edu

J.B. West et al. (eds.), *Isoscapes: Understanding Movement, Pattern, and Process on Earth Through Isotope Mapping*, DOI 10.1007/978-90-481-3354-3_12,

to one study may be less useful for another; in nature no single geographic location is expected to produce exactly the same isotope value for every organism using resources there, nor is any location value expected to stay the same from year to year. Isoscapes must be custom-tailored to individual forensic studies not only for best results, but also in order to effectively explore mechanistic hypotheses for explaining differences in efficacy among studies.

Perhaps for the sake of convenience, deviations from mean isoscape values are rarely formally addressed in models, but they are occasionally documented. Because of this, many sources of within-location variance in isoscapes are well known and the magnitudes of these sources of variance can be easily estimated. This can be extremely useful for not only characterizing certainty in geographic assignments (Wunder and Norris 2008a), but also for providing insight into the most fruitful directions for future research (Bowen and Revenaugh 2003).

Along with work presented elsewhere in this volume, this chapter concerns the application of, rather than the generation of, isoscapes. In contrast, however, the ideas presented here are centered primarily on the consideration of variances rather than of means. Because of this, I de-emphasize prediction in favor of probabilistic assignment, which marks this work as fundamentally different from the many examples using GIS-based isoscapes for wildlife forensics reported in the literature (e.g. Wassenaar and Hobson 1998; Hobson et al. 1999, 2006, 2007; Meehan et al. 2001; Cryan et al 2004; Norris et al. 2004; Bearhop et al. 2005; Bowen et al. 2005; DeLong et al. 2005; Lott and Smith 2006; Paxton et al. 2007). I describe here the use of variance estimates directly to generate probability surfaces and to identify gaps in knowledge. I discuss approaches for both discrete and continuous frameworks to characterize the probability of specific geographic origins and I discuss the differences between such characterizations for individuals and for populations.

This chapter is intended as a proof-of-concept work, and will not prescribe when or where to apply or avoid various isoscapes. It is intended to provide generalized guidance for using isoscapes in any research that features geographic forensics as a goal. In an effort to carry along the chapter and the ideas that shape the approach, I refer to a generalized example problem of assigning summering locations to birds sampled during winter via a precipitation-based hydrogen isoscape, a widely-reported application of isoscapes. I constrain the presentation in this way to highlight the relevant features of the approach without distraction from the unavoidable list of caveats that riddle any particular case-study and without the added complexity of addressing issues of covariance and added dimensionality that arise from considering multiple isoscapes and other information sources simultaneously. However, I point out that the efficacy of the approach is considerably improved by using multiple isoscapes and higher-dimension covariates in case-specific applications; the exploration and reporting of such extended applications are strongly encouraged.

12.2 Example Problem

The example here concerns the use of stable isotope compositions of bird feathers to infer cross-seasonal geographic connectivity in North American bird migration systems, the basic examples of which were first presented by Chamberlain et al. (1997) and Hobson and Wassenaar (1997). The premise is that we can use an isoscape to find the geographic location where bird feather or claw material (keratin) was synthesized. Bird feathers and claws are useful in this regard because they are metabolically inert once formed, and so in theory the stable isotope values of the keratin will stay the same as the bird migrates to a new location. The idea is to link two different points in time and space as part of the migratory history of an individual bird using isotopes in keratin.

Migratory birds typically molt feathers once or twice per year, often depending on the type of feather in question. For example, many North American migratory birds molt flight feathers (wings and tail) on the summer grounds late in the breeding cycle and rely on these feathers to get them to the wintering grounds and back (Pyle 1997). Thus, by sampling flight feathers during winter, one can determine locations within the breeding region where the feather was likely synthesized during the previous summer. It is worth noting that many of the same migratory species molt their contour feathers (the body feathers) twice per year; once into basic (winter) plumage near the end of the breeding cycle, and again into alternate (breeding) plumage just prior to spring migration to the breeding grounds (Pyle 1997), suggesting that it might be possible to also determine winter locales for the same species of birds sampled during summer. The point in either case is that feathers can be used to infer geographic linkages between summer and winter regions by sampling in the alternate season from when the feather was grown. The goal of such migratory bird studies is to learn how geographic dependencies within species are shaped through the course of a full year in seasonal systems (Webster and Marra 2005).

12.2.1 Study Design and Model Development

For the migratory bird example, I calibrate an available precipitation-based isoscape using freshly grown feathers sampled from young and adult birds across the target range (the range of isoscape values spanning the spatial extent of the breeding range). I then sample feathers during winter that are known to have been synthesized the summer before. The calibrated isoscape is used to estimate the otherwise unknown breeding origins of birds sampled during winter. The list of assumptions and expectations necessary for this plan include (1) the assumption that the precipitation-based hydrogen isoscape provides a reasonable process-model for the expected spatial pattern in hydrogen isotopes found at the base of avian food webs, (2) the assumption that values in that precipitation isoscape are

fixed and known (e.g. model-based variance around the mean spatial pattern is negligible), (3) the expectation that "nice" transfer functions modeling water isotope values through the food web to bird keratin isotopes can be estimated empirically, (4) the assumption that carbon-bound (non-exchangeable) hydrogen isotope values of organic keratin do not change with time, (5) the expectation that lab practices reliably calibrate hydrogen measurements in organic keratin to Vienna Standard Mean Ocean Water (VSMOW) using multiple organic keratin standards, (6) the assumption that keratin is synthesized by birds during summer prior to migration, (7) the expectation that age of bird influences isotope values of keratin, and (8) the expectation that all other factors influencing keratin isotope values are either unknown or un-measurable for birds sampled during winter. This list of assumptions and design plans is nearly universal in these types of studies. Study design and model construction follow directly: In order to understand the extent to which the precipitation-based isoscape model is reasonable (assumption 1), points 2–7 must be supported either directly or from the literature, and data models must incorporate points 3, 7 and 8.

12.3 Model Aim and Overview

Isoscapes describe average spatial patterns in isotope values; that is, an isoscape provides an expected isotope value, given a geographic coordinate. This is useful for studying and understanding processes that lead to changes in isotope values over space. The distinguishing problem in forensics is to determine the extent to which isotope patterns can differentiate among locations when the isoscape model is *inverted*. That is, we want probabilistic statements about the geographic coordinate, given an isotope value. This implies that the goal in most forensic applications of isoscapes is to determine geographic origins for *individual* organisms or samples; rarely are we interested in making inferences about population means. Therefore it is useful to understand the extent to which distributions of isotope values from different locations are the *same*, which is different from understanding the extent to which mean values differ among locations. For example, if there are statistically significant differences between the means from different locations, but the observed ranges of isotope values of feathers from those different locations overlap substantially, it is difficult to reliably assign individual birds to one of these discrete locations (Wunder and Norris 2008a). Often, these statistically significant but pragmatically insignificant differences among mean values for locations result from large sample sizes (in cases where means are proximal in isotope space).

Because GIS-based isoscape models define only one isotope value for each geographic location, we need more than the isoscape to determine the probability that a feather was grown at a given location. The typical work-around solutions have been to either (1) arbitrarily describe large geographic ranges a priori and summarize isoscape values within each range (e.g. Royle and Rubenstein 2004), or (2) to arbitrarily determine a minimum magnitude that is on the order of the

measurement (analytical) error for measuring δ^2H. The former is appealing in terms of simplicity but may be unnecessarily conservative, whereas the latter ignores heterogeneity among individuals at a given location and is therefore not conservative enough. The modeling approach described here provides another alternative by combining a stochastic component based on known, estimated, or hypothesized residual variance with a calibrated isoscape.

The calibration function can be based on theory (i.e. represent mechanistic understanding of the system) or it can be empirically based (i.e. use a generalized linear model to relate feather values to isoscape values). As the simplest example, consider early exploratory studies that suggested δ^2H of feathers is related to that of precipitation by constant linear shift of −25‰ (Rubenstein and Hobson 2004). If we assume this to be true, then we would calibrate a precipitation-based hydrogen isoscape by subtracting 25‰ from the value of each modeled value in the isoscape for use as the calibrated isoscape. Calibrations will rarely be this simple; many applied studies will allow for the construction of far more complex calibrations and I point out that the calibration can be (and should be) as complex or as simple as the state of the science allows.

The stochastic component models unknown or un-measurable random processes for every point in the isoscape; it represents all sources of uncertainty associated with the state of the science. As with the calibration, the stochastic model structure can be based on theory (i.e. constructed hierarchically), or it can be empirically estimated from the residuals of the calibration step. This coupled model forms the basis for generating geographically-explicit probability densities (probability surfaces) for isotope values from any sample of unknown origin.

12.3.1 Model Assembly, Deterministic Calibration

Because isoscapes are average representations of spatial processes, they operate as the deterministic component of the model framework here. Ideally, isoscapes combine data with results from experiments and theory that together identify relevant factors governing the isotopic variance among individual samples and over space. Failing any underlying mechanistic theory, however, the spatial model can be entirely data-based and fit using ordinary kriging, inverse distance weighting, etc., but the universality of the resultant model is compromised by comparison. Once fit to the data, the isoscape is a deterministic model that depends on the sample at hand. In many cases the sample material of interest is available from across the full extent of the geographic range of interest; in such cases, the isoscape can be modeled directly and no specific calibration is needed. The alternative for cases where saturated sampling of the material of interest is not possible, an existing isoscape developed for other applications can be calibrated from a smaller sample of known-origin material relevant to the study at hand. The basic idea for practitioners is that the deterministic isoscape should reflect as much as is known about baseline patterns (spatial and otherwise) in the system of interest.

The example migratory problem relies on a calibrating an isoscape for hydrogen in precipitation. The general form of this calibration is flexible and can be written in simplest form as $y_{ij} = f(x_j) + \varepsilon_{ij}$ where y_{ij} is the observed isotope value for feather i that was known to have been synthesized at location j, $f(x_j)$ is the function that relates the expected value for the isoscape ($x = \delta^2 H$) at location j to δ^2H of the feather ij, and ε_{ij} is the distance between the expectation of that function for location j and the measured δ^2H for feather ij. For example, we might calibrate the precipitation isoscape via a simple linear regression of measured summer-grown feather values on predicted water values. The calibration model is $y_{ij} = \beta_0 + \beta_1 x_j + \varepsilon_{ij}$ where x_j is the expected δ^2H for precipitation at location j and where y_{ij} and ε_{ij} are as above. The regression coefficients are estimated from the feather data and the isoscape model output. Notice that the calibration $f(x_j)$ need not be so simple; it can be multidimensional and non-linear. It almost always should include structure not only from the modeled isoscape (the universal geographic influences), but also from covariates that are relevant to the study organism or material (e.g. based on natural history, experimental results and/or theory). Our migration problem assumed that young developing birds use resources for synthesizing keratin differently than do adults (c.f. Meehan et al. 2003). Adding an indicator function for the adult age group, we have:

$$y_{ij} = \left(\beta_{a0} + \beta_{a1} x_j\right) I_{[adult]}(\varphi) + \left(\beta_{c0} + \beta_{c1} x_j\right)\left(1 - I_{[adult]}(\varphi)\right) + \varepsilon_{ij} \qquad (12.1)$$

where $I(\varphi) = 1$ if the feather y_{ij} is from an adult bird and $I(\varphi) = 0$ if it is from a chick; β_0 and β_1 are additionally indexed with a and c to differentiate regression coefficients for adults and chicks respectively. Figure 12.1 shows this model for a simulated dataset of adult and young birds sampled across a landscape with water isoscape δ^2H values from −125‰ to −45‰. For the simulated data, $\beta_{a0} = -22$, $\beta_{c0} = -24$, $\beta_{a1} = 0.85$, $\beta_{c1} = 0.92$, and $\varepsilon_{ij} \sim N(0, \sigma^2)$ where $\sigma^2 = 196$, values selected to fall within the range of published values for studies of migratory birds (reviewed by Wunder 2007).

So far, most studies coupling water δ^2H isoscapes with bird feather data to determine geographic origins of migratory birds have used simple linear regressions like this to calibrate precipitation isoscapes (see Wunder and Norris 2008b for a review). In this literature, there has been much discussion about so-called discrimination factors (the intercept in these simple linear regressions; e.g. Hobson and Wassenaar 1997; Meehan et al. 2001; Rubenstein and Hobson 2004; Lott and Smith 2006). However, the more important factor to consider for linear calibrations is the scaling (the slope parameter estimate). This is especially true for hydrogen models because few measurements actually occur near the origin; most are 50 or more units away. For example, a calibration function with $\beta_0 = -20$‰ and $\beta_1 = 1.0$ gives −120‰ for isoscape values of −100‰ whereas a calibration with the same −20‰ intercept but with scaling of 0.9 gives −110‰ for the same isoscape value, a difference of 10‰, which is five times greater than the typical magnitude of analytical uncertainty. This simple rule of scaling has been generally underappreciated thus far, perhaps

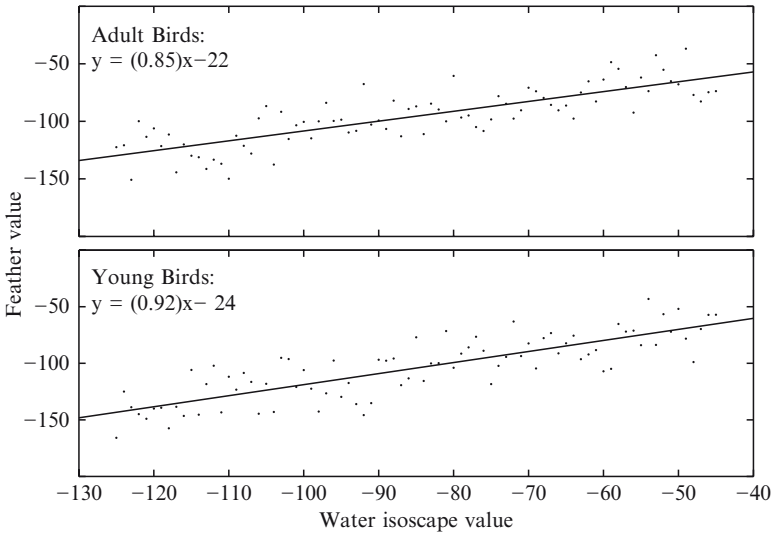

Fig. 12.1 Simulated δ^2H data for feathers of known origin from birds of two different age classes. Lines are regressions of δ^2H in feathers on predicted values for δ^2H at the known origins from a water-based isoscape (Bowen et al. 2005). Simulated data were generated from the equations shown along with error structure given by the Normal distribution $N(\mu,\sigma^2)$ with $\mu = 0$ and $\sigma^2 = 196$ for both age classes. The linear models shown were used to calibrate the water-based isoscape from Bowen et al. (2005) for use in determining spatially explicit probability densities for feathers of unknown origin. See text for details

because it implies that we still really need to calibrate isoscapes using tissue of known origin for every case study application. For this reason, I encourage every effort to calibrate isoscapes using known-origin samples from as much of the target range as possible, and discourage the use of fixed offsets to adjust isoscapes.

12.3.2 Model Assembly, Stochastic Component

Obviously, we would like ε_{ij} to be small for all samples at all locations in the isoscape. Small ε would indicate that we have modeled the relevant mechanistic processes that govern change in isotope values across geographic and covariate space. Such understanding remains a distant goal for most organic systems, and almost certainly will never be fully realized for any system. In the meantime, studying the shape and magnitude of the distribution on ε for sample populations helps to quantify exactly how far away from that understanding we are.

Because even the most carefully calibrated isoscapes are (thus far) static models, they provide only a single value for each geographic location. This geographically indexed set of values is the best guess for long-term, large-population

average values, given the model structure used to generate the isoscape surface. That is, the isoscape is a *population*-level inference; given a population of observed isotope values for a single pixel, the isoscape value for that pixel should be proximal to the mean of the values for that population. Because of this, few individual isotope data observed at a single geographic location are expected to align exactly with the isoscape value for that locale. So long as the distribution of feather values at a location in the isoscape has a single mode, the value of the rescaled isoscape for any locale will put us generally in the correct region of the isotope space for feathers from that location. However, it will not tell us how far from that point we can wander before we have enough reason to believe that the feather was grown elsewhere.

In problems of forensics, it is far more common to seek inference about the geographic origin of a single sample than it is to be concerned with the origin associated with the mean of a population of samples. Even in cases where we have a sample population, such as with the wintering bird example, we are most often interested in understanding the structure of geographic origins within the sample, as opposed to the geographic location associated with the sample mean, a point I discuss in more detail later. This is why it is useful to carefully consider the how the stochastic term relates the isoscape to observed samples.

Often, the stochastic term is called error or noise. Such terminology invokes the sense that there are problems, abnormalities, or mistakes in our data or model, but these terms are really just used to describe the difference between observed nature and models for nature. They represent random processes and are considered as random variables. Sometimes these processes (variables) have known structure. For example, the Normal random variable circumscribes the familiar bell-shaped curve. Given values for the mean and variance for the Normal random process, the probability density for any value of y is

$$f(y) = \frac{e^{-\frac{(y-\mu)^2}{2\sigma^2}}}{\sigma\sqrt{2\pi}} \tag{12.2}$$

where y is the observed value and μ is the population mean scaled by σ. This model is often written more succinctly as $Y \sim N(\mu\ ,\ \sigma^2)$. This simple Normal structure can be used as the stochastic component for the calibration model given by Eq. 12.1; we just need estimates for μ and σ^2. Following from the calibration model in Eq. 12.1, the mean value for δ^2H of feathers at location x_j is an estimate for μ:

$$\mu = \left(\beta_{a0} + \beta_{a1}x_j\right)I_{[adult]}(\varphi) + \left(\beta_{c0} + \beta_{c1}x_j\right)\left(1 - I_{[adult]}(\varphi)\right) \tag{12.3}$$

Substituting into Eq. 12.2, we have:

$$Y_j \left| x_j, \beta_{a0}, \beta_{a1}, \beta_{c0}, \beta_{c1}, \beta \sim N\left(\left\{\left(\beta_{a0}+\beta_{a1}x_j\right)I_{[adult]}(\varphi)+\left(\beta_{c0}+\beta_{c1}x_j\right)\left(1-I_{[adult]}(\varphi)\right)\right\}, \sigma^2\right) \right. \quad (12.4)$$

leaving σ^2 to be structured by one of many different methods. Once a structure for σ^2 is determined, the model given by Eq. 12.4 describes a weighted distribution of feather isotope values for each location x_j in the calibrated isoscape, thus overcoming the limitations of using a single value for any given location. Although $f(x)$ can vary in scaling of expected feather values over individual locations in an isoscape (constant variance is not a requirement), in practice it is often better to try to adjust $f(x)$ for homogeneity of variance in the residuals so that they have the same overall form across geographic space. For example, the residuals from the model for the simulated feather data are homoscedastic across the sampled range (Fig. 12.1); maximum likelihood unsurprisingly returns $\sigma^2 = 196$ for the residuals in both adult and young bird feathers, which was the value used to simulate the data.

It is important to recognize that the distribution of errors need not be normal; the structure can be informed from the observed distribution of the calibration residuals. Error structures can take any shape, ranging from a simple uniform distribution with support over some narrow pre-determined range, to an unknown complex hierarchical structure that cannot be written in closed form with support over an infinite range. Most isoscape applications in the literature thus far have defaulted to a uniform distribution. For example, Lott and Smith (2006) used $U(\mu - 8, \mu + 8)$ where μ is the feather value; this model evenly distributes the nonzero probability density over all isoscape locations that have values within 8‰ of the observed feather value and assigns a probability density of 0 to all outside this range. Limiting the support to a range of 16‰ was reasoned by comparing model output with the model-generating data. They could just as easily have used 4‰ as an estimate for σ in a Gaussian kernel to similarly constrain approximately 95% of the density to a range of 16‰ centered on the observed feather value. In either case however, as well as in the example problem discussed here so far, the estimated error structure is relevant only to the study at hand. More importantly, because this structure is modeled as a single all-inclusive process we gain little to no insight about mechanisms that generate differences from the expectation of the isoscape model. A more informed approach is to partition the variance in ways that reflect the state of understanding for the study system. I discuss this in more detail in Section 12.3.4.

12.3.3 Model Application, Bayes Rule Inversion

In our example so far, we have a probability distribution function for feather values, given any location. But ultimately we are interested in probability distribution functions for locations, not feathers. Let J be a random variable defining the probability

distribution for all locations j, given a feather value. It usually makes sense to constrain the potential region of origin to some a priori suspected range; for our case, we would clearly want to restrict the range of possible geographic locations to within the known breeding range for the species in question. To accomplish this, let the prior distribution on J be defined by an indicator function identifying the breeding range: $f_J(j) = I_{[range]}(j)$. This prior on location assigns a multiplier of zero to all locations outside the known summer range and a multiplier of one to all locations within the range. Note that again the general form of this prior is flexible and it can be written to reflect any and all non-isoscape information about the probability of any location as an origin. For example, Royle and Rubenstein (2004) advocate using relative abundance of various locations when available; this would extend the indicator function above such that the prior probability is not evenly distributed across the breeding range.

Bayes' rule defines conditional probability inversions. Following from above,

$$f_{J|Y,X}\left(J = j \middle| Y = y_{ij}, X = x_j\right) = \frac{f_{Y|X}\left(Y = y_{ij} \middle| X = x_j\right) f_J\left(J = j\right)}{\int f_{Y|X}\left(Y = y_{ij} \middle| X = x_\zeta\right) f_J\left(J = \zeta\right) d\zeta} \tag{12.5}$$

where $f_{Y|X}$ is the function associated with the calibration for feathers of known origin (Eq. 12.4, the conditional distribution on Y_j from the previous section) for an isoscape over ξ locations. This equation describes the posterior probability density function for location j as the true origin given the measured δ^2H value for a feather and the calibrated isoscape. The denominator integrates out to a constant, so that the probability density is proportional to the numerator. Using this relation and substituting detail from Eqs. 12.2 and 12.4, we have:

$$P\left(J = j \middle| y, \overline{\beta}, \varphi, x_j, \sigma^2\right) \propto \left(\frac{1}{\sqrt{2\pi\sigma^2}} e^{-\frac{\left(y - \left\{\left(\beta_{a0} + \beta_{a1} x_j\right) I_{[adult]}(\varphi) + \left(\beta_{c0} + \beta_{c1} x_j\right)\left(1 - I_{[adult]}(\varphi)\right)\right\}\right)^2}{2\sigma^2}}\right) I_{[range]}^{(j)} \tag{12.6}$$

where j is a geographic location, y is δ^2H for a feather of unknown origin (from the individual bird of interest), $\overline{\beta}$ is the vector of regression coefficients from the calibration function, ϕ is the age class for the bird from which the feather came, x_j is the expected value for δ^2H at location j from the original (precipitation) isoscape, and σ^2 is variance observed in the residuals from the calibration.

For large geographic areas or for isoscapes with fine-scale resolution, the resultant probability density surface can be comprised of very small values for the map locations. Because of this and for ease of interpretation, it is often useful to project these values onto the unit scale on a per-location basis using either a logistic transformation or by rescaling all values relative to the largest observed density value.

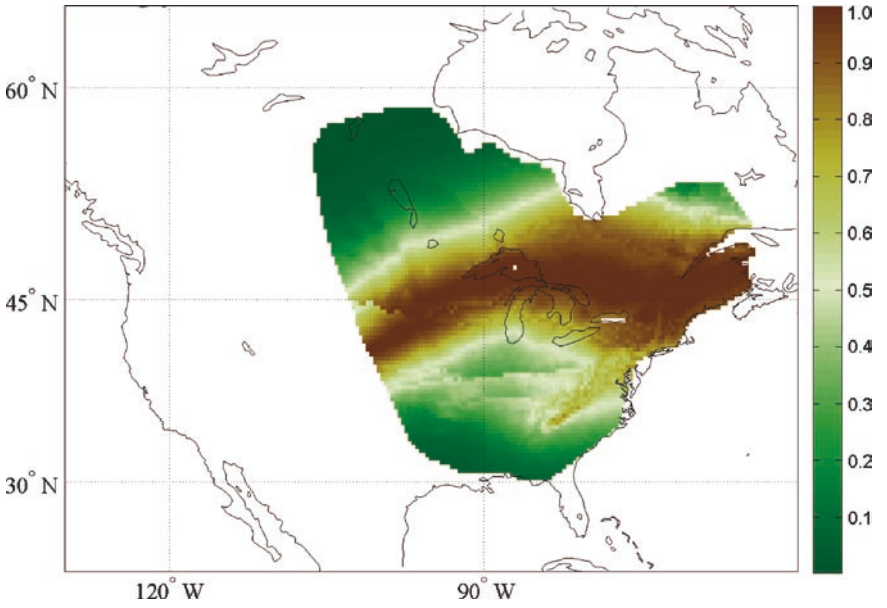

Fig. 12.2 Probability density surface for a hypothetical adult bird feather of unknown origin with $\delta^2H = -75‰$ modeling bulk variance from the calibration shown in Fig. 12.1. The geography of possible origins for the feather is restricted to the hypothetical breeding range chosen to represent a generic migratory bird that breeds in the eastern deciduous forests of North America. For presentation purposes, the density value for each pixel in the probability surface has been rescaled by the largest observed density value. Fig. 12.2, see Appendix 1, Color Section

Figure 12.2 shows the geographically explicit probability surface for a feather with $\delta^2H = -75‰$ from the model just described fitted with the simulated adult bird data and the isoscape for water δ^2H from Bowen et al. (2005). The posterior density surface in Fig. 12.2 has been rescaled on a per-location basis relative to the largest observed density value among all locations.

12.3.4 Partitioning the Variance

Although it is convenient to estimate the variance structure of the model directly from the calibration residuals as just described in Sections 12.3.2 and 12.3.3, it can be more informative to structure the model from first principles. For example, we might consider a two-tiered hierarchy that models two independent sources of error, one from lab measurement (analytical) errors and another from individual heterogeneity in physiology, diet, and behavior (within population variance). The assumption of independence in variances implies that measurement error does not change proportional to the magnitude of within population variance. This independence assumption also implies that the variances are additive as long as they are similarly

distributed, giving $\sigma^2 = \sigma^2_a + \sigma^2_p$, where the subscripts a and p indicate analytical and within-population variance, respectively.

Because continuous-flow isotope ratio mass spectrometry (CF-IRMS) depends on linear calibrations using multiple lab standards to estimate δ^2H for samples, one can use these calibration curves to estimate the value of the standards and quantify the difference between those estimated values and the accepted values for the standards. Similarly, an estimate of σ^2 can be made from observed isotope values for known-origin feathers collected at single sites, from which σ^2_a can be subtracted to find σ^2_p (since the observed data include analytical error).

I will again assume Gaussian kernels for illustrating the isoscape calibration function, this time incorporating the hierarchical structure from the two independent components of variance. Let y_{ij} be the observed δ^2H for a feather i at location j which includes measurement error. Let z_{ij} be the true value of feather i at location j. We can then adjust the model for Y_j to reflect the new structure using the following hierarchy:

$$Z_j \left| x_j, \overline{\beta}, \varphi, \sigma^2_p \sim N\left(\left\{ \left(\beta_{a0} + \beta_{a1} x_j \right) I_{[adult]}(\varphi) + \left(\beta_{c0} + \beta_{c1} x_j \right) \left(1 - I_{[adult]}(\varphi) \right) \right\}, \sigma^2_p \right) \right. \tag{12.7}$$

$$Y_j \left| z_j, \sigma^2_a \sim N\left(z_j, \sigma^2_a \right) \right. \tag{12.8}$$

In this formulation, Z_j is the expected distribution of feather values for location j, including among-individual variance and centered on the value predicted for precipitation from the original isoscape; this is the distribution we would observe if there were no additional variance from the process of obtaining lab measurements. The next level in the hierarchy, Y_j, incorporates uncertainty from CF-IRMS measurements. The hierarchy can be represented in the probability model for J (Eq. 12.6) as:

$$P\left(J = j \left| y, \overline{\beta}, \varphi, x_j, \sigma^2_p, \sigma^2_a \right. \right) \propto$$
$$N\left(N\left(\left\{ \begin{array}{l} \left(\beta_{a0} + \beta_{a1} x_j \right) I_{[adult]}(\varphi) + \\ \left(\beta_{c0} + \beta_{c1} x_j \right) \left(1 - I_{[adult]}(\varphi) \right) \end{array} \right\}, \sigma^2_p \right), \sigma^2_a \right) I_{[range]}(j) \tag{12.9}$$

One can continue in this way to add additional components of variance that are either known from the literature or estimated from data. In this simplified example, only variances associated with feather values are considered. However, it should be clear the calibration function coefficients (β_{a0}, β_{a1}, β_{c0}, β_{c1}) are estimated with error, the model used to generate the isoscape value x_j also involves param-

eters that are estimated with error, and so too might the determination of age class (ϕ) be done with some estimable degree of error. All of these sources of variance can be incorporated hierarchically (Clark 2007).

This hierarchical arrangement provides a key advantage over the use of a single estimate for bulk variance: it provides the flexibility to ask questions about relative effects on uncertainty in geographic assignments from measurement error and from among-individual differences. For example, the standard deviation associated with the population of errors for δ^2H measurements on typical instrumentation (σ_a) is about 2‰ (Wassenaar 2008). Using this value for σ_a we can compute σ_p for the migration example as being about 12‰ (using the value of $\sigma^2 = 196$ from the simulation data). Plugging these values into the hierarchical model above produces the same probability density as was produced by the non-hierarchical model with $\sigma^2 = 196$ (e.g. Fig. 12.2). Figure 12.3a shows the same density as in Fig. 12.2 but derived from this hierarchical model and left on the natural scale (the pixel values sum to unity). The hierarchically structured model provides the flexibility to let $\sigma^2_a = 0$ to ask the question "How would my geographic inference change if I were to completely remove all measurement error?" Figure 12.3b shows the probability surface for this case. Alternately, we can let $\sigma^2_p = 0$ and leave $\sigma^2_a = 4$ to ask what things would look like if measurement error were the only source of variance (e.g. for the unlikely event that our calibrated isoscape captured all of the natural processes influencing variation in isotope values among individuals across space). The probability density surface for that case is given in Fig. 12.3c. In this example, it is clear that efforts to minimize measurement error will result in virtually no improvement in geographic precision of assignment, and that future research would be better directed at understanding mechanisms of individual heterogeneity. To the extent possible, I discourage the use of case-study-specific estimates for bulk variance terms; most progress will come from first principles-based hierarchical models that partition the estimable variance in thoughtful ways that help prioritize future research needs.

12.4 Discrete and Continuous Frameworks

Technically, because isoscapes are often distributed as GIS grids at fixed geographic resolution, all applications of these isoscapes are discrete; the GIS grids give values for a discrete set of points. Therefore, the distinction I make here is one of resolution and applies to whether the interest is in estimating kernels for every possible grid point (continuous framework) or in estimating kernels from a collection of points that fall within some geographic boundaries that are imposed a priori (discrete framework). Discussion thus far has involved continuous frameworks, cases where interest was in kernels for individual geographic coordinates. Discrete frameworks are coarser and address the question of whether sampled material derived from jurisdiction A or jurisdiction B. For discrete frameworks, the collection of points within each jurisdiction is treated as a population of distributions and Monte Carlo methods

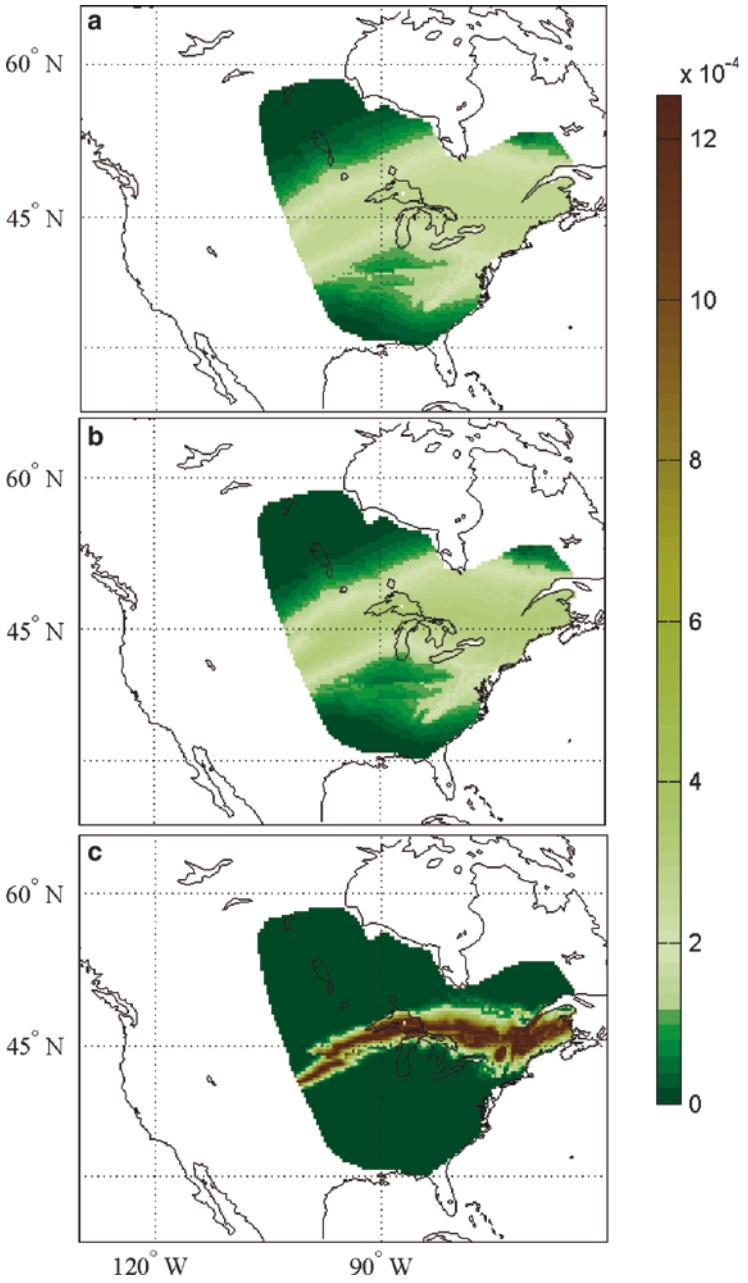

Fig. 12.3 (**a**) Probability density surface for an adult bird feather of unknown origin with measured $\delta^2H = -75‰$ using a hierarchical model for two sources of variance; one from measurement errors in the lab and the other from among individual differences at a single location. The geography of possible origins for the feather is additionally restricted as described in Fig. 12.2. (**b**) Probability density surface for the same adult bird feather ($\delta^2H = -75‰$) and hierarchical model,

are used simulate the posterior distribution from the population of distributions. Wunder and Norris (2008a) illustrate an extension for just such a case (Norris et al. 2006).

The limitations of a discrete framework are generally that the boundaries defining the regions can be somewhat arbitrary and may not nicely divide the isotope space (e.g. Fig. 12.4). If the isotope space is not nicely divided, the distributions of values for the defined regions are likely to overlap widely, or result in some wide geographic regions getting mapped to narrow regions in isotope space, thereby reducing the efficacy of discerning among potential regions of origin. For example, regions B and D in Fig. 12.4 are geographically vast, but isotopically narrow. Thus, these regions are not expected to end up as assigned origins for many samples despite the broad geographic coverage. Also notice that adjacency in geographic space does not necessarily translate to adjacency in isotope space: isotopic neigh-

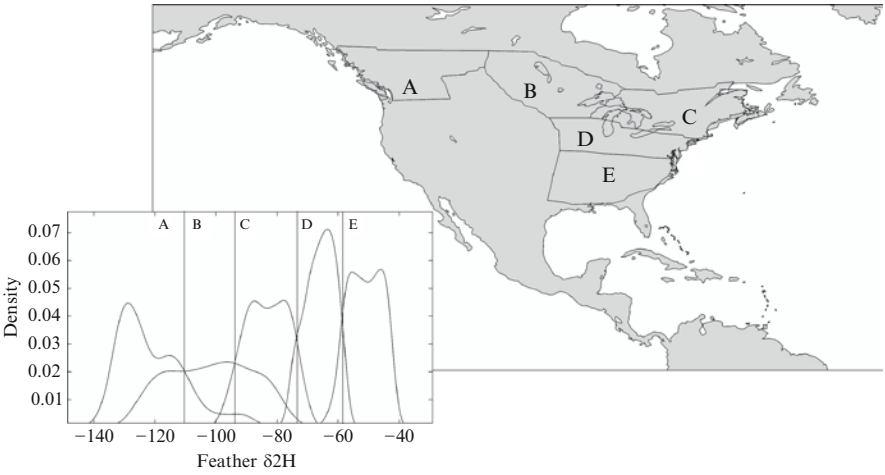

Fig. 12.4 Map showing broadly-circumscribed geographic target ranges for assigning as breeding origins to American redstarts (*Setophaga ruticilla*) sampled during winter as described in Norris et al. (2006) and Wunder and Norris (2008a). Inset shows empirical probability density (smoothed histogram) for each labeled geographic region in hydrogen isotope space, using values from the isoscape in Bowen et al. (2005). *Vertical lines* occur at assignment cutoff thresholds for distinguishing between neighboring regions

Fig. 12.3 (continued) but setting the parameter for analytical error to zero. This illustrates the gains in geographic precision from improving lab practices for measuring δ^2H to the point of perfect repeatability among samples. (**c**) Probability density surface for the same adult bird feather ($\delta^2H = -75‰$) and hierarchical model, but setting the parameter for within-location variance to zero, and restoring the original parameter value for analytical error (see text). This illustrates the gains in geographic precision from improving mechanistic understanding of the variance-generating processes to the point of perfect prediction, but still allowing for measurement error in the lab. All probability densities appear on the same scale as defined by the color bar

bors are not necessarily geographic neighbors. Another potential limitation of the discrete approach is that each jurisdiction of potential origin must be fully characterized, ideally with sample material of known origin. Otherwise any uncharacterized region is considered with probability zero as the origin.

The advantages of a discrete framework are likewise obvious: in many cases, we simply do not have enough training data to adequately calibrate the full extent of the isoscape of interest; a conservative workaround is to use the discrete framework to define regions at broad resolutions that capture the extent of the limited training sample. In other cases, there may be applied management or otherwise politically-motivated situations where the real interest is in fact to determine the weight of evidence for one region as the origin relative to another. In such cases, it makes sense to adopt a discrete framework. However, for many, if not most cases, it is generally more desirable to apply a continuous framework.

12.5 Origin of Populations versus That for Individuals

It is tempting to think that we can improve our models (gain better geographic precision) by increasing sample sizes. However, because isoscape calibrations are not always 1:1 mappings, the geographic location of the sample mean is not the same as the mean of the geographic locations, a point to which I alluded earlier. Furthermore, in cases where the true sample structure is multi-modal, mapping the location for the arithmetic mean will describe a geographic region from which none of the samples actually derived. In other words, for research seeking to find spatial structure, it is universally more advantageous to first generate the probability density surfaces for each individual in the sample and then summarize over the set of spatially explicit surfaces. It is generally uninformative to generate a single spatially explicit probability density surface from population-level summary statistics.

To illustrate this effect, I simulated a bimodal distribution to represent a sample population of unknown-origin birds. The simulated population was a mixture of two normal random variables, one centered on −50‰ and the other centered on −115‰. Figure 12.5a shows the bimodal density associated with this mixture and also the density assuming a normal structure, which has a mean of −92‰ for the mixture. Already, it is clear that by falsely assuming all samples are from the same random process (e.g. are normally distributed) the mean is nowhere near the sample values.

Figure 12.5b and c show the geographically indexed posterior probability densities for the two different approaches. In Fig. 12.5b, the density was generated by first modeling a probability density for each individual sample simulated from the mixture, then computing the mean field from these densities. The density in Fig. 12.5c was generated as a single surface for the mean value of the simulated samples (−92‰). The model presented in Section 12.3.3 was used in both cases.

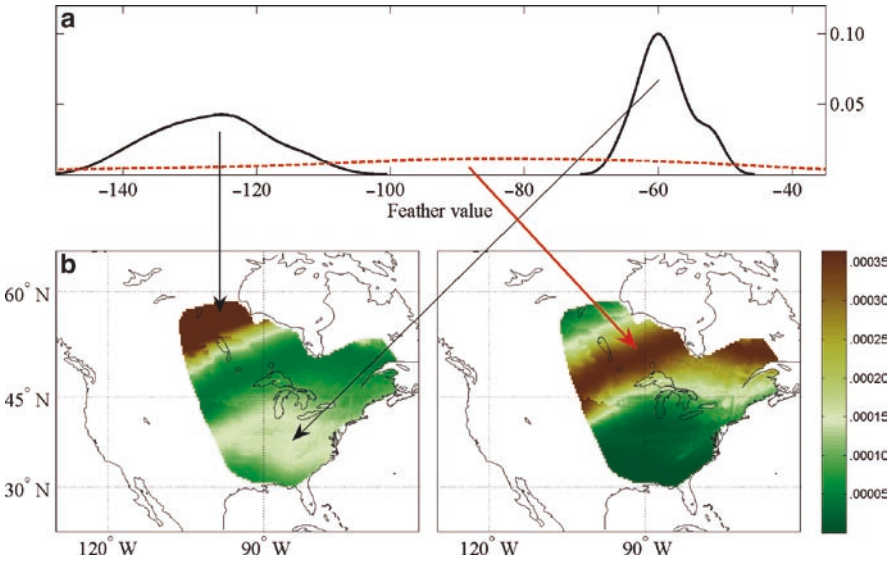

Fig. 12.5 (**a**) Simulated feather δ^2H data from a mixture of two normal random variables. *Solid black line* shows the probability density for δ^2H based on the true bimodal distribution for the simulated feather data. *Dashed red line* indicates the probability density for δ^2H when assuming a normal distribution with a single mode. (**b**) Probability density surface constructed from densities modeled separately for each individual sample. Posterior density shown is average of all individual densities normalized by the sum of all individual densities, clearly showing bimodal structure in geographic space corresponding to bimodal structure in isotope space. *Black arrows* link modes in isotope space with those in geographic space. (**c**) Probability density surface using mean and standard deviation of simulated samples, showing single geographic mode corresponding to single mode in isotope space, with most of the mass where no actual data exist. *Red arrow* links center of mass in isotope space with that in geographic space. Fig. 12.5, see Appendix 1, Color Section

That is, the kernel parameters depended on the isoscape calibration using *known*-origin samples. The simulated data in the mixture shown in Fig. 12.5 represent samples of *unknown* origin that are assumed to individually follow the random process models used in the calibration.

The geographic structure in Fig. 12.5b reflects the true bimodal structure of the mixture. The gradients in Fig. 12.5b faithfully translate variance shape in isotope space to variance shape in geographic space. By contrast, Fig. 12.5c shows the probability density associated with the mean of the simulated samples. Notice that not only does the density for the mean value put most of the probability density in a geographic location from where no samples actually derived, but it also appears more peaked, giving a false sense of heightened precision. The gradients in Fig. 12.5c do not reflect the variance structure in isotope space among the simu-

lated samples. Clearly, the probability surface model for the mean is not the same as the mean of the probability surface models. It is also clear that the more informative approach is to find the geographic structure using individual level probability surfaces, rather than assuming the population structure from the start.

12.6 Concluding Remarks

Wonderfully predictable geographic patterns emerge in many isoscapes. In order to best see these geographic patterns, it is important to focus acutely on the mean value from the isoscape model. Considering variances around the mean isotope pattern can easily obscure pattern elucidation and theory formulation and therefore is of less value for theoretical work. However, for applied problems, patterns from isoscape models are only as useful as their inverses. The most informative inversions will include direct consideration of uncertainty in the original model construct and will provide for an unbiased two-way translation of information. Inverting models without considering variance can lead to very biased results, especially when variances are large and causes of those variances are poorly understood.

I suggest the following points for consideration in the early stages of designing a study using isoscapes to determine origins. Whenever possible, build the isoscape with material that has a known history in space and time; that is, use material of known geographic and temporal origins. Think about how best to characterize variance among sample material synthesized at the same place and time. Is there theory to suggest ways to partition the variance or does the structure of the calibration residuals suggest some particular process or mechanism? Partition the variance whenever possible as this is the shortest way to develop strong feedback between experimental results and applied observational work; reserve the use of single estimates of bulk variance to case-specific studies that feature some pressing applied need. It rarely makes sense to find the probability density for the mean of a population of samples of unknown origin. Because there is not a 1:1 mapping from isotope space to geographic space, it is universally more advantageous to find probability densities for individual samples prior to aggregating over the population of interest.

Isoscapes are powerful constructs for applied studies with geographic forensics as a goal because of their potential to translate isotopic measurements into geographic locations. The goal in this chapter was to determine specific geographic locations from which sampled tissue may have derived, given isotope measurements for the tissue. The isoscape in this case was the translator; it was used to translate the tissue isotope value for a single feather sample into a geographic value. The trick from an applied standpoint is in understanding how much is lost in such a translation and how best to recover the lost information. It is my hope that the methods described in this chapter provide a simple first step in that direction, and that the framework presented here can be readily extended to cases where much more information is at hand.

Acknowledgements I thank the editors for the opportunity to write this chapter. Comments from Gabe Bowen, Jason West, and two anonymous reviewers substantially improved earlier versions of this manuscript. I thank Mirgate and Basin for funding my travel to the Isoscapes meeting in Santa Barbara, CA where I presented the methods described here. In addition, I am grateful to Fritz Knopf, Colleen Webb, Cyndi Kester, Craig Stricker, Craig Johnson, Len Wassenaar, Keith Hobson, Ryan Norris, Pete Marra, Jeff Kelly, and Carlos Martinez del Rio for discussions that shaped both the direction and presentation of this work.

References

Bearhop S, Fiedler W, Furness RW, Votier SC, Waldron S, Newton J, Bowen GJ, Berthold P, Farnsworth K (2005) Assortative mating as a mechanism for rapid evolution of a migratory divide. Science 310:502–504

Benson S, Lennard C, Maynard P, Roux C (2006) Forensic applications of isotope ratio mass spectrometry – a review. Forensic Sci Int 157:1–22

Bowen GJ, Revenaugh J (2003) Interpolating the isotopic composition of modern meteoric precipitation. Water Resour Res 39:1–13

Bowen GJ, Wassenaar LI, Hobson KA (2005) Global application of stable hydrogen and oxygen isotopes to wildlife forensics. Oecologia 143:337–348

Chamberlain CP, Blum JD, Holmes RT, Feng X, Sherry TW, Graves GR (1997) The use of isotope tracers for identifying populations of migratory birds. Oecologia 109:132–141

Clark JS (2007) Models for ecological data: an introduction. Princeton University Press, Princeton, NJ

Cryan PM, Bogan MA, Rye RO, Landis GP, Kester CL (2004) Stable hydrogen isotope analysis of bat hair as evidence for seasonal molt and long-distance migration. J Mammal 85:995–1001

DeLong JP, Meehan TD, Smith RB (2005) Investigating fall movements of hatch-year flammulated owls (*Otus flammeolus*) in central New Mexico using stable hydrogen isotopes. J Raptor Res 39:19–25

Ehleringer JR, Casale JF, Lott MJ, Ford VL (2000) Tracing the geographical origin of cocaine. Nature 408:311–312

Fraser I, Meier-Augenstein W, Kalin RM (2006) The role of stable isotopes in human identification: a longitudinal study into the variability of isotopic signals in human hair and nails. Rapid Commun Mass Spectrom 20:1109–1116

Giuliani G, Chaussidon M, Schubnel HJ, Piat DH, Rollion-Bard C, France-Lanord C, Giard D, deNarvaez D, Rondeau B (2000) Oxygen isotopes and emerald trade routes since antiquity. Science 287:631–633

Hobson KA, Wassenaar LI (1997) Linking breeding and wintering grounds of neotropical migrant songbirds using stable hydrogen isotopic analysis of feathers. Oecologia 109:142–148

Hobson KA, Wassenaar LI, Taylor OR (1999) Stable isotopes (δD and δ13C) are geographic indicators of natal origins of monarch butterflies in eastern North America. Oecologia 120:397–404

Hobson KA, Wilgenburg SV, Wassenaar LI, Hands H, Johnson WP, O'Meilia M, Taylor P (2006) Using stable hydrogen isotope analysis of feathers to delineate origins of harvested sandhill cranes in the central flyway of North America. Waterbirds 29:137–147

Hobson KA, Wilgenburg SV, Wassenaar LI, Moore F, Farrington J (2007) Estimating origins of three species of neotropical migrant songbirds at a gulf coast stopover site: combining stable isotope and GIS tools. Condor 109:256–267

Lott CA, Smith JP (2006) A geographic-information-system approach to estimating the origin of migratory raptors in North America using stable hydrogen isotope ratios in feathers. Auk 123:822–835

Meehan TD, Lott CA, Sharp ZD, Smith RB, Rosenfield RN, Stewart AC, Murphy RK (2001) Using hydrogen isotope geochemistry to estimate the natal latitudes of immature Cooper's hawks migrating through the Florida Keys. Condor 103:11–20

Meehan TD, Rosenfield RN, Atudorei VN, Bielefeldt J, Rosenfield LJ, Stewart AC, Stout WE, Bozek MA (2003) Variation in hydrogen stable-isotope ratios between adult and nestling Cooper's hawks. Condor 105:567–572

Muller W, Fricke H, Halliday AN, McColluoch MT, Wartho JA (2003) Origin and migration of the Alpine Iceman. Science 302:862–866

Norris DR, Marra PP, Montgomerie R, Kyser TK, Ratcliffe LM (2004) Reproductive effort, molting latitude, and feather color in a migratory songbird. Science 306:2249–2250

Norris DR, Marra PP, Bowen GJ, Ratcliffe LM, Royle JA, Kyser TK (2006) Migratory connectivity of a widely distributed songbird, the American redstart (*Setophaga ruticilla*). Ornithol Monogr 61:14–28

Paxton KL, vanRiper IIIC, Theimer TC, Paxton EH (2007) Spatial and temporal migration patterns in Wilson's warbler (*Wilsonia pusilla*) in the southwest as revealed by stable isotopes. Auk 124:162–175

Pyle P (1997) Identification guide to North American birds. Slate Creek Press, Bolinas, CA

Royle JA, Rubenstein DR (2004) The role of species abundance in determining breeding origins of migratory birds with stable isotopes. Ecol Appl 14:1780–1788

Rubenstein DR, Hobson KA (2004) From birds to butterflies: animal movement patterns and stable isotopes. Trends Ecol Evol 19:256–263

Sharp ZD, Atudorei V, Panarello HO, Fernandez J, Douthitt C (2003) Hydrogen isotope systematics of hair: archeological and forensic applications. J Archaeol Sci 30:1709–1716

Wassenaar LI (2008) An introduction to light stable isotopes for use in terrestrial animal migration studies. In: Hobson KA, Wassenaar LI (eds) Tracking animal migration with stable isotopes. Academic, San Diego, CA

Wassenaar LI, Hobson KA (1998) Natal origins of migratory monarch butterflies at wintering colonies in Mexico: new isotopic evidence. Proc Natl Acad Sci U S A 95:15436–15439

Webster MS, Marra PP (2005) Importance of understanding migratory connectivity and seasonal interactions. In: Greenberg R, Marra PP (eds) Birds of two worlds: the ecology and evolution of migratory birds. Johns Hopkins University Press, Baltimore, MD

Wunder MB (2007) Geographic structure and dynamics in mountain plover. Ph.D. Dissertation, Colorado State University

Wunder MB, Norris DR (2008a) Improved estimates of certainty in stable isotope-based methods for tracking migratory animals. Ecol Appl 18:549–559

Wunder MB, Norris DR (2008b) Analysis and design for isotope-based studies of migratory animals. In: Hobson KA, Wassenaar LI (eds) Tracking animal migration with stable isotopes. Academic, San Diego, CA

Part III
Multidisciplinary Applications of Isoscapes

Chapter 13
Using Isoscapes to Track Animal Migration

Keith A. Hobson, Rachel Barnett-Johnson, and Thure Cerling

13.1 Introduction

Animal migration is a phenomenon that has captured the imagination of scientist and layperson alike and continues to fascinate as new insights into the biological mechanisms behind these movements are uncovered. No less fascinating have been the myriad of innovative tools researchers have used to monitor animal movements and to establish linkages between individuals and populations as they move throughout their annual cycles. These tools can broadly be categorized as exogenous and endogenous (reviewed by Hobson and Norris 2008). Exogenous markers are those devices affixed to an animal for later retrieval and so facilitating a mark-recapture approach or as active transmitters that broadcast the location of an animal via radio- or satellite-based technology. More recently, geographic locator tags have been developed that monitor time and daylight cycles that can ultimately be translated into latitude and longitude once downloaded at recapture. However, the most widely used and versatile exogenous marker has been a simple numbered tag or leg band and to date, millions of migratory birds have been so marked. This approach has been moderately successful for those individuals with a high probability of recapture such as hunted species, those with high site fidelity, or those that congregate in large numbers (Hobson 2003). However, the technique is clearly inadequate for most of the world's migratory organisms. This has led to a great deal of interest

K.A. Hobson (✉)
Environment Canada, 11 Innovation Blvd, Saskatoon, SK, S7N 3H5, Canada
e-mail: Keith.Hobson@ec.gc.ca

R. Barnett-Johnson
Institute of Marine Sciences, University of California Santa Cruz, 100 Schaffer Road, Santa Cruz, CA 95060
e-mail: Barnett-Johnson@biology.ucsc.edu

T. Cerling
Department of Geology, University of Utah, Salt Lake City, Utah
e-mail: Thure.cerling@utah.edu

J.B. West et al. (eds.), *Isoscapes: Understanding Movement, Pattern, and Process on Earth Through Isotope Mapping*, DOI 10.1007/978-90-481-3354-3_13,

in the utility of naturally occurring endogenous markers such as stable isotopes and genetic markers. The primary advantage of such approaches is that they do not require initial marking of the organism and so are not biased by the nature of the often limited marked population. Stable isotope markers rely on the principle that, in equilibrium situations, animal tissues reflect the isotopic structure of local foodwebs. Since isotopic patterns in foodwebs can differ spatially, the measurement of isotopic profiles in animal tissues can provide information on animal origins. Thus, animals are linked through foodwebs to underlying isoscapes. This realization has led to a renaissance of interest in describing and predicting isoscapes from local to continental scales as a means to track animal migration (West et al. 2006; Hobson and Wassenaar 2008).

13.2 The Three Principles of Isotopic Tracking

The successful use of isoscape information in animal tracking relies on some simple principles. The first is that the "isoscape terrain" through which the animal of interest moves must be known. In some cases, this can be a relatively easy criterion to meet. Some animals may simply move between biomes with different photosynthetic pathways (e.g. C3, C4, CAM) and so are exposed to foodwebs differing in isotope (especially ^{13}C and ^{2}H) abundance (e.g. Alisauskas et al. 1998; Wolf and Martinez del Rio 2000). Alternatively, they may move across a geological substrate that is a gradient between young and old formations that in turn represents a gradient in relative abundance of ^{87}Sr (Barnett-Johnson et al. 2008). However, in many cases, isoscapes are less well categorized and moreover, the researcher may be unaware of all *possible* isoscapes visited by the organism prior to capture.

The second principle is that isotopic values in animals can be offset from baseline isoscape values due to isotopic discrimination and such discrimination factors need to be known for the tissue of interest (Hobson and Clark 1992a). Other physiological processes should be known as well, including metabolic routing of specific macronutrients from diet to specific animal tissues, and other processes that can change tissue isotope ratios once the animal is in equilibrium with a foodweb. The third principle is that the time period of spatial integration corresponding to a particular animal tissue is known. For metabolically active tissues, the time period over which the spatial information is available will differ due to different tissue elemental turnover rates. Fast turnover tissues will represent short periods of dietary information and slow turnover tissues will represent longer periods (Hobson and Clark 1992b). For metabolically inactive tissues like feathers, hair and nail, a longitudinal isotopic record of previous origins is possible. The successful application of isoscapes to animal tracking requires, then, an understanding of baseline isoscape pattern, tissue-specific isotopic discrimination and patterns of turnover. Not all applications of the stable isotope method to tracking animal movements will meet all of these criteria. This is not to suggest that they cannot still provide useful information that might, for example, eliminate *possible* origins. However, we should

all strive to improve our understanding and consideration of these principles in future work. The following sections will address each of these components in turn.

13.3 Isoscapes

We primarily consider terrestrial and freshwater isoscapes that have potential in animal tracking studies. There is also a great deal of interest in the development of marine isoscapes in order to assist the tracking of marine mammal and fish stocks but this field is less advanced currently (but see Graham et al. 2009, this volume). The extent of the world's oceans and complexity of processes influencing baseline foodweb isotope values makes this a challenging area deserving its own treatment. We refer the interested reader to consider the detailed zooplankton marine isoscapes for $\delta^{13}C$ and $\delta^{15}N$ developed for the Bering, Chukchi and Beaufort seas by Schell et al (1998) and to the use of the subtropical convergence isotopic threshold in the Southern Ocean for tracking movements of the Southern Right Whale (*Eubalaena australis*, Best and Schell 1996). Other researchers have inferred feeding origins of seabirds in the southern hemisphere based on a pronounced depletion in foodweb ^{13}C with latitude (Cherel and Hobson 2007; Quillfeldt et al. 2005). Elsewhere, researchers have broadly inferred inshore and offshore feeding of marine vertebrates based on relatively ^{13}C depleted pelagic vs. benthic marine foodwebs (Hobson et al. 1994; Reich et al. 2007). Recently, Popp et al. (2007) investigated compound-specific analyses of individual amino acids in Yellowfin Tuna (*Thunnus alnacares*). That study did not address marine isoscapes per se but did reveal that it may be possible to infer marine isoscape patterns more readily by using isotopic analyses of essential amino acids of top predators since these amino acids should not be affected by trophic level and so will be more directly related to baseline source values.

13.3.1 C3/C4/CAM ($\delta^{13}C$, δD)

Isoscapes related to photosynthetic physiology of plants have received much attention and are covered in greater detail elsewhere in this book. These isoscapes involve the use of $\delta^{13}C$ measurements to distinguish C3, C4 and CAM metabolism which is, in turn, influenced largely by climatic factors and so can vary spatially across continents or with altitude. CAM plants can additionally be distinguished from C4 plants through the use of δD measurements (e.g. Wolf and Martinez del Rio 2000). Similarly, plant $\delta^{15}N$ values can be modeled based on climate variables known to influence plant metabolism but this isotope is inherently more difficult to model as an isoscape due to numerous other factors such as agriculture and anthropogenic landscape changes and modification of soils (Nadelhoffer and Fry 1994; Pardo and Naddelhoffer 2009, this volume). Additionally, because trophic position strongly influences animal tissue $\delta^{15}N$ values, placing organisms to $\delta^{15}N$ isoscapes requires a good understanding of isotopic discrimination.

Some of the earliest terrestrial studies involving the forensic use of isotopes in investigations involving animal tissues were based on the use of $\delta^{13}C$ measurements to track relative use of C3 and C4 plants. Initially, these applications dealt with archaeological investigations of the use of corn by ancient human populations in the New World (Burger and Van der Merwe 1990). The use of corn by migratory birds can also provide information on previous movements since corn-growing regions are often well known at continental scales (Alisauskas et al. 1998). The development of C4 agricultural isoscapes based on corn production (and to a lesser extent on production of other C4 crops like sorghum and sugar cane) are feasible and could be used to track those species known to use agricultural landscapes. This would be particularly useful when combined with δD measurements that could provide latitudinal information. For example, Wassenaar and Hobson (2000) showed a strong segregation between two groups of Red-winged Blackbirds (*Agelaius phoeniceus*) clearly related to corn consumption in agricultural areas and further associated those corn areas with more northern latitudes in the USA using feather δD values. Such agricultural isoscapes based on corn production might be particularly dynamic given recent interest in using corn for ethanol production in North America and so it will probably require year-specific isoscape information for any given animal tracking study of interest.

Mapping discrete distributions of C4 crops in an otherwise C3 landscape, while useful for some applications, will be generally less important than the use of isotopic gradients associated with large spatial scales. In such cases, animals of interest will be associated with more natural plant communities. In North America we generally expect an increase in $\delta^{13}C$ values in plant communities with decreasing latitude and increasing altitude (Graves et al. 2002; Hobson et al. 2003). However, in their development of a combined $\delta^{13}C$ and δD isoscape of Monarch Butterfly (*Danaus plexippus*) wing chitin for the eastern North American breeding population, Hobson et al. (1999) found that monarch wing $\delta^{13}C$ increased with latitude, a phenomenon presumably associated with the isotopic composition of host milkweed (*Asclepia* spp.). Thus, some ecological situations will clearly require the ground truthing of expected isoscape patterns.

Isoscapes modeled on the expected proportion of C3 and C4 plants across landscapes is one product of use to researchers interested in tracking migratory animals. However, enrichment in C3 plant $\delta^{13}C$ values due to mechanisms associated with water-use efficiency have also proved useful. The classic example of this was provided by Marra et al. (1998) who showed that American Redstarts (*Setophaga ruticilla*) wintering in xeric habitats in Jamaica were enriched in ^{13}C compared to those wintering in moist habitats. Such differences in habitat occupancy on the wintering grounds were connected to departure times and actual expected breeding success. This concept of seasonal interactions established through the isotopic measurement of bird tissues grown on the wintering grounds has led to great interest in using stable isotopes to infer past habitat use by migrant species (Hobson 2008; Marra et al. 2006). Further development of $\delta^{13}C$ isoscapes associated with the wintering grounds is needed as well as refinements in our understanding of how this isotope can be used to infer habitat conditions. Certainly, any $\delta^{13}C$ isoscape that models expected average plant community values due to a variety of biogeographic and physiological processes will potentially assist with animal tracking.

13.3.2 Deuterium and ^{18}O in Precipitation and Surface Waters

It has long been recognized that deuterium and ^{18}O abundance in precipitation in North America show a continent-wide pattern with a general gradient of relatively enriched values in the southeast to more depleted values in the northwest (Sheppard et al. 1969; Taylor 1974). These patterns, populated largely by data from the long-term International Atomic Energy Agency (IAEA) Global Network of Isotopes in Precipitation (GNIP) database are among those now described for most regions of the world (Bowen et al. 2005). While this program was never designed to create regional isoscapes for these elements, it has nonetheless by default provided the backbone for the use of such isoscapes in animal tracking. The first major linkage between the abiotic precipitation isoscapes and plant material was provided by Yapp and Epstein (1982). Cormie et al. (1994) then showed an excellent correlation between δD in deer bone collagen and average growing season precipitation δD. That work inspired Chamberlain et al. (1997) and Hobson and Wassenaar (1997) to examine how well such precipitation isotope values were passed on to birds growing feathers at known locations at a continental scale across North America. The strong correlation ($r^2 = 0.89$) measured by Hobson and Wassenaar (1997) between feather δD and the mean growing season average precipitation δD for forest songbirds across the central part of the North American continent indicated the immense potential seemingly too good to be true. Fortunately, that large-scale spatial pattern has since been confirmed by several other researchers on various avian species (Hobson 2008) as well as bats (Cryan et al. 2004).

Few measurements of $\delta^{18}O$ have been conducted on tissues of migratory organisms due primarily to the only recent developments using pyrolysis combustion allowing such measurements. However, Fourel et al. (1998) showed a strong relationship between δD and $\delta^{18}O$ for chitin in wings of Monarch Butterflies demonstrating that the meteoric relationship between these two elements can be passed on up the foodweb. This opens up the possibility of inferring environmental and spatial information by measuring both isotopes in tissues of migratory animals. Recently, Ehleringer et al. (2008) showed excellent agreement between drinking water δD and $\delta^{18}O$ measurements and those in human hair across the United States. The current challenge is that oxygen can be fixed in animal tissues through diet, air, and drinking water and it is just not clear how departures from the meteoric relationship should be interpreted. Nonetheless, heat stress in animals and evapotranspiration in local environments are expected to change the relationship between tissue δD and $\delta^{18}O$ in animal tissues and so may be useful in identifying those individuals coming from specific habitats like deserts.

13.3.3 Strontium Isotopes ($^{87}Sr/^{86}Sr$) and the Heavy Element Advantage

The natural variation in strontium isotopes ($^{87}Sr/^{86}Sr$) is becoming increasingly used in animal migration research, especially to track movements of fish among aquatic

ecosystems (Kennedy et al. 2002; reviewed by Rubenstein and Hobson 2004; Barnett-Johnson et al. 2008). One advantage in using a heavy isotope system to track animal movements compared to light isotopes is that there is usually negligible or no isotopic fractionation from geologic sources through foodwebs and into tissues. The lack of Sr isotope fractionation between dietary inputs and tissues has been shown for a variety of different animals and skeletal tissues including antlers from reindeer (Aberg 1995), elephant, mammoth, and mastodon bone and tusks (Vogel et al. 1990; Koch et al. 1995; Hoppe et al. 1999), marine and freshwater fish teeth, vertebrae, and otoliths (Koch et al. 1992; Kennedy et al. 1997; Ingram and Weber 1999), and human teeth and bones (Ezzo et al. 1997). For some freshwater vertebrates, such as fish, dissolved Sr in water is the primary source of Sr in tissues, although prey and water Sr sources are usually isotopically identical (for exception due to aquaculture see Ingram and Weber 1999; Walther and Thorrold 2006; Kennedy et al. 2000). Thus, the use of $^{87}Sr/^{86}Sr$ as a tracer for animal migrations has explicitly focused on identifying geographic regions that an animal has inhabited based on different regional geologies.

There are three stable isotopes of Sr: ^{88}Sr (82.53%), ^{86}Sr (9.87%), and ^{84}Sr (0.56%). The ^{87}Sr isotope of Sr (7.04%) is radiogenic and is produced by the beta decay of ^{87}Rb (half-life = 48.8×10^9 years), which contributes to the distinctly different ^{87}Sr abundances and $^{87}Sr/^{86}Sr$ ratios across different parts of the landscape. It is well known from over three decades of geologic research that variations in $^{87}Sr/^{86}Sr$ are a function of both the age of the crust and distinctive Rb/Sr ratios in rock types. For example, rocks that are older and ones that have high Rb/Sr ratios (e.g., sandstone, shale and granites) have higher $^{87}Sr/^{86}Sr$ ratios than younger rocks or rock types with low Rb/Sr ratios (e.g., basaltic lavas, limestone, and marble; Faure 1977; Aberg 1995).

Sr isotopes are ideal markers for the development and use of isotope mapping because of the lack of biotic fractionation, well-documented geologic mechanisms creating spatial variation across the landscape, and low temporal variability (Graustein 1989; Blum et al. 2000; Kennedy et al. 2000). The only published example of a large-scale Sr isoscape models bedrock $^{87}Sr/^{86}Sr$ of the United States as a function of rock age (Beard and Johnson 2000). This approach is particularly useful for constraining the location and habitat of migrants at a large-scale. However, many studies have empirically measured $^{87}Sr/^{86}Sr$ and found significant variation on finer spatial scales largely due to variation in rock type (Kennedy et al. 1997; Hoppe et al. 1999; Barnett-Johnson et al. 2008). Not quantifying $^{87}Sr/^{86}Sr$ variation on small-scales can confound classifications and limit the utility of Sr isoscapes depending on the scale of migration of an animal.

Several characteristics of $^{87}Sr/^{86}Sr$ incorporation and analyses may limit its broad use across taxa (reviewed by Wassenaar 2008). Sr occurs at low concentrations in non calcium-bearing tissues like bird feathers (<20 μg Sr/ g) and requires costly and extensive wet chemistry to isolate Sr for isotopic analyses typically on a thermal ionization mass spectrometer (TIMS; Kennedy et al. 1997; Font et al. 2007). These constrains have limited their use over light isotopes in bird migration research. In contrast, Sr occurs in much higher concentrations (e.g., > ten times that of feathers)

in bony tissues (e.g., teeth, bones, otoliths) and is growing in use in fish migration research, wildlife forensics (e.g., deer), and human migration applications (Beard and Johnson 2000). Kennedy et al. (1997) found that different bony tissues within individual juvenile Atlantic salmon (*Salmo salar*) in a river have the same Sr isotopic values (e.g., otoliths, vertebrae), although overall Sr/Ca may vary and turn-over rates for different tissue types may need to be considered once individuals migrate into areas characterized by different $^{87}Sr/^{86}Sr$ sources.

Recent advancements in analytical instrumentations have contributed to the elevation of $^{87}Sr/^{86}Sr$ from a specialized assay to large sample size applications (Hobbs et al. 2005; Walther and Thorrold 2008). Precise measurements of $^{87}Sr/^{86}Sr$ can be achieved with multi-collector inductively coupled plasma mass-spectrometry (MC-ICPMS) in geologic and biologic samples thereby significantly decreasing analytical costs, increasing sample throughput and eliminating the need for extensive wet chemistry (Ramos et al. 2004). In addition several new applications in fisheries science can be pursued because of laser ablation capabilities with MC-ICPMS which allow reconstructions of fish migrations from the daily growth rings recorded in otoliths at high temporal resolutions of movement (e.g., 10 days; Barnett-Johnson et al. 2005; Woodhead et al. 2005).

13.4 Isotopic Discrimination and Physiological Considerations

For many elements, only slight changes in stable isotope ratios occur between trophic levels after they are fixed by plant tissues. Isotopes of sulfur and possibly hydrogen fall into this category along with the heavier elements like Sr. While overall ^{13}C discrimination between diet and the whole body of animals is relatively small (i.e. of the order of 1‰), tissues differ in the amount of isotopic discrimination and absolute values for keratinous tissues can be significant. Trophic discrimination associated with ^{15}N is substantial (of the order of 3.4‰; Post 2002) and has been used as a trophic indicator. Relating animal tissues to ^{15}N isoscapes will therefore require careful consideration of the trophic level of the animal of interest. Also, stable nitrogen isotopes in the tissues of consumers really represent a means of tracing protein pathways derived from diet since this element is largely absent in lipids and carbohydrates. For essential amino acids, nitrogen will largely be incorporated with little isotopic discrimination into the protein pool of the consumer. Non-essential amino acids typically involve more opportunities for isotopic discrimination during protein synthesis and so the net discrimination we see for $\delta^{15}N$ measurements in consumers will reflect the degree to which the diet meets the amino acid requirement of the consumer (Robbins et al. 2005). Isotopic discrimination associated with $\delta^{15}N$ will also depend on the means of voiding nitrogenous waste. Here, a major difference is found between aquatic invertebrates that void nitrogen via ammonia compared to terrestrial vertebrates (Post 2002). Hobson et al. (1993) also determined that birds that fast and undergo significant protein catabolism during incubation, like geese breeding at high latitudes, also experience an increase in body $\delta^{15}N$

values. Knowledge of these sorts of physiological processes is necessary, then, when using tissue $\delta^{15}N$ values of migratory organisms to infer origins. The current consensus is that researchers should strive to use the most parsimonious value associated with their specific organism of interest. The review of isotopic discrimination in $\delta^{15}N$ across several taxa by Vanderklift and Ponsard (2003) identified mode of excretion and environment (marine, freshwater aquatic, terrestrial) as important factors (see also Post 2002).

Isoscapes of ^{15}N for use in tracking migratory animals are complicated by the fact that ^{15}N in foodwebs can be influenced by several factors, not the least of which is the trophic level of the target individual or species. Plant ^{15}N is influenced by the mode of nitrogen fixation but also by ambient temperature and moisture. In addition, anthropogenic influences such as land clearing and use of fertilizer influence plant $\delta^{15}N$ values (Pardo and Naddelhoffer 2009, this volume).

13.5 Isotopic Turnover

The concept of isotopic turnover in animal tissues is fundamental to understanding how stable isotope values can be interpreted as a temporal record of past movements. Such information, together with an understanding of the isotopic differences between isoscapes used by individuals can define the statistical power of inference applicable to a particular question of tracking (Hobson 2008). The larger the isotopic difference between any two isoscapes and the slower the turnover in tissues of interest, the greater the time over which previous use of one isoscape over the other can be detected. Previous researchers have attempted to experimentally derive isotopic turnover using diet-switch experiments. Recently, this field has received more attention as different ways of interpreting patterns of isotopic turnover in animals have been explored. These include a move away from fitting a simple exponential decay function to the data. These new approaches have identified that in some situations more than one nutrient pool is involved in tissue synthesis and this has important ramifications for tracking migrants.

A first order rate constant is:

$$\frac{dN}{dt} = -\lambda N \tag{13.1}$$

where N is the number of atoms or molecules in the system being described, t is time (s), and λ is the rate constant (s^{-1}). Integrated, this is:

$$N = N_0 e^{-\lambda t} \tag{13.2}$$

For isotope ratios, this in analogous to:

$$\frac{R_A^t - R_A^{eq}}{R_A^{init} - R_A^{eq}} = e^{-\lambda t} \tag{13.3}$$

where R_A^{init} is the initial isotope ratio ($t = 0$), R_A^{eq} is the isotope ratio at equilibrium (t = infinity), and R_A^t is the isotope ratio at time t, respectively. Using the δ-notation, this becomes:

$$\frac{\delta_A^t - \delta_A^{eq}}{\delta_A^{init} - \delta_A^{eq}} = e^{-\lambda t} \tag{13.4}$$

multiple components that contribute to the system

By treating the system as having first-order reaction kinetics, it is often possible to resolve multiple components that contribute to the system. Experiments designed to derive turnover rate constants usually involve a diet or water "switch" from the initial conditions to those with a very different isotope ratio. Recent work has shown that some tissues exhibit "multiple turnover pools" (e.g., hair, liver, or muscle; Ayliffe et al. 2004; Zazzo et al. 2007; Sponheimer et al. 2006; Martinez del Rio and Anderson-Sprecher 2008) whereas other body tissues or fluids exhibit only one turnover pool (e.g., blood plasma, red blood cells, bodywater/breath; Podlesak et al. 2008). Many experiments have not been designed to identify multiple pools, in part because of the difficulty in obtaining many samples immediately following a diet or water switch and more fundamentally because a single exponential decay function was assumed to adequately fit the data; we expect that this will change in the next decade as experiments are designed to detect multiple turnover pools. Likewise, compound specific analyses may show that individual components of tissue may have different turnover rates (e.g., essential versus non-essential amino acids).

The understanding of isotope turnover is particularly useful in interpreting dietary histories from sequential samples. This can help place an individual on an "isoscape" at a particular time, or can otherwise show changes in diet or water resource use. For a first-order reaction, each isotope pool changes with time as (from Cerling et al. 2007):

$$\delta_j^t = \delta_j^{(t-1)} \mathrm{e}^{-\lambda_j(\Delta t)} + \delta^{eq}(1 - \mathrm{e}^{-\lambda_j(\Delta t)}) \tag{13.5}$$

where $\delta_j^{(t-1)}$ is the isotope value of pool j at time $(t - 1)$, and Δt is the difference in time between "$t - 1$" and "t". For a change in isotope input value, the isotope value δ_j^t can be calculated as a function of time using this equation if δ^{eq} is known. For the case where the δ^{eq} can be related to a known fractionation factor α, a dietary history can be reconstructed from a sequence of hair samples by (Cerling et al. 2007). The following equation is for the case of three isotope turnover pools:

$$\delta_D^{(t)} = \frac{\left(\frac{\delta_H^{(t)} + 1000}{\alpha_{HD}} - 1000\right) - \left(\sum_{j=1}^{3} f_i \delta_j^{t-1} e^{-\lambda_j \Delta t}\right)}{\left(\sum_{j=1}^{3} f_i \left(1 - e^{-\lambda_j \Delta t}\right)\right)} \tag{13.6}$$

where $\delta_D^{(t)}$ is the isotopic composition of diet at time "t", $\delta_H^{(t)}$ is the isotopic composition of an individual hair segment in a sequence of hair samples at time "t", α_{HD} is the isotope fractionation factor between tissue and diet (written as enrichment), f_j is the fractional contribution of each isotope turnover pool, $\delta_j^{(t-1)}$ is the isotope composition of the hair segment older than the one being measured ($t - 1$), and Δt is the difference in time between segment "i" and segment "$i,t - 1$". In this analysis it is often the case that the shortest turnover pools equilibrate very rapidly (within one or two sampling intervals) whereas the longest turnover pools never reach equilibrium; therefore it is necessary to make a best "guess" for the isotopic composition of the longest pool: Cerling et al (2007) suggest that the long term average value for that pool is appropriate unless other knowledge of the dietary history is known.

How important is the detailed knowledge of the various fractional contributions and the values of the various turnover pools? Is a "close approximation" good enough for "isoscape location?" We provide an example that compares several different models for turnover times of two pools. For the case of hair, various research groups have found that multiple pools contribute to the isotopic composition of carbon in hair: in particular they find that there is one (or more) pool(s) with a half-life of a few days or less, and a pool that is much longer. Further, most groups have found that these contributions are subequal (between the proportions 70/30 and 50/50). Ayliffe et al (2004), Zazzo et al. (2007), and Podlesak et al. (2008) found the long pool to have half-lives of ca. 140, 70, and 140 days for horses, cows, and woodrats, respectively. The half-lives and turnover of ^{15}N is not known for these studies because none of them had a large enough $\delta^{15}N$ difference in the starting and final conditions; however, the observed isotope enrichment for most herbivorous mammals is ca. 3‰ for normal or poor-protein diets (i.e., excluding high protein diets; Sponheimer et al. 2006). We model the diet input for an individual elephant (*Loxodonta africana*) known to occupy two regions: semi-arid bushland to montane forest (Cerling et al. 2006). We calculate the diet as described above for four models: one is the instantaneous equilibrium with the environment ($t_{1/2} < 2$ days for all pools), and three models with a short half-life (< 2 days) and a long half life (70, 100, or 140 days, respectively). All models use equal contributions (50:50). Figure 13.1 shows calculated diets for the four different models given above; it is evident that for this case, what is important is that both "long" and "short" pools exist but that the absolute half-lives of the "long" pools are relatively unimportant.

The individual elephant occupied two regions, spending most of his time in one region with short "expeditions" to another region where he resides, at most, a few months a year. Tracking the isotope composition of the "long" and "short" pools shows that the "short" pool is always in equilibrium with the local environment, while the long pool is strongly dominated by the long-term resident environment and that the relatively short visits to the new environment are not long enough to change the isotopic ratio of the "long" pool. The net result of this is that all models, including instantaneous equilibrium with the environment, predict a similar diet for the region where the individual spends most of his time; however, the "instantaneous" equilibrium model predicts a different environment than all dual-pool models

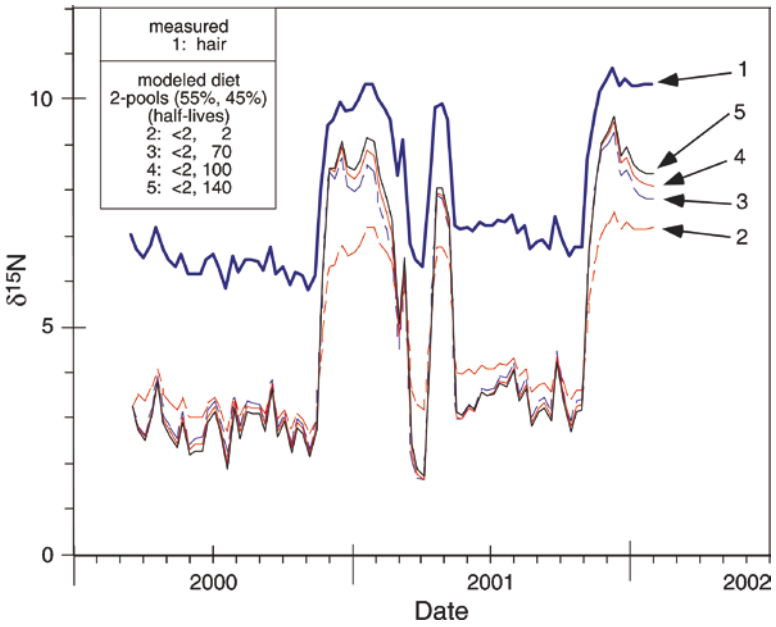

Fig. 13.1 Measured hair values from a migrating African elephant and modeled diets using the 2-pool model described in text. Migration was from a region of high $\delta^{15}N$ values to one of low $\delta^{15}N$ values; transit time between the regions was less than 12 h based on GPS observations (Cerling et al. 2006). Model results are for "one-pool" (all half-lives less than sampling interval), and three scenarios where the long pool had 50% contribution but half-lives of 70, 100, and 140 days, respectively. This sensitivity study shows that the multiple pool model is different than the single pool model, but that the length of the long pool is less important than the fact that there are two pools present. Fig. 13.1, see Appendix 1, Color Section

which do not differ substantially. This exercise illustrates that the "apparent" enrichment between diet and tissues is different in the different environments, and that this is a result of a non-equilibrium condition where the long turnover times for one of the pools contributes differentially to the tissue being studied. Clearly, appropriate models should be used to determine the environmental "isoscapes" occupied during migration of animals. Fortunately, however, this model shows that the exact parameters of all models do not have to be determined in all cases to make good estimates of the environmental history of individuals.

13.6 Some Key Case Studies

13.6.1 Birds and Insects

Bird feathers and insect wing chitin are two very useful materials for isotopic tracking of movements because they are essentially inert following formation and so provide information on origin during the relatively short period of formation.

Once considerations of the importance of single vs. multiple pool nutrient sources are resolved (and it has generally been assumed but rarely shown explicitly that bird feathers overwhelmingly reflect diet during feather growth, but see Fox et al. 2009) the molt phenology, and hence choice of feather for analysis, of a particular species will be crucial to interpretation. Unfortunately and somewhat surprisingly, molt phenology is often not well understood for all species, particularly at the population or sub-species level and some researchers have confused problems with isotope data and problems with their understanding of molt (Larson and Hobson 2009). However, when details of molt are known, researchers have been able to use more than one feather type per individual to infer origins at different periods of the annual cycle (Mazerolle and Hobson 2005). Similar arguments apply to periods of hair growth in mammals (Britzke et al. 2009).

The first true animal isoscape was produced by Hobson et al. (1999) who investigated where Monarch Butterflies that wintered in Mexico originated in their eastern North American breeding areas. That study created an isotopic basemap or isoscape corresponding to δD and $\delta^{13}C$ values in butterfly wing chitin. Interestingly, that isoscape was produced with the help of 80 elementary schools across the range. Young students raised butterflies from eggs on host milkweed plants in gardens receiving only natural precipitation. Wing chitin isotope values were then measured from 1,300 individuals collected at all known roost sites in Mexico the winter following the creation of the isoscape (i.e. corresponding directly to the production year of interest). So, these authors created the δD and $\delta^{13}C$ isoscape relevant to the period of interest. Since this isoscape was based on the actual tissue measured (i.e. wing chitin) no correction was required linking abiotic or foodweb isotope values to butterfly wing isotope values. This approach, although laborious, satisfied the three principles of tracking using isoscapes. Unfortunately, the creation of a species-specific tissue isoscapes for the year of interest is beyond the realm of possibility for most applications.

Since then, relatively few studies have used stable isotopes to track migratory insects (but see Brattström et al. 2008) despite the fact that a great deal of potential exists for this taxon. One complicating variable with insects is that many species of interest are agricultural pests and originate in cropland that has been irrigated with groundwater. This potentially undermines the use of the water isoscape products based primarily on the GNIP precipitation dataset.

The greatest advances in using isoscapes to track migration has been those concerned with birds and chiefly using the continental deuterium in precipitation patterns. Two key papers are noteworthy. The first by Kelly et al. (2002) showed that western North American populations of Wilson's Warbler (*Wilsonia pusillus*) undergo a leapfrog migration to their wintering grounds in Central America whereby more northern breeding populations fly over more southern populations to winter the furthest south. The other study involved an establishment of migratory connectivity between breeding and wintering grounds of Black-throated Blue Warblers (*Dendroica caerulescens*). In that study, Rubenstein et al. (2002) also made use of a longitudinal gradient in feather $\delta^{13}C$ values to better delineate origins. These studies were important because they represented insights into the migratory connectivity of

these populations that simply could not be achieved without the use of stable isotope measurements and an *a priori* knowledge of isoscape pattern. However, neither study attempted to provide a rigorous statistical treatment of the confidence of assignment of individuals and this remains an area of much needed development (see below).

In an extensive analysis of over 700 individuals taken throughout the autumn migratory central flyway in North America, Hobson et al. (2006) delineated origins of both adult and young-of-the-year Sandhill Cranes (*Grus canadensis*). That study revealed that the region with greatest production of young contributing to the flyway differed spatially from the area from which adult birds were derived (Fig. 13.2). This result has profound consequences for the management of this species. The approach used by Hobson et al. (2006) in that and other studies (Wassenaar and Hobson 2001a; Hobson et al. 2007) was to consider a fixed discrimination factor between the deuterium growing season average precipitation isoscape and feathers and use this in an additive fashion in GIS to produce a feather δD isoscape. That discrimination factor was derived from previous experimental and observational studies and reinforced from analysis of regression results of modeled precipitation and measured feather δD values (Hobson 2008). They then delineated those regions on the feather isoscape corresponding only to the breeding distribution of this species and then further depicted origins as falling within isocontours defined by percentiles (Fig. 13.2). That approach is straightforward and has considerable appeal. However, the approach does not propagate error associated with our estimate of a precipitation to feather discrimination. Hobson et al. (2006) performed a sensitivity analysis on their results to determine the effect of altering their discrimination factor by ±5‰ but more advanced statistical approaches are now possible to propagate error associated with tissue isoscapes and, more appropriately, to depict probability of origin surfaces (Wunder and Norris 2008).

13.6.2 Mammals

Like bird feathers and claws or whale baleen plates, animal hair, claws and hooves can provide an isotopic chronology of past movements, diets, and biomes (Barnett 1994; Drucker et al. 2008). Sequential sampling of such tissues holds great promise when combined with knowledge of isoscape patterns encountered by migratory mammals. These studies will be enhanced by investigations of tissue growth rates and how these change seasonally and with diet quality.

There has been considerable interest in using isoscapes to infer previous origins of mammals. An early seminal study involving Bowhead Whale (*Balaena mysticetus*) migration from the Beaufort to the Bering Chukchi seas using $\delta^{13}C$ and $\delta^{15}N$ measurements of the baleen plates of these animals (Schell et al. 1988). That study was also based on a clear understanding of the marine isoscape through which whales moved (see Schell et al. 1998). More recently, other isotopes and trace elements have been used to see how well they correlate with annual movements of western

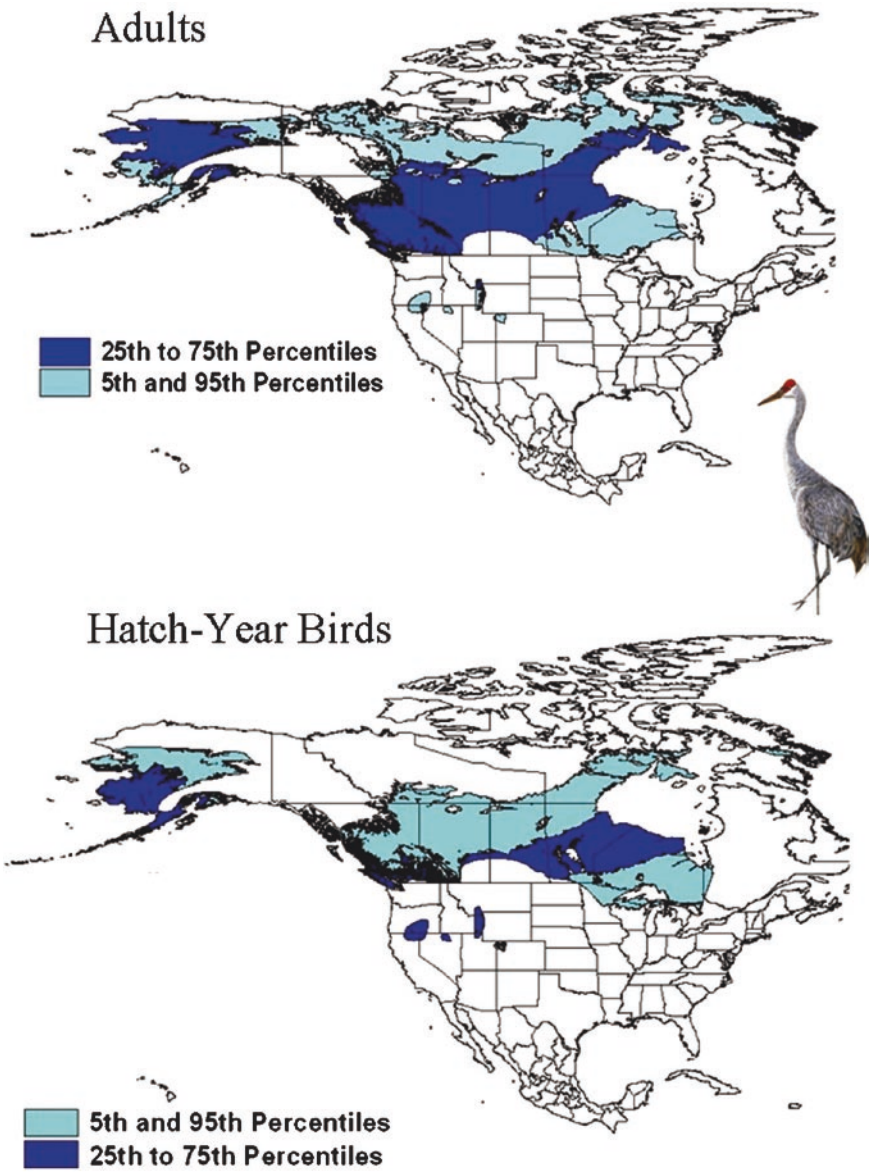

Fig. 13.2 Depictions of the origins of adult and young-of-the-year Sandhill Cranes based on the distributions of their feather δD values and the use of a feather δD isoscape in turn derived primarily from the GNIP database. This figure illustrates one means of depicting origins of migratory organisms without error propagation. Results are based on Hobson et al. (2006) who examined over 700 individuals harvested by hunters in the Central Flyway and provide important conservation information on where most young were produced. Fig. 13.2, see Appendix 1, Color Section

Bowhead Whales. Hobson and Morrison examined δD values along the plate of a Western Bowhead Whale taken in the Beaufort Sea region of western Canada. That individual showed characteristic oscillations in baleen δD consistent with its annual migration between relatively deuterium depleted waters of the Beaufort to the more enriched values of the Bering and Chukchi seas where these whales winter (Fig. 13.3). A positive drift in baleen δD values between more recent and older portions of the baleen may have been due to increased freshwater input from the Mackenzie River in more recent times but that remains to be tested. Importantly, this example illustrates that isotopic baselines associated with isoscape patterns may change due to biotic and abiotic processes (see also Cullen et al. 2001; Schell 2001). We suspect that δD and $\delta^{18}O$ measurements may be useful markers at high latitudes in marine systems.

In terrestrial applications, early attempts to trace origins of African ivory using isotopes of light and heavy elements based on measured values of source populations at specific reserves or national parks did not involve the use of isoscapes *per se* but did rely on isotopically defined source populations. That approach is also amenable to the use of trace element analyses (Szép et al. 2003) because populations of interest can be typed or categorized since baseline values, in turn determined by soils or geological substrates, are expected to remain relatively unchanged.

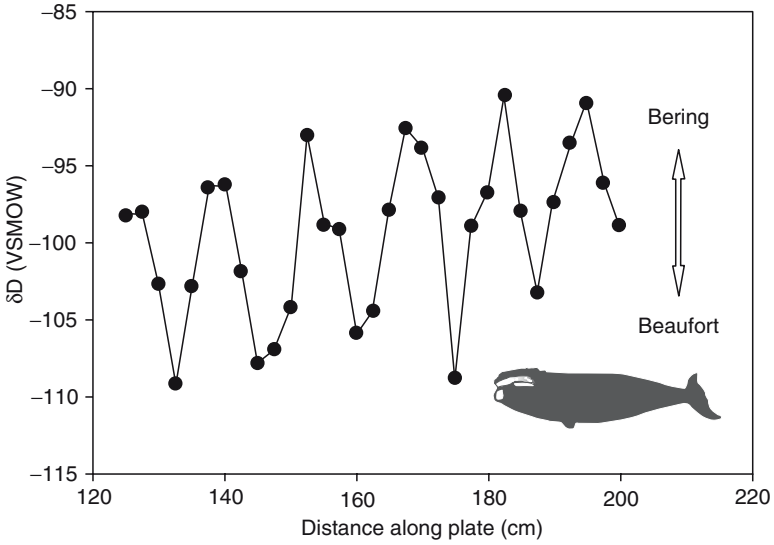

Fig. 13.3 Baleen δD values from a western Bowhead Whale annually moving between the eastern Beaufort and the Bering and Chuckchi seas. This illustrates that high-latitude marine isoscapes are a possible resource for tracking migratory marine mammals and fish

Cormie et al. (1994) was the first to associate bone collagen δD values of deer to those expected from the mean growing season average precipitation surface. Since then, relatively few applications to questions of terrestrial animal migration have been conducted although Cerling et al. (2006) have continued to look at individual movements of animals relative to expected or measured isoscapes. An exception has been the investigation of Cryan et al. (2004) who derived a regression between hair δD values of bats and the precipitation δD isoscape for North America. That study should encourage further use of a bat hair δD isoscape to infer origins (e.g. Britzke et al. 2009). One of the fundamental problems with the application of the stable isotope tracking technique to bats is that their hair growth periods are often poorly understood and their ability to revert to torpor and their active mobilization of body nutrients during lactation renders them a problematic group.

13.6.3 Fish

Otoliths are structures in the inner ears of fishes which grow by the daily deposition of calcium carbonate and protein layers throughout the life of a fish. Elements (e.g., Sr) in the surrounding waters substitute for calcium and get incorporated into the fish otolith. Since otoliths are metabolically inert, their isotopic composition can provide a permanent chronology of different water masses or habitats occupied by a fish and are ideal structures for reconstructing movement patterns.

Sr isotope ($^{87}Sr/^{86}Sr$) ratios in otoliths are powerful tools to address fundamental questions in fish ecology, conservation, and fisheries management. $^{87}Sr/^{86}Sr$ in otoliths have been used to identify natal freshwater habitats (Kennedy et al. 1997; Ingram and Weber 1999; Barnett-Johnson et al. 2008), track small-scale freshwater movement patterns (Kennedy et al. 2000), and chronicle timing of migration between marine and freshwater environments (Koch et al. 1992; Bacon et al. 2004; McCulloch et al. 2005). Kennedy et al. (1997) first demonstrated the potential of using $^{87}Sr/^{86}Sr$ measurements to identify key production rivers contributing to the adult population of Atlantic salmon. Their work showed that the water in the majority of rearing streams for Atlantic salmon in the Connecticut River differed significantly in their $^{87}Sr/^{86}Sr$ signatures, based on watershed geology and the same isotopic values were transferred to fish tissues (Fig. 13.4). This work inspired the application of $^{87}Sr/^{86}Sr$ in otoliths to track other species of anadromous and freshwater fishes in different systems.

The recent advancement of analytical instrumentation using laser ablation MC-ICPMS allows spatial coordination of $^{87}Sr/^{86}Sr$ measurements in the daily growth rings recorded in otoliths. This allows reconstruction of fish migrations through geochronology at high resolutions and high sample throughput necessary for many fisheries applications. Using this analytical breakthrough, Barnett-Johnson (2007) was able to conduct a mixed-stock analysis and link the natal identity of Chinook salmon *Oncorhynchus tshawytcha* caught off the central California coast to their

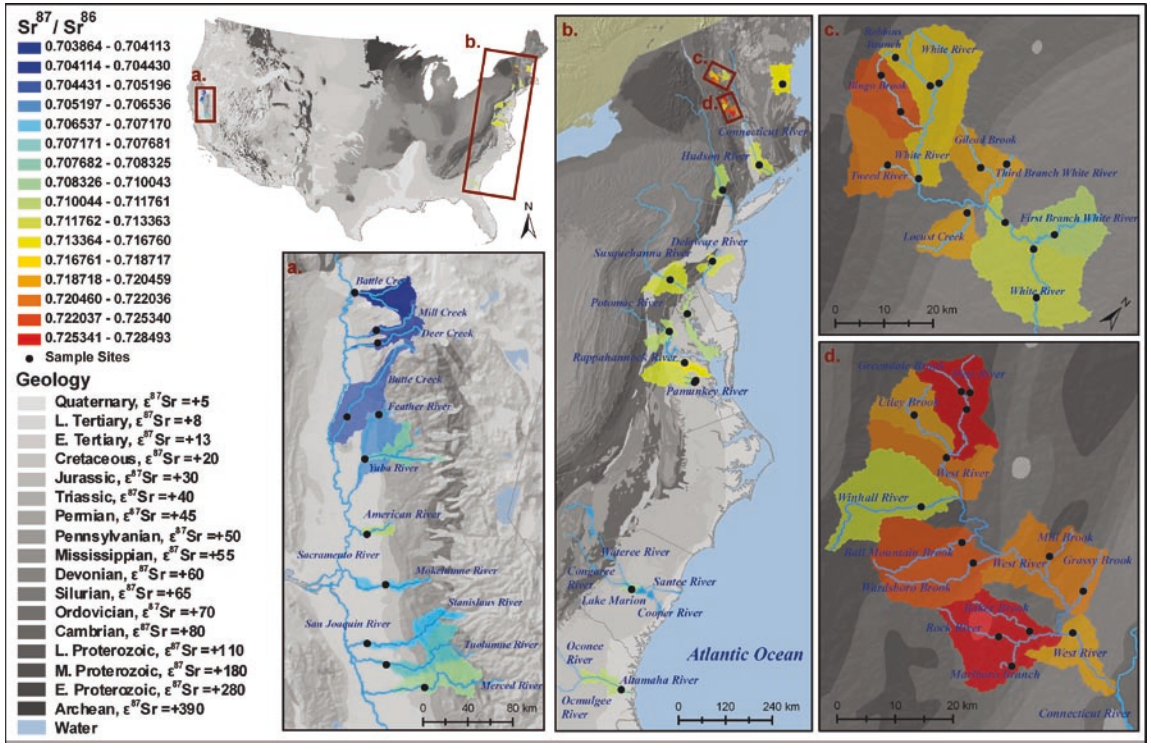

Fig. 13.4 Strontium isoscape highlighting first-order Sr variations ($\varepsilon^{87}Sr$) inferred by age variations in basement rocks (grey-scale; modified from Beard and Johnson 2000) and empirical measures of $^{87}Sr/^{86}Sr$ for watersheds (black circles and grey-scale) in insets from studies on Chinook salmon (*Oncorhynchus tshwaytcha*) in the California Central Valley (**a**; Barnett-Johnson et al. 2008), American shad (*Alosa sapidissima*) along the Atlantic coast (**b**; Walther and Thorrold 2008), and Atlantic salmon (*Salmo salar*) in the Connecticut River Basin, Vermont (**c** and **d**; Kennedy et al. 2000). Data synthesis and GIS map courtesy of Corey Phillis and Matthew Jones. Note: $\varepsilon^{87}Sr$ notation defined by Beard and Johnson (2000) as: $\varepsilon^{87}Sr = [(^{87}Sr/^{86}Sr)_{predicted}/(^{87}Sr/^{86}Sr)_{bulk\ earth} - 1] \times 10{,}000$ where $[^{87}Sr/^{86}Sr]_{predicted}$ is the $^{87}Sr/^{86}Sr$ value modeled by assuming a fixed initial $^{87}Sr/^{86}Sr$ and ^{87}Rb and Sr content and using the known decay rate for ^{87}Rb and rock ages and $[^{87}Sr/^{86}Sr]_{bulk\ earth}$ is equal to 0.7045, see Appendix 1, Color Section

rivers and hatcheries of origin in California's Central Valley. They found that only 10% (±6%) of Chinook salmon were from wild sources with a single hatchery largely supporting the fishery, suggesting that hatchery supplementation may be playing a greater role than previously thought. Walther and Thorrold (2008) found that American shad (*Alosa sapidissima*) returning to spawn in the York River were homing to their natal river, but that there was much less fidelity to individual tributaries. By reconstructing natal $^{87}Sr/^{86}Sr$ and Sr/Ca in adult otoliths, they found that small-scale straying could allow fish from the Mattaponi River to subsidize spawning in the Pamunkey River, which has experienced persistent recruitment failure. Here, we compile for the first time empirical measures of $^{87}Sr/^{86}Sr$ from three key fish studies to create an aquatic-focused Sr isoscape from Kennedy et al. (2000), Barnett-Johnson et al. (2008), and Walther and Thorrold (2008). These studies were chosen to provide empirical measures of $^{87}Sr/^{86}Sr$ in natal tributaries for different fish species on small and coast-wide scales for the east and west coast of the United States to highlight the utility of Sr isoscapes for fisheries applications. These empirical values from water and or fish otoliths are placed within the context of a baseline U.S. continental-scale map with predicted $^{87}Sr/^{86}Sr$ developed by Beard and Johnson 2000 (Fig. 13.4).

The baseline map highlights first-order Sr variations ($\varepsilon^{87}Sr$) inferred by age variations in basement rocks (Beard and Johnson 2000). Empirical measures of $^{87}Sr/^{86}Sr$ from the key fish studies are extrapolated to the scale of watersheds, as the $^{87}Sr/^{86}Sr$ values in otoliths and water are likely influenced by geology at this scale (Barnett-Johnson et al. 2008).

The small-scale variations in $^{87}Sr/^{86}Sr$ among rivers (e.g., natal sites) captured by empirical measurements have been used to track natal origins in a variety of fish species and systems. In California's Central Valley, $^{87}Sr/^{86}Sr$ ratios and daily growth bands recorded in otoliths of Chinook salmon from all major natural and hatchery spawning sites can be used to identify river and hatchery of origin of Central Valley fall-run adults in the ocean with high accuracy (94–98%; Fig. 13.4a; Barnett-Johnson et al. 2008). The north to south isotopic gradient is driven by young volcanic rocks influencing watershed values in the northern part of the Central Valley river system and older granitic rocks, which predominate in the south. Along the east coast of the United States, $^{87}Sr/^{86}Sr$ ratios vary among natal rivers for American shad across their spawning distribution (Fig. 13.4b; Walther and Thorrold 2008). Atlantic salmon in the White River in Vermont can be identified to tributary of origin by using $^{87}Sr/^{86}Sr$ and ^{15}N variation reflecting differences in geologic and agricultural inputs into salmon streams (Fig. 13.4c; Kennedy et al. 2000).

While geologic age used by Beard and Johnson (2000) explains some observed variation in measured isotopic values, there is significant disagreement between predicted and measured values (Fig. 13.4). For example, several tributaries off the Sacramento River in California have measured values of $^{87}Sr/^{86}Sr$ that are lower than any values predicted by the analysis conducted by Beard and Johnson (2000). This disagreement between observed and predicted values is likely explained by the role that lithology plays in Sr geochemistry that remains unquantified in the Beard and Johnson model and is an area primed for future research. By placing spatial variation in Sr isotope ratios in the context of bedrock geology, a mechanistic and

quantitative framework can be developed to determine how particular rock types contribute to patterns of $^{87}Sr/^{86}Sr$ variability in watersheds and otoliths. Developing these geologic models to inform Sr isoscapes across systems will assist in evaluating whether general characteristics in geology (in addition to age) emerge in explaining $^{87}Sr/^{86}Sr$ variability in otoliths and aid in forecasting the efficacy of Sr isotopes as natural tags of origin.

13.7 Current Limitations and Future Research

With few exceptions (e.g. Hobson et al. 1999; Barnett-Johnson et al. 2008), terrestrial isoscapes have not typically been created for the purposes of tracking migratory animals. Rather, ecologists and wildlife managers have made use of isotopic patterns derived for other purposes, especially those related to expected patterns based on plant physiology or long-term precipitation datasets. Ideally, available isoscapes would include those for each species and tissue of interest and include a spatial resolution appropriate to the movement patterns of the organism of interest ranging from local to continental scales. This requires huge effort and expense and so, in the near term then, we will continue to infer movement patterns of animals based on imperfect isoscape information.

Another problem with current isoscape models is that they are static and it is usually unclear just how much variance is associated with baseline or foodweb isoscapes used by animals at any particular location. While this can be accommodated to some degree by defining isotopic variance, based on long-term datasets, those data are typically unavailable for a number of isotopes. Such retrospective analyses of variance also are not particularly useful if future climatic conditions escape the natural range of variability and this in particular presents a challenge for the long-term GNIP precipitation dataset for δD and $\delta^{18}O$ measurements. Ideally, isoscapes based on the GNIP dataset and the associated variance surface would be updated annually and be flexible enough to accommodate additional sampling. Farmer et al. (2008) recently analyzed GNIP data for selected stations and years for sites in North America and Europe. They then used these estimates of variance to derive so-called fundamental limits to the resolution of origins of migratory birds using the feather δD approach. Unfortunately, those authors failed to realize that the predicted feather δD value from the long-term GNIP record refers to precipitation-weighted growing season averages and is not based on raw GNIP data. Their exercise should be repeated using the correct weighting approach. However, of more use will be regional analyses that attempt to explain the source of variance in the GNIP (or GNIP supplemented with other precipitation data sources) dataset. So, the influence of departures in precipitation amount from the long-term average and other meteorological data on the measured precipitation δD values will allow us to potentially account for departures from the web-based models of Bowen et al. (2005). Some authors are now carefully considering factors which contribute to departures in feather δD from long-term modeled averages (e.g. Coulton et al. 2009).

This research is urgently needed in regions of the continent where variance in weather patterns from long-term averages are most pronounced (e.g. the Great Plains of North America).

For isotopes such as ^{13}C and ^{15}N, recent advances in the potential for using remote sensing data to refine isoscape models presents an intriguing possibility of deriving annual isoscape models. Of course, for the heavier isotopes like those of Sr linked to geological substrates and presumed small temporal variability, the possibility exists for the establishment of relatively permanent isoscapes following some concerted effort of ground truthing. Developing a Sr isoscape in aquatic systems based on water sampling in defined watersheds and streams is feasible for fish movement and production studies since there is no significant fractionation between water $^{87}Sr/^{86}Sr$ values and otoliths in fish, as long as prey sources are in equilibrium with water. The need for modeling error propagation in assigning regions of origin for individuals across years using Sr isotopes will be dictated by the extent to which temporal variability confounds spatial differences in $^{87}Sr/^{86}Sr$ values.

For a number of animal tracking applications, the precipitation δD and $\delta^{18}O$ isoscapes will be the most useful. This suggests that particular effort be placed on refining the use of these isotopes. Apart from encouraging further analyses of the long-term GNIP dataset and refining our understanding of similar surface water datasets, much more research is needed to understand mechanisms of isotopic discrimination between foodwebs and animal tissues of interest. It seems clear that a single precipitation to tissue isotopic discrimination factor for animal δD (and presumably $\delta^{18}O$) is not appropriate. Currently, the influence of thermoregulation and work on the hydrogen isotope budget in animals and how this influences animal tissue δD values is much needed for several taxa. Fortunately, such investigations are amenable to controlled laboratory studies (McKechnie et al. 2004). Measurement of δD in animal tissues is also more complicated than the other light isotopes due to exchange with ambient laboratory water vapor due to weak N–H and O–H bonds. Wassenaar and Hobson (2003; 2006) discuss this issue at length and urge isotopists to adopt means of reporting δD values in animal tissues using a comparative equilibration technique so that data can be readily compared among laboratories. As we refine applications of $\delta^{18}O$ measurements, similar concerns are appropriate since there are currently no international standards available for $\delta^{18}O$ in organics.

The development of a Sr isoscape is in its infancy relative to light-isotope mapping for animal tracking efforts on continental scales. As such, there are several avenues for refinement and future research. A significant advancement will be to derive a quantitative geologic model that incorporates both age and rock type into $^{87}Sr/^{86}Sr$ predictions that could be scaled to both large and fine-scale resolutions. Barnett-Johnson et al. 2008 was successful at explaining 95% of the $^{87}Sr/^{86}Sr$ variation in salmon otoliths across watersheds in California's Central Valley by measuring the area of a watershed comprised of granitic rocks. However, in this system, both rock type and age co-varied so a quantitative assessment of the influence of age and lithology could not be accounted for independently. The ability to accurately characterize *unsampled* areas through the use of a geologic proxy would go far in fulfilling the first principle in an ideal isoscape. In practice, the relationship between geology

and empirical measures of $^{87}Sr/^{86}Sr$ may be challenging to model on a large-scale. For example, sedimentary rocks may contain multiple age and lithologic components and weathering rates differ among rock types. Similarly, local-scale phenomena may be necessary to consider in areas where atmospheric deposition plays a significant role in Sr addition from dust with different $^{87}Sr/^{86}Sr$ than local bedrock.

Further refinement may be necessary in the art of graphically mapping $^{87}Sr/^{86}Sr$ variation in aquatic systems. Unlike light-isotope mapping of abiotic processes where an interpolation algorithm can be used to represent neighboring areas that have not been explicitly sampled, a successful Sr isoscape will need to incorporate geologic variations that may occur on relatively small spatial scales. One current challenge is in determining the best way to display $^{87}Sr/^{86}Sr$ for rivers. The approach taken in this chapter extrapolates measured values of water [and fish] at the scale of a watershed. However, $^{87}Sr/^{86}Sr$ can vary within a river from headwaters to downstream sources and especially at the confluence with rivers characterized by different $^{87}Sr/^{86}Sr$ values (Weber 2002). This form of isotopic variation for rivers is difficult to represent graphically and needs further development.

Finally, more development is required to formulate standard protocols for depicting origins of animals based on isoscapes. Ideally, such approaches will be amenable to web-based tools and well-defined algorithms. Wunder and Norris (2008) have advocated approaches which more honestly incorporate error propagation and the ultimate derivation of probability of origin surfaces. However, much more work is required on this front to make these techniques more accessible to researchers and to test the consequences of depicting origins using a variety of GIS and spatial statistical methods. Currently, this remains as one of the biggest frontiers to the field of isotopic tracking of migratory organisms (Kelly et al. 2008).

Acknowledgments KAH thanks John Morrison for providing early δD measurements of Bowhead Whale baleen depicted here. Steve van Wilgenburg assisted with figures and GIS methods. RB thanks Corey Phillis for compiling $^{87}Sr/^{86}Sr$ values from the literature and Matthew Jones for creating the GIS map displaying $^{87}Sr/^{86}Sr$ data. We thank the organizers of the ISOSCAPE meeting in Santa Barbara for their kind invitation to present his work.

References

Aberg G (1995) The use of natural strontium isotopes as tracers in environmental studies. Water Air Soil Poll 79:309–322

Alisauskas RT, Klaas EE, Hobson KA, Ankney CD (1998) Stable-carbon isotopes support use of adventitious color to discern winter origins of lesser snow geese. J Field-Ornith 69:262–268

Ayliffe LK, Cerling TE, Robinson T, West AG, Sponheimer M, Passey BH, Hammer J, Roeder B, Dearing MD, Ehleringer JR (2004) Turnover of carbon isotopes in tail hair and breath CO_2 of horses fed an isotopically varied diet. Oecologia 139:11–22

Bacon CR, Weber PK, Larson KA, Reisenbichler R, Fitzpatrick JA, Wooden JL (2004) Migration and rearing histories of chinook salmon (*Oncorhynchus tshawytscha*) determined by ion microprobe Sr isotope and Sr:Ca transects of otoliths. Can J Fish Aquat Sci 61:2425–2439

Barnett BA (1994) Carbon and nitrogen ratios of caribou tissues, vascular plants, and lichens from Northern Alaska. M.Sc. Dissertation, University of Alaska

Barnett-Johnson R (2007) Spatial scales of mixing and natal source contributions of salmon populations in the coastal ocean detected by otolith and genetic signatures of origin. Ph.D. Dissertation, University of California, Santa Cruz

Barnett-Johnson R, Ramos FC, Grimes CB, MacFarlane RB (2005) Validation of Sr isotopes in otoliths by laser ablation multicollector inductively coupled plasma mass spectrometry (LA-MC-ICPMS): opening avenues in fisheries science applications. Can J Fish Aquat Sci 62:2425–2430

Barnett-Johnson R, Ramos FC, Pearson T, Grimes CB, MacFarlane RB (2008) Tracking natal origins of salmon using isotopes, otoliths, and landscape geology. Limnol Oceanog 53:1633–1642

Beard BL, Johnson CM (2000) Strontium isotope composition of skeletal material can determine the birth place and geographic mobility of humans and animals. J Forens Sci 45: 1049–1061

Best PB, Schell DM (1996) Stable isotopes in Southern Right Whale (*Eubalaena australis*) baleen as indicators of seasonal movements, feeding and growth. Mar Biol 124:483–494

Blum JD, Taliaferro EJ, Weisse MT, Holmes RT (2000) Changes in the Sr:Ca, Ba:Ca, and ^{87}Sr:^{86}Sr ratios between trophic levels in two forested ecosystems in the northeastern, USA. Biogeochem 49:87–101

Bowen GJ, Wassenaar LI, Hobson KA (2005) Application of stable hydrogen and oxygen isotopes to wildlife forensic investigations at global scales. Oecologia143:337–348

Brattström O, Wassenaar LI, Hobson KA, Åkesson S (2008) Placing butterflies on the map – testing resolution of three stable isotopes within Sweden using the monophagous peacock Inachis io. Ecography 31:490–498

Britzke ER, Loeb SC, Hobson KA, Romanek CS, Vonhof, MJ (2009) Assessing origins of bats using stable hydrogen isotope analysis: an investigation of four species in the eastern United States. J Mammal 90:743–751

Burger RL, Van der Merwe MJ (1990) Maize and the origin of highland Chavin civilization: an isotopic perspective. Am Anthropol 92:85–95

Cerling TE, Wittemyer G, Rasmussen HB, Vollrath F, Cerling CE, Robinson TJ, Douglas-Hamilton I (2006) Stable isotopes in elephant hair documents migration patterns and diet changes. Proc Nat Acad Sci U S A 103:371–373

Cerling TE, Ayliffe LK, Dearing MD, Ehleringer JR, Passey BH, Podlesak DW, Torregrossa A-M, West AG (2007) Determining biological tissue turnover using stable isotopes: the reaction progress variable. Oecologia 151:175–189

Chamberlain CP, Blum JD, Holmes RT, Feng X, Sherry TW, Graves GR (1997) The use of isotope tracers for identifying populations of migratory birds. Oecologia 109:132–141

Cherel Y, Hobson KA (2007) Geographical variation in stable carbon isotope signatures of marine predators: a tool to investigate their foraging areas in the Southern Ocean. Mar Ecol Prog Ser 329:281–287

Cormie AB, Schawarcz HP, Gray J (1994) Relationship between the hydrogen and oxygen isotopes of deer bone and their use in the estimation of relative humidity. Geochim Cosmochim Acta 60:4161–4166

Coulton DW, Clark RG, Hobson KA, Wassenaar LI, Hebert, CE (2009) Temporal sources of deuterium (δD) variability in waterfowl feathers across a prairie to boreal gradient. Condor 111:255–265

Cryan PM, Bogan MA, Rye RO, Landis GP, Kester CL (2004) Stable hydrogen isotope analysis of bat hair as evidence for seasonal molt and long-distance migration. J Mammal 85:995–1001

Cullen JT, Rosenthal Y, Falkowski PG (2001) The effect of anthropogenic CO_2 on the carbon isotope composition of marine phytoplankton. Limnol Oceanog 46:996–998

Drucker DG, Bridault A, Hobson KA, Szuma E, Bocherens H (2008) Can carbon-13 in large herbivores track forest environments in temperate and boreal ecosystems? Evidence from modern and ancient ungulates. Paleogeog Paleoclim Paleoecol 266:69–82

Ehleringer JR, Bowen GJ, Chesson LA, West AG, Podlesak DW, Cerling TE (2008) Hydrogen and oxygen isotope ratios in human hair are related to geography. Proc Nat Acad Sci U S A 105:2788–2793

Ezzo J, Johnson A, Price CM, Price TD (1997) Analytical perspective on prehistoric migration: a case study from east-central Arizona. J Archaeol Sci 24:447–466

Farmer A, Cade BS, Torres-Dowdall J (2008) Fundamental limits to the accuracy of deuterium isotopes for identifying spatial origins of migratory animals. Oecologia 158:183–192

Faure G (1977) Principles of isotope geology, 2nd edn. Wiley, New York

Font L, Norwell GM, Pearson DG, Ottley CJ, Willis SG (2007) Sr isotope analysis of bird feathers by TIMS: a tool to trace bird migration paths and breeding sites. J Anal Atom Spectrom 22:513–522

Fourel F, Merren T, Morrison J, Wassenaar LI, Hobson KA (1998) Application of EA Pyrolysis-IRMS δD and $\delta^{18}O$ analysis to Animal Migration Patterns. Micromass UK Ltd, Application Note 300

Fox T, Hobson KA, Kahlert J (2009) Isotopic evidence for differential protein contributions to Greylag Goose (*Anser anser*) feathers. J Avian Biol 40:108–112

Graham BS, Koch PL, Newsome SD, McMahon KW, Aurioles D (2009) Using isoscapes to trace the movements and foraging behavior of top predators in oceanic ecosystems. In: West JB, Bowen G, Dawson T, Tu K (eds) Isoscapes: understanding movement, pattern, and process on Earth through isotope mapping. Springer-Verlag, New York

Graustein WC (1989) ^{87}Sr:^{86}Sr ratios measure the sources and flow of strontium in terrestrial ecosystems. In: Rundel PW, Ehleringer JR, Nagy KA (eds) Stable isotopes in ecology. Springer-Verlag, New York

Graves GR, Romanek CS, Navarro AR (2002) Stable isotope signature of philopatry and dispersal in a migratory songbird. Proc Nat Acad Sci U S A 99:8096–8100

Hobbs JA, Qing-zhu Y, Burton JE, Bennett WA (2005) Retrospective determination of natal habitats for an estuarine fish using otolith strontium isotope ratios. Mar Fresh Res 56:1–6

Hobson KA (2003) Making migratory connections with stable isotopes. In: Berthold P, Gwinner E, Sonnenschein E (eds) Avian migration. Springer-Verlag, Berlin

Hobson KA (2008) Applying isotopic methods to tracking animal movements. In: Hobson KA, Wassenaar LI (eds) Tracking animal migration using stable isotopes. Academic, London

Hobson KA, Clark RG (1992a) Assessing avian diets using stable isotopes. II: factors influencing diet-tissue fractionation. Condor 94:189–197

Hobson KA, Clark RG (1992b) Assessing avian diets using stable isotopes. I: turnover of carbon-13 in tissues. Condor 94:181–188

Hobson KA, Norris DR (2008) Animal migration: a context for using new techniques and approaches. In: Hobson KA, Wassenaar LI (eds) Tracking animal migration using stable isotopes. Academic, London

Hobson KA, Wassenaar LI (1997) Linking breeding and wintering grounds of neotropical migrant songbirds using stable hydrogen isotopic analysis of feathers. Oecologia 109:142–148

Hobson KA, Wassenaar LI (2008) Tracking animal migration using stable isotopes. Academic, London

Hobson KA, Alisauskas RT, Clark RG (1993) Stable-nitrogen isotope enrichment in avian tissues due to fasting and nutritional stress: implications for isotopic analyses of diet. Condor 95: 388–394

Hobson KA, Piatt JF, Pitocchelli J (1994) Using stable isotopes to determine seabird trophic relationships. J Anim Ecol 63:786–798

Hobson KA, Wassenaar LI, Taylor OR (1999) Stable isotopes (δD and $\delta^{13}C$) are geographic indicators of natal origins of monarch butterflies in eastern North America. Oecologia 120:397–404

Hobson KA, Wassenaar LI, Milá B, Lovette I, Dingle C, Smith TB (2003) Stable isotopes as indicators of altitudinal distributions and movements in an Ecuadorean hummingbird community. Oecologia 136:302–308

Hobson KA, Van Wilgenburg S, Wassenaar LI, Hands H, Johnson W, O'Melia M, Taylor P (2006) Using stable-hydrogen isotopes to delineate origins of Sandhill Cranes harvested in the Central Flyway of North America. Waterbirds 29:137–147

Hobson KA, Van Wilgenburg S, Wassenaar LI, Moore F, Farrington J (2007) Estimating origins of three species of neotropical migrants at a Gulf coast stopover site: combining stable isotope and GIS tools. Condor 109:256–267

Hoppe KA, Koch PL, Carlson RW, Webb SD (1999) Tracking mammoths and mastodons: reconstruction of migratory behavior using strontium isotope ratios. Geology 27:439–442
Ingram BL, Weber PK (1999) Salmon origin in California's Sacramento-San Joaquin river system as determined by otolith strontium isotopic composition. Geology 27:851–854
Kelly JF, Atudorei V, Sharp ZD, Finch DM (2002) Insights into Wilson's Warbler migration from analyses of hydrogen stable-isotope ratios. Oecologia 130:216–221
Kelly JF, Bearhop S, Bowen GJ, Hobson KA, Norris DR, Wassenaar LI, West JB, Wunder MB (2008) Future directions and challenges for using stable isotopes in advancing terrestrial animal migration research. In: Hobson KA, Wassenaar LI (eds) Tracking animal migration using stable isotopes. Academic, London
Kennedy BP, Folt CL, Blum JD, Chamberlain CP (1997) Natural isotope markers in salmon. Nature 387:766–767
Kennedy BP, Blum JD, Folt CL, Nislow KH (2000) Using natural strontium isotopic signatures as fish markers: methodology and application. Can J Fish Aquat Sci 57:2280–2292
Kennedy BP, Klaue A, Blum JD, Folt CL, Nislow KH (2002) Reconstructing the lives of fish using Sr isotopes in otoliths. Can J Fish Aquat Sci 59:925–929
Koch P, Halliday AN, Walter LM, Stearly RF, Huston TJ, Smith GR (1992) Sr isotopic composition of hydroxyapatite from recent and fossil salmon: the record of lifetime migration and diagenesis. Earth Planet Sci Lett 108:277–287
Koch PL, Heisinger J, Moss C, Carlson RW, Fogel ML, Behrensmeyer AK (1995) Isotopic tracking of change in diet and habitat use in African elephants. Science 267:1340–1343
Larson K, Hobson KA (2009) Assignment to breeding and wintering grounds using stable isotopes: a comment on lessons learned by Rocque et al. J Ornithol 150:709–712
Marra PP, Hobson KA, Holmes RT (1998) Linking winter and summer events in a migratory bird using stable carbon isotopes. Science 282:1884–1886
Marra PP, Norris DR, Haig SM, Webster MS, Royle JA (2006) Migratory connectivity. In: Crooks KR, Sanjayan MA (eds) Connectivity conservation. Cambridge University Press, New York
Martinez del Rio C, Anderson-Sprecher R (2008) Beyond the reaction progress variable: the meaning and significance of isotopic incorporation data. Oecologia 156:765–772
Mazerolle D, Hobson KA (2005) Estimating origins of short-distance migrant songbirds in North America: contrasting inferences from hydrogen isotope measurements of feathers, claws, and blood. Condor 107:280–288
McCulloch M, Cappo M, Aumend J, Muller W (2005) Tracing the life history of individual barramundi using laser ablation MC-ICP-MS Sr-isotopic and Sr:Ba ratios in otoliths. Mar Fresh Res 56:637–644
McKechnie AE, Wolf BO, Martinez del Rio C (2004) Deuterium, stable isotope ratios as tracers of water resources use: an experimental test with rock doves. Oecologia 140:191–200
Nadelhoffer KJ, Fry B (1994) Nitrogen isotope studies in forest ecosystems. In: Lajtha K, Michener RH (eds) Stable isotopes in ecology and environmental science. Blackwell Scientific, Oxford
Pardo LH, Naddelhoffer KJ (2009) Using nitrogen isotope ratios to assess terrestrial ecosystems at regional and global scales In: West JB, Bowen G, Dawson T, Tu K (eds) Isoscapes: understanding movement, pattern, and process on Earth through isotope mapping. Springer-Verlag, New York
Podlesak DW, Torregrossa AM, Ehleringer JR, Dearing MD, Passey BH, Cerling TE (2008) Turnover of oxygen and hydrogen isotopes in the body water, CO2, hair and enamel of a small mammal after a change in drinking water. Geochim Cosmochim Acta 72:19–35
Popp BN, Graham BS, Olson RJ, Hannides CCS, Lott MJ, Lopez-Ibarra GA, Galvan-Magana F, Fry B (2007) Insight into the trophic ecology of Yellowfin Tuna, *Thunnus albacares*, from compound-specific nitrogen isotope analysis of proteinaceous amino acids. In: Dawson TE, Siegwolf RTW (eds) Stable isotopes as indicators of ecological change. Academic, London
Post DM (2002) Using stable isotopes to estimate trophic position: models, methods and assumptions. Ecology 83:703–718

Quillfeldt P, McGill RAR, Furness RW (2005) Diet and foraging areas of Southern Ocean seabirds and their prey inferred from stable isotopes: review and case study of Wilson's storm-petrel. Mar Ecol Prog Ser 295:295–304

Ramos FC, Wolff JA, Tollstrup DL (2004) Measuring ^{87}Sr:^{86}Sr variations in minerals and groundmass from basalts using LA-MC-ICPMS. Chem Geol 211:135–158

Reich KJ, Bjorndal KA, Bolten AB (2007) The "lost years" of green turtles: using stable isotopes to study cryptic life stages. Biol Lett 3:712–714

Robbins CT, Felicetti LA, Sponheimer M (2005) The effect of dietary protein quality on nitrogen isotope discrimination in mammals and birds. Oecologia 144:534–540

Rubenstein DR, Hobson KA (2004) From birds to butterflies: animal movement patterns and stable isotopes. Trends Ecol Evol 19:256–263

Rubenstein DR, Chamberlain CP, Holmes RT, Ayres MP, Waldbauer JR, Graves GR, Tuross NC (2002) Linking breeding and wintering ranges of a migratory songbird using stable isotopes. Science 295:1062–1065

Schell DM (2001) Carbon isotope ratio variations in Bering Sea biota: the role of anthropogenic carbon dioxide. Limnol Oceanog 46:999–1000

Schell DM, Saupe SM, Haubenstock N (1988) Natural isotope abundances in bowhead whale (*Balaena mysticetus*) baleen: markers of aging and habitat usage. In: Rundel PW, Ehleringer JR, Nagy KA (eds) Stable isotopes in ecological research. Springer Verlag, New York

Schell DM, Barnett BA, Vinette K (1998) Carbon and nitrogen isotope ratios in zooplankton of the Bering, Chukchi and Beaufort Seas. Mar Ecol Prog Ser 162:11–23

Sheppard SMF, Neilsen RL, Taylor HP (1969) Oxygen and hydrogen isotope ratios of clay minerals from porphyry copper deposits. Econ Geol 64:755–777

Sponheimer M, Robinson TF, Cerling TE, Tegland L, , Roeder BL, Ayliffe L, Dearing MD, Ehleringer, JR (2006) Turnover of stable carbon isotopes in the muscle, liver, and breath CO_2 of alpacas (*Lama pacos*). Rapid Commun Mass Spectrom 20:1395–1399

Szép T, Møller AP, Vallner J, Kovacs B, Norman D (2003) Use of trace elements in feathers of sand martin *Riparia riparia* for identifying moulting areas. J Avian Biol 34:307–320

Taylor HP Jr (1974) An application of oxygen and hyrdrogen isotope studies to problems of hydrothermal alteration and ore deposition. Econom Geol 69:843–883

Vanderklift MA, Ponsard S (2003) Sources of variation in consumer-diet $\delta^{15}N$ enrichment: a meta analysis. Oecologia 136:169–182

Vogel JC, Eglington B, Auret JM (1990) Isotope fingerprints in elephant bone and ivory. Nature 346:747–749

Walther BD, Thorrold SR (2006) Water, not food, contributes the majority of strontium and barium deposited in the otoliths of a marine fish. Mar Ecol Prog Ser 311:125–130

Walther BD, Thorrold SR (2008) Geochemical signatures in otoliths record natal origins in American shad. Trans Am Fish Soc 137:57–69

Wassenaar LI (2008) An introduction to light stable isotopes for use in terrestrial animal migration studies. In: Hobson KA Wassenaar LI (eds) tracking animal migration with stable isotopes. Academic, New York

Wassenaar LI, Hobson KA (2000) Stable-carbon and hydrogen isotope ratios reveal breeding origins of red-winged blackbirds. Ecol Appl 10:911–916

Wassenaar LI, Hobson KA (2001a) A stable-isotope approach to delineate geographical catchment areas of avian migration monitoring stations in North America. Env Sci Technol 35:1845–1850

Wassenaar LI, Hobson KA (2001b) Comparative equilibration and online technique for determination of non-exchangeable hydrogen of keratins for use in animal migration studies. Isotopes Environ Health Stud 39:1–7

Wassenaar LI, Hobson KA (2006) Stable-hydrogen isotope heterogeneity in keratinous materials: mass spectrometry and migratory wildlife tissue sampling strategies. Rapid Comm Mass Spectrom 20:1–6

Weber PK (2002) Geochemical markers in the otoliths of Chinook salmon in the Sacramento-San Joaquin river system, California. Ph.D. Dissertation, University of California, Berkeley, CA

West JB, Bowen GJ, Cerling TE, Ehleringer JR (2006) Stable isotopes as one of nature's ecological recorders. Trends Ecol Evol 21:408–414

Wolf B, Martinez del Rio C (2000) Use of saguaro fruit by white-winged doves: isotopic evidence of a tight ecological association. Oecologia 124:536–543

Woodhead J, Swearer S, Hergt J, Maas R (2005) In situ Sr-isotope analysis of carbonates by LA-MC-ICP-MS: interference corrections, high spatial resolution and an example from otolith studies. J Anal At Spectrom 20:22–27

Wunder MB, Norris DR (2008) Improved estimates of certainty in stable-isotope based methods for tracking migratory animals. Ecol Appl 18:549–559

Yapp CJ, Epstein S (1982) Climatic significance of the hydrogen isotope ratios in tree ring cellulose. Nature 297:636–639

Zazzo A, Harrison SM, Bahar B, Moloney AP, Monaghan FJ, Scrimgeour CM, Schmidt O (2007) Experimental determination of dietary carbon turnover in bovine hair and hoof. Can J Zool 85:1239–1248

Chapter 14
Using Isoscapes to Trace the Movements and Foraging Behavior of Top Predators in Oceanic Ecosystems

Brittany S. Graham, Paul L. Koch, Seth D. Newsome, Kelton W. McMahon, and David Aurioles

14.1 Introduction

The inability to directly observe the long distant movements of marine predators and the vast extent of their pelagic habitat has hindered our understanding of their movements, distribution, and foraging behavior. Recently these challenges have spurred the development of new methods to examine animal movements remotely, including advancements in electronic tags (Holland et al. 1990; Stewart and DeLong 1995; Lutcavage et al. 1999; Biuw et al. 2007). Electronic tagging is generally limited to studying individual movements of a relatively small number of large individuals. However, the launch of extensive tagging campaigns (e.g., Block et al. 2005) and advancements in tag-to-tag communication could circumvent the

B.S. Graham (✉)
Department of Oceanography, University of Hawai'i, Honolulu, HI, 96822, USA

P.L. Koch
Dept. of Earth & Planetary Sciences, University of California, Santa Cruz, CA, 95064, USA
e-mail: pkoch@pmc.ucsc.edu

S.D. Newsome
Carnegie Institution of Washington, Geophysical Laboratory, Washington DC, 20015, USA
e-mail: snewsome@ciw.edu

K.W. McMahon
MIT-WHOI Joint Program in Biological Oceanography, Woods Hole Oceanographic Institution, Woods Hole, MA, 02543, USA
e-mail: kmcmahon@whoi.edu

D. Aurioles
Centro Interdisciplinario de Ciencias Marinas, Instituto Politécnico Nacional, La Paz Baja California Sur, 23060 Mexico,
e-mail: daurioles@hotmail.com

B.S. Graham
Current address: Stable Isotopes in Nature Laboratory (SINLAB), Canadian Rivers Institute, University of New Brunswick, Fredericton, NB, Canada E3B 5A3
e-mail: grahamb@unb.ca

J.B. West et al. (eds.), *Isoscapes: Understanding Movement, Pattern, and Process on Earth Through Isotope Mapping*, DOI 10.1007/978-90-481-3354-3_14,

difficulties of interpreting population-level movement patterns based on only a small number of individuals.

The stable isotope composition of animal tissues can provide intrinsic tags to study the foraging and migratory ecology of elusive or highly migratory species, such as top marine predators (Hobson 1999; Hobson et al. this volume). This method can be applied to track the movements of juvenile stages of marine vertebrates that are not amenable to current electronic tagging technologies. In addition, stable isotope analysis can provide retrospective information on the movement patterns and foraging ecology in both modern (Hobson et al. 1997; Burton and Koch 1999) and prehistoric marine predators (e.g., Burton et al. 2001; Newsome et al. 2007a, b). While foraging in specific environments, individuals acquire the isotopic composition of their local prey. By comparing the isotope composition of the animal to its local prey or the local environmental isotope composition (i.e., local primary producer isotopic composition), information can be gained on residency and movements patterns. In other words, an animal's isotopic composition can be used as a natural "tag" to track their movements through isotopically distinct habitats.

There are several requirements for applying this approach to study the movements and habitat use of top predators in the open ocean. First, the isotopic turnover rates for tissues of interest must be determined for each predator, because these rates provide a temporal framework in which to interpret predator stable isotope compositions. Turnover rates have been determined for carbon and nitrogen isotope ($\delta^{13}C$ and $\delta^{15}N$) values in different tissues for a variety of marine top predators, including seabirds, seals, penguins, tropical tuna, and sharks (Hobson et al. 1996; Bearhop et al. 2002; Kurle 2002; Cherel et al. 2005; Kim et al. 2008; Graham et al. in review). A second critical requirement is to construct maps of the geographical distribution of isotope values in the environment on temporal and spatial scales that are ecologically relevant to movements of the animal of interest. This is especially challenging for isotopic studies examining the movements of highly-mobile, marine predators because of their potentially vast foraging ranges. One approach has been to generate isotopic mapst (i.e., isoscapes) based either on sources that integrate marine production at the base of the food web (e.g., annually integrated phytoplankton, zooplankton, the organic matter in surface sediments), or control taxa at the same trophic level, but with known migratory and habitat preferences. Both approaches require intensive sampling to establish spatial and temporal isotopic patterns, and both necessitate assumptions about food web structure, animal physiology, and animal behavior that should be supported by independent datasets. Given these assumptions, however, if an individual has a similar isotopic value as the local isotopic baseline, then the predator is a resident, whereas if the individual and baseline isotopic values are distinctly different, the predator is an immigrant from another, isotopically distinct region.

14.1.1 Mechanisms That Shape the Isotopic Baseline

The carbon isotope compositions of open ocean consumers reflect those of algae at the base of the food web. At the most general level, higher $\delta^{13}C$ values are associated

with rapid growth rates whereas lower values are associated with slow growth rates (Goericke and Fry 1994; Popp et al. 1998). At relatively small scales within oceanic basins $\delta^{13}C$ values track productivity, with higher values in productive nearshore regions, such as upwelling zones, compared to less productive offshore regions. Because of the preferential uptake of ^{12}C by phytoplankton during photosynthesis, nutrient-driven phytoplankton blooms in upwelling zones increase the $\delta^{13}C$ value of aqueous CO_2 by a few per mil as they draw down its concentration. Low aqueous [CO_2] can itself lead to lower isotopic discrimination during photosynthesis. In offshore regions, especially equatorial regions where the water column is strongly stratified, low nutrient levels lead to low growth rates, so [CO_2] is less of a factor and $\delta^{13}C$ values in primary producers are lower. The gradient in $\delta^{13}C$ values between primary producers in nearshore versus offshore pelagic ecosystems has other, additive causes, including the effects of phytoplankton size and geometry, and taxonomic differences on isotopic fractionation (Bidigare et al. 1997; Pancost et al. 1997; Popp et al. 1998; Rau et al. 2001). Finally, macroscopic marine plants, such as kelp and sea grass, have substantially higher $\delta^{13}C$ values than phytoplankton. Using data compiled from the literature, Clementz and Koch (2001) showed that major marine and marginal marine habitat types have distinct $\delta^{13}C$ values (i.e., seagrass habitat > kelp forest > nearshore marine > offshore marine).

The $\delta^{13}C$ values of primary producers also vary predictably among ocean basins. High-latitude pelagic ecosystems typically have much lower $\delta^{13}C$ values than pelagic ecosystems at lower latitudes. In colder regions, aqueous [CO_2] is high due to seasonally low photosynthetic rates caused by light and trace metal limitation, vertical mixing of a weakly stratified water column, and the greater solubility of CO_2. Under high aqueous [CO_2], the fractionation associated with photosynthetic uptake of CO_2 is strongly expressed, leading to low $\delta^{13}C$ values. The converse applies in the warm, well lit, stratified waters of temperate and tropical latitudes. Finally, taxon-specific biological variables and local environmental conditions must be important, since meridional gradients in particulate organic matter (POM) $\delta^{13}C$ values are significantly different in oceans in the southern versus northern hemisphere (Goericke and Fry 1994).

Nitrogen isotope compositions of primary producers set the $\delta^{15}N$ value at the base of the food web and are dependent upon the $\delta^{15}N$ values of their nutrient source (e.g., nitrate, ammonium, N_2), subsequent biological transformations (e.g., N_2-fixation in subtropical gyres and denitrification in oxygen minimum zones), isotopic fractionation associated with nitrogen assimilation, nutrient pool size, and the degree to which primary producers drawdown the nitrogen pool (see reviews by Sigman and Casciotti 2001; Montoya 2007). N_2-fixation by cyanobacteria is an important source of new nitrogen to oligotrophic high-nutrient, low-chlorophyll regions such as the North Pacific Subtropical Gyre. N_2-fixation generates organic matter with low $\delta^{15}N$ values (−3 to 3‰), because the $\delta^{15}N$ value of dissolved N_2 is near 0‰ and there is little isotopic fractionation associated with its biological uptake by phytoplankton (Dore et al. 2002; Montoya 2007). The relative importance of N_2-fixation fluctuates seasonally. In the winter to spring, the erosion of the thermocline promotes the entrainment of nitrate into the euphotic zone, whereas in the summer to early fall the surface ocean tends to stratify and N_2 fixation dominates new nitrogen and influences the $\delta^{15}N$ value of the primary producers (Montoya 2007).

In most oceanic regions, however, marine primary production is based on nitrate (NO_3^-) supply. The $\delta^{15}N$ values of phytoplankton in these regions reflects two major factors: (1) the $\delta^{15}N$ value of NO_3^- supplied to the euphotic zone, especially via upwelling of nitrate-rich deep water, and (2) the degree of NO_3^- uptake by phytoplankton. Where NO_3^- uptake is complete (the predominant case), the annually integrated $\delta^{15}N$ value of primary production equals the $\delta^{15}N$ value of inputs (*sensu* Eppley and Peterson 1979). The vast sub-surface NO_3^- pool that mixes and is entrained into the euphotic zone averages ~5–7‰ in most regions (Sigman and Casciotti 2001). However below highly productive regions, deep water can become suboxic to anoxic, such as in the Eastern Tropical Pacific oxygen minimum zone. In the absence of adequate O_2, bacteria turn to nitrate to respire organic matter (denitrification), which preferentially removes ^{15}N-depleted NO_3^- and leaves residual nitrate strongly ^{15}N-enriched (+15 to +20‰; Voss et al. 2001). Geographic differences in upwelling intensity and the extent of sub-surface denitrification contribute to large-scale spatial differences in the $\delta^{15}N$ value of phytoplankton. Finally, if the pool of NO_3^- is large and uptake of nitrate is incomplete (e.g., Southern Ocean), then phytoplankton will have lower $\delta^{15}N$ values, because they preferentially assimilate ^{14}N-depleted nitrate. However, as uptake continues and the NO_3^- pool is drawn down, the $\delta^{15}N$ value of phytoplankton will increase, approaching the $\delta^{15}N$ value of the source NO_3^- pool.

14.1.2 Marine Isoscapes in the Pacific and Atlantic Ocean Basins

These differences among and within oceanic regions in nutrient cycling at the base of food web produce geographical gradients in the carbon and nitrogen isotope composition. Both surface POM and deep-sea sediments are proxies for the base of the food web, and their $\delta^{15}N$ values show large isotopic variation and coherent geographical patterns in the Pacific Ocean. For example, a 9‰ variation was observed in the $\delta^{15}N$ values of deep-sea sediments in the eastern equatorial Pacific (Farrell et al. 1995) and a 16‰ variation was observed in the $\delta^{15}N$ values of surface POM along a north-south transect in the central equatorial Pacific (Altabet 2001). In the northeast Pacific Ocean there is approximately a 2–3‰ decrease in baseline $\delta^{13}C$ and $\delta^{15}N$ values from temperate (~30–35° N) to high-latitude (~50° N) pelagic ecosystems (Saino and Hattori 1987; Goericke and Fry 1994; Aurioles et al. 2006). Higher temperatures and extensive upwelling lead to higher phytoplankton growth rates (and higher $\delta^{13}C$ values) in the California Current (CC) relative to the Gulf of Alaska. Higher productivity in coastal systems along the entire eastern Pacific and southern Bering Sea leads to higher ecosystem $\delta^{13}C$ values than in offshore systems. Nitrogen isotope values are also higher at lower latitudes in the eastern north Pacific because intermediate waters in the CC are sourced from the eastern tropical Pacific Ocean, where there is substantial denitrification at depth (Altabet et al. 1999; Voss et al. 2001). This ^{15}N-enriched nitrate is carried northward at depth via

the California Undercurrent and is an important source of nitrogen to surface waters in the CC. Finally, both $\delta^{13}C$ and $\delta^{15}N$ values decrease from east to west in the southeastern Bering Sea (Schell et al. 1998). These isotopic gradients are most likely due to differences in the extent of vertical mixing and the degree of utilization of nutrients in the western Bering Sea.

Constructing maps of isotope values at the base of the food web that are relevant to the movements of marine predators is challenging because in many cases it must be completed on a basin-wide scale. McMahon et al. (in review) generated a baseline isoscape for the Atlantic Ocean based on a meta-analysis of published plankton $\delta^{13}C$ and $\delta^{15}N$ values (Fig. 14.1). The broad spatial patterns observed in these plankton and zooplankton isoscapes reflect the processes described in Section 14.1. For example, in the subtropical gyres, zooplankton $\delta^{15}N$ values are low and reflect the incorporation of fixed-N_2 into the food web. The low $\delta^{15}N$ and $\delta^{13}C$ values observed at high latitudes relate to the utilization rate of NO_3^- by phytoplankton and the high aqueous [CO_2], respectively. These geographical variations in stable isotope values (or isoscapes) provide a means to track the foraging and migration of top marine predators within and between regions on an ocean-basin scale. This approach has recently been used to describe the foraging behavior and movements of a wide variety of marine predators, such as marine mammals, diving seabirds, procellariforms, and tropical tunas (e.g., Lee et al. 2005; Newsome et al. 2007b; Cherel and

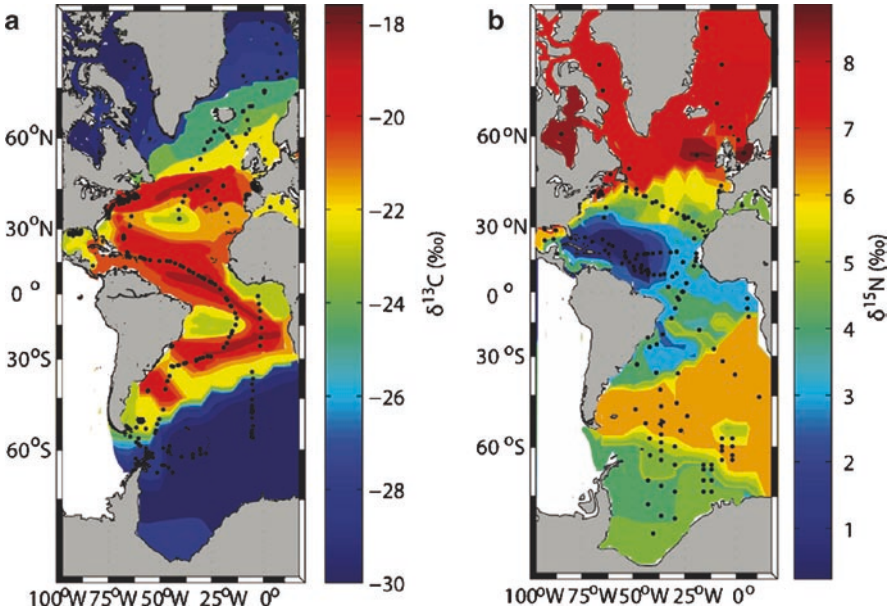

Fig. 14.1 Contour plots of isotope values in the Atlantic Ocean from a meta-analysis of published data. (**a**) $\delta^{13}C$ values of plankton from the upper ocean (0–500 m; n = 425) and (**b**) $\delta^{15}N$ values of zooplankton, primarily calanoid copepods, from the upper ocean (0–500 m; n = 198). *Black dots* indicate sample locations (Data are from McMahon et al. (in review)). Fig. 14.1, see Appendix 1, Color Section

Hobson 2007; Menard et al. 2007; Olson et al. unpublished; Graham et al. 2009). Here we broadly review case studies on two groups of top predators, pinnipeds and tropical tunas.

14.2 Case Studies – Marine Isoscapes and Top Predator Movements

14.2.1 Marine Mammals

Migration and habitat use by marine mammals have been studied extensively and are reviewed in Newsome et al. (in press). Schell et al.'s (1989) pioneering work on bowhead whales (*Balaena mysticetus*) demonstrated that large $\delta^{13}C$ and $\delta^{15}N$ gradients in high-latitude food webs could be exploited to study seasonal migratory patterns between the Bering and Beaufort Seas. Rau et al. (1992) conducted another study examining diet and residence patterns in a range of taxa, including several species of seals, in the Weddell Sea. Hobson et al. (1997) were among the first to suggest that isotopic differences between marine mammal species, in this case harbor seals (*Phoca vitulina*) and Steller sea lions (*Eumetopias jubatus*), were due to coastal/benthic versus offshore/pelagic foraging. Most marine mammal studies have relied on gradients in carbon and nitrogen isotopes, though Stewart et al. (2003) and Outridge et al. (2003) have done elegant work on the movement patterns of walruses (*Odobenus rosmarus*) using patterns of lead isotope variation in different tissues. Here, we will focus on case studies exploring modern and archaeological pinniped populations in the northeastern Pacific Ocean.

Do the isotopic patterns described above for the northeastern Pacific Ocean cascade up to label top consumers in a reliable way, or do differences in trophic level and physiology, as well as prey migration, obscure these basic patterns? We used data from Burton and Koch (1999), Burton et al. (2001), and Newsome et al. (2007a, b) to investigate this issue by studying the isotopic composition of extant pinnipeds with well-understood and geographically-distinct foraging habitats. The key "control" species are harbor seals and northern fur seals (*Callorhinus ursinus*). Harbor seals are relatively sedentary, living along rocky coasts and sloughs from Baja California to the Aleutian Islands. They undertake short, shallow dives and feed nearshore. Northern fur seals, by contrast, forage offshore at the shelf-slope break or beyond. Males and females from the small rookery on San Miguel Island (SMI), California, forage offshore in the CC system, whereas males from the large Pribilof Island rookeries forage in the Bering Sea and Gulf of Alaska. Females from the Pribilof rookeries are highly migratory, and thus not useful as "buoys" to sample any one oceanographic region.

Figure 14.2 presents means (±1 standard deviation) of the $\delta^{13}C$ and $\delta^{15}N$ values for bone collagen or tooth dentin from harbor seals and northern fur seals, separated by geographic region (Alaska vs. California). Bone collagen is a bulk tissue with a

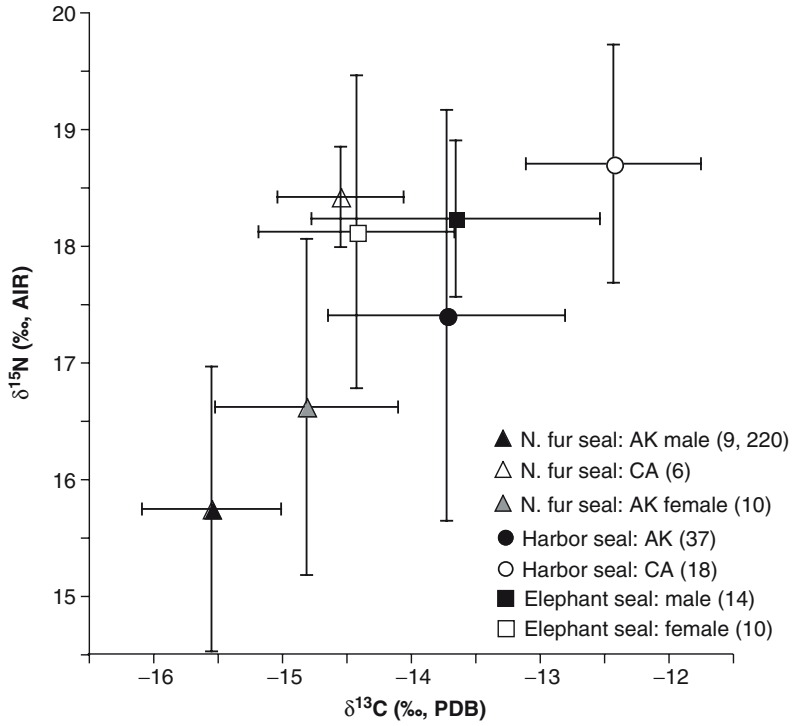

Fig. 14.2 Bivariate plot of collagen carbon and nitrogen isotope values (means ± 1 standard deviation) for three modern pinniped species that breed and feed at different locations in the northeastern Pacific. Number of samples analyzed is indicated in parentheses. For N. fur seal: AK male, the first number is number of bone samples, the second is number of dentin samples; for all other samples only bone was analyzed (Data are from Burton and Koch (1999), Burton et al. (2001), and Newsome et al. (2007b))

slow turnover rate that integrates animal diet over several years. Tooth dentin, which was measured for a large suite of male northern fur seals from the Pribilof Islands, grows by accretion and has conspicuous growth bands. It can be sub-sampled to yield more discrete time periods in an animal's life. For the study by Newsome et al. (2007b), the source of our tooth dentin data, dentin accreted in the third year of life was milled from each tooth.

In both Alaska and California, nearshore-foraging harbor seals had higher $\delta^{13}C$ values than offshore-foraging northern fur seals, as expected. The $\delta^{15}N$ values were not significantly different between nearshore and offshore foragers, which supports the conclusion that animals are feeding at roughly the same trophic level and that $\delta^{15}N$ values do not differ predictably between coastal and pelagic ecosystems in this region. Intra-specific comparisons reveal that high latitude populations in Alaskan waters have lower $\delta^{13}C$ and $\delta^{15}N$ values than temperate latitude populations from California. Thus, isotopic patterns in higher trophic level foragers mirror those observed in plankton and organic matter at the base of the food web. Harbor seals

were not available from sites further west along the Aleutians, so it could not be determined if the large isotopic shifts across the island chain are transmitted up the food web in modern taxa.

With increased confidence that isotopic values from marine mammal tissues track variations in the marine isoscape, we will discuss several case studies that have examined foraging zone or migration in extant northeastern Pacific pinnipeds. First, as noted earlier, female northern fur seals from the Pribilof rookeries are highly migratory (Ream et al. 2005). During the 4-month breeding season females feed in the Bering Sea, as they need to remain near the rookery to nurse their pups. For the 8 months they are off the rookery at sea, many females migrate southward, crossing the Gulf of Alaska to forage as far south as the shelf-slope break from British Columbia to southern California. Other females forage in the open ocean at highly productive sites associated with the transition from subarctic-subtropical waters (35–40° N, 140–180° W; North Pacific Convergence Zone). Not surprisingly, northern fur seal females from the Pribilofs have $\delta^{13}C$ and $\delta^{15}N$ values intermediate between those for males from Alaska and conspecifics feeding off California, consistent with their foraging in both high and middle latitudes during the course of a year (Fig. 14.2; Burton and Koch 1999).

Our other modern case studies focus on northern elephant seals (*Mirounga angustirostris*). These seals breed on islands or isolated mainland beaches from central Baja to northern California, with one outlying rookery on Vancouver Island. The smaller females (~600 kg) are on land for approximately 1 month in winter to give birth and nurse, and for 1 month in summer to molt. The larger males (~2,000 kg) are on land for three winter months to breed, and again for approximately one summer month to molt. Animals fast while breeding and molting. Both sexes are highly migratory when off their rookeries. Satellite tracking data from animals at rookeries on SMI and Point Año Nuevo (PAN), CA, show that the animals undertake long migrations between foraging locations and breeding and molting grounds (Stewart and DeLong 1995; LeBoeuf et al. 2000). At both PAN and SMI, males migrate rapidly to the north, where they feed on benthic prey on the continental shelf from Oregon to the western Aleutians. Females exhibit a greater range of migratory and foraging behaviors. Many females from SMI forage in pelagic waters at the northern edge of the subarctic-subtropical transition (45–50° N, 130–180° W); others forage on benthic prey on the continental shelf from California to Washington. Some PAN females show similar movement patterns, but others forage benthically further north (like males) or in pelagic sub-arctic waters north of the subarctic-subtropical transition. While individuals from the same rookery may have very different migratory patterns, the limited data available from multiple years suggest that individuals return to the same locations each year.

Bone collagen isotope data from males and females at PAN lead to interpretations of foraging and migratory behavior entirely consistent with tracking data. Males from PAN have values similar to harbor seals from Alaska, who also forage benthically at high latitude (Fig. 14.2). Female northern elephant seals from PAN have isotopic values indistinguishable from northern fur seals from California, who also forage pelagically, chiefly in or south of the transition zone to subarctic waters.

We note that these isotopic interpretations of elephant seal migratory behavior for PAN were reached by Burton and Koch (1999) before extensive tracking data were available (LeBoeuf et al. 2000). High-resolution satellite tracking data have since offered independent confirmation of interpretations based on marine isoscapes, albeit interpretations informed by earlier, less extensive tracking and observational data on elephant seal movements.

Aurioles et al. (2006) present another study of foraging location in northern elephant seals. While a great deal is now known about the migratory behavior of animals from the PAN and SMI rookeries, the migratory patterns for elephant seals in Mexico, such as those from the San Benitos Islands (SBI) off Baja California, are largely unknown. To track feeding grounds of SBI elephant seals, Aurioles et al. (2006) measured $\delta^{13}C$ and $\delta^{15}N$ values in hair of recently weaned elephant seal pups at SBI and PAN, assuming that their isotopic values reflect those of mothers' milk and therefore mothers' diets over the preceding few months. Mean $\delta^{13}C$ and $\delta^{15}N$ values (±1 standard deviation) for SBI pups (−16.1 ± 0.9‰ and 17.7 ± 0.9‰, respectively) were significantly higher than those for PAN pups (−17.6 ± 0.4‰ and 15.6 ± 1.0‰, respectively). From data on environmental isotope gradients along the eastern Pacific Rim, Aurioles et al. (2006) estimated that the difference in pup isotope values was consistent with the hypothesis that SBI females foraged, on average, ~8° south of females from PAN.

This hypothesis has gained support from an ongoing study of whiskers from female northern elephant seals at PAN and SBI by Aurioles and Newsome (unpublished data). Whiskers grow continuously, and while the rate of growth is not yet well calibrated for northern elephant seals at this time, and may vary seasonally, it is likely that each whisker represents slightly less than 1 year's growth based on the sinusoidal trends in isotope values along individual whiskers. Considering the average isotopic values for each whisker, mean $\delta^{13}C$ and $\delta^{15}N$ values (± one standard deviation) for SBI females (−15.1 ± 0.5‰ and 17.4 ± 0.8‰, respectively) are indeed higher than those for PAN females ((−15.8 ± 0.2‰ and 15.5 ± 1.0‰, respectively). In Fig. 14.3, every data point from each whisker is plotted for the nine SBI and ten PAN individuals. There is considerable overlap among samples from the two rookeries, but many samples from PAN have lower $\delta^{13}C$ and $\delta^{15}N$ values than observed at SBI, and many samples from SBI have values higher than observed at PAN. From this isotopic pattern, we hypothesize that there are tracks for PAN individuals that extend north of any tracks for SBI individuals, and tracks for individuals from SBI that extend south of any tracks for PAN individuals. This hypothesis is being tested through the collection of tracking data on SBI individuals and further analysis of whiskers collected from both rookeries.

Historical data provide a baseline against which to judge the significance of recent ecological shifts. Burton et al. (2001) and Newsome et al. (2007a) explored the historical ecology of northern fur seals. This species is common in archaeological sites from southern California to the Aleutian Islands, yet today it breeds almost exclusively on offshore islands at high latitudes. In all sites where they co-occur, prehistoric adult female northern fur seals have lower $\delta^{13}C$ values than nearshore-foraging harbor seals (Fig. 14.4), as is the case today (Fig. 14.2), suggesting that the female fur

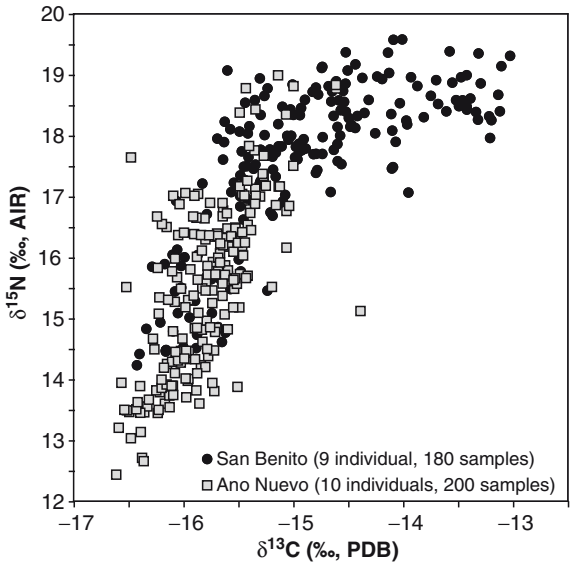

Fig. 14.3 Bivariate plot of whisker carbon and nitrogen isotope values from female northern elephant seals from Pt. Año Nuevo, CA, (ten individuals) and San Benito Island, Baja California, Mexico (nine individuals). Nearly twenty samples were collected from evenly spaced positions along the length of each whisker. Data are from Newsome and Aurioles (unpublished data)

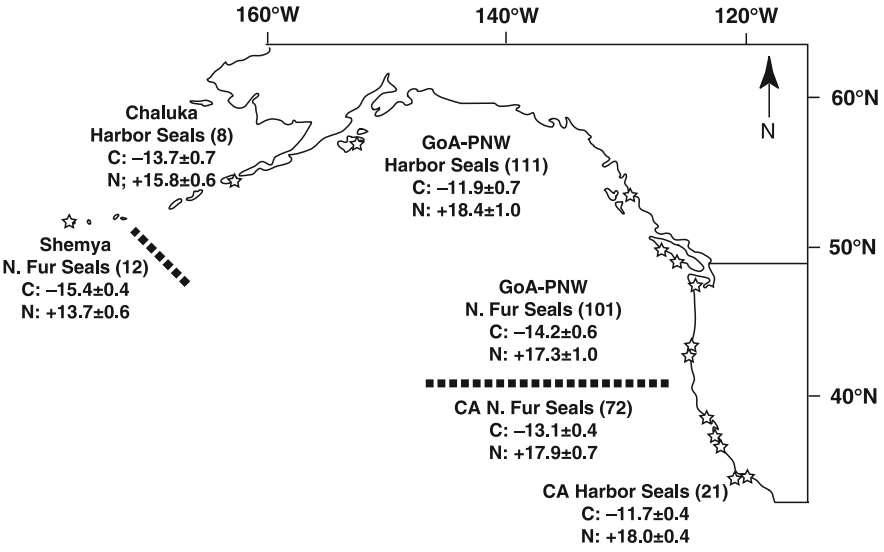

Fig. 14.4 Mean (±1 standard deviation) for $\delta^{13}C$ (*upper numbers*) and $\delta^{15}N$ (*lower numbers*) values for pinniped bone collagen from archaeological sites along the northeast Pacific margin. Number of samples analyzed is indicated in parentheses. Sites from which samples were analyzed are indicated by *star symbols*. *Thick dashed lines* separate sites that combined to calculate values for northern fur seals: Shemya, Gulf of Alaska/Pacific Northwest (GoA/PNW), California. Harbor seals were clustered into the following groups: California, Gulf of Alaska/Pacific Northwest, Chaluka (Data are from Newsome et al. (2007a) as well as Newsome (unpublished) for Chaluka harbor seals)

seals were foraging in deep, offshore waters over their entire range. The availability of fur seals to prehistoric human hunters was not because they foraged close to shore. Furthermore, prehistoric adult female northern fur seals cluster into three geographically-defined groups: a southern group (California) with high $\delta^{13}C$ and $\delta^{15}N$ values, a northern group (eastern Aleutian/Gulf of Alaska/Pacific Northwest) with intermediate values, and a western Aleutian group with very low isotope values (Fig. 14.4). This third group is the first indication in our marine mammal data of the low $\delta^{13}C$ and $\delta^{15}N$ values that characterize the marine isoscape of the western Aleutians. These isotopic distinctions among seals from different regions suggest that ancient northern fur seal females were less migratory than animals from the modern Pribilof rookery, and confirm that prehistoric fur seals from California were not immigrants from northern waters but instead were year-round residents. This conclusion is supported by archaeometric data showing that archaeological sites contain many unweaned pups, confirming the presence of temperate-latitude breeding colonies in California, the Pacific Northwest, and the eastern Aleutian Islands. The relative roles of human hunting versus climatic factors in explaining the loss of these temperature-latitude rookeries are unclear; more paleoclimatic and paleoceanographic data are needed to explore alternative hypotheses for this change in ecosystem state.

14.2.2 Tropical Tunas

Commercial fisheries have removed approximately 50 million tons of tuna from the Pacific Ocean since the 1950s (Sibert et al. 2006). The majority of this exploited biomass has been tropical tunas taken from the equatorial zone (20° N to 20° S). In order to determine population dynamics and develop the most successful fisheries management for tropical tunas, movement patterns of these highly mobile predators must be accurately determined. Tropical tuna form schooling aggregations and some species associate to fixed (e.g., seamounts, fish aggregating devices) or dynamic (e.g., fronts, meso-scale eddies) oceanographic features (Holland et al. 1990, 1999; Polovina et al. 2001). Tuna movements between these sometimes distant oceanic features are not well understood. On a basin-wide scale, there is some evidence from tag and recapture programs of restricted mixing between the eastern Pacific Ocean and the western and central Pacific Ocean. Hence, integrated stock assessments of tropical tunas in the Pacific Ocean are developed for either the entire tropical Pacific basin (Sibert et al. 2006) or for the eastern and western-central management regions (e.g., Hampton 2002; Hoyle and Maunder 2006). If tropical tuna movements are further restricted within these large oceanic regions, where commercial fishing effort is spatially patchy, then current exploitation rates could be locally unsustainable. Stock assessment models can incorporate additional spatial structure, but these models require more observational data on tuna movements to define mixing rates at finer resolutions. The main objective of the following case study was to determine if bulk $\delta^{15}N$ values of tropical tuna could be used as intrinsic tags to examine their habitat use and movements in the equatorial Pacific Ocean.

Marine mammals and seabirds often return annually to specific breeding grounds or rookeries, which provides an opportunity to tag individuals and collect tissue samples. Tropical tuna do not have well-defined spawning regions, but rather, spawn almost continuously in waters near the equator (10° N–10° S), with some individuals spawning in subtropical waters (Itano 2000). With their expansive spawning region and our lack of knowledge on their seasonal or annual movement patterns, sampling tropical tuna must occur opportunistically and the coverage must encompass much of the equatorial and subtropical Pacific Ocean. Commercial fishing of tunas is widespread in the equatorial Pacific and, therefore, can provide a unique sampling platform to collect samples from many individuals over large regions. In the work described below, yellowfin (*Thunnus albacares*) and bigeye (*T. obesus*) tuna were captured by purse-seine and long-line fishing vessels, and were sampled on vessels by fisheries observers from the Inter-American Tropical Tuna Commission and from the national fisheries observer programs in the central and western Pacific. As a result of this international collaboration between scientists, observer programs, and fishers, muscle samples were collected from tuna across much of the equatorial Pacific, allowing for the construction of tuna isoscapes (Graham et al. 2009).

The $\delta^{15}N$ values of yellowfin (YFT) and bigeye (BET) tuna demonstrate highly variable, but spatially coherent structure in the equatorial Pacific Ocean (Fig. 14.5a and b). The overall range in $\delta^{15}N$ values of YFT and BET is 13.7‰ (n = 387) and 12.5‰ (n = 196), respectively. This large isotopic variation could result from geographical variations in (a) their trophic level (TL) or (b) the isotopic baseline value, which is reflected in the tuna $\delta^{15}N$ values. If shifts in the trophic levels of tuna were the primary mechanism producing this 12–14‰ spatial variation, then there would be regional variations of approximately four to five trophic levels. Not only is a TL variation of this magnitude unrealistic in marine ecosystems, which generally have a total of four to five TLs (Fry 1988; Olson and Watters 2003), but stomach content studies conducted in the Pacific Ocean have revealed little foraging specialization in tropical tunas (Reintjes and King 1953; Alverson 1963). It is more likely that these geographical variations in the $\delta^{15}N$ values of tuna reflect differences in nutrient dynamics and subsequent $\delta^{15}N$ values at the base of the marine food web. Popp et al. (2007) used compound-specific nitrogen isotope analysis of individual amino acids from tissues of YFT to test this hypothesis and showed that spatial variations in tuna bulk $\delta^{15}N$ values in the eastern tropical Pacific are controlled by variations in $\delta^{15}N$ values at the base of the food web and not TL. Thus, the $\delta^{15}N$ values of tropical tunas and the resulting isoscapes appear to be driven, in large part, by the geographical variations in nutrient dynamics at the base of the food web (Popp et al. 2007; Menard et al. 2007; Olson et al. unpublished; Graham et al. 2009).

If a predator migrated extensively in the equatorial Pacific, then little geographical isotopic variation would be expected in its tissues because regional differences in baseline $\delta^{15}N$ values would be integrated and homogenized over time. The large isotopic variation observed in YFT and BET throughout the equatorial Pacific suggests these tuna must reside and forage within a region for a long enough period to reflect the baseline $\delta^{15}N$ structure. Tissue turnover rates estimated for juvenile YFT

indicate that the nitrogen in the white muscle represents an accumulated foraging history of approximately 2 months (Graham et al. 2009). Turnover rates are likely slower in larger individuals (Martínez del Rio et al. 2009). Accordingly, the $\delta^{15}N$ values of tuna incorporated into these isoscapes (Fig. 14.5a and b) should represent an integrated foraging history of at least 2–4 months. This intrinsic tag approach reveals that tropical tunas are not 'highly migratory' and suggests a high degree of regional residency on the order of several months in the equatorial Pacific Ocean. These isotope-based conclusions corroborate conventional and electronic tagging studies that reveal restricted movements (e.g., <1,000 km/month) in individual BET tracked in the Coral Sea (Gunn et al. 2005), YFT and BET tracked around the

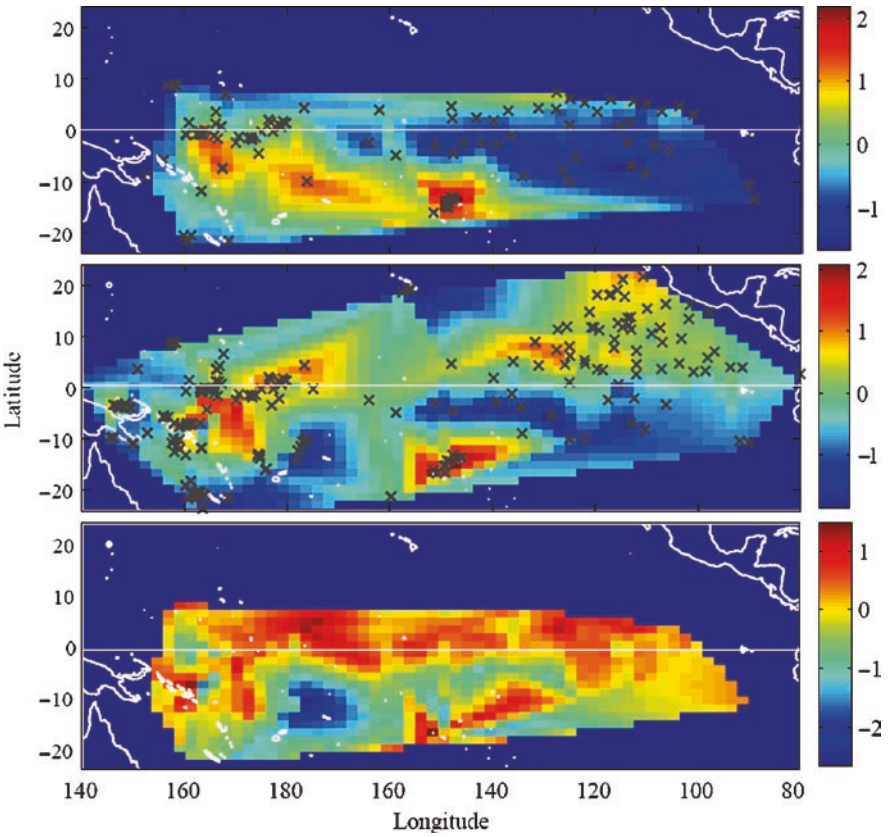

Fig. 14.5 $\delta^{15}N$ isoscapes for (**a**) bigeye (n = 196) and (**b**) yellowfin (n = 387) tuna. *Crosses* indicate sample locations. Samples collected in the eastern tropical Pacific represent a composite of ~five individuals. The $\delta^{15}N$ values for each species were normalized against the average value for that species within the study region. (**c**) A map of the residuals between the interpolated $\delta^{15}N$ values for the two species (i.e., observable difference between the normalized values). Regions with positive residuals represent areas where the $\delta^{15}N$ values of YFT are greater than BET and negative residuals represent areas where the $\delta^{15}N$ values of BET are greater than YFT (Data are from Graham et al. (2009)). Fig. 14.5, see Appendix 1, Color Section

Hawaiian Islands (Adam et al. 2003; Sibert et al. 2003), and YFT tracked near Baja California (Schaefer et al. 2007), but also show that this residency behavior in tuna exists at a population level and over a much larger spatial scale than previously documented. Accordingly, these results suggest that managing tuna fisheries on a basin-wide or sub-basin scale could lead to localized depletions in certain regions because these tuna demonstrate higher site fidelity than previously recognized.

The next step in the study of tuna isoscapes should be to develop a model that quantifies tuna movements. Coupling tissue turnover rates and isoscapes can provide broad constraints on the maximum net directional movements required to maintain the tuna isotopic gradients (Graham et al. 2009). Tuna movements, however, are not simply directed or unidirectional, but include random or diffusive movements. Applying an advection-diffusion reaction model (Sibert and Hampton 2003) to isotopic datasets should better approximate fish movements. Once quantitative estimates of tuna movements can be derived from a synthesis of isotope datasets, these movement rates should be validated with extrinsic tagging datasets and, ultimately, incorporated into stock assessment models to improve the spatial resolution of tuna fisheries management.

Comparing isoscapes of different species over the same geographical range can provide insight into interspecific differences in their resource and habitat utilization. In the equatorial Pacific Ocean, large-scale differences occur in the $\delta^{15}N$ isoscapes of BET and YFT (Fig. 14.5c), however, a significant linear relationship exists between the interpolated (or estimated) $\delta^{15}N$ values of the BET and YFT isoscapes (p-value < 0.01) (Fig. 14.6). This correlation between the two species suggests that although their $\delta^{15}N$ values vary spatially, there is a consistent relationship between their $\delta^{15}N$ values. The interpolated values of the two species of tuna deviate from a direct 1:1 relationship, because at low $\delta^{15}N$ values, YFT have slightly higher $\delta^{15}N$

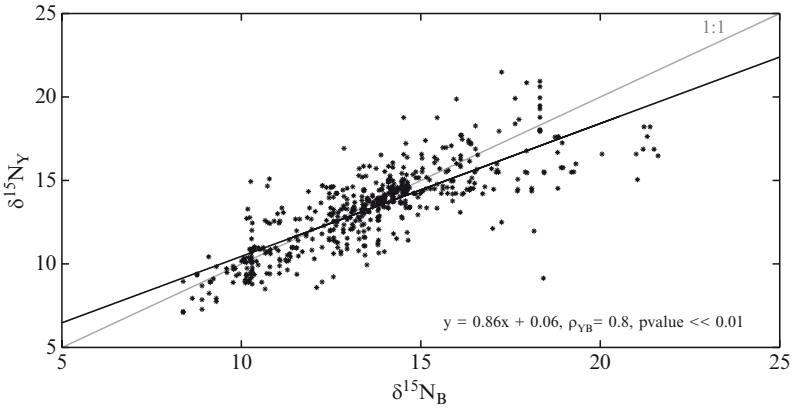

Fig. 14.6 Bivariate plot of the interpolated (estimated) $\delta^{15}N$ values of bigeye ($\delta^{15}N_B$) and yellowfin tuna ($\delta^{15}N_Y$). The *black line* represents the correlation between $\delta^{15}N_Y$ and $\delta^{15}N_B$ values (Pearson correlation coefficient (ρ_{YB})). The *gray line* represents the 1:1 relationship (Data are from Graham et al. (2009))

values than BET, and at high $\delta^{15}N$ values BET have higher values than YFT (Fig. 14.6). We hypothesize that this interspecific pattern relates to differences in their foraging behavior. In the eastern tropical Pacific Ocean, Olson and Watters (2003) assessed trophic levels for upper-trophic level predators with an Ecopath model and estimated the TL to be 5.3 and 4.8 for large BET and YFT, respectively. Large BET generally feed at greater depths than YFT, and while at depth BET can feed on squids and fish species that are at higher trophic levels (e.g., Menard et al. 2006). Small BET and YFT had similar TLs (Olson and Watters 2003). Consequently, small BET and YFT should have similar $\delta^{15}N$ values and large BET should have higher values than larger YFT. We hypothesize that this size-related variation in the trophic dynamics of YFT and BET explains the deviation of the relationship between their $\delta^{15}N$ values from a direct 1:1 relationship. Comparing the interpolated $\delta^{15}N$ values of yellowfin and bigeye tuna suggests that there are components of their foraging behavior that are consistent across the equatorial Pacific Ocean.

In the central and eastern equatorial Pacific Ocean, just a few degrees north of the equator, YFT $\delta^{15}N$ values are higher than BET $\delta^{15}N$ values (Fig. 14.5c). Unless YFT forage at a higher trophic level in this area relative to all other regions, this isotopic difference could represent deviations in BET and YFT habitat utilization. We would predict the baseline $\delta^{15}N$ values to be low at the upwelling area along the equator because of the large pool of NO_3^- and the low rate of utilization by phytoplankton. If BET forage more exclusively in these equatorial waters, then BET $\delta^{15}N$ values would reflect the low baseline values. Additionally, if YFT spent more time foraging at higher latitudes, where there are higher baseline $\delta^{15}N$ values associated to the utilization of nitrate that advects north from the equator, then the $\delta^{15}N$ values of YFT would be higher in these regions. The deviation between YFT and BET $\delta^{15}N$ values at the boundary between low $\delta^{15}N$ values in the equatorial region and higher values at higher latitudes might reflect their relative residency at the equator.

Schaefer et al. (2007) suggested that reproductively mature YFT in the eastern Pacific make seasonal movements to the equator during spawning periods and smaller or non-reproductive individuals remain at higher latitudes. The isotopic difference observed between the YFT and BET isoscapes could result from YFT moving into equatorial regions from subtropical latitudes (higher $\delta^{15}N$ values) to use the warm surface waters for spawning, whereas BET reside and forage within the equatorial region (lower $\delta^{15}N$ values) during spawning and non-spawning periods. Hence, yellowfin and bigeye could exhibit population-level niche separation, where these tunas share habitat along the equator during spawning, but otherwise separate their main foraging regions. Overall, tuna isoscapes provide large-scale, population-level information that then can be tested with high-resolution extrinsic tracking techniques.

14.3 Summary and Future Directions

Over the past two decades, marine ecologists have spent considerable resources developing and deploying electronic and satellite tagging technologies. Recent initiatives such as TOPP (Tagging of Pacific Pelagics, www.topp.org) have amassed

tremendous amounts of high-resolution three-dimensional tracking data that has have given us incredible insight into the movement patterns and foraging strategies of elusive animals difficult to study in their natural environments. Furthermore, tagging programs are beginning to collaborate with biological and physical oceanographers to map the vertical temperature and chemical structure of remote pelagic regions by placing instrumentation on large marine animals (e.g., Biuw et al. 2007). These activities represent a unique opportunity for isotope ecologists to calibrate and expand their tool in marine ecology, specifically in the creation and eventual utilization of $\delta^{13}C$ and $\delta^{15}N$ marine isoscapes. While isoscapes will never achieve the fine-spatial scale details obtained with satellite tags and on-board instrumentation (e.g., time-depth recorders), they provide a cost-effective alternative and may be more suitable for answering population-level questions (i.e., stock discrimination) than tagging technologies or even genetic markers. For example, a typical satellite tag costs ~$4,000, and satellite time costs ~$8/tag per day. With a standard 3-month deployment, researchers invest nearly $5,000 just for the hardware to study the movements of one individual, and these costs do not reflect the personnel and logistical costs associated with the deployment of each tag. By contrast, for $5,000 the $\delta^{13}C$ and $\delta^{15}N$ values of approximately 400 individuals can be determined. Ultimately, research objectives and budget should incorporate the added knowledge gained by the union of extrinsic and intrinsic tagging approaches.

The construction of marine isoscapes from the top-down and bottom-up will take time, as there are numerous factors that must be considered in the accurate interpretation of isotopic time series from behaviorally complex predators (e.g., Wunder, this volume). Briefly, these factors can be categorized into two general types, those that relate to physiological and behavioral changes of the consumer itself, and those that result in temporal and spatial variability in isotope values at the base of the food web (i.e., baseline effects). With respect to the former, physiological condition (i.e., anabolic vs. catabolic state), isotopic turnover/growth rates, trophic enrichment factors between prey and predator, isotopic fractionation among tissues that relate to differences in amino acid composition (i.e., tissue-dependent fractionations), and intra-specific variation in trophic level must be considered as potential sources of isotopic variability when attempting to create spatial and/or temporal isoscapes with data derived from top predators.

Baseline variations result from temporal changes in physical (e.g., temperature), chemical (e.g., nutrient supply), and biological (e.g., algae species composition) variables known to control the isotopic composition of primary producers and consumers in the open ocean. A crucial step in the advancement of using isoscapes to track the movement of ancient and modern predators in oceanic ecosystems retrospectively is to determine the temporal stability of baseline values. As described in detail above, seasonal fluctuations in baseline isotope values depend upon changes in nutrient sources, species composition, biogeochemical cycling rates, and biological productivity. For instance, both annual and decadal variations in $\delta^{13}C$ and $\delta^{15}N$ values have been observed in zooplankton collected from the Gulf of Alaska in the northeast Pacific Ocean (Kline 1999; Kline et al. 2008). Similarly, Hannides et al. (2009) found nearly a 10‰ variation in the bulk $\delta^{15}N$ values of zooplankton

collected over 5 years from a single location in the subtropical Pacific Ocean. To some degree, seasonal isotopic variations at lower trophic levels will be dampened as this primary production signal is transferred up food chains to top predators (Bump et al. 2007), but careful consideration of the nutrient dynamics, temporal lags between the lower and upper trophic levels, and isotopic turnover rates will be essential to interpret baseline and predator isoscapes. We suggest that future work on assessing the isotopic baseline should focus on the development of biogeochemical models that incorporate the mechanistic processes involved in controlling the isotope values at the base of the food web. Eventually, careful consideration of these two types of factors will not only yield a temporally and spatially sensitive isoscape of the ocean, but will also teach us more about the ecology and physiology of top marine consumers.

Acknowledgements We thank B. Fry, B. Popp, R. Olson, V. Allain, F. Galvan, A. Lorrain, and J. Sibert for invaluable and continual support of the tuna research. Tuna research and BSG were funded by the Cooperative Agreement NA17RJ1230 between the Joint Institute for Marine and Atmospheric Research (JIMAR) and the National Oceanic and Atmospheric Administration (NOAA) to the Pelagic Fisheries Research Program. Marine mammal work was funded by NSF Grants EAR-0000895 and OCE-0345943, as well as by a grant from UCMEXUS.

References

Adam SM, Sibert J, Itano D, Holland K (2003) Dynamics of bigeye (*Thunnus obesus*) and yellowfin (*T. albacares*) tuna in Hawaii's pelagic fisheries: analysis of tagging data with a bulk transfer model incorporating size-specific attrition. Fish Bull 101:215–228

Altabet M (2001) Nitrogen isotopic evidence for micronutrient control of fractional NO_3^- utilization in the equatorial Pacific. Limnol Oceanogr 46:368–380

Altabet MA, Pilskaln C, Thunell R, Pride C, Sigman D, Chavez F, Francois R (1999) The nitrogen isotope biogeochemistry of sinking particles from the marine of the Eastern North Pacific. Deep-Sea Res 46:655–679

Alverson F (1963) The food of yellowfin and skipjack tunas in the eastern tropical Pacific Ocean. I-ATTC Bull 7:293–396

Aurioles D, Koch PL, Le Boeuf BJ (2006) Differences in foraging location of Mexican and California elephant seals: evidence from stable isotopes in pups. Mar Mamm Sci 22:326–338

Bearhop S, Waldron S, Votier SC, Furness RW (2002) Factors that influence assimilation rates and fractionation of nitrogen and carbon stable isotopes in avian blood and feathers. Physiol Biochem Zool 75:451–458

Bidigare RR, Fleugge A, Freeman KH, Hanson KL, Hayes JM, Hollander D, Jasper JP, King LL, Laws EA, Milder J, Millero FJ, Pancost R, Popp BN, Steinberg PA, Wakeham SG (1997) Consistent fractionation of ^{13}C in nature and in the laboratory: growth-rate effects in some haptophyte algae. Glob Biogeochem Cycles 11:279–292

Biuw M, Boehme L, Guinet C, Hindell M, Costa D, Charrassin J-B, Roquet_ F, Bailleul F, Meredith M, Thorpe S, Tremblay Y, McDonald B, Park Y-H, Rintoul SR, Bindoff N, Goebel M, Crocker D, Lovell P, Nicholson J, Monks F, Fedak MA (2007) Variations in behavior and condition of a Southern Ocean top predator in relation to in situ oceanographic conditions. Proc Nat Acad Sci Am U S A 104:13705–13710

Block BA, Teo SL, Walli A, Boustany A, Stokesbury MJ, Farwell CJ, Weng KC, Dewar H, Williams TD (2005) Electronic tagging and population structure of Atlantic bluefin tuna. Nature 434:1121–1127

Bump JK, Fox-Dobbs K, Bada JL, Koch PL, Peterson RO, Vucetich JA (2007) Stable isotopes, ecological integration, and environmental change: wolves record atmospheric carbon isotope trend better than tree rings. Proc Royal Soc B: Biol Sci 274:2471–2480

Burton RK, Koch PL (1999) Isotopic tracking of foraging and long-distance migration in northeastern Pacific pinnipeds. Oecologia 119:578–585

Burton RK, Snodgrass JJ, Gifford-Gonzalez D, Guilderson T, Brown T, Koch PL (2001) Holocene changes in the ecology of northern fur seals: insights from stable isotopes and archaeofauna. Oecologia 128:107–115

Cherel Y, Hobson KA (2007) Geographical variation in carbon stable isotope signatures of marine predators: a tool to investigate their foraging areas in the Southern Ocean. Mar Ecol Prog Ser 329:281–287

Cherel Y, Hobson KA, Hassani S (2005) Isotopic discrimination between food and blood and feathers of captive penguins: implications for dietary studies in the wild. Physio Biochem Zool 78:106–115

Clementz MT, Koch PL (2001) Differentiating aquatic mammal habitat and foraging ecology with stable isotopes in tooth enamel. Oecologia 129:461–472

Dore JE, Brum JR, Tupas LM, Karl DM (2002) Seasonal and interannual variability in sources of nitrogen supporting export in the oligotrophic subtropical North Pacific Ocean. Limnol Oceanogr 47:1595–1607

Eppley RW, Peterson BJ (1979) Particulate organic matter flux and planktonic new production in the deep ocean. Nature 282:677–680

Farrell JW, Pedersen TF, Calvert SE, Nielsen B (1995) Glacial-interglacial changes in surface nitrate utilization in the equatorial Pacific Ocean. Nature 377:514–517

Fry B (1988) Food web structure on Georges Bank from stable C, N, and S isotopic compositions. Limnol Oceanogr 33:1182–1190

Goericke R, Fry B (1994) Variations in marine plankton $\delta^{13}C$ with latitude, temperature, and dissolved CO_2 in the world ocean. Glob Biogeochem Cycles 8:85–90

Graham BS, Fry B, Popp BN, Olson RJ, Holland KN (2009) Tissue turnover rates in captive and wild populations of an endothermic teleost, yellowfin tuna, in captivity and in the wild. J Exp Mar Biol Ecol

Gunn J, Hampton J, Evans K, Clear N, Patterson T, Bigelow K, Langley A, Leroy B, Williams P, Miyabe N, Sibert J, Bestley S, Hartmann K (2005) Migration and habitat preferences of bigeye tuna, *Thunnus obesus*, on the east coast of Australia. CSIRO Mar Res Bull 199

Hampton J (2002) Stock assessment of yellowfin tuna in the western and central Pacific Ocean. 2002 SCTB Working Paper.

Hannides CCS, Popp BN, Landry MR, Graham BS (2009) Quantitative determination of zooplankton trophic position using amino acid-specific stable nitrogen isotope analysis. Limnol Oceanogr 54:50–61

Hobson KA (1999) Tracing origins and migration of wildlife using stable isotopes: a review. Oecologia 120:314–326

Hobson KA, Schell DM, Renouf D, Noseworthy E (1996) Stable carbon and nitrogen isotopic fractionation between diet and tissues of captive seals: implications for dietary reconstructions involving marine mammals. Can J Fish Aquat Sci 53:528–533

Hobson KA, Sease JL, Merrick RL, Piatt JF (1997) Investigating trophic relationships of pinnipeds in Alaska and Washington using stable isotope ratios of nitrogen and carbon. Mar Mammal Sci 13:114–132

Holland KN, Brill RW, Chang RC (1990) Horizontal and vertical movements of yellowfin and bigeye tuna associated with fish aggregating devices. Fish Bull 88:493–507

Holland KN, Kleiber P, Kajiura SM (1999) Different residence times of yellowfin tuna, *Thunnus albacares*, and bigeye tuna, *T. obsesus*, found in mixed aggregations over a seamount. Fish Bull 97:392–395

Hoyle SD, Maunder MN (2006) Status of yellowfin tuna in the eastern Pacific Ocean in 2005 and outlook for 2006. I-ATTC Stock Assessment Report 7, pp 144

Itano, DG (2000) The reproductive biology of yellowfin tuna (*Thunnus albacares*) in Hawaiian waters and the western tropic Pacific Ocean: project summary. SOEST-JIMAR # 00-328, pp 69

Kim S, Casper D, Koch PL (2008) Calibrating isotopic methods to study shark ecology. In: Abstract of the 6th international conference on applications of stable isotope techniques to ecological studies, Honolulu, Hawaii, 25–29 August 2008

Kline TC (1999) Temporal and spatial variability of $^{13}C/^{12}C$ and $^{15}N/^{14}N$ in pelagic biota of Prince William Sound, Alaska. Can J Fish Aquat Sci 56:94–117

Kline TC, Boldt JL, Farley EV, Haldorson LJ, Helle JH (2008) Pink salmon (*Oncorhynchus gorbuscha*) marine survival rates reflect early marine carbon source dependency. Prog Oceanogr 77:194–202

Kurle CM (2002) Stable-isotope ratios of blood components from captive northern fur seals (*Callorhinus ursinus*) and their diet: applications for studying the foraging ecology of wild otariids. Can J Zool 80:902–909

LeBoeuf BJ, Crocker DE, Costa DP, Blackwell SB, Webb PM, Houser DS (2000) Foraging ecology of northern fur seals. Ecol Monogr 70:353–382

Lee SH, Schell DM, McDonald TL, Richardson WJ (2005) Regional and seasonal feeding by bowhead whales (*Balaena mysticetus*) as indicated by stable isotope ratios. Mar Ecol Progr Ser 286:271–287

Lutcavage ME, Brill RW, Skomal GB, Chase BC, Howey PW (1999) Results of pop-up satellite tagging on spawning size class fish in the Gulf of Maine: do North Atlantic bluefin tuna spawn in the mid-Atlantic? Can J Fish Aquat Sci 56:173–177

Martínez del Rio C, Wolf N, Carleton SA, Gannes LZ (2009) Isotopic ecology ten years after a call for more laboratory experiments. Biol Rev 84:91–111

Menard F, Labrune C, Shin Y, Asine A, Bard F (2006) Opportunistic predation in tuna: a size-based approach. Mar Ecol Prog Ser 323:223–231

Menard F, Lorrain A, Potier M, Marsac F (2007) Isotopic evidence of distinct feeding ecologies and movement patterns in two migratory predators (yellowfin tuna and swordfish) of the western Indian Ocean. Mar Biol 153:141–152

Montoya JP (2007) Natural abundance of ^{15}N in marine planktonic ecosystems. In: Michener R and K. Lajtha (eds) Stable isotopes in ecology and environmental science, 2nd ed. Blackwell, Malden, MA, pp 176–201

Newsome SD, Etnier MA, Gifford-Gonzalez D, Phillips DL, van Tuinen M, Hadly EA, Costa DP, Kennett DJ, Guilderson TP, Koch PL (2007a) The shifting baseline of northern fur seal ecology in the northeast Pacific Ocean. Proc Nat Acad Sci 104:9709–9714

Newsome SD, Etnier MA, Kurle CM, Waldebauer JR, Chamberlain CP, Koch PL (2007b) Historic decline in primary productivity in western Gulf of Alaska and eastern Bering Sea: isotopic analysis of northern fur seal teeth. Mar Ecol Prog Ser 332:211–224

Newsome SD, Clementz MR, Koch PL (in press) Using stable isotope biochemistry to study marine mammal ecology. Mar Mamm Sci

Olson RJ, Watters GM (2003) A model of the pelagic ecosystem in the eastern tropical Pacific Ocean. I-ATTC Bull 22:135–218

Olson RJ, Popp BN, Graham BS, López-Ibarra GA, Galván-Magaña F, Lennert-Cody CE, Bocanegra-Castillo N, Wallsgrove NJ, Gier E, Alatorre-Ramírez V, Balance LT, Fry B (in press) Food web inferences of stable isotope spatial patterns in copepods and yellowfin tuna in the pelagic eastern Pacific Ocean. Prog Oceanogr

Outridge PM, Davis WJ, Stewart RE, Born EW (2003) Investigation of the stock structure of Atlantic walrus (*Odobenus rosmarus rosmarus*) in Canada and Greenland using dental Pb isotopes derived from local geochemical environments. Arctic 56:82–90

Pancost RD, Freeman KH, Wakeham SG, Robertson CY (1997) Controls on carbon isotope fractionation by diatoms in the Peru upwelling region. Geochim Cosmochim Acta 61:4983–4991

Polovina JJ, Howell E, Kobayashi DR, Seki MP (2001) The transition zone chlorophyll front, a dynamic global feature defining migration and forage habitat for marine resources. Progr Oceanogr 49:469–483

Popp BN, Laws EA, Bidigare RR, Dore JE, Hanson KL, Wakeham SG (1998) Effect of phytoplankton cell geometry on carbon isotopic fractionation. Geochim Cosmochim Acta 62:69–77

Popp BN, Graham BS, Olson RJ, Hannides CCS, Lott MJ, Lopez-Ibarra GA, Galvan-Magana F, Fry B (2007) Insight into the trophic ecology of yellowfin tuna, *Thunnus albacares*, from compound-specific nitrogen isotope analysis of proteinaceous amino acids. In: Dawson T, R. Siegwolf (eds) Stable isotopes as indicators of ecological change. Elsevier Academic Press, San Diego, CA, pp 173–190

Rau GH, Ainley DG, Bengtson JL, Torres JJ, Hopkins TL (1992) $^{15}N/^{14}N$ and $^{13}C/^{12}C$ in Weddell Sea birds, seals, and fish – implications for diet and trophic structure. Mar Ecol Prog Ser 84:1–8

Rau GH, Chavez FP, Friederich GE (2001) Plankton $^{13}C/^{12}C$ variations in Monterey Bay, California: evidence of non-diffusive inorganic carbon uptake by phytoplankton in an upwelling environment. Deep-Sea Res I 48:79–94

Ream RR, Sterling JT, Loughlin TR (2005) Oceanographic features related to northern fur seal migratory movements. Deep-Sea Res II 52:823–843

Reintjes J, King J (1953) Food of yellowfin tuna in the central Pacific. Fish Bull 54:90–110

Saino T, Hattori A (1987) Geographical variation of the water column distribution of suspended particulate organic nitrogen and its ^{15}N natural abundance in the Pacific and its marginal seas. Deep-Sea Res 34:807–827

Schaefer KM, Fuller DW, Block BA (2007) Movements, behavior, and habitat utilization of yellowfin tuna (*Thunnus albacares*) in the northeastern Pacific Ocean, ascertained through archival tag data. Mar Biol 152:503–525

Schell DM, Saupe SM, Haubenstock N (1989) Bowhead Whale (*Balaena mysticetus*) growth and feeding as estimated by $\delta^{13}C$ techniques. Mar Biol 103:433–443

Schell DM, Barnett BA, Vinette KA (1998) Carbon and nitrogen isotope ratios in zooplankton of the Bering, Chukchi and Beaufort seas. Mar Ecol Prog Ser 162:11–23

Sibert J, Hampton J (2003) Mobility of tropical tunas and the implications for fisheries management. Mar Policy 27:87–95

Sibert JR, Musyl MK, Brill RW (2003) Horizontal movements of bigeye tuna (*Thunnus obesus*) near Hawaii determined by Kalaman filter analysis of archival tagging data. Fish Oceanogr 12:1–11

Sibert J, Hampton J, Kleiber P, Maunder M (2006) Biomass, size, and trophic status of top predators in the Pacific Ocean. Science 314:1773–1776

Sigman DM, Casciotti KL (2001) Nitrogen isotopes in the ocean. In: Steele JH, Turekian KK, Thorpe SA (eds) Encyclopedia of ocean sciences. Academic, London, pp 2449

Stewart BS, DeLong RL (1995) Double migrations of the northern elephant seal, *Mirounga angustirostris*. J Mamm 76:196–205

Stewart REA, Outridge PM, Stern RA (2003) Walrus life-history movements reconstructed from lead isotopes in annual layers of teeth. Mar Mamm Sci 19:806–818

Voss M, Dippner JW, Montoya JP (2001) Nitrogen isotope patterns in the oxygen-deficient waters of the Eastern Tropical North Pacific Ocean. Deep-Sea Res 48:1905–1921

McMahon KW, Lysiak N, Brin L, Buckman K, Kneeland J, Gibbons F, Thorrold SR (in review) Ocean ecogeochemistry applied to connectivity analyses in marine populations. Estuar Coast Shelf Sci

Chapter 15
Toward a $\delta^{13}C$ Isoscape for Primates

Margaret J. Schoeninger

15.1 Introduction

Within the field of anthropology, stable isotope data have contributed to several lines of investigation including diet reconstruction and forensics (see Ehleringer and Schwarcz this volume), residential mobility (Knudson and Price 2007), management of domestic animals (Balasse et al. 2003), and reconstructing paleoenvironmental conditions (Wynn 2000) among others. In studies that use $\delta^{13}C$ data, it is most common to assume that the value in human or animal tissue or in paleosols reflects an integration of C_3 and/or C_4 inputs where both C_3 and C_4 plant components are assigned a particular average value depending on the expected $\delta^{13}C$ value of atmospheric CO_2 (see Still this volume for an example of this in modeling continental-scale distributions of plant $\delta^{13}C$ values).

Yet while the distribution of $\delta^{13}C$ values across all plant species is bimodal (C_3 and C_4), herbaceous vegetation, trees, and cool season grasses (C_3 plants) display $\delta^{13}C$ values that range from −31‰ to −23‰ (O'Leary 1988), and much of this variation is associated with the level of canopy cover where these plants grow (see Heaton 1999). Data from a series of studies on nonhuman primates (Schoeninger et al. 1997, 1998, 1999; McGee and Vaughn 2003; Sponheimer et al. 2006; Loudon et al. 2007), summarized below, suggest that within C_3-feeding primates, $\delta^{13}C$ values vary with canopy cover as well. Directions for future research, anticipated impacts for conservation, and the implications for interpreting behavior within a group of fossil humans (Neanderthals) and earlier members of the human lineage (australopithecines and *Homo habilis*) are considered at the end of this presentation.

M.J. Schoeninger (✉)
Department of Anthropology, University of California at San Diego, La Jolla, CA, 92093-0532, USA
e-mail: mjschoen@ucsd.edu

J.B. West et al. (eds.), *Isoscapes: Understanding Movement, Pattern, and Process on Earth Through Isotope Mapping*, DOI 10.1007/978-90-481-3354-3_15,

15.2 $\delta^{13}C$ Variation in Plants and the Animals That Feed on Them

Patterned differences in $\delta^{13}C$ variation of C_3 plants have been known for almost two decades (van der Merwe and Medina 1989; Broadmeadow et al. 1992). Such differences are due to variations in: (1) the $\delta^{13}C$ value in the carbon dioxide available to the plant during photosynthesis and (2) a set of isotope effects that occur during the process of photosynthesis (including the overall rate of photosynthesis). The $\delta^{13}C$ value of well-mixed atmospheric carbon dioxide today is around −7.8‰ (Wahlen 1994), that reported in deciduous tropical forests (i.e., open canopies) is similar (−8.3 to −7.8‰) to the atmospheric value; but that within semievergreen tropical forests (i.e., more closed canopies) has been reported as low as −9.9‰ (Broadmeadow et al. 1992). The more negative values within forests are partially due to the addition of ^{12}C-enriched carbon dioxide respired from microbial activity on soil organic detritus (van der Merwe and Medina 1989). In open areas such as savannas or deciduous bush/woodlands, the carbon dioxide available to plants should be around −7.8‰ whereas that available to plants in forests varies according to the amount of soil-respired carbon dioxide and the amount of mixing with atmospheric carbon dioxide. The carbon isotope ratios of this respired CO_2, vary dramatically both temporally and spatially within C_3 environments (Pataki et al. 2003), yet plant leaves (and presumably fruits and nuts) monitor these fluxes poorly (Bowling et al. 2003) probably because plant parts integrate the variation within the CO_2 available to the plants during photosynthesis. The $\delta^{13}C$ values in top predators (e.g., wolves) clearly monitor large-scale trends in atmospheric carbon dioxide presumably by integrating the variation in their prey herbivores, which in turn integrate intra- and inter-annual variation in the $\delta^{13}C$ of plants (Bump et al. 2007).

Although much inter-annual and inter-seasonal variation in plant tissues is not yet understood (see Cerling et al. 2003; Bowling et al. 2008), there are some generalities that apply. Increased concentrations of the carbon dioxide available to plants, such as occur in closed canopies due to the addition of soil-respired carbon dioxide and low light levels, associate with more negative leaf values (Broadmeadow et al. 1992), and high light levels, such as occur in more open canopies, and lower CO_2 concentrations associate with less negative leaf $\delta^{13}C$ values (Yakir and Israeli 1995). There is also variation within forests such that leaves at the top of the highest trees have the highest $\delta^{13}C$ values while those at the very base have the lowest values.

These relationships in plants have been reported as present and consistent from every continent, and data from a wide range of animals species (mostly large herbivorous mammals) demonstrate that they are recorded in the animals feeding on these plants (see Krigbaum 2003 for a recent summary). Data from a large study comprising several bovid species in East Africa (Cerling et al. 2003) demonstrate a correlation between the $\delta^{13}C$ values in hair and other keratinaceous tissues, and the level of canopy cover. Suni antelope, bongo and bushbuck, which all lived in closed canopy forests have values around −25‰. Although the bongo is reported to come from an open forested region, this species is noted for its closed forest preferences

and probably fed within such forests. In contrast, two duiker species also from a closed canopy have values that are approximately 1–2‰ higher (−24‰ and −22‰). Whether the apparent contradiction of these two duiker species is due to the particular feeding habits of duikers (fruits) or to the specific structure of their forest is not clear. Different populations of two species of duiker from deciduous, open woodlands have an average of −23.5‰. Gerenuk, two species of dikdik, and eland living in areas with open canopies have average values between −21.6‰ and −20.4‰.

15.3 A Primate $\delta^{13}C$ Isoscape?

Primates should integrate the $\delta^{13}C$ variation in plants within the band of tropical environments. The order primates includes largely tropical species although today some members of the Old World monkey subfamily, cercopithecine, live in temperate regions (e.g., Japanese macaques). Further, most species feed on a wide range of foods with marked seasonal variation in contrast to many other herbivorous mammalian species. Many species are arboreal, feeding throughout canopies and should integrate intra-canopy variation in plant $\delta^{13}C$ values (Heaton 1999). Significantly, most primates feed largely on C_3 foods (Milton 1987), although several cercopithecine species consume significant quantities of grass seeds and grass corms as well (Jolly 1970; Codron et al. 2005). This combination of factors led my colleagues and me to expect that the $\delta^{13}C$ values in primate tissues would associate with gross-level differences in canopy cover in forests and woodlands.

A series of studies across several species of extant primates (including prosimians, monkeys and apes) demonstrate that their hair $\delta^{13}C$ values correlate with canopy cover irrespective of their specific diets or phyletic assignment (Schoeninger et al. 1997; Schoeninger et al. 1998, 1999), and more recent work by others, summarized below, supports those findings. Gross metabolic differences appear to have little effect as body size varied dramatically across the species from small galagos (prosimians) and capuchins (monkeys) to larger monkeys (howling monkeys and muriquis) to very large apes (chimpanzees). Geographic variation in plant species also appeared to have little effect as samples were taken from Central and South American, Africa, and Madagascar.

Reference to a primate $\delta^{13}C$ isoscape involves a question mark because for each study reported, the sample size for each species is small. Most primate species are either endangered or virtually extinct and obtaining tissues for analysis is nontrivial. Obtaining hair samples from monkeys and prosimians required the trapping of individual animals that were collected as part of larger, long-term behavioral studies, which included routine capture for assessing physiological status (Glander et al. 1991). None of the chimpanzee populations sampled was habituated to the presence of humans; therefore hairs for analysis were taken from night nests. Care was taken to avoid sampling the same animal twice by collecting hairs from fresh nests. Since chimpanzees nest high in trees, obtaining hair samples required extensive tree-climbing.

Further, separating the influence of diet from that of canopy cover requires extensive dietary information on each primate population sampled. The number of long-term field studies on habituated populations where feeding can be observed, recorded, and analyzed are limited. Tracking devices are required to obtain feeding data for nocturnal primates like galagos and lepilemur; such studies are limited. In the primary cases discussed here, feeding behavior was recorded and comparative information was available on each individual animal in several of the behavioral studies. For the unhabituated chimpanzee populations, fecal material or other proxy indicators were evaluated in order to determine diet. The results from the primary studies are shown graphically in Fig. 15.1.

Two species of Central American monkeys, spider monkey (*Ateles geoffroyi*) and the capuchin monkey (*Cebus capucinus*), come from closed canopy forest consisting of evergreen and semievergreen tree stands. The forest (La Selva, Costa Rica) exhibits low seasonality in rainfall with average rainfall around 4,000 mm/year (Janzen 1983). The two monkey species have identical $\delta^{13}C$ values (Schoeninger et al. 1997 and see Fig. 15.1) although their diets differ markedly. The spider

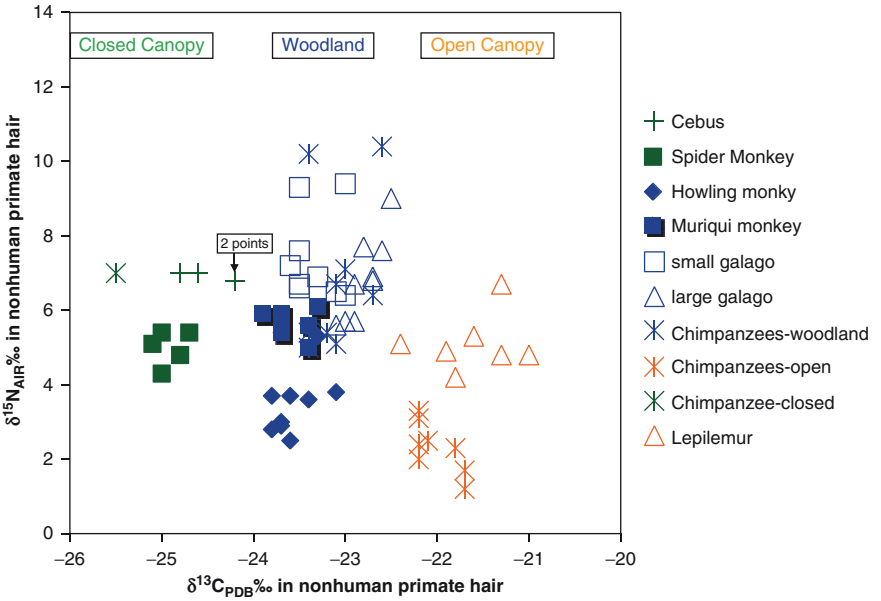

Fig. 15.1 $\delta^{13}C$ values in hair from across primate species reflect the level of canopy cover in the areas in which the animals lived irrespective of their specific diets (indicated by $\delta^{15}N$ values, see text for discussion). Two species of New World monkeys from closed canopies show values around −26‰ to −24.5‰. Two other species of New World monkeys, two species of African prosimians, and a population of chimpanzees, which all live in deciduous woodland regions show values around −24‰ to −23‰. One species of prosimian from Madagascar and a population of chimpanzees living in open canopy savanna-woodland habitats have values between −22 and −21‰ (Data from Schoeninger et al. 1997, 1998, 1999). Fig. 15.1, see Appendix 1, Color Section

monkey is a highly selective fruit-eater with merely 20% of their diet consisting of young leaves; mature leaves are avoided (Strier 1992). This adaptation is confirmed by their tooth morphology (Kay 1975), digestive tract morphology (Chivers and Hladik 1980), and rapid food assimilation rates (Milton 1984) in addition to behavioral observations on the population sampled. In contrast, the capuchin monkey is a noted omnivore with a diet that includes a significant weight percent of insects with ranges in different populations reported from 20% to over 50% (data cited in Fedigan et al. 1985). Tooth morphology, as well as time spent feeding, indicates that fruit is also preferred food (Kay 1975; Fedigan et al. 1985). The $\delta^{15}N$ values in these two species are consistent with behavioral observations. The omnivorous capuchin has values that are 1.5–2.5‰ higher than those in the spider monkey or about that expected due to the trophic level offset in their diets (Schoeninger and DeNiro 1984). Yet, even with these dietary differences and even though fruit is eaten in greater amounts (relative to body size) by the spider monkey, the two species show very similar average $\delta^{13}C$ values in hair (−25‰). This average value is similar to the majority of East African bovid species in closed canopy forests; but contrasts with the fruit-eating forest duikers, which had higher $\delta^{13}C$ values (Cerling et al. 2003). The hair from a single chimpanzee living in a closed canopy forest in West Africa shows $\delta^{15}N$ values similar to those of the capuchins; but a slightly lower $\delta^{13}C$ value than those of the two New World monkey species.

Five extant primate species with extensive information on diet were available from deciduous woodlands. These include two New World monkey species, two sympatric species of African prosimians, and a population of Tanzanian chimpanzees (Schoeninger et al. 1999). Their $\delta^{13}C$ values are similar to each other (Fig. 15.1) and are higher than those species from the closed canopy forests. The two New World monkey species include the mantled howler monkey (*Alouatta palliata*) from Costa Rica, and the muriqui (*Brachyteles arachnoides*) from Brazil. The mantled howler monkeys showed seasonal differences in hairs collected from the rainy and dry seasons at a low level of significance even though they show no significant differences between the sampling years nor was there any difference between sexes (Schoeninger et al. 1997). Howler monkeys have the tooth morphology of a folivore (Kay 1975), with the digestive tract morphology and function of a primary leaf-eater that includes fruit in its diet (Chivers and Hladik 1980; Milton 1984). The specific troop that was sampled for stable isotope analysis also spends approximately 40% of its feeding time ingesting leguminous plant parts (Glander 1981). In contrast, muriqui molar size and morphology suggests a greater emphasis on fruit-eating (Rosenberger 1992) and observations indicate that they prefer fruit when available (Strier 1992). The two African prosimian species are both galagos (*Galgago zanzibaricus* and *Otolemur garnettii*) that live in a lowland, dry forest in the Gedi Ruins National Monument in Kenya. Both species are omnivorous and focus on insects and fruits; the larger species (*O. garnettii*) eats relatively less animal prey than does the smaller species (*G. zanzibaricus*) (Harcourt and Nash 1986).

The last species from deciduous woodland is the chimpanzee. This particular population, from the Democratic Republic of the Congo (DRC), lives along a

perennially flowing river lined by trees comprised mainly of deciduous with some evergreen species. Superficially, the area looks very similar to that inhabited by the mantled howler monkey species. Tree fruits are considered the basic food for chimpanzees (Wrangham 1977; Teleki 1981; McGrew et al. 1988) but actual intake levels vary. When preferred fruits are less available, individuals may add hard seeds (Suzuki 1969), stems (McGrew et al., 1988) or pith (Wrangham et al. 1991). Leaves generally provide protein; but seeds, insects or meat (McGrew 1983; Boesch 1994; Stanford 1996) can also be eaten. Analysis of 113 fecal samples showed that for this particular population, the most common foods were the fleshy fruits from trees and shrubs along the forest margins (Steklis et al. 1992).

The $\delta^{15}N$ values agree with the feeding observations and fecal analyses. The howling monkeys, which ate significant amounts of leguminous vegetation, have the lowest values. The frugivorous folivore, the muriqui, has values about two per mil higher and quite similar to the frugivorous spider monkey. The omnivorous galagos and the chimpanzees are, on average, higher and show a wider range of values, between 6‰ and 10‰. Insect-eating in the galagos explains the high values in these two species. Meat- and insect-eating may also explain the values in the chimpanzees (Stanford 1996) although because this population is unhabituated, observations of feeding were not available and fecal analyses under-represent both types of intake. In contrast to the marked variation in $\delta^{15}N$ values, this set of five extant species, all have $\delta^{13}C$ values between −24‰ and −23‰. Thus, even though they represent different subsistence strategies (folivore, frugivore, and omnivore), different continents (Central and South America, and Africa), and different taxonomic units (prosimians, monkeys, and apes), they have very similar $\delta^{13}C$ values that are 1–1.5‰ higher than those of the monkey species from closed canopy forests. Their values are similar to bovid species from similar types of forests.

Two final primate species were sampled from two different open canopy woodlands that were significantly drier and more open than the two previous types of habitats. Both regions had broken canopies with grass growing beneath the trees. As with the previous comparisons, these two species have values similar to each other even though their diets differed dramatically (Fig. 15.1). The two species are the prosimian, *Lepilemur leucopus*, from a region of Madagascar that had been subjected to lengthy drought conditions (Schoeninger et al. 1998) and a population of chimpanzees from a dry, open savanna-woodland in the Ugalla region of the Tongwe Forest Reserve of Tanzania (Schoeninger et al. 1999). Approximately 250 hours of focal follows on individual lepilemurs revealed that all feeding was on leaves, stems, or flowers; seeds were found in only one of 69 fecal pellets (Nash 1998); two individuals observed feeding on CAM plants are not considered here. As discussed above, chimpanzees focus on tree fruits although 194 fecal samples collected from a region similar to Ugalla commonly included seeds from leguminous trees that are ubiquitous in both areas (Suzuki 1969).

The $\delta^{15}N$ values from the two species agree with dietary expectations. The chimpanzees have the lower values as expected for feeding on legumes. Their values are very similar to those of the troop of mantled howling monkeys that also fed on

leguminous plants. The lepilemurs have higher $\delta^{15}N$ values that are similar to those in fruit-eating monkeys from deciduous woodlands and closed canopy forests. The majority of individuals in both species have $\delta^{13}C$ values between −22‰ and −21‰ even though they differ in terms of diet (leaves, stems and flowers versus fruit- and leguminous seed-eating) and taxonomy (prosimian versus ape). Their hair $\delta^{13}C$ values most strongly reflect the type of habitat in which they lived.

More recent studies of primate hair support these earlier findings although extensive feeding data are not available from these studies. A brief abstract (McGee and Vaughn 2003) reports the average values from three populations of sifakas (prosimians) living in different regions within the Ranomafana National Park in southeastern Madagascar. Sifakas are arboreal, fruit- and seed-eaters although the specific diets of these three populations were not discussed. The region experiences high rainfall, yet extensive logging and other human disturbance have removed tree cover to a marked extent. All of the populations have average $\delta^{13}C$ values around −23.5‰, which compares well to the primate species living in Woodland environments.

Data from three different populations of ring-tailed lemurs (*Lemur catta*), a relatively large, semi-terrestrial prosimian from the Beza Mahafaly Special reserve in Madagascar also shows a correlation between canopy cover and hair $\delta^{13}C$ values (Loudon et al. 2007; see Fig. 15.2). The ring-tailed lemur is an omnivorous primate that eats mostly fruits and leaves, and their $\delta^{15}N$ values show a range of values. No specific information was given on the diets of these three populations so it is not possible to compare average $\delta^{15}N$ value with population diet. Each population's $\delta^{13}C$ values, however, plot nearly as expected from the ecology of each population's home range. The Teal group lives in the most forested region, and plots with the New World monkeys from closed canopy woodlands. The Blue group, which has a home range that includes the most disturbed habitats, overlaps with the monkeys, prosimians and the chimpanzee population that lived in open, deciduous woodlands. The Orange group has a home range that includes forest edge regions as well as disturbed forests. They plot intermediate between the other two groups of ring-tailed lemurs within the overall range of the Central American monkeys living in closed canopy environments.

Another recent study reports $\delta^{13}C$ values from a chimpanzee population from the Fongoli site in Senegal in West Africa (Sponheimer et al. 2006, see Chimpanzee-Open #2 on Fig. 15.3) that lives in an open canopy savanna-woodland similar to that of the chimpanzees from Ugalla in Tanzania (see Chimpanzee-Open #1 on Fig. 15.3). The newer study shows greater variation in $\delta^{13}C$ values than appears in the Ugalla chimpanzees. In fact, the West African chimpanzee data overlap with the chimpanzee population from the deciduous woodland environment in the DRC (see Chimpanzee-Woodland on Fig. 15.3). It would be interesting to determine if the data vary along the lines of ecological variation within Fongoli; but it is not yet possible to assess the data in this manner. Pictures of the site show areas of large trees bounded by open canopy woodland and open savanna grassland.

Although the data from different studies are not identical to expectations based on the baseline data sets discussed originally, this could be due to multiple factors

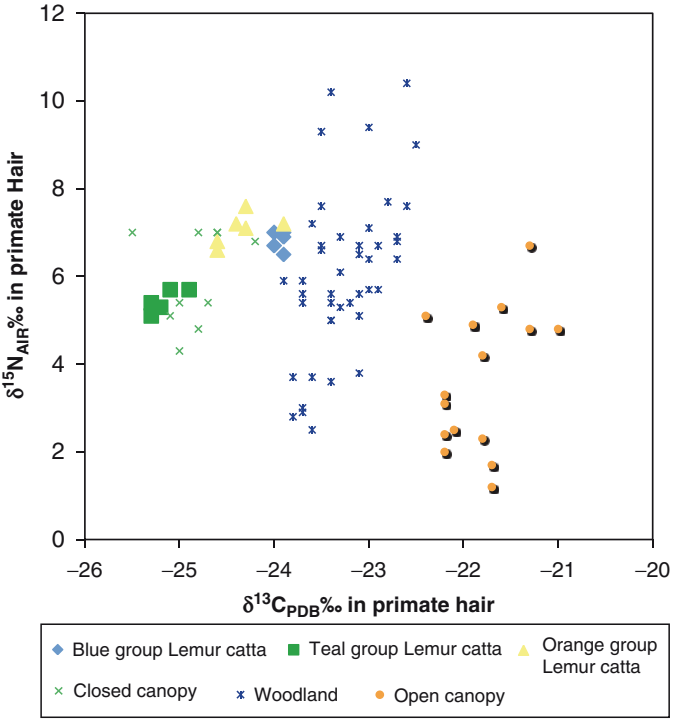

Fig. 15.2 Comparison of $\delta^{13}C$ values in three populations of ring-tailed lemurs from Madagascar (Loudon et al. 2007). The Teal group from undisturbed habitats compares favorably with closed canopy primates discussed for Fig. 15.1 and replotted here. The Blue group from the most disturbed habitat compares well with deciduous woodland canopy primates replotted here from Fig. 15.1. The Orange group comes from forest edge and disturbed habitats and plots between the other two groups. Fig. 15.2, see Appendix 1, Color Section

including hair preparation methods or other differences between laboratories. Larger samples taken from a wider range of habitats are needed to determine whether or not a primate isoscape can be developed. Hair samples from additional long-term field studies that have recorded, if not reported, diet information are critical to this endeavor. Comparison of these data with other isoscape data (e.g., Still and Powell this volume) or with GIS maps of extant vegetation and of canopy cover, if such exist, could refine our understanding of the relationships between primate hair $\delta^{13}C$ values and canopy cover. Once the relationship is clarified additional samples could be drawn from collections of primate pelts and skeletons housed in natural history museums in this and other countries. Such collections often lack specific information on habitat characteristics, including canopy cover. If, however, they could be 'fit' to probable habitat locations on the basis of their $\delta^{13}C$ values, it could expand our understanding of the original expanse of various primate populations before the present decimation of so many species.

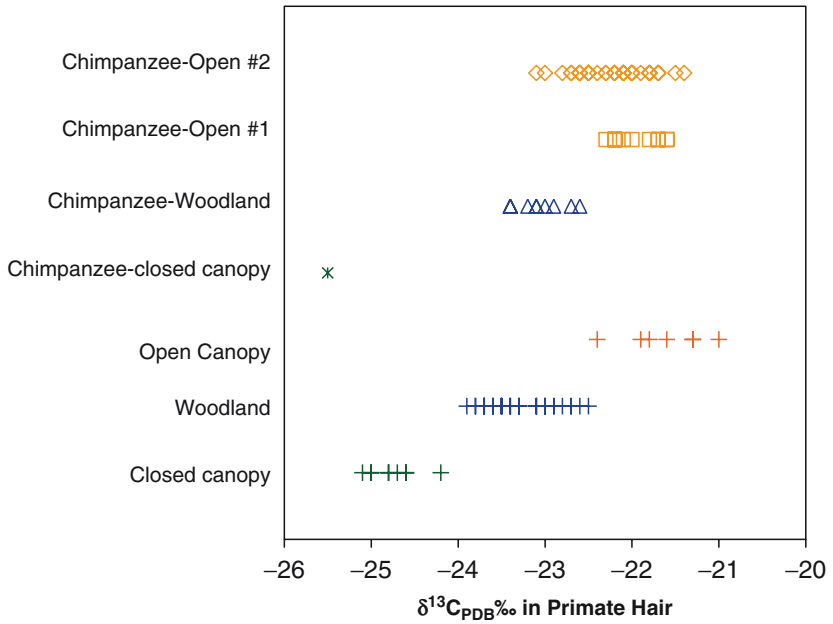

Fig. 15.3 Comparison of $\delta^{13}C$ values in chimpanzees from the open canopy savanna-woodland habitat of Fongoli in Senegaal (Sponheimer et al. 2006) with those of other chimpanzee populations discussed for Fig. 15.1 and replotted here. The Fongoli chimpanzee data overlap those from the Ugalla, Tanzania site, which also a savanna-woodland and those from Ishasha, DRC, which is a deciduous woodland habitat. Pictures of the Fongoli site show areas of tall trees as well as open woodland and open grassland regions. Regrettably, it is not possible to compare the chimpanzee hair values with specific regions at Fongoli. Fig. 15.3, see Appendix 1, Color Section

15.4 Implications for Diet Reconstruction in Early Members of the Human Lineage

Reconstructing the life ways of earlier human populations and those of our fossil ancestors and relatives is critical for testing various hypotheses regarding the course of human evolution. One required aspect for such reconstructions is the species subsistence strategy. This requires consideration of the types of habitats in which the early populations lived because habitat characteristics constrain the food items available to a primate species. Commonly, identifications of the accompanying fauna recovered from fossil sites serves to indicate whether the region was forested, woodland, bushland or savanna (e.g., Reed 1997); but in some cases, the fauna are secondarily deposited from multiple, different environments, and may not be associated with the fossil human relatives (e.g., Coffing et al. 1994). Further complicating such approaches is the fact that many terrestrial species use multiple environments during life. Plant remains are seldom preserved, which means that direct environmental or ecological reconstructions are not possible.

Other methods use the $\delta^{13}C$ values in various materials in order to reconstruct general aspects of paleoecological situations. Early methods attempted to estimate the presence of C_3 and C_4 plant types during the period of time that the earliest human ancestors appeared in eastern Africa by analyzing the $\delta^{13}C$ values in the bone mineral of various ungulate species (e.g., Cerling 1979; Cerling et al. 1988; Kingston et al. 1994) using assigned endpoints for C_3 and C_4 plants. Carbon isotope ratios in paleosols and in carbonate nodules were also used at many sites; but these are not always available or well-preserved (Wynn 2000; Cerling et al. 1988; Kingston 2007).

For reconstructing diets in extinct populations and species, the tissues analyzed most commonly are bone collagen, bone apatite and tooth enamel. Bone collagen will closely match the values in hair since both are proteins although bone collagen provides an averaging of a decade or more of diets whereas hair represents a much shorter period of time. In considering the diets of European Neandertals, the $\delta^{13}C$ values in collagen are compared directly to those in hair although 1.5‰ is added to the data from the extant species to offset the ^{12}C enrichment in the modern atmosphere (Friedli et al. 1986). The $\delta^{13}C$ values in bone collagen from European Neandertals (Bocherens, in press) compared with the estimated $\delta^{13}C$ values in primate bone collagen (Fig. 15.4) demonstrate that Neandertals foraged in open country habitats.

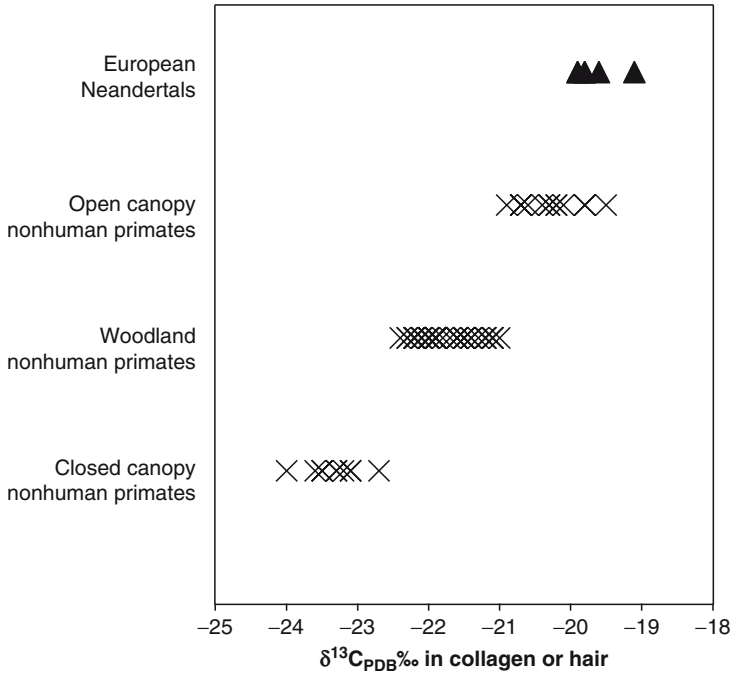

Fig. 15.4 Comparison of $\delta^{13}C$ values in collagen from four individual European Neandertals (Boucherens 2009) with estimated collagen values for the C_3-feeding primates discussed in Fig. 15.1 and replotted here. The comparison demonstrates clearly that Neandertals obtained their food (animal and plant) in regions characterized by open canopies. This contrasts with expectations that they lived in heavily forested regions

Although previous studies have attempted to reconstruct the actual species hunted by the Neandertals, the clearest signal is that they hunted and gathered in open areas even though the regions they inhabited could have been forested. This is most likely due to the fact that forest fauna seldom move in large herds and are more difficult to locate and hunt than are open country herd animals.

In considering the diets in earlier members of the human lineage, only tooth enamel is available and it is necessary to establish the expected offset between hair $\delta^{13}C$ values and those in tooth enamel. For that, we turn to the only study that measured both tissues in the same animals. In extant browsing bovids, enamel shows variable offsets from keratin (hair, hoof, and horn; Cerling et al. 2003); but in both enamel and keratin, those species from closed canopy forests have lower $\delta^{13}C$ values than do those from open Woodlands. Across eight species the average offset between keratin and enamel $\delta^{13}C$ values is 9.5‰. Therefore in estimating the tooth values for the extant primates for whom we have only hair $\delta^{13}C$ values, I added 10‰ to hair values. In addition, 1.5‰ is added to the data from the extant species to offset the ^{12}C enrichment in the modern atmosphere (Friedli et al. 1986). One more factor must be considered, i.e., diagenesis (postmortem alteration of the carbonate fraction), which can be a significant problem (Koch et al. 1997) with no generally accepted measure of assessment (although see Shemesh 1990) in fossil tooth enamel. In East Africa, some 3.9 million year old tooth enamels were extensively altered mineralogically whereas others, from the same excavation site, were not (Kohn et al. 1999). The altered enamels showed $\delta^{13}C$ values that were 1‰ to several per mil more similar to the values in sediments than was true of the unaltered enamels (Schoeninger et al. 2003). Alteration toward the sediment values results in higher $\delta^{13}C$ values than in the living animal. In South Africa, diagenetic alteration of 1–2‰ occurs (Lee-Thorp 2000) and is the value used when evaluating fossil data below.

In a comparison of published data in tooth enamel from East African *Homo habilis* and *Paranthropus boisei* (van der Merwe et al. 2008) and South African *Australopithecus africanus* and *Paranthropus robustus* (Sponheimer et al. 2005) with the estimated $\delta^{13}C$ values in primate tooth enamel (Fig. 15.5), it is clear that all these species foraged in open country or drought-type habitats rather than in closed canopy situations. Some individuals apparently added foods with a C_4 signal to their diets although what those foods may have been is still the subject of much discussion.

15.5 Final Thoughts on a Primate Isoscape

Although the preliminary data presented earlier in this manuscript supports reasonable expectations that primate $\delta^{13}C$ values could result in a tropical band isoscape, much work remains to be done in order to make such an isoscape useful. With more samples from long-term field studies in different habitats, the promise could well be fulfilled. In that event, the patterns will be useful in reconstructing habitat distributions of primates collected between the eighteenth and twentieth centuries.

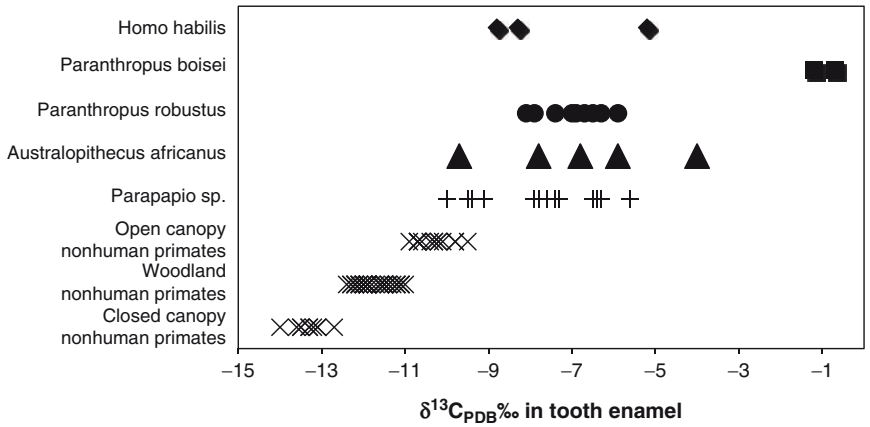

Fig. 15.5 Comparison of published $\delta^{13}C$ values from tooth enamel of several species of South and East African fossil hominines (spouheimer et al. 2005; van der Merwe et al. 2008) with estimated tooth enamel values for the C_3-feeding primates discussed in Fig. 15.1 and replotted here. Due to the changes in the d13C value of atmospheric Co2, modern primate values should be shifted 1.5‰–2‰, from 9‰ in open canopy situations to 7.5–6‰. In addition, diagenetic alteration of 1–2‰ would change the values from 7.6–6‰ to 6.5–5‰, means many could have eaten only C_3 foods; but in an open canopy savanna-woodland habitat. Some individuals, however, including both individuals of *Paranthropus robustus* appear to have eaten some foods with a C4 signal

Isotope data from primates killed illegally today as part of the bushmeat trade might also be able to identify the habitats where the poachers are working. Finally, such an isoscape would be very useful in evaluating data on fossil human populations and earlier members of our lineage in making diet estimates that consider the inherent variation in canopy cover across habitats.

Acknowledgements Thank you to Gabriel Bowen for inviting me to attend Isoscapes 2008 and to present something from the physical anthropology perspective. I probably learned more than did my audience. Also, Todd Dawson handled the review process, and I greatly appreciate the time and effort given by Brittany Graham in this regard. To Jason West, a special thanks for multiple email discussions, which opened a whole new research vista for some of my students and myself. None of the studies summarized in this manuscript would have been possible without support from multiple divisions within the National Science Foundation.

References

Balasse M, Smith A, Ambrose S, Leigh SR (2003) Determining sheep birth seasonality by analysis of tooth enamel oxygen isotope ratios: the Late Stone Age site of Kasteelberg (South Africa). J Archaeol Sci 30:205–215

Bocherens, Herve (2009) Neanderthal dietary habits: Review of the isotopic evidence. In: Hublin, Jean-Jacques and Michael P. Richards (eds) The Evolution of Hominin Diets: Integrating Approaches to the Study of Palaeolithic Subsistence. Springer pp. 241–250.

Boesch C (1994) Chimpanzees-red colobus monkeys: a predator-prey system. Anim Behav 47:1135–1148

Bowling DR, Pataki DE, Ehleringer JR (2003) Ecolsystem isotope exchange and whole-canopy discrimination in *Medicago sativa*. Agric For Meteorol 116:159–179

Bowling DR, Pataki DE, Randerson JT (2008) Carbon isotopes in terrestrial ecosystem pools and CO_2 fluxes. New Phytol 178:24–40

Broadmeadow MSJ, Griffiths H, Maxwell C, Borland AM (1992) The carbon isotope ratio of plant organic material reflects temporal and spatial variations in CO_2 within tropical forest formations in Trinidad. Oecologia 89:435–441

Bump JK, Fox-Dobbs K, Bada JL, Koch PL, Peterson RO, Vucetich JA (2007) Stable isotopes, ecological integration and environmental change: wolves record atmostpheric carbon isotope trend better than tree rings. Proc R Soc B 274(1624):2471–2480

Cerling TE (1979) Paleochemistry of Plio-Pleistocene Lake Turkana, Kenya. Palaeogeogr Palaeoclimatol Palaeoecol 27:247–285

Cerling TE, Bowman JR, O'Neil JR (1988) An isotopic study of a fluvial-lacustrine sequence: the Plio-Pleistocene Koobi-Fora sequence, East Africa. Palaeogeogr Palaeoclimatol Palaeoecol 63:335–356

Cerling TE, Harris J, Passey B (2003) Diets of East African bovidae based on stable isotope analyses. J Mammal 84(2):456–470

Chivers DJ, Hladik CM (1980) Morphology of the gastrointestinal tract in primates: comparisons with other mammals in relation to diet. J Morphol 166:337–386

Codron D, Luyt J, Lee-Thorp J, Sponheimer M, de Ruiter D, Codron J (2005) Utilization of savanna-based resources by Plio-Pleistocene baboons South African. J Sci 101:245–248

Coffing K, Feibel C, Leakey M, Walker A (1994) Four-million-year-old hominids from East Lake Turkana, Kenya. Am J Phys Anthropol 93:55–65

Fedigan LM, Fedigan L, Chapman C (1985) Census of *Alouatta palliata* and *Cebus capucinus* monkeys in Santa Rosa National Park, Costa Rica. Brenesia 23:309–322

Friedli H, Lotscher H, Oeschger H, Siegenthaler U, Stauffer B (1986) Ice core record of the $^{13}C/^{12}C$ ratio of atmospheric CO_2 in the past two centuries. Nature 324:237–238

Glander KE (1981) Feeding patterns in mantled howling monkeys. In: Kamil AC, Sargent TD (eds) Foraging behavior: ecological, ethological, and psychological approaches. Garland Press, New York, pp 231–257

Glander KE, Fedigan LM, Fedigan L, Chapman C (1991) Capture techniques and measurements of three monkey species in Costa Rica. Folia Primatol 57:70–82

Harcourt CS, Nash LT (1986) Species differences in substrate use and diet between sympatric Galagos in two Kenyan coastal forests. Primates 27(1):41–52

Heaton THE (1999) Spatial, species, and temporal variations in the $^{13}C/^{12}C$ ratios of C_3 plants: implications for palaeodiet studies. J Archaeol Sci 26:637–649

Janzen DH (1983) Costa Rican natural history. University of Chicago Press, Chicago, IL

Jolly CJ (1970) The seed-eaters: a new model of hominid differentiation based on a baboon analogy. Man 5(1):5–26

Kay RF (1975) The functional adaptations of primate molar teeth. Am J Phys Anthropol 43:195–216

Kingston JD (2007) Shifting adaptive landscapes: progress and challenges in reconstructing early hominid enviornments. Am J Phys Anthropol 134(S45):20–58

Kingston JD, Marino BD, Hill A (1994) Isotopic evidence for Neogene hominid paleoenvironments in the Kenya Rift Valley. Science 264:955–959

Knudson KJ, Price TD (2007) Utility of multiple chemical techniques in archaeological residential mobility studies: case studies from Tiwanaku- and Chiribaya-afficiated sites in the Andes. Am J Phys Anthropol 132:25–39

Koch PL, Tuross N, Fogel ML (1997) The effects of sample treatment and diagenesis on the isotopic integrity of carbonate in biogenic hydroxylapatite. J Archaeol Sci 24:417–429

Kohn MJ, Schoeninger MJ, Barker WW (1999) Altered states: effects of diagenesis on fossil tooth chemistry. Geochim Cosmochim Acta 63(18):2737–2747

Krigbaum J (2003) Neolithic subsistence patterns in northern Borneo reconstructed with stable carbon isotopes of enamel. J Anthropol Archaeol 22:292–304

Lee-Thorp JA (2000) Preservation of biogenic carbon isotopic signals in Plio-Pleistocene bone and tooth mineral. In: Ambrose SH, Katzenberg MA (eds) Biogeochemical approaches to paleodietary analysis. Kluwer/Plenum, New York, pp 89–115

Loudon JE, Sponheimer M, Sauther ML, Cuozzo FP (2007) Intraspecific variation in hair delta C-13 and delta N-15 values of ring-tailed lemurs (*Lemur catta*) with known individual histories, behavior, and feeding ecology. Am J Phys Anthropol 133(3):978–985

McGee EM, Vaughn SE (2003) Variations in stable isotope composition of *Propithecus diadema edwardsi* from disturbed and undisturbed rainforest habitats in Ranomafana National Park, Madagascar. Am J Phys Anthropol 120(S36):149

McGrew W (1983) Animal foods in the diets of wild chimpanzees (*Pan troglodytes*): why cross-cultural variation? J Ethol 1:46–61

McGrew WC, Baldwin PJ, Tutin CEG (1988) Diet of wild chimpanzees (*Pan troglodytes verus*) at Mt. Assirik, Senegal: I. Composition. Am J Primatol 16:213–226

Milton K (1984) The role of food-processing factors in primate food choice. In: Rodman PS, Cant JGH (eds) Adaptations for foraging in nonhuman primates: contributions to an organismal biology of prosimians, monkeys, and apes. Columbia University Press, New York, pp 249–279

Milton K (1987) Primate diets and gut morphology: implications for hominid evolution. In: Harris M, Ross EB (eds) Food and evolution. Temple University Press, Philadelphia, PA, pp 93–115

Nash LT (1998) Vertical clingers and sleepers: seasonal influences on the activities and substrate use of *Lepilemur leucopus* at Beza Mahafaly Special Reserve, Madagascar. Folia Primatol 69(1):204–217

O'Leary MH (1988) Carbon isotopes in photosynthesis. BioScience 38(5):328–336

Pataki DE, Ehleringer JR, Flanagan LB, Yakir D, Bowling DR, Still CJ, Buchmann N, Kaplan JO, Berry JA (2003) The application and interpretation of Keeling plots in terrestrial carbon cycle research. Global Biogeocheml Cycles 17(1):1022:1021–1015

Reed KE (1997) Early hominid evolution and ecological change through the African Plio-Pleistocene. J Hum Evol 32:289–322

Rosenberger AL (1992) Evolution of feeding niches in New World monkeys. Am J Phys Anthropol 88(6):525–562

Schoeninger MJ, DeNiro MJ (1984) Nitrogen and carbon isotopic composition of bone collagen from marine and terrestrial animals. Geochim Cosmochim Acta 48:625–639

Schoeninger MJ, Iwaniec UT, Glander KE (1997) Stable isotope ratios monitor diet and habitat use in New World monkeys. Am J Phys Anthropol 103:69–83

Schoeninger MJ, Iwaniec UT, Nash LT (1998) Ecological attributes recorded in stable isotope ratios of arboreal prosimian hair. Oecologia 113:222–230

Schoeninger MJ, Moore J, Sept JM (1999) Subsistence strategies of two 'savanna' chimpanzee populations: the stable isotope evidence. Am J Primatol 47:297–314

Schoeninger MJ, Reeser H, Hallin K (2003) Paleoenvironment of Australopithecus anamensis at Allia Bay, East Turkana, Kenya: evidence from mammalian herbivore enamel stable isotopes. J Anthropol Archaeol 22:200–207

Shemesh A (1990) Crystallinity and diagenesis of sedimentary apatites. Geochim Cosmochim Acta 54:2433–2438

Sponheimer M, Lee-Thorp J, de Ruiter D, Codron D, Codron J, Baugh AT, Thackeray F (2005) Hominins, sedges, and termites: new carbon isotope data from Sterkfontein valley and Kruger National Park. J Hum Evol 48:301–312

Sponheimer M, Loudon JE, Codron D, Howells ME, Pruetz JD, Codron J, de Ruiter DJ, Lee-Thorp JA (2006) Do "savanna" chimpanzees consume C_4 resources? J Hum Evol 51:128–133

Stanford CB (1996) The hunting ecology of wild chimpanzees: implications for the evolutionary ecology of Pliocene hominids. Am Anthropol 98:96–113

Steklis HD, Sept JM, Harris JWK, Cachel S (1992) Ethnoarchaeological investigations of chimpanzees in a gallery forest in eastern Zaire. Research Report submitted to National Geographic Society

Strier KB (1992) Atelinae adaptations: behavioral strategies and ecological constraints. Am J Phys Anthropol 88(4):515–524

Suzuki A (1969) An ecological study of chimpanzees in a savanna woodland. Primates 10:103–148

Teleki G (1981) The omnivorous diet and eclectic feeding habits of chimpanzees in Gombe National Park, Tanzania. In: Harding RSO, Teleki G (eds) Omnivorous primates: gathering and hunting in human evolution. Columbia University Press, New York, pp 303–343

van der Merwe N, Masao F, Bamford MK (2008) Isotopic evidence for contrasting diets of early hominins *Homo habilis* and *Australopithecus boisei* of Tanzania. S Afr J Sci 104:153–156

van der Merwe NJ, Medina E (1989) Photosynthesis and $^{13}C/^{12}C$ ratios in Amazonian rain forests. Geochim Cosmochim Acta 53:1091–1094

Wahlen M (1994) Carbon dioxide, carbon monoxide and methane in the atmosphere: abundance and isotopic composition. In: Lajtha K, Mitchener RH (eds) Stable isotopes in ecology and environmental science. Blackwell Scientific, Oxford, pp 93–113

Wrangham RW (1977) Feeding behaviour of chimpanzees in Gombe National Park, Tanzania. In: Clutton-Brock TH (ed) Primate ecology: studies of feeding and ranging behavious in lemurs, monkeys and apes. Academic, London, pp 504–538

Wrangham RW, Conklin NL, Chapman CA, Hunt KD (1991) The significance of fibrous foods for Kibale Forest chimpanzees. Phil Trans R Soc London 334:171–178

Wynn JG (2000) Paleosols, stable carbon isotopes, and paleoenvironmental interpretation of Kanapoi, Northern Kenya. J Hum Evol 39:411–432

Yakir D, Israeli Y (1995) Reduced solar irradiance effects on net primary productivity (NPP) and the $\delta^{13}C$ and $\delta^{18}O$ values in plantations of *Musa* sp., *Musaceae*. Geochim Cosmochim Acta 59(10):2149–2151

Chapter 16
Stable and Radiogenic Isotopes in Biological Archaeology: Some Applications

Henry P. Schwarcz, Christine D. White, and Fred J. Longstaffe

16.1 Introduction

Isotopic analysis has been an important tool in several fields of anthropology: archaeology, skeletal biology, zooarchaeology, paleoanthropology, primatology, ethnobotany, and forensic anthropology all of which are concerned with the history, evolution, culture, biology, and dispersal of the human species. Both non-radiogenic and radiogenic stable isotopes have been applied to these topics. In this review we shall summarize briefly the main areas of application of these methods to bioarchaeology (the study of ancient biological remains) and forensic anthropology, and provide a few illustrations. Isotopic methods are being applied to three discrete kinds of problems in the social sciences:

Isotopic tracers : both stable and radiogenic isotopes can be used to associate human remains and, in some cases, artifactual materials, to a specific source or region.

Paleodiet: stable isotopes of C and N have been analysed in human tissues to learn about consumption habits of ancient and modern peoples: "you are what you eat".

Paleoclimate: some stable isotope distribution patterns are affected by temperature, rainfall, humidity and other climatic factors; these can have direct impact on human culture and biology, and can also be used to reconstruct ancient mobility.

Each of these methods has been applied over the entire span of evolution of our species, and on all the continents except Antarctica. The scope of these efforts is vast and this brief review will be able only to touch on those aspects related to isoscapes. Little attention will be paid to analytical methods which can be found

H.P. Schwarcz (✉)
School of Geography and Earth Sciences, McMaster University, Hamilton, ON, Canada L8S 3Z7
e-mail: Schwarcz@mcmaster.ca; white2@uwo.ca; flongsta@uwo.ca

C.D. White
Department of Anthropology, The University of Western Ontario, London, Ont., Canada N6A 5C2

F.J. Longstaffe
Department of Earth Sciences, The University of Western Ontario, London, Ont., Canada N6A 5C2

J.B. West et al. (eds.), *Isoscapes: Understanding Movement, Pattern, and Process on Earth Through Isotope Mapping*, DOI 10.1007/978-90-481-3354-3_16,

well-presented in other texts including Sharp (2007). We shall also assume a general familiarity on the part of the reader with the basic concepts of stable isotopes and the definitions of terms such as $\delta^{18}O$, etc.

16.2 Growth History Reflected in Skeletal Materials

The combination of isotopic analysis with growth differences among human tissues enables the reconstruction of a wide variety of mobility patterns as well as changes in diet or climate over lifespans. Throughout life, the skeleton actively remodels, with the result that the isotopic record obtained from bone reflects the diet through the last years of life history. Therefore, isotopic tracing using bone only allows us to reconstruct long term diet, and to identify first-generation migrants who have recently relocated. Obviously, their children and later generations will acquire the isotopic labels of their place of residence. The rate of bone turnover is higher in children (5–15%/year at age 10–15) vs 3–4%/year for adult females and 1.5 – 3%/year for males (Hedges et al. 2007).

Tissues that are formed incrementally, e.g. teeth, hair and nails and do not remodel can be used to identify short term changes in isotopic composition. This record allows us to reconstruct not only seasonality of diet or climate, but also to identify the occurrence and timing of geographic relocations. Because teeth are preferentially preserved, they are most commonly used for these purposes. Serial sections of dentine and enamel are analyzed using microdrilling or laser sampling techniques (e.g. Balasse et al. 2003; Fuller et al. 2003; Richards et al. 2008). The first molars (M1) begin to form in utero, while all other permanent teeth except M3 form in childhood, up to age 8 years. The third molar (M3) forms between age 8 and 17. Dentin formation follows that of enamel, and can be partly remodeled during later life if the tooth is subject to attrition or trauma. Sequential analyses of hair and nails have enriched our understanding of the lives of mummies (Schwarcz and White 2004) as well as contributed to forensic studies (Ehleringer et al. 2008). Note that, unlike apatite, a significant fraction of the unexchangable O and H in proteins such as keratin (hair, nails) is derived from food which may not be at equilibrium with the local environmental water pool, especially for modern humans. This mixed-source dependence of O, H isotopes has been modeled recently for hair by Ehleringer et al. (2008).

16.3 Isotopic Tracers and Migration

With the exception of F, all the light elements (H to Ca) have multiple isotopes which exhibit variations in their relative abundances in nature arising as a result of various fractionation processes. The daughter isotopes of some long-lived radioisotopes also vary in abundance, as a result of variations in the relative abundance of parent to daughter (e.g., Rb/Sr) coupled with variations in the age of the bedrock exposed at the earth's surface.

The surface of the earth exhibits a wide range of variations in isotopic ratios, some of which show regular regional trends. Living organisms, including humans tend to acquire isotopic compositions corresponding to the isotope ratios in ingested food and water of the region(s) in which they lived. Analyses of these ratios in the skeletal remains of the people can be use to determine if the individuals are local to the place where they were found or, if not, to test hypotheses as to whence they have come. People move about the landscape for many reasons, amongst them being intermarriage, resource acquisition, trade, warfare, colonization, pilgrimage, etc. We therefore expect that many archaeological populations will include some individuals who are not from their burial site.

16.3.1 Oxygen Isotopes

Although in principle we could use isotopes of all the light elements (e.g., C, N, H, S) to trace geographically varying sources of food and drink, most emphasis has been placed on the use of oxygen isotopes in bones and teeth, principally because we know that the O in bone mineral (hydroxyapatite or HA) is derived from body water, most of which is in turn derived from local meteoric water (Luz et al. 1984; Longinelli 1984). Intra-populational variation for individuals thought to represent local controls is thought to be about ±1‰ (White et al. 1998, 2000; Prowse et al. 2007; see also Longinelli 1984 for animals). The $\delta^{18}O$ of precipitation ($\delta^{18}O_{ppt}$) generally decreases with: (a) distance from a marine coastline; (b) increase in elevation of a site; (c) decreasing temperature of precipitation, and (d) increasing latitude (Ayliffe and Chivas 1990; Yurtsever and Gat 1981), Detailed maps of the distribution of $\delta^{18}O_{ppt}$ have been compiled for the US (Bowen et al. 2007), and parts of Europe (e.g., Italy: Longinelli and Selmo 2003). Bowen and Revenaugh (2003) present a model for predicting $\delta^{18}O_{ppt}$ over the entire earth.

To the extent that humans use purely local water supplies, regional distributions of $\delta^{18}O_{ppt}$ can be used to test whether a person lived their entire life at a given site or migrated during some part of their life. This is done through the analysis of $\delta^{18}O$ of skeletal HA. The formula of this mineral is approximately $Ca_{10}(PO_4, CO_3)_3(OH, CO_3)$. O atoms occur at four different lattice sites, but we assume that that they are all equilibrated with body water at the ambient body temperature of 37°C. Two different approaches have been followed to determine $\delta^{18}O$ by analysis of either phosphate (PO_4) or structural carbonate (CO_3) molecular ions. Phosphate can be extracted from bone or tooth enamel and converted to silver phosphate, $AgPO_4$, which is usually analysed by fluorination (Clayton and Mayeda 1963; Crowson et al. 1991). The precision of analysis is about ±0.5‰. Alternately, we can determine $\delta^{18}O$ of the structural CO_3 component of HA by reacting it with 100% phosphoric acid and analyzing the liberated CO_2 (Koch et al. 1997). For well preserved samples (unaffected by diagenesis) these two methods give equivalent information; the CO_2 liberated by acid from HA is 8.5‰ higher than that obtained by fluorina-

tion of phosphate (Iacumin et al. 1996b). There is some concern that structural CO_3 ions in HA may be affected by exchange with HCO_3^- ions in soil water during burial (Zazzo et al. 2004). The crystallinity index of the HA can be determined to assure that it has not been recrystallized (Wright and Schwarcz 1996).

The $\delta^{18}O$ of bone phosphate ($\delta^{18}O_p$) of animals in general, and humans in particular has been shown to be linearly related to $\delta^{18}O_{ppt}$, although the form of the relationship varies between species. For humans, Longinelli (1984) found that

$$\delta^{18}O_p = 0.67\,\delta^{18}O_{ppt} + 22.5 \tag{16.1}$$

where both $\delta^{18}O$ values are given in relation to Standard Mean Ocean Water (SMOW).

In practice, many studies of human migration have dealt with regions where little is known about the regional variation in $\delta^{18}O_{ppt}$, and have instead made comparison of $\delta^{18}O_p$ among populations at different sites and/or over time.

16.3.2 Strontium Isotopes

Strontium substitutes for Ca in the HA structure and is not strongly excluded during uptake of Ca from the diet. Therefore the $^{87}Sr/^{86}Sr$ ratio of unaltered bone and tooth enamel reflects the ratio in the diet and, in turn, reflects the ratio in soils in the source region of the diet (Price et al. 2002). Bone that has been buried in soil absorbs significant amounts of Sr from the soil that cannot be removed by chemical leaching, and which obscures the primary dietary signal (Trickett et al. 2003; Molleson 1988). Tooth enamel is much less affected by Sr uptake during burial and provides the best indication of dietary $^{87}Sr/^{86}Sr$.

^{87}Sr is the daughter of ^{87}Rb (half-life = 10^{10} years), while ^{86}Sr is non-radiogenic. Sr in soils is derived from the weathering of ancient rocks whose $^{87}Sr/^{86}Sr$ ratio increases with increasing Rb/Sr ratio and geological age. Typically, $^{87}Sr/^{86}Sr$ ratios vary between approximately 0.702 (in young, low Rb-rocks such as oceanic basalt) to >0.740 in old Rb-rich granitic rocks. Areas underlain by marine-derived limestones display ratios similar to that of ancient seawater, which varied widely through the Phanerozoic. In glaciated areas, the soil may be derived from glacial till which is a homogenized mixture of bedrock types derived upstream from the site in the direction of glacial transport. Therefore the $^{87}Sr/^{86}Sr$ ratio may differ from that of local bedrock. Sr is also taken up from seafood, fish, and sea-salt. This will impart a $^{87}Sr/^{86}Sr$ ratio close to that of modern seawater (0.7092). When trying to characterize the $^{87}Sr/^{86}Sr$ ratio available to humans at a site, it is advisable to measure biologically available Sr in plants and animals from the site, rather than to sample the bedrock or even the soil directly. The relevant $^{87}Sr/^{86}Sr$ ratio is that of Sr available to the biological system through leaching of soil by surface waters, whereas total analysis of the soil or bedrock will include Sr bound in mineral components that are not readily leachable.

16.3.3 Paleodietary Isotopes

Isotopic ratios of carbon ($\delta^{13}C$) and nitrogen ($\delta^{15}N$) in bone collagen (col) were shown by DeNiro and Epstein (1978, 1981) to reflect the corresponding ratios in ingested foods. However, there are offsets of +5‰ between $\delta^{13}C$(diet) and $\delta^{13}C$(col), and +3‰ between $\delta^{15}N$(diet) and $\delta^{15}N$(col). The latter relationship reflects the *trophic level effect* which results from the preferential loss of ^{14}N during catabolic breakdown of protein and excretion of nitrogen. The origin of the collagen-diet fractionation is not well known, but probably arises from the fact that collagen is dominantly composed of the amino acids glycine and proline which are ^{13}C-enriched with respect to other amino acids. The $^{13}C/^{12}C$ ratio of the total diet (i.e., lipids, proteins, carbohydrates) is also reflected in $\delta^{13}C$ of structural CO_3 in the hydroxyapatite of bones and teeth (Koch 1998). The offset between diet and CO_3 is not well established but appears to be about 11‰ (see Passey et al. 2005)

Variation in $\delta^{13}C$ in human diet mainly arises as a result of consumption of two types of ^{13}C-enriched foods: (1) plants which use the Hatch-Slack, C_4 photosynthetic pathway: all tissues of C_4 plants have $\delta^{13}C$ values about 17‰ higher than for corresponding components of C_3 plants; and (2) marine foods with $\delta^{13}C$ values ~7‰ higher than terrestrial foods. The most important C_4 foods are maize (*Zea mays*) in the New World, and millet and sorghum in Europe, Africa and Asia. Many of the most important cultigens such as wheat, barley, and rice are C_3 plants, which cannot be distinguished from one another using C isotopes, nor can we easily distinguish their consumption from that of animal derived protein (including aquatic fish) using C isotopes alone. (Fig. 16.1)

Krueger and Sullivan (1984) suggested that the amino acids of collagen were dominantly derived from amino acids in the diet, and therefore the $\delta^{13}C$ values of collagen would mainly reflect proteins and the carbohydrates and lipids in the diet would be under-represented. This was experimentally demonstrated using mice by Ambrose and Norr (1993). Schwarcz (2000) noted, however, that 80% of the amino acids in collagen are non-essential, that is, can be synthesized in the human body and could therefore be constructed from the total carbon pool in the body, especially when protein is scarce. This could account for the exceptionally high $\delta^{13}C$ values of collagen in North American consumers of maize, even though most of their protein came from fish and C_3-consuming herbivores.

Much of the variation in $\delta^{15}N$ largely arises as a result of the trophic level effect: carnivores have higher $\delta^{15}N$ values than herbivores. The number of trophic levels in the marine and aquatic realms is higher than on land (since lower trophic-level carnivorous organisms are eaten by higher-level organisms). Therefore, the highest $\delta^{15}N$ values in humans are observed where marine or aquatic foods are important in the diet (Schoeninger and DeNiro 1984)

The δD values of collagen reflect the δD of drinking water (Cormie et al. 1994), although about 20% of the H atoms quickly exchange with environmental water vapor, an effect which can be corrected for during isotopic analysis. The δD of collagen appears to be partly controlled by the trophic level of the consumer

(Reynard and Hedges 2008). δD values of bone collagen should, in principle, reflect regional variations in δD of meteoric precipitation, but diagenetic effects have not yet been carefully evaluated. The isotopes of extraosseous proteins such as collagen in skin or keratin of hair reflect the δD and $\delta^{18}O$ of local drinking water (Bowen et al. 2007) but these tissues are rarely preserved in non-mummified human remains.

Paleodietary isotopes can seldom be used as tracers of migration because the isotopic characteristics of food are generally too widespread and do not exhibit regional gradients. Maize appears as a dietary component at various times in New World populations but patterns of maize dispersal, if they exist, have not yet been worked out (Schwarcz 2006). No C_4 foods were widely used as human sources of nutrition in Europe or Asia. Therefore the carbon isotopic composition of human bone (both collagen and apatite) is not expected to exhibit regional gradients in the Old World. Tracing of the inland dispersal of high $\delta^{15}N$, $\delta^{13}C$ marine foods from coastal areas is confounded by the use of widely transported dried fish and other marine foods. Given these limitations, no comprehensive studies have yet been made of the geographic distributions of paleodietary isotopes, and we will not discuss this topic further.

16.4 Oxygen Isotopic Studies of Migration

The first study to trace the geographic origins of people using O isotopes was an attempt to trace the origins of U.S. Army victims of the War of 1812 found buried in Canada (Schwarcz et al. 1993). Subsequently, $\delta^{18}O$ analyses of bone and teeth have been applied to a wide range of archaeological problems and, more recently, to a few forensic cases (largely unpublished as yet). We shall provide a few

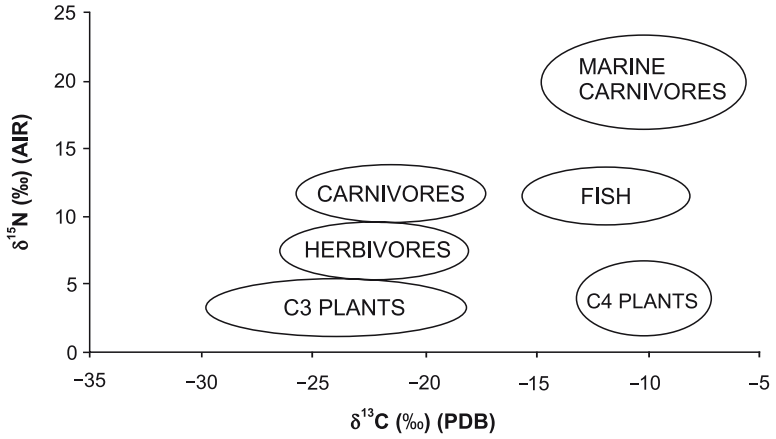

Fig. 16.1 Ranges of $\delta^{13}C$ and $\delta^{15}N$ values in common food sources

examples from both the New and Old Worlds, three of which are roughly contemporaneous (Teotihuacan, Rome, Dahkleh Oasis).

16.4.1 Mesoamerica

Isotopic reconstructions of mobility have enabled hypothesis testing related to urban and state growth, forms of imperialism (conquest, colonization), economic and military organization, marriage patterns, and ethnic relationships. Archaeologists have long known that there was extensive movement of cultural materials throughout Mesoamerica, but the main issues have been whether people as well as material goods were moving, and if people had moved, who had moved. The feasibility of research using phosphate oxygen isotopes in this part of the world was established by investigating diagenesis (Stuart-Williams et al. 1996), and establishing isotopic baselines at key sites in a variety of Mesoamerican regions, e.g., Oaxaca, Maya Lowlands and Highlands, West Mexico, Pacific Coast (White et al. 1998). The goal of this research was to understand how power was exercised by the earliest state in the Americas (Teotihuacan). The approach taken was to reconstruct: (1) its internal relationships (through the ethnic structure of its neighborhoods), (2) the way(s) in which it controlled the rest of the Mesoamerican world (through its military structure, sacrifices associated with monumental architectures), and (3) the origins of individuals at foreign sites.

Enamel-bone comparisons from Tlailotlacan, a barrio of Zapotecs, indicated that this group maintained its ethnic identity since its arrival in the early phases of the city by taking children to their ethnic homelands and sojourning them there (presumably to be enculturated) before returning them to the city. The ethnic structure of the city was further investigated with analyses of what was believed to have been a local population of lapidary workers and later state controlled ceramic manufacturers (Tlajinga 33), but which actually included a significant number of assimilated immigrants, probably from West Mexico (White et al. 2004b; see Patzquaro in Fig. 16.2.). Data from another neighborhood inhabited by merchants indicated that their movement was mainly unidirectional, i.e., they came to the city to live permanently while operating their trading houses across generations (Spence et al. 2005; White et al. in press). Their diets also indicated they were less assimilated than those at Tlajinga 33.

The $\delta^{18}O_p$ values from the sacrifices at the Feathered Serpent and Moon Pyramids in the city, and people living at foreign sites suggest that Teotihuacan used several strategies for control. The hypothesis that Teotihuacan conquered and installed its own rulers at Kaminaljuyú, Guatemala and at Altun Ha, Belize has not been supported by $\delta^{18}O_p$ at either site (White et al. 2000, 2001a,b). However, one high status individual from Kaminaljuyú appears to have been sent to Teotihuacan during his adolescence, one might speculate for training. By contrast, many of the individuals (male and female) in the Pacific Coast sites of Montana and Balberta

have isotopic compositions consistent with Teotihuacan, which supports the hypothesis that this area was colonized by the state (White et al. in prep).

Although the foreign sites have not provided evidence for military conquest, analysis of sacrificed soldiers at the Feathered Serpent Pyramid indicates that Teotihuacan had a military organization that included local recruits, but was mainly comprised of men from diverse regions of Mesoamerica who had lived in the city for many years (White et al. 2002). Teeth from the human trophy maxillae that were worn by the soldiers contained teeth of individuals who had also came from different locations; which provides evidence for the violent and widespread exercise of power (Spence et al. 2004). However, there are also many sacrificed individuals in both the Feathered Serpent and Moon Pyramids who were high status foreigners, some of whom appear to have been Maya (White et al. 2002; 2007) and whose mortuary treatment indicates respect, which suggests that Teotihuacan also wielded significant ideological power.

16.4.2 Rome

In the period of dominance of the Roman empire, cemeteries were mainly located just outside the walls of the larger cities, including Rome itself, with the result that few burials from this period have been recovered. An exception is the site of Isola Sacra at the mouth of the Tiber River, where more than 2,000 burials covered by later sandy deposits were discovered. The burials were of people who had lived in the nearby former city of Portus in the first and second centuries AD. As a part of a study of the skeletal characteristics of these remains (Prowse et al. 2003; 2005), an oxygen isotopic study of tooth enamel from this site was focused on the geographic origin of the buried people (Prowse et al. 2007). The $\delta^{18}O$ of CO_3 of HA was measured. A reference set of deciduous teeth from modern natives of Rome was used to define the range of $\delta^{18}O_{sc}$. About one third of the 61 individuals appeared to have originated from outside of Rome, in a region with a lower $\delta^{18}O_{ppt}$ than that providing drinking water to Rome (Fig. 16.3). The authors surmised that these low-$\delta^{18}O_{sc}$ individuals had immigrated to the city from the nearby Apennine Mountains where $\delta^{18}O_{ppt}$ values are known to be substantially lower (Fig. 16.4). Comparison of M1 and M3 molars showed that the majority of these immigrants arrived in Rome as children.

One individual at Isola Sacra displayed higher $\delta^{18}O_{sc}$ values than the modern population. He was inferred to have come from North Africa, which is consistent with the fact that shipments of grain from Roman colonies at Alexandria and elsewhere in North Africa arrived continuously at Portus.

The large proportion of immigrants in the burial population is consistent with the high mortality rate known to have existed in Rome in the Imperial period, partly as a result of endemic malaria present on the coastal plain of Latium. Although the size of the population does not appear to have been growing, we might infer from

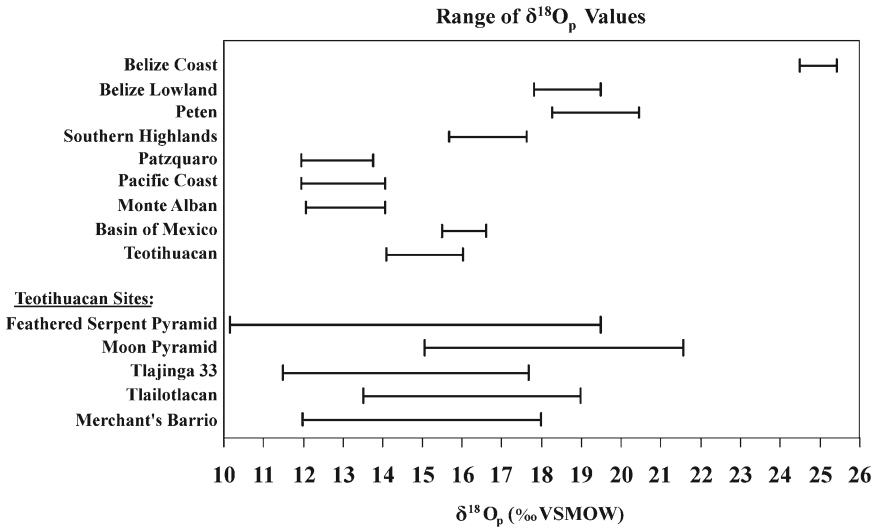

Fig. 16.2 $\delta^{18}O$ values of bone apatite from humans recovered from different barrios at Teotihuacan compared with the Teotihuacan baseline and other regions in Mesoamerica

the large proportion of the population that appears isotopically to be non-indigenous that the arrival of outsiders was restocking a population with a continuously high mortality rate caused by endemic diseases. This demographic model is analogous to the dynamics of population maintenance in contemporaneous Teotihuacan, where Storey (1992) speculated that immigration was necessary to compensate for the high infant mortality associated with urbanism, and the $\delta^{18}O_p$ values of her study population indicated an immigration level of about one third (White et al. 2004b).

16.4.3 Nile and Sahara Desert

In a study of an AD 250 Roman period cemetery population from the Dakhleh Oasis, Egypt, Dupras and Schwarcz (2001) found that the $\delta^{18}O_{sc}$ in teeth of most individuals at this site indicated that their water source was local (wells derived from an ancient aquifer, the value of which is stable) and that their $\delta^{15}N$ collagen values were significantly enriched (consistent with low rainfall and saline soils). Two outliers had lower $\delta^{15}N$ and higher $\delta^{18}O_{sc}$ values indicative of recent arrival from the Nile valley where such values have been previously recorded in Nubian populations (Iacumin et al. 1996a; White et al. 2004a). Similarly, White et al. (2004a)

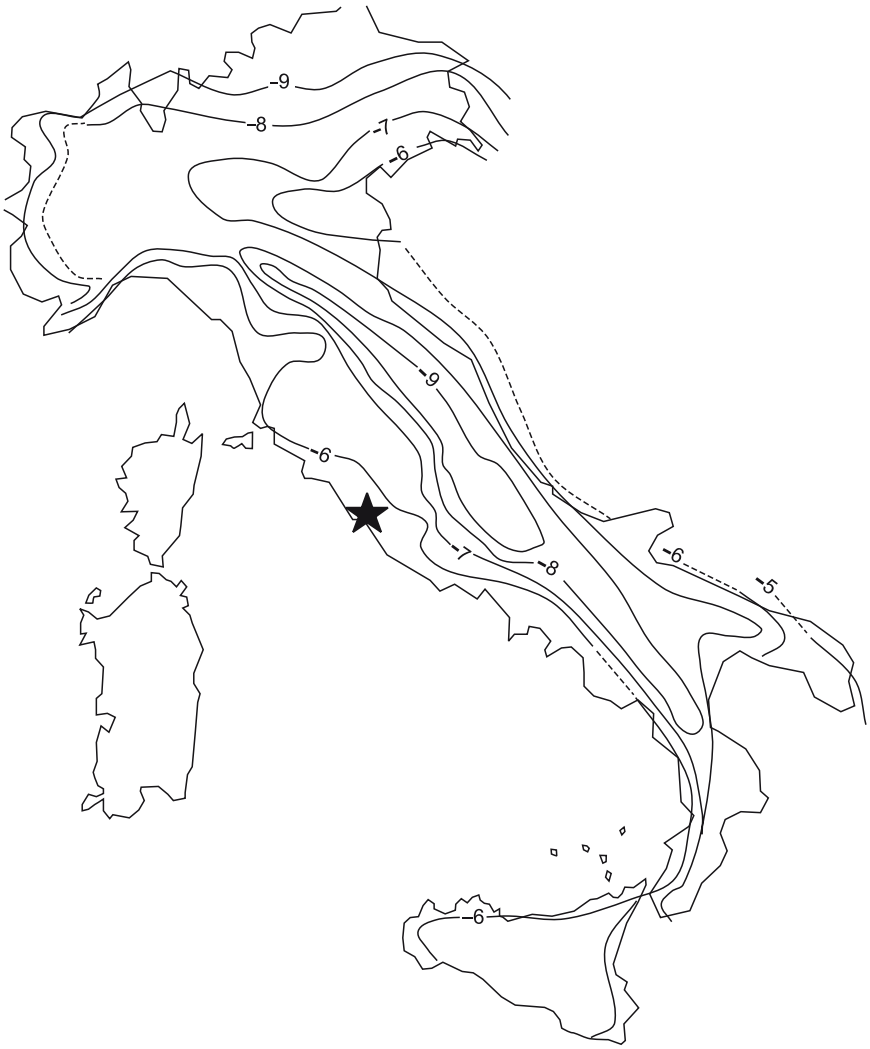

Fig. 16.3 Variation in $\delta^{18}O$ of precipitation over Italy, adapted from Longinelli and Selmo (2003). *Black circle* shows location of the cemetery of Isola Sacra at the mouth of the Tiber River, near Rome. Contours are in ‰ with respect to VSMOW

found inter tooth and bone-enamel differences in $\delta^{18}O_p$ values within individuals suggestive of movement expected along the Nile corridor and probably related to origins from different locations upstream and downstream as Nile $\delta^{18}O_w$ reflects increasing evaporation as it moves away from its source. Furthermore, combined records indicate that the $\delta^{18}O_w$ of the Nile had decreased from predynastic to

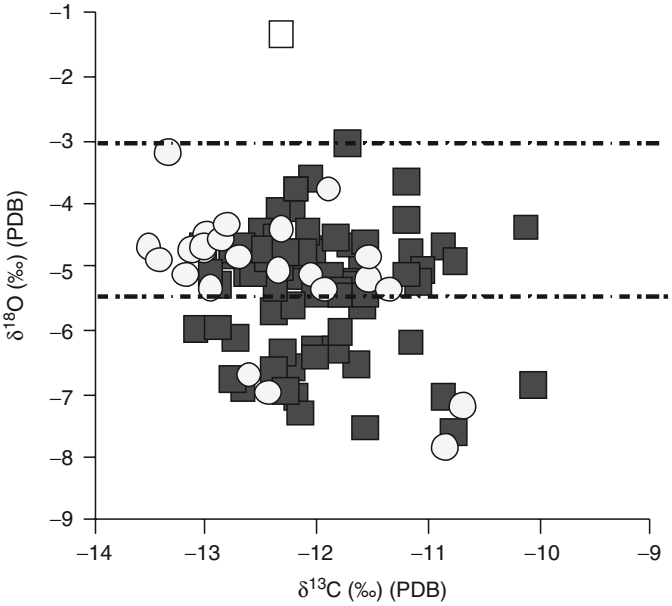

Fig. 16.4 Oxygen and carbon isotope ratios of teeth of people buried at Isola Sacra. *Open circles*: deciduous teeth of modern children from Rome. *Open square*: outlier with higher $\delta^{18}O$, believed to originate in North Africa (Prowse et al. 2007). *Dashed lines* identify values expected for lifetime residents of Rome

Medieval times (Iacumin et al. 1996a; White et al. 2004b). Regardless of the locational or temporal variation in Nile $\delta^{18}O_w$ values, the Nile and oasis water values are still much lower.

16.5 Strontium Isotopic Studies

A number of studies have focused on the use of $^{87}Sr/^{86}Sr$ ratios alone as an indicator of human provenance. Notably, Price and his colleagues have studied sites in Europe and South America and shown that judicious use of Sr isotopes can reveal the presence of outsiders in an otherwise locally derived population. While earlier studies included analyses of bone and teeth, it appears likely that bone tends to adsorb Sr from the soil in which it is buried and thus exhibit apparently "local" $^{87}Sr/^{86}Sr$ ratios, whereas tooth enamel, due to its larger crystal size and lower organic content, is less likely to be altered isotopically during burial (Bentley et al. 2004). Tooth analyses, however, will only record human mobility during childhood or (for the third molar) adolescence.

Fig. 16.5 Map of central Europe showing sites studied by Price et al. (2001). Linear Bandkeramik culture was found within shaded area

The Linearbandkeramik (LBK) is a complex of artifactual methods and materials characteristic of the early Neolithic in Central Europe (Fig. 16.5). As Price et al. (2001) state, "The…LBK... has traditionally been regarded as the initial phase of the Neolithic of Central Europe and a classic example of prehistoric migration." Analyses are given of Sr in teeth from two German sites, Flomborn and Schweitzingen (Fig. 16.6). Local values were estimated based on the mean ±2 s.d. of the total population at each cemetery. Of the 11 skeletons at Flomborn, seven appear to be outsiders (>2 s.d. from the mean), while seven out of 21 at Schweitzinger are outside the local range. This appears to confirm the notion that a significant fraction of the people buried at this site had migrated there, although the localities from which they had arrived are unclear. Bentley et al. (2004) recommended the use of local animals to estimate the "local" signal, rather than the average of the cemetery population.

In an attempt to define possible source regions, Bentley and Knipper (2005) used archaeological pig teeth from a large region of Southern Germany to assess biologically available Sr and determine local $\delta^{18}O_{ppt}$. They succeeded in finding sites in this region which matched data from the study by Price et al. (2001) and provided a data base for similar further studies of the German Neolithic.

The $^{87}Sr/^{86}Sr$ ratio method has also been used in the New World. At the Andean site of Tiwanaku, Peru, Knudson et al. (2004) showed that some of the individuals at the site had been born and raised away from other nearby, identifiable regions. At the Mayan site of Tikal, Guatemala, Wright (2005) analyzed 83 individuals of whom all but 8 had values around 0.70812 (Fig. 16.7). Tikal lies geographically

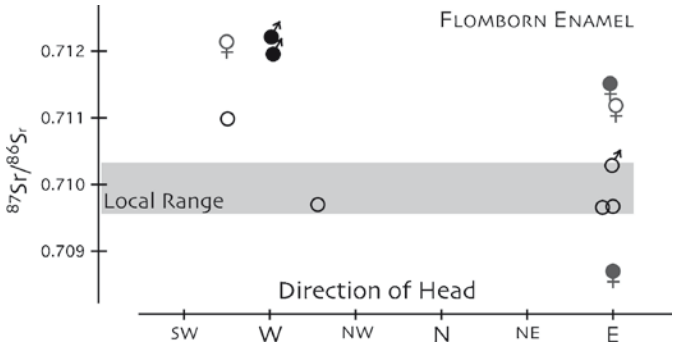

Fig. 16.6 $^{87}Sr/^{86}Sr$ ratios in teeth from Neolithic people buried at the Neolithic German site of Flomborn (Price et al. 2001)

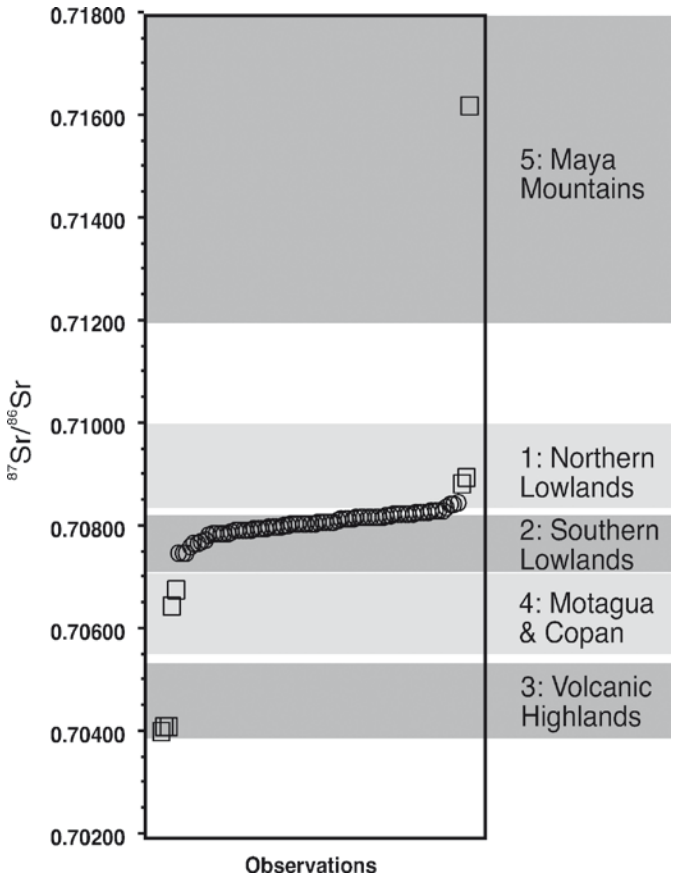

Fig. 16.7 Sr isotope data for Tikal, Guatemala in relation to expected values for this and other regions in Guatemala and Belize (Wright 2005)

well within the southern lowlands, for which a somewhat lower $^{87}Sr/^{86}Sr$ ratio is expected (supported by data from local fauna [rodents, snails] where $^{87}Sr/^{86}Sr$ = 0.7078 – 0.7081). Wright suggests that the higher mean value for humans arises from consumption of small amounts of sea-salt containing traces of Sr with a $^{87}Sr/^{86}Sr$ ratio of 7092. Consumption of marine foods was also invoked by Knudson et al. (2004) to account for high Sr isotope ratios in some individuals.

The use of multiple isotopic methods increases the resolution with which we can point to a place of origin for an individual. For example, many of the sacrificial victims from the Moon Pyramid, Teotihuacan, would appear to be local if only $\delta^{18}O$ or $^{87}Sr/^{86}Sr$ were analyzed, but when both data sets were combined, all of the victims appeared to have come from elsewhere (White et al. 2007; Fig. 16.8).

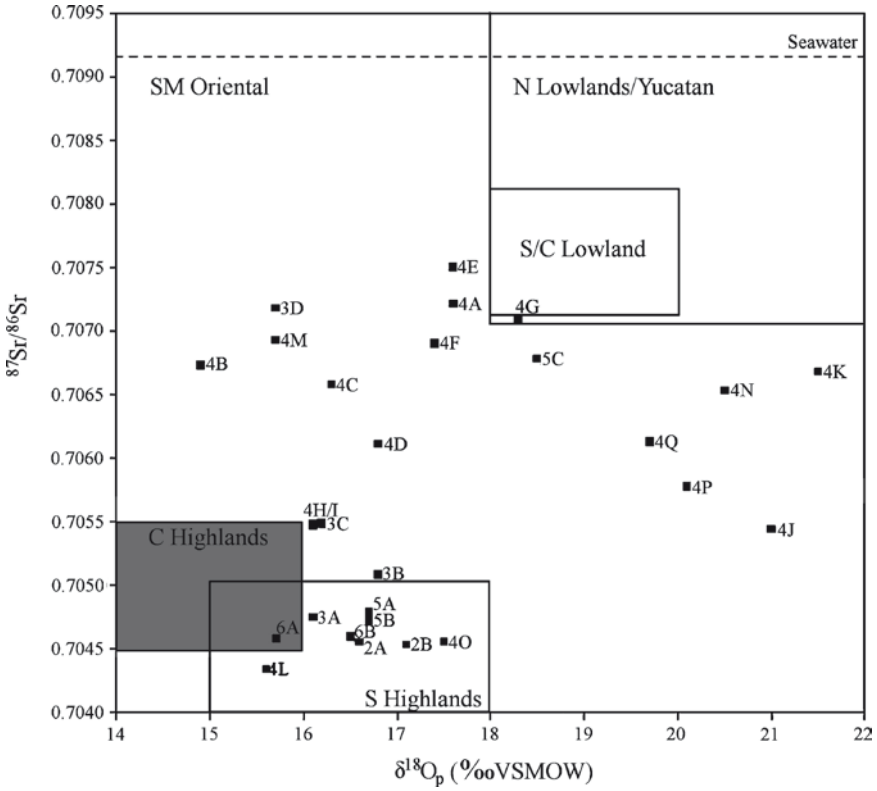

Fig. 16.8 Oxygen and strontium isotope ratios for sacrificial victims from the Pyramid of the Moon, Teotihuacan. Also shown (*grey square*) is the expected range of natives of this location (White et al. 2007)

16.6 Overview of Migration Studies Using Isotopes

Isotopic tracing of human skeletal remains has been shown to be an effective method for addressing important archaeological issues. It is possible to demonstrate whether a population is isotopically homogeneous and, if not, who the outliers are. Reasons for mobility can be inferred by examining the demographic patterning of local and "foreign" individuals and the age(s) at which they relocated. For example, are men moving and marrying local women? Are people moving to improve their financial status, or is high economic status needed in order to move? Are people being moved for purposes of colonization? Are movements permanent or temporary? Was movement required/encouraged by the state to replenish a population with a high mortality rate? Are foreigners or local individuals selected for ritual purposes (e.g. sacrifice)?

The precision of location could be further improved if we had more comprehensive maps of the geographical distribution of these isotope ratios. The distribution of $\delta^{18}O_{ppt}$ and δD over the US is now well documented (Bowen et al. 2007), less well known over Europe, and extremely poorly known over other continental areas including Africa, Asia, Mesoamerica, and South America. Distributions of biologically available $^{87}Sr/^{86}Sr$ ratios are hardly known except in specific areas where intensive archaeological interest has led to their study. The $^{143}Nd/^{144}Nd$ and Pb isotope ratios ($^{206}Pb/^{207}Pb$, etc.) are potentially of use in tracing skeletal remains along with Sr isotopes, but have not been mapped to any extent. To some extent these ratios can be inferred from corresponding regional values in bedrock, with the caveat regarding biological available isotope ratios as noted earlier.

16.7 Forensic Applications of Stable and Radiogenic Isotopes

The use of isotopes in forensic analysis of human remains is gaining recognition. One application is determining whether the victim was a local resident and, if not, to attempt to define the region of their origin. For example, recently Schwarcz (2007) used a combination of paleodietary and $\delta^{18}O_{sc}$ analyses to demonstrate that a woman found in Mammoth Lakes, CA, was probably a Native American, and that she had not lived for long at Mammoth Lakes. The $\delta^{18}O_{sc}$ of her teeth was consistent with her having been raised as a child in a small village in Oaxaca, Mexico, whence she was traced through DNA analysis (Fig. 16.9). Isotopic analyses of hair

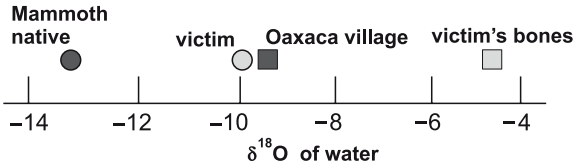

Fig. 16.9 Isotopic tracing of an unidentified murder victim from Mammoth Lakes, California. Data represent $\delta^{18}O$ values of drinking water corresponding to analyses of teeth and bone (Based on unpublished data from HPS)

segments can also be used to determine a victim's recent movement, and a large database to be used for this application has been constructed by Ehleringer et al. (2008)

16.8 Paleoclimate

Climate change has had a large impact on human existence. Throughout human history and prehistory, the survival and flourishing of human populations at specific localities has been contingent on climate, i.e., temperature, rainfall and advances and retreats of continental ice sheets.

The long term record of climate change, the alternation between glacial and interglacial stages, has been recorded most faithfully through oxygen isotopic variations in two archives: foraminifera in deep sea cores; and ice cores from the Antarctic and Greenland (Bradley 1999). Less extensive and more localized records are preserved in lake sediments, coral reefs, and speleothems (stalagmites).

The basis of isotopic paleoclimate studies was established by the discovery that we could recover growth temperatures of calcareous organisms (mollusks, corals) from the fractionation of ^{18}O between $CaCO_3$ and water (Epstein et al. 1951). That concept has been extended to environmental studies involving many other materials. The $\delta^{18}O$ of teeth and bones records changes in $\delta^{18}O_{ppt}$, which can be related, in

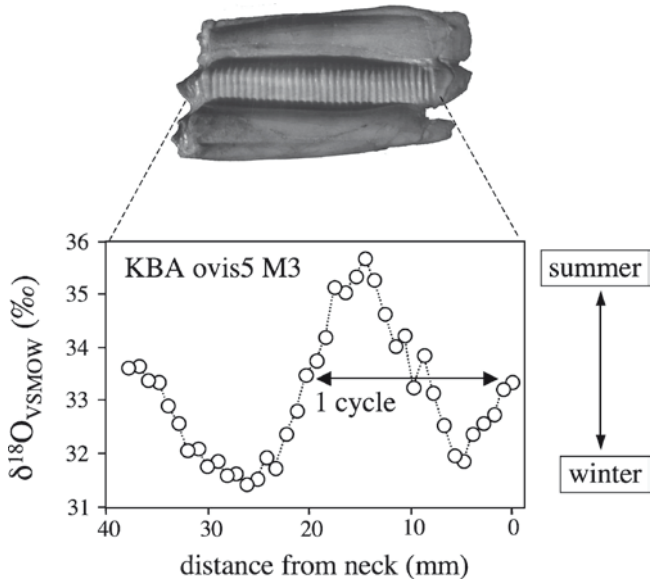

Fig. 16.10 Variation in $\delta^{18}O$ of carbonate in a tooth from second molar (M2) of a sheep from Kasteelsberg, South Africa, showing seasonal variation. δ18O values with respect to SMOW (From Balasse et al. 2003)

turn, to environmental temperature (Longinelli 1984). Because mammalian body temperature is constant, $\delta^{18}O_p$ is determined by $\delta^{18}O_{ppt}$. In temperate locations $\delta^{18}O_{ppt}$ increases with temperature (T); where average $T > 20$, $\delta^{18}O_{ppt}$ is negatively dependent on volume of rain ("the amount effect"). Fricke et al. (1998) have shown how seasonal variation in $\delta^{18}O_{ppt}$ can be recovered from serial samples of ungulate teeth (Fig. 16.10). Attempts to use $\delta^{18}O_p$ of bones or teeth from archaeological sites to reconstruct paleotemperatures have mainly been unsuccessful, however, due to uncertainties in the T–$\delta^{18}O_{ppt}$ relationship.

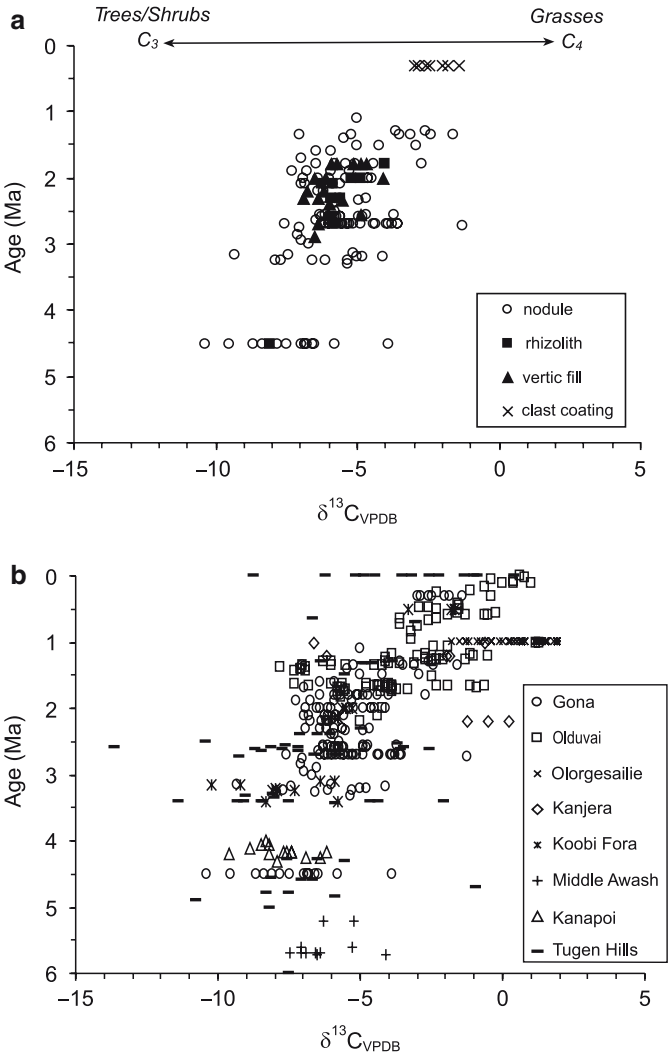

Fig. 16.11 Variation in $\delta^{13}C$ of soil carbonates from E. Africa during the late Cenozoic, showing the effect of a gradual decrease in soil moisture and consequent expansion of C_4 –grass-dominated savanna (Levin et al. 2004). a) Gona, Ethiopia; b) East Africa.

The isotopic composition of plant tissues responds to changes in $\delta^{18}O_{ppt}$ and to relative humidity. Thus isotopic values of cellulose of fossil wood and leaves may be used to track changes in relative humidity and temperature (Richter et al. 2008; Webb and Longstaffe 2006).

The abundance of C_4 grasses relative to C_3 species increases with decreasing humidity and increasing temperature. This leads in turn to an increase in the $\delta^{13}C$ of both soil organic matter and calcretes developed in the soils of arid and subarid environments. A striking long-term shift has been observed in $\delta^{13}C$ of soil carbonates in East Africa, which is believed to correspond to the shift from a flora dominated by shrubs and trees, to more open grasslands (Levin et al. 2004; Fig. 16.11). The same soils also show a parallel though less well-defined trend of increasing $\delta^{18}O$, which these authors attribute to lowered humidity leading to increased evaporative fractionation of soil water.

These changes in aridity must inevitably have affected human evolution. The evolution of our species in Africa is believed to have been stimulated in part by the effect of climate on landscape, leading to a creation of open grasslands for which bipedal locomotion was more appropriate (Klein 1999).

16.9 Conclusions

We have shown that stable isotope ratios of the light elements C, N, O and H as recorded in materials from archaeological sites all over the world have added a great deal to our understanding of human history. Most of this work has been carried on by teams of isotope geochemists and/or archaeologists and physical anthropologists. Isotopic analyses are now demanded routinely in archaeological research programs and specialized sessions in isotopic anthropology are commonly included in major meetings of anthropological and archaeological organizations. Researchers at work excavating sites are increasingly alert to possibilities of using isotopes to address archaeological issues, and the growing ability to micro-sample is enabling better access to museum collections.

In each of these areas of study, it is important for the isotopic researcher to be aware of complementary kinds of data and use multiple lines of evidence where possible. For example, when reconstructing the geographic origins of individuals, it is useful to analyze multiple isotopes, and combine biological data (e.g., intentional skeletal modifications, skeletal morphology and metrics, phenotypic genetic traits, DNA) with archaeological data (e.g., mortuary treatment, grave goods, etc.).

In the future, new analytical methods will probably be adapted to some of the problems described above. Non-standard stable isotope methods are now becoming more widely used in biological systems. For example isotopes of Ca, Fe, Mg, Cu and B are all potentially usable as tracers in tooth enamel (Farkas et al. 2007; Johnson et al. 2004).

Acknowledgements We acknowledge the contribution to our research as cited here by the Natural Sciences and Engineering Research Council of Canada (NSERC: HPS and FJL:) and the Social Sciences and Humanities Research Council of Canada (SSHRC: HPS AND CDW).

References

Ambrose S, and Norr L (1993) Experimental evidence for the relationship of the carbon stable isotope ratios of whole diet and dietary protein to those of bone collagen and carbonate. In: Lambert JB and Grupe G (eds) Prehistoric human bone: archaeology at the molecular level. Springer, Berlin/Heidelberg/New York, pp 1–38

Ayliffe LK, Chivas AR (1990) Oxygen isotope composition of the bone phosphate of Australian kangaroos: potential as a palaeoenvironmental recorder. Geochim Cosmochim Acta 54:2603–2609

Balasse M, Smith A, Ambrose S, Leigh SR (2003) Determining sheep birth seasonality by analysis of tooth enamel oxygen isotope ratios: the Late Stone Age site of Kasteelberg (South Africa). J Archaeol Sci 30:205–215

Bentley R A, Price TD, and Stephan E (2004) Determining the 'local' $^{87}Sr/^{86}Sr$ range for archaeological skeletons: a case study from Neolithic Europe, J Archaeol Sci, 31: 365–75.

Bentley RA, Knipper C (2005) Geographical patterns in biologically available strontium, carbon and oxygen isotope signatures in prehistoric SW Germany. Archaeometry 47:629–644

Bowen GJ, Revenaugh J (2003) Interpolating the isotopic composition of modern meteoric precipitation. Water Resour Res 39:1299

Bowen GJ, Ehleringer JR, Chesson LA , Stange E and Cerling TE (2007) Stable isotope ratios of tap water in the contiguous United States. Water Resour Res 43:W03419

Bradley RS (1999) Paleoclimatology. Academic, New York

Clayton RN, Mayeda TK (1963) The use of bromine pentafluoride in the extraction of oxygen from oxides and silicate for isotopic analysis. Geochim Cosmochim Acta 27:43–52

Cormie A, Schwarcz HP, Gray J (1994) Determination of the hydrogen isotopic composition of bone collagen and correction for hydrogen exchange. Geochim Cosmochim Acta 58:365–376

Crowson RA, Showers WJ, Wright EK, Hoering TC (1991) Preparation of phosphate samples for oxygen isotope analysis. Anal Chem 63:2397–2400

DeNiro MJ, Epstein S (1978) Influence of diet on the distribution of carbon isotopes in animals. Geochim Cosmochim Acta 42:495–506

DeNiro MJ, Epstein S (1981) Influence of diet on the distribution of nitrogen isotopes in animals. Geochim Cosmochim Acta 45:341–351

Dupras T, Schwarcz HP (2001) Strangers in a strange land: stable nitrogen and oxygen isotope evidence for human migration in the Dakhleh Oasis, Egypt. J Archaeol Sci 28:1199–1208

Epstein S, Buchsbaum R, Lowenstam HA Urey HC1951: Carbonate-water isotopic temperature scale, Bull Geol Soc Amer, 62:417–426

Ehleringer JR, Bowen GJ, Chesson LA, West AG, Podlesak DW, Cerling T (2008) Hydrogen and oxygen isotope ratios in human hair are related to geography. Proc Natl Acad Sci U S A 105:2788–2793

Farkas J, Boehm F, Wallmann K, Blenkinsop J, Eisenhauer A, van Geldern R, Munnecke A, Voigt S, Veizer J (2007) Calcium isotope record of Phanerozoic oceans; implications for chemical evolution of sea water and its causative mechanisms. Geochim Cosmochim Acta 71:5117–5134

Fricke HC, Clyde WC, O'Neil JR (1998) Intra-tooth variations in $\delta^{18}O(PO_4)$ of mammalian tooth enamel as a record of seasonal variations in continental climate variables. Geochim Cosmochim Acta 62:1839–1850

Fuller BT, Richards MP, Mays SA (2003) Stable carbon and nitrogen isotope variations in tooth dentine serial sections from Wharram Percy. J Archaeol Sci 30(2003):1673–1684

Hedges REM, Clement JGC, Thomas DL, O'Connell TC (2007) Collagen turnover in the adult femoral mid-shaft: modeled from anthropogenic radiocarbon tracer measurements. Am J Phys Anthropol 133:808–816

Iacumin P, Bocherens H, Mariotti A, Longinelli A (1996a) An isotopic palaeoenvironmental study of human skeletal remains from the Nile Valley. Paleogeog Paleoclim Paleoecol 126:15–30

Iacumin P, Bocherens H, Mariotti A, Longinelli A (1996b) Oxygen isotope analyses of co-existing carbonate and phosphate in biogenic apatite: a way to monitor diagenetic alteration of bone phosphate? Earth Planet Sci Lett 142:1–6

Johnson CM, Beard BL, and Albarede F (eds) (2004) Geochemistry of non-traditional stable isotopes. Mineral Society of America and the Geochemical Society, Rev Mineral 55 454

Klein RG (1999) The human career : human biological and cultural origins University of Chicago Press, Chicago, IL, 810 p

Knudson KJ, Price TD, Buikstra JE, Blom DE (2004) The use of strontium isotope analysis to investigate Tiwanaku migration and mortuary ritual in Bolivia and Peru. Archaeometry 46:5–18

Koch PL (1998) Isotopic reconstruction of past continental environments. Annu Rev Earth Planet Sci Lett 26:573–613

Koch PL, Tuross N, Fogel ML (1997) The effects of sample treatment and diagenesis on the isotopic integrity of carbonate in biogenic hydroxylapatite. J Archeol Sci 24:417–429

Krueger HW and Sullivan CH (1984) Models for carbon isotope fractionation between diet and bone, In: Turnlund JE and Johnson PE (Eds) Stable isotopes in nutrition. American Chemical Society Symposium Series 258, Washington DC, pp 205–222

Levin NE, Quade J, Simpson SW, Semaw S, Rogers M (2004) Isotopic evidence for Plio-Pleistocene environmental change at Gona, Ethiopia. Earth Planet Sci Lett 219:93–110

Longinelli A (1984) Oxygen isotopes in mammal bone phosphate: a new tool for paleohydrological and paleoclimatological research? Geochim Cosmochim Acta 48:385–390

Longinelli A, Selmo E (2003) Isotopic composition of precipitation in Italy: a first overall map. J Hydrol 270:75–88

Luz B, Kolodny Y, Horowitz M (1984) Fractionation of oxygen isotopes between mammalian bone-phosphate and environmental drinking water. Geochim Cosmochim Acta 48:385–390

Molleson T (1988) Trace elements in human teeth. In: Grupe G, Hermann B (eds) Trace elements in environmental history. Springer-Verlag, Berlin/Heidelberg/New York, pp 67–82

Passey BH, Robinson TF, Ayliffe LK, Cerling TE, Sponheimer M, Dearing MD, Roeder BL, Ehleringer JR (2005) Carbon isotope fractionation between diet, breath CO2, and bioapatite in different mammals. J Archaeol Sci 32:1459–1470

Price TD, Bentley RA, Gronenborn D, Lüning J, Wahl J (2001) Human migration in the Linearbandkeramik of Central Europe. Antiquity 75:593–603

Price TD, Burton JH, Bentley RA (2002) The characterization of biologically available strontium isotope ratios for the study of prehistoric migration. Archaeometry 44:117–35

Prowse T, Schwarcz HP, Saunders S, Macchiarelli R, Bondioli L (2003) Isotopic paleodiet studies of skeletons from the Imperial Roman-age cemetery of Isola Sacra, Rome, Italy. J Archaeol Sci 31:259–272

Prowse T, Schwarcz HP, Saunders S, Macchiarelli R, Bondioli L (2005) Isotopic Evidence for Age-related Variation in Diet from Isola Sacra, Italy. Am J Phys Anthropol 128:2–13

Prowse T, Schwarcz HP, Garnsey P, Knyf M, Macchiarelli R, Bondioli L (2007) Isotopic evidence for large scale immigration to imperial Rome. Am J Phys Anthropol 132:510–519

Reynard LM, Hedges REM (2008) Stable hydrogen isotopes of bone collagen in palaeodietary and palaeoenvironmental reconstruction. J Archaeol Sci 35:1934–1942

Richards M, Harvati K, Grimes V, Smith C, Smith T, Hublin J, Karkanas P, Panagopoulou E (2008) Strontium isotope evidence of Neanderthal mobility at the site of Lakonis, Greece using laser-ablation PIMMS. J Archaeol Sci 35:1251–1256

Richter SL, Johnson AH, Dranoff MM, LePage BA, Williams CJ (2008) Oxygen isotope ratios in fossil wood cellulose: isotopic composition of Eocene to Holocene-aged cellulose. Geochim Cosmochim Acta 72:2744–2753

Schoeninger MJ, DeNiro MJ (1984) Nitrogen and carbon isotopic composition of bone collagen from marine and terrestrial animals. Geochim Cosmochim Acta 48:625–639

Spence M, White CD, Rattray ED, Longstaffe FJ (2004) Un análysis de las proportiones de los isótopos en los entieros del Barrio de los Commerciantes. La Segunda Mesa Redonda de Teotihuacan. Centro de Estudios Teotihuacanos, Instituto Nacional de Anthropologia e Historia, Mexico City, pp 453–492

Spence M, White CD, Rattray ED, Longstaffe F (2005) Past lives in different places: The origins and relationships of Teotihuacan's foreign residents. In: Richard E. Blanton (ed) Early civilizations, settlement, and subsistence: Essays in honour of Jeffrey R. Parsons, Cotsen Institute, University of California, Los Angeles, pp 155–197

Schwarcz HP (2000) Some biochemical aspects of carbon isotopic paleodiet studies. In: Ambrose S, Katzenberg MA (eds) Biogeochemical approaches to paleodietary analysis. Kluwer, New York, pp 189–210

Schwarcz HP (2006) Stable carbon isotope analysis and human diet: a synthesis. In: Tykot R et al. (eds) Histories of maize. Amsterdam, Elsevier, pp 315–324

Schwarcz HP (2007) Tracing unidentified skeletons using stable isotopes. Forensic Magazine, June/July 2007

Schwarcz HP, White CD (2004) The grasshopper or the ant?: cultigen-use strategies in ancient Nubia from C-13 analyses of human hair. J Archaeol Sci 31:753–762

Schwarcz HP, Gibbs L and Knyf M (1993) Oxygen isotope analysis of bones from Snake Hill as indicator of place of origin. In: Pfeiffer S, Williamson R (eds) Snake Hill burial, an investigation of a military cemetery from the war of 1812. Dundurn Press, Toronto, pp 263–268

Sharp Z (2007) Principles of stable isotope geochemistry. Pearson/Prentice Hall, Upper Saddle River, NJ

Storey R (1992) life and death in the ancient city of Teotihuacan. University of Alabama Press, Tuscaloosa.

Stuart-Williams H, Schwarcz HP, White CD, Spence M (1996) The isotopic composition and diagenesis of human bone at Teotihuacan and Oaxaca, Mexico. Paleogeog Paleoclim Paleoecol 126:1–14

Trickett MA, Budd P, Montgomery J, Evans J (2003) An assessment of solubility profiling as a decontamination procedure for the $^{87}Sr/^{86}Sr$ analysis of archaeological human skeletal tissue. App Geochem 18:653–658

Webb EA, Longstaffe FJ (2006) Identifying the $\delta^{18}O$ signature of precipitation in grass cellulose and phytoliths: refining the paleoclimate model. Geochim Cosmochim Acta 70:2417–2426

White CD, Spence MW, Stuart-Williams HL, Schwarcz HP (1998) Oxygen isotopes and the identification of geographical origins: the Valley of Oaxaca versus the Valley of Mexico. J Archaeol Sci 25:643–655

White CD, Longstaffe FJ, Spence MW, Law K (2000) Testing the nature of Teotihuacan imperialism at Kaminaljuyu' using phosphate oxygen-isotope ratios. J Anthro Res 56:535–558

White CD, Longstaffe FJ, Law K, Pendergast DM (2001a) Revisiting the Teotihuacan connection at Altun Ha: oxygen isotope analysis of Tomb F-8/1. Ancient Mesoam 12:65–72

White CD, Pendergast DM, Longstaffe FJ, Law K (2001b) Social complexity and food systems at Altun Ha, Belize: the isotopic evidence. Lat Am Antiq 12:371–393

White CD, Spence MW, Longstaffe FJ (2002) Geographic identities of the sacrificial victims at the Feathered Serpent Pyramid: implications for the nature of state power. Lat Am Antiq 13:217–236

White CD, Longstaffe FJ, Law K (2004a) Exploring the effects of environment, physiology and diet on oxygen–isotope ratios in ancient Nubian bones and teeth. J Archaeol Sci 31: 233–250

White CD, Storey R, Longstaffe FJ, Spence MJ (2004b) Immigration, assimilation and status in the ancient city of Teotihuacan: stable isotopic evidence from Tlajinga 33. Lat Am Antiq 15:176–198

White CD, Price TD, Longstaffe FJ (2007) Residential histories of the human sacrifices at the Moon Pyramid, Teotihuacan. Ancient Mesoam 18:159–172

White CD, Spence MW, Longstatte FJ (2009) The Teotihuacan Dream: An isotopic study of economic organization and immigration. Ontario Archaeological Society, Toronto, in press

Wright LE (2005) Evidence from oxygen and strontium isotopes in identifying immigrants to Tikal, Guatemala: defining local variability in strontium isotope ratios of human tooth enamel. J Archaeol Sci 32:555–566

Wright L, Schwarcz HP (1996) Infrared evidence for diagenesis of bone apatite at Dos Pilas, Guatemala: paleodietary implications. J Archaeol Sci 23:933–944

Yurtsever Y and Gat JR (1981) Atmospheric waters. In: Gat JR, Gonfiantini R (eds) Stable isotope hydrology: deuterium and oxygen-18 in the water cycle, Technical Report Series, No 210. International Atomic Energy Agency, Vienna, pp 103–142

Zazzo A, Lecuyer C, Sheppard SMF, Grandjean P, Mariotti A (2004) Diagenesis and the reconstruction of paleoenvironments; a method to restore original $\delta^{18}O$ values of carbonate and phosphate from fossil tooth enamel. Geochim Cosmochim Acta 68:2245–2258

Chapter 17
A Framework for the Incorporation of Isotopes and Isoscapes in Geospatial Forensic Investigations

James R. Ehleringer, Alexandra H. Thompson, David W. Podlesak, Gabriel J. Bowen, Lesley A. Chesson, Thure E. Cerling, Todd Park, Paul Dostie, and Henry Schwarcz

17.1 Introduction

Stable isotope ratio analyses have been commonplace in the environmental, biological, and geological fields for many decades (Ehleringer et al. 1993; Griffiths 1998; Rundel et al. 1988, Sharp 2006; West et al. 2006). However, the extension and application of stable isotopes into forensic investigations is relatively new and rapidly expanding because of the many ways this analytical approach can help with law enforcement investigations (Benson et al. 2006; Ehleringer et al. 2007, 2008b;

J.R. Ehleringer (✉) and L.A. Chesson
IsoForensics Inc., 423 Wakara Way, Suite 205, Salt Lake City, UT, 84108, USA
e-mail: jim@isoforensics.com, lesley@isoforensics.com

A.H. Thompson, D. Podlesak and T.E. Cerling
Department of Biology, University of Utah, 257 S 1400 E, Salt Lake City, UT, 84112, USA
e-mail: ahthompson@biology.utah.edu, podlesak@biology.utah.edu, thure.cerling@utah.edu

G.J. Bowen
Department of Earth and Atmospheric Sciences, Purdue University, 550 Stadium Mall Drive, West Lafayette, IN, 47907, USA
e-mail: gabe@purdue.edu

T. Park
Salt Lake County Sheriff's Office, 3365 S 900 W, Salt Lake City, UT, 84119, USA
e-mail: tpark@slco.org

P. Dostie
Mammoth Lakes Police Department, 568 Old Mammoth Road, Mammoth Lakes, CA, 93546, USA
e-mail: pdostie@aol.com

H. Schwarcz
School of Geography and Earth Sciences, McMaster University, Hamilton, ON, Canada L8S 3Z7
e-mail: schwarcz@mcmaster.ca

J.B. West et al. (eds.), *Isoscapes: Understanding Movement, Pattern, and Process on Earth Through Isotope Mapping*, DOI 10.1007/978-90-481-3354-3_17,

Meier-Augenstein and Fraser 2008; Meier-Augenstein and Liu 2004). As is clear from the contributions in this volume, stable isotope analyses complement other analytical approaches to chemical identification in an investigation (e.g., HPLC, GC/MS, LC/MS), because stable isotope analyses provide an additional "fingerprint" that further characterizes a piece of forensic evidence. Stable isotope analyses provide a means of relating or distinguishing between two pieces of evidence that have exactly the same chemical composition (e.g., drug specimen found at a crime scene and at the suspect's residence). The study of stable isotopes as a forensic tool is based on the analytical ability to precisely measure naturally-occurring differences in the amounts of the heavy-to-light stable isotopes in evidentiary material and to relate that composition to other specimens or other evidence. In this chapter, our interest is in comparisons involving specific consideration of geographic location of origin and isotopic "fingerprints" associated with specific locations. This is a new field and area of active research, applicable now to providing information that will help guide law-enforcement investigations. In the future as our ability to model geographic isotopic variation for substrates of forensic interest improves, these analytical tools should find greater impacts in law enforcement investigations and as scientific information in prosecution efforts. The forensic evidence under consideration can be in the form of specific compounds (e.g., cocaine), mixtures (e.g., heroin), and/or biological tissues (e.g., bird feathers, hair, teeth).

17.2 Breadth of Isotope Applications in Forensics

Stable isotope ratio analyses yield potentially unique information for forensic investigations, complementing other approaches by adding a "stable isotope signature" to compounds or materials that are identified as identical by other methods. Consider the three questions illustrated in Fig. 17.1.

First, consider the utility of isotope analyses in the comparative approach: do the isotope ratios of two or more specimens have indistinguishable or distinguishable isotope ratio values? Non-spatial applications of stable isotope analyses can involve comparing the stable isotope ratios of a specimen with that of other specimens associated with the forensic incident or comparing the stable isotope ratios of a specimen with specimens of known origin contained within a database (Fig. 17.1). With limited information about an evidence specimen, the main applications of stable isotope ratios here include sample matching within a database, sample processing information if fractionation effects are well known, and/or source location identification if there is an exhaustive database of samples of known origin. Consider several specimens of a material of interest (e.g., illicit drugs, counterfeit money, toxins) that may be obtained by investigators with the intent of identifying related groups, sources, or regions-of-origin of the material (Casale et al. 2006; Ehleringer et al. 2000). Biological samples obtained from the same location and time will have experienced the same environmental conditions and therefore should have similar stable isotope ratios. Chemical processing of materials can also result in distinctive stable isotope ratios, as can impurities left behind during the production

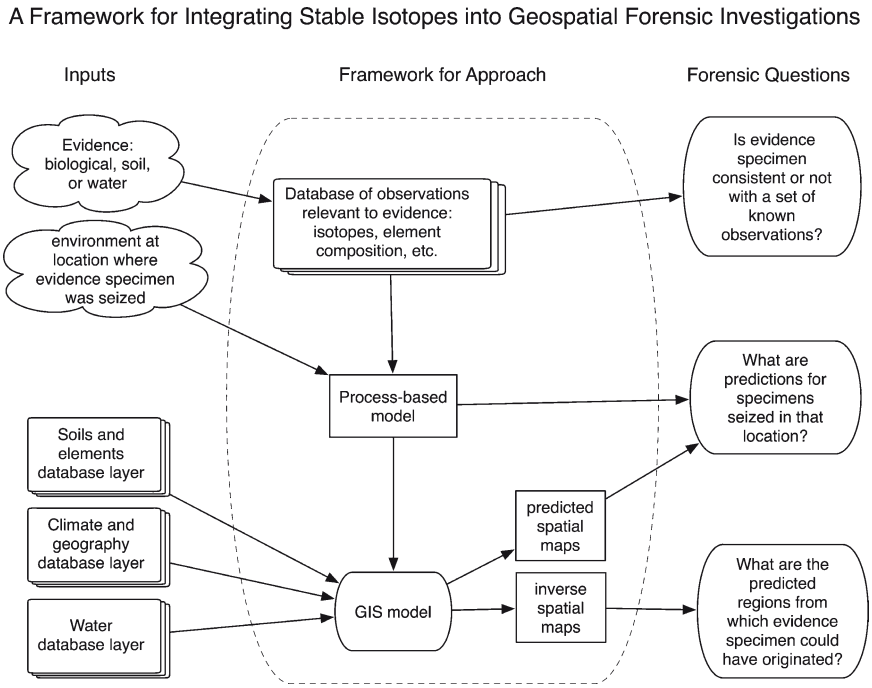

Fig. 17.1 A framework for the stable isotope ratio analysis of forensic samples. Three primary classes of information can be provided for seized evidence specimens based on stable isotope ratio data that allow investigators to address three questions (far right). Evidence specimens can be matched either to other evidence specimens seized, or to known authentics and previously acquired evidence specimens recorded in a database. If the database is sufficiently extensive or if other modeling has been completed (see text), then two additional questions can be addressed: (1) what are the expected stable isotope ratios of specimens from a given location and (2) given a specimen's stable isotope ratios, from where might that sample have originated?

of derived products (Benson et al. 2006; Toske et al. 2006). Because of this, "like" samples may be readily grouped based on their stable isotope ratio values. In addition to matching samples, forensic workers can compare individual samples to databases of stable isotope ratio information obtained from authentic samples (e.g., Casale et al. 2006). In this case, a sample of unknown origin could be assigned probable source location by comparison with an authentic stable isotope ratio database, or a previously made assignment of origin could be corroborated by database comparison. Although this can be considered a spatial application, it is limited in its utility because the approach has limited predictive power. In most cases, stable isotope observations will provide an insight into whether a specimen is "consistent with" or "not consistent with" another specimen(s) or locations(s).

A second class of questions and applications of stable isotopes in forensic studies are based on the predictive power of models, once the mechanisms and isotope effects influencing the isotopic composition of a material are understood for that material, compound, or organism. Alternatively, linear regression models may describe the relationships. Here a modeling approach may make a specific prediction of the stable isotope

ratio expected for a material in a specific environment. By combining first-principles or process-based models of stable isotope fractionation in organisms with the spatial modeling capacity of Geographic Information Systems (GIS), spatial maps of predicted stable isotope ratios can be constructed (Bowen et al. 2005b, 2007; Ehleringer et al. 2008a; West et al. 2007). The results of stable isotope ratio analyses on a specimen can then be compared to the geographical predictions, and potential source locations identified. Climate conditions and other parameters needed to make these predictions are often not unique globally. Therefore, it is uncommon for models to uniquely predict a single region or origin for a specimen, because the climate drivers influencing the predicted stable isotope ratios of a material are not unique. Rather a set of stable isotope analyses often identifies one or more "geographic zones" or "geographic bands" from which a specimen could have originated.

These advances represent cutting edge applications of stable isotope ratios to forensics that will continue to develop over the coming years. As databases and fundamental understandings of stable isotope ratios grow, the process-based models can be refined, increasing accuracy. If so, then the combination of process-based models, verifiable databases, and GIS modeling will aid in forensic work. Here we expect new applications to develop that relate to both biological organisms and to materials synthesized or produced using local water or biological materials as starting materials. Examples related to biological materials, such as microbes, plants, and animals, are discussed further in this chapter. However not further discussed, because of page limitations, are synthetic and biosynthetic products, ranging from beeswaxes to hydrogen peroxide solutions, where aspects of the isotopic composition of the products are likely to be directly related to water-related isoscapes.

Lastly, two additional isotope approaches are being applied to the forensic sciences. First, isotope ratios of heavy elements exhibit detectable patterns across the landscape associated with geological features in some cases and anthropogenic activities in others. The abundances of isotopes in these heavy elements have become additional important tools in geolocating the region-of-origin of individuals. Heavy elements, such as lead, neodymium and strontium often exhibit distinct geographic patterns that can be used to provenance the origins of humans and biological materials (Beard and Johnson 2000; Crittenden et al. 2007; English et al. 2001; Ghazi and Millette 2004; Gulson et al. 1997; Pye and Croft 2004). Another useful technical approach is the measurement of ^{14}C content of modern biological tissues to indicate the year of formation of a tissue, organ, and/or individual (e.g., Spalding et al. 2005). This technique, often referred to as carbon-14 bomb dating, capitalizes on the extensive aboveground nuclear testing in the early 1960s, ending with the adoption of the Nuclear Test Ban Treaty.

17.2.1 A Framework Based on Process-Based Models

During the past several decades, extensive theoretical and experimental progress has been made towards understanding the biochemical and physical basis of naturally

occurring variations in the stable isotope abundances of different biological tissues and materials. These include many aspects of carbon, hydrogen, and oxygen stable isotopes in plant, animal, and microbe systems. For the forensic applications discussed in this chapter, it is the constructive combination of process-based models with the geospatial information associated with water isotopes that provides the basis of forensic geo-location applications (Fig. 17.1).

In the plant sciences, models have been developed to predict variations in the carbon (Ehleringer et al. 1993; Farquhar et al. 1989) and hydrogen and oxygen (Roden et al. 2000; Yakir and DeNiro 1990) isotope ratios of plant tissues (see also West et al. this volume). Similar progress has been made in understanding the basis for isotope ratio variations in microbes (Jarman et al. 2008; Kreuzer-Martin et al. 2003, 2004) and animals (Gretebeck et al. 1997; Kohn 1996; Podlesak et al. 2008). The chapter in this volume by Still and colleagues nicely shows how carbon isotope ratios of plants vary geographically and how this information might be useful in provenancing plant material. Here, of primary forensic interest is the application of hydrogen and oxygen isotope models to understanding how water and cellulose in plant tissues vary geographically, because both parameters are important components of food, wood, paper, and/or security documents. Yapp and Epstein (1982) established that there are strong correlations between the hydrogen isotopic composition of wood and environmental water; more recently Richter et al. (2008) have expanded on these observations. A first critical step in interpreting these patterns is an appreciation of the Craig–Gordon model that describes evaporative enrichment of a pool of water (Craig and Gordon 1965; Gat 1996). The second critical step is extending this theory to both the hydrogen and oxygen isotope ratios of plant tissue water (Dongmann et al. 1974; Flanagan et al. 1991; Lai et al. 2008) and eventually to the labile signal of water that might be recorded in plant organic matter (Richter et al. 2008; Roden et al. 2000). Understanding how environmental factors drive changes in the isotopic composition of plant-tissue water in stems, leaves, and fruits is essential to understanding hydrogen and oxygen isotope ratio variations in cellulose, but are also significant in their own right because product adulteration often occurs in fruit juices, wine, and other plant-based beverages (Breas et al. 1994; Pupin et al. 1998; Simpkins et al. 2000). Provenancing of wines and juices is already of significant forensic, commercial, and regulatory interest in the EU (Breas et al. 1994; Rossmann et al. 1999).

There are shared structural features that relate to the processes influencing the hydrogen and oxygen isotope ratios in biological organisms – insects, mammals, birds, plants, or microbes – that suggest forensic applications (Fig. 17.2). Understanding the processes occurring in biological systems that influence different pools of water within biological organisms is fundamental to determining the extent to which a biological signal might be useful in reconstructing aspects of geo-location information. By appreciating the common features of biological water within plants and animals, it is possible to examine how the same environmental processes and fractionation events might or might not influence the isotope ratios of an equivalent water pool.

Figure 17.2 shows the essential water pools of higher terrestrial organisms. Water is taken up in liquid form. That source water carries a geo-location signal and

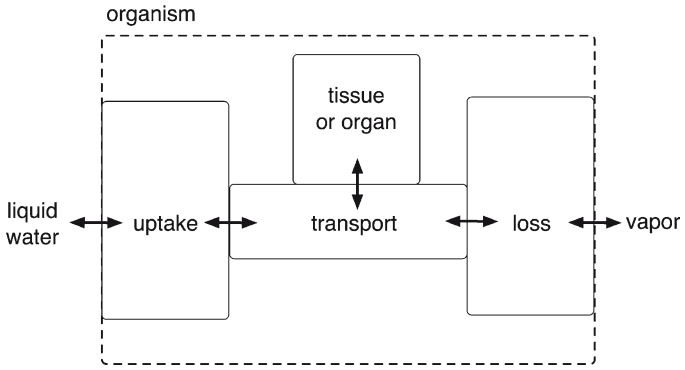

Fig. 17.2 Biological organisms can be thought of as consisting of water pools that interact differently with their surrounding environment. As such, the four distinct but common pools of water within biological organisms influence how hydrogen and oxygen isotopes of water provide information that is useful in reconstructing aspects of geo-location

is transported to different internal tissues or to external tissues where an evaporative fractionation event might occur (i.e., lungs in animals or leaves in plants). Evaporative processes governed by humidity (another geo-location signal) affect the degree to which the hydrogen and oxygen isotopes of a water pool become evaporatively enriched. Here we see one distinction between plants and animals. Water that is isotopically enriched continues to circulate within animals (i.e., through blood or circulatory systems; sometimes referred to as "body water") and therefore should be isotopically enriched above the "input" drinking water, but the xylem of plants is effectively a one-way transport system. Thus, the isotopic composition of xylem conduits is not evaporatively enriched. The isotopic analyses of water in the transport tissues of animals and plants in a common environmental setting provide distinctly different but complementary isotopic information.

Internal plant and animal tissues not directly exposed to evaporative enrichment are not necessarily experiencing a water environment that is isotopically identical to that of the transport (plants) or circulatory system (animals; Fig. 17.2). Carbohydrate metabolism should tend to increase the oxygen isotope ratios of water pools within cells because the oxygen isotope ratio values of both diatomic oxygen and carbohydrates will always be higher than those of water in the existing pools. To the degree that water transport through aquaporins and/or water diffusion across plasma membranes is rapid in these tissues, the concentrations of metabolically-enriched cellular water will be tend to be diluted by the net inward movement of surrounding circulatory water (e.g., body water in multi-cellular animals and aqueous media in microbes). However, if metabolically distinct water pools exist in plant, animal or microbe tissues, this implies that a 2-pool model should be applied to interpret the hydrogen and oxygen isotopic composition of fixed organic matter of tissues of forensic interest (e.g., actin-myosin or keratin in animals, cellulose in plants, or spore walls in microbes). The likelihood of a 2-pool versus a 1-pool water system in biological organisms should be a function of metabolic rate relative to

aquaporin influences over water movement across the plasma membrane. Experimental evidence supports the possibility of two isotopically distinct pools in cells with high metabolic rates of both microbes (Kreuzer-Martin et al. 2005b, 2006) and animals (Podlesak et al. 2009b). No evidence is available to suggest that such gradients exist in cells with low metabolic rates (Kreuzer-Martin et al. 2005b).

As implied in Fig. 17.2, the hydrogen and oxygen isotope ratios of water in plants, animals and microbes or of the organic products produced by these organisms can contain information that is of forensic interest. It is important to recognize that the isotope ratio information in water pools is subject to evaporative influences unless measures are taken to ensure that subsequent evaporation or isotopic exchange do not occur following sample collection. These limitations do not necessarily apply to organic matter where there is a distinct likelihood that the hydrogen and oxygen atoms of the water pool environment have become recorded within the organic molecule.

17.3 Topics of Forensic Interest That Use Hydrogen and Oxygen Isotope Ratios

17.3.1 Hydrogen and Oxygen in Tapwater and Bottled Water

The majority of hydrogen and oxygen atoms in the body water pool of most organisms is derived from water taken up directly from their environment, and as a result the hydrogen and oxygen isotopic composition of environmental water can have a strong influence on the isotopic composition of body tissues. In some natural systems, this source water can be considered to be relatively "pristine" local meteoric water, and its isotopic composition estimated using geostatistical models for spatial distributions of precipitation water isotope ratios (Bowen, this volume). Within human systems, however, water can be derived from a complex blend of local and non-local, surface and subsurface systems that may contain waters with widely differing source locations, recharge ages, and residence times (and hence isotopic compositions). Human drinking water, for example, may include a blend of private, public, and commercial drinking waters and water-based beverages that each contributes to the total pool of hydrogen and oxygen atoms in human body water. In some cases, waters and beverages may be of forensic interest in and of themselves in cases where water rights, trademarks, or authenticity concerns are involved. Several studies have attempted to characterize the isotopic composition of water and beverage sources to human systems and investigate how variation within and among sources might be a useful or confounding factor in forensic investigations.

The complex blend of water sources exploited by humans introduces isotopic complexities that may be relevant to forensic interpretations of hydrogen and oxygen isotope data. Extensive research on groundwater systems has shown that fresh groundwater typically has an isotopic composition similar to the time-averaged

composition of rainwater in recharge areas (Ingraham et al. 1991; Ingraham and Taylor 1991; Kortelainen and Karhu 2004; Smith et al. 2002). In many cases these isotope ratios may be similar to those predicted from precipitation sampling networks. However, in large aquifer systems where recharge and extraction sites are separated by considerable distance or elevation and fossil groundwater systems where recharge may have occurred under different climate regimes, modern precipitation isotope ratios can be very different from those of human water sources (Fritz et al. 1974; Sultan et al. 2007; Thiros 1995; Zuber et al. 2004). Surface water sources are fed by a combination of groundwater discharge and surface runoff, and may transport water across great distances encompassing large gradients in the isotopic composition of local precipitation. Both transport and evaporation from arid-region river, lake and reservoir systems can lead to large differences between surface water isotopic compositions and those of other water resources available at any particular geographic location (Dutton et al. 2005; Fekete and Gibson, this volume; Kendall and Coplen 2001). Additional complexity arises from the large-scale diversion of water by humans, sometimes across large geographic distances, in arid climate regions. These diversions transport water across natural hydrological and isotopic barriers, and can contribute to regionally "anomalous" water resource isotopic compositions both through direct supply and through purposeful or accidental introduction to groundwater pools (Coplen et al. 1999; Williams 1997).

Despite this complexity, a survey of tap waters across the continental USA, which included data from a wide range of municipal water sources, does indicate the presence of strong, systematic, geographic gradients that mimic the general patterns characteristic of modern precipitation (Bowen et al. 2007; Fig. 17.3). The magnitude of these regional patterns relative to local isotopic heterogeneity in tap water can be assessed by examining the reduction of variance in the tap water data with a model that relates tap water isotope data to both spatial variation in incident precipitation isotope composition and to spatially coherent deviations between precipitation and tap water values. Although the complexities described above may be important factors in specific locations, this model explains 92–95% of the tap water isotopic variance, suggesting that on average they impart a relatively small uncertainty relative to the geographic gradients in North America at scales of thousands of kilometers. The implication for forensic studies is that generalized models of water resource isotope distributions, such as that presented by Bowen et al. (2007), may provide a reasonable baseline for large-scale geo-location of the origin of materials or humans, particularly in cases where the water consumed is a mixture of locally available water (e.g., for a person drinking water at home, work, and local restaurants). Still, significant improvements to the precision of such applications should be possible if the spatial distribution of specific water resource types can be incorporated into water isotope base maps in order to develop more sophisticated representations of the characteristic values and heterogeneity of local waters.

Significant attention has also been given to the stable isotopic composition of bottled waters and beverages, both as a source of water consumed by humans and as a commodity where authentication of provenance is of commercial interest. In the first regard, bottled beverages clearly represent a potential source of non-local hydrogen and oxygen that may be introduced to the human body and complicate

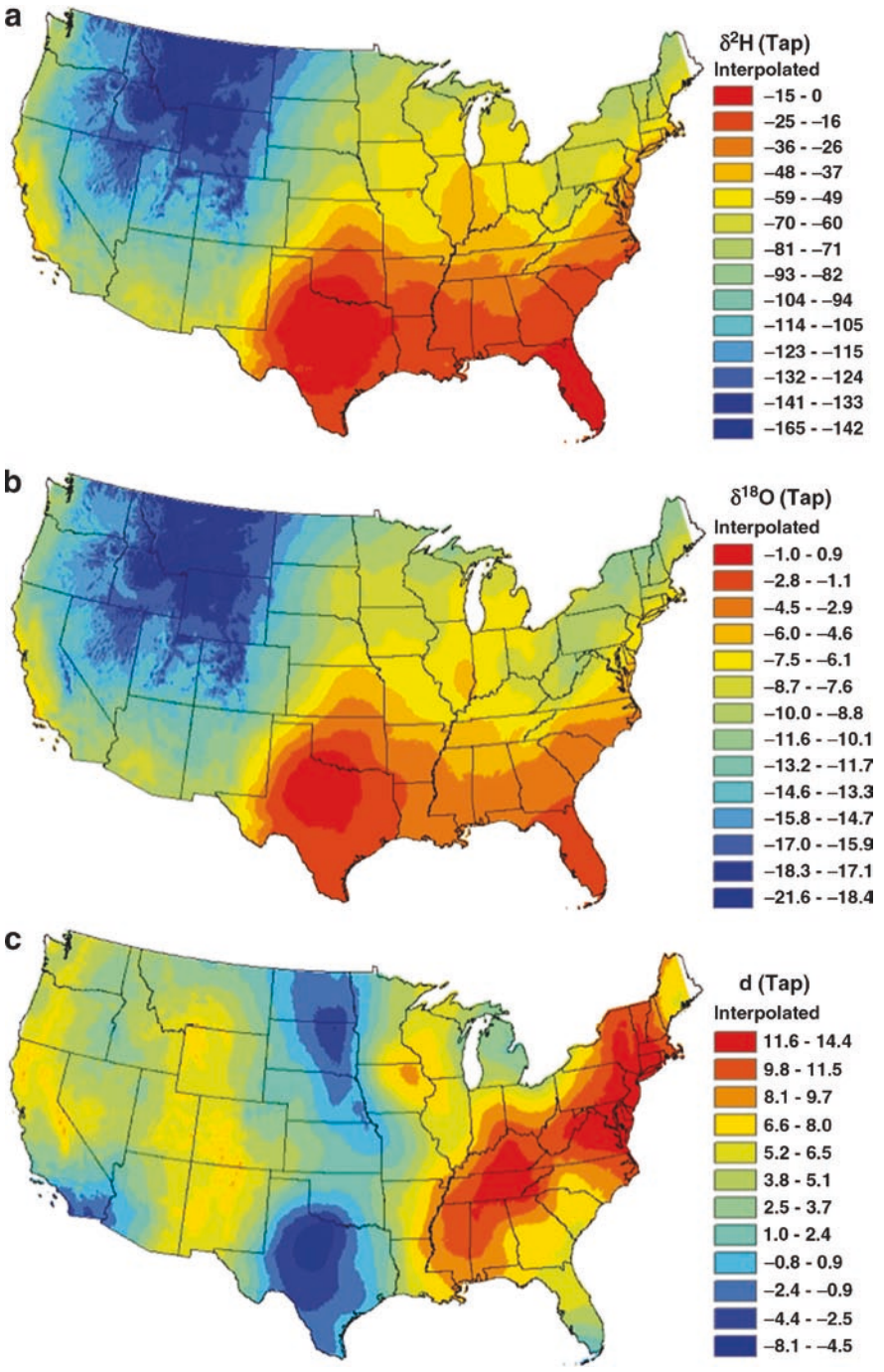

Fig. 17.3 Prediction maps showing estimated isotope ratios (**a**: δ^2H, **b**: $\delta^{18}O$) and deuterium excess values (**c**) for tap water in the contiguous United States (Methods details are available in Bowen et al. 2008 and at http://waterisotopes.org). Fig. 17.3, see Appendix 1, Color Section

interpretations of the geographic movements of individuals. A broad survey of 234 bottled water samples representing at least 136 brand names, however, found that the isotopic composition of these waters was strongly correlated ($r^2 > 0.5$) with the composition of local meteoric water at the location of purchase (Bowen et al. 2005c). This likely reflects the widespread availability of bottled waters produced from filtered tap water and packaged regionally. Although "specialist" consumers of single-source bottled water brands may take in large quantities of water having atypical hydrogen and oxygen isotope ratios for their location of residence, this is not likely to be a significant factor for most bottled water consumers who consume primarily local or regional products. In the second regard, several studies have demonstrated that stable isotopes can be conservative tracers of the source of bottled waters and beverages (Bowen et al. 2005c; Brencic and Vreca 2006; Ingraham et al. 2004; West et al. 2007), although modification of isotope ratios during production (Brencic and Vreca 2006; Ingraham and Caldwell 1999) and storage (Spangenberg and Vennemann 2008) must be considered.

17.3.2 Hydrogen and Oxygen in the Body Water of Animals

The isotope composition of body water in animals is distinctly related to region of origin through drinking water sources, diet, and local influences of climate (Gretebeck et al. 1997; Kohn 1996; Longinelli and Padalino 1980; Podlesak et al. 2008). Recent modeling efforts have combined process-based models of the isotopic composition of human body water with GIS software to produce spatial maps of human body water isotopes (Podlesak et al. 2009a). These maps can be used forensically to identify region of origin for a specific sample, or as a parameter in predictive models of organic tissues such as hair and tooth enamel (see section on organic tissues).

Process-based models of body water isotopes are mass balance models based on the influx and efflux of hydrogen and oxygen through an organism (Kohn 1996; Luz et al. 1984; Schoeller et al. 1986). Detailed models of mammalian body water isotopes include all sources of hydrogen and oxygen such as drinking water, free water in food, hydrogen and oxygen bound in ingested organic molecules (food), atmospheric O_2, and atmospheric water vapor. Models also include the effluxes of hydrogen and oxygen in the form of urine and sweat, water vapor loss associated with breathing and evaporation across the skin, and carbon dioxide loss. Evaporation across the skin and the lungs is influenced by temperature and humidity. Carbon dioxide loss, as well as metabolic water formation, is influenced by diet composition. Metabolic water and carbon dioxide are produced during the catabolism of energy (food) at the cellular level, influencing the isotope composition of the body water pool. The formation of metabolic water incorporates relatively ^{18}O-enriched atmospheric O_2 and food oxygen into the body water pool, and the loss of oxygen as carbon dioxide will tend to deplete the body water pool in ^{18}O (CO_2 is isotopically enriched relative to body water: $\alpha = 1.038$; Bottinga 1968; Brenninkmeijer et al. 1983). Detailed process-based models of body water isotopes include the

above variables as well as estimates for the isotopic composition of each influx and efflux, and estimates for the molar quantity of each influx and efflux.

Recently, Podlesak et al. (2009a) created a detailed process-based model for the isotopic composition of human body water. This model was created for an adult male that ate an average American diet. The authors used published studies on human energetics, metabolism, and water balance to estimate the molar quantities of each source of hydrogen and oxygen, and to also test the model. The model was subsequently input into ArcGIS 9.1 ModelBuilder© and combined with source layers for mean relative humidity, mean average temperature (CRU CL 2.0; 10′ × 10′; www.cru.uea.ac.uk), δ^2H and $\delta^{18}O$ values of drinking water, and δ^2H and $\delta^{18}O$ values of food to produce a spatial map of the equilibrium δ^2H and $\delta^{18}O$ values of human body water for the contiguous USA (Fig. 17.4).

Figure 17.4 displays the spatial map for equilibrium δ^2H and $\delta^{18}O$ values of body water for an adult male. In this version of the model, the source layer for drinking water values was the spatial tap water map produced by Bowen et al. (2007) for the contiguous USA, and the δ^2H and $\delta^{18}O$ values of food were linked to local drinking water. Values ranged from −147‰ to +4‰ for δ^2H and from −16.3‰ to +1.4‰ for $\delta^{18}O$ (Fig. 17.4). The most enriched δ^2H and $\delta^{18}O$ values were in interior Texas and along the Gulf Coast and the most depleted values were in the higher latitudes and elevations of the interior West (Fig. 17.4). Drinking water supplies >55% of the hydrogen atoms and >40% of the oxygen atoms in the body water, and as a result, the isotopic composition of the body water values reflects the isotopic composition of tap water. However, the correlation between the isotope composition of drinking water and body water is not 1:1 due to the influence of climate through evaporation, the incorporation of food hydrogen and oxygen, and the incorporation of atmospheric O_2 into the body water pool. Atmospheric O_2 is responsible for >20% of the oxygen atoms in the body water. Thus, accurate spatial predictions of δ^2H and $\delta^{18}O$ values of body water require detailed process models that incorporate all sources of hydrogen and oxygen and the influence of climate.

Podlesak et al. (2009a) also created a second parameterization of the model to determine the influence of drinking water source layer on body water isotope values. The first parameterization of the model used a spatial map of tap water values as the source for drinking water values. At this time, there are few areas of the world that have detailed spatial maps of tap water isotope values, and the isotopic composition of local tap water and local precipitation can be >40‰ and >7‰ different in hydrogen and oxygen isotope ratios, respectively (Bowen et al. 2007). The authors compared the δ^2H and $\delta^{18}O$ values of body water created using a spatial map of tap water with the values created using a spatial map of precipitation. Body water isotope values were up to 40‰ and up to 5.5‰ different for hydrogen and oxygen isotope ratios, respectively, between the two spatial maps. In areas such as Texas, where tap water is more enriched than local precipitation, estimated δ^2H and $\delta^{18}O$ body water values were more enriched, and in areas where local tap water was more depleted than local precipitation, body water values were more depleted than those estimated using local precipitation values. Thus, reliable spatial maps of human body water and organic tissues will require detailed spatial maps of drinking water.

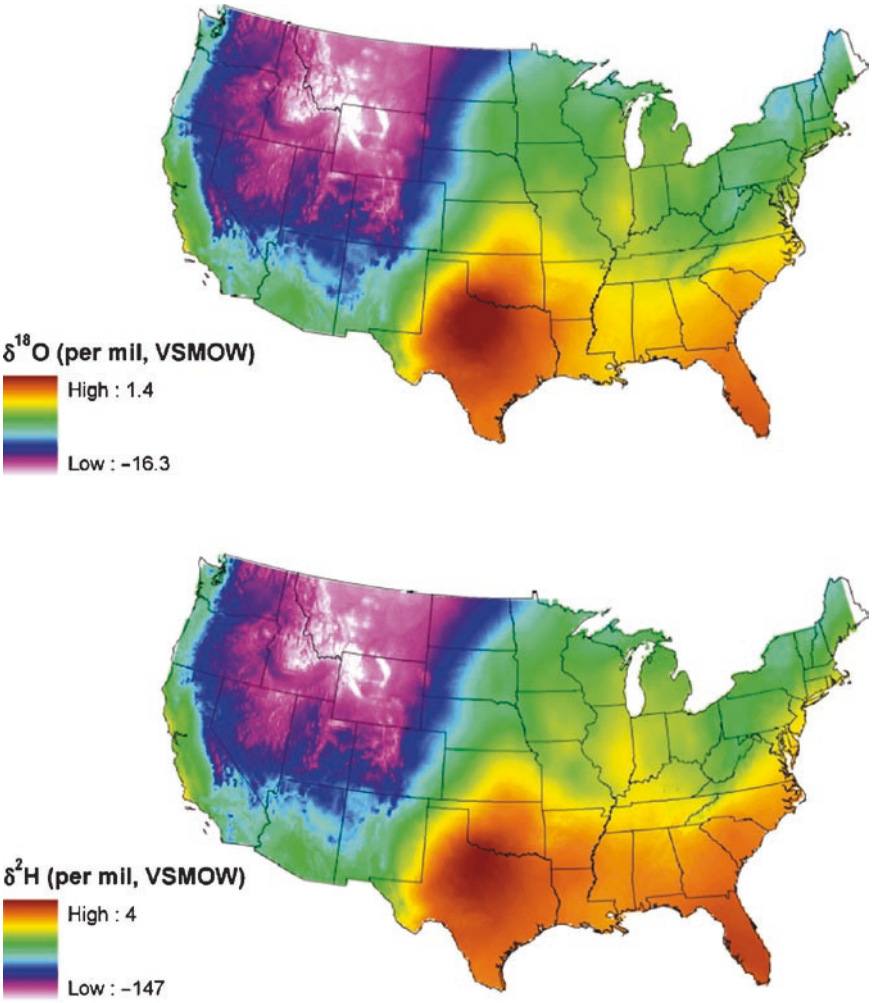

Fig. 17.4 Predicted average hydrogen and oxygen isotope ratios of body water across the USA (After Podlesak et al. in review), see Appendix 1, Color Section

Spatial maps of the isotopic composition of human body water have multiple uses in forensics. First, the spatial map can be used as an input to other models (such as a hair model, discussed later). Secondly, a spatial map of δ^2H and $\delta^{18}O$ values of body water may be used to identify a local resident from a visitor. For example, the isotope composition of body water varies significantly across the USA (Fig. 17.4). A person traveling from one isotopically distinct region to another would be distinguishable from a local for a specific length of time, depending on the rate of body water turnover (half-life of body water ~6 days) and the isotopic difference between the regions.

17.3.3 Oxygen Isotopes in Inorganic Matter

The carbon isotopic composition of carbonate and phosphate in bioapatite found in mammalian tooth enamel and bone is linked to the isotopic composition of the diet (Longinelli 1984; Passey et al. 2007; Podlesak et al. 2008), and the oxygen isotopic composition is linked to the isotopic composition of the body water (Podlesak et al. 2009a). Carbon analysis of mammalian carbonates has been used to reconstruct diet in animals and humans (Ambrose and Norr 1993; Luz et al. 1990; Passey and Cerling 2002; Passey et al. 2005a, b; Stevens et al. 2006). The oxygen analysis of carbonates has been used to reconstruct climate and to identify region of origin for animals. In general, carbonate is enriched in ^{13}C between +9‰ and +15‰ relative to diet. The enrichment in ^{13}C is likely the result of fractionation during the precipitation of bioapatite mineral from dissolved inorganic carbon within the blood. Similarly, carbonate is enriched in ^{18}O also due to the precipitation of the mineral at normal mammalian body temperatures. As a result, the carbon isotope analysis of tooth enamel for humans can be used to identify geographic differences in diet related to the consumption of C_3 or C_4 crops. C_3 plants, such as wheat, are the basis of most agriculture in Europe and the Middle East, whereas, C_4 plants such as corn are the basis of much of the agriculture in North America. Similarly, latitudinal and elevational gradients in oxygen isotopes of precipitation are reflected in tooth enamel and the oxygen isotopic composition can be used to geo-locate samples.

As a first attempt at using carbonates in tooth enamel forensically to identify location of origin for modern human samples, we measured a group of teeth collected from across the contiguous USA. We measured teeth from California, North Carolina, New York, and Utah using methods described by Passey and colleagues. We used linear regression to compare oxygen isotopes of carbonate ($\delta^{18}O_c$) with oxygen isotopes of drinking water ($\delta^{18}O_{dw}$). The relationship was highly significant ($\delta^{18}O_c = 0.350\delta^{18}O_{dw} + 27.6‰$, $r^2 = 0.85$, $P < 0.0001$; Fig. 17.5).

Next, we input the above regression relationship between local drinking water and tooth carbonate into ArcGIS 9.1 ModelBuilder© to produce a spatial representation of the $\delta^{18}O$ values of carbonate for the contiguous USA (Fig. 17.6). As expected, the distribution of carbonate $\delta^{18}O$ values closely reflected the variations in $\delta^{18}O$ values of tap water (Fig. 17.3). The regression in Fig. 17.5 compares well with previous observations for humans in Europe published earlier that were based on phosphate observations (D'Angela and Longinelli 1990; Longinelli 1984). At this initial stage of development, the exact slope and intercept are less important because these parameters are likely to change as the magnitude and diversity of the teeth observations increases. There is undetermined uncertainty in any individual observation, but a clear, linear pattern is suggested by the available data. We feel that the relevant take-home message here is that the same forces shaping the distributions of water isotopes across the USA are likely to be reflected in isoscapes of both hair and tooth isotope ratios.

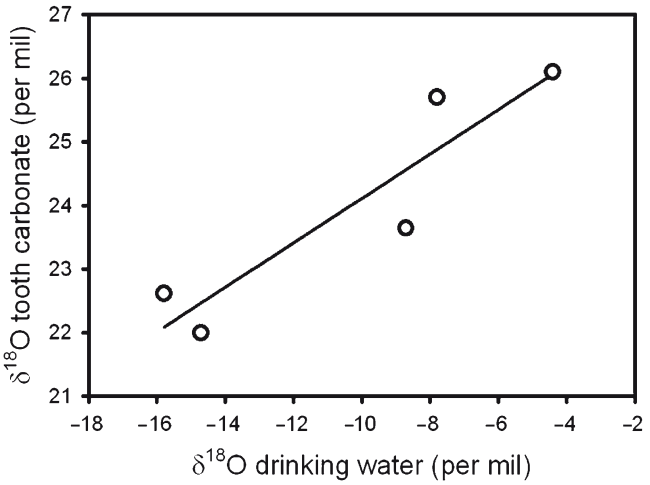

Fig. 17.5 A plot of the relationship between oxygen isotope ratios of tap water in a region versus the oxygen isotope ratios of carbonate in human teeth from that region. Specimens were prepared as described by Passey et al. (2002, 2005a, b). The linear regression is y = 0.350x + 27.6‰ ($r^2 = 0.85$, $P < 0.0001$)

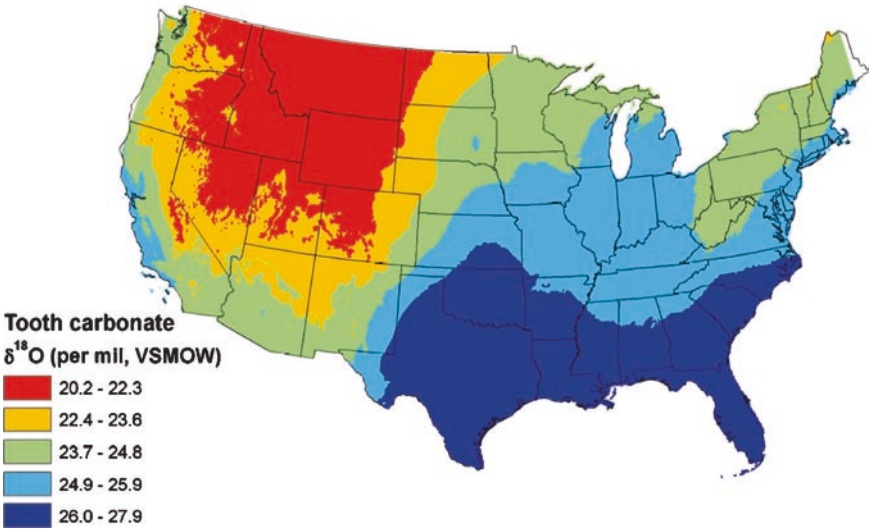

Fig. 17.6 The predicted distribution of oxygen isotope ratios of carbonates in enamel from human teeth across the contiguous USA, see Appendix 1, Color Section.

17.3.4 Hydrogen and Oxygen Isotopes in Organic Matter

Exchange processes during biosyntheses provide opportunities for the hydrogen and oxygen isotopes of cellular water to become incorporated into proteins, carbohydrates, and fatty acids. Each of these classes of biological compounds may have a forensic

application. Predicting spatial patterns to address a spatial forensic issue requires that at least some process-based understanding of isotope fractionation events is understood. Given the large variations seen in the hydrogen and oxygen isotopes of precipitation waters (Bowen this volume), there is an expectation that the isotopic composition of organic matter should, to some degree, reflect these broad spatial patterns if fractionation events during biosynthesis indeed incorporate a cellular water signal.

For several decades, supporting correlational data have been available. For example, the continental-scale correlations of hydrogen isotope ratios in tree-ring cellulose with local water by Yapp and Epstein (1982) provide evidence that the variations in hydrogen isotopes of cellulose are closely associated with changes in environmental waters. On the other hand, Roden et al. (2005) observed that cellulose isotope values in conifers did not follow a similar pattern along a climatic gradient from coastal to interior Oregon. The apparently conflicting patterns of both studies are resolved with the process-based model of Roden et al. (2000), which recognizes that both water source and humidity are important determinants of the final hydrogen isotope ratio values in cellulose. In some situations, the isotopic influences of humidity gradients and water sources result in a diminished correlation between water source and cellulose isotope ratios. It is our foundational premise that the spatial patterns of hydrogen and oxygen isotopes in biological systems are most consistently predictable by combining process-based models with spatially explicit climate data, which will both predict and explain apparent anomalies in correlational data.

Many of the key insights into how hydrogen and oxygen isotopes of the water environment become recorded into biological materials originate with the pioneering studies by DeNiro, Epstein, Fogel, Hoering, Sternberg, Yakir, and others from UCLA, Cal Tech, and the Carnegie Institution of Washington. It was the initial observations by DeNiro and Epstein (1977) that provided the mechanistic underpinnings of the fractionation processes associated with lipid synthesis. Experimental studies of plants by Sternberg et al. (1986) and Yakir and DeNiro (1990) helped define fractionation processes during synthesis of carbohydrates. Roden et al. (2000) later integrated many of the reactions to provide an overall model that linked source water, environment, fractionation processes, and carbohydrate movement among tissues to describe how the hydrogen and oxygen isotope ratios of cellulose reflected a combination of discrete steps where both source water and evaporated water could influence the isotope ratios of cellulose, the final carbohydrate product (Fig. 17.2). One relevant point with respect to Fig. 17.2 is that the leaf water and plant cellulose models do not use or require a 2-pool concept to predict hydrogen and oxygen isotope ratios of leaf water or of cellulose (or of carbohydrates in general). Two different tissues can be involved in carbohydrate synthesis, such as with sugar synthesis in autotrophic cells, transportation within the plant, and its subsequent incorporation into cellulose in heterotrophic cells. However, each of these are single pools that do not interact because water movement in xylem is unidirectional and therefore not a circulatory system.

Kreuzer-Martin et al. (2005a, 2003) extended the carbohydrate-model observations to show that microbial spores, a combination of protein and carbohydrates, would also reflect variations in the stable isotope ratios of water sources. Their interest was a forensic application: to source microbial spores, such as the anthrax

spores mailed in letters in late 2001 (http://en.wikipedia.org/wiki/2001_anthrax_attacks). Kreuzer-Martin and colleagues showed that the hydrogen and oxygen isotope ratios of spores record the isotopic composition of the culture medium and of the water in which these microbes were cultured, providing a potential geo-location signal. In *Bacillus* spores, approximately 74% of the oxygen atoms in a spore were derived from its source water. The utility of the stable isotope approach here is to allow investigators to both eliminate possible sources by showing that spore hydrogen and oxygen isotope values are not consistent with a region and to further guide investigations by indicating that stable isotope ratio values are consistent with particular geographical regions. Later studies by Kreuzer-Martin and Jarman (2007) showed that these relationships held, as expected, across *Bacillus* species.

The hair of humans and other mammals is composed predominately of the protein keratin, which in its isotope chemistry records information about food and water sources consumed by individuals. Perhaps most well documented are the patterns in the carbon, nitrogen, and sulfur isotope ratios of hair related to geographically distinct dietary preferences. European and Japanese hair is often distinct from USA hair, as is Chilean, Canadian, and German hair (Bol and Pflieger 2002; McCullagh et al. 2005). While these studies imply a geographical pattern, the pattern is based on culturally-related dietary preference and not fundamental climatic or environmental characteristics of a particular location.

The move to understand stable hydrogen and oxygen isotopes in proteins is a logical extension of the earlier plant cellulose and microbial studies. Human hair and fingernails should also record water source information, and in so doing provide geographic information for forensic studies. Several recent studies have suggested that isotope ratio differences in human hair exist and can be used to distinguish individuals of different geographic origin (Fraser et al. 2006; O'Connell and Hedges 1999; Sharp et al. 2003). A recent study of public interest involving stable isotopes was the case of the Ice Man discovered on the border between Austria and Italy (Hoogewerff et al. 2001; Macko et al. 1999).

Ehleringer et al. (2008a) developed a process-based model to explain hydrogen and oxygen isotope ratio values in proteins, assuming steady state conditions. Their particular application was to human hair and to the region-of-origin of that hair (Fig. 17.7), but it is a general model that is applicable to all proteins. Three predictions of that model are useful to point out here. First, essentially all oxygen atoms in a protein have exchanged with animal body water. Body water isotopes are influenced by drinking water, diatomic oxygen, and oxygen from energy sources. Second, a two-pool water model is required to explain water-environment patterns because water transport in animals is a circulatory system (not a one-way transport system as in plants). Third, the hydrogen atoms in R-groups do not interact with the aqueous media if the amino acid remains intact; thus they have the potential to provide food-source information. If the model adequately captures the essence of human biology, then this implies that oxygen isotope ratio analyses of protein can be used to infer geo-location information if body water isotopes can be adequately modeled. The model also suggests that simultaneous measurements of hydrogen and oxygen isotope ratio in protein can be used to extend the region-of-origin

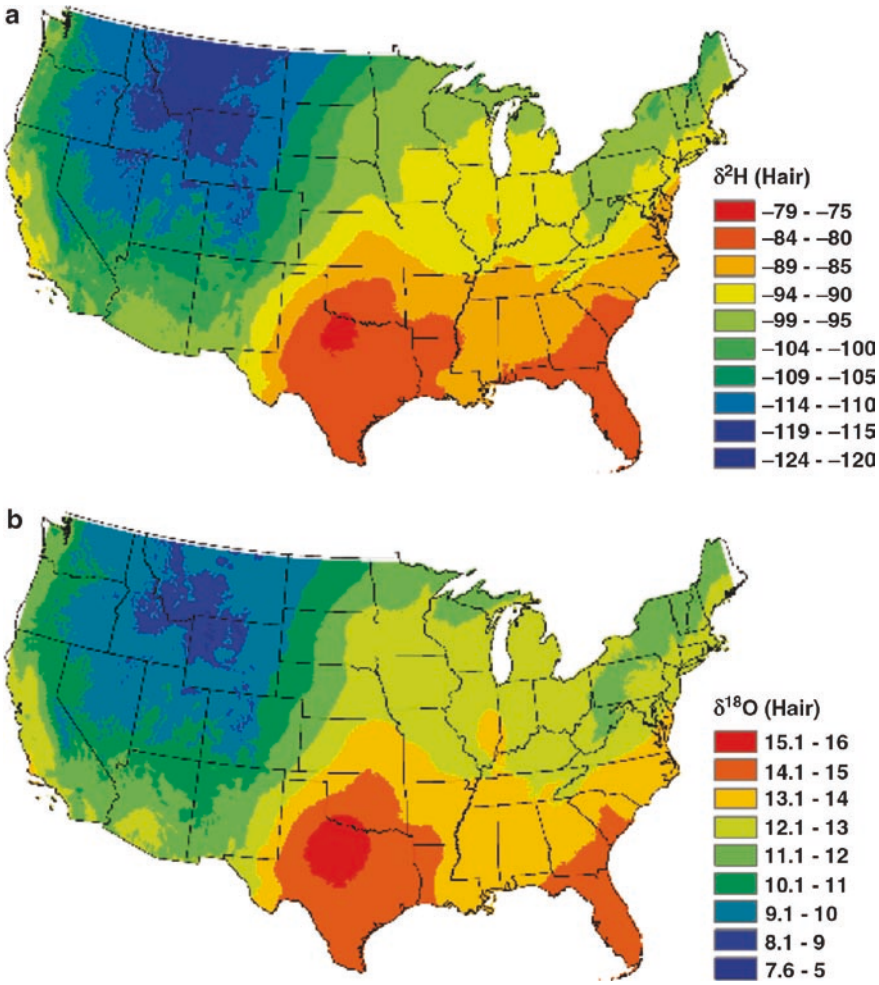

Fig. 17.7 The predicted geographic distribution of the hydrogen (**a**) and oxygen (**b**) isotope ratios in human hair across the USA (From Ehleringer et al. 2008), see Appendix 1, Color Section

model to assess non-steady state conditions and to infer dietary conditions. While the Ehleringer et al. model was developed for steady state conditions, the multi-pool turnover concepts developed by Cerling et al. (2007) can be applied to extend this steady state model into more dynamic and realistic situations.

Four evaluations of the Ehleringer et al. (2008a) model have been made to date. Each independent set of observations provides support for the region-of-origin spatial model predictions. First, Ehleringer et al. (2008a) provide an evaluation based on random hair collections from 65 geographically distributed cities across the USA traversing a broad water-isotope gradient. The model accurately predicts the region-of-origin for 86% of the hair samples. Second, Chesson et al. (2008)

observed hydrogen and oxygen isotope ratios of delipified hamburgers from fast-food meals collected throughout the USA. The correlations of the two isotopes in this protein are similar to those predicted by the Ehleringer et al. model. Third, Bowen et al. (2009) examined the hydrogen and oxygen isotope ratios of ancestral human populations in a diverse set of regions around the globe. The predictions of the model were in agreement with their observations, provided a local food component was added. Lastly, Thompson et al. (2009) examined hydrogen and oxygen isotope ratios along a geographical transect from southern India north through Mongolia. Their observations were fully predictable on the basis of parameters in the Ehleringer et al. model. Based on the model and the result of its four initial evaluations, we now apply this region-of-origin model to explore a forensic application – the geographical movements of unidentified murder victims prior to death.

17.4 Application of Stable Isotope Analysis to Unsolved Murder Investigations

In cases of unidentified human remains where traditional methods of establishing an individual's identity such as documentation, known samples of DNA and recognition by family members are not available, stable isotope analysis can provide useful information regarding an individual's recent and previous regions of residence. To investigators, reconstruction of movements across isotopic gradients can help to focus an investigation and enable the direction of valuable resources to the most promising geographic region. Isotopic evidence may answer a number of questions such as: Was this individual a resident in the region prior to death? Where was the childhood region of residence? Did the victim move prior to death? Was the diet of this individual unusual in any way? Two cases are detailed below that highlight the application of hydrogen and oxygen isotope ratio analyses to human hair and oxygen isotope ratio analysis to tooth enamel from unidentified human remains.

At this stage of the applications of stable isotope analyses to forensic applications, the focus is on patterns consistent with mean model predictions. Uncertainty in model projections and statistical patterns are unknown. Thus, none of the projections that follow should be construed as the definitive or ultimate patterns to be predicted. Instead they represent our best projections based on currently available models. To capture some of the uncertainty in model predictions, we have expanded the ranges of values used in model predictions by a factor of 2. Therefore, model predictions for where an individual may have traveled from represent broader geographic trends than predicted based on isotope measurement precision. Whether or not the model projections are sufficiently accurate to capture the actual trends will become known as the individual cases are solved now and in the future.

17.4.1 The Case of "Saltair Sally", Found in Utah

In October 2000, the unidentified remains of a young female, approximately 17–20 years of age, were discovered in a shallow grave in the desert close to Interstate Highway 80 at Saltair, west of Salt Lake City, Utah. The decomposed, scattered remains consisted only of incomplete skeletal elements, including the cranium and teeth, the victim's scalp and hair and a few distinctive personal effects. Physical examination provided an estimate of 12–24 months since death. An estimation of stature indicated a short individual with strikingly long hair. Despite efforts by police to establish the identity of this individual through the local media, no response from family or friends was elicited. A missing person report was not filed and the victim's identity remained unknown. The individual has been referred to as "Saltair Sally" and the case eventually became a cold case.

In 2007, the Utah State Medical Examiner released approximately 26 cm of hair for isotope ratio analysis along its length in order to provide information about the potential travel moments of this individual. Several hairs were aligned, sectioned, and analyzed for hydrogen and oxygen isotope ratios following established methods (Bowen et al. 2005a; Ehleringer et al. 2008a). Using an average growth rate of 0.4 mm/day (Saitoh et al. 1967), the hair length was estimated to represent approximately 22 months prior to death. The most recent proximal hair segment was also converted to CO_2 and sent for ^{14}C analysis to establish a year of death using the "bomb-spike" signal, estimated as 1996, several years earlier than previously thought.

The oxygen isotope ratios from the hair showed periodic changes before death (Fig. 17.8). The oxygen isotope ratios demonstrated a cycle, reaching two peaks of approximately 10‰ at months 22 and 10 and a plateau of approximately 10‰ around 4 months prior to death.

It is estimated that oxygen isotope ratios measured from hair will attain complete equilibrium within 3 months (Ehleringer et al. 2008a). This corresponded well with the period between month 8 and month 4 prior to death, where the values increased until they reached a plateau and remained constant until death. Prior to this, the data indicated that the victim was not resident of a single location for long enough to reach complete isotopic equilibrium and moved across an isotopic gradient, possibly at least twice each year. The data suggested at least three movement events in the past 22 months followed by a period in one location just before death. These patterns suggest that this individual was mobile rather than being a long-term resident in one location.

While both hydrogen and oxygen isotope ratios should be correlated with the isotopes of water in the region, we feel that it is more appropriate to consider oxygen isotope ratios when inferring information about the geographical movements of an individual across isotopically distinct regions (isoscapes). This is because the Ehleringer et al. (2008a) model predicts complete oxygen isotope exchange of amino acids with the environment during protein hydrolysis, but only partial hydrogen isotope exchange (because of the non-exchangeable hydrogen on the R-groups

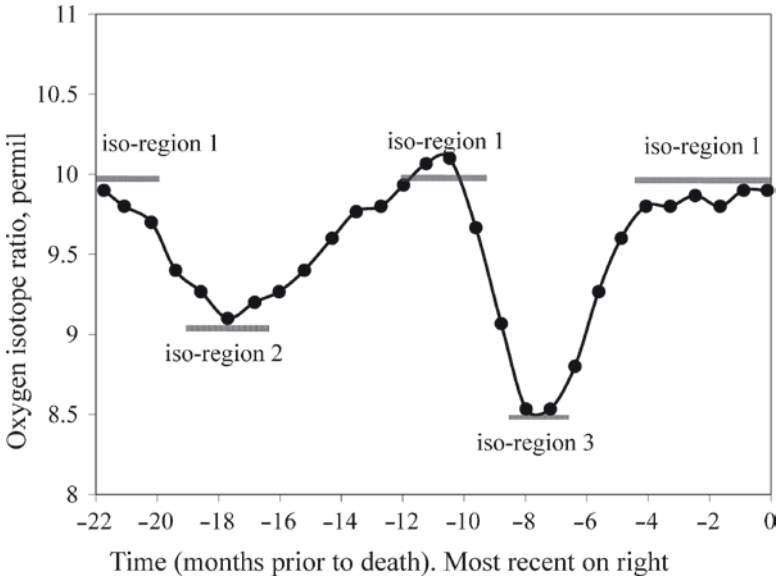

Fig. 17.8 Identification of locations on a plot of the oxygen isotope ratios measured from "Saltair Sally" as a function of time before the victim's death. Time was calculated based on an average growth rate of 0.4 mm/day. Data are 3-point running means. Three iso-regions are noted where it is suggested that the victim had resided for a period of time. Iso-region 1 is tentatively identified as corresponding to three points along the time line corresponding to the 4, 12 and 22 months prior to death. Iso-region 2 is tentatively identified as the minimum in the time line at months 19–17 prior to death. Iso-region 3 is tentatively identified as the minimum in the time line at months 12–8 prior to the victim's death

of amino acids). Five points along the oxygen isotope ratios measured along the length of the hair that was considered to represent three different geographical locations were chosen (Fig. 17.8). Predictions of the semi-mechanistic model of Ehleringer et al. (2008a) were inverted to predict the drinking water input that would produce the observed patterns of oxygen isotope ratios in hair. Using an isoscape of oxygen isotope ratios in drinking water (Bowen et al. 2007), with a margin of ±0.5‰ added to either side of the modeled value per location, maps of the geographic regions were produced to predict where this individual had traveled in the last 22 months of her life (Fig. 17.9a–c).

Iso-region 1 was consistent with three periods of time along the hair and suggested that at 22 months before death the victim could have been in an area consistent with the area where her remains were discovered (Fig. 17.9a). Immediately after this she moved to Iso-region 2, a smaller geographic area consistent with somewhat more depleted oxygen isotope values to the north of Iso-region 1 (Fig. 17.9b). Movement back to an area consistent with iso-region 1 occurred approximately 18 months prior to death, followed by movement to iso-region 3 approximately 6 months later. Iso-region 3 was consistent with a smaller geographical area further to the north of Iso-region 1, corresponding to significantly

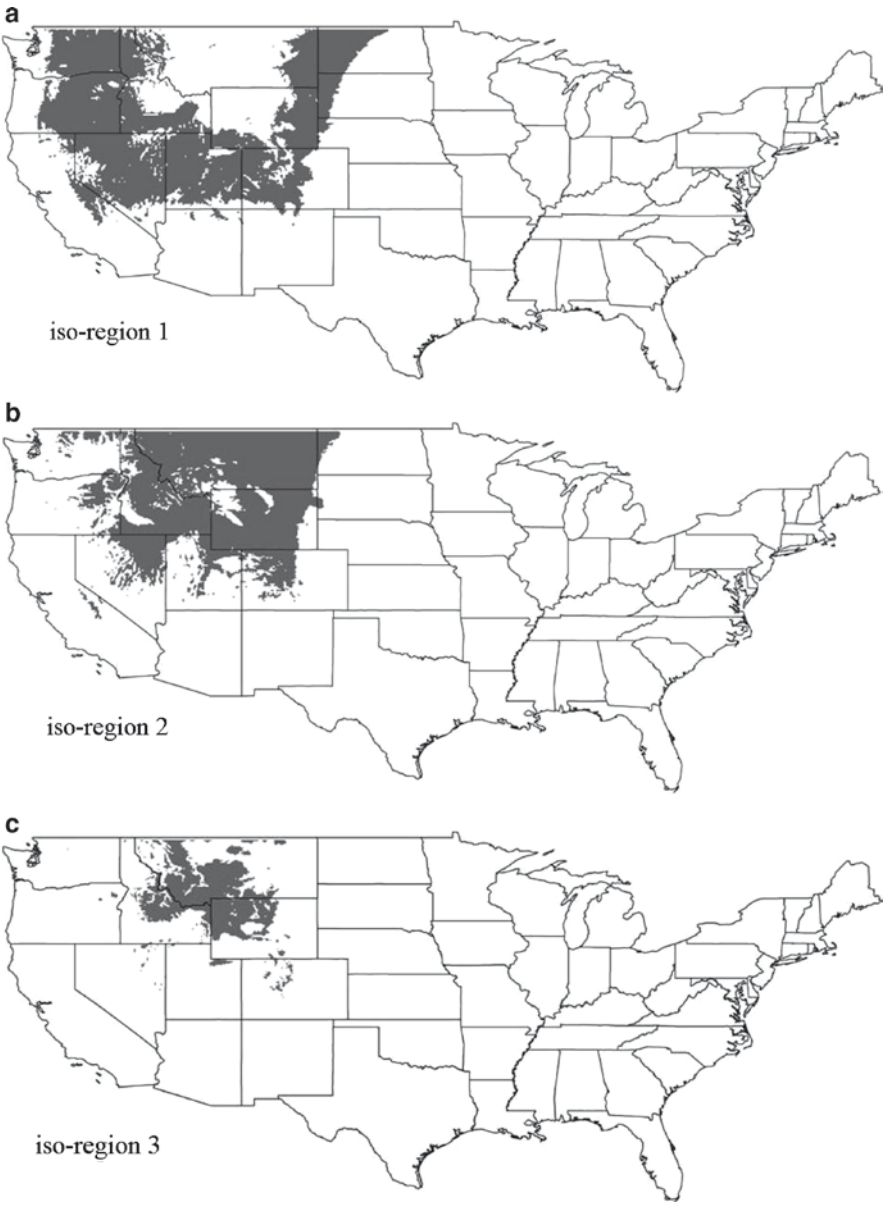

Fig. 17.9 A Geographic Information System (GIS) representation of those geographic regions that are associated with iso-region 1 (**a**), iso-region 2 (**b**), and iso-region 3 (**c**). For these predictions, we used a range of $\delta^{18}O$ values that spans ±0.5‰ of the predicted mean $\delta^{18}O$ value for different regions

more depleted oxygen isotope values (Fig. 17.9c). Subsequently, the victim moved back to Iso-region 1 approximately 8 months before death and remained resident in this area until her death.

In order to establish whether Saltair Sally was local to the Intermountain West region of the USA during her childhood, tooth enamel from the upper left incisor and the upper left second molar was analyzed for oxygen isotope ratios. It was estimated that these teeth mineralized between 8 to 9 and 12 to 13 years of age, respectively, based on published measurement and modeling approaches (Nakamura et al. 2007; Spalding et al. 2005). The oxygen isotope values measured from both teeth were very similar (23.0‰ and 23.1‰, respectively), suggesting that the victim did not move across an isotopic gradient between approximately 8 and 13 years of age. The relationship between oxygen isotopes in tooth enamel carbonate and oxygen isotope values in local water was used to calculate a predicted water oxygen isotope value and the corresponding geographic region of origin where the victim was likely resident while her teeth mineralized (Fig. 17.6). This region of residence was estimated to be consistent with a childhood in the Intermountain West, and is predicted to be the same region that she was a resident of just before and at the time of her death (as predicted from oxygen isotope analysis of her hair).

17.4.2 An Unidentified Victim from Mammoth Lakes, California

In May 2003, a hiker and his dog discovered a human skull in the Sierra Nevada near Mammoth Lakes, California and alerted the police. Soon afterwards a shallow grave was uncovered by police containing the fragmented remains of a female homicide victim and her clothing (Dostie 2007). The medical examiner reported that she was between 30 to 40 years of age, short in stature, slight of build and possibly of Southeast Asian origin. She had been buried for between 6 and 9 months under the snowpack since her death. An appeal to establish her identity was made by the police through the local media outlets. A US Forest Service employee responded and recalled a woman matching the victim's description had been in the area with a man thought to be her husband in the fall of 2002 and that she had confided she was afraid of him. Based on their description, a forensic artist produced a reconstruction of the victim that was circulated, however no family members contacted the police and a missing person report matching the victim was not filed. The investigation continued but the victim's identity remained unknown.

In this case, DNA analysis was applied to establish the victim's ethnic ancestry rather than as a comparative method to directly establish identity. The results suggested that she was of Native American rather than Asian origin, and this was further supported by a physical anthropologist who examined the remains. Further analysis of both mitochondrial and nuclear (HLA loci) DNA showed the victim's origins were likely to have been in the Oaxaca region of southern Mexico.

Carbon and oxygen isotope ratios were previously carried out on the victim's hair, tooth enamel and a bone sample (Schwarcz 2007). The ^{13}C-enriched carbon isotope ratios suggested that the victim's diet contained significantly more maize derived carbon than the average US resident, supporting a Mexican or Central American origin. Oxygen isotope ratios of the tooth enamel and bone carbonate

showed values that corresponded to regions with highly enriched oxygen isotope values, indicative of a very warm climate and consistent with both a childhood and subsequent adulthood in southern Mexico.

In light of the above information, oxygen and carbon isotope ratios were measured along the length of the hair in order to reconstruct the victim's movements prior to death (Fig. 17.10). Almost 25 cm of hair was received for analysis, which corresponded to approximately the last 21 months of the victim's life. The oxygen isotope ratios showed relatively subtle but clear changes along the length of the hair that suggested movement across isotopic gradients by this individual (Fig. 17.10). The carbon isotope data were consistent with the values from previous analyses (Schwarcz 2004, 2008), and showed much more ^{13}C enrichment along the whole length of the hair than is typically seen in USA residents (McCullagh et al. 2005; unpublished data).

When the oxygen isotope ratios were compared to the carbon isotope ratio data, both datasets showed corresponding depletions in values from approximately

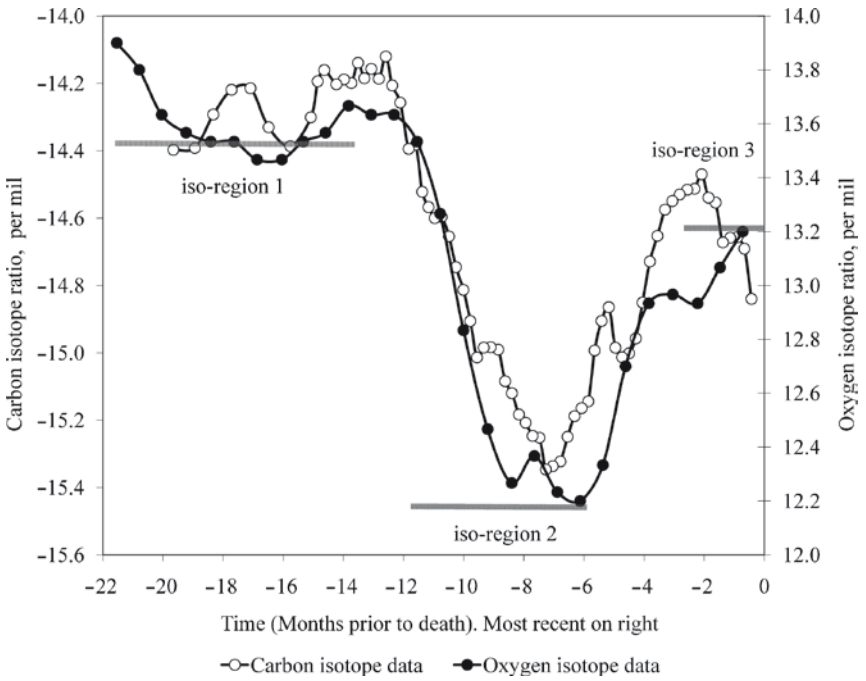

Fig. 17.10 A plot of the carbon and oxygen isotope data measured from hair from the Sierra Nevada murder victim as a function of time prior to the victim's death with three regions marked. Time was calculated based on an average growth rate of 0.4 mm/day. Data are 3-point running means. Three regions are marked where it is suggested the victim resided for a period of time. Iso-region 1 is tentatively identified as corresponding to the plateau at months 22–12 prior to death; iso-region 2 is as the minimum in the time line at months 12–6 prior to death and iso-region 3 as the maximum in the time line immediately prior to the victim's death

month 12 to month 7 prior to death (Fig. 17.10). The hair carbon and oxygen isotope values for the period between 22 and 12 months prior to death were relatively steady, suggesting that the individual did not cross any significant isotopic gradients during this period. The data suggested that approximately a year before death the victim traveled from a warmer region, where a more ^{13}C-enriched diet (likely due to maize) was also consumed, to a cooler region, where the ^{13}C-enriched input to the diet decreased slightly. The depletion in hair oxygen isotope ratios was rapid but she did not remain in this region for long enough for oxygen isotope ratios to reach full equilibrium with local water-isotope values, evidenced by the lack of a plateau. About 6 months before death another travel event took place and both oxygen and carbon isotope ratios became more enriched again, suggesting movement to a warmer place and increased consumption of ^{13}C enriched foods. Immediately prior to death, the isotopic values appeared to be in flux and were still increasing.

In order to assess what the expected oxygen isotope ratios of the hair of a Mammoth Lakes resident were, water from the site was collected, analyzed and used as the input to the Ehleringer et al. (2008a) model. The calculated oxygen isotope ratios predicted for hair were between 9.5‰ and 10.1‰. Even with an allowance of ±0.5‰, at no time did the values in the victim's hair reach these depleted values. The isotopic data therefore strongly suggested that this individual was a recent visitor to the Mammoth Lakes area and had not been a resident at any time in the last 2 years.

The shifts in isotope ratios suggested that the victim had moved across isotopic gradients at least twice in the last 2 years; 12 months before death, again at approximately 6 to 8 months before death and finally possibly 2 months prior to her death. Three points where shifts were seen in the oxygen isotope ratios measured from the hair were chosen and the oxygen isotope ratios were used to predict the corresponding geographic regions (Fig. 17.11). Predictions of regions-of-origin were made using the hair oxygen isotope ratios measured at these points as input to the inversion calculations in the Ehleringer et al. (2008a) model. Regions of the USA and Mexico with corresponding hair oxygen isotope ratios in drinking water and precipitation respectively were then selected as detailed above and maps were produced (Fig. 17.11a–c). These regions suggested geographical movements that may have involved crossing the USA–Mexican border. The supporting evidence from these and other analyses suggested that the victim was resident in or close to the Oaxaca to Sonora regions of Mexico in the 22–12 months before her death (Fig. 17.11a). She then moved north to a region that included northern Sonora and the USA side of the border, where she remained until 6 months prior to her death (Fig. 17.11b). At this point she may have traveled south again to the southern side of the USA–Mexico border, possibly as far as central Mexico (Fig. 17.11c), before her death and subsequent discovery in the Sierra Nevada of California.

Oxygen isotope ratios of carbonate within the tooth enamel of this individual have been analyzed by Schwarcz (2007). From its value of +22.0‰, the geo-location information for this individual is consistent with iso-region 2 in Fig. 17.11. This datum is consistent with an individual who may have grown up in Mexico before moving to the USA.

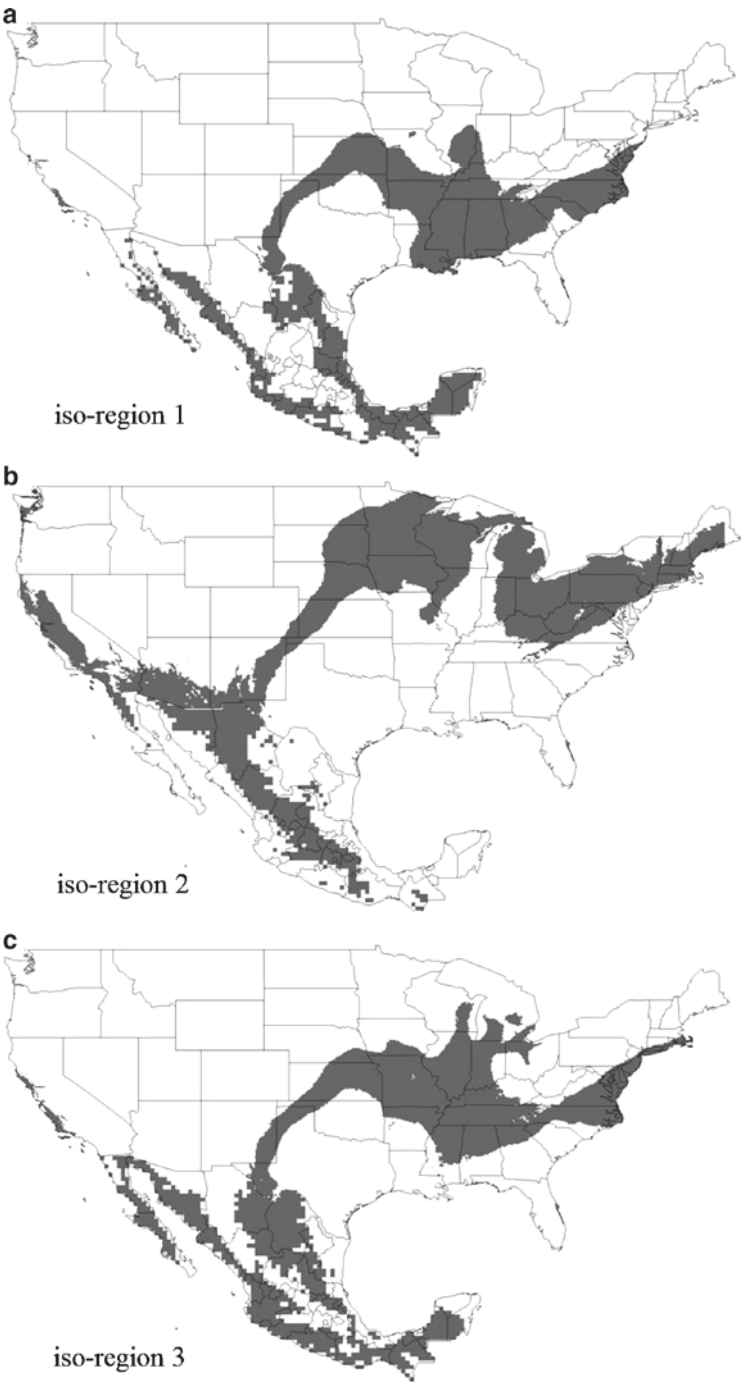

Fig. 17.11 A Geographic Information System (GIS) representation of those geographic regions that are associated with iso-region 1 (**a**), iso-region 2 (**b**), and iso-region 3 (**c**) for the Sierra Nevada murder victim. For these predictions, we used a range of $\delta^{18}O$ values that spans ±0.5‰ of the predicted mean $\delta^{18}O$ value for each region

Stable isotope analyses of hair and teeth have proved useful in other forensic investigations, confirming other forensic data and contributing to efforts that resulted in the identification of previous cold cases. However, at the time of submission of this publication, the identities of these two murder victims remain unknown.

17.5 Emerging Opportunities

The application of stable isotopes in forensic sciences is new (Meier-Augenstein and Liu 2004); the expansion into spatial forensic patterns is even newer (Ehleringer et al. 2008b; Meier-Augenstein and Fraser 2008). However, the need for stable isotope information that is relevant to broad spatial scales is already evident (Bowen et al. 2005b). As our understanding of both spatial patterns in water isotopes and of biological fractionation processes improves, it is expected that more applications will emerge where stable isotope analyses play an important role in guiding an investigation. When the use of both stable isotopes of light elements, reflecting biological process as described here, is combined with stable isotope analyses of heavy elements, reflecting soil parameters, finer-resolution provenancing capacities should be achievable. The heavy-element foundation in geosciences clearly establishes the forensic utility of strontium and neodymium isotopes in quantifying the region-of-origin of individuals and products of interest (Crittenden et al. 2007; Garcia-Ruiz et al. 2007; Pye and Croft 2004). In some cases, it is expected that stable isotope ratio data will provide key information that becomes part of the prosecution evidence introduced into the judicial court system. In other cases, the isotope data will serve to guide investigations, confirm suspected relationships, and reject others. Stable isotopes may well become an increasingly important component of food provenancing and its commercial and regulatory implications, as implied by the recent TRACE studies in the EU (http://www.trace.eu.org/) and by studies from Chesson et al. (2008). As our appreciation of natural, biosynthetic, and synthetic fractionation factors increases over time, the forensic applications of stable isotope are likely to play a greater role in forensic investigations and in criminal prosecution.

References

Ambrose SH, Norr L (1993) Experimental evidence for the relationship of the carbon isotope ratios of whole diet and dietary protein to those of bone collagen and carbonate. In: Lambert JB, Grupe G (eds) Prehistoric human bone: archaeology at the molecular level. Springer-Verlag, Berlin, pp 1–37

Beard BL, Johnson CM (2000) Strontium isotope composition of skeletal material can determine the birth place and geographic mobility of humans and animals. J Forensic Sci 45:1049–1061

Benson S, Lennard C, Maynard P, Roux C (2006) Forensic applications of isotope ratio mass spectrometry – a review. Forensic Sci Int 157:1–22

Bol R, Pflieger C (2002) Stable isotope (C-13, N-15 and S-34) analysis of the hair of modern humans and their domestic animals. Rapid Commun Mass Spectrom 16:2195–2200

Bottinga Y (1968) Calculation of fractionation factors for carbon and oxygen exchange in the system calcite-carbon dioxide-water. J Phys Chem 72:800–808

Bowen GJ, Chesson L, Nielson K, Cerling TE, Ehleringer JR (2005a) Treatment methods for the determination of δ^2H and $\delta^{18}O$ of hair keratin by continuous-flow isotope-ratio mass spectrometry. Rapid Commun Mass Spectrom 19:2371–2378

Bowen GJ, Wassenaar LI, Hobson KA (2005b) Global application of stable hydrogen and oxygen isotopes to wildlife forensics. Oecologia 143:337–348

Bowen GJ et al (2005c) Stable hydrogen and oxygen isotope ratios of bottled waters of the world. Rapid Commun Mass Spectrom 19:3442–3450

Bowen GJ, Ehleringer JR, Chesson LA, Stange E, Cerling TE (2007) Stable isotope ratios of tap water in the contiguous USA. Water Resour Res 43:W03419

Bowen GJ, Ehleringer JR, Chesson LA, A.H. Thompson, Podlesak DW, Cerling TE (2009) Dietary and physiological controls of the hydrogen and oxygen isotope ratios of hair from mid-20th century indigenous populations. Am J Phys Anthropol 139:494–504

Breas O, Reniero F, Serrini G (1994) Isotope ratio mass spectrometry: analysis of wines from different European countries. Rapid Commun Mass Spectrom 8:967–970

Brencic M, Vreca P (2006) Identification of sources and production processes of bottled waters by stable hydrogen and oxygen isotope ratios. Rapid Commun Mass Spectrom 20: 3205–3212

Brenninkmeijer CAM, Kraft P, Mook WG (1983) Oxygen isotope fractionaltion between CO_2 and H_2O. Isotope Geosci 1:181–190

Casale J, Casale E, Collins M, Morello D, Cathapermal S, Panicker S (2006) Stable isotope analyses of heroin seized from the merchant vessel Pong Su. J Forensic Sci 51:603–606

Cerling TE et al (2007) Determining biological tissue turnover using stable isotopes: the reaction progress variable. Oecologia 151:175–189

Chesson LA, Thompson AH, Podlesak DW, Cerling TE, Ehleringer JR (2008) Variation in hydrogen, carbon, nitrogen, and oxygen stable isotope ratios in the modern American diet: fast food meals. J Agric Food Chem 56:4084–4091

Coplen TB, Herczeg AL, Barnes C (1999) Isotope engineering – using stable isotopes of the water molecule to solve practical problems. In: Cook PG, Herczeg AL (eds) Environmental tracers in subsurface hydrology. Kluwer, Boston, MA, pp 79–110

Craig H, Gordon LI (1965) Deuterium and oxygen 18 variations in the ocean and the marine atmosphere. In: Tongiorgi E (ed) Stable isotopes in oceanographic studies and paleotemperatures. Consiglio Nazionale Delle Ricerche Laboratorio di Geologia Nucleare, Pisa, Italy, pp 9–130

Crittenden RG, Andrew AS, LeFournour M, Young MD, Middleton H, Stockmann R (2007) Determining the geographic origin of milk in Australasia using multi-element stable isotope ratio analysis. Int Dairy J 17:421–428

D'Angela D, Longinelli A (1990) Oxygen isotopes in living mammal's bone phosphate: further results. Chem Geol 86:75–82

DeNiro MJ, Epstein S (1977) Mechanism of carbon isotope fractionation associated with lipid synthesis. Science 197:261–263

Dongmann G, Nurnberg HW, Forstel H, Wagener K (1974) On the enrichment of H_2O_{18} in the leaves of transpiring plants. Rad Environ Biophys 11:41–52

Dostie P (2007) Case number 03–0929 murder in Mammoth lakes. Forensic Mag 4:1_2–^{18}

Dutton A, Wilkinson BH, Welker JM, Bowen GJ, Lohmann KC (2005) Spatial distribution and seasonal variation in $^{18}O/^{16}O$ of modern precipitation and river water across the conterminous United States. Hydrol Process 19:4121–4146

Ehleringer JR, Hall AE, Farquhar GD (eds) (1993) Stable isotopes and plant carbon/water relations. Academic, San Diego, CA

Ehleringer JR, Casale JF, Lott MJ, Ford VL (2000) Tracing the geographical origin of cocaine. Nature 408:311–312

Ehleringer JR, Cerling TE, West JB (2007) Forensic science applications of stable isotope ratios. In: Blackledge RD (ed) Forensic analysis on the cutting edge: new methods for trace evidence analysis. Wiley, San Diego, CA, pp 399–422

Ehleringer JR, Bowen GJ, Chesson LA, West AG, Podlesak DW, Cerling TE (2008a) Hydrogen and oxygen isotope ratios in human hair are related to geography. Proc Natl Acad Sci U S A 105:2788–2793

Ehleringer JR, Cerling TE, West JB, Podlesak DW, Chesson LA, Bowen G (2008b) Spatial considerations of stable isotope analyses in environmental forensics. In: Hester RE, Harrison RM (eds) Issues in environmental science and technology, vol 26. Royal Society of Chemistry Publishing, Cambridge, pp 36–53

English NB, Betancourt JL, Dean JS, Quade J (2001) Strontium isotopes reveal distant sources of architectural timber in Chaco Canyon, New Mexico. Proc Natl Acad Sci U S A 98: 11897–11896

Farquhar GD, Ehleringer JR, Hubick KT (1989) Carbon isotope discrimination and photosynthesis. Annu Rev Plant Physiol Plant Mol Biol 40:503–537

Flanagan LB, Comstock JP, Ehleringer JR (1991) Comparison of modeled and observed environmental influences on the stable oxygen and hydrogen isotope composition of leaf water in *Phaseolus vulgaris* L. Plant Physiol 96:588–596

Fraser I, Meier-Augenstein W, Kalin RM (2006) The role of stable isotopes in human identification: a longitudinal study into the variability of isotopic signals in human hair and nails. Rapid Commun Mass Spectrom 20:1109–1116

Fritz P, Drimmie RJ, Render FW (1974) Stable isotope content of a major prairie aquifer in Central Manitoba, Canada. In: Isotope techniques in groundwater hydrology, vol I. IAEA, Vienna, pp 379–398

Garcia-Ruiz S, Moldovan M, Fortunato G, Wunderli S, Alonso JIG (2007) Evaluation of strontium isotope abundance ratios in combination with multi-elemental analysis as a possible tool to study the geographical origin of ciders. Anal Chim Acta 590:55–66

Gat JR (1996) Oxygen and hydrogen isotopes in the hydrologic cycle. Annu Rev Earth Planet Sci 24:225–262

Ghazi AM, Millette JR (2004) Environmental forensic application of lead isotope ratio determination: a case study using laser ablation sector ICP-MS. Environ Forensics 5:97–108

Gretebeck RJ et al (1997) Adaptation of the doubly labeled water method for subjects consuming isotopically enriched water. J Appl Physiol 82:563–570

Griffiths H (ed) (1998) Stable isotopes integration of biological, ecological, and geochemical processes. BIOS Scientific Publishers, Oxford

Gulson BL, Jameson CW, Gillings BR (1997) Stable lead isotopes in teeth as indicators of past domicile – a potential new tool in forensic science? J Forensic Sci 42:787–791

Hoogewerff J et al (2001) The last domicile of the Iceman from Hauslabjoch: a geochemical approach using Sr, C and O isotopes and trace element signatures. J Archaeol Sci 28:983–989

Ingraham NL, Caldwell EA (1999) Influence of weather on the stable isotopic ratios of wine: tools for weather/climate reconstruction? J Geophys Res 104:2185–2194

Ingraham NL, Taylor BE (1991) Light stable isotope systematics of large-scale hydrologic regimes in California and Nevada. Water Resour Res 27:77–90

Ingraham NL, Lyles BF, Jacobson RL, Hess JW (1991) Stable isotopic study of precipitation and spring discharge in Southern Nevada. J Hydrol 125:243–258

Ingraham NL, Matthews RA, McFadyen R, Franks AL (2004) The use of stable isotopes to identify the hydrologic source of bottled water: Baxter, California. Environ Eng Geosci 10:361–365

Jarman KH et al (2008) Bayesian-integrated microbial forensics. Appl Environ Microbiol 74:3573–3582

Kendall C, Coplen TB (2001) Distribution of oxygen-18 and deuterium in river waters across the United States. Hydrol Process 15:1363–1393

Kohn MJ (1996) Predicting animal $\delta^{18}O$: Accounting for diet and physiological adaptation. Geochim Cosmochim Acta 60:4811–4829

Kortelainen NM, Karhu JA (2004) Regional and seasonal trends in the oxygen and hydrogen isotope ratios of Finnish groundwaters: a key for mean annual precipitation. J Hydrol 285: 143–157

Kreuzer-Martin HW, Lott MJ, Dorigan J, Ehleringer JR (2003) Microbe forensics: Oxygen and hydrogen stable isotope ratios in *Bacillus subtilis* cells and spores. Proc Natl Acad Sci U S A 100:815–819

Kreuzer-Martin HW, Chesson LA, Lott MJ, Dorigan JV, Ehleringer JR (2004) Stable isotope ratios as a tool in microbial forensics. I. Microbial isotopic composition as a function of growth medium. J Forensic Sci 49:954–960

Kreuzer-Martin HW, Chesson LA, Lott MJ, Ehleringer JR (2005a) Stable isotope ratios as a tool in microbial forensics. Part 3. Effect of culturing on agar-containing growth media. J Forensic Sci 50:1372–1379

Kreuzer-Martin HW, Ehleringer JR, Hegg EL (2005b) Oxygen isotopes indicate most intracellular water in log-phase *Escherichia coli* is derived from metabolism. Proc Natl Acad Sci U S A 102:17,337–317,341

Kreuzer-Martin HW, Lott MJ, Ehleringer JR, Hegg EL (2006) Metabolic processes account for the majority of intracellular water in log-phase *Escherichia coli* cells as revealed by hydrogen isotopes. Biochemistry 45:13622–13630

Kreuzer-Martin HW, Jarman KH (2007) Stable isotope ratios and forensic analysis of microorganisms. Appl Environ Microbiol 73:3896–3908

Lai CT, Ometto J, Berry JA, Martinelli LA, Domingues TF, Ehleringer JR (2008) Life form-specific variations in leaf water oxygen-18 enrichment in Amazonian vegetation. Oecologia 157:197–210

Longinelli A (1984) Oxygen isotopes in mammal bone phosphate: a new tool for paleohydrological and paleoclimatological research? Geochim Cosmochim Acta 48:385–390

Longinelli A, Padalino AP (1980) Oxygen isotopic composition of water from mammal blood: first results. Europ J Mass Spectrom 1:135–139

Luz B, Kolodny Y, Horowitz M (1984) Fractionation of oxygen isotopes between mammalian bone-phosphate and environmental drinking water. Geochim Cosmochim Acta 48:1689–1693

Luz B, Cormie AB, Schwarcz HP (1990) Oxygen isotope variations in phosphate of deer bones. Geochim Cosmochim Acta 54:1723–1728

Macko SA, Lubec G, Teschler-Nicola M, Andrusevich V, Engel MH (1999) The Ice Man's diet as reflected by the stable nitrogen and carbon isotopic composition of his hair. FASEB J 13:559–562

McCullagh JSO, Tripp JA, Hedges REM (2005) Carbon isotope analysis of bulk keratin and single amino acids from British and North American hair. Rapid Commun Mass Spectrom 19:3227–3231

Meier-Augenstein W, Fraser I (2008) Forensic isotope analysis leads to identification of a mutilated murder victim. Sci Justice 48:153–159

Meier-Augenstein W, Liu RH (2004) Forensic applications of isotope ratio mass spectrometry. In: Yinon J (ed) Advances in forensic applications of mass spectrometry. CRC Press, Boca Raton, FL, pp 149–180

Nakamura T et al (2007) Application of AMS C-14 measurements to criminal investigations. J Radioanal Nucl Chem 272:327–332

Nardoto GB et al (2006) Geographical patterns of human diet derived from stable-isotope analysis of fingernails. Amer J Phys Anthropol 131:137–146

O'Connell TC, Hedges REM (1999) Investigations into the effect of diet on modern human hair isotopic values. Am J Phys Anthropol 108:409–425

Passey BH, Cerling TE (2002) Tooth enamel mineralization in ungulates: implications for recovering a primary isotopic time-series. Geochim Cosmochim Acta 66:3225–3234

Passey BH, Cerling TE, Schuster GT, Robinson TF, Roeder BL, Krueger SK (2005a) Inverse methods for estimating primary input signals from time-averaged isotope profiles. Geochim Cosmochim Acta 69:4101–4116

Passey BH et al (2005b) Carbon isotope fractionation between diet, breath CO_2, and bioapatite in different mammals. J Archaeol Sci 32:1459–1470

Passey BH, Cerling TE, Levin NE (2007) Temperature dependence of oxygen isotope acid fractionation for modern and fossil tooth enamels. Rapid Commun Mass Spectrom 21: 2853–2859

Podlesak DW, Torregrossa AM, Ehleringer JR, Dearing MD, Passey BH, Cerling TE (2008) Turnover of oxygen and hydrogen isotopes in the body water, CO_2, hair, and enamel of a small mammal. Geochim Cosmochim Acta 72:19–35

Podlesak DW, Bowen GJ, Cerling TE, Ehleringer JR (2009a) δ^2H and $\delta^{18}O$ of human body water: a GIS model to distinguish residents from nonresidents in the contiguous United States. Isotopes Env Health Stud (in review)

Podlesak DW et al. (2009b) Stable isotopes reveal distinct, metabolically-based pools in mammals (in review)

Pupin AM, Dennis MJ, Parker I, Kelly S, Bigwood T, Toledo MCF (1998) Use of isotopic analyses to determine the authenticity of Brazilian orange juice (*Citrus sinensis*). J Agric Food Chem 46:1369–1373

Pye K, Croft DJ (eds) (2004) Forensic geoscience: principles, techniques, and applications. The Geological Society, London

Richter SL, Johnson AH, Dranoff MM, Taylor KD (2008) Continental-scale patterns in modern wood cellulose δ18O: implications for interpreting paleo-wood cellulose δ18O. Geochim Cosmochim Acta 72:2735–2743

Roden JS, Lin GG, Ehleringer JR (2000) A mechanistic model for interpretation of hydrogen and oxygen isotope ratios in tree-ring cellulose. Geochim Cosmochim Acta 64:21–35

Roden JS, Bowling DR, McDowell NG, Bond BJ, Ehleringer JR (2005) Carbon and oxygen isotope ratios of tree ring cellulose along a precipitation transect in Oregon, United States. J Geophys Res Biogeosci 110, G02003. doi:1029/2005JG000033

Rossmann A, Reniero F, Moussa I, Schmidt HL, Versini G, Merle MH (1999) Stable oxygen isotope content of water of EU data-bank wines from Italy, France and Germany. Z Lebensm Unters Forsch A-Food Res Technol 208:400–407

Rundel PW, Ehleringer JR, Nagy KA (eds) (1988) Stable isotopes in ecological research. Springer-Verlag, New York

Saitoh MS, Uzuka M, Sakamoto M, Kobaro T (1967) Rate of hair growth. In: Montagna W, Dobson RL (eds) Hair growth, vol IX. Pergamon Press, Oxford, pp 183–201

Schoeller DE, Ravussin E, Schutz Y, Acheson KJ, Baertschi P, Jequier E (1986) Energy expenditure by doubly labeled water: validation in humans and proposed calculation. Am J Physiol 250:R823–R830

Schwarcz HP (2007) Tracing unidentified skeletons using stable isotopes. In: Forensic Magazine 4: June/July Vicon Publishing, Amherst, MA/New Hampshire

Sharp Z (2006) Principles of stable isotope geochemistry. Pearson Prentice Hall, Upper Saddle River, NJ

Sharp ZD, Atudorei V, Panarello HO, Fernandez J, Douthitt C (2003) Hydrogen isotope systematics of hair: archeological and forensic applications. J Archaeol Sci 30:1709–1716

Simpkins WA, Patel G, Harrison M, Goldberg D (2000) Stable carbon isotope ratio analysis of Australian orange juices. Food Chem 70:385–390

Smith GI, Friedman I, Veronda G, Johnson CA (2002) Stable isotope compositions of waters in the Great Basin, United States 3. Comparison of groundwaters with modern precipitation. J Geophys Res 107:4402. doi:4410.1029/2001JD000567

Spalding KL, Buchholz BA, Bergman LE, Druid H, Frisen J (2005) Age written in teeth by nuclear tests. Nature 437:333–334

Spangenberg JE, Vennemann TW (2008) The stable hydrogen and oxygen isotope variation of water stored in polyethylene terephthalate (PET) bottles. Rapid Commun Mass Spectrom 22:672–676

Sternberg LdSL, DeNiro MJ, Savidge RA (1986) Oxygen isotope exchange between metabolites and water during biochemical reactions leading to cellulose synthesis. Plant Physiol 82:423–427

Stevens RE, Lister AM, Hedges REM (2006) Predicting diet, trophic level and palaeoecology from bone stable isotope analysis: a comparative study of five red deer populations. Oecologia 149:12–21

Sultan M et al (2007) Natural discharge: a key to sustainable utilization of fossil groundwater. J Hydrol 335:25–36

Thiros SA (1995) Chemical composition of ground water, hydrological properties of basin-fill material, and ground water movement in Salt Lake Valley, UT. In: Utah Department of Natural Resources Technical Publication No 110-A

Thompson AH et al. (2009) Stable isotope analysis of modern human hair collected along an Asian geographic transect. Am J Phys Anthropol (in press)

Toske SG, Cooper SD, Morello DR, Hays PA, Casale JF, Casale E (2006) Neutral heroin impurities from tetrahydrobenzylisoquinoline alkaloids. J Forensic Sci 51:308–320

West JB, Bowen GJ, Cerling TE, Ehleringer JR (2006) Stable isotopes as one of nature's ecological recorders. Trends Ecol Evol 21:408–414

West JB, Ehleringer JR, Cerling TE (2007) Geography and vintage predicted by a novel GIS model of wine $\delta^{18}O$. J Agric Food Chem 55:7075–7083

Williams A (1997) Stable isotope tracers: natural and anthropogenic recharge, Orange County, California. J Hydrol 201:230–248

Yakir D, DeNiro MJ (1990) Oxygen and hydrogen isotope fractionation during cellulose metabolism in *Lemna gibba* L. Plant Physiol 93:325–332

Yapp CJ, Epstein S (1982) Climatic significance of the hydrogen isotope ratios in tree cellulose. Nature 297:636–639

Zuber A, Weise SM, Motyka J, Osenbruck K, Rozanski K (2004) Age and flow pattern of groundwater in a Jurassic limestone aquifer and related Tertiary sands derived from combined isotope, noble gas and chemical data. J Hydrol 286:87–112

Chapter 18
Stable Isotopes in Large Scale Hydrological Applications

John J. Gibson, Balázs M. Fekete, and Gabriel J. Bowen

18.1 Introduction

The seminal water budget studies of L'vovich et al. (1990), Baumgartner and Reichel (1975), and Korzoun et al. (1978) provided the first practical synthesis of global-scale variations in climatology of major water budget components. Although based on limited data, these studies presented fairly consistent first-approximations of the long-term continental water fluxes; estimates that are still being refined today, both spatially and temporally, using a variety of observational and modeling techniques (Browning and Gurney 1999; Oki et al. 1999; Vörösmarty et al. 1998; Fekete et al. 2002; Raschke et al. 2001). Early on, the establishment of global patterns and recognition of continental, regional (and local) variability in water budgets provided a unifying framework and context for widespread analysis of water cycling processes.

While it can be argued that a similar conceptual framework has been established for global isotope balance processes, the practical (quantitative) closure of the modern-day isotope mass balance for the continents has not yet been achieved, due mainly to a lack of long-term systematic measurements for the riverine fluxes to the oceans. As a result, a perspective of isotope variations in hydrological systems has emerged

J.J. Gibson (✉)
Alberta Research Council, University of Victoria, Vancouver Island Technology Park, 3 - 4476 Markham St, Victoria, BC, Canada, V8Z 7X8
e-mail: jjgibson@uvic.ca

B.M. Fekete
Global Water Center of the CUNY Environmental Crossroads Initiative, The City College of New York at the City University of New York, 160 Convent Avenue, New York, NY, 10031, USA
e-mail: bfekete@ccny.cuny.edu

G.J. Bowen
Department of Earth and Atmospheric Sciences, Purdue Climate Change Research Center, Purdue University, West Lafayette, IN, 47907, USA
e-mail: gabe@purdue.edu

J.B. West et al. (eds.), *Isoscapes: Understanding Movement, Pattern, and Process on Earth Through Isotope Mapping*, DOI 10.1007/978-90-481-3354-3_18,

from piecemeal studies, predominantly via small-scale and short-term measurement programs, from analysis of local variations of paleoclimate archives recording deep time variations of the Earth's water cycle, and from analysis of modern-day global-scale precipitation patterns. This perspective, until recently, has not included a sophisticated understanding of climatological-scale runoff patterns, despite the added value that closure of the isotope mass balance provides as an integrated, cumulative indicator of water cycling and related processes.

Hydrological studies primarily rely on the stable isotopes of oxygen and hydrogen (^{18}O, ^{2}H), which are incorporated within the water molecule ($H_2{}^{18}O$, $^{1}H^{2}H^{16}O$), and exhibit systematic variations as a result of isotope fractionations that accompany water-cycle phase changes and diffusion. The broad features of global isotope variations were reported shortly after the discovery of the heavy isotope water molecules in the 1930s, followed by more systematic descriptions of the global isotope climatology in the 1950s and 1960s (Craig 1961; Dansgaard 1964; Friedman et al. 1964; Craig and Gordon 1965; Gat and Gonfiantini 1981). Isotope fractionation produces a natural labeling effect within the global water cycle, which has been applied to study a wide range of hydrological and climatic processes at the local, regional, and global scales.

A relatively sophisticated understanding of global isotope variations in precipitation processes and related modeling capabilities has emerged in recent years (Jouzel and Merlivat 1984; Hoffmann et al. 1998, 2000; Ciais and Jouzel 1994; Rozanski et al. 1993; Cole et al. 1993, 1999), primarily as an outgrowth of concerted efforts at the national and international level to systematically monitor the isotope composition of precipitation (IAEA/WMO Global Network for Isotopes in Precipitation (Birks et al. 2002; Aggarwal et al. this volume). Considerable advances have also been made to apply precipitation isotope data to the study of regional atmospheric water balance (Gat 1980, 1996; Gat and Gonfiantini 1981; Gat et al. 1994; Merlivat and Jouzel 1979), and the use of more localized (point) datasets for the study of paleoclimatic trends (Jouzel et al 2000; von Grafenstein et al. 1999) and water budget and runoff studies at the micro- to meso-scale (Kendall and McDonnell 1998). This dataset has provided the basis for a growing body of work focused on interpolation, prediction, and analysis of the spatial distribution of precipitation isotopic composition at national to global scales (Birks et al. 2002; Bowen and Revenaugh 2003; Lykoudis and Argiriou 2007; Bowen this volume). The large-scale patterns in the precipitation isotopic distribution reflect the transport of vapor from the tropics to higher latitudes, while going through repeated cycles of precipitating and evaporating resulting in increasing depletion of the heavier isotope species. The precipitation is depleted in the heavy isotopes of H and O at high latitudes (exceeding −300‰ and −40‰ for $\delta^{2}H$ and $\delta^{18}O$, respectively), and resembles more closely the reference ocean water (Vienna Standard Mean Ocean Water, VSMOW) near the Equator. The difference between minimum and maximum monthly values indicates strong seasonal variations in isotopic composition, such that winter precipitation tends to be more depleted than summer precipitation, which is also more pronounced at high latitudes (Fig. 18.1; Bowen 2008).

The principal uncertainty in closure of the isotope mass balance for the continents, however, remains a lack of systematic measurements of some of the important budget components, such as the isotope composition of river discharge and atmospheric moisture (Gat 2000). Notwithstanding notable contributions from individual scientists and research groups, systematic sampling within efforts by national programs, such as the U.S. Geological Survey's National Stream Quality Accounting Network (Kendall and Coplen 2001), and more recent international initiatives, such as the International Atomic Energy Agency's coordinated research project on large river basins (Gibson et al. 2002), have sought to build capacity for a network for monitoring the isotope composition of river discharge. Isotopes of water (^{18}O and ^{2}H) have also been part of a suite of tracers measured in the six major rivers flowing to the Arctic Ocean within a U.S. National Science Foundation sponsored program called PARTNERS (Pan-Arctic River Transport of Nutrients, Organic Matter and Suspended Sediments) to constrain the riverine input amounts used to assess the freshwater balance of the Arctic Ocean (McClelland et al. 2008). Among the important contributions of such programs is their ability to build consensus on sampling and data analysis techniques for improving the closure of the isotope balance for large river basins.

This chapter describes the rationale and potential benefits of incorporating isotope tracer measurements in existing hydrological monitoring networks as a complimentary tool for understanding some of the underlying causes of hydrological and biogeochemical variability, and for tracking future impacts due to land use changes, deforestation, and climate change. Notably, closure of the isotope balance for stable isotopes of water permits a sharper focus on variations in contributions and interaction between various water sources such as: surface water and groundwater, their contributions to flow in major rivers, the role of these interactions as biogeochemical regulation mechanisms, and partitioning of vapor losses by evaporation and transpiration, the latter being the quintessential link between the water and carbon cycles via photosynthesis. These are among the key mechanisms not routinely described from field-based data collected within current observational networks, nor are they readily discernible from today's remote sensing satellite observations. As with the water budget studies, fundamental characterization of integrated isotope signals at the continental scale may be of paramount importance to understanding the global climate system.

18.2 Theoretical Background

The use of stable oxygen and hydrogen isotopes as tracers in hydrologic studies has expanded over the past half-century following initial characterization of variations in world precipitation (Craig 1961; Dansgaard 1964), development of theory describing isotopic fractionation during evaporation (Craig and Gordon 1965; Gibson et al. 2008b) and testing and validation of process studies under a range of

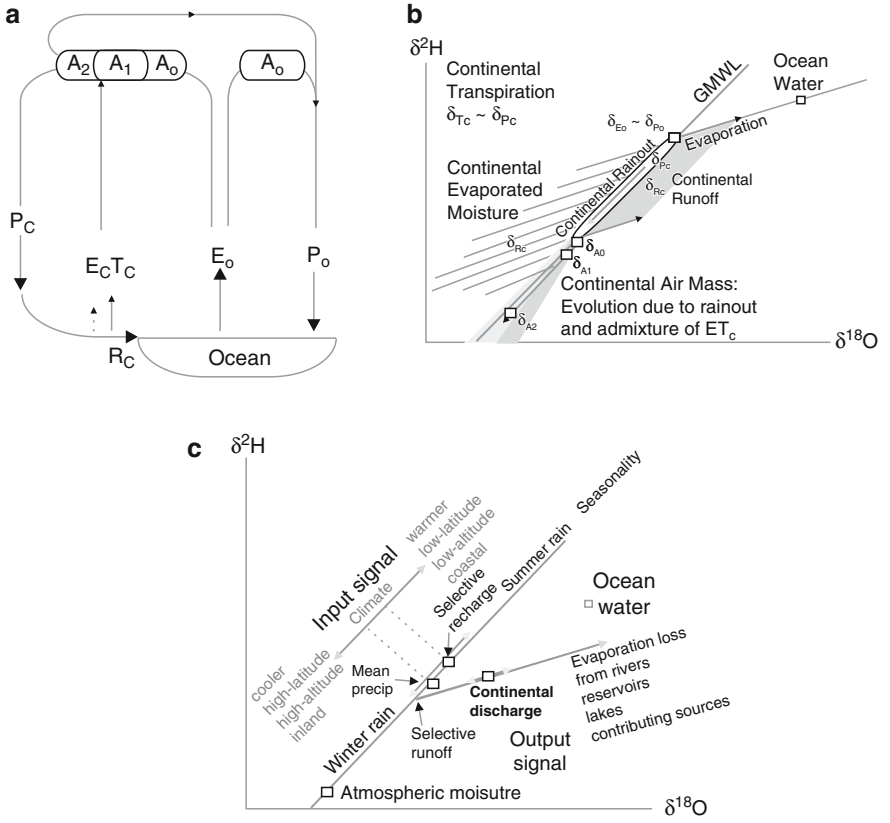

Fig. 18.1 Conceptual model of the ocean-continent water cycle. (**a**) Schematic of the global water cycle fluxes. (E_o and P_o are the oceanic evaporation and precipitation, E_c, T_c, R_c and P_c are the continental evaporation, transpiration, runoff and precipitation, A_o, is water vapour transport over the oceans, and A_1 to A_2 denotes water vapour composition over continental areas as modified by evaporation and transpiration feedback and moisture recycling. (**b**) Isotope signatures (δ values) for the ocean-continent system, where subscripts denote signature of components shown in (**a**). GMWL = global meteoric water line, ET = evapotranspiration. (**c**) Primary forcings on isotope composition of hydrological inputs and outputs from large river basins

field conditions (Gat and Gonfiantini 1981; Gat 1996; Clark and Fritz 1997; Kendall and McDonnell 1998; Gibson and Prowse 2000).

International programs, such as the recently completed IAEA coordinated research project on "Isotope tracing of hydrological processes in large river basins," have increased scientific awareness of the potential value of incorporating isotope tracers in large-scale water cycling studies to trace water origin and residence times, snowmelt processes, surface-groundwater exchange, evaporation–transpiration partitioning, precipitation variability, and climate/land use changes (Gibson et al.

2002; Vitvar et al. 2007). Although isotope techniques have been widely tested and are operationally applied at the small catchment-scale, theoretical development and testing of isotope-mass balance approaches at the continental scale are still in progress.

We begin by presenting a quantitative framework within which isotopic variation can be related to large scale land-surface hydrological processes (Fekete et al. 2006). Tracing stable isotopes in the hydrological cycle is analogous to the tracing of conservative constituents, except that fractionation mechanisms during phase changes must also be computed and tracked. While the mathematically correct computation of isotopic composition mixing using absolute concentrations is desirable for its accuracy, particularly over large ranges of isotopic composition, we adopt the common approximation of isotopic composition as δ values for notational simplicity. Herein we use $\delta = \frac{R}{R_{ref}} - 1$, where R, R_{ref} values refer to $^{2}H/^{1}H$ or $^{18}O/^{16}O$ in sample and V-SMOW standard, respectively).

For long time periods, the mass and isotope balances for the oceans and continents, respectively, are given by

$$P_O = E_O - P_C \tag{18.1}$$

$$\delta_{P_O} P_O = \delta_{E_O} E_O - \delta_{P_O} P_O \tag{18.2}$$

and

$$P_C = R_C + E_C + T_C \tag{18.3}$$

$$\delta_{P_C} P_C = \delta_{R_C} R_C + \delta_{E_C} E_C + \delta_{T_C} T_C \tag{18.4}$$

where P_O and E_O is oceanic precipitation and evaporation, and P_C, R_C, E_C and T_C are continental precipitation, runoff, evaporation, and transpiration (Fig. 18.1a). Changes in atmospheric moisture are expected due to admixture of evaporated and transpired moisture to air masses over the continents. Oceanic moisture in coastal areas is shown as A_O which becomes subsequently modified as it moves across the continent to inland areas (shown here as ranging from A_1 to A_2).

The approximate isotope compositions (δ) of components are shown in Fig. 18.1b. Long-term differences in precipitation arise from Rayleigh-type fractionation of atmospheric moisture and precipitation during rainout over the continents. Transpired moisture is expected to be isotopically similar to precipitation or groundwater recharge for a given location, whereas evaporated moisture will be heavy-isotope depleted (plotting on or above the MWL) and river discharge will tend to be heavy-isotope enriched (plotting on or below the MWL). Figure 18.1c shows specific hydro-climate forcings on ^{2}H and ^{18}O isotopic compositions, including those related to long-term precipitation input signals (temperature, latitude, altitude, distance from ocean source), seasonal signals (temperature, monsoon

cycles, moisture sources, glacial melt), bias in recharge due to selection of high-precipitation or thaw-season events, and seasonal oscillations in evaporative enrichment from the river or contributing sources (soil water, lakes, reservoirs, wetlands, etc.). In addition to the monitoring of volumetric fluxes, the characterization of long-term and seasonal isotope signals is expected to provide additional insight into hydro-climatic changes in each hydrologic regime. In some cases, such as rainfall-runoff climates, primary precipitation signals may be preserved in river discharge. In others, such as arid or seasonally arid climates, the selection processes and evaporative enrichment effects often result in more pronounced differences between river discharge and precipitation. A more quantitative description of this difference is presented below.

While systematic surveys of flux-weighted isotope signatures of discharge are not very common, the anticipated long-term separation can be postulated based on the isotope and mass balance shown in Fig. 18.1b and depicted in Eqs. 18.3 and 18.4. The isotope separation between flux-weighted continental runoff and continental precipitation $\left(\delta_{R_C} - \delta_{P_C}\right)$ is expected to depend on

$$\delta_{R_C} - \delta_{P_C} = \frac{E_c\left(\delta_{R_C} - \delta_{E_C}\right) + T_c\left(\delta_{R_C} - \delta_{T_C}\right)}{P_c} \tag{18.5}$$

which is obtained by rearranging Eq. 18.4 with substitution of $R_c = P_c - E_c - T_c$ from Eq. 18.3. If it is also assumed that continental transpiration is similar to continental precipitation, i.e. $\delta_{Tc} \approx \delta_{Pc}$ then this further simplifies to

$$\delta_{R_C} - \delta_{P_C} = \frac{E_c\left(\delta_{R_C} - \delta_{E_C}\right)}{P_c - T_c} \tag{18.6}$$

Equation 18.6 demonstrates that the long-term isotope separation between runoff and precipitation will approach zero only as $E_c \to 0$ or as $\delta_{R_C} \to \delta_{E_C}$. While very low (free-surface) evaporation may be characteristic of some humid areas dominated by vegetation, the latter condition where

$$\delta_{R_C} \approx \delta_{E_C} \tag{18.7}$$

is not expected to occur due to isotope effects associated with evaporation. This can be shown by substitution of the Craig and Gordon model (Craig and Gordon, 1965):

$$\delta_{E_C} \approx \frac{\alpha^* \delta_{R_C} - h\delta_{A_C} - \varepsilon}{1 - h + 10^{-3}\varepsilon_K} \tag{18.8}$$

into Eq. 18.7 assuming $\delta^* \approx 1$, which shows that $\delta_{R_C} \to \delta_{E_C}$ only as:

$$\delta_{R_C} \rightarrow \frac{h\delta_{A_C} + \varepsilon}{h - 10^{-3}\varepsilon_K} \tag{18.9}$$

which is the limiting isotope enrichment under prevailing atmospheric conditions. Note that in this case δ_{A_C} is the average isotope composition of continental atmospheric moisture over the continent as comprised of a mixture of δ_{A_0}, δ_{A_1} and δ_{A_2} δ_{A_0} being oceanic moisture, and δ_{A_1} and δ_{A_2} representing oceanic moisture altered by progressive rainout and potential feedback of of re-evaporated continental moisture). Limiting enrichment is only expected to occur under conditions where waters evaporate to dryness and is therefore unlikely for the case of sustained discharge. Variation in evaporative enrichment of heavy isotopes in continental discharge is therefore expected to depend mainly on the fraction of water loss by (free-surface) evaporation in the river basin, as well as on the atmospheric humidity, its isotope composition and the ambient temperature.

The isotope fractionation $\varepsilon = \varepsilon_{V/L} + \varepsilon_K$ is the sum of the equilibrium fractionation ($\varepsilon_{V/L}$) and the kinetic (diffusive transport) fractionation (ε_K). The equilibrium fractionation is given by Majoube (1971) as:

$$\varepsilon_{V/L} = e^{c_0 + \frac{c_1}{T} + \frac{c_2}{T^2}} - 1 \tag{18.10}$$

where c_0, c_1, c_2 are coefficients and T is the air temperature (in kelvin). The kinetic fractionation is:

$$\varepsilon_K = (1 - h_N)(1 - \frac{\rho_i}{\rho}) \tag{18.11}$$

where controlling factors include relative humidity (h_N), the atmospheric resistances to diffusion of water molecules containing the rare, heavy (ρ_1) and common, light (ρ) water molecules, where ρ_1 / ρ is close to 1.0125 for deuterium and 1.0142 for oxygen (Gat 1996).

This conceptual model provides an example at the global scale for development of quantitative approaches to examining river discharge signals. Specifically, it provides an initial basis for understanding and quantifying the hydrological significance of the long-term precipitation-runoff isotope separation, which is expected to vary with the ratio of $E_c / E_c T_c$. Such information is not available via conventional hydrometric monitoring. One key assumption of this derivation is that the isotopic composition of continental groundwater is similar to that of precipitation, although due to selective recharge and storage effects this may not be an appropriate representation for some large river basins. Other long-term storages such as glaciers need to be explicitly included in some areas. This, and similar models, need to be developed and tested to account for seasonal variations in the hydrological processes and specific influences of long-term storage reservoirs such as groundwater and glacier melt. A recent review by Gat and Airey (2006) provides additional discussion on scaling issues related to working with stable isotopes at the continental scale.

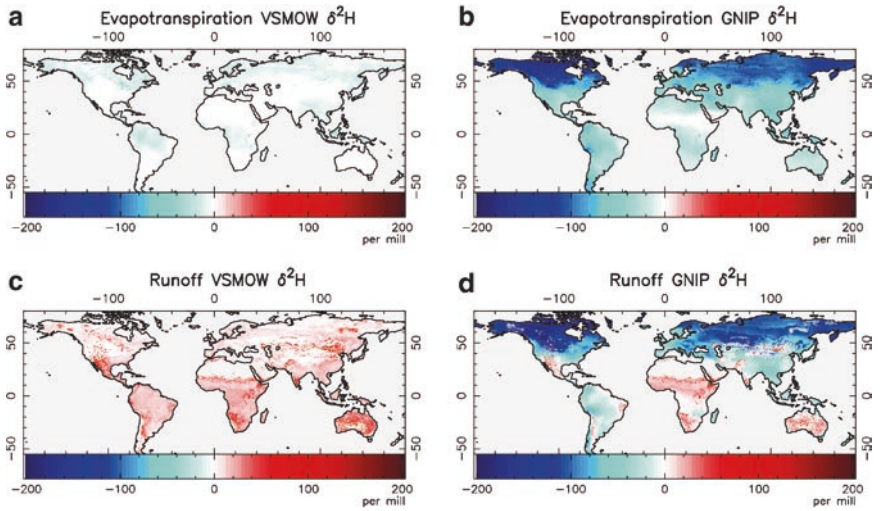

Fig. 18.2 Global isotope simulations using the iWBM distributed hydrology model. Shown are the isotopic composition of evapotranspiration using (**a**) constant V-SMOW precipitation, (**b**) GNIP precipitation climatology, runoff (**c**) constant V-SMOW precipitation and (**d**) GNIP precipitation climatology. The *left panels* illustrate modeled isotopic separation from precipitation, whereas the *right panels* show predicted isotopic compositions that might be measured in nature. These effectively constitute a spatial hypothesis awaiting verification when global observations become available (Reprinted from Fekete et al. 2006, Application of isotope tracers in continental scale hydrological modeling, Journal of Hydrology, vol. 330, p. 452, Copyright 2006, with permission from Elsevier). Fig. 18.2, see Appendix 1, Color Section

These isotopic processes were implemented in the continental scale hydrological model iWBM by Fekete et al. (2006). Figure 18.2 shows the simulated mean annual deuterium composition of the evapotranspiration and runoff under isotopically uniform (V-SMOW) and spatially and temporally varying precipitation forcings (Birks et al. 2002). The salient features of these simulation results include: (1) the dominant control of spatial variation in precipitation isotopic composition on that of the evapotranspiration and runoff, particularly at high latitudes, and (2) pronounced heavy isotope enrichment in runoff, which is a function of fractionation during evaporation and the runoff ratio (the ratio of runoff to precipitation).

18.3 Large Scale Isotopic Patterns

18.3.1 Sources and Generation of Runoff

A limited number of traditional, basin-scale isotope hydrology studies have explicitly considered the spatial variation in precipitation isotope ratios (e.g., McGuire et al. 2005). At these scales, the primary spatial signal of interest is variation in precipitation

isotopic composition with elevation, which must be considered in hydrograph separation studies that attempt to quantify the contribution of storm event water to runoff, in that the isotopic composition of storm water may vary significantly throughout high-relief catchments. At the scale of major catchments to continents, these spatial patterns are often significant and are useful means to identify water source areas. Figure 18.3 illustrates a hypothetical example: the runoff weighted mean annual isotopic composition is shown for a 30′ gridded stream network (Vörösmarty et al. 2000) in the Yenisei basin, Mongolia and Siberia. Isotopically heavier runoff originating from the mid-latitude headwaters is transported downriver through the main channel, and maintains a characteristically different isotopic composition from the surrounding lower-order streams that more closely reflect the isotopic composition of local precipitation.

River water and tap water datasets from the contiguous U.S.A. illustrate the potential for water isotopes to be used as an indicator of runoff sources (Dutton et al. 2005; Bowen et al. 2007b). Both studies show that meteoric waters across large, high-relief areas of the western U.S.A. tend to be ^{2}H- and ^{18}O-depleted relative to local precipitation due to the altitude effect on the isotopic composition of high-elevation precipitation contributing to runoff. Unambiguous identification and

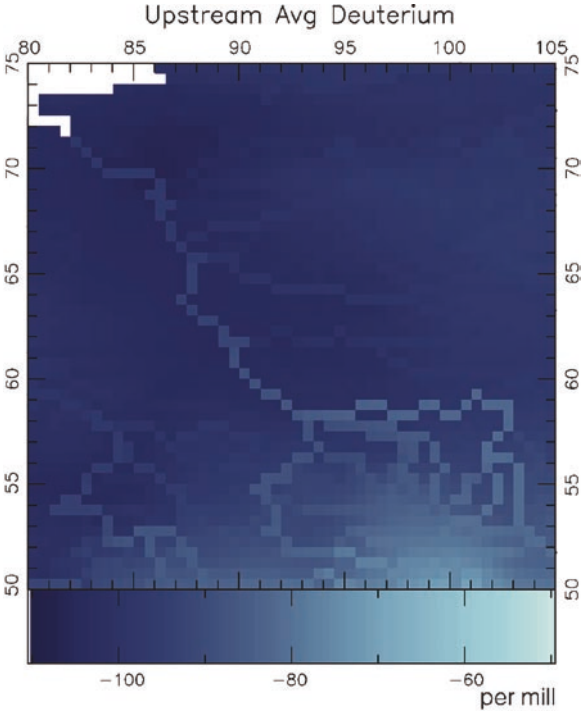

Fig. 18.3 Average, runoff weighted hydrogen isotopic composition of the precipitation in the Yenisei basin in Mongolia and Siberia, propagated down a river network derived from a 30′ digital elevation model. Fig. 18.3, see Appendix 1, Color Section

quantification of these effects is only possible for watersheds and continental areas when both $\delta^{18}O$ and $\delta^{2}H$ are applied together to identify isotope effects of evaporation.

An additional factor that may contribute to the observed pattern is the selective (e.g., seasonally-biased) generation of runoff. The influence of this effect on large-scale isotopic patterns can be observed in the Fekete et al. (2006) simulations, where contrary to the theory presented above the isotopic composition of evapotranspired water in some snow-dominated regions is predicted to be isotopically heavier than annual average precipitation whereas the excess water (that forms surface runoff and groundwater recharge) is lighter (Fig. 18.2). Winter precipitation is more depleted than summer precipitation due to the greater degree of rainout between relatively warm ocean vapor source regions and cool wintertime continents, supplemented by enhanced equilibrium fractionation at lower temperature (Eq. 18.10). This heavy-isotope depleted precipitation is more prone to form excess water, due to the lower evaporation rates in winter time, therefore the excess water weighted mean annual isotopic composition of the surface runoff and groundwater recharge forming water surplus carries more of the winter precipitation signal than the summer precipitation that tends to evaporate more. In addition to its significance for understanding seasonal water balance, this process of selective excess water generation also has implications for hydrograph separation in that the isotopic composition of groundwater will gravitate towards the mean precipitation value weighted by the temporally varying runoff ratio.

18.3.2 Evaporative Processes

Isotope ratios measured in surface waters have provided important information on evaporative processes and their impact on hydrological mass balance across a wide range of spatial scales. Among the unique and important potential contributions of isotopic data is their ability to partition evaporation (fractionating) and transpiration (non-fractionating) fluxes and their capacity to quantify evaporative loss in ungauged areas.

Gibson and Edwards (2002) applied spatially distributed sampling of lake water isotope ratios to quantify land surface evaporation across a large region (275,000 km^2) of northern Canada, illustrating systematic, spatial patterns in the ratios of evaporation to transpiration and evaporation to inflow. Within some parts of the study domain, as much as 60% of catchment-integrated precipitation was lost as evaporation, leading to substantial heavy-isotope enrichment in runoff. The larger-scale manifestation of this pattern is apparent in early data from the PARTNERs program, which show that river discharge in Arctic rivers deviates strongly from the Global Meteoric Water Line of Craig (1961), particularly for the North American rivers (Mackenzie and Yukon R.) draining catchments containing extensive lakes and wetlands. The comparative proximity to the GMWL of the four Eurasian rivers sampled (Ob', Yenisey, Lena and Kolyma, see Fig. 18.4) suggests more

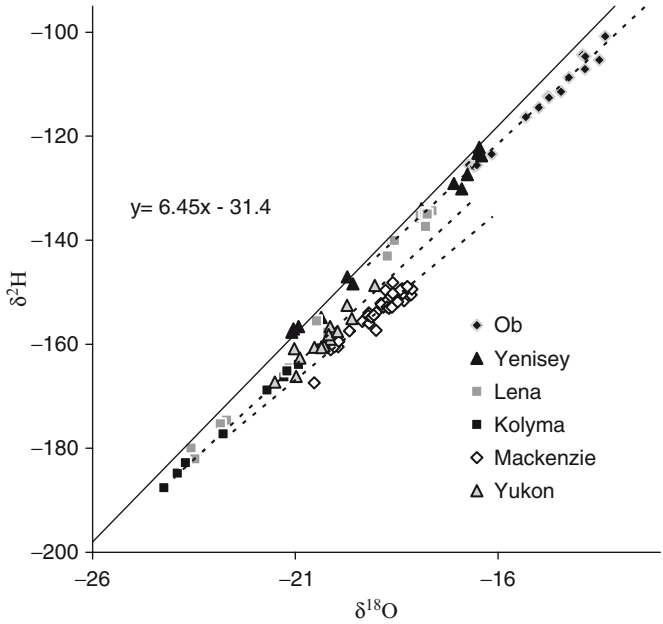

Fig. 18.4 δ^2H-$\delta^{18}O$ plot showing isotopic data for major Arctic flowing rivers collected during the PARTNERS study. *Solid line* is the Global Meteoric Water Line. *Dashed lines* represent best fit lines through individual river datasets. Slopes range from 6.5 to 8 reflecting mixing between evaporated and non-evaporated sources (Based on unpublished provisional data, http://ecosystems.mbl.edu/partners/)

limited wetland/lake sources, and potentially more atmospheric recycling of evapotranspired water crossing the Asian landmass relative to the North American rivers (Yukon and Mackenzie) where the distance to humid, saturated air masses at sea level is shorter. Drainage to the Arctic Ocean represents 10% of global runoff and therefore is a critical component of the global water budget, which may be better understood through continued isotopic monitoring (McClelland et al. 2008; Cooper et al. 2008).

In contrast to the Arctic flowing rivers, for which evaporative isotopic signals are strongly linked to wetland sources distributed widely across the watershed, some dryland rivers such as the Barwon-Darling River, Southeastern Australia display isotopic signals which are more consistent with evaporative enrichment of water from the river channel and floodplain itself (Fig. 18.5). Gibson et al. (2008a) described a technique for evaluating reach water balance using isotopic enrichment signals and applied it to the Barwon-Darling River dataset. Among the most interesting outcomes of this study is the development of a potential tool for characterizing the monthly dynamics of ungauged water losses and gains for individual river reaches based on a combination of physical and isotopic monitoring. Notably, ungauged inflows to upper, middle and lower reaches of the river, expressed as

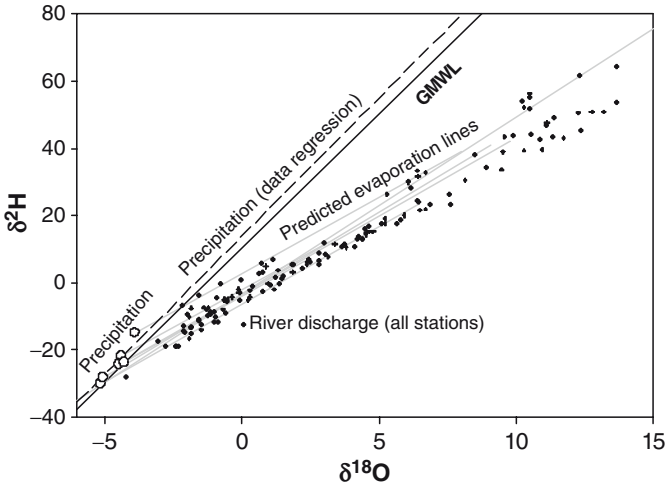

Fig. 18.5 δ^2H-δ^{18}O plots showing Barwon-Darling River discharge data at nine stations. Global Network for Isotopes in Precipitation (GNIP) annual data for Australian stations and a linear regression are shown in comparison to the Global Meteoric Water Line (GMWL). Predicted evaporation lines for GNIP input are simulated using an evaporation flux-weighting technique assuming an ideal precipitation-fed open-water reservoir as discussed in Gibson et al. (2008b). Agreement between data and modeled slopes close to 4 suggests dominance of evaporation by open-water rather than soil evaporation processes, the latter characterized by lower evaporation slopes

runoff ratios (Fig. 18.6), were found to be consistent and vary systematically in time within the expected range of between 0% and 10% of incident precipitation. Although requiring additional real-time isotopic data for operational use, the method demonstrated potential as a complimentary tool for detecting and quantifying water contributions and diversions, one that can be easily incorporated within existing water quality monitoring networks.

Strong deviations from the GMWL also characterize some surface and tap water samples from the U.S.A., although these effects are highly regionalized. The survey of Kendall and Coplen (2001) demonstrated both low deuterium excess values and temporal isotopic variation along evaporation lines for many rivers within the Rocky Mountain and western Great Plains regions. Given the diverse collection of rivers represented in the dataset, it is not clear the extent to which in-stream evaporation versus evaporation from natural lakes and reservoirs contributes to the observed patterns. Isotopic values of tap waters samples from the contiguous U.S.A., many of which were derived from surface water sources, reflect a similar pattern of variation in deuterium excess (Bowen et al. 2007b). Comparison of isotopic values (hydrogen and oxygen) and deuterium excess values with those of local precipitation suggest that some of the spatial structure in deuterium excess

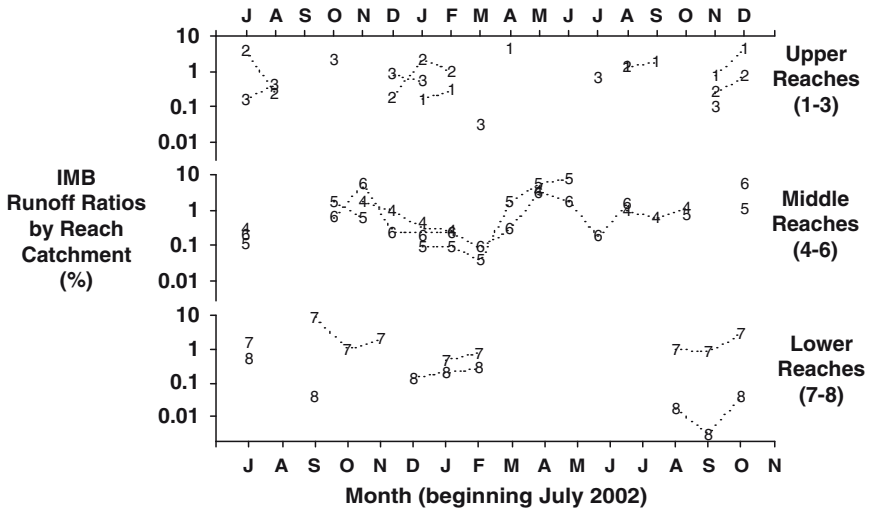

Fig. 18.6 Derived runoff ratios by month based on isotopic estimates of ungauged inflow over reach catchments along upper, middle and lower reaches of the Barwon-Darling River (Modified from Gibson et al. 2008b).

observed in U.S.A. tap and river waters is inherited directly from precipitation, but that particularly strong evaporative effects can be observed in the western Great Plains. The semiarid climate and relatively low relief of this region may contribute to relatively intense evaporation from surface water systems, reflected as strong evaporative enrichment of the heavy isotopes and deviation from the GMWL. Estimates of the fraction of catchment water lost as evaporation based on tap water data from reservoir-fed sites in central Texas and Oklahoma are as high as 45% (Bowen et al. 2007a). In addition to improved understanding of natural systems, quantification of the evaporative water flux in these human-managed systems provides information in support of planning and management decisions.

18.4 Concluding Remarks

As scientists contemplate the future of hydrology and potential for monitoring large river discharge from space (Alsdorf et al. 2003), there is still considerable insight to be gained in the present and future by improving ground-based observational networks to target many of the poorly understood interactions between the hydrospheric, atmospheric, and biospheric cycles. Isotopic and geochemical measurement programs, such as the U.S. Geological Survey's National Stream Quality Accounting Network (Hirsch 2001), and IAEAs coordinated rivers project (Gibson et al. 2002; Vitvar et al. 2007), serve as more than an exercise in validation for

land-atmosphere-ocean modeling, but rather as a resource of new information to understand the factors that contribute to water and biogeochemical variability. Some of the key processes controlling water, carbon, and nutrient cycling remain to be adequately understood for homogeneous landscapes, let alone for the complex melange of terrain types that typify regional and continental scales. Variations in contributions and interaction between various water sources such as surface water and groundwater, their contributions to flow in major rivers, the role of these interactions as biogeochemical regulation mechanisms, and partitioning of vapor losses by evaporation and transpiration, the latter being the quintessential link between the water and carbon cycles via photosynthesis, are examples of key mechanisms that are not routinely described from field-based data collected within current observational networks, nor are they readily discernible from today's remote sensing satellite observations. Fundamental characterization of integrated signal is nevertheless of paramount importance to understanding the global climate system.

Only 60% of runoff (Fekete et al. 2002; Bjerklie et al. 2003) from the continents is currently monitored, and some important regions such as the Pan-Artic drainages have experienced widespread declines in hydrological monitoring, which have seriously limited the potential for study of global change impacts (Shiklomanov et al. 2002; Vörösmarty et al. 2002). The importance of modeling and prediction in ungauged basins is an obvious target for future analysis. But optimizing the array of parameters measured in field-based surveys is as important now as ever to develop an understanding of the response of the key hydrological processes to climate changes at the continental scale. The IAEA proto-network of large rivers will monitor drainage from approximately 23% of the land surface. Improved coverage through widespread integration of water quality and water quantity networks will be required to close the stable isotope balance of the continents with accuracy similar to the early climatological water balance studies of the early 1970s.

The success of large scale applications of stable isotopes in surface hydrology also hinges on adequate monitoring of the isotopic composition of precipitation. Whereas surface and subsurface waters act as integrator in hydrological processes, and are therefore ideal targets for point measurement (since the measurement is less sensitive to the density and the exact location of the sampling locations), monitoring of the isotopic composition of precipitation with "in-situ" observations is more challenging. In order for isotope hydrology to fulfill its promise in large scale applications, continued improvement in techniques for measuring precipitation isotopic composition and generating time-explicit precipitation isoscapes are needed. Recent advancements such as the use of the Tropospheric Emission Sensor (TES) on NASA's Aura satellite to estimate the deuterium contents of the atmospheric vapor (Worden et al. 2007; Helliker and Noone this volume), and improvements in isotope-enabled GCM simulations, including nudged simulations that replicate time-explicit isotope climate, (Noone and Sturm this volume) may in combination with surface-based monitoring networks (Aggarwal et al. this volume) and statistical data assimilation tools (Bowen this volume) fill critical data gaps and advance large scale isotope hydrology from an experimental research topic to an operational tool in monitoring the water cycle.

References

Alsdorf DE, Lettenmaier DP, Vörösmarty CJ, the NASA Surface Water Working Group (2003) The need for global, satellite-based observations of terrestrial surface waters. AGU EOS Trans 84(269):275–276

Baumgartner A, Reichel E (1975) The world water balance. Elsevier, Amsterdam

Bennett KE, Gibson JJ, McEachern P (2008) Water yield estimates for critical loadings assessment: comparisons of gauging methods vs. an isotopic approach. Can J Fish Aquat Sci 65:83–99

Birks SJ, Gibson JJ, Gourcy L, Aggarwal PK, Edwards TWD (2002) Maps and animations offer new opportunities for studying the global water cycle. AGU EOS Trans 83(37):406

Bjerklie DM, Dingman SL, Vörösmarty CJ, Bolster CH, Congalton RG (2003) Evaluating the potential for measuring river discharge from space. J Hydrol 278:17–38

Bowen GJ (2008) Spatial analysis of the intra-annual variation of precipitation isotope ratios and its climatological corollaries. J Geophys Res 113:D05113

Bowen GJ, Cerling TE, Ehleringer JR (2007a) Stable isotopes and human water resources: signals of change. In: Dawson TE, Siegwolf R (eds) Stable isotopes as indicators of ecological change. Elsevier, Amsterdam, pp 285–300

Bowen GJ, Ehleringer JR, Chesson LA, Stange E, Cerling TE (2007b) Stable isotope ratios of tap water in the contiguous USA. Water Resour Res 43:W03419

Bowen GJ, Revenaugh J (2003) Interpolating the isotopic composition of modern meteoric precipitation. Water Resour Res 39:1299

Browning, KA, Gurney RJ (1999) Global energy and water cycles. Cambridge University Press, Cambridge, UK

Ciais P, Jouzel P (1994) Deuterium and oxygen-18 in precipitation: isotopic model, including mixed cloud processes. J Geophys Res 99(D8): 16793–16803

Clark ID, Fritz P (1997) Environmental isotopes in hydrogeology. CRC Press, Boca Raton, FL

Cole JE, Rind RS, Fairbanks RG (1993) Isotopic responses to interannual climate variability simulated by an atmospheric general circulation model. Guaternary Sci Rev 12:387–406

Cole JE, Rind RS, Jouzel J, Healy R (1999) Climate controls on the interannual variability of precipitation O-18: simulated influence of temperature, precipitation amount, and vapor source region. J Geophys Res 104:14223–14235

Coplen TB, Kendall C (2000) Stable hydrogen and oxygen isotope ratios for selected sites of the U.S. geological survey's NASQAN and benchmark surface-water networks.

Cooper LW, McClelland JW, Holmes RM, Raymond PA, Gibson JJ, Guay CK, Peterson BJ (2008) Flow-weighted values of runoff tracers (δ18O, and concentrations of DOC, Ba, alkalinity) from the six largest Arctic rivers. Geophys Res Lett 35. doi: 10.1029/2008GL035007.

Craig H (1961) Standard for reporting concentrations of deuterium and oxygen-18 in natural waters. Science 133:1833–1834

Craig H, Gordon LI (1965) Deuterium and oxygen-18 variation in the ocean and the marine atmosphere. Mar Geochem 3:277–374

Dansgaard W (1964) Stable isotopes in precipitation. Tellus 16:436–468

Dutton A, Wilkinson BH, Welker JM, Bowen GJ, Lohmann KC (2005) Spatial distribution and seasonal variation in $^{18}O/^{16}O$ of modern precipitation and river water across the conterminous United States. Hydrol Process 19:4121–4146

Fekete BM, Vörösmarty CJ, Grabs W (2002) High resolution fields of global runoff combining observed river discharge and simulated water balances. Global Biochem Cycles 16(3):15–16

Fekete BM, Gibson JJ, Aggarwal P, Vörösmarty CJ (2006) Application of isotope tracers in continental scale hydrological modeling. J Hydrol 330:444–456

Friedman I, Redfield AC, Schoen B, Harris J (1964) The variation of the deuterium content of natural waters in the hydrological cycle. Rev Geophys 2:177–224

Gat JR (1980) The isotopes of hydrogen and oxygen in precipitation. In: Fritz P, Fontes J-Ch (eds) Handbook of environmental isotope geochemistry, vol. 1, the terrestrial environment. A. Elsevier, Amsterdam, pp 21–48

Gat JR (1996) Oxygen and hydrogen isotopes in the hydrological cycle. Annu Rev Earth Planet Sci 24:225–262

Gat JR (2000) Atmospheric water balance – the isotopic perspective. Hydrol Process 14(8): 1367

Gat JR, Airey P (2006) Stable water isotopes in the atmosphere/biosphere/lithosphere interface: scaling-up from the local to continental scale, under humid and dry conditions. Global Planet Change 51:25–33

Gat JR, Gonfiantini R (1981) Stable isotope hydrology: deuterium and oxygen-18 in the water cycle. IAEA technical report series #210. Vienna, 337 p

Gat JR, Bowser CJ, Kendall C (1994) The contribution of evaporation from the Great Lakes to the continental atmosphere; estimate based on stable isotope data. Geophys Res Lett 21:556–560

Gibson JJ, Aggarwal P, Hogan J, Kendall C, Martinelli LA, Stichler W, Rank D, Goni I, Choudhry M, Gat J, Bhattacharya S, Sugimoto A, Fekete B, Pietroniro A, Maurer T, Panarello H, Stone D, Seyler P, Maurice-Bourgoin D, Herczeg A (2002) Isotope studies in large river basins: a new global research focus. AGU EOS Trans 83(52): 613, 616–617

Gibson JJ, Prowse TD (2000) ISOBALANCE special issue. Hydrol Process 14(8):1341–1536

Gibson JJ, Sadek MA, Stone DJM, Hughes C, Hankin S, Cendon DI, Hollins SE (2008a) Evaporative isotopic enrichment as a constraint on reach water balance along a dryland river. Isot Environ Health Stud 44:83–98

Gibson JJ, Birks SJ, Edwards TWD (2008b) Global prediction of δA and δ^2H-δ^{18}O evaporation slopes for lakes and soil water accounting for seasonality. Global Biochem Cycles 22: GB2031. doi: 10.1029/2007GB002997

Gibson JJ, Edwards TWD (2002) Regional water balance trends and evaporation-transpiration partitioning from a stable isotope survey of lakes in northern Canada. Global Biogeochem Cycles 16(2). 1026, doi:10.1029/2001GB001839

Henderson-Sellers A, McGuffie K, Noone D, Irannejad P (2005) Using stable water isotopes to evaluate Basin-Scale Simulations of Surface Water Budgets. J Hydrometeorol 5:805–822

Hirsch RM (2001) Water quality of large U.S. rivers: results from the U.S. Geological Survey's National Stream Quality Accounting Network. Hydrol Process 17(7):1085–1414

Hoffmann G, Jouzel J, Masson V (2000) Stable water isotopes in atmospheric general circulation models. Hydrol Process 14:1385–1406

Hoffmann G, Werner M, Heimann M (1998) The water isotope module of the ECHAM atmospheric general circulation model – a study on time scales from days to several years. J Geophys Res 103(D14):16871-16896

Jouzel J, Merlivat L (1984) Deuterium and oxygen 18 in precipitation: modelling of the isotopic effects during snow formation. J Geophys Res 89:11749–11757

Jouzel J, Hoffman G, Koster RD, Masson V (2000) Water isotopes in precipitation: data/model comparison for present-day and past climates. Quatern Sci Rev 19(1–5):363–379

Kendall C, McDonnell JJ (1998) Isotope tracers in catchment hydrology. Elsevier Science B. V., Amsterdam

Kendall C, Coplen TB (2001) Distribution of oxygen-18 and deuterium in river waters across the United States. Hydrol Process 15:1363–1393

Korzoun VI, Sokolov AA, Budyko MI, Voskrensensky KP, Kalinin GP, Konoplyantsev AA, Korotkevich ES, L'vovich MI (1978) Atlas of the World Water Balance. UNESCO, Paris, France

Koster RD, de Valpine DP, Jouzel J (1993) Continental water recycling and $H_2{}^{18}O$ concentrations. Geophys Res Lett 20(20):2215–2218

L'vovich MI, White GF, Belyaev AV, Kindler J, Koronkevic NI, Lee TR, Voropaev GV (1990) Use and transformation of terrestrial water systems.

Lykoudis SP, Argiriou AA (2007) Gridded data set of the stable isotopic composition of precipitation over the eastern and central Mediterranean. J Geophys Res 112:D18107

Majoube M (1971) Fractionnement en oxygéne-18 at en deuterium entre l'eau et la vapeur. J Chem Phys 68:1423–1436

McClelland JM, Holmes RM, Peterson BJ, Amon R, Brabets T, Cooper LW, Gibson JJ, Gordeev VV, Guay CK, Mulburn D, Raymond PA, Shiklomanov I, Staples R, Striegl R, Zhulidov AV, Zimov SA (2008) Development of a Pan-Arctic Database on for River Chemistry. AGU EOS Trans 89(24). doi:10.1029/2008EO240001

McGuire KJ et al (2005) The role of topography on catchment-scale water residence time. Water Resour Res 41:W05002

Merlivat L, Jouzel J (1979) Global climatic interpretation of the deuterium-oxygen-18 relationship for precipitation. J Geophys Res-Atmos 84(NC8) 5029–5033

Oki T, Nishimura T, Dirmeyer P (1999) Assessment of annual runoff from land surface models using total runoff integrating pathways (TRIP). J Meterorol Soc Jpn 77(1):235–255

Raschke E, Meywerk J, Warrach K, Andrea U, Bergstroem S, Beyrich F, Bosveld F, Bumke K, Fortelius C, Graham LP, Gryning SE, Halldin S, Hasse L, Heikinheimo M (2001) The Baltic Sea Experiment (BALTEX): a European contribution to the investigation of the energy and water cycle over a large drainage basin. Bull Am Meteorol Soc 82(11):2389–2414

Rozanski K, Araguas-Araguas L, Gonfiantini R (1993) Isotopic patterns in modern global precipitation. Isotope records, American Geophysical Union 1–36

Shiklomanov AI, Lammers RB, Vörösmarty CJ (2002) Widespread decline in hydrological monitoring threatens pan-Arctic research. AGU EOS Trans 83:16–17

Vitvar T, Aggarwal PK, Herczeg AL (2007) Global network is launched to monitor isotopes in rivers. AGU EOS Trans 88(33):325

von Grafenstein U, Erlenkeuser H, Brauer J, Jouzel J, Johnsen S (1999) A mid-European decadal isotope-climate record from the 15, 500 to 5000 years B.P. Science 284:1654–1657

Vörösmarty CJ, Askew A, Barry R, Birkett C, Döll P, Grabs W, Hall A, Jenne R, Kitaev L, Landwehr J, Keeler M, Leavesley G, Schaake J, Strzepek K, Sundarvel SS, Takeuchi K, Webster F (2002) Global water data: a newly endangered species. AGU EOS Trans 82(5):54,56,58

Vörösmarty CJ, Fekete BM, Meybeck M, Lammers RB (2000) Global system of rivers: its role in organizing continental land mass and defining land-to-ocean linkages. Global Biochem Cycles 14(2):599–621

Vörösmarty CJ, Federer CA, Schloss AL (1998) Potential evaporation functions compared on US watersheds: possible implications for global-scale water balance and terrestrial ecosystem modeling. J Hydrol 207:147–169

Worden J, Noone D, Bowman K, the Tropospheric Emission Spectrometer science team and data contributors (2007) Importance of rain evaporation and continental convection in the tropical water cycle. Nature 445: 528–532

Chapter 19
The Carbon Isotope Composition of Plants and Soils as Biomarkers of Pollution

Diane E. Pataki, James T. Randerson, Wenwen Wang, MaryKay Herzenach, and Nancy E. Grulke

19.1 Introduction

Urban environments have been compared to the global environment predicted at the end of the twenty-first century, in that urban areas are currently experiencing elevated atmospheric CO_2 concentrations, warmer temperatures, increased nitrogen loads, and elevated concentrations of pollutants (Grimm et al. 2000). It is extremely difficult to predict ecosystem responses to multiple atmospheric and climatic perturbations (Norby and Luo 2004), yet such predictions are critical, both for understanding global change as well as for quantifying critical ecosystem processes in urban areas in which large numbers of people live and work. Plants and soils in urban areas provide important ecosystem services for urban residents which may be adversely impacted by multiple pollutants in the urban environment. There is a great need for methodology to understand the effects of multiple pollutants on plants, soils, and ecosystem services, as well as for mapping ecosystem pollutant exposure and the distribution of pollutants at municipal, regional, and continental scales.

D.E. Pataki (✉) and J.T. Randerson
Department of Earth System Science, University of California, Irvine, CA
e-mail: jranders@uci.edu

D.E. Pataki and W. Wang
Department of Ecology and Evolutionary Biology, University of California, Irvine, CA
e-mail: dpataki@uci.edu
e-mail: wenwenw@uci.edu

M. Herzenach
Department of Ecology and Evolutionary Biology, University of Colorado, Boulder, CO
e-mail: marykay.herzenach@colorado.edu

N.E. Grulke
Pacific Southwest Research Station, USDA Forest Service, Riverside, CA
e-mail: ngrulke@fs.fed.us

J.B. West et al. (eds.), *Isoscapes: Understanding Movement, Pattern, and Process on Earth Through Isotope Mapping*, DOI 10.1007/978-90-481-3354-3_19,

Stable isotopes in organic matter are affected by exposure to many environmental pollutants and disturbances. Plants that utilize pollution-derived nitrogen (N) have been shown to have distinct nitrogen isotope ratios ($\delta^{15}N$) from plants using natural N sources (Ammann et al. 1999; Saurer et al. 2004; Stewart et al. 2002). Plant exposure to elevated CO_2 and oxidant pollutants such as ozone and sulfur dioxide have been shown to affect stable carbon isotope ratios ($\delta^{13}C$) (Boeckx et al. 2006; Dongarrà and Varrica 2002; Grams et al. 2007; Jedrysek et al. 2003; Lichtfouse et al. 2003; Norra et al. 2005; Novak et al. 2007; Saurer et al. 2003; Savard et al. 2002). However, both the magnitude and direction of reported isotope effects (both enrichments and depletions) have been reported in different experiments and regions, such that it can be difficult to extract general trends.

A somewhat newer application is the use of radiocarbon (^{14}C) to quantify uptake of fossil fuel-derived CO_2 by plants and to track plumes of fossil fuel CO_2 in surface air. Here we review the basis for the use of radiocarbon as a pollution tracer, recent studies that quantified spatial and temporal distributions of radiocarbon in plant "biomarkers," and the relationships between radiocarbon and other isotope tracers in polluted environments.

19.2 Radiocarbon Methodology and Notation

Radiocarbon is most widely known as a method of dating due to its half life of 5700 ± 30 years. Another common application utilizes anthropogenic levels of radiocarbon that were introduced into the atmosphere by aboveground atomic weapons testing in the 1950s and 1960s. Detonations of hydrogen bombs in the late 1950s and early 1960s introduced a "spike" in atmospheric $^{14}CO_2$ that abruptly declined following the 1963 Test Ban Treaty, primarily due to dilution by gross ocean-atmosphere and biosphere-atmosphere carbon exchange (Levin and Hesshaimer 2000; Randerson et al. 2002). Because organic material created in the last several decades contains detectable, elevated levels of ^{14}C relative to the pre-atomic testing period, the ^{14}C "bomb spike" has become a very useful tracer of the age of organic matter in ecosystems and the turnover time of carbon in soils (Trumbore, 1996, 2000; Wang and Hsieh 2002).

In urban areas, atmospheric CO_2 is elevated in concentration due to combustion of fossil fuel (Idso et al. 1998, 2001; Koerner and Klopatek 2002; Pataki et al. 2003a, 2005a, b, 2007). Because fossil fuels are much older than the half life of ^{14}C, the application of radiocarbon methods for mapping fossil fuel exposure is somewhat different than its application as a tracer of carbon age and turnover time. Fossil fuels are old enough to contain virtually no ^{14}C, as all of the ^{14}C present in the original organic matter has decayed to ^{14}N. This creates a very distinct tracer of fossil-fuel derived CO_2. To fully describe this tracer, we must review the notation of radiocarbon isotope ratios, which differs from the notation for stable isotopes.

The radiocarbon fraction modern (F) compares the $^{14}C/^{12}C$ ratio of the sample to $^{14}C/^{12}C$ of the standard NIST Oxalic Acid I:

$$F = \frac{\frac{^{14}C}{^{12}C_{sample[-25]}}}{0.95\frac{^{14}C}{^{12}C_{oxalic[-19]}}} \tag{19.1}$$

The $^{14}C/^{12}C$ ratio of the oxalic acid standard is multiplied by 0.95 to correct for radioactive decay between the pre-industrial atmosphere of 1895 and 1950, which is considered "modern" by definition (Stuiver and Polach 1977; Trumbore 1996). The notation [−25] and [−19] refer to corrections for mass dependent fractionation. Because radiocarbon is principally used for dating and for geochemical applications in which mass dependent fractionation is not the process of interest, $^{14}C/^{12}C$ ratios are corrected for mass dependent fractionation based on stable carbon isotope ratios, with the assumption that mass dependent fractionation of ^{14}C in relation to ^{12}C is twice as large as fractionation of ^{13}C relative to ^{12}C. The Oxalic Acid standard has a stable carbon isotope ratio of −19‰ in conventional δ notation relative to V-PDB, while all other samples are corrected to an average, C_3 $\delta^{13}C$ of −25‰ by convention:

$$\frac{^{14}C}{^{12}C_{sample[-25]}} = \frac{^{14}C}{^{12}C_{sample[\delta]}}\left[1 - \frac{2(25+\delta)}{1000}\right] \tag{19.2}$$

where δ is the measured $\delta^{13}C$ of the sample relative to V-PDB. Based on measurements of the specific activity of the oxalic acid standard, its $^{14}C/^{12}C$ is 1.231×10^{-12} (1950 value), or 1.245×10^{-12} after correction to a $\delta^{13}C$ of −19‰ (Karlén et al. 1964; Roberts and Southon 2007). Direct determination of $^{14}C/^{12}C$ of the standard by accelerator mass spectrometry has yielded slightly different values and the discrepancy is still under investigation (Roberts and Southon 2007).

Mass fractionation-corrected F can be used to calculate the radiocarbon isotope ratio ($\Delta^{14}C$):

$$\Delta^{14}C = [F * e^{\lambda(y-1950)} - 1] * 1000 \tag{19.3}$$

where λ is 1/8267 based on the ^{14}C half life and y is the measurement year. This expression corrects for the decay of the oxalic acid standard since 1950 (Stuiver and Polach 1977).

Using this notation, fossil fuels containing no radiocarbon have a $\Delta^{14}C$ of −1,000‰. In contrast, CO_2 in the modern atmosphere has a $\Delta^{14}C$ of ~50‰ as of 2007 (Levin et al. 2008), with distinct latitudinal gradients that include a maximum in the tropics and minima in mid-latitudes of the northern hemisphere and over the Southern Ocean (Krakauer et al. 2006). Even with contemporary latitudinal gradients, the difference in $\Delta^{14}C$ between remote atmospheric sites and fossil emissions provides a very large range of end members for tracing the dispersal of CO_2 from urban sources. In contrast, the end members for CO_2 source apportionment using stable carbon isotopes are approximately −24 to 60–‰ for fossil fuel, depending on the fuel type, versus ~−8‰ for CO_2 in the background atmosphere (Andres et al. 2000; Pataki et al. 2003a, 2005a; Tans 1981).

19.3 Isotope Ratios of Vegetation in Polluted Air

Several studies have noted isotopic depletion in organic matter near fossil fuel combustion sources using $\delta^{13}C$. Lichtfouse et al. (2003) reported depleted $\delta^{13}C$ in grasses growing near highways in Paris in comparison to grasses growing in rural areas. They also noted a trend toward greater depletion with decreasing distance to the highway in samples collected from 0–50 m from the road. Dongarrà and Varrica (2002) reported a depletion of 3.6‰ in tree rings sampled in Palermo, Italy representing the period 1880–1998, which they attributed to CO_2 concentrations elevated above the global background in the urban area. Boeckx et al. (2006) showed depletion of $\delta^{13}C$ of urban soils in Belgium, although a wide range of values were reported across soil and land use types.

In addition to the effects of uptake of isotopically depleted, fossil-fuel derived CO_2, $\delta^{13}C$ of organic matter is also strongly influenced by physiological processes in C_3 plants, particularly the ratio of intercellular to ambient CO_2 concentrations, which is determined by the relationship between stomatal conductance and photosynthesis (Farquhar et al. 1989). Therefore, it can be difficult to distinguish uptake of isotopically depleted CO_2 in polluted air from plant physiological responses to pollution and other related environmental factors. Jędrysek et al. (2003) and Šantrůčková et al. (2007) reported enrichment rather than depletion in $\delta^{13}C$ of tree rings in trees exposed to urban and industrial pollution, which they attributed to the effects of acid deposition and sulfur emissions on plant gas exchange. This is consistent with Savard et al. (2002), who reported an enrichment of 3.5‰ in tree rings following the construction of a copper smelter which emitted SO_2 in a boreal forest in Canada. One potential cause of pollution-derived isotopic enrichment is an increase in the importance of PEP carboxlyase, which has a much smaller fractionation factor than Rubsico, and has been found to increase in activity under elevated ozone concentrations (Saurer et al. 1995). Norra et al. (2005) showed enrichment of $\delta^{13}C$ of soils downwind versus upwind of pollution sources in Germany, which they related to the physiological effects of pollution on local vegetation. Many other environmental factors such as climate variability, soil moisture, and nutrient availability may also influence $\delta^{13}C$, such that stable carbon isotopes of C_3 plants alone cannot provide a definitive tracer of atmospheric pollution.

The stable carbon isotope ratio of C_4 plants is less affected by physiology than C_3 plants; in regions with C_4 vegetation these species can be used to trace the isotope ratio and in turn the concentrations of anthropogenic CO_2. Marino and McElroy (1991) showed that $\delta^{13}C$ of cellulose nitrate in *Zea mays* was a reliable indicator of $\delta^{13}C$ of the atmosphere in samples dating back to 1948. This method has subsequently been used to estimate the contribution of fumigation CO_2 to the canopies of elevated CO_2 experiments (Pataki et al. 2003b) such as a Swiss experiment in a mature forest (Pepin and Körner 2002). In addition, $\delta^{13}C$ of C_4 plants was used to identify and map areas of high anthropogenic CO_2 concentrations in the city of Cotonou, Benin (Kèlomé et al. 2006).

Radiocarbon can also be used to detect the amount of anthropogenic carbon in plants, which should be directly analogous to the isotopic composition of the

atmosphere during periods of photosynthesis. Because mass-dependent, photosynthetic fractionation is accounted for in $\Delta^{14}C$, variations in plant $\Delta^{14}C$ directly correspond to the radiocarbon content of atmospheric CO_2 at the time of fixation, and therefore can be more straightforward to interpret than measurements of plant $\delta^{13}C$ in polluted areas. In addition, $\Delta^{14}C$ is very sensitive to small variations in CO_2 caused by fossil fuel emissions, given the large isotopic difference between CO_2 derived from fossil-fuel combustion and CO_2 in the modern atmosphere. This difference is so great that an increase in mixing ratio of fossil fuel-derived CO_2 of only 1 ppm at contemporary atmospheric levels (−8‰, 380 ppm) results in a depletion of $\Delta^{14}C$ by 2.8‰. Hence, Alessio et al. (2002) detected a significant depletion of oak leaves, i.e. an elevated level of CO_2 exposure, within 300 m of a major roadway in Rome using radiocarbon, despite the fact that $\delta^{13}C$ changed by less than 1‰ on average and showed a high degree of variability.

As another illustration, Fig. 19.1 shows both leaf stable carbon and radiocarbon isotope ratios measured across a well-studied pollution gradient in the San Bernardino Mountains of southern California. Arbaugh et al. (2003) described the San Bernardino Mountains Air Pollution Gradient network, which has been measured for ozone concentrations, nitrogen deposition, and their effects on mixed conifer ecosystems since the 1960s. The western portion of this gradient is adjacent to the Los Angeles Basin and experiences high concentrations of photochemical oxidant pollution as well as elevated nitrogen inputs which decline in the eastern portion of the gradient (Arbaugh et al. 2003; Fenn and Bytnerowicz 1997; Lee et al. 2003). Based on diurnal leaf gas exchange measurements, in 1995 early morning CO_2 concentrations averaged 500–600 ppm at polluted sites, compared to mid morning to early afternoon concentrations of 325–350 ppm (N.E. Grulke, unpublished data).

We sampled needles of four conifer species at three sites across the pollution gradient in the winter and spring of 2005. Current year shoots of *Pinus ponderosa*, *Abies concolor*, *Calocedrus decurrens*, and *Pinus lambertiana* were sampled from the mid-canopy of mature trees at highly polluted Camp Paivika (34°14.021″ N, 117°19.338″ W, 1,800 m.a.s.l.), moderately polluted Strawberry Peak (34°14.058″ N, 117°13.955″ W, 2,240 m.a.s.l.) and relatively unpolluted Miller Canyon (34°16.116 N, 117°17.060″ W, 1,178 m.a.s.l.). Needles were dried at 70° for at least 48 h and ground to a fine powder. Nitrogen isotope ratio ($\delta^{15}N$) and $\delta^{13}C$ were measured with an elemental analyzer coupled to an Isotope Ratio Mass Spectrometer (Delta Plus IRMS, Thermofinnigan, San Jose, CA. To measure $\Delta^{14}C$, ground samples were converted to graphite according to Santos et al. (2004) and analyzed by Accelerator Mass Spectrometry (AMS) at the W.M. Keck Carbon Cycle AMS Facility at the University of California, Irvine. This facility has been described in detail by Southon et al. (2004).

While there were species differences in $\delta^{13}C$ of leaves measured across the San Bernardino Gradient, there were no significant site differences (Fig. 19.1, ANOVA, $p > 0.05$). This is in contrast to Grulke and Balduman (1999) who found significant differences in $\delta^{13}C$ of leaf cellulose between the more polluted sites Strawberry Peak and Camp Paivika and an atmospherically cleaner site at Lassen National Forest at the eastern end of the San Bernardino Mountains. In contrast, there were

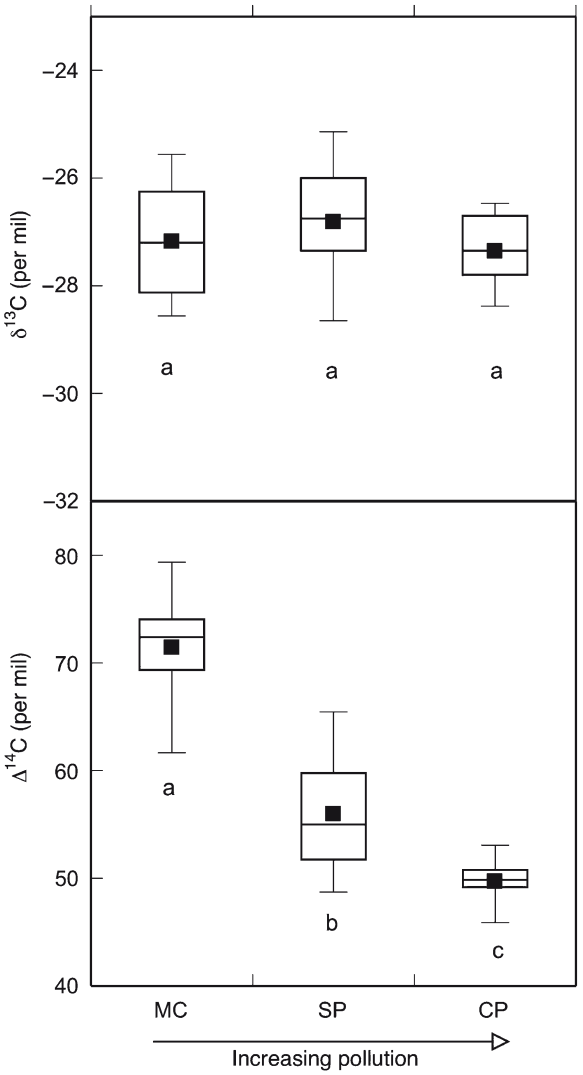

Fig. 19.1 Box plots of leaf stable carbon isotope ratio ($\delta^{13}C$) and radiocarbon isotope ratio ($\Delta^{14}C$) in conifer trees sampled across a known ozone and nitrogen deposition gradient in the San Bernardino Mountains in California, USA. MC refers to Miller Canyon, SP is Strawberry Peak, and CP is Camp Paivika. The *square* shows the mean value, the *lower line* of the box shows the bottom quartile of the data, the *middle line* shows the median, the *upper line* shows the top quartile, and the *bars* show the 10th and 90th percentile. *Letters* show significant differences among sites with an LSD post-doc test of an ANOVA, $p < 0.05$

no significant species differences in $\Delta^{14}C$ (ANOVA, $p > 0.05$) in the current study. However, there was a significant decline in leaf $\Delta^{14}C$ from the control site at Miller Canyon to the most polluted site at Camp Paivika (Fig. 19.1, ANOVA, $p < 0.05$).

Hence, atmospheric CO_2 concentrations appear to vary across the gradient along with ozone and nitrogen concentrations. To quantify this effect, we can calculate the proportion of fossil fuel-derived CO_2 in plants (f_F), which should correspond to the average, photosynthate-weighted proportion of fossil fuel versus background CO_2 in the atmosphere:

$$f_F = \frac{(\Delta^1 4C_P - \Delta^1 4C_B)}{(\Delta^1 4C_F - \Delta^1 4C_B)} \tag{19.4}$$

where $\Delta^{14}C_P$ is the radiocarbon content of the leaf expressed in Δ notation, $\Delta^{14}C_B$ is the radiocarbon content of the background atmosphere, and $\Delta^{14}C_F$ is the radiocarbon content of fossil fuel-derived CO_2, which was specified as −998‰. According to measurements at Pt. Barrow, AK by X. Xu et al. (unpublished data), $\Delta^{14}C_B$ was 65.1 ± 2.4‰ in 2004, where the error refers to the standard deviation of bi-monthly measurements. The concentration of atmospheric CO_2 at Pt. Barrow during this period was 378 ppm (Conway et al. 2007). The station at Pt. Barrow is located 8 km from Barrow, AK and has a prevailing east-northeast wind with a largely marine influence (http://www.esrl.noaa.gov/gmd/obop/brw/index.html). Hence, air samples from this station are often used as indicators of the composition of unpolluted air (e.g. Keeling et al. 2005). Assuming that background and fossil fuel combustion were the only major sources of CO_2 at the San Bernardino sites, leaves at Miller Canyon contained no anthropogenic CO_2, whereas leaves at Camp Paivika contained 1.2% of locally-added fossil fuel CO_2, equivalent to a photosynthate-weighted average CO_2 mixing ratio of 383 ppm. This is similar to direct measurements of atmospheric CO_2 concentrations at this site (N.E. Grulke, unpublished data).

19.4 The Spatial Distribution of $\Delta^{14}C$ Plant Biomarkers

The distribution of leaf $\Delta^{14}C$ at Miller Canyon shows some values that were higher than the estimated background value for atmospheric CO_2 of 65.1‰ (Fig. 19.1). While this may be due to measurement errors and variability in $\Delta^{14}C$ of the background atmosphere and local sources, it is also very possible that the organic matter present in current year leaf tissue contained carbon fixed in a previous year when the atmosphere contained more ^{14}C, as $\Delta^{14}C$ of atmospheric CO_2 has been declining since the 1960s. Retention of older carbon may be particularly prevalent at more arid sites where leaves are long-lived (Grulke and Balduman 1999). This illustrates a potential complication of using perennial plants as indicators of current atmospheric pollution. For this reason, several studies that have used plants to map spatial variations in $\Delta^{14}C$ and locally-added fossil fuel CO_2 have used annual plants, whose period of carbon fixation is more constrained. Hsueh et al. (2007) collected samples of corn plants (*Zea mays*) from throughout the United States in the summer of 2004 and measured their radiocarbon composition. They sent packets to residents at varying locations and instructed them to collect corn samples with the following

protocol: samples were collected more than 1.6 km away from highways, more than 45 m from paved roads, and more than 20 m away from buildings that may emit CO_2 from combustion furnaces. Potential point sources of pollution such as power plants were avoided to utilize the radiocarbon content of the samples as integrators of transport of fossil fuel CO_2 over large areas in the well-mixed boundary layer.

Figure 19.2 shows the data from this study plotted as a $\Delta^{14}C$ anomaly, or the difference between the background $\Delta^{14}C$ of CO_2 estimated from Pt. Barrow, AK air samples in 2004 and measured values in *Zea mays*, rather than the absolute values. This will allow comparison with data collected in other years when the background atmosphere has a different $\Delta^{14}C$ value. The results show two regions of depleted plant $\Delta^{14}C$ that correspond to elevated atmospheric CO_2 concentrations. In the northeastern U.S., plant $\Delta^{14}C$ was depleted by as much 13‰ relative to atmospheric CO_2 at Pt. Barrow, while in California, plant $\Delta^{14}C$ was depleted by as much as 28‰. To confirm that this depletion was due primarily to the addition of fossil fuel-derived CO_2 to the atmosphere, Hsueh et al. (2007) used the Model of Atmospheric Transport and Chemistry (MATCH) to independently estimate atmospheric CO_2 derived from fossil fuel releases and the Carnegie-Ames-Stanford Approach (CASA) biogeochemical model to simulate the influence of terrestrial biosphere and marine CO_2 fluxes on atmospheric CO_2 and $\Delta^{14}C$. The modeling results

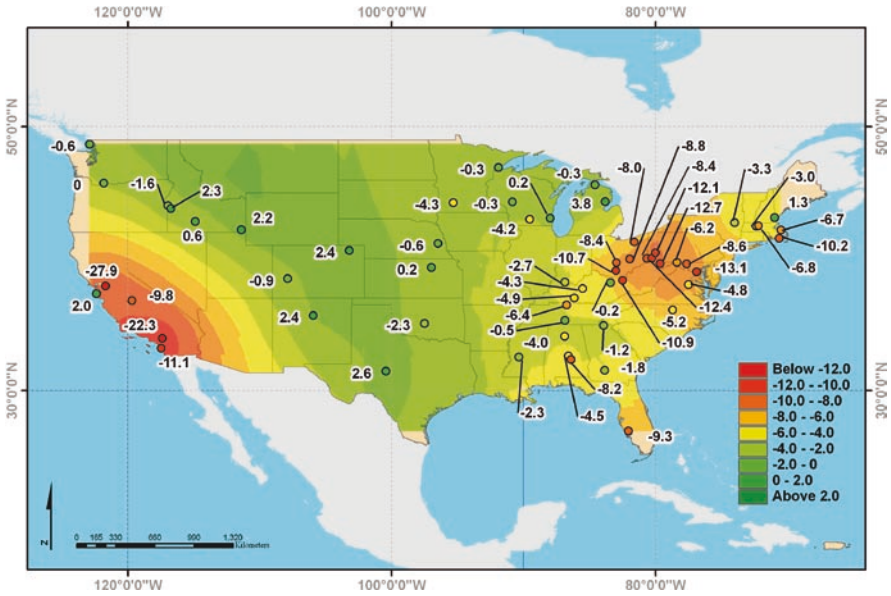

Fig. 19.2 The difference between $\Delta^{14}C$ of CO_2 in clear air measured in Pt. Barrow, Alaska, and in leaves of corn plants sampled throughout the United States in 2004. Units are per mil (‰) relative to the Oxalic Acid standard (Modified from Hsueh et al. 2007). Fig. 19.2, see Appendix 1, Color Section

confirmed that fossil fuel emissions were the dominant influence on $\Delta^{14}C$ variability across North America, although biogenic respiration of ^{14}C-enriched CO_2 partially offset the depletion in atmospheric $\Delta^{14}C$, particularly in the eastern U.S. Overall, the model predicted a mean difference of 8.5‰ between $\Delta^{14}C$ of background CO_2 and actual CO_2 over the northeast, which was similar to the 7.5 ± 2.9‰ difference observed in the *Zea mays* samples.

As a follow-up to this study, Riley et al. (2008) measured $\Delta^{14}C$ of annual grasses throughout California in 2005. Unlike *Zea mays*, which grows during the summer months in North America, the grasses sampled in the California study were winter annuals with a growing season around February, March, and April. The sampling protocol in this study focused on samples collected more than 3.2 km from highways, more than 45 m from roads, and more than 20 m from buildings in rural areas. Because this study focused more intensively on urban areas than in the national study, samples were collected on residential streets, neighborhood parks, or abandoned parking lots when it was not possible to collect urban samples in the absence of buildings and roads. At this higher spatial resolution, the anomalies from background $\Delta^{14}C$ of CO_2 were larger than in the national study, and showed a depletion of up to 62‰ in the Los Angeles Basin and 31‰ in the San Francisco Bay Area (Fig. 19.3). This study also compared observations and modeled estimates of atmospheric $\Delta^{14}C$ of CO_2 by modeling transport of fossil fuel CO_2 with the MM5 meteorological model integrated with the LSM1 land-surface model. The $\Delta^{14}C$ of heterotrophic respiration was estimated with functions derived from the CASA model. The modeled and measured $\Delta^{14}C$ of grasses agreed within 1‰ in the North Coast and Los Angeles regions, and within 5‰ in the Central Valley and San Francisco regions.

Given the agreement between measured and modeled values, Riley et al. (2008) further applied this approach to model the transport of fossil fuel CO_2 across and out of California to trace its fate and dispersion into the larger atmospheric volume. This analysis indicated that 21%, 39%, and 35% of fossil fuel CO_2 left the region to the north, east, and south of California, respectively. This is a particularly useful application of biomarkers and atmospheric models as atmospheric monitoring of CO_2 emissions has become increasingly important both in carbon cycle science and in the implementation of policy to regulate greenhouse gas emissions. In addition, because other pollutants associated with combustion are likely transported along with fossil fuel-derived CO_2, these results have important ramifications for tracking dispersion of other pollutants of interest for human health (e.g. carbon monoxide, ozone, NO_x, and aerosols) across state and national borders.

A detailed evaluation of the data from the Los Angeles Basin using data reported in Riley et al. (2008) and also Wang and Pataki (2009) provides information at an even finer spatial resolution. In this analysis, the $\Delta^{14}C$ anomaly (deviation from background) of winter annual plants collected in the 2004 and 2005 growing seasons were mapped in region in and surrounding the Los Angeles metropolitan area. This dataset showed the greatest influence of fossil fuel-derived CO_2 relative to the $\Delta^{14}C$ of atmospheric CO_2 at Pt. Barrow, with depletion of more than 100‰ in a sample collected near downtown Los Angeles (Fig. 19.4).

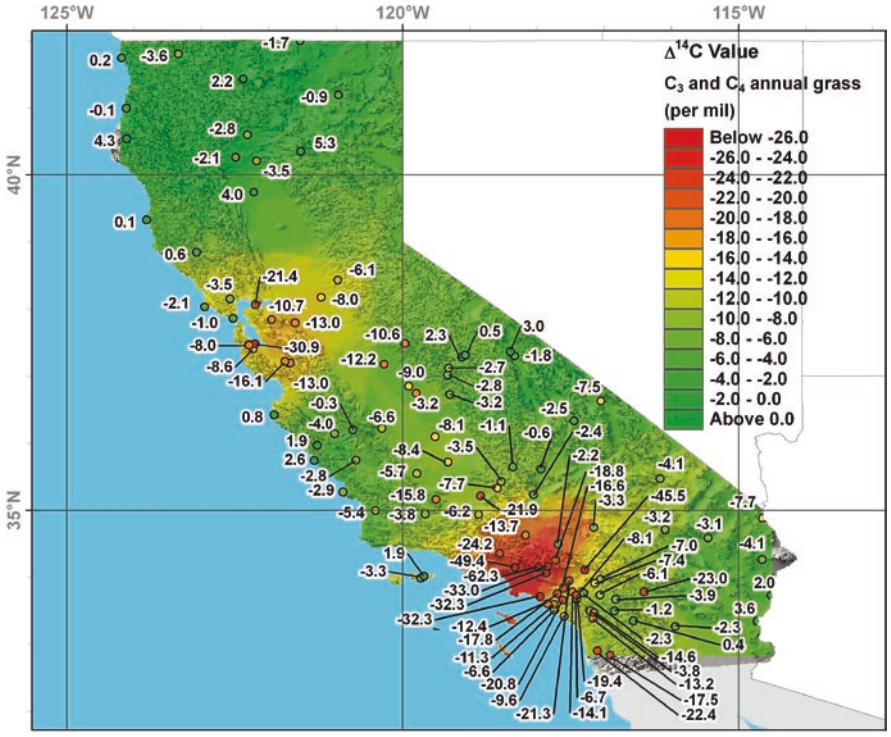

Fig. 19.3 The difference between $\Delta^{14}C$ of CO_2 in clear air measured in Pt. Barrow, Alaska, and in leaves of winter annual plants sampled throughout California in 2005. Units are per mil (‰) relative to the Oxalic Acid standard (Modified from Riley et al. 2008). Fig. 19.3, see Appendix 1, Color Section

This corresponds to a photosynthate-weighted, average CO_2 concentration of 437 ppm. Moving westward away from the densely populated urban area, plant samples showed increasingly less depletion with several samples within 5‰ of the $\Delta^{14}C$ at Pt. Barrow in rural areas of Orange and Riverside Counties. When the spatial distribution of plant $\Delta^{14}C$ was evaluated in relation to population density, geography, meteorological variables, and criteria air pollutants in a multiple regression model, $\Delta^{14}C$ was found to be significantly related to population density, distance to major roads, atmospheric carbon monoxide concentrations, and in particular to atmospheric ozone concentrations as measured by the local air quality monitoring agency. These four variables explained 53% of the spatial variability in leaf $\Delta^{14}C$, further supporting the application of $\Delta^{14}C$ as an integrator of atmospheric pollution that may complement and enhance traditional air quality monitoring networks.

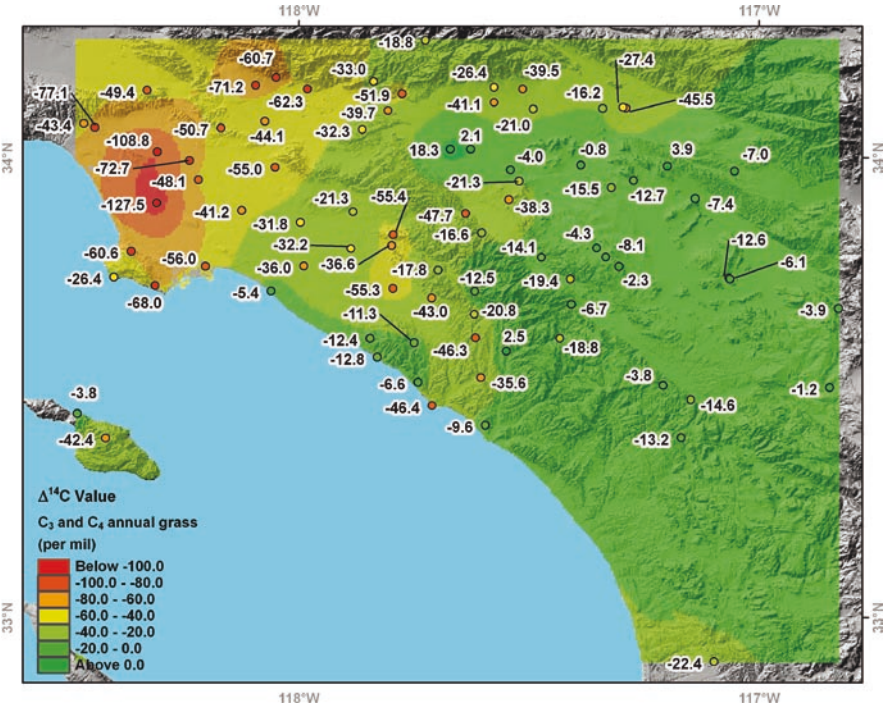

Fig. 19.4 The difference between $\Delta^{14}C$ of CO_2 in clear air measured in Pt. Barrow, Alaska, and in leaves of winter annual plants sampled throughout the Los Angeles Basin in 2004 and 2005. Units are per mil (‰) relative to the Oxalic Acid standard (Modified from Wang and Pataki 2009). Fig. 19.4, see Appendix 1, Color Section

19.5 The Temporal Distribution of $\Delta^{14}C$ Biomarkers

Because there is a good record of the $\Delta^{14}C$ of remote atmospheric CO_2 during the industrial period (Levin and Hesshaimer 2000), $\Delta^{14}C$ of archived organic samples from polluted areas can provide a record of changes in local $\Delta^{14}C$ and concentrations of CO_2 over time. Rakowski et al. (2004, 2005) showed depletion in $\Delta^{14}C$ of tree rings in Nagoya, Japan and Krakow, Poland over several decades relative to $\Delta^{14}C$ of CO_2 in clean air samples from Germany. This corresponded to CO_2 mixing ratios that were elevated above background levels by 5.6–12.6 ppm in Nagoya and 5.9–6.5 ppm in Krakow. In a novel application of organic matter archives as biomarkers of fossil fuel CO_2, Shibata and Kawano (1994) and Shibata et al. (2005) measured $\Delta^{14}C$ of rice grains harvested throughout Japan over a 17 year period. They found significant correlations between $\Delta^{14}C$ and population density as a proxy for local emissions. $\Delta^{14}C$ varied by more than 40‰ in rural areas versus large cities. With a long enough record, it may be possible to determine whether the slope of

this relationship is changing over time, which may provide very useful information about changes in CO_2 emissions and concentrations per capita. It is likely that this information will be increasingly needed for monitoring compliance with CO_2 emissions reductions programs and regulations in the future.

Long-term records of CO_2 mixing ratios during the industrial period have many applications and are an important new application of measurements of $\Delta^{14}C$. There is increasing interest in resolving high resolution CO_2 emissions inventories and in linking emissions more quantitatively to urban ecosystem processes in order to understand the mechanistic drivers of emissions, which are both socioeconomic and biophysical (Pataki et al. 2006). There is great potential to better link isoscapes near CO_2 emissions sources with interdisciplinary studies of urban expansion, demography, changes in infrastructure, and other factors that may improve our understanding of the human carbon cycle and improve future CO_2 emissions scenarios.

19.6 Combining Carbon and Nitrogen Tracers

While $\delta^{13}C$ is one of the most commonly used tracers in natural ecosystems due to the well-described relationship between plant gas exchange and $\delta^{13}C$, $\delta^{15}N$ has been shown to be a very useful tracer in polluted environments. There are many factors that influence fractionation of nitrogen isotopes in plants and soils, including enzymatic fractionation in soil microbial processes, fractionation in volatilization of gaseous N, mycorrhizal transfers, and nitrogen transformations within plants (Evans 2001; Högberg 1997; Robinson 2001). This complexity can make the interpretation of variations in $\delta^{15}N$ of organic matter difficult. However, there are now many studies that show consistent differences between $\delta^{15}N$ of organic matter in more versus less human-impacted environments. Ammann et al. (1999) showed $\delta^{15}N$ enrichment of spruce needles near a highway in Switzerland which they attributed to uptake of NO_2 pollution-derived dry deposition. Stewart et al. (2002) reported $\delta^{15}N$ depletion of plants growing near industrial pollution sources in Brazil where the pollution source was dominated by isotopically depleted NH_3 and NH_4^+. Norra et al. (2005) mapped $\delta^{15}N$ of both vegetation and soil in an urban area in Germany and found that $\delta^{15}N$ of both types of organic matter was more strongly correlated with land use than with soil parent material or meteorology. These results were supported by a subsequent study in Belgium which showed that the spatial distribution of plant and soil $\delta^{15}N$ was also most strongly influenced by land use, with depleted values in unfertilized urban soils containing N-fixing species and enriched values in fertilized agricultural areas and wetlands associated with large gaseous losses (Boeckx et al. 2006).

In the study in the San Bernardino Mountains in California, leaf $\delta^{13}C$ did not show any trends across the pollution gradient (Fig. 19.1); however, there were significant trends in $\delta^{15}N$ (Fig. 19.5) and C:N (Fig. 19.6). Both site and species significantly influenced leaf $\delta^{15}N$ (two-way ANOVA, $p < 0.05$), with most species showing depleted values of $\delta^{15}N$ at the more polluted sites, although the trend

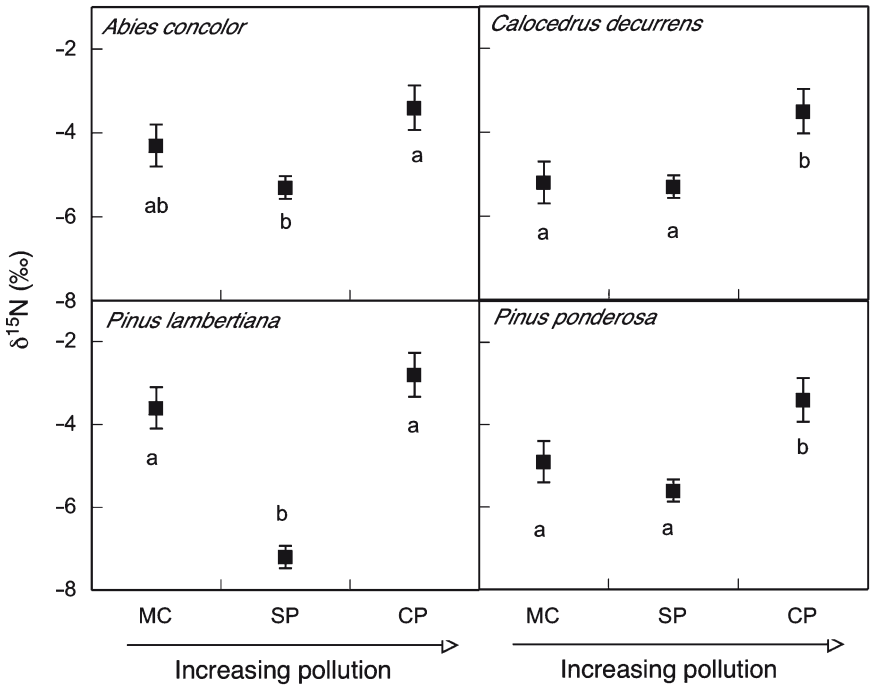

Fig. 19.5 Leaf nitrogen isotope ratio ($\delta^{15}N$) in four species of conifer trees sampled across a known ozone and nitrogen deposition gradient in the San Bernardino Mountains in California, USA. *Letters* show significant differences among sites with an LSD post-doc test of an ANOVA, $p < 0.05$

was complex in some species and showed the most depleted values at the intermediate site (Fig. 19.5). Leaf C:N was lowest at the most polluted site in three of the four species (Fig. 19.6), supporting increased plant uptake of pollution-derived N at sites of high anthropogenic N deposition. These results suggest that $\Delta^{14}C$, $\delta^{15}N$, and C:N are very promising tracers of anthropogenic tracers that show strong gradients in urbanized regions. To date, natural abundance ^{14}C and ^{15}N tracers have been applied in a relatively small number of urban ecological studies, but there is great potential to evaluate trends and mechanisms of isotope distribution in a wide variety of urban areas.

19.7 Conclusions

While $\delta^{13}C$ of organic matter can be difficult to interpret in polluted areas due to opposing effects of fossil fuel $^{13}CO_2$ dilution and the effects of secondary combustion products on physiology, radiocarbon can be used to distinguish between these

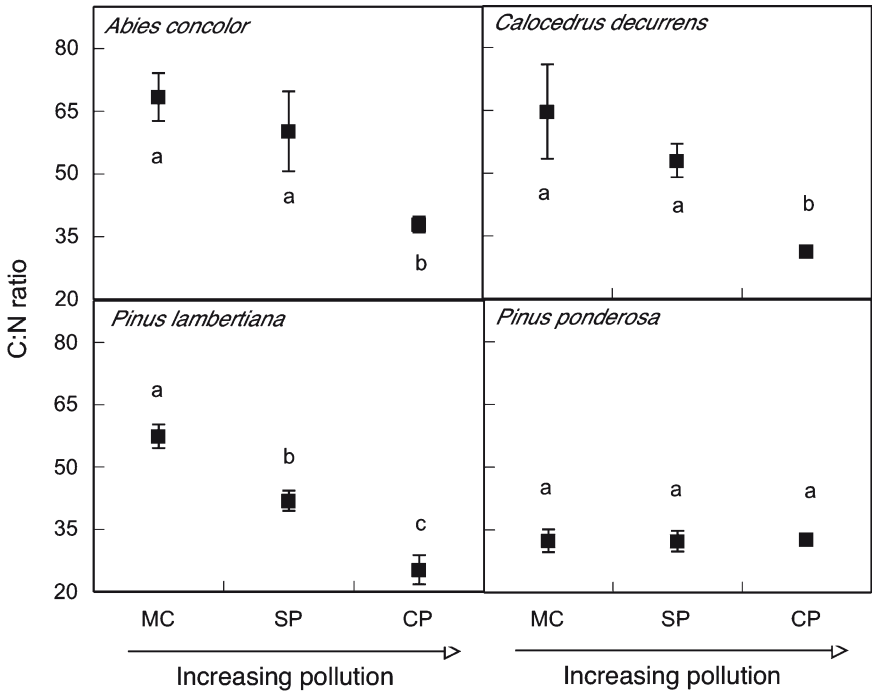

Fig. 19.6 Leaf carbon:nitrogen (C:N) in four species of conifer trees sampled across a known ozone and nitrogen deposition gradient in the San Bernardino Mountains in California, USA. *Letters* show significant differences among sites with an LSD post-doc test of an ANOVA, $p < 0.05$

effects. Plant $\Delta^{14}C$ is solely influenced by $\Delta^{14}C$ of atmospheric CO_2 at the time of fixation, and therefore can be used to infer atmospheric CO_2 mixing ratios in areas where locally-added fossil fuel-derived CO_2 contributes to elevated CO_2. Studies at many different spatial scales, from transects a few hundred meters from roadways to mapping studies at regional and national scales, have demonstrated that $\Delta^{14}C$ is a robust measure of anthropogenic CO_2. Statistical correlations between isotope ratios and environmental variables can help resolve the complexity of the effects of multiple disturbances in urban environments on plant physiology. These studies can be further informed by detailed studies of mechanistic relationships between altered urban environments and physiological responses, and by comparative studies across varying regions, which are currently at an early stage. Recent interest in developing new applications of isoscapes at varying spatial and temporal scales can greatly contribute to improving our understanding of plant–soil–environment interactions and associated ecosystem services in highly human-dominated and disturbed environments, which are a rapidly increasing proportion of the landscape.

Acknowledgements This work was supported by U.S. National Science Foundation grant 0620176. We thank Dachun Zhang, Greg Cane, and Xiaomei Xu for their assistance in the laboratory and Kristine Adan and Neeta Bijoor for their assistance in the field.

References

Alessio M, Anselmi S, Conforto L, Improta S, Manes F, Manfra L (2002) Radiocarbon as a biomarker of urban pollution in leaves of evergreen species sampled in Rome and in rural areas (Lazio-Central Italy). Atmos Environ 36:5405–5416

Ammann M, Siegwolf R, Pichlmayer F, Suter M, Saurer M, Brunold C (1999) Estimating the uptake of traffic-derived NO_2 from ^{15}N abundance in Norway spruce needles. Oecologia 118:124–131

Andres RJ, Marland G, Boden T, Bischof S (2000) Carbon dioxide emissions from fossil fuel consumption and cement manufacture, 1751–1991, and an estimate of their isotopic composition and latitudinal distribution. In: Wigley TML, Schimel DS (eds) The carbon cycle. Cambridge University Press, Cambridge, pp 53–62

Arbaugh M et al (2003) Photochemical smog effects in mixed conifer forests along a natural gradient of ozone and nitrogen deposition in the San Bernardino Mountains. Environ Int 29:401–406

Boeckx P, Van Meirvenne M, Raulo F, van Cleemput O (2006) Spatial patterns of $\delta^{13}C$ and $\delta^{15}N$ in the urban topsoil of Gent, Belgium. Org Geochem 37:1383–1393

Conway TJ, Lang PM, Masarie KA (2007) Atmospheric carbon dioxide dry air mole fractions from the NOAA ESRL carbon cycle cooperative global air sampling network, 1968–2006, Version: 2007-09-19. In, ftp://ftp.cmdl.noaa.gov/ccg/co2/flask/event/

Dongarrà G, Varrica D (2002) $\delta^{13}C$ variations in tree rings as an indication of severe changes in the urban air quality. Atmos Environ 36:5887–5896

Evans RD (2001) Physiological mechanisms influencing plant nitrogen isotope composition. Trends Plant Sci 6:121–126

Farquhar GD, Ehleringer JR, Hubick KT (1989) Carbon isotope discrimination and photosynthesis. Annu Rev Plant Physiol Plant Mol Biol 40:503–537

Fenn ME, Bytnerowicz A (1997) Summer throughfall and winter deposition in the San Bernardino Mountains in southern California. Atmos Environ 31:673–683

Grams TEE, Kozovits AR, Häberle K-H, Matyssek R, Dawson TE (2007) Combining $\delta^{13}C$ and $\delta^{18}O$ analyses to unravel competition, CO_2 and O_3 effects on the physiological performance of different-aged trees. Plant Cell Environ 30:1023–1034

Grimm NB, Grove JM, Pickett STA, Redman CL (2000) Integrated approaches to long-term studies of urban ecological systems. BioScience 50:571–584

Grulke NE, Balduman L (1999) Deciduous conifers: high N deposition and O_3 exposure effects on growth and biomass allocation in Ponderosa pine. Water Air Soil Pollut 116: 235–248

Högberg P (1997) ^{15}N natural abundance in soil-plant systems. New Phytol 137:179–203

Hsueh DY, Krakauer N, Randerson JT, Xiaomei X, Trumbore SE, Southon JR (2007) Regional patterns of radiocarbon and fossil fuel-derived CO_2 in surface air across North America. Geophys Res Lett 34. doi:10.1029/2006GL027032

Idso CD, Idso SB, Balling RC (1998) The urban CO_2 dome of Phoenix, Arizona. Phys Geogr 19:95–108

Idso CD, Idso SB, Balling RC (2001) An intensive two-week study of an urban CO_2 dome in Phoenix, Arizona, USA. Atmos Environ 35:995–1000

Jędrysek MO, Krępiec M, Skrzypek G, Kałuny A (2003) Air pollution effect and paleotemperature scale versus $\delta^{13}C$ records in tree rings and in a peat core (southern Poland). Water Air Soil Pollut 145:359–375

Karlén I, Olsson IU, Källberg P, Kilicci S (1964) Absolute determination of the activity of two ^{14}C dating standards. Arkiv för Geofysik 4:465–471

Keeling CD et al. (2005) Atmospheric CO_2 and $^{13}CO_2$ exchange with the terrestrial biosphere and oceans from 1978 to 2000: observations and carbon cycle implications. In: Ehleringer JR, Cerling TE, Dearing MD (eds) A history of atmospheric CO_2 and its implications for plants, animals, and ecosystems. Springer, New York, pp 83–113

Kèlomé NC, Lévêque J, Andreux F, Milloux M-J, Oyédé L-M (2006) C_4 plant isotopic composition ($\delta^{13}C$) evidence for urban CO_2 pollution in the city of Cotonou, Benin (West Africa). Sci Total Environ 366:439–447

Koerner B, Klopatek J (2002) Anthropogenic and natural CO_2 emission sources in an arid urban environment. Environ Pollut 116:S45–S51

Krakauer NY, Randerson JT, Primeau FW, Gruber N, Menemenlis D (2006) Carbon isotope evidence for the latitudinal distribution and wind speed dependence of the air–sea gas transfer velocity. Tellus 58B:390–417

Lee EH, Tingey DT, Hogsett WE, Laurence JA (2003) History of tropospheric ozone for the San Bernardino Mountains of Southern California, 1963–1999. Atmos Environ 37:2705–2717

Levin I, Hesshaimer V (2000) Radiocarbon – a unique tracer of global carbon cycle dynamics. Radiocarbon 42:69–80

Levin I, Hammer S, Kromer B, Meinhardt F (2008) Radiocarbon observations in atmospheric CO_2: determining fossil fuel CO_2 over Europe using Jungfraujoch observations as background. Sci Total Environ 391:211–216

Lichtfouse E, Lichtfouse M, Jaffrezic A (2003) $\delta^{13}C$ values of grasses as a novel indicator of pollution by fossil-fuel-derived greenhouse gas CO_2 in urban areas. Environ Sci Technol 37:87–89

Marino BD, McElroy MB (1991) Isotopic composition of atmospheric CO_2 inferred from carbon in C_4 plant cellulose. Nature 349:127–131

Norby RJ, Luo Y (2004) Evaluating ecosystem responses to rising atmospheric CO_2 and global warming in a multi-factor world. New Phytol 162:281–293

Norra S, Handley LL, Berner Z, Stüben D (2005) ^{13}C and ^{15}N natural abundances of urban soils and herbaceous vegetation in Karlsruhe, Germany. Eur J Soil Sci 56:607–620

Novak K et al (2007) Ozone air pollution effects on tree-ring growth, $\delta^{13}C$, visible foliar injury and leaf gas exchange in three ozone-sensitive woody plant species. Tree Physiol 27:941–949

Pataki DE, Bowling DR, Ehleringer JR (2003a) The seasonal cycle of carbon dioxide and its isotopic composition in an urban atmosphere: anthropogenic and biogenic effects. J Geophys Res 108:4735

Pataki DE et al (2003b) Tracing changes in ecosystem function under elevated carbon dioxide conditions. BioScience 53:805–818

Pataki DE, Bush SE, Ehleringer JR (2005a) Stable isotopes as a tool in urban ecology. In: Flanagan LB, Ehleringer JR, Pataki DE (eds) Stable isotopes and biosphere–atmosphere interactions: processes and biological controls. Elsevier, San Diego, CA, pp 199–216

Pataki DE, Tyler BJ, Peterson RE, Nair AP, Steenburgh WJ, Pardyjak ER (2005b) Can carbon dioxide be used as a tracer of urban atmospheric transport? Journal of Geophysical Research Atmospheres 110. doi:10.1029/2004JD005723

Pataki DE et al (2006) Urban ecosystems and the North American carbon cycle. Global Change Biol 12:1–11

Pataki DE, Xu T, Luo Y, Ehleringer JR (2007) Inferring biogenic and anthopogenic carbon dioxide sources across an urban to rural gradient. Oecologia 152:307–322

Pepin S, Körner C (2002) Web-FACE: a new canopy free-air CO_2 enrichment system for tall trees in mature forests. Oecologia 133:1–9

Rakowski AZ, Nakamura T, Pazdur A (2004) Changes in radiocarbon concentration in modern wood from Nagoya, central Japan. Nucl Instrum Methods Phys Res B 223–224:507–510

Rakowski AZ, Kuc T, Nakamura T, Pazdur A (2005) Radiocarbon concentration in an urban area. Geochronometria 24:63–68

Randerson JT, Enting IG, Schuur EAG, Caldiera K, Fung IY (2002) Seasonal and latitudinal variability of troposphere $\Delta^{14}CO_2$: Post bomb contributions from fossil fuels, oceans, the stratosphere, and the terrestrial biosphere. Global Biogeochem Cycles 16. doi:10.1029/2002GB001876

Riley WJ et al. (2008) Where do fossil fuel carbon dioxide emissions from California go? An analysis based on radiocarbon observations and an atmospheric transport model. Journal of Geophysical Research Biogeosciences 113. doi:10.1029/2007JG000625

Roberts ML, Southon JR (2007) A preliminary determination of the absolute $^{14}C/^{12}C$ ratio of OX-1. Radiocarbon 49:441–445

Robinson D (2001) $\delta^{15}N$ as an integrator of the nitrogen cycle. Trends Ecol Evol 16:153–162

Santos GM, Southon JR, Druffel-Rodriguez KC, Griffin S, Mazon M (2004) Magnesium perchlorate as an alternative water trap in AMS graphite sample preparation: a report on sample preparation at KCCAMS at the University of California, Irvine. Radiocarbon 46:165–173

Šantrůčková H, Šantrůček J, Šetlík J, Svoboda M, Kopáček J (2007) Carbon isotopes in tree rings of Norway spruce exposed to atmospheric pollution. Environ Sci Technol 41:5778–5782

Saurer M, Maurer S, Matyssek R, Landolt W, Gundthardt-Goerg MS, Siegenthaler U (1995) The influence of ozone and nutrition on $\delta^{13}C$ in *Betula pendula*. Oecologia 103:397–406

Saurer M, Cherubini P, Bonani G, Siegwolf R (2003) Tracing carbon uptake from a natural CO_2 spring into tree rings: an isotope approach. Tree Physiol 23:997–1004

Saurer M, Cherubini P, Ammann M, De Cinti B, Siegwolf R (2004) First detection of nitrogen from NOx in tree rings: a $^{15}N/^{14}N$ study near a motorway. Atmos Environ 38:2779–2787

Savard MM, Begin C, Parent M (2002) Are industrial SO_2 emissions reducing CO_2 uptake by the boreal forest? Geology 30:403–406

Shibata S, Kawano E (1994) Effects of latitude and population density in the growing districts on ^{14}C content of rice grains. Appl Radiat Isot 45:815–816

Shibata S, Kawano E, Nakabayashi T (2005) Atmospheric [14C]CO2 variations in Japan during 1982–1999 based on 14C measurements of rice grains. Appl Radiat Isot 63:285–290

Southon J et al (2004) The Keck Carbon Cycle AMS laboratory, University of California, Irvine: initial operation and a background surprise. Radiocarbon 46:41–49

Stewart GR, Aidar MPM, Joly CA, Schmidt S (2002) Impact of point source pollution on nitrogen isotope signatures ($\delta^{15}N$). Oecologia 131:468–472

Stuiver M, Polach H (1977) Reporting of ^{14}C data. Radiocarbon 19:355–363

Tans PP (1981) $^{13}C/^{12}C$ of industrial CO_2. In: Bolin B (ed) Carbon cycle modelling, vol 16. Wiley, Chichester, IL

Trumbore SE (1996) Applications of accelerator mass spectrometry to soil science. In: Boutton TW, Yamasaki S (eds) Mass spectrometry of soils. Marcel Dekker, New York, pp 311–340

Trumbore S (2000) Age of soil organic matter and soil respiration: radiocarbon constraints on belowground C dynamics. Ecol Appl 10:399–411

Wang W, Pataki DE (2009) The spatial distribution of radiocarbon and stable isotope biomarkers in the Los Angeles Basin. Landscape Ecol (in press), doi: 10.1007/s10980-099-9401-5

Wang Y, Hsieh Y-P (2002) Uncertainties and novel prospects in the study of the soil carbon dynamics. Chemosphere 49:791–804

Chapter 20
Isoscapes in a Rapidly Changing and Increasingly Interconnected World

Gabriel J. Bowen, Jason B. West, and Todd E. Dawson

20.1 Introduction

"Isoscapes" have recently emerged as a coherent framework for the analysis, visualization, distribution, and application of environmental isotope data and have already created new disciplinary and interdisciplinary research opportunities. The chapters in this volume document the diverse and important roles that spatial monitoring and data analysis play in the application of isotope chemistry within contemporary science. The authors of this volume demonstrate how isoscapes serve as a tool for basic research, a template for data analysis and visualization, and a common platform and language for establishing a dialogue among specialists and non-specialists. The diversity and depth of the work demonstrates the relevance of isoscapes-based research to the needs of science and society in the twenty-first century, especially where problems are recognized to involve complex systems with widely distributed impacts, necessarily studied at large spatial scales (also see Bowen et al. 2009). Many chapters also highlight the significant challenges and gaps in understanding that must be overcome if the potential of these methods are to be realized. These are clear targets for future research that promise to expand discovery through improved understanding and application of spatio-temporal isotope variability.

G.J. Bowen
Department of Earth and Atmospheric Sciences, Purdue Climate Change Research Center, Purdue University, West Lafayette, IN, 47907, USA
e-mail: gabe@purdue.edu

J.B. West (✉)
Texas AgriLife Research and Department of Ecosystem Science & Management, Texas A&M University, College Station, TX, 77843-2138, USA
e-mail: jbwest@tamu.edu

T.E. Dawson
Center for Stable Isotope Biogeochemistry, Department of Integrative Biology, University of California, Berkeley, CA, 94720, USA
e-mail: tdawson@berkeley.edu

J.B. West et al. (eds.), *Isoscapes: Understanding Movement, Pattern, and Process on Earth Through Isotope Mapping*, DOI 10.1007/978-90-481-3354-3_20,

Isoscapes have shown their strength in addressing basic research problems within the Earth and atmospheric sciences, ecology, and to a growing extent in anthropology. Considering isotope data within a spatial context can reveal otherwise obscure patterns indicative of mechanistic processes. For example, the integration of individual tree-ring isotope records within a spatio-temporal network offers unique opportunities to identify and characterize linkages between local and regional climate (e.g., aridity in the southwestern USA) and annular climate modes such as the ENSO (Leavitt et al. this volume). Isotopes can be sensitive bio-monitors, and analysis of isotopic data within its spatial context increases our ability to identify localized perturbations to biogeochemical systems (e.g., effects of mixing-induced algal blooms on aquatic nitrogen biogeochemistry; Kendall et al. this volume). Incorporation of isotopes within 'comprehensive' climate system models provides a unique indication of the importance and spatial distribution of below-cloud 'recycling' of water from falling raindrops on the atmospheric water cycle (Noone and Sturm this volume; Worden et al. 2007).

Isoscapes have further enabled a new generation of isotope-based approaches to applied science questions by facilitating the transfer of isotopic data and theory to non-specialists through the generation and distribution of derived data products (isotope maps). Scientists and managers working on a wide range of problems have a largely unsatisfied need for basic information on the spatiotemporal history (origin and/or movement over time) of plants, animals, and products. Isotopic tracers now provide capabilities of this type and are even adopted operationally in some areas. Inferring the tributary of origin of wild-born salmon or travel history of a 'Jane Doe' from isotope data offers unprecedented information for decision support in a variety of management or law enforcement goals (Hobson et al.; Ehleringer et al. this volume). The transfer of these methods from experimental to operational use would arguably be impossible were it not for the development of relevant isoscapes that provide capabilities for the use of isotopic information by non-specialists.

The unifying concept of isoscapes-based research is a natural extension of the basic recognition of spatiotemporal variation in environmental isotope systems to the principle that this variation is *mechanistic* and *predictable*. These two properties underlie the power of isoscapes. That the spatiotemporal variation is mechanistic implies that, with adequate understanding, observed patterns of isotopic variation can be 'inverted' to reveal aspects of the underlying Earth systems processes. This approach has been the root of much of the research on global carbon cycle dynamics highlighted by Vaughn et al. (this volume) and, in a less formal sense, many process-level studies of the water cycle (Helliker and Noone this volume) and biogeochemistry (Kendall et al. this volume). The mechanistic nature of isotope fractionation and mixing processes is also the foundation of isoscape predictability, with many practical consequences for isoscape-based research. Predictability enables research that uses isoscapes to assign Earth materials to sources or source locations, whether in studies of hydrological systems (Gibson et al. this volume), ecological systems (Hobson et al. this volume; Graham et al. this volume), or

anthropological systems (Schoeninger this volume; Schwarcz et al. this volume; Ehleringer et al. this volume). Predictability also allows researchers to probe isoscapes for perturbations, elucidating the patterns of natural or anthropogenic processes such as climate modes (Noone and Sturm this volume) or pollutant releases (Pataki et al. this volume).

As the work presented here illustrates, the scope, impact, and information return of isoscapes-based research are expanding rapidly. To sustain this momentum there is a need for improved mechanistic understanding and ability to predict isotope distributions across a growing range of isotopic and environmental systems, and temporal and spatial scales.

20.2 The Search for Mechanistic Relationships

As recognition of the potential uses of isoscapes has grown, it has driven demand for spatial analyses and isotope maps for new materials, new isotope systems, and new spatial and temporal scales. As several chapters in this volume illustrate, this demand is currently pushing the limits of mechanistic understanding for many systems. This in turn feeds back to suggest new process-based research to help explain underlying pattern. For example, in some systems, such as soil and plant $\delta^{15}N$, a large body of work exists but a mechanistic synthesis has not yet been accomplished (Pardo and Nadelhoffer this volume; Craine et al. 2009). For others, such as $\delta^{2}H$ and $\delta^{18}O$ in plant tissues (West et al. this volume) or marine isoscapes (Graham et al. this volume), theory is available but not yet sufficiently general to allow widespread application (e.g., to a wide range of species). And in others such as $\delta^{2}H$ and $\delta^{18}O$ in heterotroph tissues, the demand for models describing isotopic variation as a function of location is pushing development of theory in previously underexplored areas (Ehleringer et al. this volume).

Regardless of the specifics of the system, the growing interest in studying and understanding large-scale isotopic patterning should promote an increased emphasis on data synthesis and the identification of generalizable mechanistic relationships that drive isotopic variation. The history of isotope chemistry offers some key examples of transformational mechanistic syntheses, for example the pioneering work of Craig and Gordon (1965), which has influenced most subsequent work on water isotopes, and the work on photosynthetic carbon isotope fractionation of Farquhar et al. (1982). Not coincidentally, the greatest progress in isoscapes-based research has thus far been in areas that benefit directly from the theory developed by these authors. Further advances will require new syntheses and improved mechanistic understanding, work that could bring with it the simultaneous benefits of advancing understanding of Earth systems processes and supporting isoscape generation with application to a wide range of questions. Conversely, isoscapes-based research may itself play a role in the development of new theory as the depth of this work increases. Spatial data can be a powerful resource for diagnosis and refinement of spatial prediction models, as has been the case for isotope-enabled

general circulation models (Noone and Sturm this volume), and could be useful for improving models for systems as diverse as surface hydrology and mammalian digestive physiology. With appropriate mechanistic understanding, inversion approaches previously applied to spatially integrated fluxes in the carbon cycle could be applied to the same system at different scales or to other biogeochemical or pollutant systems (e.g., nitrogen deposition; Kendall et al. this volume) and assignment applications could be refined to better capitalize on multiple data types or extended to new ecological systems or geographic regions.

20.3 Better Data, Better Predictions

A common theme highlighted throughout this volume is the need for improved predictive ability, particularly with respect to temporal variation of environmental isoscapes. Time-explicit isotope maps are needed to run carbon cycle inversions (Vaughn et al. this volume), improve geographic assignments (Hobson et al. this volume), drive surface hydrology models (Gibson et al. this volume), and detect change in Earth systems over time (Bowen et al. 2007; Hemming et al. 2007; Williams et al. 2007; Schwarcz et al. this volume). In most cases, a major limiting factor for the production of time-explicit isoscapes is the low density and poor continuity of spatial datasets over multi-year timescales (Bowen this volume). The move towards production and application of time-explicit isoscapes will require new approaches to isotope monitoring (Ehleringer and Dawson 2007) that enable improved continuity of measurements in space and time and/or modeling techniques that produce isoscapes based on existing data streams with high spatial and temporal fidelity.

The chapters of this volume offer a wide range of possible solutions for the problem of temporal prediction, many of which may be realized within the coming years. Water isoscapes, which to this point have been intimately anchored to spatial isotope monitoring databases, may benefit from novel techniques and technology allowing retrospective and future measurement of isotope distributions to supplement the existing network of IAEA observations (Agarwaal et al. this volume; Helliker and Noone this volume). From the modeling standpoint, improved parameterizations for statistical models that use independent variables derived from satellite observations or climate model simulations and the continued improvement of isotope-enabled GCMs, including the development and validation of nudging schemes for isotope enabled GCMs, may, to some extent, circumvent the limitations of current methodologies that depend strongly on the isotope monitoring data (Bowen this volume; Noone and Sturm this volume). For other systems (e.g., $\delta^{13}C$, $\delta^{15}N$), predictive models have been developed largely without the benefit of (or dependence on) large-scale isotope monitoring data, and are, or theoretically could be, applied to predict temporal variability within the bounds of the data sources used (Wang et al. this volume; Still et al. this volume). In all cases, however, some level of continued isotope monitoring will be required for purposes of validation of new models and data products, as well as model calibration or refinement.

Isotope monitoring networks have been developed under a range of conditions and data availability, many of which are described in section 1 of this book. These range from coordinated, long-term networks with prescriptive sampling and data analysis protocols (e.g., Agarwaal et al. this volume) to organic, application-oriented collaborative networks (e.g., Vaughn et al. this volume) to opportunistic and post-hoc databasing efforts (e.g., Kendall et al. this volume; Leavitt et al. this volume). Each of these approaches has merits and drawbacks and each has contributed to advancing disciplinary science objectives, as described by the chapter authors. The long-term sustainability of monitoring networks is never certain, however, and in most cases network administrators must regularly secure support for continued operations through demonstration of value to stakeholders and funding agencies. Such networks form the backbone for isoscapes modeling and mapping studies and isoscapes should, in turn, contribute value to monitoring networks through their role as a bridge between disciplinary data collection efforts and multidisciplinary data consumers. For example, application of meteoric water data to ecological, anthropogenic and forensic applications has been widely advanced through recent efforts to translate monitoring data into predictive isoscapes, resulting in significant increases in data usage. Continued efforts like this can be of great value in demonstrating the broad impact of network activities.

20.4 Limitations and Challenges

Isoscapes are the product of models, and, like all model products, they have inherent limitations. Models distill complex natural phenomena into mechanisms that can be generalized across space and time. Isoscapes models make predictions of isotope effects associated with fractionation and mixing processes based on spatiotemporal data of limited resolution and accuracy and mechanistic understandings that are continuing to develop and evolve. The modeling process involves decisions and trade-offs – for any given system no single isoscape can be generated that is 'optimal' for all applications. Most isoscapes are produced with specific applications in mind, and compromises accepted during this process may reduce the usefulness of the end product for non-target applications. Two of the most critical trade-offs encountered in work with isoscapes, and highlighted throughout this volume, involve compromises between *specificity* and *generality* and those between *resolution* and *scale*.

As the use of isoscapes grows and expands into new fields, the demand for more substrate-specific analyses and models has increased. Already, geographic assignment applications, which have to this point relied on isoscapes of 'generic' environmental materials (e.g., precipitation water, bedrock strontium), are testing the boundaries of the method's accuracy and precision. Improved assignment will require explicit treatment of multiple, specific substrates (water, food, air) and their uptake and processing by organisms (e.g., Ehleringer et al. this volume; Hobson et al. this volume; Wunder this volume). This intensified focus has yielded an important

recognition of the need for critical evaluation of the appropriateness of generalized isoscapes for specific applications. However, the need for substrate-specific, or even organism or individual-specific isoscapes, can exceed the limits of existing theory and data (see above) and would be expected to require compromises in terms of the general applicability of the modeling results. Isoscapes documenting deep groundwater or cotton cellulose isotope ratios may be of great benefit for specific applications, but also require specific sampling and/or model calibration efforts and are not as broadly applicable as more generalized source-water data products (e.g., meteoric precipitation). The efforts and activities involved in creation of isoscapes and isoscapes models of higher-order specificity are critical to the advancement of isoscapes-based science, and will ultimately provide data and theory of broad benefit. Particularly in their early stages, however, these systems-specific investigations will likely be more difficult to organize as community-level activities and will often fall on the shoulders of individual investigators without the benefit of support from coordinated sampling networks or large agencies.

For many isoscapes developers and users achieving higher spatial and temporal resolution in isoscape data products and models represents a critical goal, but often this involves trade-offs with respect to scale or 'extent'. This is particularly evident in the development of monitoring programs, where network designers are faced with the challenge of identifying sample substrates that integrate information over spatial scales appropriate to the systems and processes targeted by the network. Taking examples from within this volume, tall tower networks that sample trace gas isotope ratios in the free troposphere provide little information on field-scale processes (Vaughn et al. this volume), whereas $\delta^{15}N$ values of riverine POM are likely to yield more information about local in-stream biogeochemical processes than large-scale source/sink patterns (Kendall et al. this volume). With respect to models, resolution and scale limitations derive primarily from two factors – computational demand and the extent and resolution of data used to define boundary conditions (or used as 'predictor variables'). For example, global simulations of water isotope distributions using atmospheric models running at cloud-resolving resolutions cannot currently be run at the global scale (Noone and Sturm this volume), and meter-scale plant $\delta^{13}C$ estimation is impractical at the global scale but is being accomplished for small regions (Still et al. this volume; Wang et al. this volume). Fortunately, these limitations are not fundamental but practical in nature, and with continued technological innovation, adequate investments in computational and earth-observing infrastructure, and solid theory for resolving small-scale processes there is every reason to expect that model resolution will increase. In this event, isoscapes models may play an increasingly important role in up- and downscaling, for example to leverage spatially integrated tropospheric CO_2 isotopic measurements (Vaughn et al. this volume) with meter-scale predictions of plant and soil $\delta^{13}C$ values (Wang et al. this volume) to link large-scale changes in regional carbon budgets with spatially heterogeneous ecosystem processes.

Recognition of the strengths, trade-offs and potential inaccuracies of individual isoscapes or isoscapes modeling approaches is the first step to their informed use, and together with proper analysis of error constitute a necessary basis for robust

applications of these data products that recognize relevant limitations. In order to support this process, there is a critical need for increased error analysis and documentation within the community that works with the spatial analysis of isotope data and generation of isoscapes. With a small number of exceptions (e.g., Bowen and Revenaugh 2003; Lykoudis and Argiriou 2007; van der Veer et al. 2009), isotope maps that have appeared in the literature or are currently being distributed electronically and reused by researchers lack any documentation or grid-based analysis of error (although this is becoming more common). Analytical or numerical quantification of prediction uncertainty in isoscapes should be requisite for any analysis that produces reusable data products, and these estimates should be quantitatively assimilated, together with realistic estimates of other uncertainties, in subsequent analyses (e.g., Wunder this volume). In the short term, honest assessment of error will reveal limitations inherent in the current generation of isoscapes and isoscape-based applications. Recognition of these limitations, however, will lead to more robust application of isoscapes data products and guide the continued efforts of researchers in ways that address the most critical uncertainties and fundamental challenges associated with this work.

20.5 Opportunities for Isoscapes in a Networked World

The isoscapes concept has developed and matured in the context of a world that is becoming increasingly interconnected and networked: from the free flow of people and products across borders to the exchange of information through digital data networks to cross-disciplinary connections among scientists, agencies, and corporations. Isoscapes are, at their core, a spatiotemporal fingerprint of the chemical and physical processes that shape the environment and society in which we live. Networking has facilitated the exchange of data and ideas that allow us to document and map isotope distributions, and as interconnections between cities and nations grow through travel, trade, and human interaction with the biosphere, atmosphere and hydrosphere, isoscapes will become increasingly important in documenting and understanding the patterns and processes of human-induced changes (also see Ehleringer and Dawson 2007). Understanding the consequences of this interconnectedness is one of the major promises of isoscapes that has had limited exploration until now and which we anticipate will be an area of active growth in the future.

Many of the elements required to advance this work are already developing or in place, but sustained progress in isoscapes-based research will inevitably require sustained intellectual and financial commitments in several areas, including:

1. Continued emphasis on basic research on isotope biogeochemistry
2. Expanded Earth systems monitoring programs involving both isotopic and non-isotopic measurements
3. Increased collaboration with GIS theoreticians, geostatisticians and software developers

4. Continued support for application-based, proof-of-concept research, including multi-element, multi-system studies
5. Conscientious documentation and unrestricted distribution of isoscapes data products

The chapters of this volume demonstrate the breadth of what isoscapes have contributed across a remarkable range of domains, and hint and what they have to offer in the future. Their history has largely been one of organic and opportunistic discovery, primarily driven by individual scientists pursuing knowledge in their respective fields. As the networking of science and society continues to grow, concerted efforts to understand movement, pattern, and process on Earth through the study of isotope landscapes may help us unravel and understand our dynamic and connected world.

References

Bowen GJ, Revenaugh J (2003) Interpolating the isotopic composition of modern meteoric precipitation. Water Resour Res 39:1299

Bowen GJ, Cerling TE, Ehleringer JR (2007) Stable isotopes and human water resources: signals of change. In: Dawson TE, Siegwolf RTW (eds) Stable isotopes as indicators of ecological change. Academic-Elsevier, San Diego, CA, pp 285–300

Bowen GJ et al (2009) Isoscapes to address large-scale Earth science challenges. Eos 90:109–110

Craig H, Gordon LI (1965) Deuterium and oxygen-18 variations in the ocean and the marine atmosphere. In: Tongiorgi E (ed) Proceedings of a conference on stable isotopes in oceanographic studies and paleotemperatures, vol 9–130. Spoleto, Italy

Craine JM, Elmore AJ, Aidar MPM, Bustamante M, Dawson TE, Hobbie EA, Kahmen A, Mack MC, McLauchlan KK, Michelsen A, Nardoto GB, Pardo LH, Peñuelas J, Reich PB, Schuur EAG, Stock WD, Templer PH, Virginia RA, Welker JM, Wright IJ (2009) Global patterns of foliar nitrogen isotopes and their relationships with climate, mycorrhizal fungi, foliar nutrient concentrations, and nitrogen availability. New Phytol 183:980–992

Ehleringer JR, Dawson TE (2007) Stable isotopes record ecological change, but a sampling network will be critical. In: Dawson TE, Siegwolf RTW (eds) Stable isotopes as indicators of ecological change. Academic-Elsevier, San Diego, CA, pp 19–24

Farquhar GD, O'Leary MH, Berry JA (1982) On the relationship between carbon isotope discrimination and the intercellular carbon dioxide concentration in leaves. Aust J Plant Physiol 9:121–137

Hemming D, Griffiths H, Loder NJ, Marca A, Robertson I, Williams D, Wingate J, Yakir D (2007) The future of large-scale table isotope networks. In: Dawson TE, Siegwolf RTW (eds) Stable isotopes as indicators of ecological change. Academic-Elsevier, San Diego, CA, pp 361–382

Lykoudis SP, Argiriou AA (2007) Gridded data set of the stable isotopic composition of precipitation over the eastern and central Mediterranean. J Geophys Res 112:D18107

van der Veer G, Voerkelius S, Lorentz G, Heiss G, Hoogewerff JA (2009) Spatial interpolation of the deuterium and oxygen-18 composition of global precipitation using temperature as ancillary variable. J Geochem Explor 101:175–184

Williams DG, Evans RD, West JB, Ehleringer JR (2007) Applications of stable isotope measurements for early-warning detection of ecological change. In: Dawson TE, Siegwolf RTW (eds) Stable isotopes as indicators of ecological change. Academic-Elsevier, San Diego, CA, pp. 399–405

Worden J, Noone D, Bowman K (2007) Importance of rain evaporation and continental convection in the tropical water cycle. Nature 445:528–532

Appendix 1: Color Section

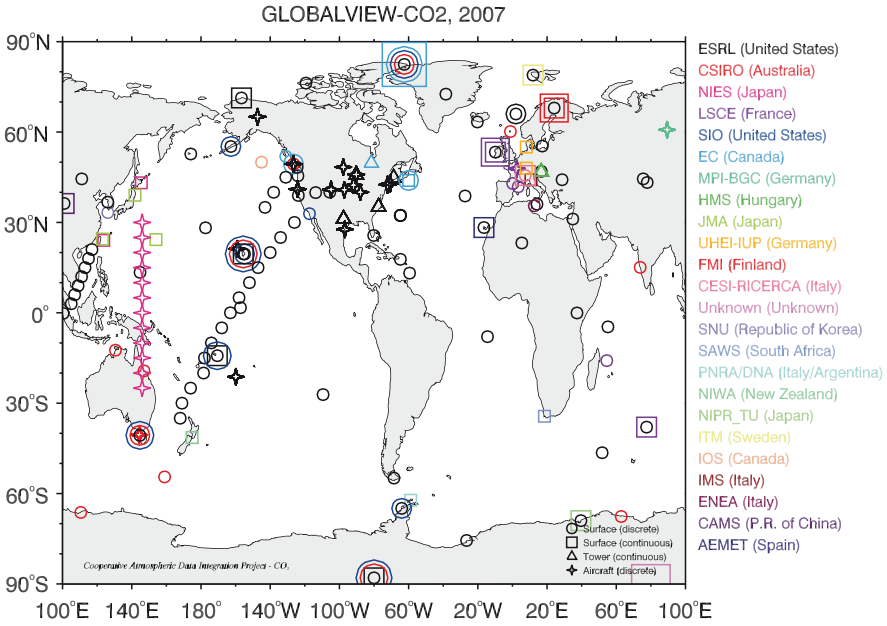

Fig. 1.1 Map of sampling sites for multiple laboratories that measure trace gas concentrations and contribute to GLOBALVIEW. A smaller subset of these labs also measure stable isotopes

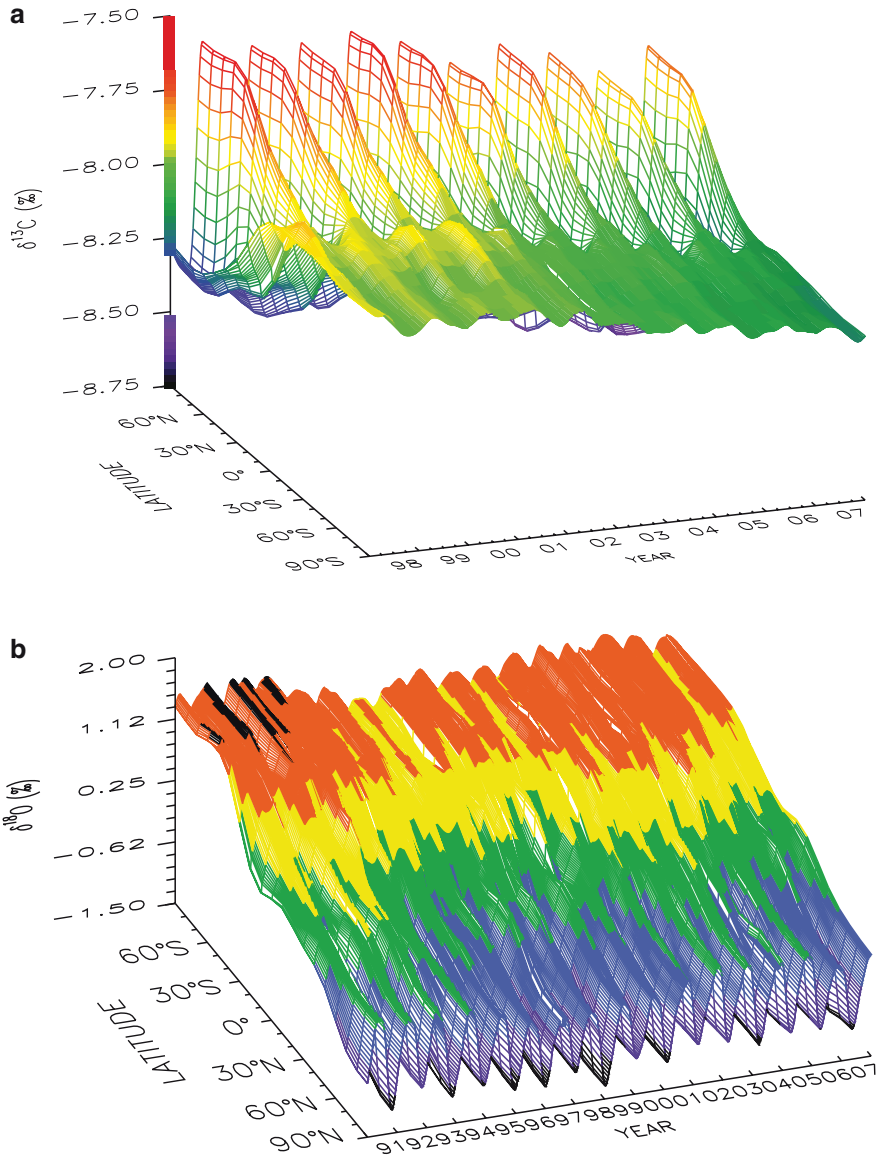

Fig. 1.4 (a) Surface plot of spatial $\delta^{13}C$-CO_2 data from the NOAA/INSTAAR global flask network through time, created from 55 sites from south to north. (b) Surface plot of spatial $\delta^{18}O$-CO_2 data from the NOAA/INSTAAR global flask network through time, created from 55 sites. Note the y-axis is reverse of the $\delta^{13}C$-CO_2 plot, from north to south, in order to better display the large latitudinal gradient

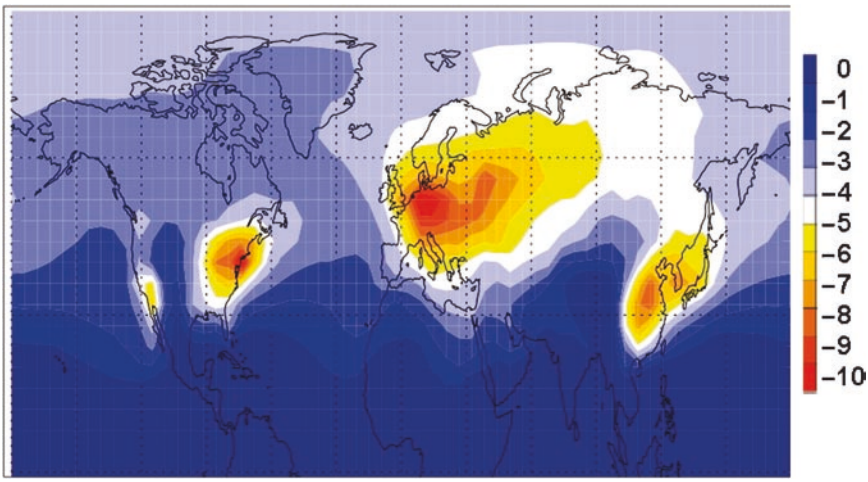

Fig. 1.7 Northern Hemisphere surface distribution of $\Delta^{14}C$ predicted by the TM5 model for 2004

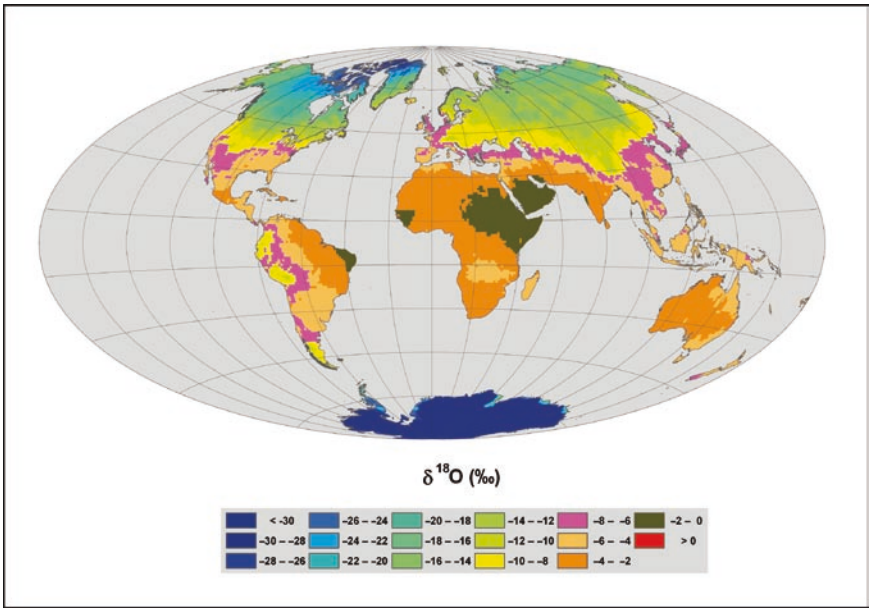

Fig. 2.5 Global interpolation map of oxygen-18 composition of precipitation (modified from Aggarwal et al. 2007)

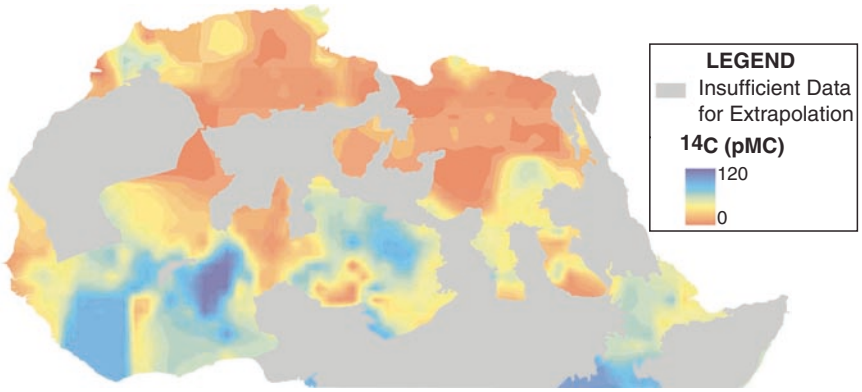

Fig. 2.7 Carbon-14 (percent of modern carbon) in deep groundwater of northern Africa (modified from Aggarwal et al. 2007)

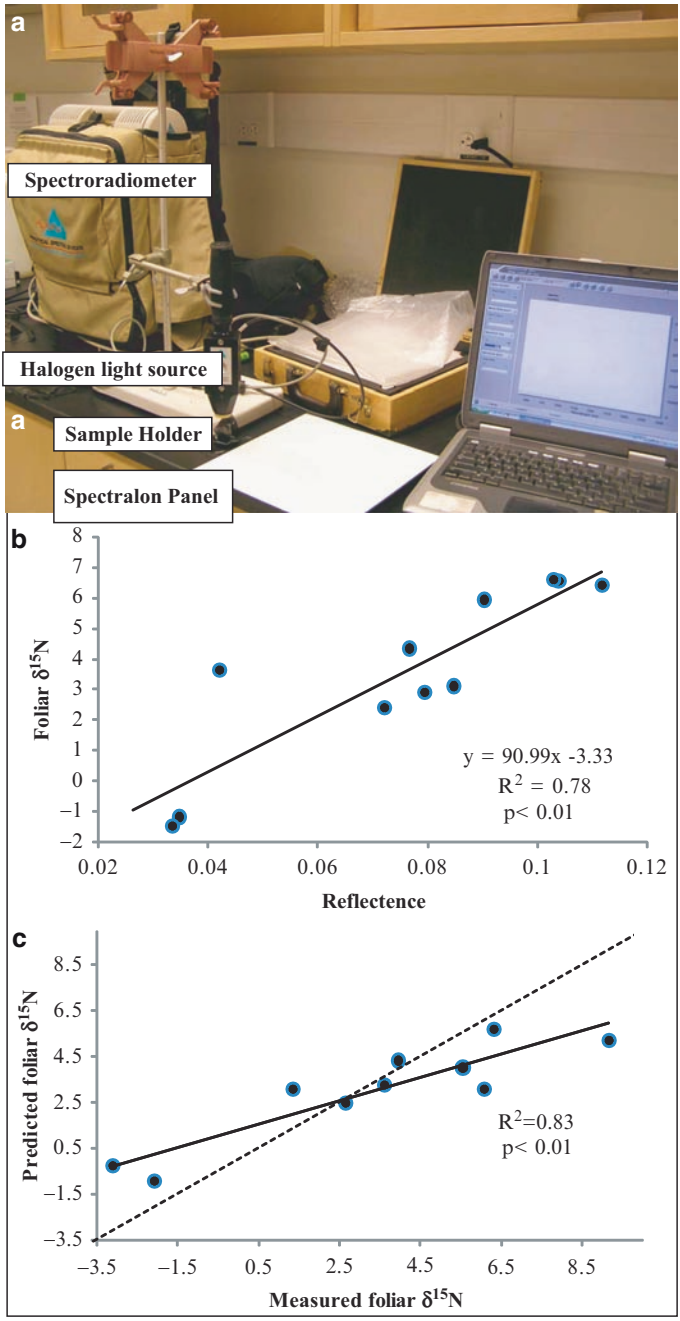

Fig. 3.4 The setup and results from the laboratory spectroscopy experiment, showing (a) the customized setup for spectra analysis in the laboratory. (b) The calibration regression between foliar spectra data (420 nm, reflectance was calculated as the ratio of the reflected radiance of the leaf to the reflected radiance of a Spectralon panel) and 15N data. (c) The predictions of foliar 15N from independent validation samples versus the measured values. The dotted line is one to one line, which shows the agreement/departure between the predicted values and measured values

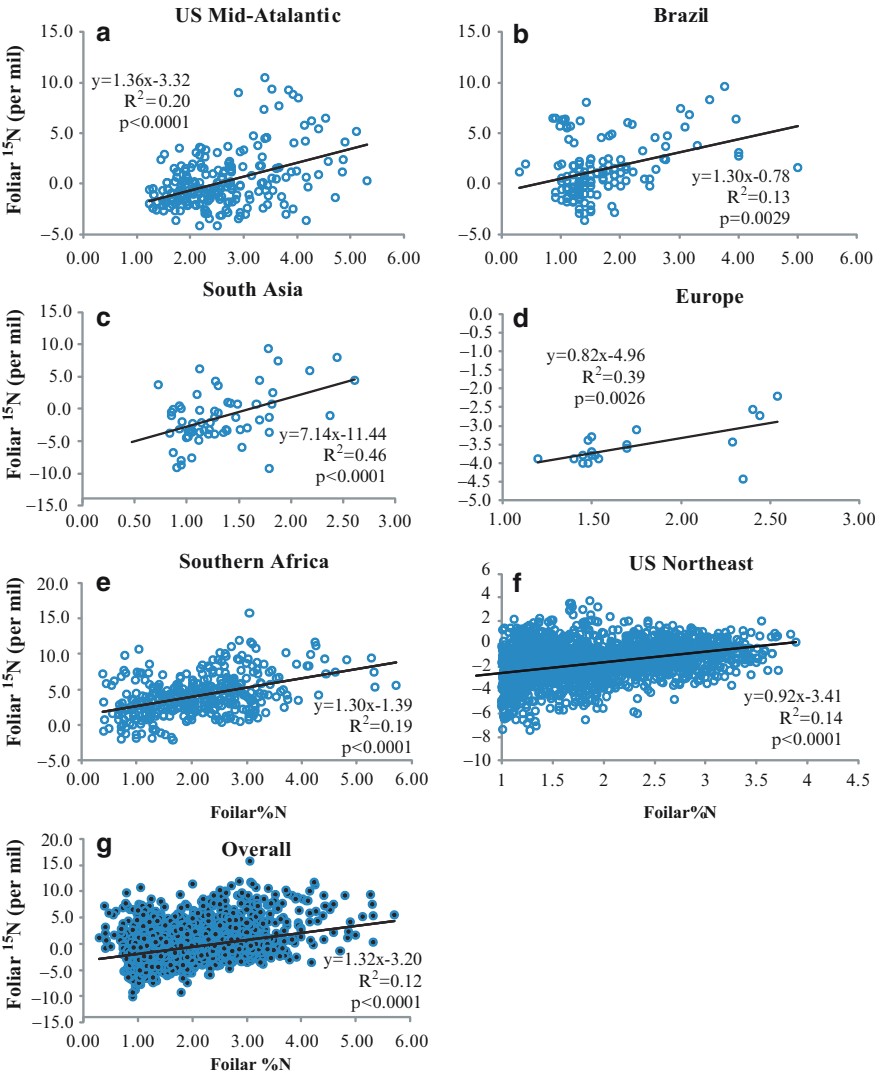

Fig. 3.5 The relationships between foliar d15N and foliar %N (excluding the nitrogen-fixing species) across different regions. Data are from (a) the US Mid-Atlantic succession fields and forests (Martinelli et al. 1999; Wang et al. 2007d), (b) the Brazilian savannas and rainforests (Bustamante et al. 2004; Martinelli et al. 1999), (c) the Asian forests and marshes (Martinelli et al. 1999; Tateno et al. 2003; Zhou et al. 2006), (d) European forests (Koerner et al. 1999; Martinelli et al. 1999), (e) the southern African savannas and woodlands (Aranibar and Macko 2005; Hogberg 1986, 1990, 1997; Hogberg and Alexander 1995; Schulze et al. 1991), (f) the US Northeast forests (Pardo et al. 2006) and (g) the overall dataset

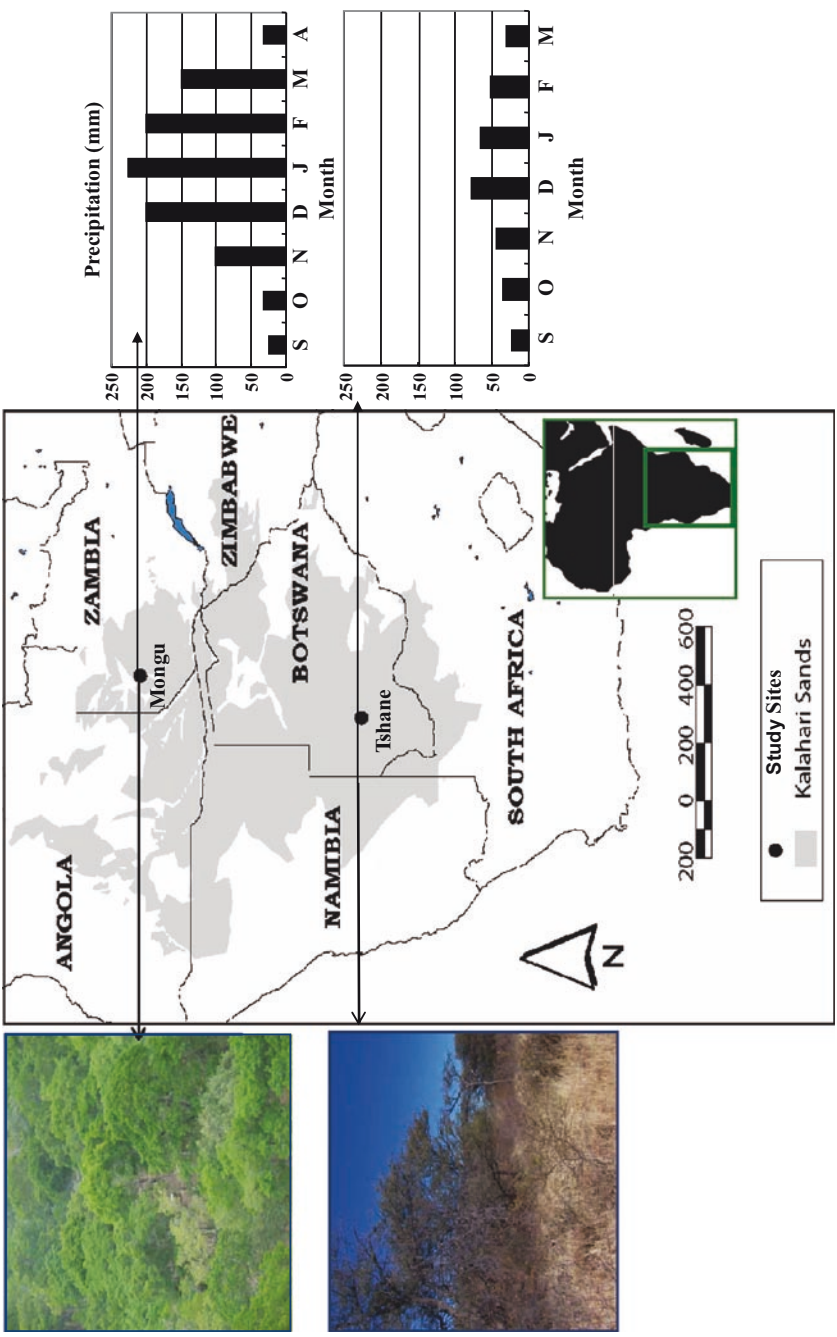

Fig. 3.6 Sampling locations, rainfall characteristics and satellite derived vegetation structure along the Kalahari Transect. The column charts are the mean annual monthly precipitation data (1961–1990) of the two sampling locations from Shugart et al. (2004)

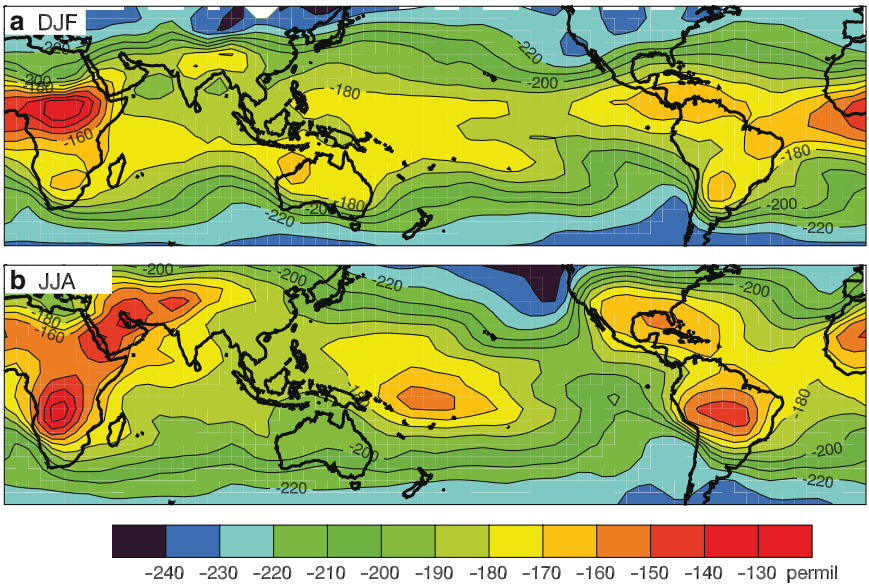

Fig. 4.6 DJF and JJA mean δD for the atmosphere between 800 and 500 hPa derived from the infrared spectra measured by the NASA Tropospheric Emission Spectrometer on the Aura spacecraft. Observations were taken between December 2004 and February 2008. Contour interval is 10‰ and the data are most reliable between 30°N and 30°S

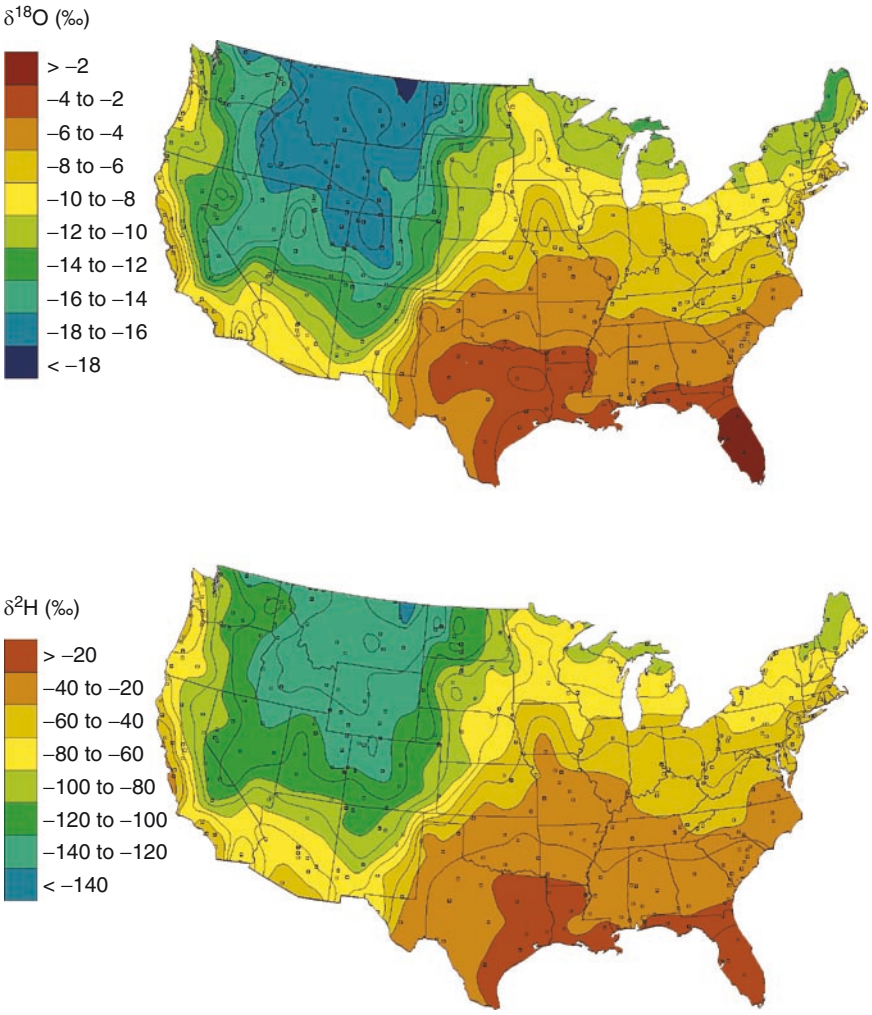

Fig. 5.2 Spatial distributions of discharge-weighted average water-$\delta^{18}O$ values for ~400 USGS NASQAN river sites, sampled 1987–1987; almost 5,000 samples were analyzed (Modified from Kendall and Coplen 2001)

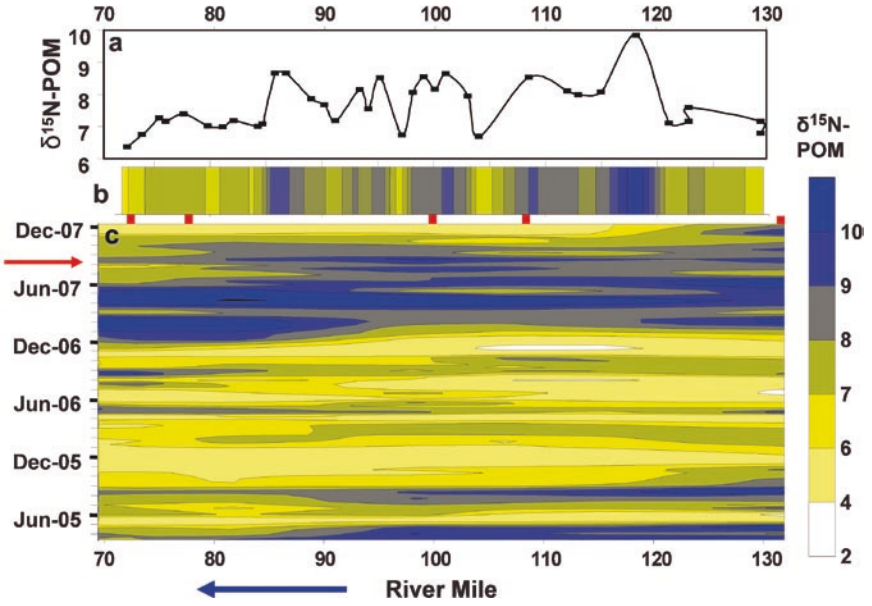

Fig. 5.3 Comparison of three different approaches for plotting $\delta^{15}N$ data for riverine POM samples from a 60 mile reach of the San Joaquin River. The lower the river mile number, the further downstream the location. The spatial distributions of $\delta^{15}N$ values from a boat synoptic in August 2007 are presented in two manners: (a) as a typical bivariate plot ($\delta^{15}N$ vs river mile), and (b) as gradational changes in color within a thin "band" representing the river channel. The spatial and temporal distributions of $\delta^{15}N$ values from five fixed-location monitoring sites (locations shown with red bars at the top of Fig. 5.3c) sampled ~ 75 times March 2005–December 2007 are shown in (c). The date of the August 2007 synoptic is shown with a red arrow to the left of the panel

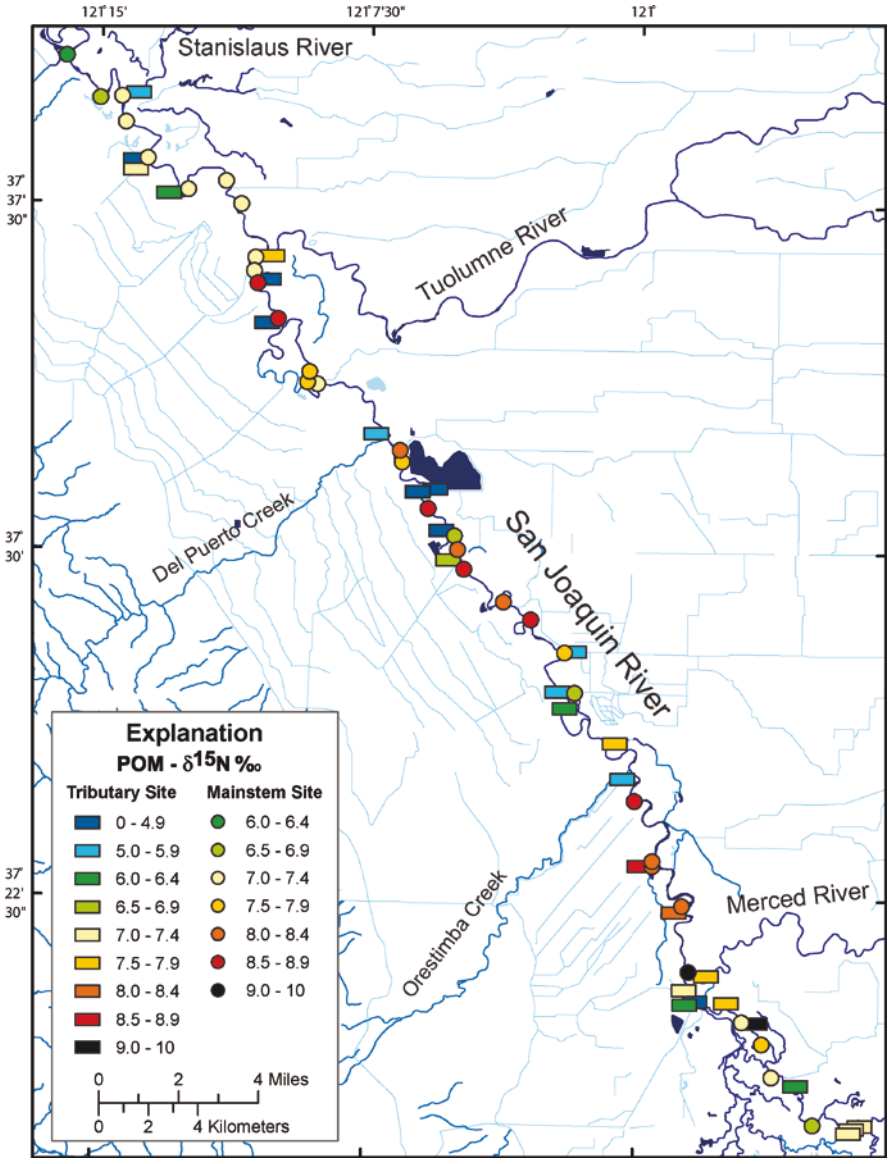

Fig. 5.4 Spatial distribution of POM-δ^{15}N values in the San Joaquin River collected during a synoptic in August 2007, plotted as a series of colored dots on a base map; these are the same data shown in Fig. 5.3a and b. δ^{15}N values for samples collected at the mouths of tributaries are plotted as colored rectangles. The positions of the rectangles relative to the San Joaquin River show whether the tributaries drain into the river from the E or W side

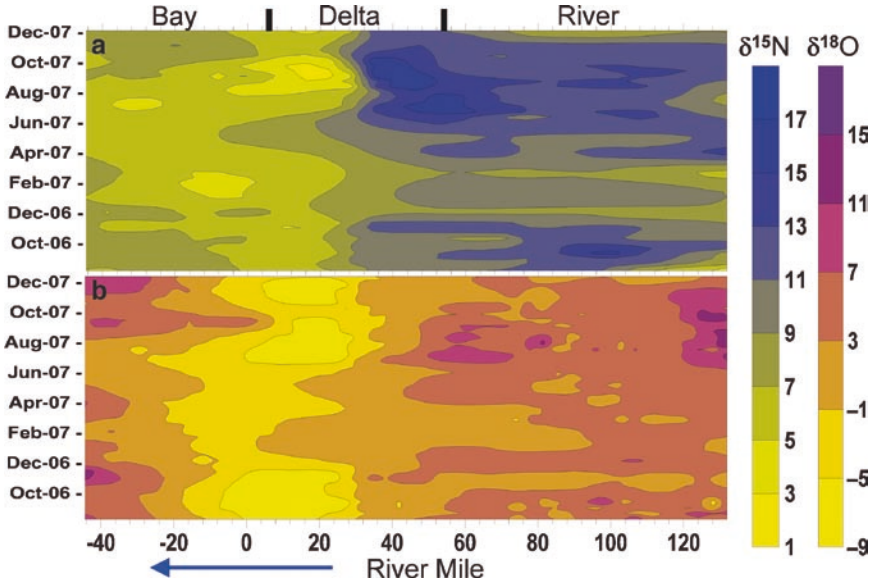

Fig. 5.5 Spatial and temporal distributions of nitrate $\delta^{15}N$ values (a) and nitrate $\delta^{18}O$ values (b) from 170 miles of river, extending from the headwaters of the San Joaquin River in agricultural return waters in the Central Valley, through the delta of the San Joaquin and Sacramento Rivers, and across the northern San Francisco Bay to where the estuary drains into the Pacific Ocean. The river miles are measured from where the river converges with the larger Sacramento River (=0). This plot reflects data from ~1,200 samples collected August 2006–December 2007)

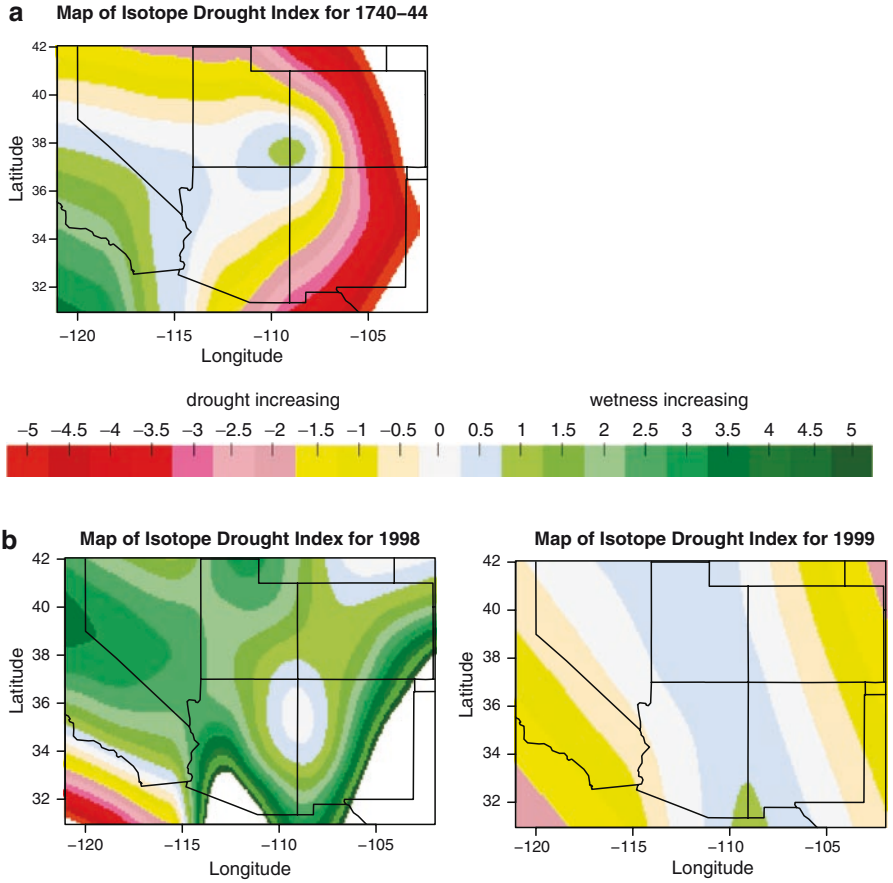

Fig. 6.3 Map of isotope "drought indices" from the initial pentad chronologies developed by Leavitt and Long (1989a) for 1740–44 (a) and for the more recently developed annual chronologies (Leavitt et al., 2007) for 1998 and 1999 (b). Maps of drought indices for 1998 when the Southwest had above-normal El Niño winter-spring precipitation prior to the 1998 growing season, and for the year 1999 when the Southwest had below-normal La Niña winter-spring prior precipitation. Outside the field of 14 sites, the high gradients of index change for 1740–44 and 1998 are extrapolations of trends within the network and may not be real; also the contouring is set to plot indices at an interval of 0.5 and only from −5 to +5

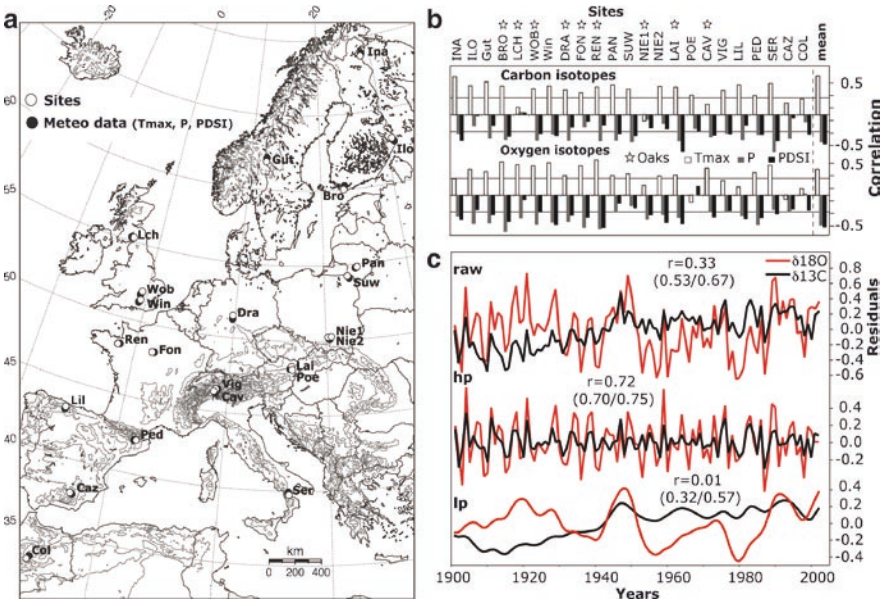

Fig. 6.6 (a) European tree sites and corresponding meteorological grid cells for the twentieth century with codes indicating site names; (b) site dependent June–August climate correlations of 'raw' carbon and oxygen isotope chronologies, with sites being latitudinally arranged (for detailed site information see Treydte et al. 2007); stars indicate oak sites (other sites are pine, and cedar in Morocco); 'mean' are correlations between mean isotope records averaged over all sites and mean meteorological data averaged over corresponding grid cells; lines are $p < 0.01$ significance levels; (c) 'European' carbon and oxygen isotope chronologies (each calculated by averaging site chronologies); 'raw' = residuals from 1901–1998 means, hp = high-pass filtered data; lp = low-pass filtered data; r = Pearson's correlation coefficient; numbers in brackets are r-values for the early AD 1901–1951 and the recent AD 1952–2002 period, respectively (from Treydte et al. 2007)

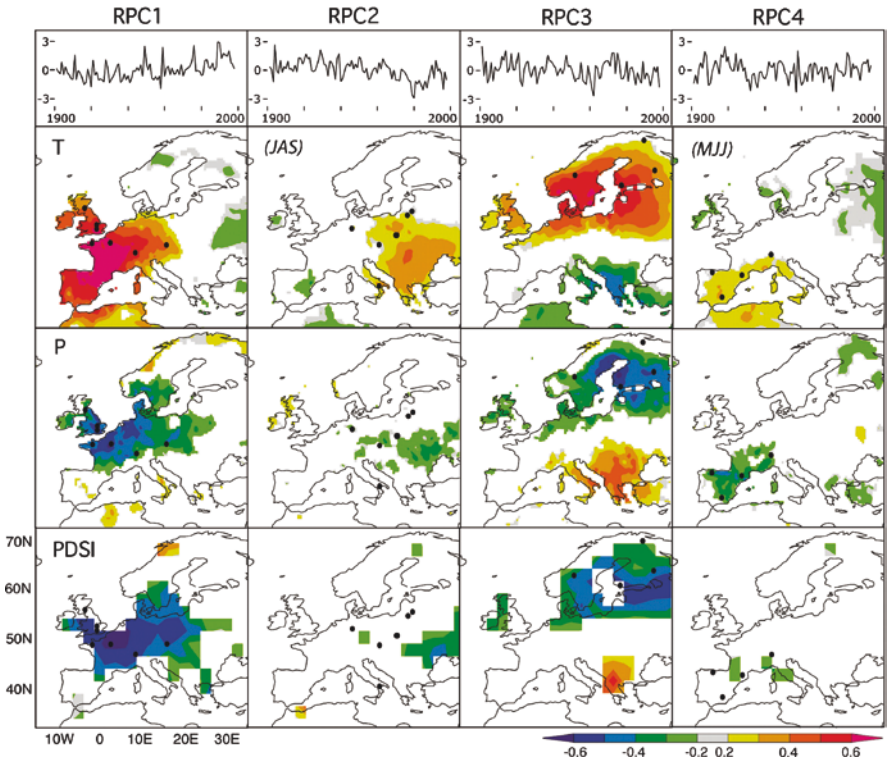

Fig. 6.7 Maps of sites with highest loading on varimax-rotated principal components, for the first four of five retained $\delta^{18}O$ chronology factors (RPC1-4) and corresponding spatial correlation fields maps for temperature (T), precipitation (P) and PDSI, calculated via the KMNI climate explorer (http://climexp.knmi.nl). Dots are sites with highest loadings at the corresponding RPCs (time series shown in the upper panel). Correlations were calculated with seasonal means of June to August (JJA), if not noted differently (JAS = July to September, MJJ = May to June). All calculations are based on the 1901–1998 common period (from Treydte et al. 2007)

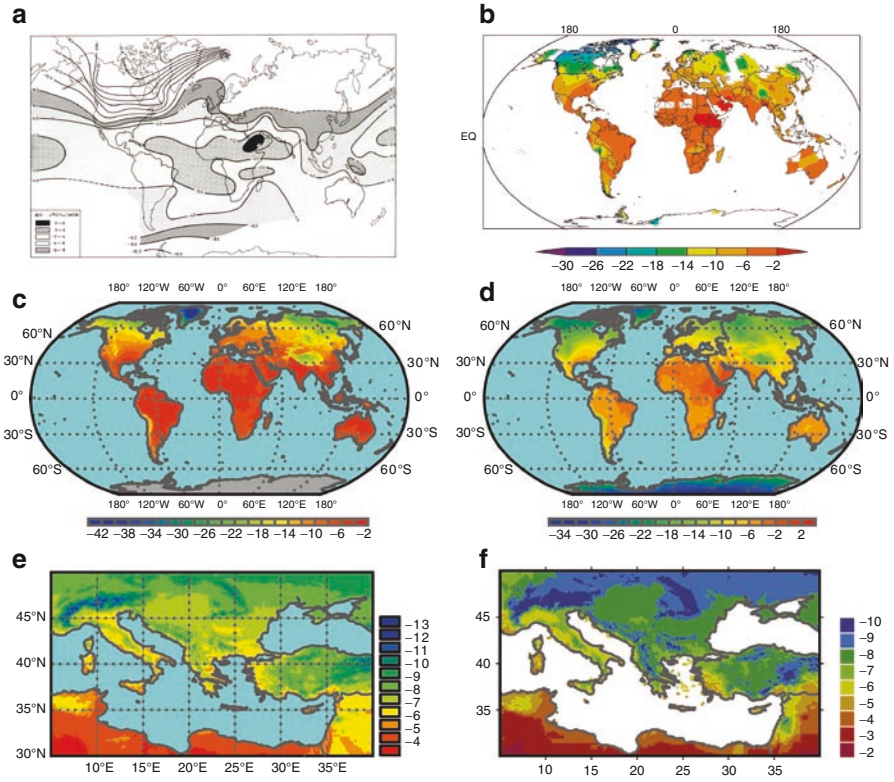

Fig. 7.4 Global and regional maps of mean annual $\delta^{18}O_p$ values. (a) An early contour map based on the GNIP station data (Yurtsever and Gat 1981). (b) Interpolated map generated by Cressman objective analysis (IAEA 2001; Birks et al. 2002). (c) A regression-model based map using the parameterization of Farquhar et al. (1993) in terms of mean annual temperature, precipitation amount, and elevation. Calculations were based on publically available gridded climate (New et al. 1999) and topographic data (U. S. National Geophysical Data Center 1998). (d) A hybrid geostatistical/regression map parameterized in terms of latitude and elevation, with interpolation by inverse distance weighting (http://waterisotopes.org; modified from Bowen and Revenaugh 2003). (e) Close-up of $\delta^{18}O_p$ values for the Mediterranean region from the map shown in panel d. (f) Regional map of $\delta^{18}O_p$ for the Mediterranean region based on a hybrid geostatistical/regression approach parameterized in terms of temperature and vapor pressure, with interpolation by ordinary Kriging with an exponential semivariogram model (Modified from Lykoudis and Argiriou 2007)

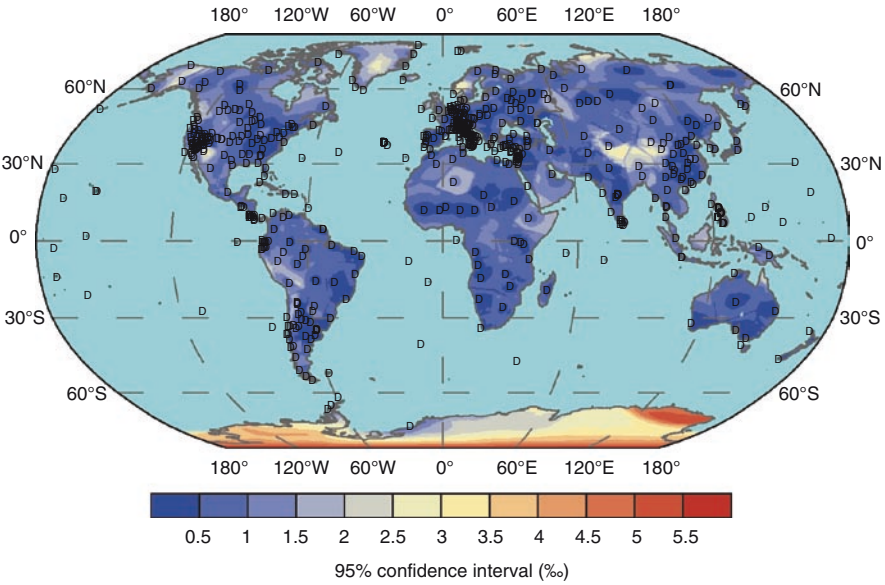

Fig. 7.7 Ninety-five percent confidence intervals for hybrid geostatistical/regression map shown in Fig. 7.4d (http://waterisotopes.org; modified from Bowen and Revenaugh 2003). Data station locations are shown by D's.

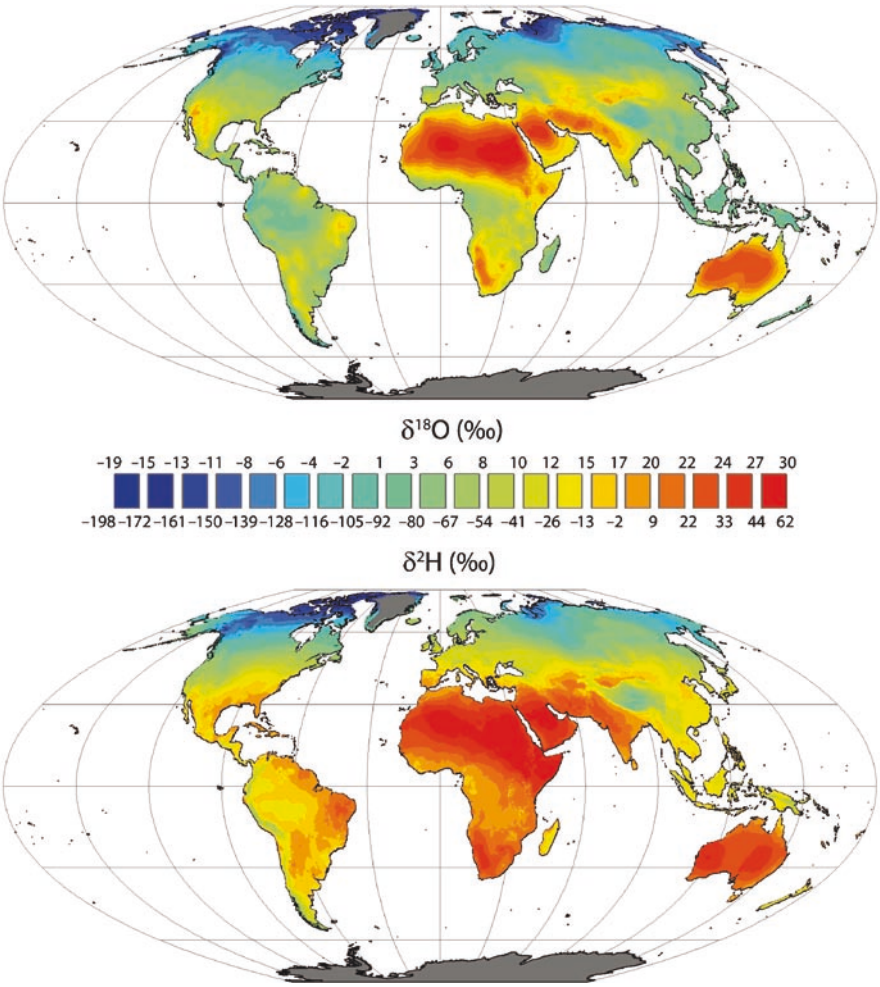

Fig. 8.1 Global mean annual average leaf water $\delta^{18}O$ and $\delta^{2}H$ isoscapes for the sites of evaporation within leaves (Eq. 8.1; reproduced with permission from West et al. 2008).

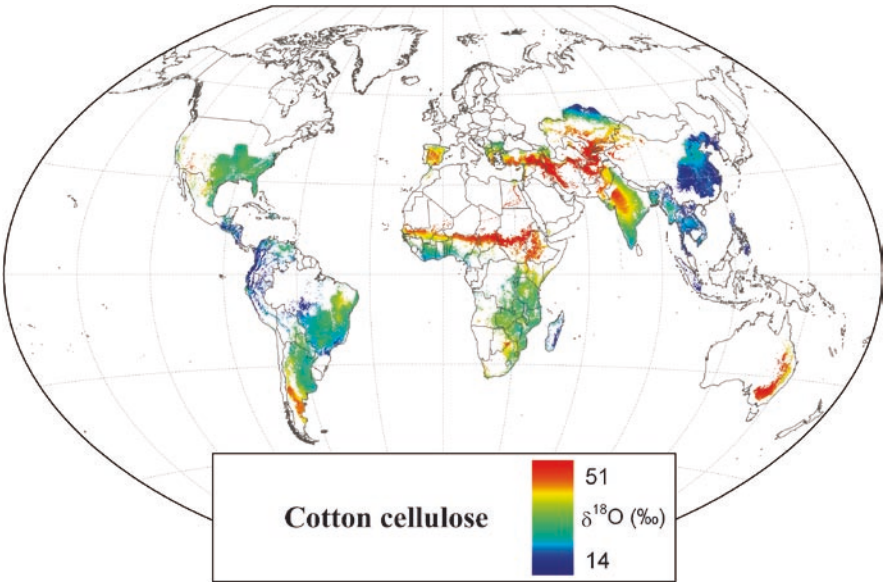

Fig. 8.2 Cotton $\delta^{18}O$ isoscape produced using a steady-state leaf water model (see Fig. 8.1), published fractionation factors for cellulose and masked for climate limitations and mapped agricultural production of cotton (see text for details).

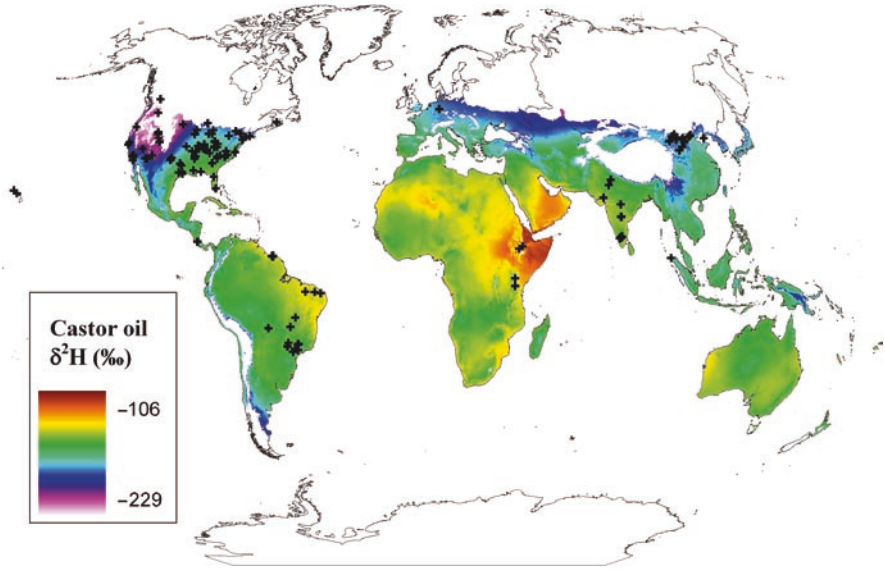

Fig. 8.3 Source water δ^2H and predicted castor oil δ^2H (‰) based on Eq. 8.5 determined from experimentally grown castor bean plants (see text). Land areas in white have mean annual temperatures below 7°C and are therefore unlikely to be regions where castor beans will grow. Continents are outlined in black. Locations of plants sampled and for which the δ^2H of extracted castor oil was determined are shown as black crosses

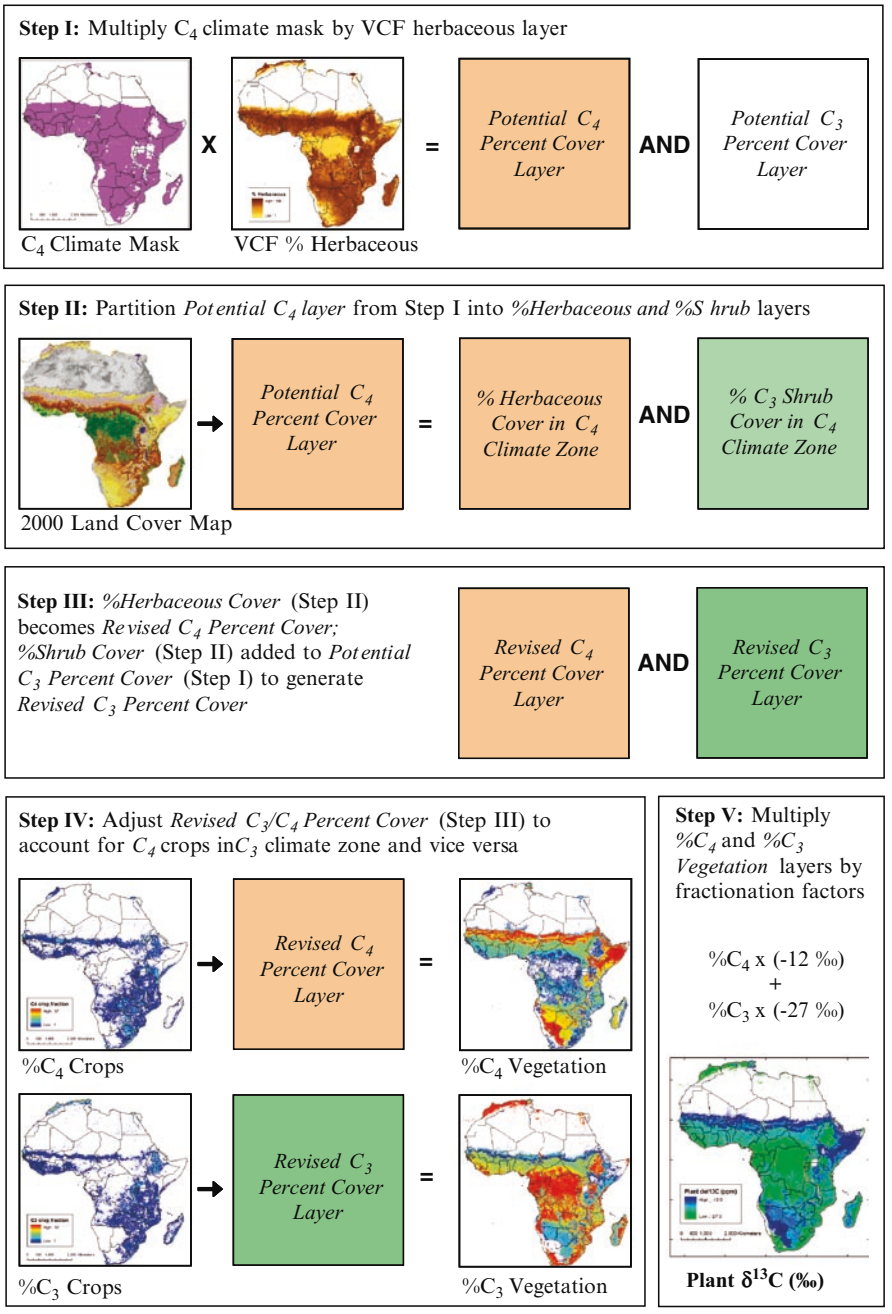

Fig. 9.1 Algorithm to predict vegetation C_3/C_4 composition and $\delta^{13}C$ (‰) content.

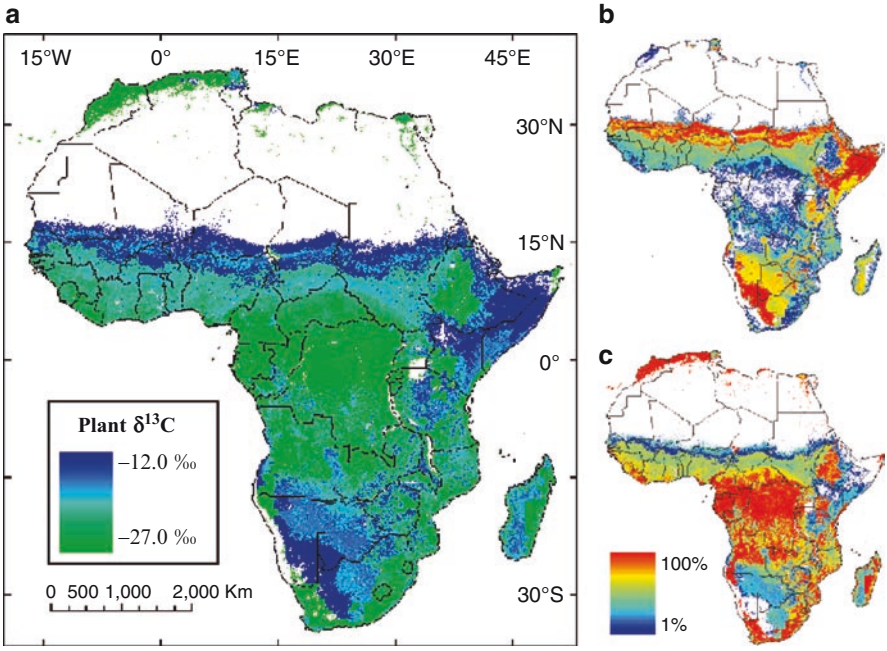

Fig. 9.2 (a) Stable carbon isotopic distribution for the African continent, (b) percentage of vegetation that uses the C_4 pathway, and (c) percentage of vegetation that uses the C_3 pathway

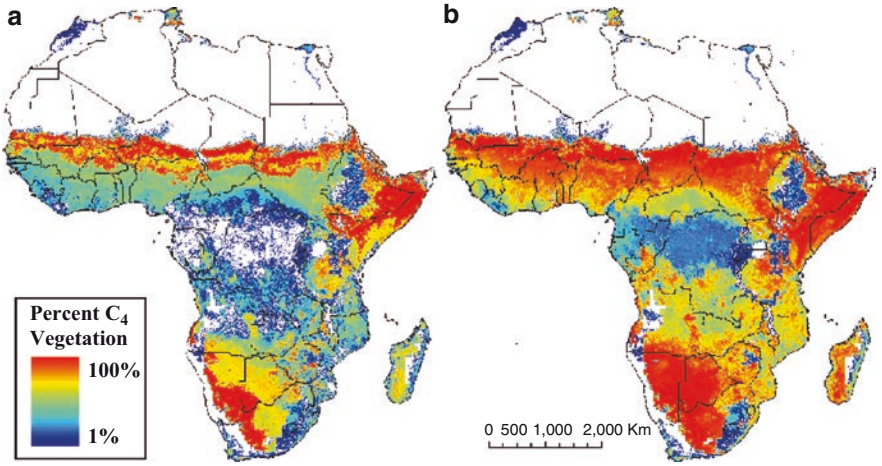

Fig. 9.3 (a) C_4 percent of vegetation with land-cover correction to partition shrubs and herbaceous cover. (b) C_4 percent of vegetation produced using the MODIS VCF herbaceous layer without land-cover correction

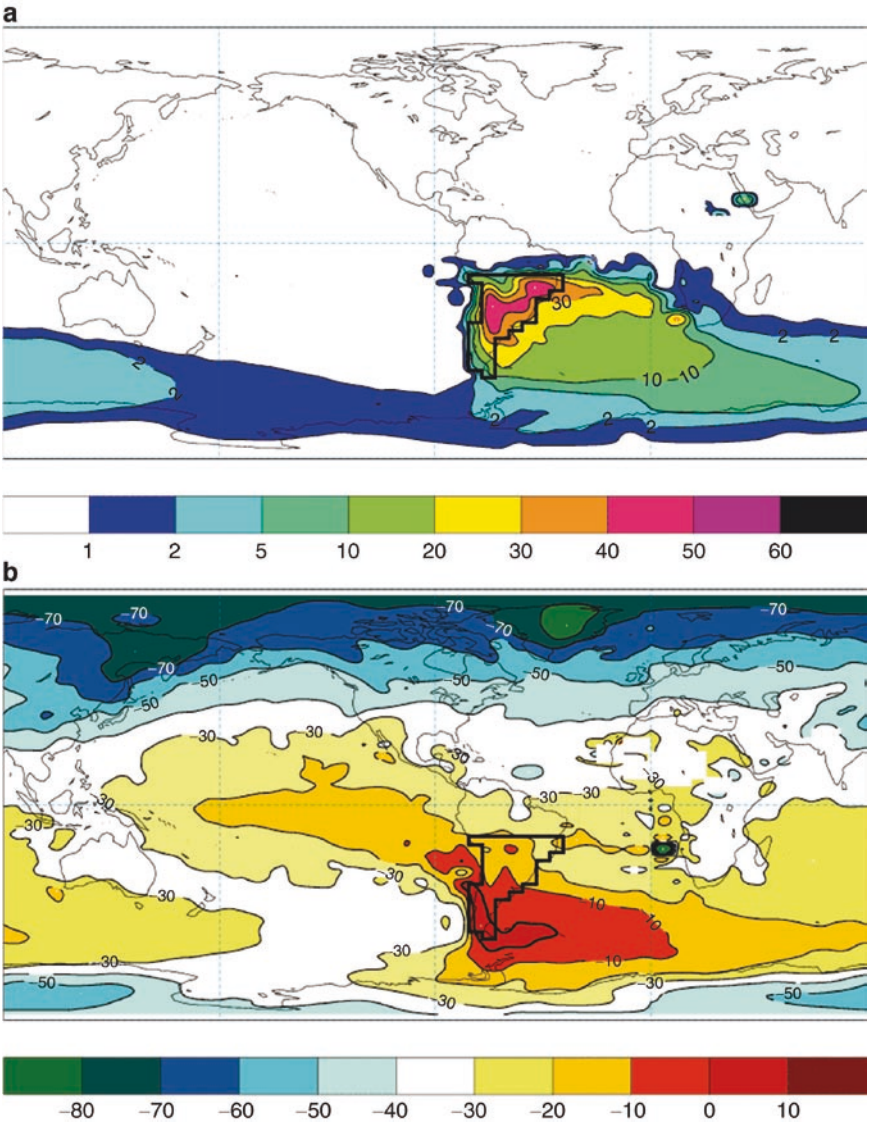

Fig. 10.1 (a) Percentage of precipitation that originated from evapotranspiration over a region in South America (shown as bold box) deduced using a non-fractionating water tracking scheme in the MUGCM (b) the isotopic composition of that water (Adapted from Noone and Simmonds 2002a)

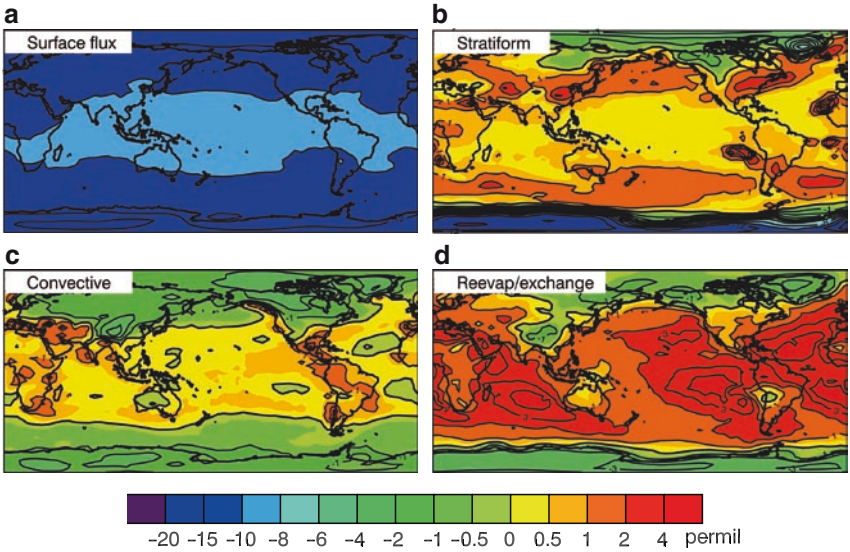

Fig. 10.2 Global model simulation of annual mean $\delta^{18}O$ in precipitation (‰) in a global isotope model with (a) fractionation only associated with surface evaporative sources and dew/frost sinks, (b) as in (a) but with fractionation also associated with stratiform condensation), (c) as in (a) but with fractionation also associated with convective condensation, and d) the influence of fractionation during exchange as raindrops fall from clouds. Panels (b) and (c) are differences relative to (a), and panel (d) is a difference relative to a control simulation that has all fractionations, and is shown in Fig. 10.4b. To the degree to which the model results are linear, the (weighted) sum of all four components composes the total isotope signal.

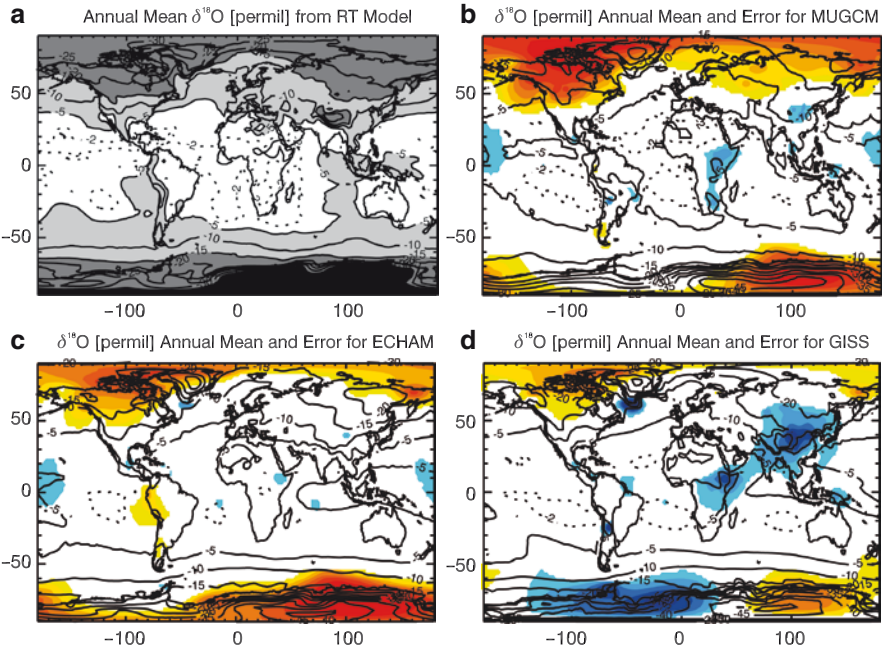

Fig. 10.4 Simulations of $\delta^{18}O$ in precipitation from three atmospheric models (MUGCM, ECHAM and GISS) participating in the first Stable Water-isotope Intercomparison Group (SWING) experiment, and from the observationally based regression model of Buenning and Noone (in review). Contour interval is 4‰ with extra contours at −2‰ and 0‰. Shading in panels (b–d) show where the models deviate from the GNIP data by more than 1‰. (red positive and blue negative) with gradations of 1‰ (Courtesy N. Buenning 2008)

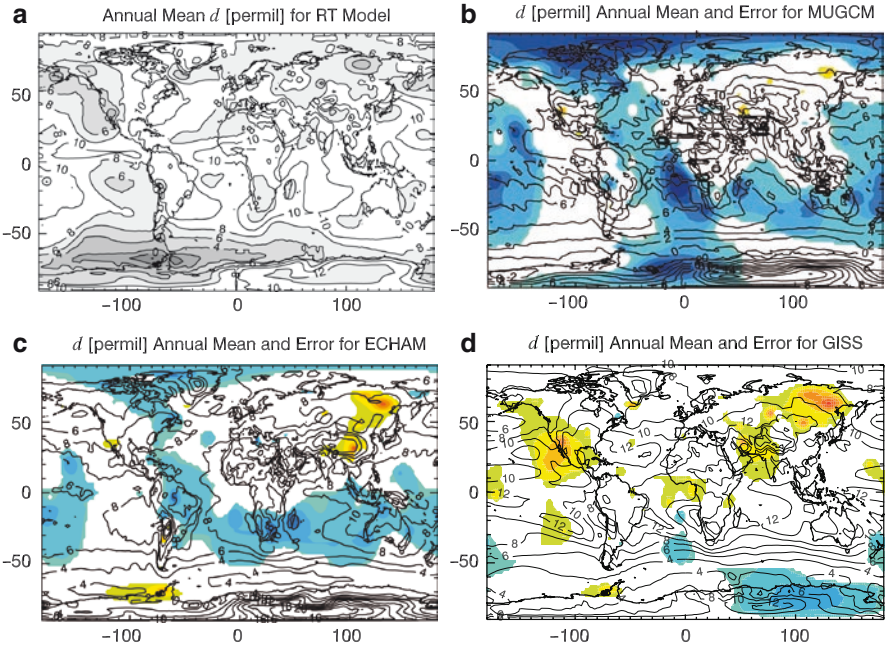

Fig. 10.5 As in Fig. 10.4 but for deuterium excess in precipitation. Contour interval is 1‰. Light shading in panels (b–d) show where the models deviate from the observations by less than −2‰, and dark shading shows where there differ by more than +2‰ with gradations of 1‰ (Courtesy N. Buenning 2008)

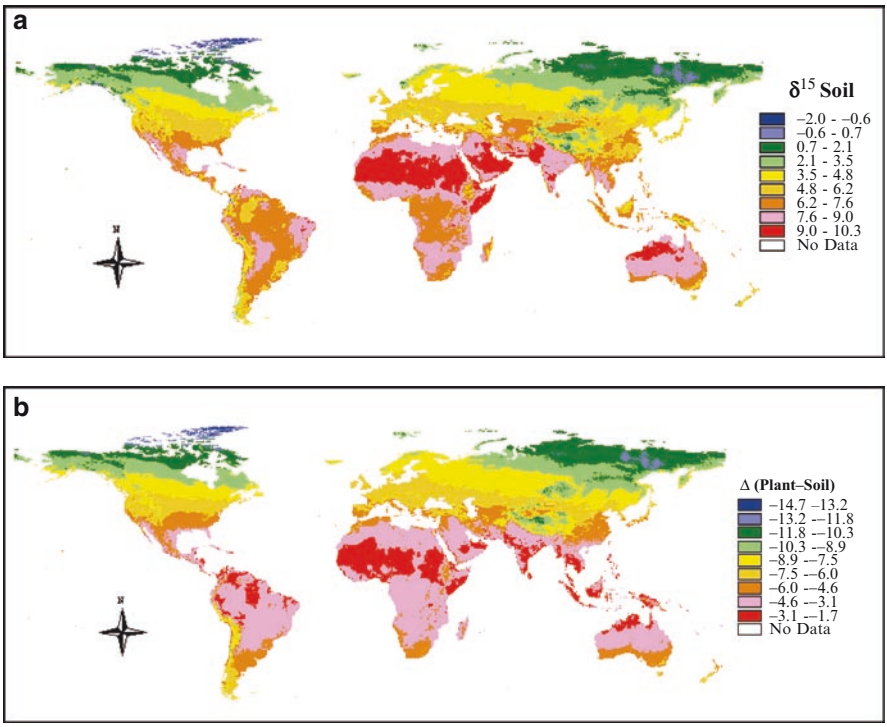

Fig. 11.5 (a) Estimated geographical distribution of soil $\delta^{15}N$ values to 50 cm (b) estimated geographical trends in $\Delta\delta^{15}N$plant-soil (From Amundson et al. 2003. Copyright (2003) American Geophysical Union. Reproduced by permission of American Geophysical Union)

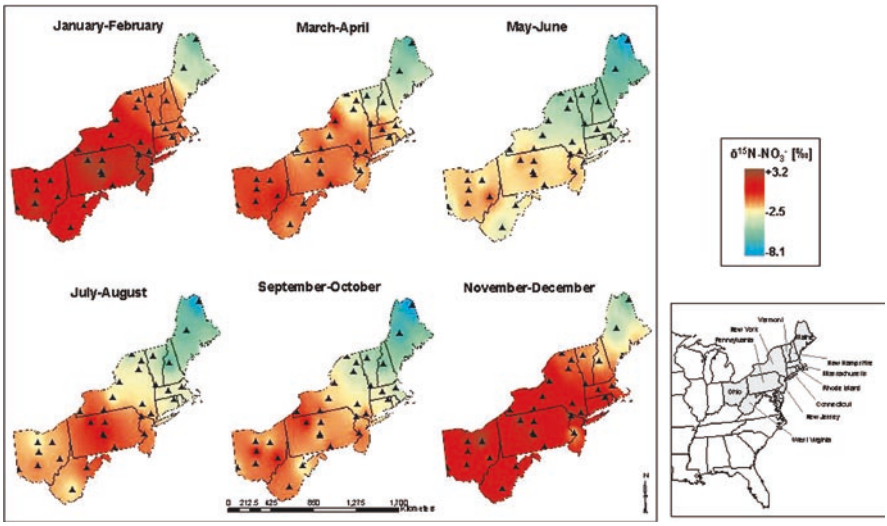

Fig. 11.6 Bimonthly, volume-weighted $\delta^{15}N$ values of precipitation NO_3^- at 30 sites in the northeastern US (From Elliott et al. 2007)

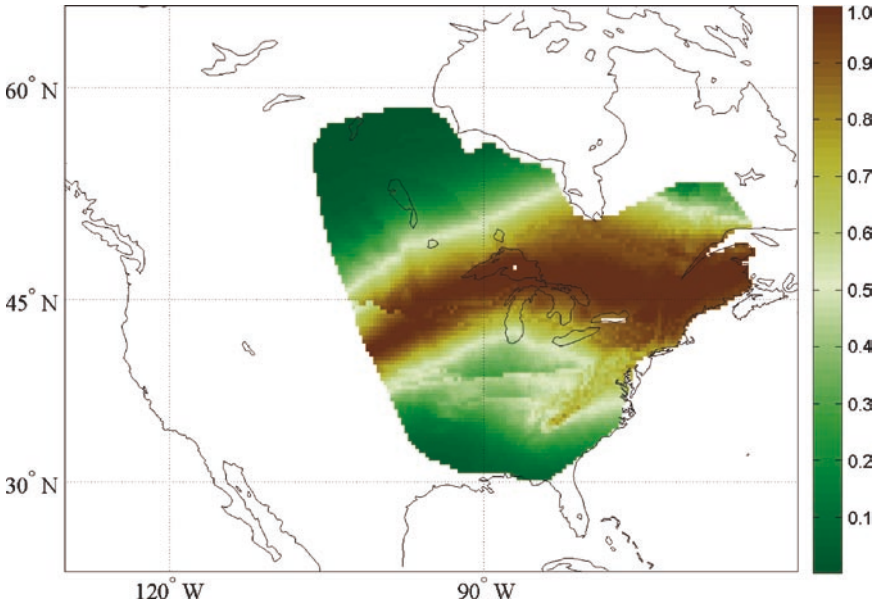

Fig. 12.2 Probability density surface for a hypothetical adult bird feather of unknown origin with $\delta^2H = -75‰$ modeling bulk variance from the calibration shown in Fig. 12.1. The geography of possible origins for the feather is restricted to the hypothetical breeding range chosen to represent a generic migratory bird that breeds in the eastern deciduous forests of North America. For presentation purposes, the density value for each pixel in the probability surface has been rescaled by the largest observed density value

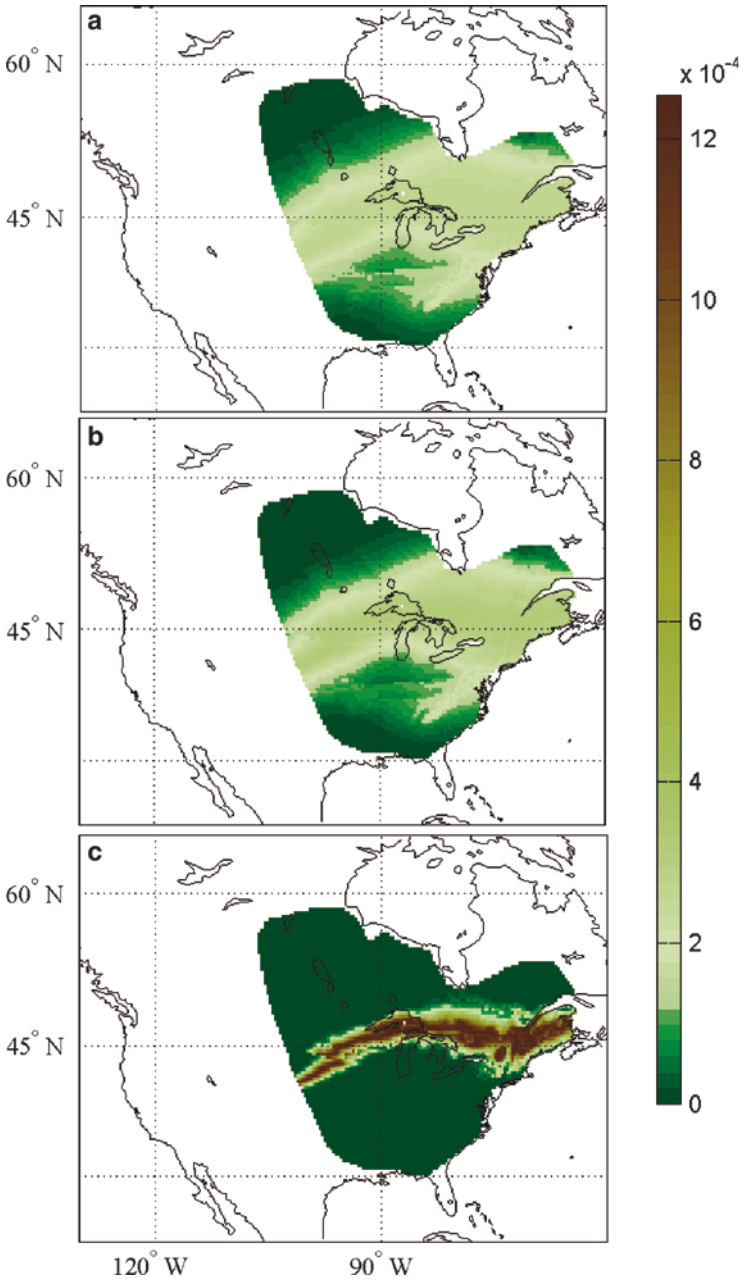

Fig. 12.3 (a) Probability density surface for an adult bird feather of unknown origin with measured $\delta^2H = -75‰$ using a hierarchical model for two sources of variance; one from measurement errors in the lab and the other from among individual differences at a single location. The geography of possible origins for the feather is additionally restricted as described in Fig. 12.2. (b) Probability density surface for the same adult bird feather ($\delta^2H = -75‰$) and hierarchical model, but setting

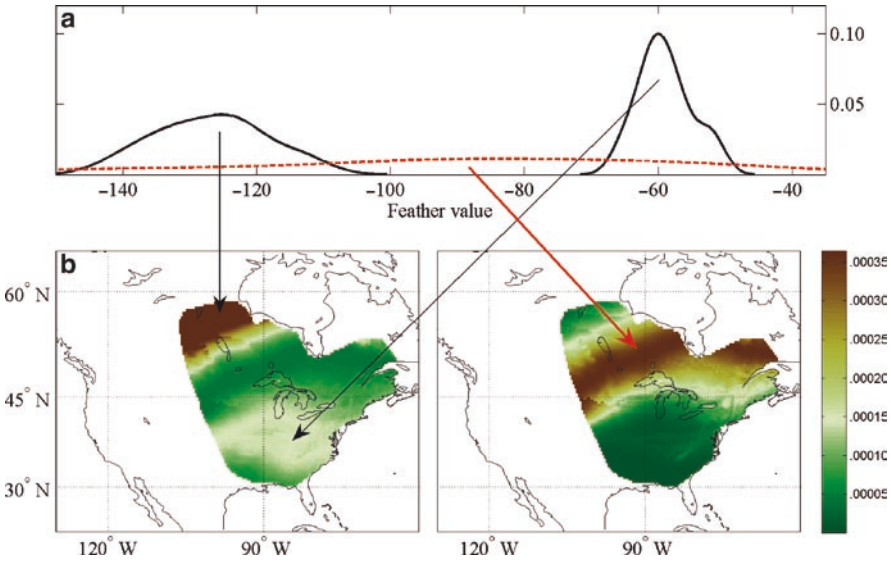

Fig. 12.5 (a) Simulated feather δ^2H data from a mixture of two normal random variables. Solid black line shows the probability density for δ^2H based on the true bimodal distribution for the simulated feather data. Dashed red line indicates the probability density for δ^2H when assuming a normal distribution with a single mode. (b) Probability density surface constructed from densities modeled separately for each individual sample. Posterior density shown is average of all individual densities normalized by the sum of all individual densities, clearly showing bimodal structure in geographic space corresponding to bimodal structure in isotope space. Black arrows link modes in isotope space with those in geographic space. (c) Probability density surface using mean and standard deviation of simulated samples, showing single geographic mode corresponding to single mode in isotope space, with most of the mass where no actual data exist. Red arrow links center of mass in isotope space with that in geographic space

Fig. 12.3 (continued) the parameter for analytical error to zero. This illustrates the gains in geographic precision from improving lab practices for measuring δ^2H to the point of perfect repeatability among samples. (c) Probability density surface for the same adult bird feather (δ^2H = −75‰) and hierarchical model, but setting the parameter for within-location variance to zero, and restoring the original parameter value for analytical error (see text). This illustrates the gains in geographic precision from improving mechanistic understanding of the variance-generating processes to the point of perfect prediction, but still allowing for measurement error in the lab. All probability densities appear on the same scale as defined by the color bar.

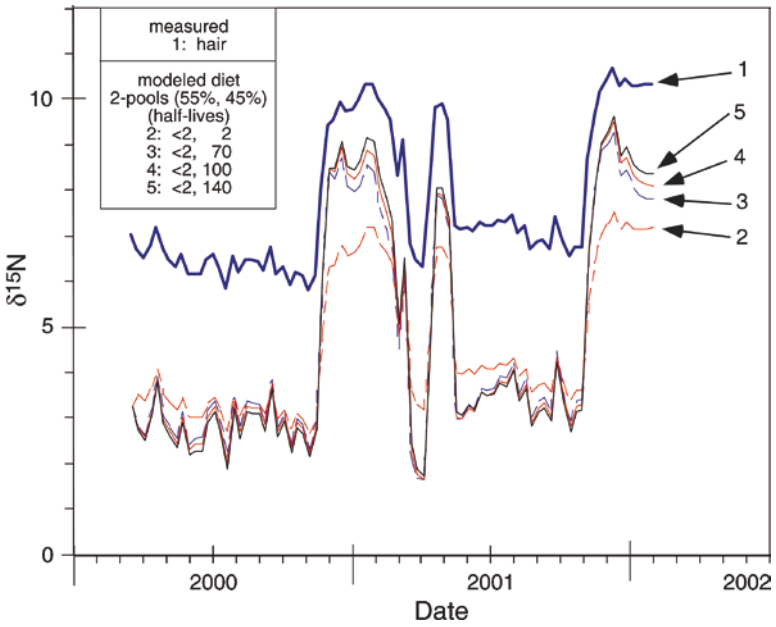

Fig. 13.1 Measured hair values from a migrating African elephant and modeled diets using the 2-pool model described in text. Migration was from a region of high $\delta^{15}N$ values to one of low $\delta^{15}N$ values; transit time between the regions was less than 12 h based on GPS observations (Cerling et al. 2006). Model results are for "one-pool" (all half-lives less than sampling interval), and three scenarios where the long pool had 50% contribution but half-lives of 70, 100, and 140 days, respectively. This sensitivity study shows that the multiple pool model is different than the single pool model, but that the length of the long pool is less important than the fact that there are two pools present

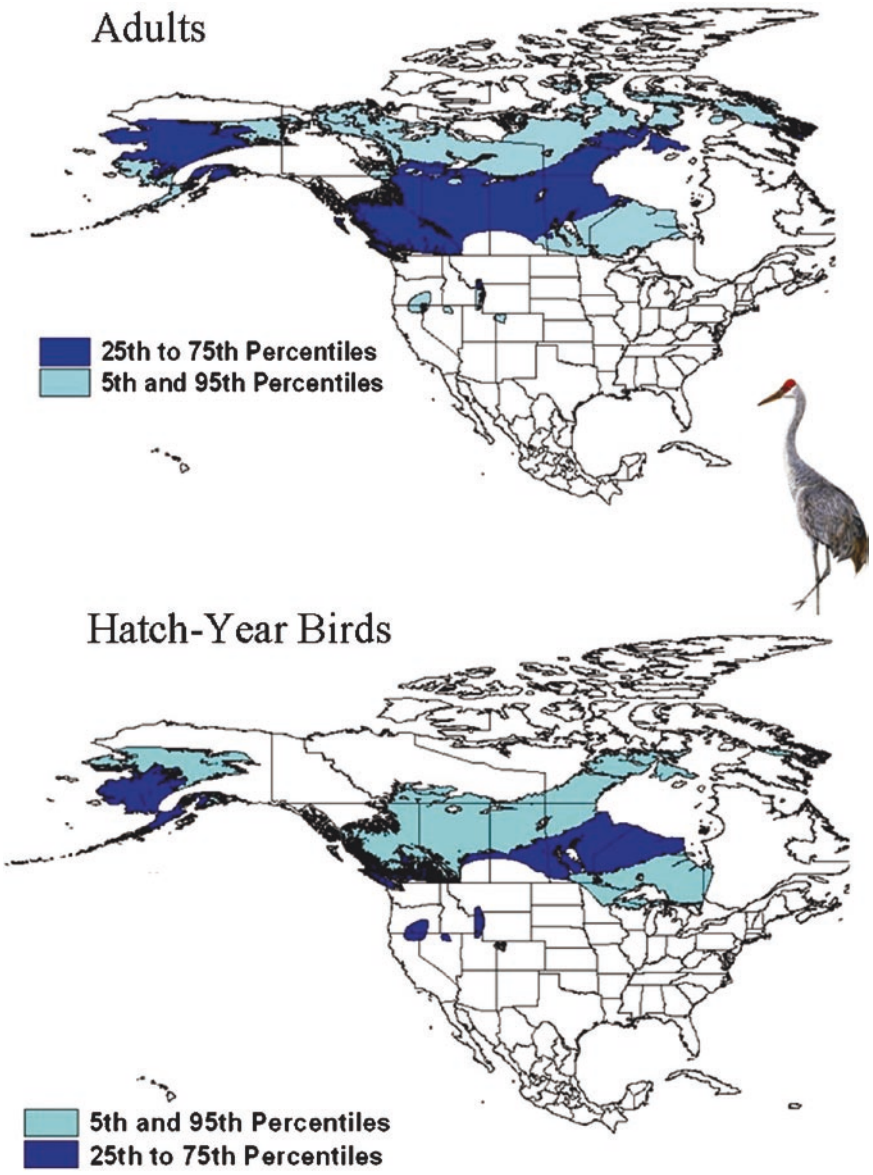

Fig. 13.2 Depictions of the origins of adult and young-of-the-year Sandhill Cranes based on the distributions of their feather δD values and the use of a feather δD isoscape in turn derived primarily from the GNIP database. This figure illustrates one means of depicting origins of migratory organisms without error propagation. Results are based on Hobson et al. (2006) who examined over 700 individuals harvested by hunters in the Central Flyway and provide important conservation information on where most young were produced

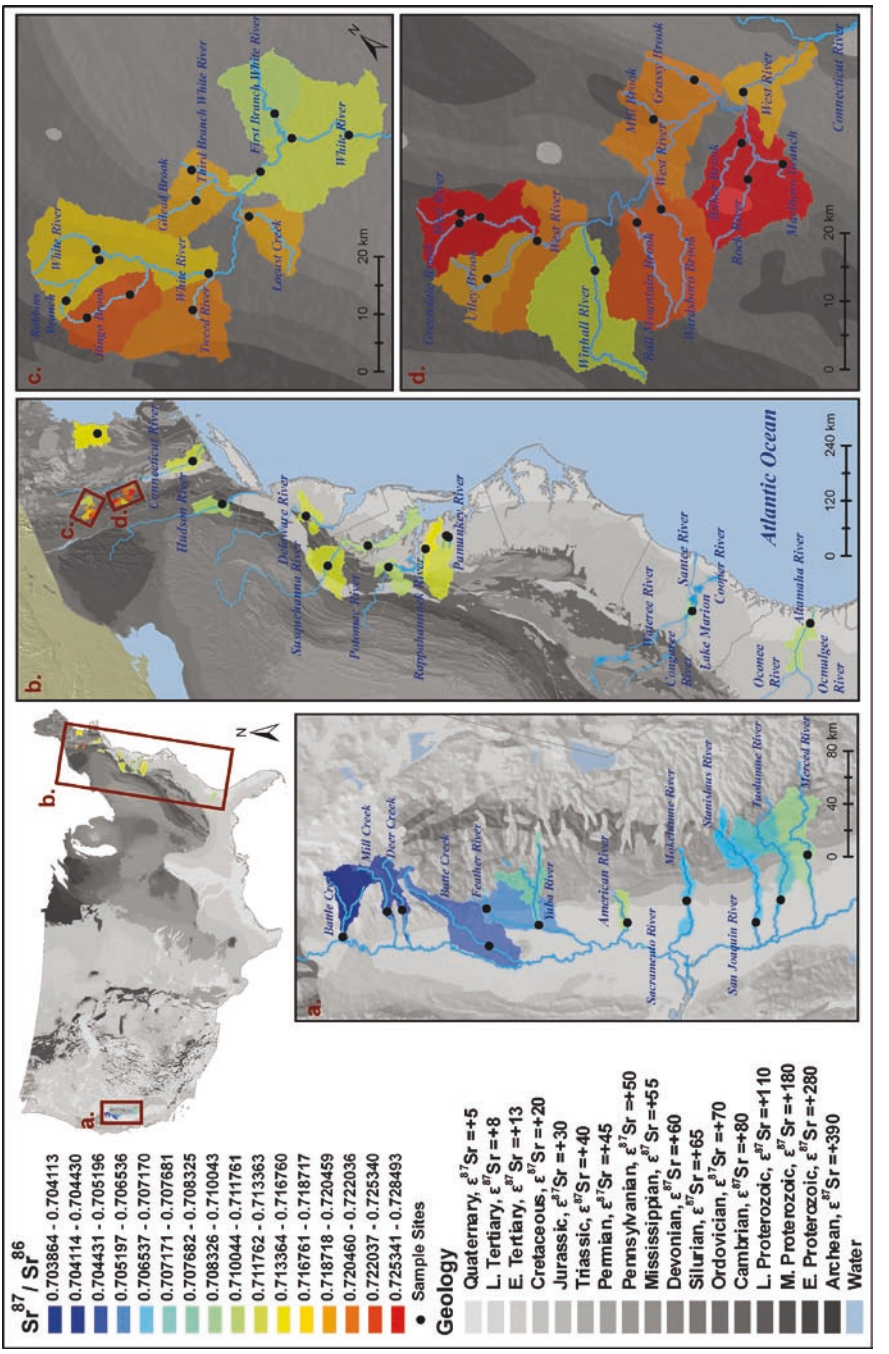
Sr^{87}/Sr^{86}
0.703864 - 0.704113
0.704114 - 0.704430
0.704431 - 0.705196
0.705197 - 0.706536
0.706537 - 0.707170
0.707171 - 0.707681
0.707682 - 0.708325
0.708326 - 0.710043
0.710044 - 0.711761
0.711762 - 0.713363
0.713364 - 0.716760
0.716761 - 0.718717
0.718718 - 0.720459
0.720460 - 0.722036
0.722037 - 0.725340
0.725341 - 0.728493
Sample Sites
Geology
Quaternary, $\varepsilon^{87}Sr$ =+5
L. Tertiary, $\varepsilon^{87}Sr$ =+8
E. Tertiary, $\varepsilon^{87}Sr$ =+13
Cretaceous, $\varepsilon^{87}Sr$ =+20
Jurassic, $\varepsilon^{87}Sr$ =+30
Triassic, $\varepsilon^{87}Sr$ =+40
Permian, $\varepsilon^{87}Sr$ =+45
Pennsylvanian, $\varepsilon^{87}Sr$ =+50
Mississippian, $\varepsilon^{87}Sr$ =+55
Devonian, $\varepsilon^{87}Sr$ =+60
Silurian, $\varepsilon^{87}Sr$ =+65
Ordovician, $\varepsilon^{87}Sr$ =+70
Cambrian, $\varepsilon^{87}Sr$ =+80
L. Proterozoic, $\varepsilon^{87}Sr$ =+110
M. Proterozoic, $\varepsilon^{87}Sr$ =+180
E. Proterozoic, $\varepsilon^{87}Sr$ =+280
Archean, $\varepsilon^{87}Sr$ =+390
Water
a.
b.
c.
d.
Battle Creek
Mill Creek
Deer Creek
Feather River
Yuba River
American River
Sacramento River
Mokelumne River
Stanislaus River
San Joaquin River
Tuolumne River
Merced River
0 40 80 km
Atlantic Ocean
Ocmulgee River
Altamaha River
Ocmulgee River
Ocmee River
Cooper River
Lake Marion
Santee River
Congaree River
Pamunkey River
Rappahannock River
Potomac River
Susquehanna River
Delaware River
Hudson River
Connecticut River
0 120 240 km
Robium Branch
White River
Unga Brook
Tweed River
White River
Gilead Brook
Third Branch White River
Locust Creek
First Branch White River
White River
0 10 20 km
Ompompanoosuc River
Ulley Brook
West River
Winhall River
Bald Mountain Brook
Barrows Brook
Rock Brook
Mill Brook
West River
Grassy Brook
West River
Meadows Branch
Connecticut River
0 10 20 km

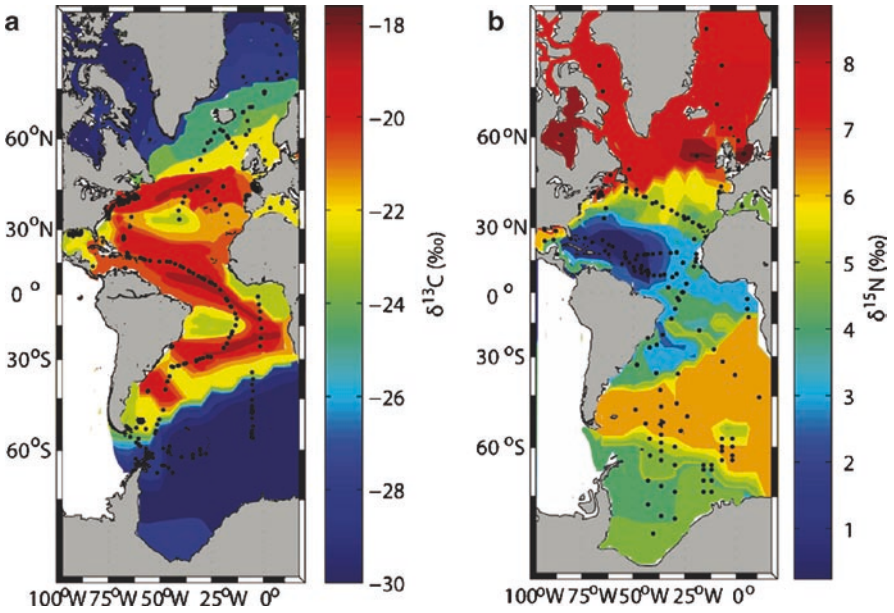

Fig. 14.1 Contour plots of isotope values in the Atlantic Ocean from a meta-analysis of published data. (a) d13C values of plankton from the upper ocean (0–500 m; n = 425) (b) d15N values of zooplankton, primarily calanoid copepods, from the upper ocean (0–500 m; n = 198). Black dots indicate sample locations (Data are from McMahon et al. (in review))

Fig. 13.4 Strontium isoscape highlighting first-order Sr variations ($\varepsilon^{87}Sr$) inferred by age variations in basement rocks (grey-scale; modified from Beard and Johnson 2000) and empirical measures of $^{87}Sr/^{86}Sr$ for watersheds (black circles and grey-scale) in insets from studies on Chinook salmon (Oncorhynchus tshwaytcha) in the California Central Valley (a; Barnett-Johnson et al. 2008), American shad (Alosa sapidissima) along the Atlantic coast (b; Walther and Thorrold 2008), and Atlantic salmon (*Salmo salar*) in the Connecticut River Basin, Vermont (**c** and **d**; Kennedy et al. 2000). Data synthesis and GIS map courtesy of Corey Phillis and Matthew Jones. Note: $\varepsilon^{87}Sr$ notation defined by Beard and Johnson (2000) as: $\varepsilon^{87}Sr = [(^{87}Sr/^{86}Sr)_{predicted}/(^{87}Sr/^{86}Sr)_{bulk\ earth} - 1] \times 10{,}000$ where $[^{87}Sr/^{86}Sr]_{predicted}$ is the $^{87}Sr/^{86}Sr$ value modeled by assuming a fixed initial $^{87}Sr/^{86}Sr$ and ^{87}Rb and Sr content and using the known decay rate for ^{87}Rb and rock ages and $[^{87}Sr/^{86}Sr]_{bulk\ earth}$ is equal to 0.7045,

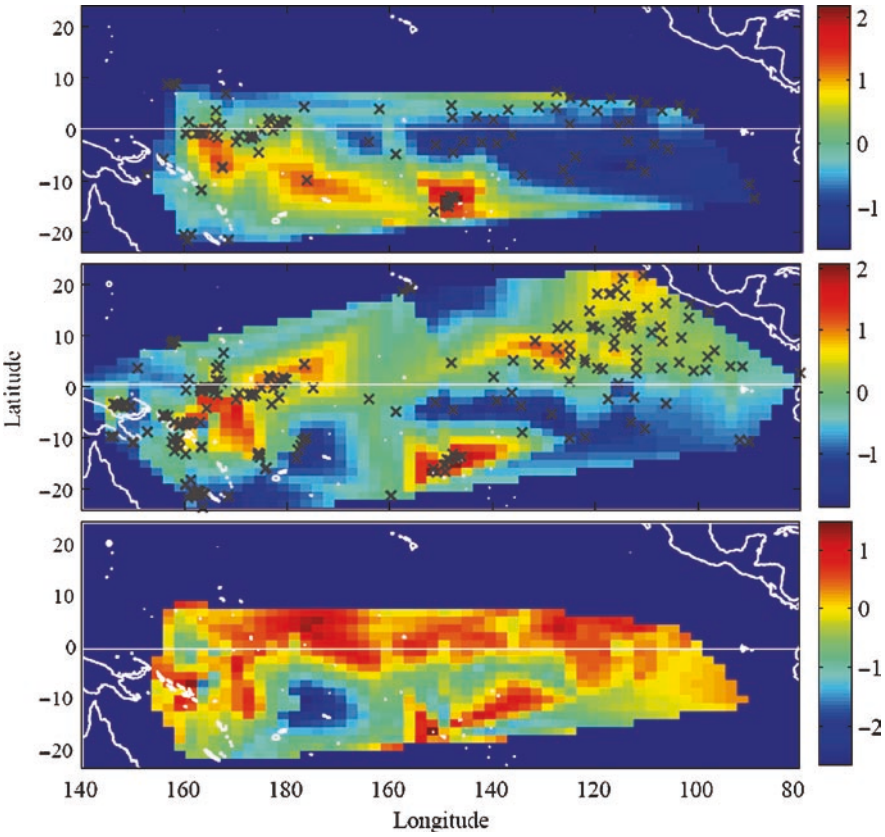

Fig. 14.5 $\delta^{15}N$ isoscapes for (a) bigeye (n = 196) and (b) yellowfin (n = 387) tuna. Crosses indicate sample locations. Samples collected in the eastern tropical Pacific represent a composite of ~five individuals. The $\delta^{15}N$ values for each species were normalized against the average value for that species within the study region. (c) A map of the residuals between the interpolated $\delta^{15}N$ values for the two species (i.e., observable difference between the normalized values). Regions with positive residuals represent areas where the $\delta^{15}N$ values of YFT are greater than BET and negative residuals represent areas where the $\delta^{15}N$ values of BET are greater than YFT (Data are from Graham et al. (2009))

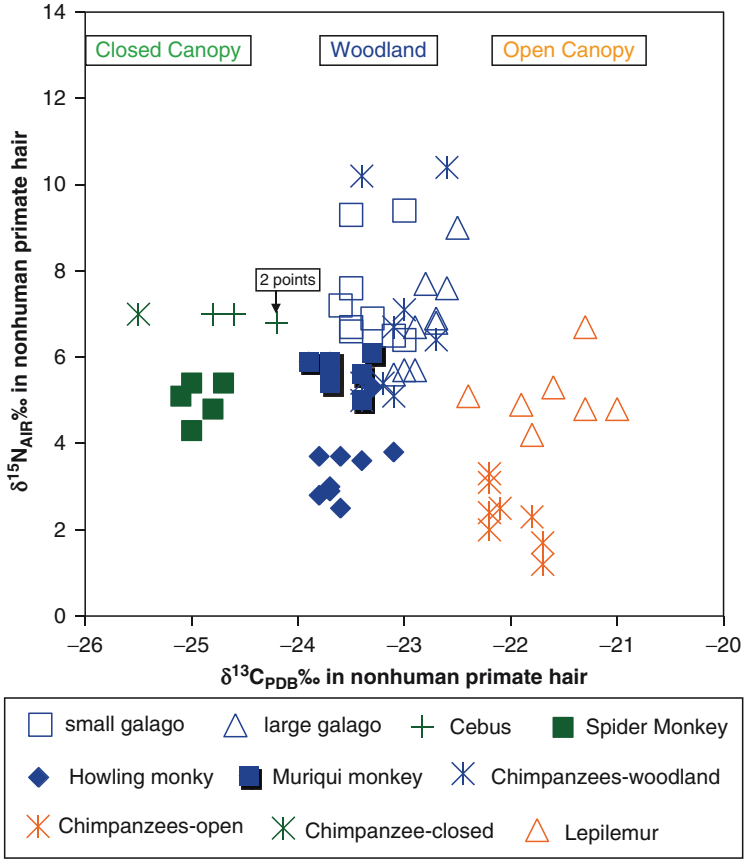

Fig. 15.1 $\delta^{13}C$ values in hair from across primate species reflect the level of canopy cover in the areas in which the animals lived irrespective of their specific diets (indicated by $\delta^{15}N$ values, see text for discussion). Two species of New World monkeys from closed canopies show values around −26‰ to −24.5‰. Two other species of New World monkeys, two species of African prosimians, and a population of chimpanzees, which all live in deciduous woodland regions show values around −24‰ to −23‰. One species of prosimian from Madagascar and a population of chimpanzees living in open canopy savanna-woodland habitats have values between −22 and −21‰ (Data from Schoeninger et al. 1997, 1998, 1999

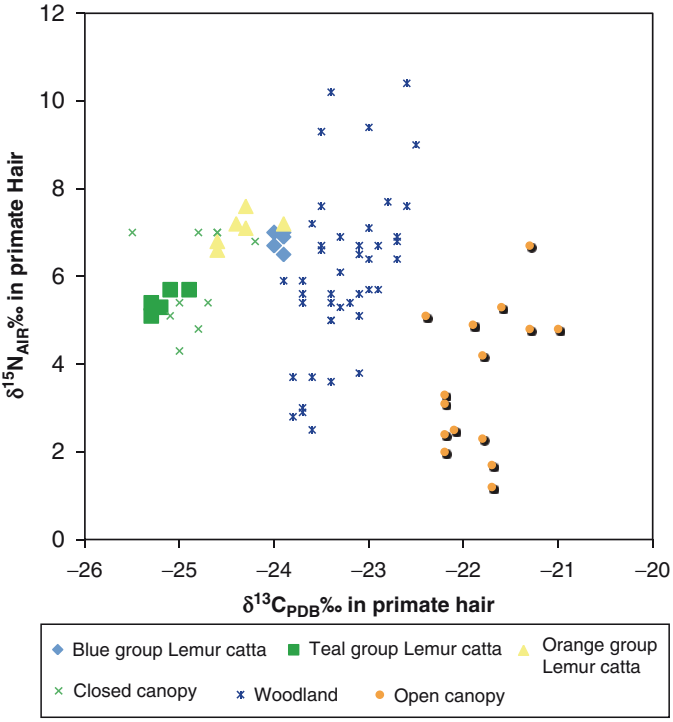

Fig. 15.2 Comparison of $\delta^{13}C$ values in three populations of ring-tailed lemurs from Madagascar (Loudon et al. 2007). The Teal group from undisturbed habitats compares favorably with closed canopy primates discussed for Fig. 15.1 and replotted here. The Blue group from the most disturbed habitat compares well with deciduous woodland canopy primates replotted here from Fig. 15.1. The Orange group comes from forest edge and disturbed habitats and plots between the other two groups

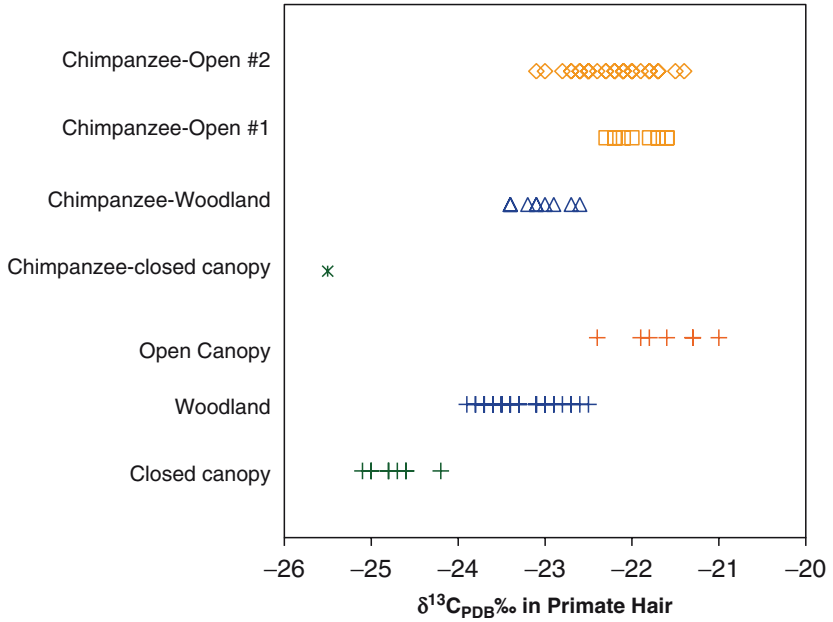

Fig. 15.3 Comparison of $\delta^{13}C$ values in chimpanzees from the open canopy savanna-woodland habitat of Fongoli in Senegaal (Sponheimer et al. 2006) with those of other chimpanzee populations discussed for Fig. 15.1 and replotted here. The Fongoli chimpanzee data overlap those from the Ugalla, Tanzania site, which also a savanna-woodland and those from Ishasha, DRC, which is a deciduous woodland habitat. Pictures of the Fongoli site show areas of tall trees as well as open woodland and open grassland regions. Regrettably, it is not possible to compare the chimpanzee hair values with specific regions at Fongoli

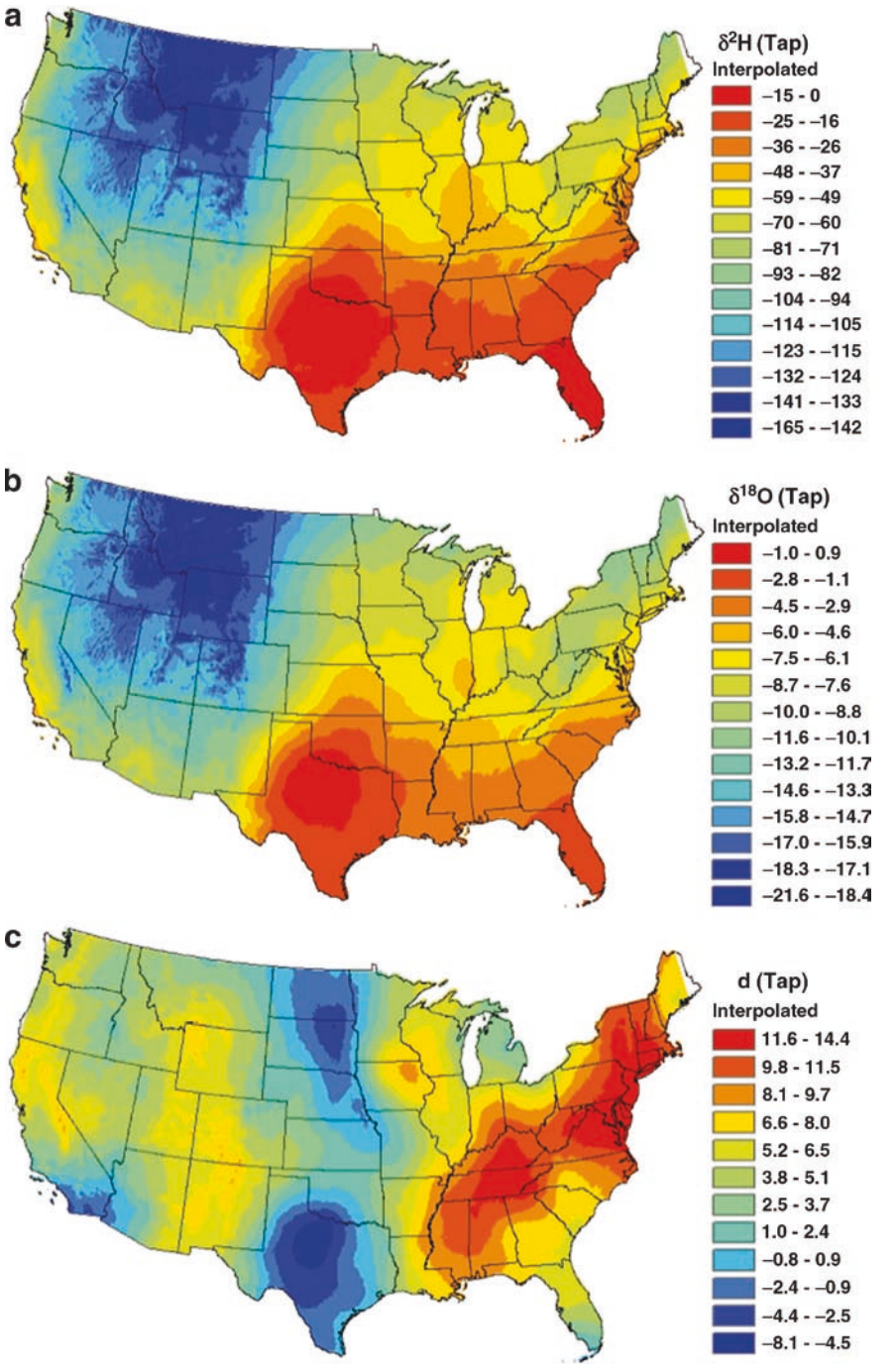

Fig. 17.3 Prediction maps showing estimated isotope ratios (a: δ^2H, b: $\delta^{18}O$) and deuterium excess values (c) for tap water in the contiguous United States (Methods details are available in Bowen et al. 2008 and at http://waterisotopes.org)

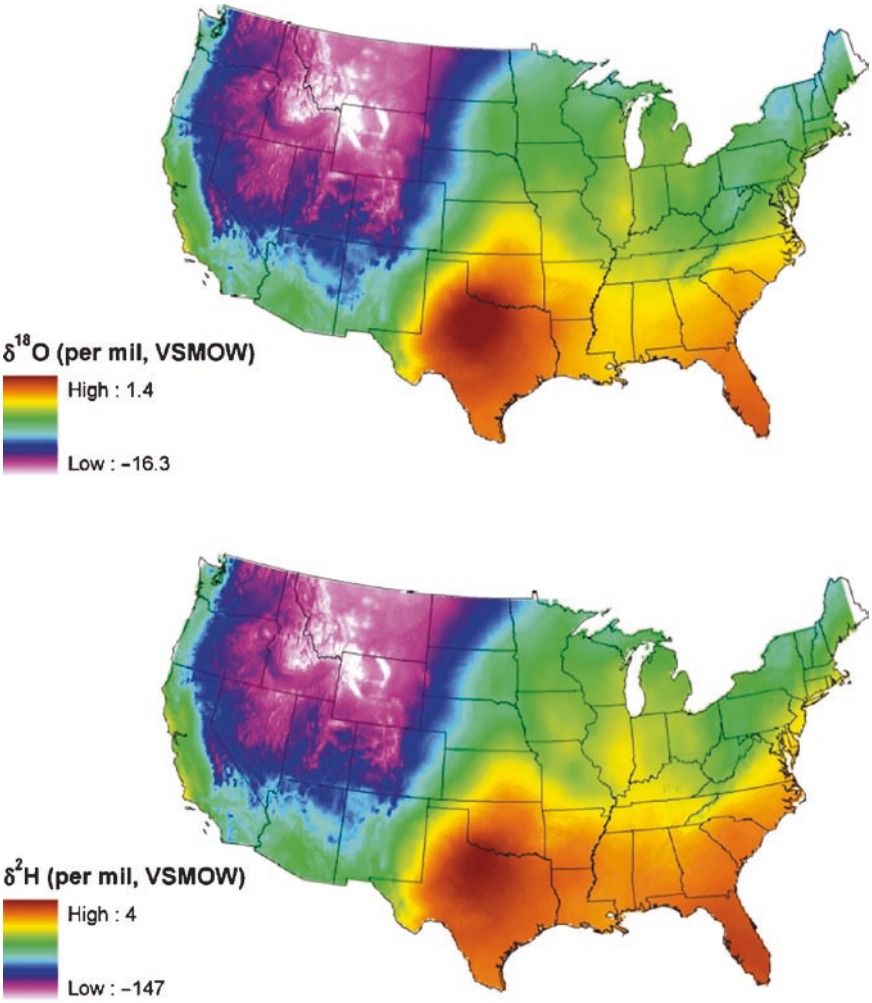

Fig. 17.4 Predicted average hydrogen and oxygen isotope ratios of body water across the USA (After Podlesak et al. in review)

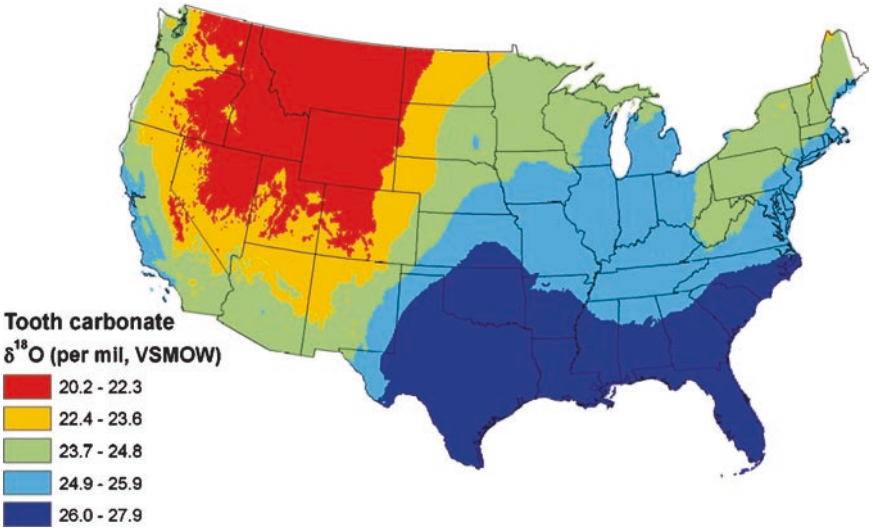

Fig. 17.6 The predicted distribution of oxygen isotope ratios of carbonates in enamel from human teeth across the contiguous USA

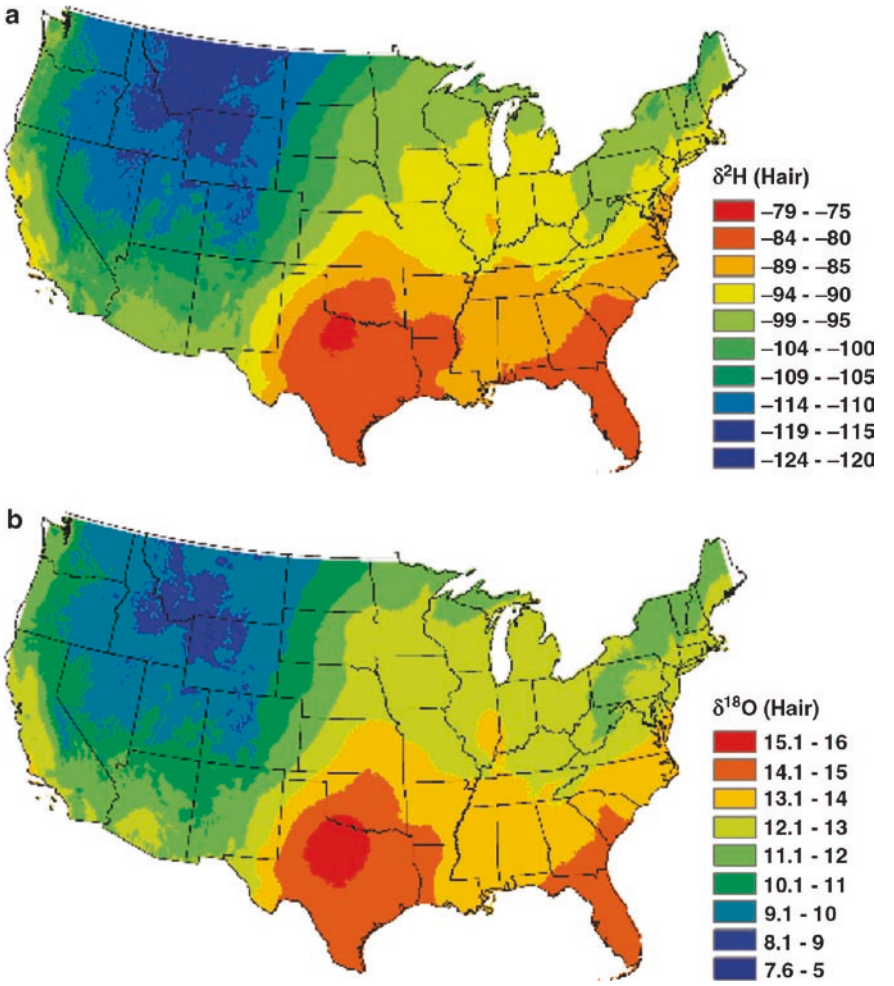

Fig. 17.7 The predicted geographic distribution of the hydrogen (a) and oxygen (b) isotope ratios in human hair across the USA (From Ehleringer et al. 2008)

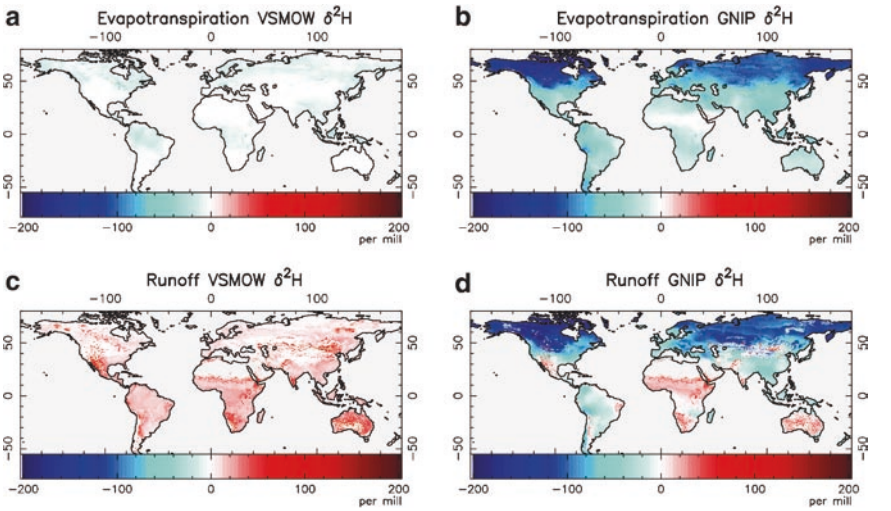

Fig. 18.2 Global isotope simulations using the iWBM distributed hydrology model. Shown are the isotopic composition of evapotranspiration using (a) constant V-SMOW precipitation, (b) GNIP precipitation climatology, runoff (c) constant V-SMOW precipitation and (d) GNIP precipitation climatology. The left panels illustrate modeled isotopic separation from precipitation, whereas the right panels show predicted isotopic compositions that might be measured in nature. These effectively constitute a spatial hypothesis awaiting verification when global observations become available (Reprinted from Fekete et al. 2006, Application of isotope tracers in continental scale hydrological modeling, Journal of Hydrology, vol. 330, p. 452, Copyright 2006, with permission from Elsevier)

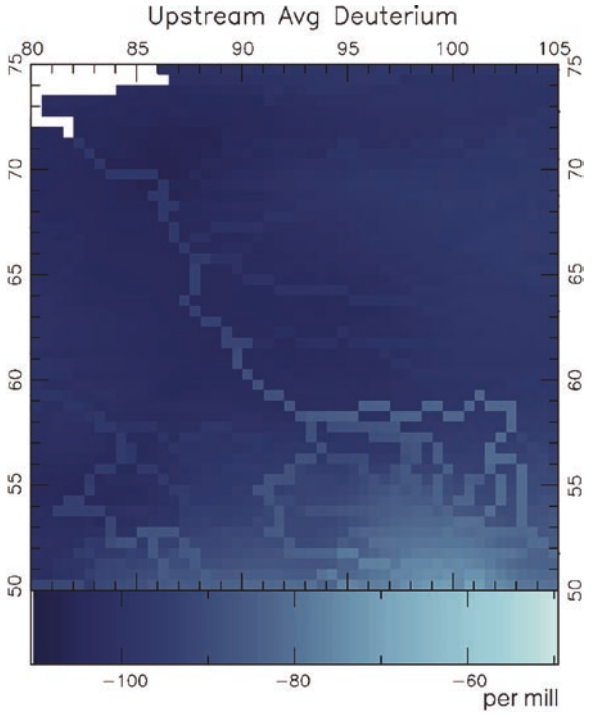

Fig. 18.3 Average, runoff weighted hydrogen isotopic composition of the precipitation in the Yenisei basin in Mongolia and Siberia, propagated down a river network derived from a 30' digital elevation model

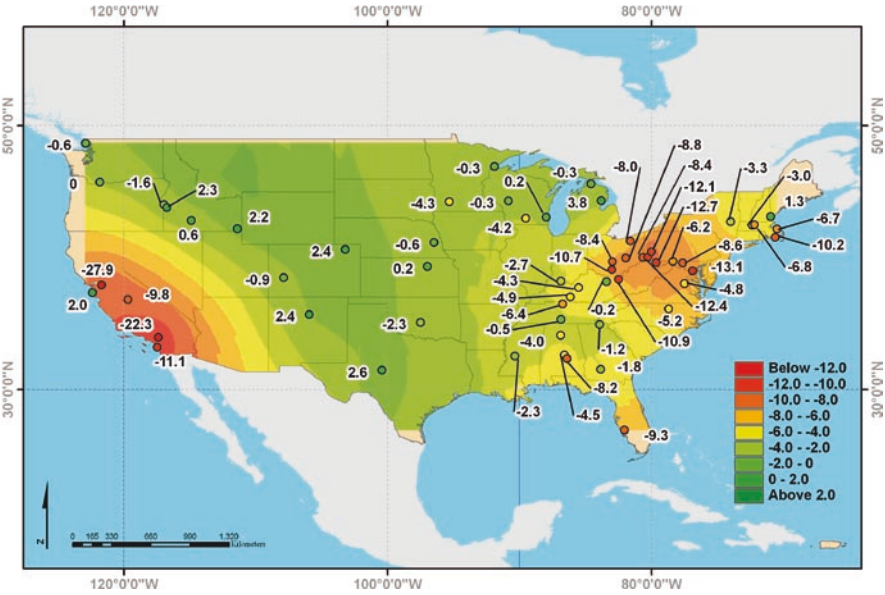

Fig. 19.2 The difference between $\Delta^{14}C$ of CO_2 in clear air measured in Pt. Barrow, Alaska, and in leaves of corn plants sampled throughout the United States in 2004. Units are per mil (‰) relative to the Oxalic Acid standard (Modified from Hsueh et al. 2007)

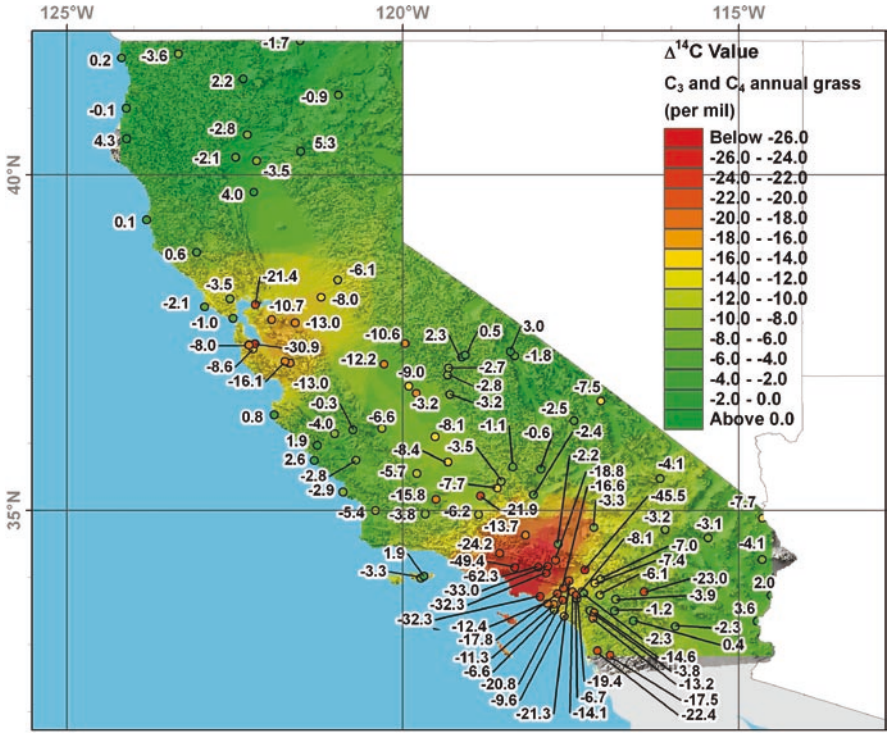

Fig. 19.3 The difference between $\Delta^{14}C$ of CO_2 in clear air measured in Pt. Barrow, Alaska, and in leaves of winter annual plants sampled throughout California in 2005. Units are per mil (‰) relative to the Oxalic Acid standard (Modified from Riley et al. 2008)

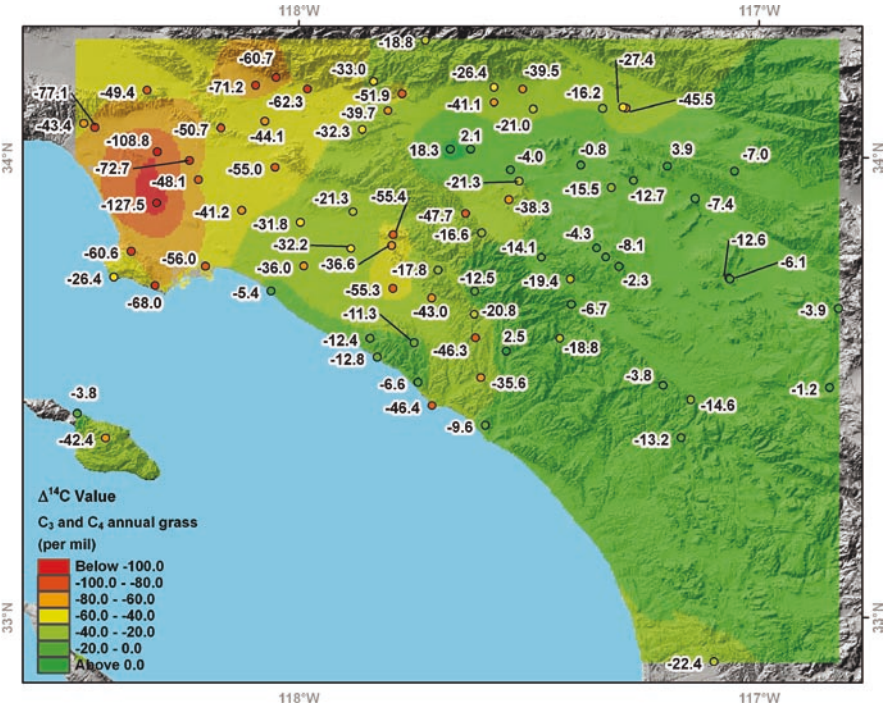

Fig. 19.4 The difference between $\Delta^{14}C$ of CO_2 in clear air measured in Pt. Barrow, Alaska, and in leaves of winter annual plants sampled throughout the Los Angeles Basin in 2004 and 2005. Units are per mil (‰) relative to the Oxalic Acid standard (Modified from Wang and Pataki 2009)

Index